Some Inorganic Chemistry of the New Carbon Cage Cluster, Buckminsterfullerene, C_{60}.

by Richard E. Douthwaite

A thesis submitted in part fulfilment of the requirements for the degree of Doctor of Philosophy at the University of Oxford.

Balliol College

Oxford

January 1995



The work described in this thesis was carried out in the Inorganic Chemistry Laboratory, South Parks Road, Oxford, from March 1992 to September 1994 under the supervision of Professor Malcolm L. H. Green FRS. All the work is my own unless stated to the contrary, and has not previously been submitted for any degree at this, or any other, university.

[Signature removed from online version of thesis]

Abstract

Some Inorganic Chemistry of the New Carbon Cage Cluster, Buckminsterfullerene, C_{60}.

Richard E. Douthwaite
Balliol College

Michaelmas Term 1994
Submitted for D. Phil.

This thesis investigates the properties and reactivity of the carbon cluster C_{60}, Buckminsterfullerene. Each chapter is self contained with experimental details and characterising data.

Chapter 1 reviews the relevant and particularly interesting chemistry of C_{60}, and includes some chemical aspects of the other recently discovered new forms of carbon including the graphitic carbon nanotubules, concentric carbon spheres and amorphous carbon networks. An experimental section describes the techniques used for the synthesis of fullerene rich soot and the subsequent isolation and purification of C_{60} as performed in the Inorganic Chemistry Laboratory, Oxford.

Chapter 2 describes the synthesis, characterisation, and some reaction chemistry of the new complex $Rh(\eta^2\text{-}C_{60})(CO)(H)(PPh_3)_2$ and its activity with respect to the catalytic hydroformylation of ethene and propene, and is compared to the industrially used catalyst $Rh(CO)(H)(PPh_3)_3$. Studies to determine the thermal stability of $Rh(\eta^2\text{-}C_{60})(CO)(H)(PPh_3)_2$ compared to $Rh(CO)(H)(PPh_3)_3$ during hydroformylation catalysis are also included.

Chapter 3 describes the synthesis and characterisation of the new complexes $NaC_{60}.5thf$, $NMe_4C_{60}.1.5thf$ and what could be the new complex $Na_{0.9}C_{60}.3thf$. These materials exhibit a magnetic transition at approximately 180K as determined by bulk static D.C. susceptibility measurements and electron spin resonance spectroscopy. This transition is discussed mainly in terms of a metal-metal or metal-insulator transition. Some reaction chemistry of these materials is also described.

Also described are studies into various aspects of the sodium C_{60} phase diagram at ambient temperature and pressure with regard to the proposed solid solution behaviour in the compositional range Na_1C_{60} to Na_3C_{60}. The synthesis of the novel hexagonal close packed compounds Na_6C_{60} and Na_9C_{60} and consequences for the phase diagram of sodium C_{60} intercalates are discussed.

Chapter 4 describes the synthesis of various alkali metal C_{60} intercalates using a microwave induced argon plasma as the heat source. The developement of this technique for the bulk synthesis of other materials and attempts at the synthesis of novel lithium and ytterbium intercalates are also described.

Acknowledgements

I would like to thank firstly Prof. Malcolm L. H. Green FRS for allowing me to work in his group and for many stimulating discussions. I would also like to apologise for my appalling spelling, and writing style, which I have inflicted upon him over the past three years.

Without the arrival of Dr. Matthew J. Rosseinsky I do not think the work in this thesis would have been possible. Countless questions regarding solid state chemistry, alkali metal fullerides, magnetism, and crystallography have been answered with a smile (at least when I was in the room). All the crystallography in this thesis is also down to him.

Other major contributors to this thesis I would like to mention are Dr. Adrian (I make my own soap) Brough (solid state NMR), Dr. Mark Green (BIOSYM work), Rochel (I've only seen him alone once, and that was in the Gent's) Lago and Dr. Edman (Every time you come down to S14 Richard, I want to hide) Tsang (catalysis elucidation), and Dr. Gavin Whittaker (Microwave expert). Other contributors include Dr. Steven Heyes, Simon ' solid state Johnny' Clarke, Adam Stephens, and all those people I have forgotten.

My partners in grime John (I'M NOT F*****G AGGRESIVE!) Turner and Adam (There's a phone call for you) Stephens for initiating me into the pleasures of C_{60} synthesis, manual chromatography with 10 litres of hexane, and subsequent rotary evaporation of those aforementioned 10 litres of hexane to get 50 mg of an ugly brown powder that would react to become an insoluble ugly brown powder.

This leads me to thank Terry and Martin for glassblowing (columns for less arduous chromatography and microwave vessels). I would also like to thank them for drilling and grinding alumina and zirconia (sorry about the diamond bit).

The basement boys (workshop and stores) Ken 'Thanking you', Steve ' Ken's gone paragliding in the Andes', Keith 'They were guilty, hang the b******s, Dave 'Did I ever tell you about the time I built a particle accelerator', and Howard and Chris.

Proof readers, John, Matt and Malcolm whose parting comment amongst others on giving back chapter 4 ('there isn't a sentence in that chapter that couldn't be improved) I will never forget.

Members of the lab who I have had the pleasure of their company throughout my years of purgatory and would like to thank are Jason 'A real gent' Hubert, Paddy 'P. C.' McGowan, Alejandra ' It's sooo big' Suarez, Rafa 'lantern jaw' Gomez (thanks for the trip to Madrid as well), Dave 'Buck, Buck' Glueck, Steve 'LASER's suck' Kuebler, Luca 'It's a disaster' Labella, John (I didn't mean it about being aggressive) Turner, Dave 'I'm getting married' White, Neil 'I've scored a pair of twenties' Popham and Gary 'Er, Er, Er, Er, Er, pint please' Diamond and all the other members of the group past and present who I have forgotten because my memory is shot to pieces.

Finally I would like to give a very special thank you to Polly for the pleasure of her company and great support over the past year or so and for experiments in natural philosophy. I also apologise for reneging on three holidays and I promise to take a trip with you as soon as this is finished.

Abbreviations

Me = methyl

$Cp^* = \eta^5\text{-}C_5Me_5$

$Cp = \eta^5\text{-}C_5H_5$

thf = tetrahydrofuran

MeCN = acetonitrile

DMSO = dimethylsulfoxide

NMR = nuclear magnetic resonance

MAS = magic angle spinning

SQUID = superconducting quantum interference device

ESR = electron spin resonance

RDE = rotating disc electrode

DSC = differential scanning calorimetry

EMF = electromotive force

IR = Infra-red spectroscopy

UV-Vis = Ultra-violet/ visible spectroscopy

HPLC = high pressure liquid chromatography

SCE = standard calomel electrode

LUMO = lowest unoccupied molecular orbital

HOMO = highest occupied molecular orbital

fcc = face centred cubic

hcp = hexagonal close packed

bct = body centred tetragonal

bcc = body centred cubic

Contents

Chapter 1 *An Introduction to C_{60} and Other New Forms of Carbon*

1.1. General Introduction.....2
1.2. Molecular Fullerenes.....2
1.2.1. Postulation, Discovery and Isolation of the Fullerenes.....2
1.2.2. Physical Properties of the Fullerene C_{60}.....3
1.3. Chemistry of the Fullerene C_{60}.....5
1.3.1. Organic Chemistry.....7
1.4. Solution Inorganic Chemistry.....12
1.5. Charge Transfer Salts.....15
1.6. Intercalation Chemistry.....16
1.6.1. Intercalation Chemistry with no Charge Transfer.....17
1.6.2. Intercalation Chemistry with Charge Transfer.....18
1.7. Polymers and Materials.....21
1.8. Mass Spectroscopic Studies.....22
1.9. Endohedral Fullerenes.....23
1.10. Other Work (Separation, Host-Guest and ESR of Organic Radicals).....24
1.11. Other Forms of Carbon Generated From the Arc Vaporisation of Graphite.....27
1.11.1. Carbon Nanotubules.....27
1.11.2. Amorphous Carbon Networks and Nanoparticles.....32
1.11.3. Concentric Carbon Spheres ('Buckyonions').....32

1.12. General Experimental Details.....33
1.13. The Preparation of C_{60}.....33
1.13.1. Soot Generation.....33
1.13.2. Column Chromatography of Fullerene Containing Soot.....36
1.13.3. Isolation of C_{60}.....37
1.13.4. Sublimation of C_{60}.....39
References.....41

Chapter 2 *C_{60} and the Hydroformylation Process*

2.1. Introduction.....54
2.2. The Industrial Hydroformylation Process.....54
2.3. The Mechanisms of Hydroformylation Catalysis Using Rhodium Tertiary Phosphine Complexes.....56
2.3.1. Factors Affecting the Rate of Hydroformylation.....59
2.3.2. Factors Affecting the Selectivity of Hydroformylation.....61
2.4. Thermal Decomposition of $Rh(CO)(H)(PPh_3)_3$.....63
2.5. The Hydroformylation of C_{60}.....64
2.6. Summary.....65

2.7. The Hydroformylation of C_{60}.....66
2.8. Synthesis of $Rh(C_{60})(CO)(H)(PPh_3)_2$.....66
2.8.1. The Single Crystal Structure of $Rh(C_{60})(CO)(H)(PPh_3)_2$.....70
2.8.2. Some Reactivity of $Rh(C_{60})(CO)(H)(PPh_3)_2$.....70
2.9. The Study of $Rh(C_{60})(CO)(H)(PPh_3)$ as a Hydroformylation Catalyst.....70
2.10. The Catalytic Hydroformylation of Ethene.....71
2.10.1. Results of Ethene Hydroformylation.....71
2.10.2. Discussion on the Hydroformylation of Ethene.....71
2.11. The Catalytic Hydroformylation of Propene.....73
2.11.1. Results of the Hydroformylation of Propene.....74
2.11.2. Discussion on the Hydroformylation of Propene.....77
2.12. Thermal Decomposition Studies.....78
2.12.1. Results of Thermal Decomposition Studies.....78
2.12.2. Disscusion on the Thermal Degradation Studies.....79
2.12.3. Reaction of $Rh(C_{60})(CO)(H)(PPh_3)_2$ with Excess C_{60}.....80
2.13. The Hydroformylation of C_{60} from $Rh(C_{60})(CO)(H)(PPh_3)_2$.....80
2.14. Summary.....81

2.15. Experimental Details for Chapter 2.....82
2.15.1. Manipulations and Solvents.....82
2.15.2. Instrumental Methods.....82
2.16. Synthesis and Reactions.....83
2.16.1. Synthesis of $Rh(CO)(H)(PPh_3)_3$. (1).....83
2.16.2. Synthesis of $Rh(C_{60})(CO)(H)(PPh_3)_2$. (2).....83
2.16.3. Reaction of $Rh(C_{60})(CO)(H)(PPh_3)_2$ with HCl.....84
2.16.4. Reaction of $Rh(C_{60})(CO)(H)(PPh_3)_2$ with $HBF_4.Et_2O$.....84
2.16.5. Reaction of $Rh(C_{60})(CO)(H)(PPh_3)_2$ with CS_2.....84
2.16.6. Reaction of $Rh(C_{60})(CO)(H)(PPh_3)_2$ with C_{60}.....84
2.17. Hydroformylation Catalysis.....84
2.17.1. Procedure for Catalytic Reactions.....84
2.17.2. Hydroformylation Catalysis of Ethene Using $Rh(CO)(H)(PPh_3)_3$ and $Rh(C_{60})(CO)(H)(PPh_3)_2$.....85
2.17.3. Hydroformylation Catalysis of Propene Using Rh(CO)(H)(PPh3)3 and $Rh(C_{60})(CO)(H)(PPh_3)_2$.....87
2.17.4. Analysis of the Products from Propene Hydroformylation.....87
2.18. Temperature-Programmed Decomposition Studies of the Catalysts.....87
2.18.1. Temperature-Programmed Decomposition of $Rh(C_{60})(CO)(H)(PPh_3)_2$ and $Rh(CO)(H)(PPh_3)_3$ in the Presence of CO and H_2.....88
2.18.2. Temperature-programmed decomposition of $Rh(C_{60})(CO)(H)(PPh_3)_2$ and Rh(CO)(H)(PPh3)3 in the presence of CO, H_2 and C_2H_4.....88
2.19. Attempted Hydroformylation of C_{60}.....89

References 90

Chapter 3 *Studies into Sodium Compounds of the Anions of C_{60} and Related Areas*

3.1. Introduction to C_{60} Anions. 93
3.1.1. Solid State Synthetic Routes to Alkali Metal C_{60} Compounds.....94
3.1.2. Solution Routes to Alkali Metal C_{60} Compounds. 96
3.2. Electrochemical Routes to C_{60} Anions. 98
3.3. The Sodium C_{60} Phase Diagram. 98
3.3.1. Postulated Binary Sodium C_{60} Phases at Room Temperature. 101

3.4. Synthesis of NaC_{60}.5thf from Solution.....105
3.4.1. Determination of the Quantity of thf Occluded in NaC_{60}. 107
3.4.2. Structural Studies on NaC_{60}.5thf.....107
3.4.3. ^{13}C and ^{23}Na MAS and Powder NMR Spectroscopic Studies of NaC_{60}.5thf.....112
3.4.4. Magnetic Measurements of NaC_{60}.5thf.....114
3.4.5. ESR Measurements of NaC_{60}.5thf.....121
3.4.6. Electrochemistry of NaC_{60}.5thf. 126
3.4.7. UV-Vis Spectroscopy of NaC_{60}.5thf. 128
3.5. Studies of the thf Insoluble Residue from the Synthesis of NaC_{60}.5thf. 128
3.5.1. Powder X-ray Crystallography and Formulation of 'The Residuals'.....128
3.5.2. ^{13}C and ^{23}Na MASNMR Spectroscopy of 'The Residuals'. 130
3.5.3. SQUID and ESR Measurements of 'The Residuals'.....132
3.6. Discussion on the Na C_{60} thf System. 137
3.7. Some Reaction Chemistry of NaC_{60}.5thf.....139
3.7.1. Synthesis of NMe_4C_{60}.1.5thf. 142
3.7.2. Powder X-ray Crystallography of NMe_4C_{60}.1.5thf. 143
3.7.3. ^{1}H Solution and ^{13}C Powder and MASNMR Spectroscopy of NMe_4C_{60}.1.5thf. 143
3.7.4. SQUID and ESR Measurements of NMe_4C_{60}.1.5thf.....148
3.7.5. Some Chemistry of NMe_4C_{60}.1.5thf. 150
3.7.6. Discussion on NMe_4C_{60}.1.5thf. 156
3.8. Investigations into the Sodium C60 Phase Diagram. 159
3.8.1. Attempted Synthesis of Na_1C_{60}. 159
3.8.2. Attempted Synthesis of $Na_{1.3}C_{60}$. 161
3.8.3. Attempted Synthesis of Na_1C60 and $Na_{1.3}C_{60}$ via Quenching. 164
3.8.4. Synthesis of $Na_{2.5}C_{60}$. 164
3.8.5. Discussion on Solid Solution Phases Between the Compositions Na_1C_{60} and Na_3C_{60}. 166
3.8.6. Synthesis of Hexagonal Close Packed Na_6C_{60} and Na_9C_{60}. 168
3.8.7. Discussion of the Sodium C_{60} Phase Diagram.....172

Experimental Details for Chapter 3 174
3.11. Preparation of $Mn(Cp^*)_2$ 175
3.12. Synthesis of $Na[Mn(Cp^*)_2]$ 176
3.13. Synthesis of Solvated Sodium Salts of C_{60} 176
3.13.1. Extraction of $NaC_{60}.5thf$ 176
3.13.2. Studies of the thf InsolublesThe Residuals'. 177
3.14. Synthesis of $NMe_4C_{60}.1.5thf$. 178
3.15. Synthesis of Some Na Phases of C_{60} Using a Furnace 180
3.15.1. Attempted Synthesis of Na_1C_{60} 180
3.15.2. Attempted Synthesis of $Na_{1.3}C_{60}$ 181
3.15.3. Attempted Synthesis of Na_1C_{60} and $Na_{1.3}C_{60}$ via Quenching. 181
3.15.4. Synthesis of $Na_{2.5}C60$. 182
3.15.5. Synthesis of hcp Na_6C_{60} and Na_9C_{60} 183
3.15.6. Reaction of hcp Na_6C_{60} and C_{60} 183
References 185

Chapter 4 *The Application of Microwave Techniques to the Synthesis of Metal Fullerides*

4.1. General Introduction to Microwave Techniques 190
4.2. The Heating Effect Caused by Dielectric Losses 190
4.3. The Heating Effect Caused by Conduction Losses 193
4.4. Thermal Runaway in Ceramics. 194
4.5. Microwave Induced Plasmas. 196
4.6. The Heating Effect Caused by a Microwave Induced Plasma. 197
4.7. Conventional Solid State and Other Synthetic Routes to Alkali Metal Fullerides. 198
4.8. Possible New Fullerides and Their Potential Properties. 199

4.9. Application of Microwave Techniques to the Synthesis of Alkali Metal Fullerides. 200
4.10. Preliminary Investigations. 200
4.10.1. The Effect of Microwave Radiation on C_{60} and Potassium. 200
4.10.2. Attempted Volumetric Heating of Potassium Metal in the Presence of C_{60} 200
4.10.3. Exposure of C_{60} to a Dinitrogen/Potassium Discharge. 201
4.10.4. Choice of Initiating Plasma Gas. 202
4.10.5. Reaction of C_{60} and Excess Potassium in an Argon/Potassium Discharge. 203
4.10.6. Reaction of a K_xC_{60} Phase Assemblage and C_{60} to form K_3C_{60} 205
4.10.7. Discussion of the Preliminary Reactions. 205
4.11. The Use of Ceramics as Microwave Furnaces. 205
4.11.1. Sublimation of Potassium from an Alumina Crucible Aided by an Argon Plasma. 206

4.12. Design of a Suitable Microwave Reactor for the Synthesis of a K_xC_{60} Phase Assemblage. 207
4.13. Synthesis of a K_xC_{60} Phase Assemblage Using a Reusable Microwave Reactor. 208
4.14. Synthesis of K_3C_{60} from C_{60} and a K_xC_{60} Phase Assemblage. 210
4.15. Synthesis of Other Alkali Metal Fullerides. 214
4.15.1. Synthesis of K_3C_{60} and K_4C_{60} from K_6C_{60} and C_{60} 215
4.15.2. Synthesis of Rb_1C_{60}, Rb_3C_{60} and Rb_4C_{60} from Rb_6C_{60} and C_{60} 220
4.15.3. Synthesis of Cs_1C_{60} and Cs_4C_{60} from Cs_6C_{60} and C_{60} 226
4.16. Reaction of hcp Na_6C_{60} With One Equivalent of C_{60} 232
4.17. Preliminary Investigations into the Synthesis of Binary Lithium C_{60} Compounds 232
4.18. Preliminary Investigations into the Synthesis of Lanthanide Fullerides Using Microwave Techniques 234
4.18.1. Reaction of Ytterbium Metal and C_{60} 235
4.19. Discussion and Summary 238

Experimental Details for Chapter 4. 239
4.20. Manipulations and Solvents 239
4.21. Instrumental Methods 239
4.22. Synthesis of the Saturated K, Rb and Cs Phases of C_{60}. 239
4.23. Conventional Thermal Synthesis of K, Rb and Cs Fullerides. 240
4.24 Synthesis of Alkali Metal Fullerides using Microwave Techniques. 240
4.25. Synthesis of a K_xC_{60} Phase Assemblage from K and C_{60} using an Argon Microwave Induced Plasma 243
4.26. Synthesis of K_3C_{60} from C_{60} and a K_xC_{60} Phase Assemblage. 244
4.27. Synthesis of K_3C_{60} and K_4C_{60} from $K_{6.7}C_{60}$ and C_{60}. 244
4.28. Synthesis of Rb_1C_{60}, Rb_3C_{60} and Rb_4C_{60} from $Rb_{6.7}C_{60}$ and C_{60}. 245
4.29. Synthesis of Cs_1C_{60} and Cs_4C_{60} from $Cs_{6.7}C_{60}$ and C_{60}. 245
4.30. Reaction of Na_6C_{60} and One Equivalent of C_{60}. 246
4.31. Reaction of Li Metal and C_{60} 246
4.32. Vaporisation of Ytterbium Metal in an Alumina Crucible using a Microwave Induced Argon Plasma. 246
4.33. Vaporisation of Ytterbium Metal in a Zirconia/Magnesia Crucible using a Microwave Induced Argon Plasma. 247
4.34. Reaction of Ytterbium Metal and Powdered C_{60} 247
4.34.1. Reaction of Ytterbium Metal and a Film of C_{60} and Subsequent Annealing. 248
References 250

Appendices

Appendix A Refinement of Cell Parameters of NaC_{60}.5thf 254

Appendix B Refinement of Cell Parameters of Na_6C_{60}.....255
Appendix C Refinement of Cell Parameters of Na_9C_{60}.....256
Appendix D Calculation of the Superconducting Sheilding Fraction of K_3C_{60}
Prepared by Microwave Techniques.....257

Abstract

Some Inorganic Chemistry of the New Carbon Cage Cluster, Buckminsterfullerene, C_{60}.

Richard E. Douthwaite
Balliol College

Michaelmas Term 1994
Submitted for D. Phil.

This thesis investigates the properties and reactivity of the carbon cluster C_{60}, Buckminsterfullerene. Each chapter is self contained with experimental details and characterising data.

Chapter 1 reviews the relevant and particularly interesting chemistry of C_{60}, and includes some chemical aspects of the other recently discovered new forms of carbon including the graphitic carbon nanotubules, concentric carbon spheres and amorphous carbon networks. An experimental section describes the techniques used for the synthesis of fullerene rich soot and the subsequent isolation and purification of C_{60} as performed in the Inorganic Chemistry Laboratory, Oxford.

Chapter 2 describes the synthesis, characterisation, and some reaction chemistry of the new complex $Rh(\eta^2\text{-}C_{60})(CO)(H)(PPh_3)_2$ and its activity with respect to the catalytic hydroformylation of ethene and propene, and is compared to the industrially used catalyst $Rh(CO)(H)(PPh_3)_3$. Studies to determine the thermal stability of $Rh(\eta^2\text{-}C_{60})(CO)(H)(PPh_3)_2$ compared to $Rh(CO)(H)(PPh_3)_3$ during hydroformylation catalysis are also included.

Chapter 3 describes the synthesis and characterisation of the new complexes $NaC_{60}.5thf$, $NMe_4C_{60}.1.5thf$ and what could be the new complex $Na_{0.9}C_{60}.3thf$. These materials exhibit a magnetic transition at approximately 180K as determined by bulk static D.C. susceptibility measurements and electron spin resonance spectroscopy. This transition is discussed mainly in terms of a metal-metal or metal-insulator transition. Some reaction chemistry of these materials is also described.

Also described are studies into various aspects of the sodium C_{60} phase diagram at ambient temperature and pressure with regard to the proposed solid solution behaviour in the compositional range Na_1C_{60} to Na_3C_{60}. The synthesis of the novel hexagonal close packed compounds Na_6C_{60} and Na_9C_{60} and consequences for the phase diagram of sodium C_{60} intercalates are discussed.

Chapter 4 describes the synthesis of various alkali metal C_{60} intercalates using a microwave induced argon plasma as the heat source. The developement of this technique for the bulk synthesis of other materials and attempts at the synthesis of novel lithium and ytterbium intercalates are also described.

Chapter 1

An Introduction to C_{60} and Other New Forms of Carbon

1.1. General Introduction

The recent discovery of several new forms of carbon including the fullerenes, graphitic nanotubules and some microporous carbon networks has opened new areas in chemistry, physics and engineering. Investigation into these new forms of carbon has increased at an astonishing pace with well over a thousand publications over the last four years. This introduction will not address every aspect of the chemistry and physical properties of these new systems, but will describe the chemistry and physics relevant to the work in this thesis and some particularly interesting developments. Also, more detailed aspects where necessary will be discussed at the beginning of each chapter.

1.2. Molecular Fullerenes.

1.2.1. Postulation, Discovery and Isolation of the Fullerenes.

Several reviews, articles, and books have documented the history of the fullerenes in copious detail, up to and including the macroscopic isolation, in 1990, of C_{60} and C_{70}.[1-9] A very brief account will be presented.

The first publication postulating a carbon cluster of sixty atoms in a truncated icosohedral arrangement was that by Osawa in 1970.[10] Fifteen years later the first physical evidence for the existence of C_{60} and C_{70} was found via mass spectrometry.[6] Kroto *et al* were attempting to gain information on long chain carbon molecules emitted by red giant stars. Utilising the recently developed cluster beam equipment of Smalley, a series of experiments were performed to mimic conditions on the surface and in the atmosphere of these stars. This led to the serendipitous discovery of the stable carbon clusters C_{60} and C_{70} and the frontpage publication[6] postulating the shape of C_{60} as that of a truncated icosohedron, as shown in figure 1.2.1.1.

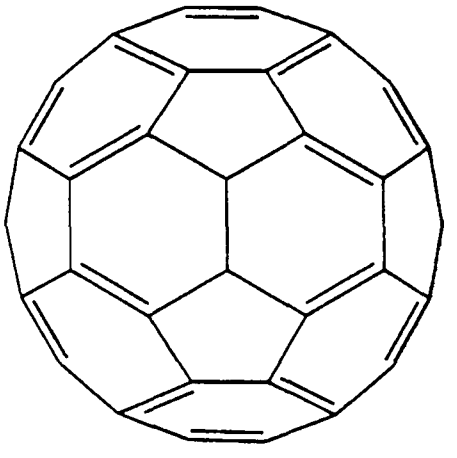


Figure 1.2.1.1. Truncated icosohedral structure of C_{60}.

The name Buckminsterfullerene was coined after the American architect Buckminsterfuller, famous for his geodesic domes and his particular use of geometry in his constructions.

This was of academic interest to the majority of chemists until in 1990 Krätchmer and Huffman announced the first macroscopic isolation of C_{60}.[7].The carbon arc vaporisation of graphite under a partial pressure of helium, gives a black sooty deposit on the walls of the reaction vessel. Infra-red measurements of this soot displayed absorption peaks at frequencies corresponding to those predicted by theory[11] for an icosohedral arrangement of sixty carbon atoms. Subsequent extraction with benzene produced a red solution which led directly, via column chromatography, to the isolation of the first few milligrams of C_{60} and C_{70}. Characterisation, by infra-red and ultra-violet absorption, agreed with theoretical calculations; mass spectroscopy gave a mass ion equivalent to sixty carbons and powder X-ray crystallography and solution ^{13}C NMR spectroscopy led to the unequivocal elucidation of the structure and molecular configuration.[7, 12] Any doubt as to the molecular configuration of C_{60} was expelled by Hawkins and coworkers who characterised the osmium tetroxide adduct OsO_4(4-*t*butylpyridine)$_2$(C_{60}) by single crystal X-ray diffraction.[13]

The smaller yield and lower symmetry (D_{6h}) of C_{70} resulted in slower unequivocal characterisation of the cluster. Single crystal derivatives are now known,[14] adding to the previous data of ^{13}C NMR, infra-red and ultra-violet spectroscopy.

Higher members of the fullerene family have been isolated in milligram quantities after very laborious chromatographic separation. A very interesting property of some fullerenes, most notably C_{76}, is that of chirality. Diederich and co-workers separated the 2 isomers of C_{76}, which have the point group D_2, by HPLC and subsequent characterisation was by ^{13}C NMR. Other higher fullerenes which have been isolated include C_{78}, C_{82}, C_{84}, C_{90} and C_{96}.[15-20]

Fullerenes are very attractive to theoreticians because of their high symmetry and the fact they are composed entirely of one simple p-block element, carbon. A catalogue containing all the possible isomers of clusters containing greater than 19 carbon atoms is in progress. Calculations as to the energy required to isomerise for instance C_{60} into one of the many possible isomers have been reported[21] but to date no reports exist claiming the isolation of any isomer other than the truncated icosohedron.

1.2.2. Physical Properties of the Fullerene C_{60}.

C_{60} consists of sixty equivalent carbon atoms in a truncated icosohedral arrangement. Geometrically, C_{60} consists of twenty hexagons and twelve pentagons arranged so that no two pentagons are adjacent, consistent with the so called 'pentagon rule'. There are thus two distinct types of bond, a 6:6 (30 bonds) and 6:5 (60 bonds) ring fusion with the bond lengths 1.41 and 1.45 Å respectively.

Hückel molecular orbital calculations[22-25] have been performed on C_{60} and are illustrated in figure 1.2.2.1.

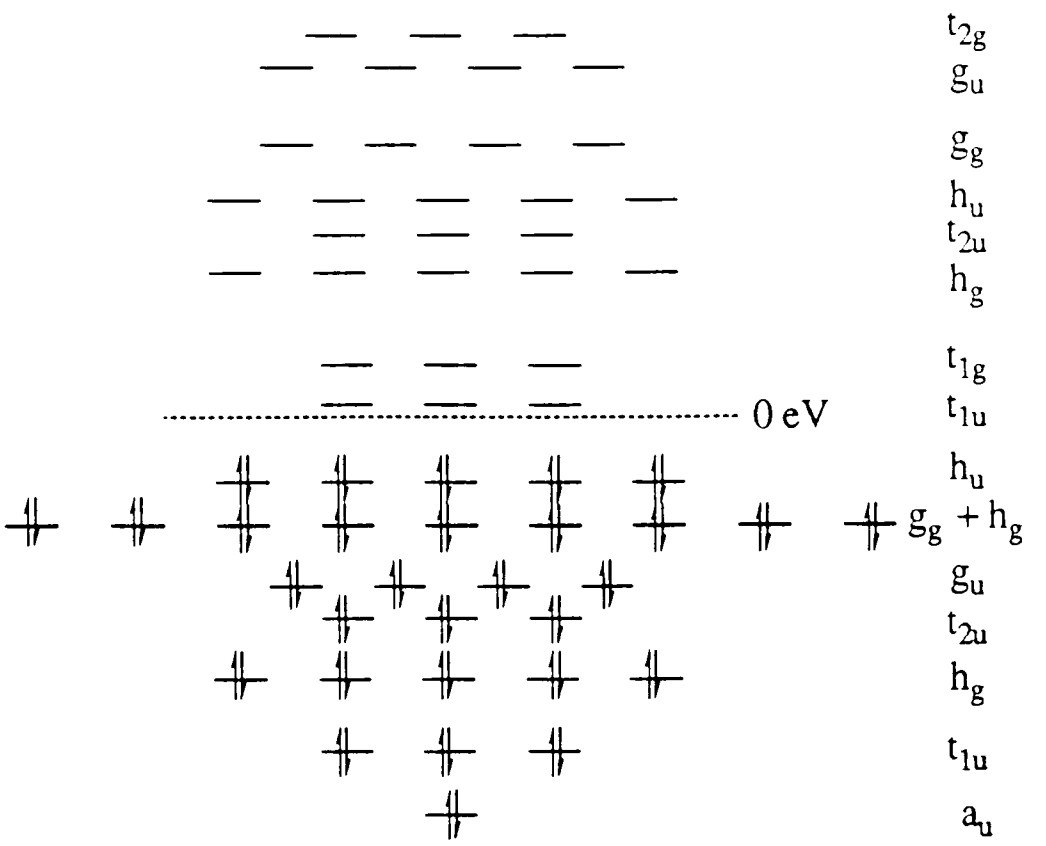


Figure 1.2.2.1. Hückel molecular orbital description of C_{60}.

The LUMO is a triply degenerate t_{1u} state capable of accepting up to six electrons as has been demonstrated by cyclic voltammetry.[10, 26] An h_u level constitutes the HOMO which contains twelve electrons and is very difficult to oxidise chemically. The LUMO is essentially non-bonding whereas the HOMO is bonding. Consequently C_{60} is much more amenable to reduction chemistry than to oxidation chemistry as can be seen from the ratio of papers published that can be classified in this manner. C_{60} has been compared to electron withdrawing olefins such as tetracyanoethylene and tetrafluoroethylene by virtue of its reactivity and has been called, amongst other things, a radical sponge.[27]

The phase diagram of carbon has a long history defined in terms of diamond, graphite and liquid and vapour phases.[28] However the introduction of fullerenes, graphitic nanotubules and particles has generated considerable interest to the workers in this field. To date, very little thermodynamic information of C_{60} is known, mainly due to the unavailability of large quantities of sufficiently pure material. The heats of formation of C_{60} and C_{70} have been determined,[29, 30] and correlate strongly with theoretical calculations.[31-34] Fullerenes are higher in energy than graphite or diamond due to there highly strained nature, but they exhibit significant kinetic stability. C_{70} is more thermodynamically stable than C_{60},[29] which can be interpreted as a consequence of a release in strain, and the first step on the asymptotic approach to a graphite structure.

In the solid state, at room temperature, C_{60} has X-ray, neutron and electron diffraction patterns which can be indexed to a face centred cubic structure with a hexagonal close packed stacking fault.[35] The space group is $Fm\bar{3}m$, which is best

formulated as a consequence of complete orientational disorder i.e the C_{60} molecules are spinning isotropically in the solid. This is also indicated using Raman scattering,[36, 37] quasielastic neutron scattering,[38] and ^{13}C solid state NMR spectroscopy.[39] At room temperature the rotational correlation time τ has been reported as 9 ps, as determined by ^{13}C powder NMR, which is only 3 times slower than expected for rotation in the gas phase and is faster than observed in solution![40]

On cooling, a first-order phase transition occurs at approximately 260K as observed, amongst other techniques, by variable temperature X-ray[41] crystallography, ^{13}C powder NMR spectroscopy,[42] Raman spectroscopy[36, 37] and differential scanning calorimetry.[43] A change, from the room temperature face centred cubic to a simple cubic structure with the space group $Pa\bar{3}$ is observed. This is best interpreted as orientational ordering due to coulombic interactions between 'electron rich' 6:6 'C-C double bond' ring fusions and pentagonal or hexagonal faces.[44] Figure 1.2.2.2. shows ^{13}C powder NMR spectra at variable temperature indicating that below the phase transition the structure is not rigid but still contains disorder. Various structural models have been proposed to account for the experimental observations but the most reasonable argues that isotropic rotation is replaced by 'ratcheting' of C_{60}'s between symmetrically equivalent orientations.[40, 42] As the temperature is lowered the ratcheting becomes progressively slower as indicated by the increase in line width of ^{13}C NMR data.

Other transitions have been postulated at various temperatures but these have been accounted for on the basis of impurities, typically solvent or C_{70}, present in the supposedly 'pure' sample. To obtain pure C_{60}, sublimation is essential because, according to mass spectral data and TGA measurements, solvent impurities acquired during chromatographic separation are retained even at temperatures above 600°C.[35, 45]

1.3. Chemistry of the Fullerene C_{60}.

Initially, based on theoretical predictions, it was thought C_{60} would be essentially inert. Within the first few months, proceeding the macroscopic isolation of the fullerenes, it became evident that C_{60} had the potential for a rich and diverse chemistry in the gas, solution and solid phases.

Before and after, the macroscopic isolation of C_{60}, numerous experiments were performed in the gas phase, usually in a mass spectrometer or similar beam equipment. Except for the case of fullerenes themselves and a few endohedral fullerenes, discussed in section 1.9, no macroscopic quantities of any of the postulated species present in the beam have been isolated in pure form.

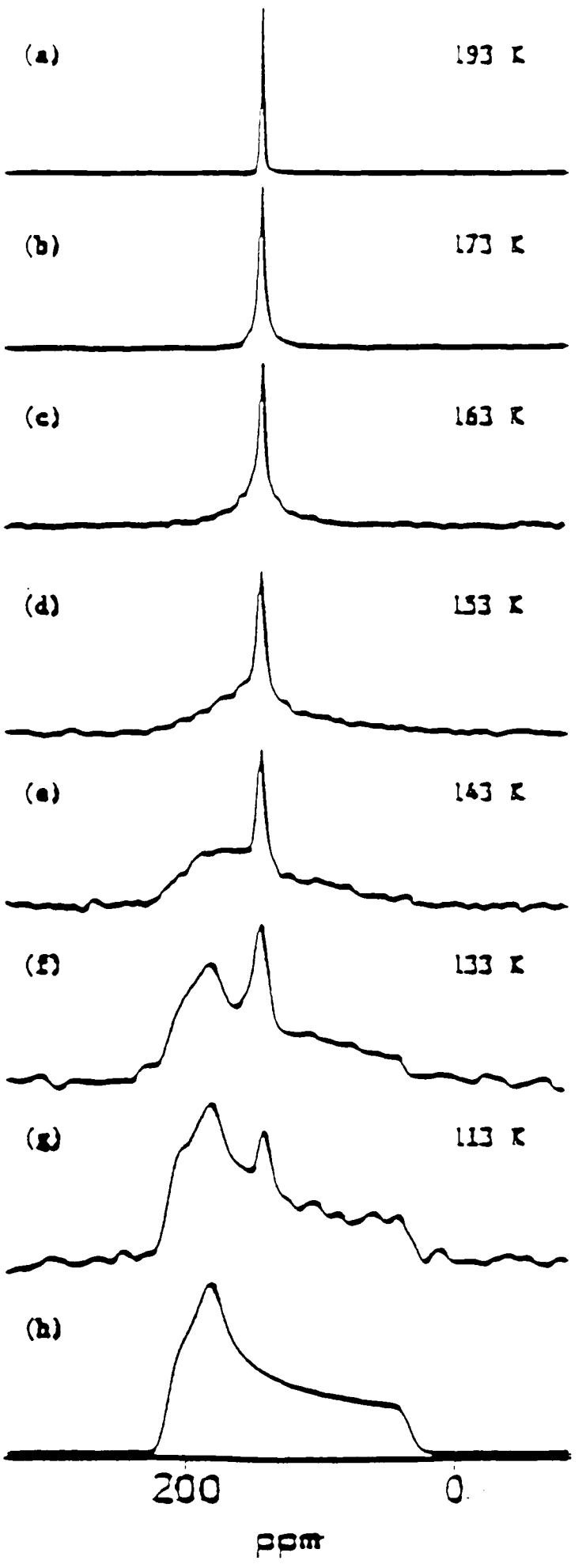


Figure 1.2.2.2. ^{13}C powder NMR spectra of solid C_{60} at indicated temperatures. Frequencies are in ppm with respect to tetramethylsilane (h) is simulated powder pattern for rigid molecules with anisotropic ^{13}C chemical shielding.

Solution chemistry has been afflicted by a number of problems, but this does not seem to have hindered rapid progress in the fields of organic, inorganic and organometallic C_{60} chemistry. Common problems encountered are the low solubility of products, and a distribution of products and their isomers. Large amounts of solvent are required and laborious separation, typically by preparative HPLC, is needed to isolate a pure compound. These problems can be obviated somewhat by judicious choice of a reactant, or derivative of it, that will impart enhanced solubility characteristics and the use of techniques which allow greater control of stoichiometry.

The relatively large molecular weight (720 a.m.u.) of C_{60} and therefore its reaction products, coupled with low solubility, and product distributions and isomers, can cause severe problems in obtaining information by traditional techniques such as NMR. It is often necessary to use relaxation agents and large diameter NMR tubes to obtain reasonable signal to noise ratios.

When a reaction involves, or results in, a compound which is moisture and/or oxygen sensitive care must be taken to use a pure form of C_{60}. It is known that the C_{60} lattice can accommodate dioxygen and solvent molecules very easily and will absorb atmospheric dioxygen if left on the open bench.[46, 47] Heating to 200°C removes dioxygen and most of any occluded solvent, but solvent has been observed in mass spectroscopy and TGA measurements on samples dried at a temperature of 600°C.[45] As a C_{60} sample will be dissolved prior to a reaction a little occluded solvent is tolerated. However, for very sensitive work, and solid state C_{60} chemistry, sublimation provides the purest form of C_{60}. Alternative evidence for impurities present, even after heating above 200°C, is shown in the observation that at least 10% of a 'C_{60}' sample is lost during the sublimation process, and sublimed C_{60} can be resublimed with no losses.

Arguably, alkali metal C_{60} phases have attracted the most attention from chemists, and especially physicists, since the discovery of superconductivity in K_3C_{60}. Solid state C_{60} chemistry has been dominated by investigations into the magnetic, optical and electronic properties of alkali metal intercalation compounds and their derivatives. Charge transfer salts of C_{60} have also been investigated widely.

Powder X-ray, neutron, and electron diffraction have allowed structural characterisation, and techniques such as ^{13}C powder and MASNMR spectroscopy, SQUID magnetometry, ESR, and DSC give valuable information when investigating the properties of C_{60} containing materials.

1.3.1. Organic Chemistry.

The discovery of C_{60} was hailed as the beginning of a renaissance in the field of organic chemistry, and the new 'three dimensional benzene', a route into a synthetic wonderland. Progress was initially slow, mainly due to the small quantities of C_{60}

available, low solubility of the products, and problems with separation and characterisation. There has also been a trend to use C_{60} as an 'R-group' in a lot of the work published to date. The chemistry of C_{60} rather than of its derivatives will be stressed.

However, a number of synthetic methodologies have been developed over the last three years.

Initially, reactions typical of aromatic systems were attempted such as Birch reduction,[48] chlorination and bromination followed by Friedel-Crafts[49], and the acid-catalysed synthesis of arylfullerenes.[50] Precise stoichiometry and isomer ratios were random due to the complete unselectivity of the reactions. Characterisation was by mass spectroscopy which in the case of the Birch reduction led to misinterpretation of the product ratios.[51]

There are four main synthetic routes which have been used successfully in the preparation of well defined fullerene containing organic molecules. These are reaction with carbenes,[52-58] dipolar cycloadditions,[59-65] Diels-Alder,[66-71] and nucleophilic addition.[49, 54, 72-74]

A development of the carbene reaction, has been the synthesis of a fullerene derivative which has shown promise as an inhibitor of the HIV-1 protease.[75] The compound is shown in figure 1.3.1.1.

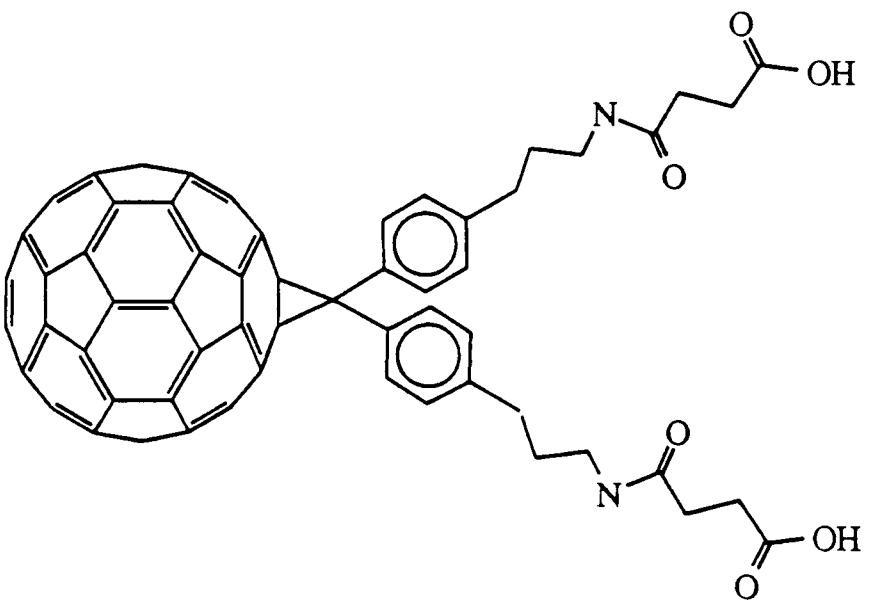


Figure 1.3.1.1. Diphenylcarbene derivative of C_{60} that has shown promise as an HIV-1 inhibitor.

Examination of the topography at the active site of the protease, reveals a cavity capable of accepting the C_{60} derivative. Introduction of this molecule into the cavity removes approximately 300Å^2 of surface area, as determined by molecular modelling, significantly reducing the activity of the protease. Chiral spiro-linked C_{60} sugars[55] have also been prepared with a view to the generation of ambiphilic C_{60} compounds with biochemical and pharmacological potential and similar potential has been postulated for the dendrimer[76] shown in figure1.3.1.2.

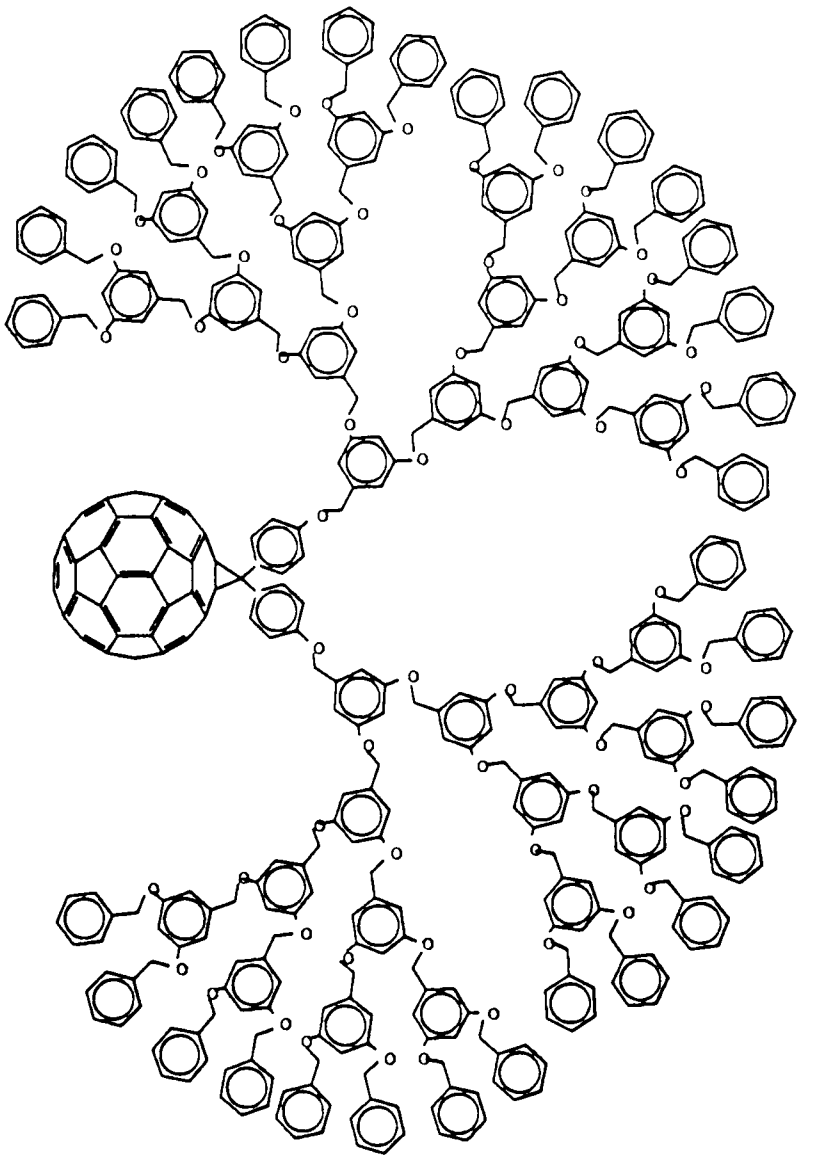


Figure 1.3.1.2. Dendrimer of C_{60}.

C_{60} can act as a dieneophile in [4+2] cycloadditions[66-71] and will also undergo [2+2] cycloadditions with benzyne[77] or more interestingly itself.[78] Diels-Alder reactions with C_{60} can be problematic due to facile decomposition via retro Diels-Alder pathways. This can be circumvented by imparting extra stability in the product by the introduction of aromaticity[68] as shown in figure 1.3.1.3. Other cyloadditions, [3+2][61, 65, 79] and [8+2][59] have also been reported.

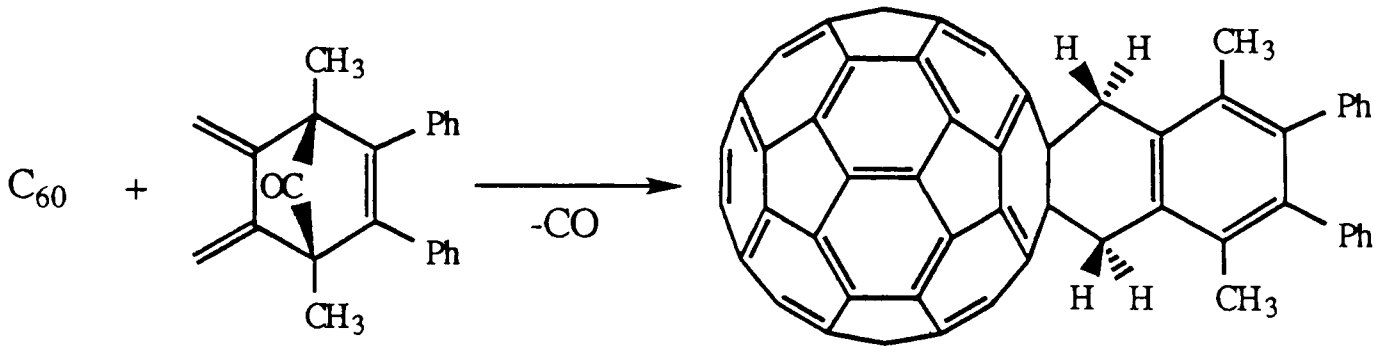


Figure 1.3.1.3. Deils-Alder adduct stabilised by adduct aromatisation.

Another class of reaction are 1,3-dipolar cycloadditions.[53, 60, 80, 81] The 1,3-dipole is usually generated in situ in the presence of C_{60} as shown in figure 1.3.1.4. for the reaction of azomethine ylides.[60]

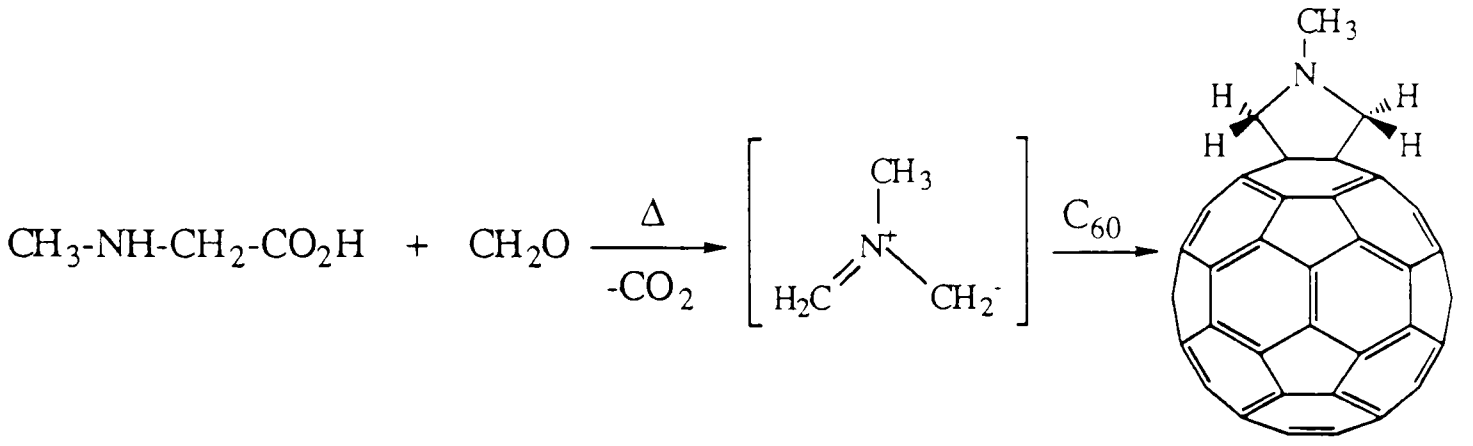


Figure 1.3.1.4. Typical 1,3-dipolar cycloaddition.

This type of reaction has been used extensively to produce five membered ring heterocycles containing two C_{60} carbons from the 6:6 ring fusion. In some compounds, such as that shown in figure 1.3.1.5, decomposition of the five membered heterocycle leads to pseudocyclopropane derivatives.[82] The compounds shown in figure 1.3.1.5, are of particular interest because they are the only two examples of addition across a 5:6 ring fusion. It is also postulated on the basis of NMR evidence that all of the C_{60} carbons are sp^2 i.e. one of the C-C bonds on C_{60} has been completely broken.

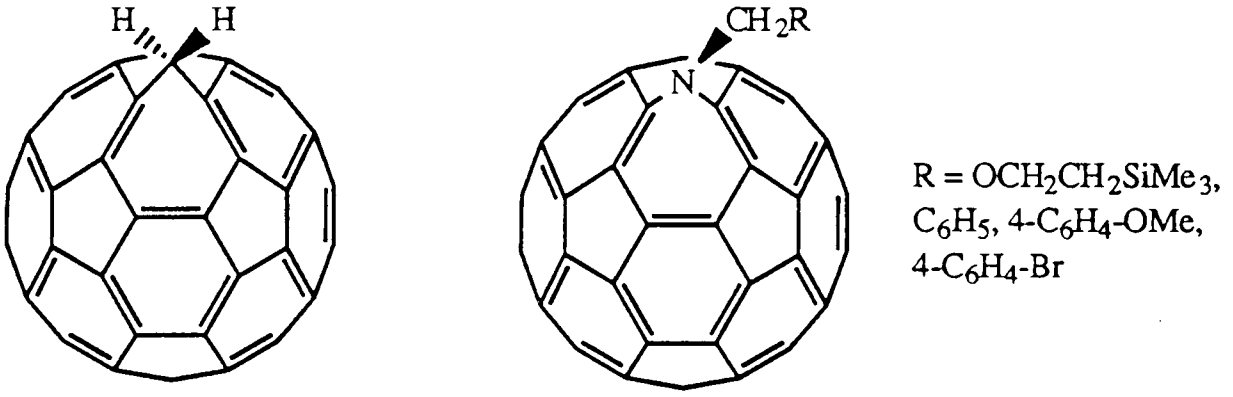


Figure 1.3.1.5. Only examples of addition across a 5:6 ring fusion.

Reaction of C_{60} with nucleophiles has produced very few well characterised compounds, probably due to indiscriminate attack and subsequent high dispersity of products and their isomers. A further possibility is concerned with the ease C_{60} anions can be oxidised to radicals which can result in dimerisation or decomposition. These characteristics are evident from reports which quote product yields as a percentage of reacted C_{60} rather than an overall yield, because typically over 50% of pure C_{60} can remain unreacted.

Two well characterised products from nucleophilic addition are the reactions with ^{t}butyl lithium[73] and borane adducts of lithiated phosphines,[74] as shown in figure 1.3.1.6. The phosphine complexes, in chiral form, have been used with a modicum of success (8% e.e.) in the asymmetric cross coupling of 1-phenyethyl magnesium bromide and β-bromostyrene. Oxidation of the ^{t}butyl-C_{60} anion with iodine to form the corresponding radical is easily achieved resulting in dimerisation. Protonation of the

^{t}butyl anion results in a hydrocarbon with a pK_a determined by quantitative electrochemistry to be 5.7 (±0.1). This ranks ^{t}butyl-C_{60}-H as one of the strongest acids known, whose composition is entirely hydrogen and carbon.

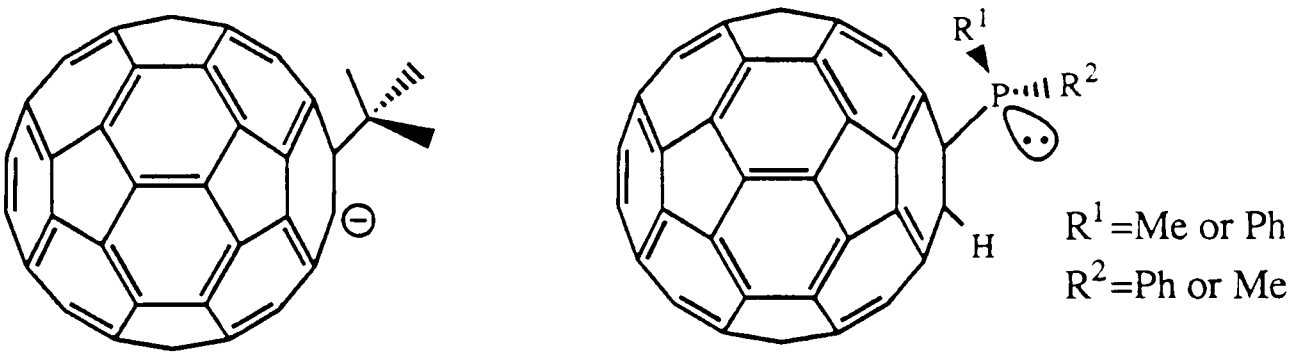
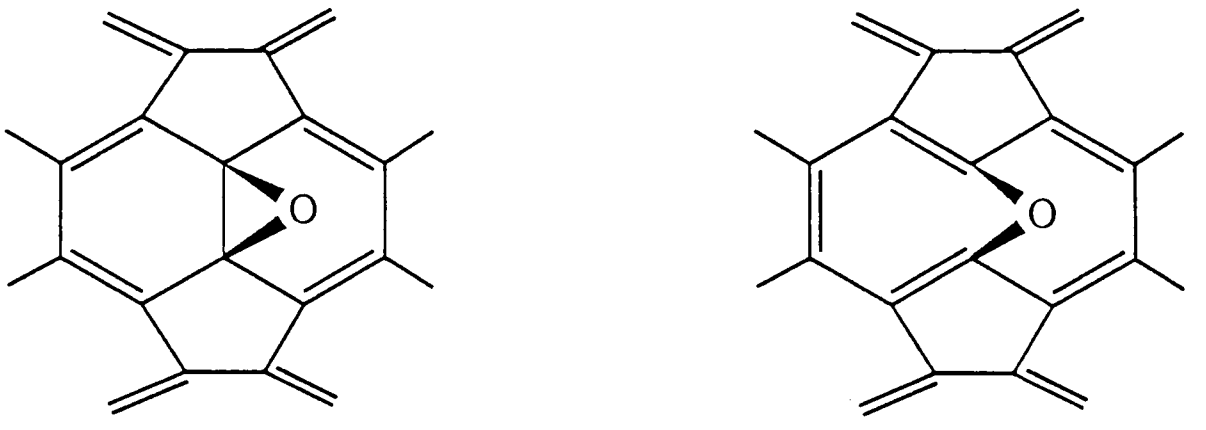


Figure 1.3.1.6. Two well characterised nucleophilic addition products.

Two other fundamentally important compounds are $C_{60}H_2$ and $C_{60}O$. There are several reports in the literature citing these compounds as components of reaction products, but reliable synthetic routes are very few in number. $C_{60}O$ has been detected as a byproduct from fullerene synthesis[83] but has been shown to decompose to C_{60} on passage down an alumina column, or on heating over *ca.* 150°C.

$C_{60}H_2$ can be synthesised from BH_3.thf[84] and using $(\eta^5C_5H_5)_2Zr(H)(Cl)$.[85] After hydrolysis of the intermediates and HPLC, ^{1}H NMR, IR, and negative ion mass spectroscopy led to the 'unequivocal' conclusion that $C_{60}H_2$ was present. No structural data to date has been reported, and so the position of the two hydrogens is unknown, but theoretical calculations lean towards addition across a 6:6 ring fusion.[86, 87]

$C_{60}O$ is most readily prepared using dimethyldioxirane[88] giving the product in 4% yield after purification via HPLC. The structure is postulated as an epoxide rather than an annulene, as shown in figure 1.3.1.7, on NMR spectroscopic evidence.



Monoepoxide of C_{60} 1,6-oxo[10]annulene structure

Figure 1.3.1.7. $C_{60}O$ is the monoepoxide rather than an annulene based on ^{13}C NMR evidence.

Another route is photooxygenation,[89] which is irradiation of an oxygen saturated benzene solution of C_{60} for several hours, followed by HPLC, giving a maximum yield of 7%. In the solid state $C_{60}O$ is orientationally disordered, but structural evidence has been reported for the product from the reaction with $Ir(CO)(Cl)(PPh_3)_2$ which forms the corresponding η^2 complex showing the presence of the epoxide at a 6:6 ring fusion.[90]

1.4. Solution Inorganic Chemistry.

This section will concentrate on C_{60} complexes of transition metal compounds and the reactions of C_{60} with the halogens. Charge transfer chemistry will be dealt with in section 1.5.

The prediction that C_{60} would be electron deficient at various potentially reactive sites, was borne out by the report of Fagan and co-workers that the electron rich platinum complex $Pt(C_2H_4)(PPh_3)_2$, reacted with C_{60}, to form the complex $Pt(\eta^2\text{-}C_{60})(PPh_3)_2$.[91] Indeed it is possible to add six $Pt(PEt_3)_2$ moieties to the surface of a single C_{60} molecule[92] as shown in figure 1.4.1.

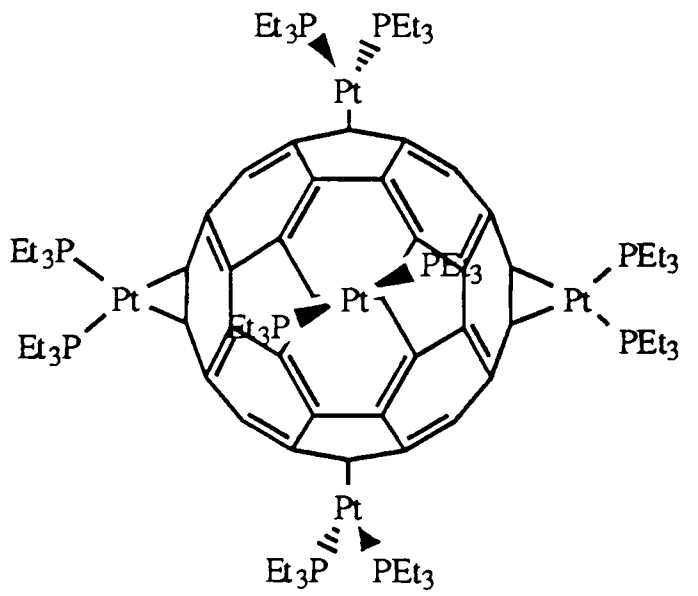


Figure 1.4.1. One of the first organometallic adducts of C_{60} structurally characterised.

Single crystal X-ray structural analysis showed that the platinum groups are arranged in a pseudooctohedral array and that the bulk of the triethylphosphines prevents further reaction beyond the sixth addition. Palladium and nickel derivatives have also been fully characterised as have derivatives of other phosphines. Electrochemistry of the platinum derivatives[93] show that it is progressively more difficult to add the electron rich metal fragment. This allows selectivity to be obtained for a required adduct to C_{60} ratio. A certain amount of reversibility is also implied to allow redistribution of metal adduct throughout the bulk C_{60} solution.

The majority of C_{60} metal complexes are based on electron rich platinum group metals. Tertiary phosphine complexes of Ir,[94-97] Ru,[98] Co,[98] and Rh[99, 100] with C_{60}

have been synthesised, mainly because the phosphine substituents impart good solubility and have a preponderance to crystallise leading to characterisation by single crystal X-ray diffraction. The complex $Rh(C_{60})(CO)(H)(PPh_3)_2$, has been shown to be an effective hydroformylation catalyst[101] and can be viewed as a transition state in the hydroformylation process. It is also noteworthy that insertion of C_{60} into the Rh-H bond does not occur. This compound and its catalytic performance form the basis of chapter 2.

Other transition metal C_{60} compounds described include $Fe(C_{60})(CO)_4$,[100] $Ru(C_{60})(CO)_4$,[102] $Mo(C_{60})(\eta^5\text{-}C_5H_5)_2$,[100] $Ta(C_{60})(\eta^5\text{-}C_5H_5)_2(H)$[100] and the first structurally characterised C_{60} complex $OsO_4(4\text{-}^t\text{butylpyridine})_2(C_{60})$ [13]shown in figure 1.4.2.

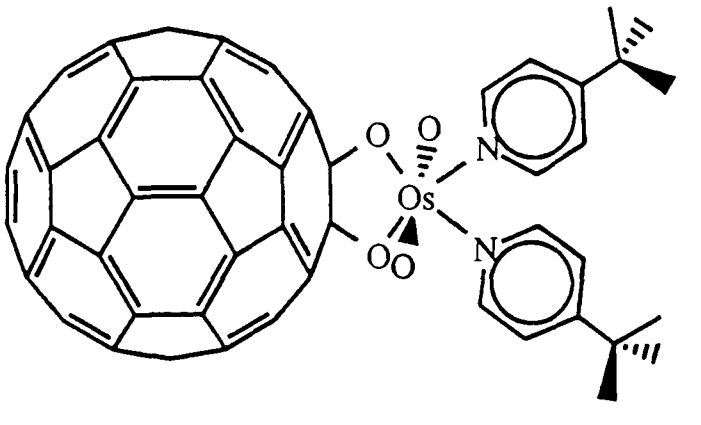


Figure 1.4.2. The first structurally characterised C_{60} complex confirming the truncated icosohedral structure of C_{60}.

C_{60} is coordinated in an η^2 mode across a 6:6 ring fusion in all of the above compounds. No other coordination mode has been observed. The iridium dimer $Ir_2Cl_2(1,5\text{-COD})_2$ forms a double addition complex of C_{60}, $[Ir_2Cl_2(1,5\text{-COD})_2]_2C_{60}$, which has been structurally characterised.[103] It has been proposed as the first η^4 C_{60} complex but , as shown in figure 1.4.3, the complex exhibits bis η^2 coordination to the C_{60}.

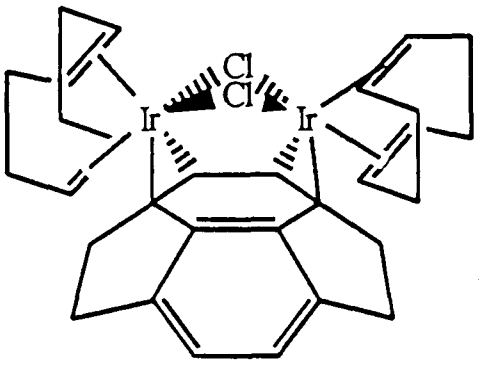


Figure 1.4.3. Bis η^2 coordination is exhibited rather than η^4.

Halogen chemistry of C_{60}, especially fluorination[104-112] has been the subject of much interest. Fluorinated buckyballs were postulated to be excellent lubricants[105] but unfortunately, so far, this has proven not to be the case. It is clear that C_{60} reacts with

fluorine or fluorinating agents, but unfortunately the products from the reaction seem to be generally inseparable, even though solubility does not appear to pose a problem. Initially it was thought that exposure of C_{60} to fluorine gave the compound $C_{60}F_{60}$[109] in high yield, but this was found to be in error.[105] There is evidence to support that cracking of C_{60} occurs, *c.f.* graphite, generating CF_2 groups in addition to the expected conventional addition products.[104, 106] The only fluorinated product of C_{60}, that has significant characterising data supporting the proposed structure, is $C_{60}F_{48}$.[108] A combination of ^{19}F-^{19}F 2D NMR spectroscopy and the use of a computer program to deconvolute the possible isomer products led to the structure determination of $C_{60}F_{48}$. However it was only approximately 60% of the analysed product.

Ambiguity over composition, has not prevented reports on the reactivity of fluorinated C_{60} from being the subject of several publications. Nucleophilic substitution of fluoride (fluorine ?) has been demonstrated with methoxide, Grignard and lithium reagents.[111] Unsurprisingly, numerous products were obtained, some containing fluorine and oxygen,[107, 112] with unknown composition or structural information.

Chlorination[49, 113, 114] and bromination[49, 115, 116] of C_{60} have yielded several well characterised derivatives and several crystal stuctures have been reported.[115, 116] Both chlorination and bromination products tend to lose the halogen at elevated temperatures and have been proposed as potential halogenating agents. A C_{60} halogenating agent should add in a *cis* arrangement because of the steric bulk of the fullerene.

The crystal structure[115] of $C_{60}Br_{24}$ vividly illustrates the beautiful symmetry possible in the chemistry of C_{60}, as shown in figure 1.4.4.

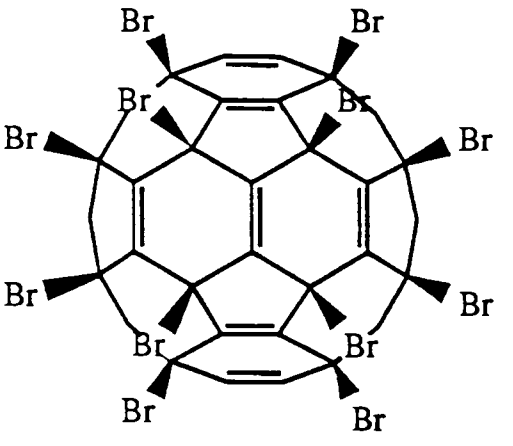


Figure 1.4.4. $C_{60}Br_{24}$ exhibits T_h symmetry

Iodine reacts with C_{60} but retains its molecular constitution. Intercalation into the C_{60} lattice occurs forming the compound $C_{60}(I_2)_2$.[117] This and other intercalation compounds will be discussed in section 1.6.

1.5. Charge Transfer Salts.

Molecular materials having interesting magnetic, optic and electronic properties have been the subject of numerous publications. Charge transfer salts are generally considered as molecular materials soluble in common organic solvents and can be prepared using standard solution chemistry techniques at moderate temperatures (< 200°C).[118]

The low lying triply degenerate LUMO of neutral C_{60} is very attractive as a basis for the preparation of molecular materials.[119] Up to six electrons can be introduced into the LUMO providing a range of possibilities and the potential to tune ensuing properties, as observed in alkali metal intercalation chemistry of C_{60}, which will be discussed in section 1.6.2. In contrast to alkali metal intercalates, a variety of donors possessing a spin, or that can contribute significantly to the electronic or magnetic wavefunction, should be amenable to chemists.

A number of charge transfer salts of C_{60} have been synthesised and characterised to varying degrees. The majority are based on transition metal organometallic or coordination compounds, and the rest on organic donors. All the charge transfer complexes of C_{60} known to date intrinsically have C_{60} as the acceptor.

Three methods have been utilised in the preparation of charge transfer salts of C_{60}. The first, is just simple addition of the neutral precursors in solution, which results in precipitation of the salt. Electrocrystallisation has been successfully used to grow single crystals of several salts, and finally salt metathesis gave single crystals of one material.

The number of electrons introduced into the C_{60} LUMO depends on a number of factors. As a primary consideration the donor must be capable of reducing the acceptor, in this case C_{60}, which can be deduced to a first approximation, by considering the relevant electrochemical data. Allowance must be made for solvent effects in the electrochemical data. Most notably, the dielectric constant of the solvent medium may determine whether charge transfer occurs or not. If the ion pair, generated after electron transfer, is insoluble in the reaction medium this tends to preclude further reduction. Therefore, judicious choice of solvent can determine if, and to what degree, charge transfer will occur.

Electrocrystallisation requires that the material deposited on the electrode surface be, at least to a small degree, conducting to allow electron transport from the electrode to the crystal surface, and of course, for the deposited salt to be insoluble in the electrolyte solution.

The first charge transfer salt to be synthesised was prepared by electrocrystallisation, and yielded a microcrystalline product which analysed as $C_{60}^{\cdot-}Ph_4P^+.(Ph_4PCl)_2$.[120] The assignment of C_{60} as the radical monoanion was based on

ESR and SQUID magnetometry data, but it is evident from close examination of the data that the material contains impurities. It is a characteristic of the vast majority of C_{60} salts known that cocrystallisation occurs, either with solvent or excess precursor, depending on the method of preparation.

Other transition metal based charge transfer salts that have been prepared by electrocrystallisation are $[(C_6H_5)_4P]_2[C_{60}][I]_x$ x~0.35,[121] $[(C_6H_5)_4P]_2[C_{60}][Cl]$,[122] $[Ru(bpy)_3^+][C_{60}^{\cdot -}]$,[123] and $[N(P(C_6H_5)_3)_2^+][C_{60}^{\cdot -}]$.[124] All have been described as crystals but only the two tetraphenylphosphonium salts have published structures. No organic salts have been synthesised by electrocrystallisation.

Solution synthesis has yielded the salts $[Cr(tpp)^+][C_{60}^{\cdot -}].3thf$ where ttp=tetraphenylporphyrin,[125] $[Fe(\eta^5\text{-}C_5H_5)(\eta^5\text{-}C_6Me_6)^+]_n[C_{60}^{n-}]$ n=1-3,[126] $[Co(\eta^5\text{-}C_5H_5)_2^+][C_{60}^{\cdot -}].PhCN$,[127] [Na(dibenzo-18-crown-6)$(thf)_2^+$][$C_{60}^{\cdot -}$].thf,[127] $[Sn(ttp)(N\text{-}MeIm)_2^{2+}][C_{60}^{\cdot -}]$,[127] where N-MeIm=N-methylimidazole, $[N(P(C_6H_5)_3)_2^+]_2[C_{60}^{2-}]$,[128] $(BEDT\text{-}TTF)_2C_{60}$ where BEDT-TTF = bis(ethylenedithio)tetrathiafulvalene,[129] $(HMTTEF)C_{60}$ where HMTTEF = hexamethylenetetratellurafulvalene,[130] and $(TDAE)C_{60}$ where TDAE = tetrakisdimethylaminoethylene.[131] Single crystal structures of these materials are limited to , $(BEDT\text{-}TTF)_2C_{60}$ and $[N(P(C_6H_5)_3)_2^+]_2[C_{60}^{2-}]$.[128] This last salt is interesting as it is the only single crystal structure of the C_{60} dianion and appears to show a Jahn-Teller distortion.

With regard to interesting properties, all the metal containing compounds exhibit Curie or Curie-Weiss behaviour at high temperature where reported. The tetraphenylphosphonium salts show different non Curie-Weiss behaviour but this has not been fully interpreted to date. Of the organic based salts, only partial charge transfer is inferred, if at all. Soft itinerant ferromagnetism has been postulated for $(TDAE)C_{60}$ below 16K, however the data is not conclusive and further experimentation is in progress.[132]

1.6. Intercalation Chemistry.

The cubic structure of C_{60} contains interstitial sites capable of accommodating guest species. Cubic structures contain one octahedral and two tetrahedral sites per molecule/atom and, assuming a C_{60} radius of 5.01Å, these have radii of 2.07 and 1.13Å respectively.

The intercalation chemistry of C_{60} can be divided into two areas where introduction of the intercalating species is accompanied by complete electron transfer or not. The former category is dominated by the alkali metals and the latter contains molecular species.

1.6.1. Intercalation Chemistry with no Charge Transfer.

Only a handful of intercalation compounds of C_{60} are known where no net electron transfer appears to take place. Of these only $(I_2)_2C_{60}$[117] and $(P_4)_2C_{60}$ have been characterised structurally.[133, 134] Both are made by exposing C_{60} powder to I_2 or P_4 vapour at elevated temperatures. $(P_4)_2C_{60}$ can also be prepared from solution by the addition of a CS_2 solution of P_4 to a toluene solution of C_{60}.[133] Both have very similar structures (space group P6/*mmm*) based on simple hexagonal stacking layers separated by layers of guest species in a A/A/A/... type arrangement, where A and / represent C_{60} and guest layers respectively. The structure of $(P_4)_2C_{60}$ is shown in figure 1.6.1.1.

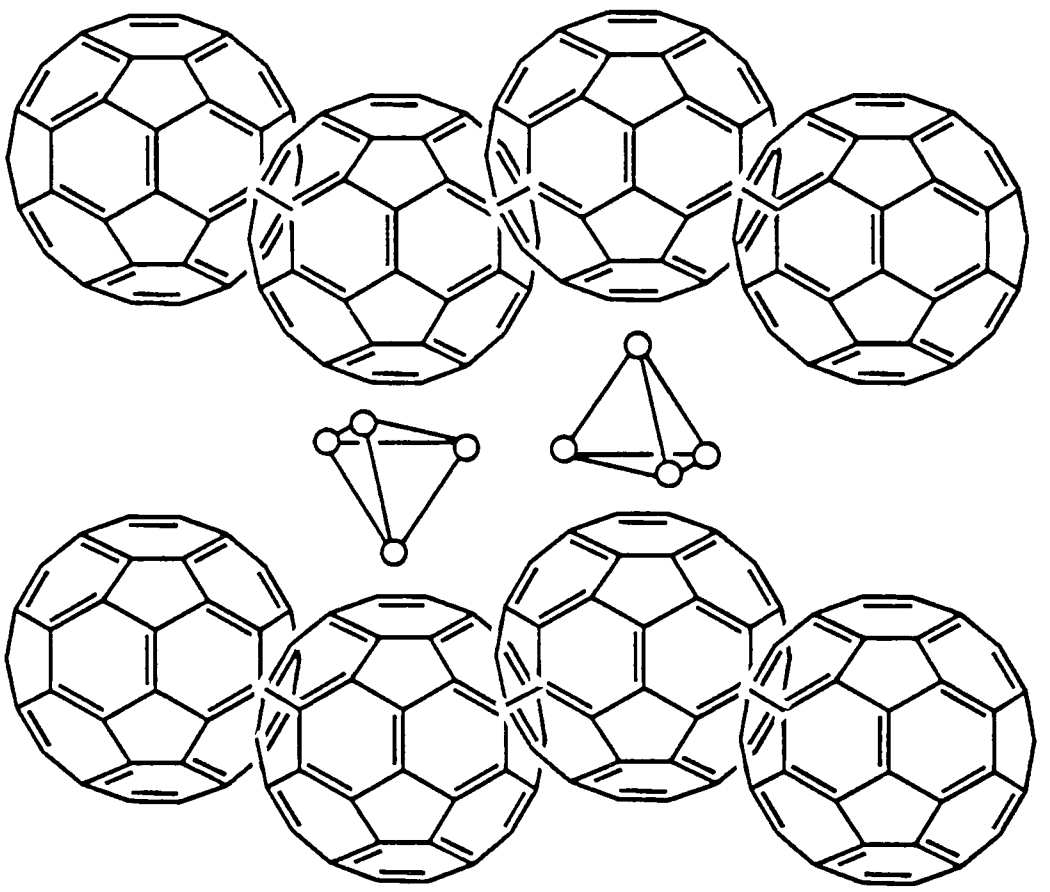


Figure 1.6.1. $(P_4)_2C_{60}$ shows a layered structure of C_{60} molecules and P_4 units.

Studies into the uptake of dihydrogen, dinitrogen and dioxygen by the C_{60} lattice at various pressures have been performed.[46] It was shown that all of these gases were readily incorporated into the interstitial sites, but no structural information is available. At ambient pressure and temperature all the gases were retained to a degree. This has important implications for the chemistry of C_{60}, where materials are expected to be oxygen sensitive. Methane did not show any significant uptake.

Several structures of C_{60} have been characterised by single crystal X-ray diffraction or electron microscopy which are not true intercalation compounds because synthesis was from a homogeneous solution. There are two reports of benzene solvated C_{60} single crystals[135, 136] exist in addition to a pentane solvated material[137] and

$[Fe(\eta^5\text{-}C_5H_5)_2]_2C_{60}$.[138] The ferrocene containing material is a cocrystal rather than a charge transfer salt, and all have lower symmetry than the intercalation materials.

1.6.2. Intercalation Chemistry with Charge Transfer.

To date, this class of materials is limited to the alkali and alkaline earth intercalates of C_{60}. Many properties have been studied ranging from electronic transport properties[139] to heterogeneous catalytic H-D exchange,[140] but by far the greatest interest lies in the superconducting phases of C_{60} intercalates.

Superconductivity is observed for several compositions of alkali metal C_{60} materials with a fcc structure,[141, 142] and the C_{60} formally triply reduced. The maximum value of the superconducting transition temperature (T_c) found so far, at atmospheric pressure, is 33K for Cs_2RbC_{60},[143] the highest value of T_c known for a material based on a simple molecular system.

In the alkali metal compounds the electron density wave function is thought to be very small at the cation and experimental evidence available corroborates this hypothesis.[144-147] The cations effectively act as spacers between C_{60} molecules. A plot of T_c versus the calculated cation volume[148] illustrates this point, as shown in figure 1.6.2.1.

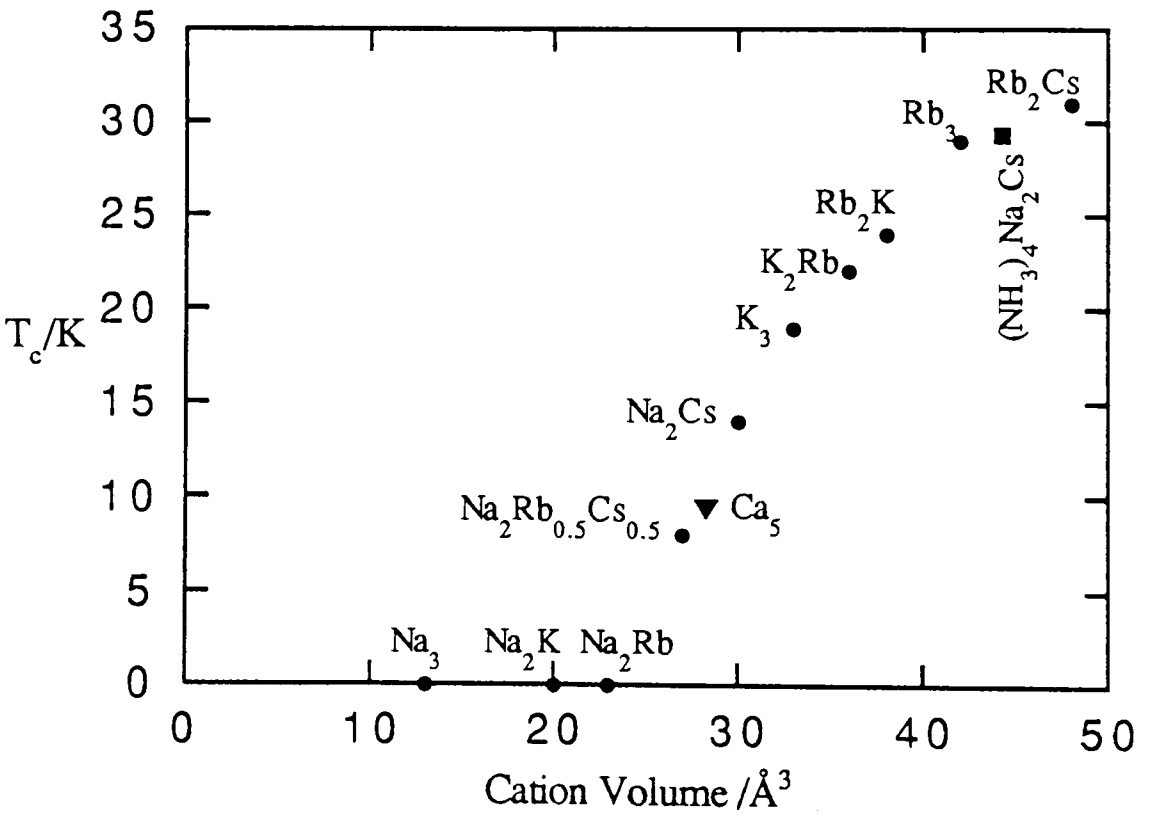


Figure 1.6.2.1. T_c's versus cation volume for various fcc superconducting phases.

This trend can be interpreted in terms of the BCS theory of superconductivity which is based on the formation of Cooper pairs due to electron-phonon coupling.[148] Increasing the cation volume decreases the overlap between neighbouring C_{60}

molecules which increases the density of states at the Fermi level and consequently results in an increase in T_c. However an anomaly appears to be present because Na_3C_{60} does not superconduct at the lowest measured temperature of 2K.[149] This is probably due to a phase change that appears to occur on cooling the sample, before the predicted onset of superconductivity at its estimated T_c of 12K.[149]

The cation volume can be manipulated by the intercalation of ammonia which ligates to a suitable cation, effectively increasing its size, and the value of T_c. Na_2CsC_{60} has a T_c of 10.5K but on exposure to ammonia and annealing, a T_c of 29.6K is observed.[150] Mass uptake indicated four moles of ammonia were present for every mole of Na_2CsC_{60} and synchrotron X-ray powder diffraction was fitted best for $Na(NH_3)_4^+$ occupying the octahedral site and the equivalent of Na and Cs occupying the remaining tetrahedral sites.

Alkali earth C_{60} phases have also been observed to superconduct in the compositions Ca_5C_{60}[151] and Ba_6C_{60}[152] with T_c's of 8.4 and 7K respectively. The formal oxidation state of the C_{60} within these materials is not known but it is interesting that Ba_6C_{60} has a bcc structure, the only non fcc superconducting C_{60} material known to date. A T_c of 8.4K for Ca_5C_{60} has also been shown to be consistent with the relation of T_c versus calculated cation volume shown in figure 1.6.2.1.

A multitude of other alkali metal C_{60} phases, both binary and ternary, are known with a variety of cubic structures as shown in figure 1.6.2.2.

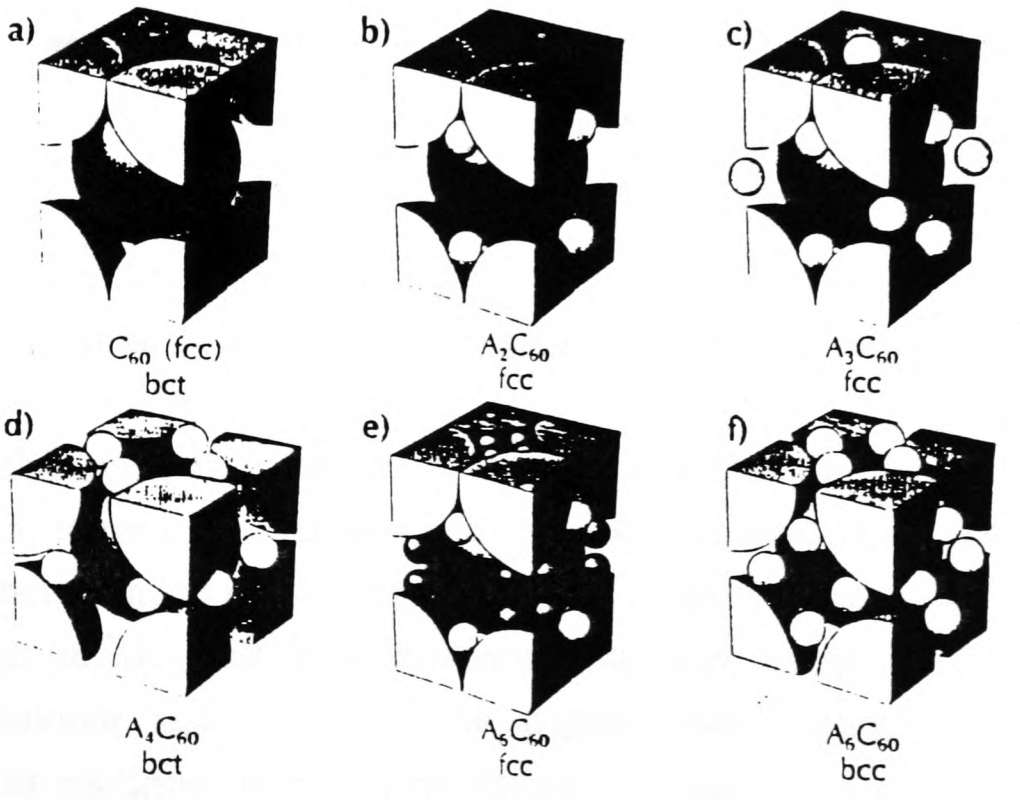


Figure 1.6.2.2. Schematic structures of C_{60} and A_xC_{60}. (a) fcc C_{60} drawn in equivalent bct representation. (b) The structure of Na_2C_{60} with Na ions in tetrahedral sites. (c) A_3C_{60} with A ions in both tetrahedral and octahedral sites. (d) The A_4C_{60} structure exhibited by K, Rb and Cs. (e) The fcc Na_6C_{60} structure with the darker Na's 50% occupied. (f) The bcc A_6C_{60} structure of K, Rb and Cs.

No binary lithium phases are known and the only lithium containing material structurally characterised is Li_2CsC_{60} which has a T_c of 12K.[153] Potassium, rubidium and caesium phases exist with the compositions A_4C_{60} and A_6C_{60}, and are semiconductiong and insulating respectively.[142] K_3C_{60} and Rb_3C_{60} are metallic before the onset of superconductivity at low enough temperatures but Cs_3C_{60} has so far not been prepared. It has a predicted T_c of approximately 50K. The t_{1u} LUMO is capable of containing 6 electrons and so the composition A_6C_{60} was thought to be limiting. However, sodium C_{60} intercalate phases are known for compositions above Na_6C_{60}, all retaining the fcc structure.[154] A phase with the composition $Na_{9.8}C_{60}$ has been structurally characterised. This is possible because of the formation of clusters of Na atoms at the octahedral site of the fcc lattice with the reduction of C_{60} not thought to proceed beyond six equivalents of electrons.

Compositions below A_3C_{60}, except for the well known Na_2C_{60} phase, have shown several very interesting phenomena. Not least of which is the recent report of 1-dimensional polymers of K_1C_{60} and Rb_1C_{60}.[155] It is possible to grow single crystalline $(KC_{60})_n$,[156] a conducting linear polymer, by coevaporation of potassium and C_{60}, however no structural information was available in this report. Polymerisation is postulated as occurring by [2+2] cycloaddition between neighbouring C_{60}'s propagated along one axis only, as shown in figure 1.6.2.3.

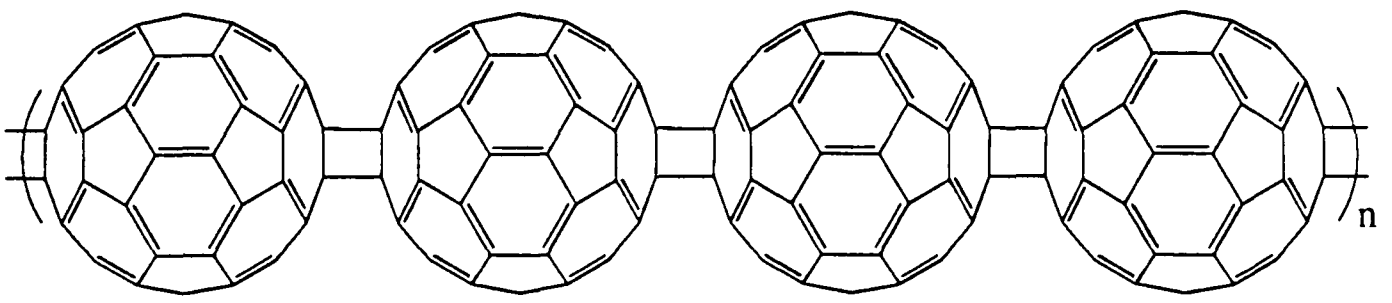


Figure 1.6.2.3. Polymer chains of C_{60} inferred in the structure refinement of Rb_1C_{60} and in pure C_{60} phases synthesised at high temperatures and pressures.

Synchrotron powder X-ray diffraction data for Rb_1C_{60} and K_1C_{60} is best interpreted in terms of a 1 dimensional polymer but remarkably polymerisation is reversible between approximately 350-450K with a change in structure from orthorhombic to rock salt. ESR measurements show evidence for 1-dimensional metallic behaviour, and a change in the magnetic spin susceptibility, which can be interpreted as resulting from polymerisation. Cs_1C_{60} also has its lattice parameter approximately 9% shorter in one direction but less work has been performed on this phase. However, Rb_1C_{60} and Cs_1C_{60} have been investigated by variable temperature powder NMR spectroscopy.[146] Measurements of the ^{13}C relaxation time, T_1, and ^{87}Rb and ^{132}Cs NMR indicate that metallic behaviour is present and that the electronic wavefunction is virtually 100% C_{60} in character.

All the compositions discussed so far are line phases with no evidence for solid solutions. At non-stoichiometric compositions disproportionation occurs. In the sodium C_{60} phase diagram it has been reported that compositions between Na_1C_{60} and Na_3C_{60} exhibit solid solution behaviour.[157] This postulation is based on synchrotron X-ray powder diffraction and DSC data. However, thermodynamic EMF measurements and experiments described in chapter 3 indicate that solid solution behaviour *may* only occur between Na_2C_{60} and Na_3C_{60} and that compositions below Na_2C_{60} disproportionate.

1.7. Polymers and Materials.

Near spherical symmetry and a pure carbon composition attracted many materials and polymer scientists to C_{60}. Problems with solubility and the number of possible products, such as cross-linking, possible within a C_{60} based material has meant that the potential has not yet been realised.

Intrinsically C_{60} is very robust to mechanical stresses but it has been shown that it is possible to crush C_{60} at 25GPa in a diamond anvil to diamond[158] and potential for optical limiting properties of C_{60} and C_{70} solutions has been shown.[159] At high pressures and temperatures C_{60} has been shown to irreversibly polymerise to give one of two structures identified so far, depending on the pressure and temperature applied.[160] A nominal fcc structure is found between 300 and 400°C at 5 GPa and a rhombohedral structure up to 800°C at the same pressure. Above 800°C the sample did not diffract indicating the sample was amorphous carbon. ^{13}C MASNMR spectroscopy revealed a broad peak with several minor peaks in contrast to the sharp sub-Hertz peak for pure C_{60}, and IR and Raman spectroscopy showed clear differences from pristine C_{60}. Powder X-ray diffraction yielded the fcc and rhombohedral structures but a full structure determination has not yet been successful. The samples were not soluble in any common organic solvents.

Reaction of C_{60} with *p*-xylylene produced a copolymer[161] of undefined weight and dispersity due to cross linking and subsequent insolubility. Other polymers have been synthesised using derivatised forms of C_{60}, such as the formation of a polyester and polyurethane of diphenylcarbene C_{60},[162] as shown in figure 1.7.1.

The polyester product is soluble in thf, benzonitrile and nitrobenzene and has a low average molecular weight of 4000, as determined by gel permeation chromatography.

Doping of polymers with C_{60} and C_{60}/C_{70} mixtures has been investigated. Several interesting observations have been noted such as the significant increase in photoconductivities of doped polyvinylcarbazole[163] and an increase in the conductivity of doped polyanilines[164] of C_{60}. These observations have been interpreted tentatively in terms of a charge transfer model where C_{60} acts as an acceptor.

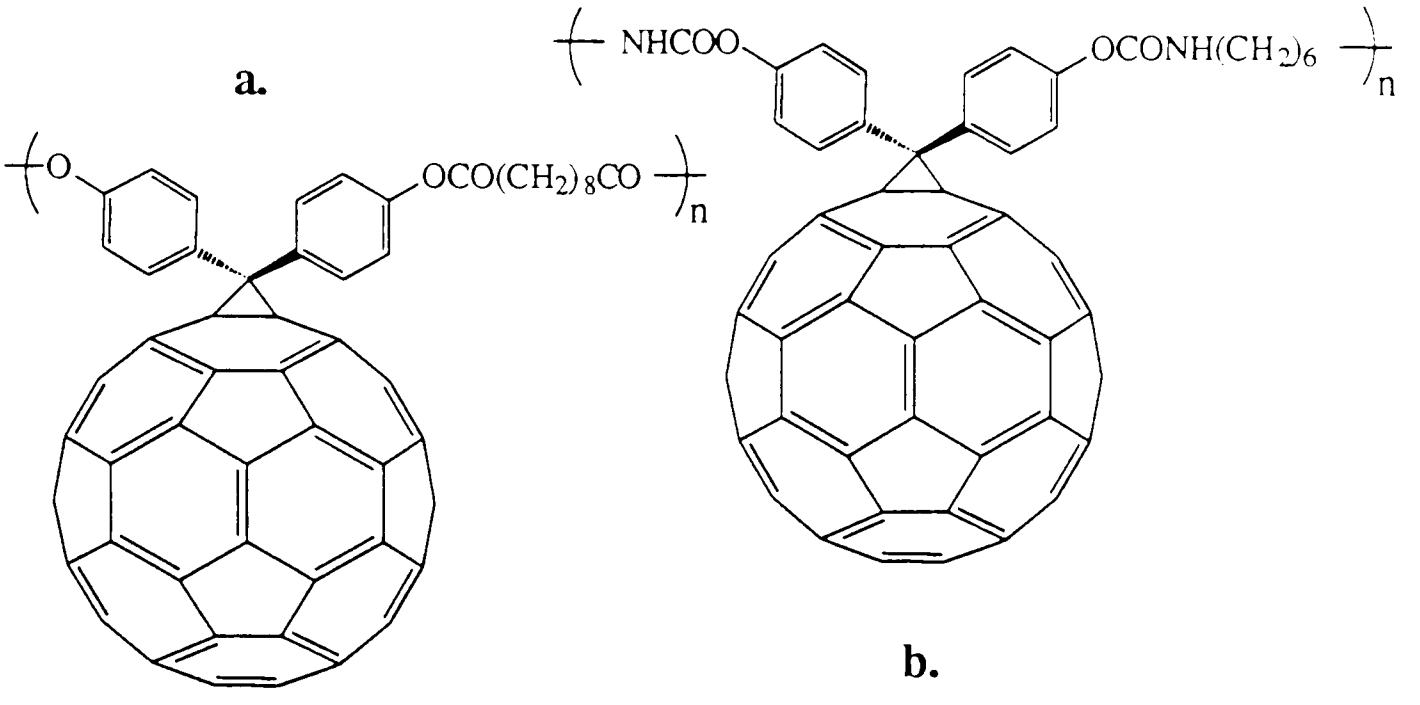


Figure 1.7.1. (a) polyester derivative of C_{60} soluble in some organic solvents. Gel permeation chromatography gives on average n = 5. (b) Polyurethane derivative is insoluble in common organic solvents and uncharacterised.

Tethering of C_{60} derivatives onto a surface has been successfully demonstrated and has potential in the modification of electrode and optical surfaces. Two approaches can be used, which entail using derivatised C_{60} or a derivatised surface capable of reaction with C_{60}. Only the later has been demonstrated to date, in for example the tethering of C_{60} onto a polyethylene surface[165] or modified oxide substrate,[166] as shown in figure 1.7.2.

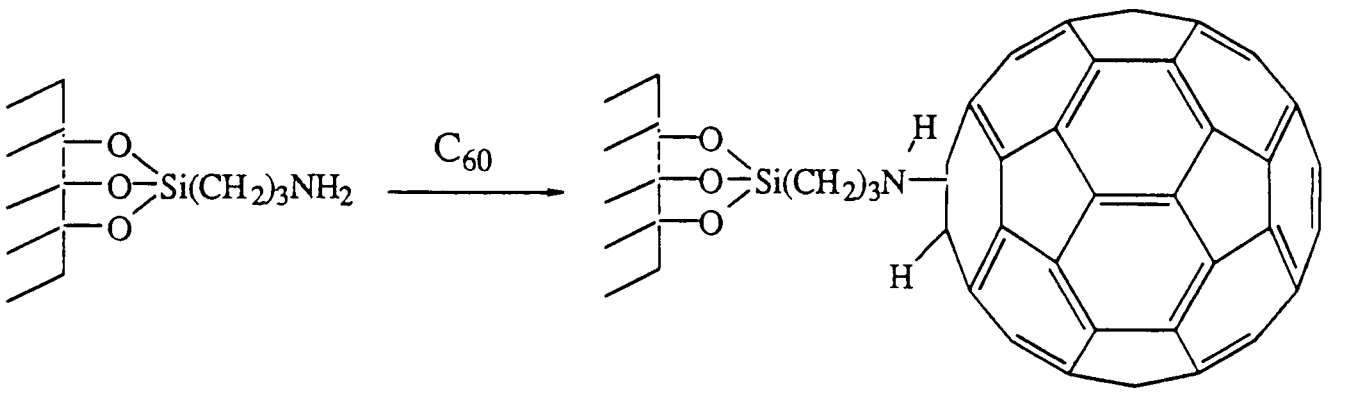


Figure 1.7.2. Modification of an oxide surface with an amine C_{60} derivative. Further reaction chemistry was performed on the tethered C_{60} molecule.

1.8. Mass Spectroscopic Studies.

Prior to the macroscopic isolation of C_{60} and C_{70} the only evidence for its existence was from the mass spectroscopy of species generated from the laser ablation of a carbon target.[6] In the intervening five years mass spectroscopists had the only access to these new carbon clusters and several papers were published describing chemistry in the gas phase, but without knowledge of the structure of the cluster the reports were regarded as academic curiosities.[167] However, once the precise structure

of C_{60} was determined, significant numbers of publications describing chemistry in the gas phase began to emerge,[168-179] and a reappraisal of pre-macroscopic isolation work, was required.

Unfortunately this does not detract from the fact that a large amount of over interpretation is possible in dealing with peaks corresponding to a certain mass/ion ratio and that macroscopic isolation from a mass spectrometer is not possible.

The greatest contribution mass spectroscopy has had, aside from being an invaluable part of the characterisation process, is in the fundamental study of endohedral fullerenes, but again definitive proof of the inclusion of species within a particular fullerene is lacking in a mass spectroscopic experiment.

To date, non of the chemistry performed in the gas phase of a mass spectrometer has been successfully transferred to macroscopic chemical synthesis apart from the production of the fullerenes themselves and some endohedral fullerenes discussed in the next section.

1.9. Endohedral Fullerenes.

Fullerenes are fully enclosed carbon cage clusters and as such possess a void volume at their centre. C_{60} has been estimated to have a void diameter of between 3.75 and 4.2Å which is easily large enough to accommodate guest species.[119] Numerous potential uses and properties have been postulated including superconductivity, lasers, ferroelectrics and even the enrichment of ^{238}U.[119]

The encapsulation of Ca, U, La, Fe, Co, Y, Sr, Sm, Eu, Sc and Yb within a C_{60} molecule has been reported either within a mass spectrometer or mass spectroscopic analysis of soot produced by the covaporisation of graphite and metal/metal oxide.[180]

By far the greatest concentration of work in this area has centred on C_{82} and C_{84} and rare earth elements, particularly scandium. A report on the isolation and preliminary characterisation of $Sc_2@C_{74}$, $Sc_2@C_{82}$ and $Sc_2@C_{84}$, where @ signifies an endohedral compound, indicates that macroscopic amounts can be obtained, but unfortunately no mention is made of product yields.[181] Transmission electron microscopy studies on $Sc_2@C_{84}$ have been reported but again no yield is given.[182] ESR measurements indicate that these dimetallofullerenes are diamagnetic in contrast to the mono and trimetallic species. Recently the compound $Y@C_{82}$ was isolated and characterised by ESR, UV-vis and cyclic voltammetry.[183] The electronic structure of this material is formulated as $Y^{3+}C_{60}^{3-}$ and theoretical calculations support this view.[184]

The mechanism of formation of endometallofullerenes, or fullerenes themselves for that matter, is not well understood but current models are based on the electron affinity of empty fullerenes. Charge transfer from central metal atoms to the

surrounding cage may cause the materials to be oxygen and water sensitive, hindering isolation, but this does not seem to be the case, given the isolation of La@C_{82}, Y@C_{82}, Sc_2@C_{74}, Sc_2@C_{82} and Sc_2@C_{84}.

One other major class of endohedral fullerenes exists, which contain the noble gases. He@C_{60} was elegantly characterised by ^{3}He NMR spectroscopy[185] and this technique has been suggested as a new tool for following fullerene chemistry.[186] Neon, argon, krypton and xenon have also been introduced with decreasing yields.[187] He inclusion was only 0.1%, at maximum, as determined by mass spectroscopy. Synthesis of these compounds was achieved by exposing C_{60} to approximately 2700 atm of the relevant noble gas at a temperature of 600°C for several hours. Approximately 50% of the C_{60} was destroyed.

1.10. Other Work (Separation, Host-Guest and ESR of Organic Radicals).

The availability of macroscopic quantities of C_{60} allowed scientists from diverse backgrounds and with a multitude of interests to partake in the birth of a new field. This led directly to a large number of disparate publications as each 'scientist' applied their knowledge to C_{60}. An attempt to cover all work, which cannot easily be classified in the sections above, would require hundreds of pages and will therefore not be attempted. Amongst others, astromomers, physicists, mathemeticians and theoreticians from every branch of science have contributed to the wealth of information available. In 1992 a paper entitled 'The Epidemic Spread of Fullerene Research' appeared in *Angew. Chem.* conservatively estimated the number of papers published as over 2000 in at least 25 major journals since the macroscopic isolation of C_{60}.[188] Two years later the rate has not decreased.

To obtain pure C_{60} it is necessary to separate it from the soot matrix and the other fullerenes, most notably C_{70}. There are two routes by which this has been achieved successfully which are column chromatography[189-197] and selective complexation.[198, 199]

Originally, the column material of choice was alumina, but developments have been made especially in the area of preparative HPLC where a very effective column, the so called 'Buckyclutcher', is now used extensively. HPLC requires fullerite, a fullerene mixture free of soot, to be effective requiring an extra separation step. By the use of a column extractor,[200] described in section 1.13.2. C_{60} can be directly separated from raw soot, albeit in lower yield than with preparative HPLC.

Host-guest complexes of C_{60} and C_{70} have been investigated not just for fundamental academic interest but also as potential as a separation technique.[198, 199,

[201] Two recent publications have reported the use of a calixarene as an effective method for the selective complexation of C_{60} which allows rapid and a comparatively cheap separation.[198, 199] However, problems of calixarene impurity seem to occur on work-up of the complex and the use of alumina, where a preparative HPLC is not available, appears still to be the method of choice. Fractional sublimation has not proved to be a viable method.

Incorporation of C_{60} into other various host lattices has been accomplished either by intercalation or cocrystallisation.[202-204] C_{60} has been incorporated into molecular sieves[204] from the gas phase and has been postulated as a possible separation technique. ^{13}C powder NMR spectroscopy showed that free rotation was still evident and N_2 sorption measurements showed that up to two thirds of the void volume was unavailable compared to an unloaded sample.

C_{60} is completely insoluble in water but by complexation with cyclodextrins or inclusion into an artificial lipid membrane significant solubility is achieved.[201, 203] The host-guest complexes of cyclodextrins and calixarenes with C_{60} show the close match in shape and size, as shown in figure 1.10.1.

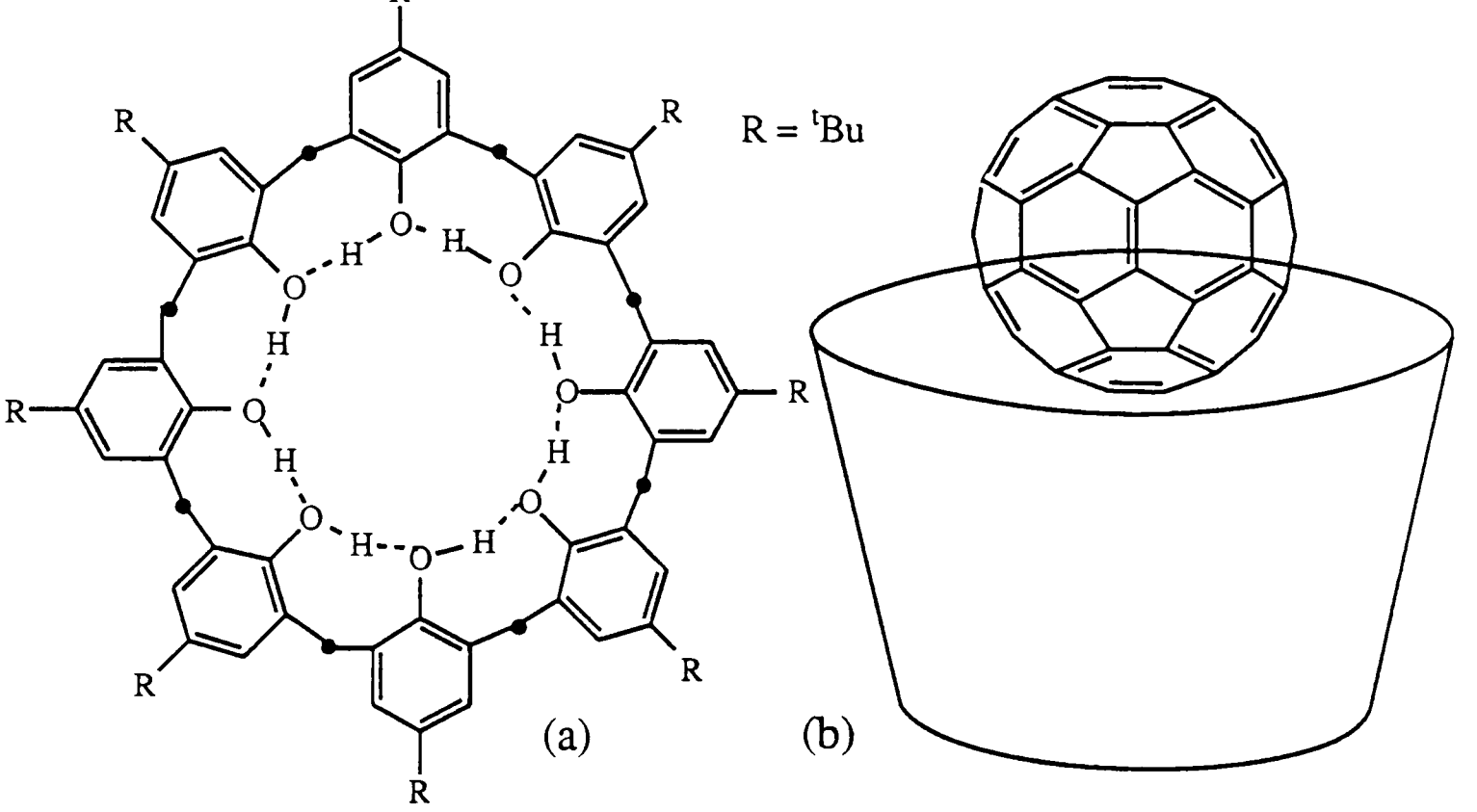
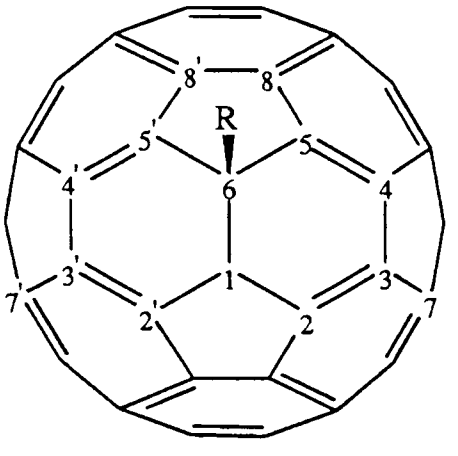


Figure 1.10.1. (a) planar representation of *p*-R-calix[8]arene which forms a 1:1 complex with C_{60} selectively in the presence of other fullerenes. (b) Schematic representation of the complex in the 'ball and socket' arrangement, believed to be structure of the C_{60} complex.

Scientists in medical research are becoming increasingly interested in the near spherical 'inert' carbon cage and its derivatives because of the possible 'lock and key' interactions, as is demonstrated in the HIV work discussed in section 1.4.

On addition of a radical to C_{60}, questions arise as to where the electron wavefunction is distributed and whether dimerisation will occur. A series of papers in 1991 and 1992 showed that reversible dimerisation did occur for certain bulkier alkyls[205-208] and that the electron resides on several carbons close to the point of radical addition, as shown in figure 1.10.2.



R = CCl_3, $(CH_3)C$ and $(CH_3)_2CH$ are believed to dimerise reversibly from variable temperature ESR measurements.

R = H, F and CH_3 could not be characterised but are beleived to form dimers irreversibly.

ESR measurements indicate that the unpaired electron resides to a degree on all the numbered atoms and on the R substituent. The greatest density is at position 1.

Figure 1.10.2.

Further work indicated that the addition of three and five equivalents of alkyl produced particularly stable species.[209] This was interpreted, on the basis of the best fit to the ESR profile, as due to pseudo allyl and cyclopentadienyl species, as shown in figure 1.10.3.

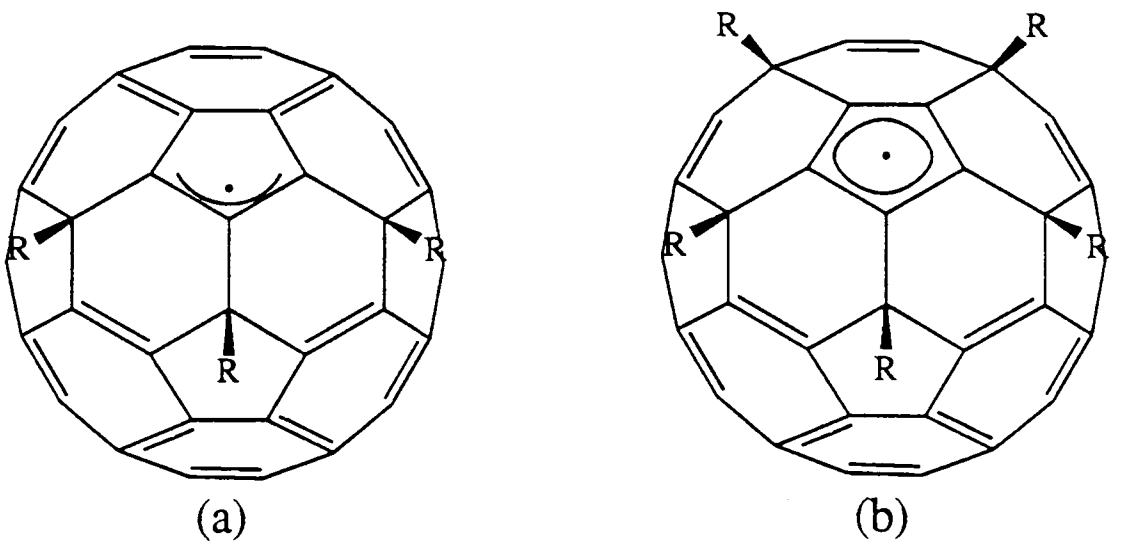


Figure 1.10.3. ESR measurements indicate that the pseudoallyl radical (a) and pseudocyclopentadienyl (b) radicals are particularly stable. They have never been macroscopically isolated.

1.11. Other Forms of Carbon Generated From the Arc Vaporisation of Graphite.

During the carbon arc vaporisation of graphite a D. C. current is generally employed allowing more controlled soot generation, and as a consequence the graphitic anode is consumed during the experiment. Due to the electric field, on the order of 300V/cm within the plasma, charged carbon species are generated and deposit is formed on the negative cathode. This deposit has been shown to contain several new forms of carbon, both structured and amorphous.

1.11.1. Carbon Nanotubules.

In 1991 Iijima,[210] utilising electron microscopy techniques, discovered closed concentric graphitic nanotubules at the centre of the cathodic deposit. These nanotubules were given the name Buckytubes and are shown schematically in figure 1.11.1.1. Interdispersed with these nanotubules are amorphous carbon networks and nanoparticles, which will both be discussed later in sections 1.11.2 and 1.11.3. The isolation of carbon nanotubules free from nanoparticles and amorphous carbon networks has yet to be achieved.

However, a fair amount of chemistry has been performed, especially with regard to opening the ends and filling the void volume.[211-213] Closed concentric nanotubules have been opened selectively using Bell's oxidation reaction which consists of heating the tubes with carbon dioxide at a temperature of 800°C, generating two equivalents of carbon monoxide.[213] Approximately 10% of the tubes were opened as observed by transmission electron microscopy. A less selective route is to effectively burn the tubes in a partial pressure of oxygen, but significant destruction of the body of the tubes occurs. By far the most efficient method appears to be mild oxidation, using boiling concentrated nitric acid.[212] Depending on the length of exposure, virtually all tube caps can be removed selectively leaving the main body intact. Carbon atoms at the end of Buckytubes are more reactive presumably because of the strain at the curved capped surface in comparison to that in the main body of the tubes.

On removing the caps, there is great interest in filling the void volume, and many potential uses have been postulated ranging from shape selective catalysis to containers for slow drug delivery. The first example of a filled tube was the inclusion of molten lead observed by electron microscopy.[211] Subsequently using the nitric acid opening technique, a variety of metals and their oxides have been introduced into the void volume[212] as is shown for one of the phases of uranium oxide in figure 1.11.1.2.

It has also been shown that by doping the graphite rods prior to vaporisation that carbides (Fe, Co, Ni, Ta, La, Sc, Y, Ce, Pr, Nd, Gd, Tb, Dy, Ho, Er, Lu) and pure metals (α-Fe, γ-Fe, hcp-Co, fcc-Co and fcc-Ni) can be incorporated into the nanotube void volume.[214] TaC and CeC_2 are interesting examples[215] because in the

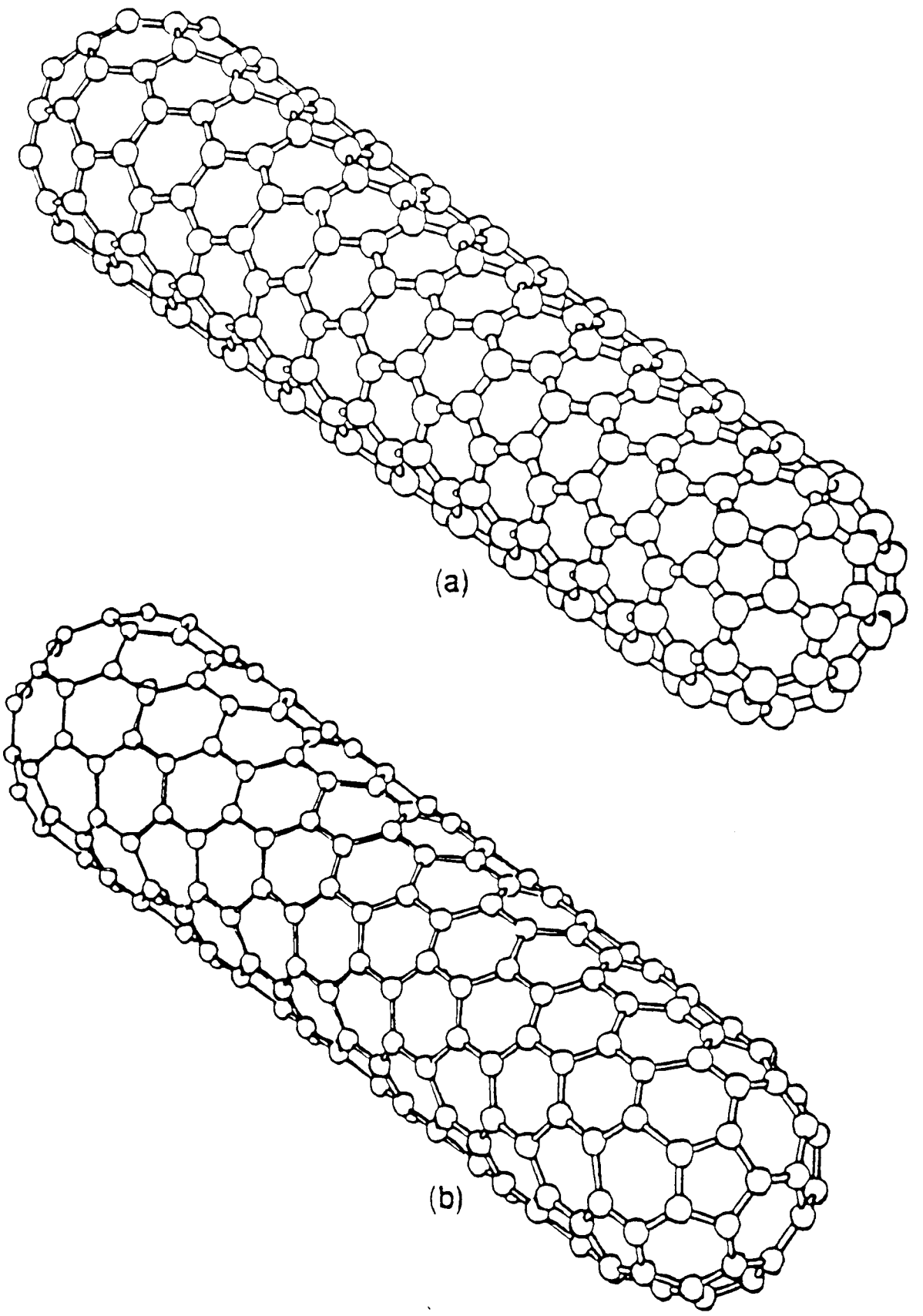


Figure 1.11.1.1. By rolling up a graphene sheet a (a single layer from a 3D graphite crystal) as a cylinder and capping each end of the cylinder with half a C_{60} molecule, a 'C_{60}-derived tubule' one layer in thickness is formed. Shown here is a schematic model for a tubule arising from (a) an 'armchair' cap with a fivefold axis and (b) a 'zigzag' cap with a three fold axis.

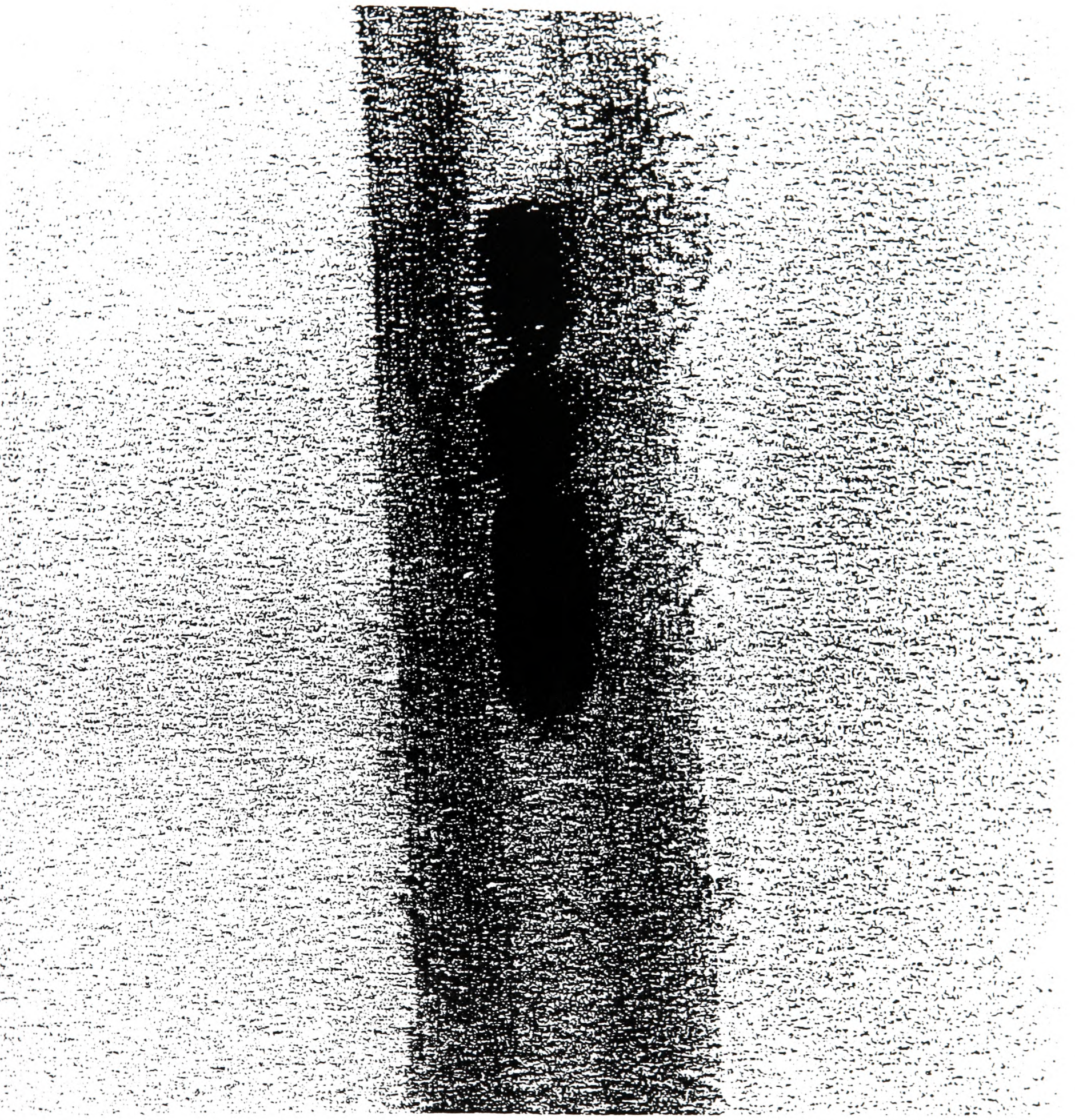


Figure 11.1.1.2. Electron micrograph of a uranium oxide phase confined inside a Buckytube. The width of the tube is approximately 50Å.

bulk they undergo superconducting and antiferromagnetic transitions respectively. Removal of metal and metal carbide, not incorporated in the tubes, was achieved by treating the samples with sulfuric acid at 180°C for 70h. Transmission electron microscopy and electron diffraction photographs showed that the encapsulated particles were typically approximately 100Å in diameter and several hundred angstroms in length. A study on the effect of particle size on these transitions was undertaken but no significant differences were observed. The major difference between these materials, and those discussed above, is that the tube ends are closed, preventing hydrolysis and oxidation of the encapsulated material.

Exposure to bromine results in the destruction of the tubes[216] but alkali metals have been intercalated with a modicum of success,[217] in between the *walls*, indicating dislocations may be present. Dislocations have also been observed in electron micrographs.

Production of tubes of defined length and size has been the object of many research efforts but to date a reproducible method is not available. Two reports[218, 219] have claimed the synthesis of single layered tubes of defined length by doping the graphite rod with a low concentration of cobalt or iron, but reproducibility in other laboratories has been difficult. In much the same way as efforts to maximise the yield of fullerene containing soot, variation in reactor design, noble gas pressure, current densities and dopant concentration, play a major role in the carbon species formed. An exotic example, is the generation of what the authors like to describe as a 'sea urchin' structure, of single layered carbon tubes projecting from an ill defined gadolinium carbide nanoparticle.[220]

Intrinsically, carbon nanotubules may have very interesting properties in their own right.[221] The majority of the tubes observed have screw axis and chirality which is imparted by the pitch and direction of the tube helix.[210] A description of the tubes is most easily afforded by considering the tube 'unzipped' and lay down as a 2-dimensional carbon network[222] and various parameters such as the chiral angle θ, can be defined as shown in figure 1.11.1.3. Theoretical considerations have shown that depending on the diameter and chiral angle, approximately a third are metallic and the rest semiconducting. This has led to the speculation of nanowires constructed purely of carbon.

The mechanism by which buckytubes grow in the soot reactor is still unknown. Various authors have proposed mechanism based on vapour deposition of C_2 units[223] in a similar way to the growth of carbon fibres, while others have postulated the 'peeling' of graphitic layers from the anode that 'curl up and snip off'.[224, 225]

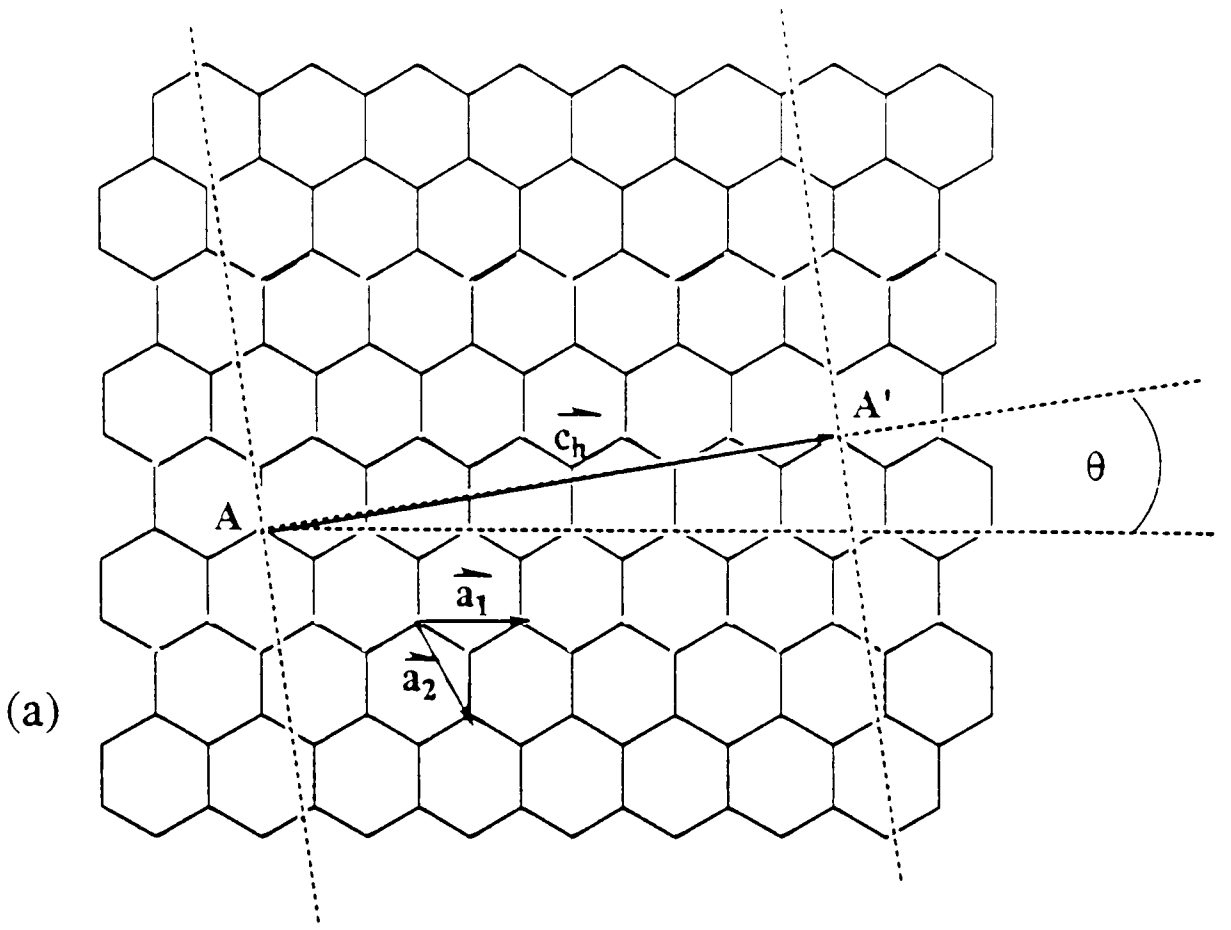


Figure 1.11.1.3. (a) The vector **AA'** or $c_h = na_1 + ma_2$ on the honeycomb lattice defined by unit vectors, a_1 and a_2, and the chiral angle θ with respect to the zigzag axis. (b) possible vectors for general tubules, including zigzag, armchair, and chiral tubules, where the numbers in brackets refer to the integers *n* and *m*. The closed and open circles denote metallic and semiconducting behaviour for each of the possible tubules.

1.11.2. Amorphous Carbon Networks and Nanoparticles.

Associated with the fullerene rich soot are amorphous carbon networks which have a very large surface area of typically 700m^2/g and are remarkably resiliant to oxidation when compared to similar carbons.[226] The concept of negative curvature formed by rings containing 7 carbon atoms was introduced.[227] A ring of 7 carbon atoms will generate a saddle point bending a graphitic type layer in the opposite direction in comparison to that of a five membered carbon ring. Gas uptake and molecular seiving properties have been demonstrated for the carbon networks generated in fullerene synthesis and its use as a catalyst support is envisaged.[226]

Nanoparticles are also found in what some authors have coined the 'carbon-zoo'. Very little is known about these structures other than what has been observed in an electron microscope.[228] Structurally, they tend to exhibit facets, whose angles at the vertices, may be interpreted as a consequence of sp^3 hybridisation, but this is unclear.

On the addition of bromine, destruction of the nanoparticles and tubes results indicating intercalation and subsequent 'explosion' has occured and that dislocations are present.[216]

1.11.3. Concentric Carbon Spheres ('Buckyonions').

On irradiation of amorphous carbon networks by a high energy electron beam Ugarte made the remarkable discovery of concentric carbon spheres,[229] so called Buckyonions, as shown in figure 1.11.3.1. The distribution of size is very narrow, within the range of 100Å in diameter, and the conversion is virtually quantitative. The mechanism for this amazing metamorphosis is to date unknown.

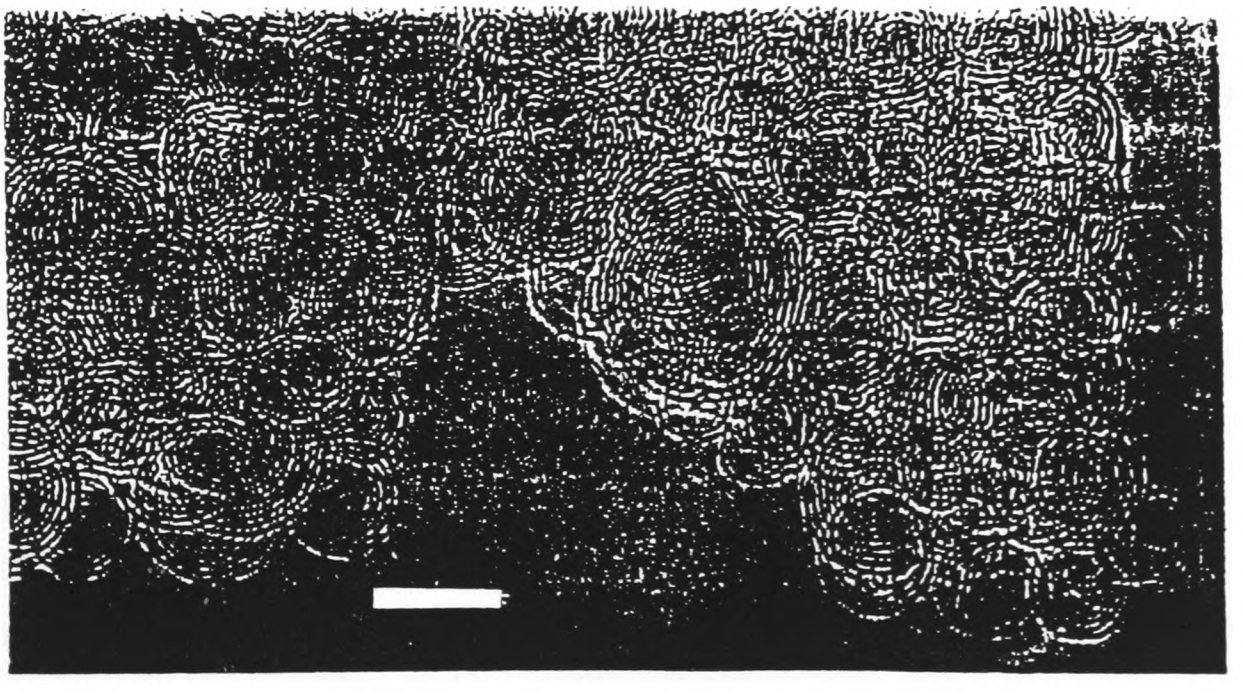


Figure 1.11.3.1. Electron micrograph of 'Buckonions'. The scale bar is 50Å.

1.12. General Experimental Details.

Manipulations were performed in air, but gloves and face masks were used in manipulation of the soot to avoid ingestion of fine carbon particulates.

Solvents (Aldrich, technical grade) were used as provided.

Helium gas (BOC) was used as provided.

Alumina (Aldrich, Brockmann grade 1, activated neutral, 150 MESH) was used as provided.

Apparatus and Materials.

Carbon rods were purchased from Ringsdorf Ltd in lengths of 1m and diameter 10mm and cut to the appropriate length.

The soot generator was made by the workshop of The Inorganic Chemistry Laboratory, Oxford.

An Edwards high vacuum pump, model EDM20A, was used to achieve a vacuum in the soot generator.

The power supply was a full bridged rectified D.C. 40V, 200A.

1.13. The Preparation of C_{60}.

1.13.1. Soot Generation.

The generation of fullerene rich soot was performed according to literature methods in a vacuum chamber of our own design, as shown in figure 1.13.1.1 and 1.13.1.1a.

10mm diameter rods of graphite were vaporised under a small dynamic pressure of helium (100 - 200 Torr, ~ 1ml/min) at 30V and 200A using a D.C. power supply.

In a typical preparation, a length of graphite rod (200 x 10mm diameter) was fitted into the water cooled copper anode and a similar graphite rod (30 x 10mm diameter) was placed into the water cooled copper cathode. A pressure of 10^{-1} mbar was achieved via a vacuum pump. Helium was then bled into the chamber continually and regulated via two needle valves, one from the helium supply and a second to the pump. A partial pressure of 150 Torr was typical. Cooling water supplying the electrodes and the walls of the chamber was circulated continually throughout the preparation at such a rate as to avoid local boiling. Initiation of the plasma was achieved by applying a potential across the electrodes of 30V and slowly bringing the two carbon rods together via the winding mechanism. During the first 30 seconds of the plasma lifetime the current would be erratic varying from 160 to 200A. After the initial 30 seconds the plasma would stabilise at 25V and 160A. The power was then increased to obtain a current of 200A. Over a period of typically 30 minutes the graphite anode was eroded by winding in the anode electrode at a steady even pace.

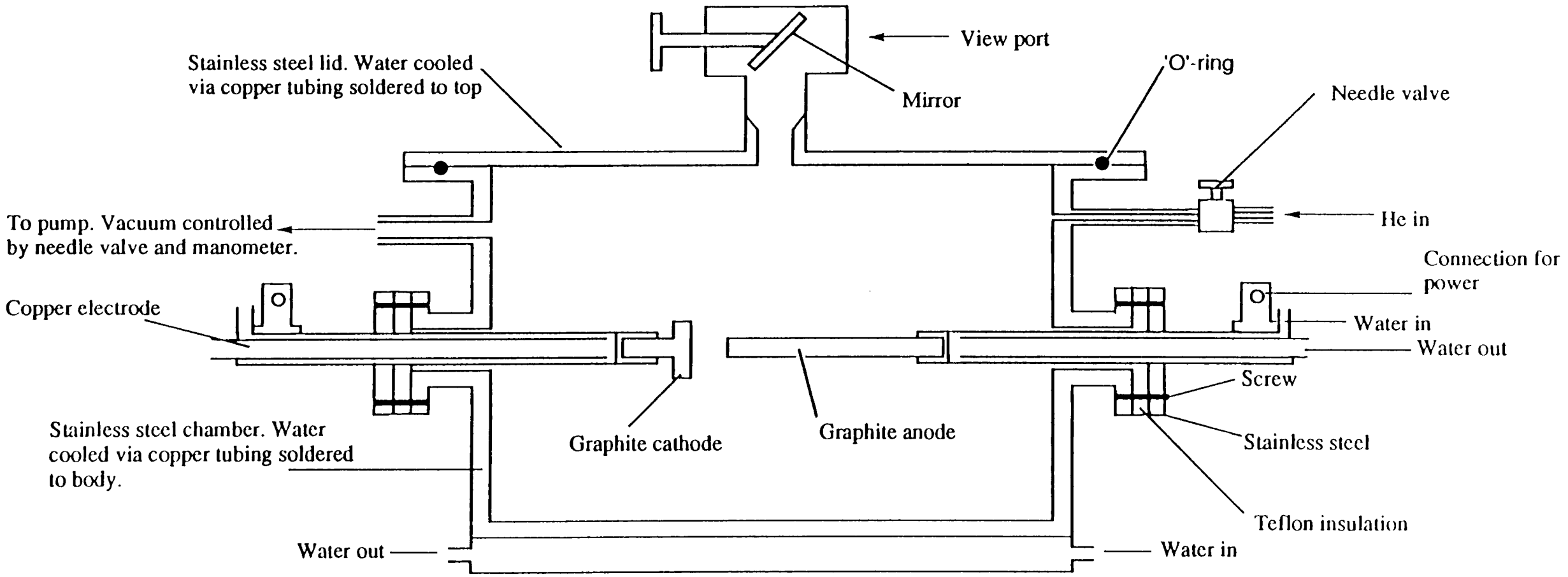


Figure 1.13.1.1. Soot generator

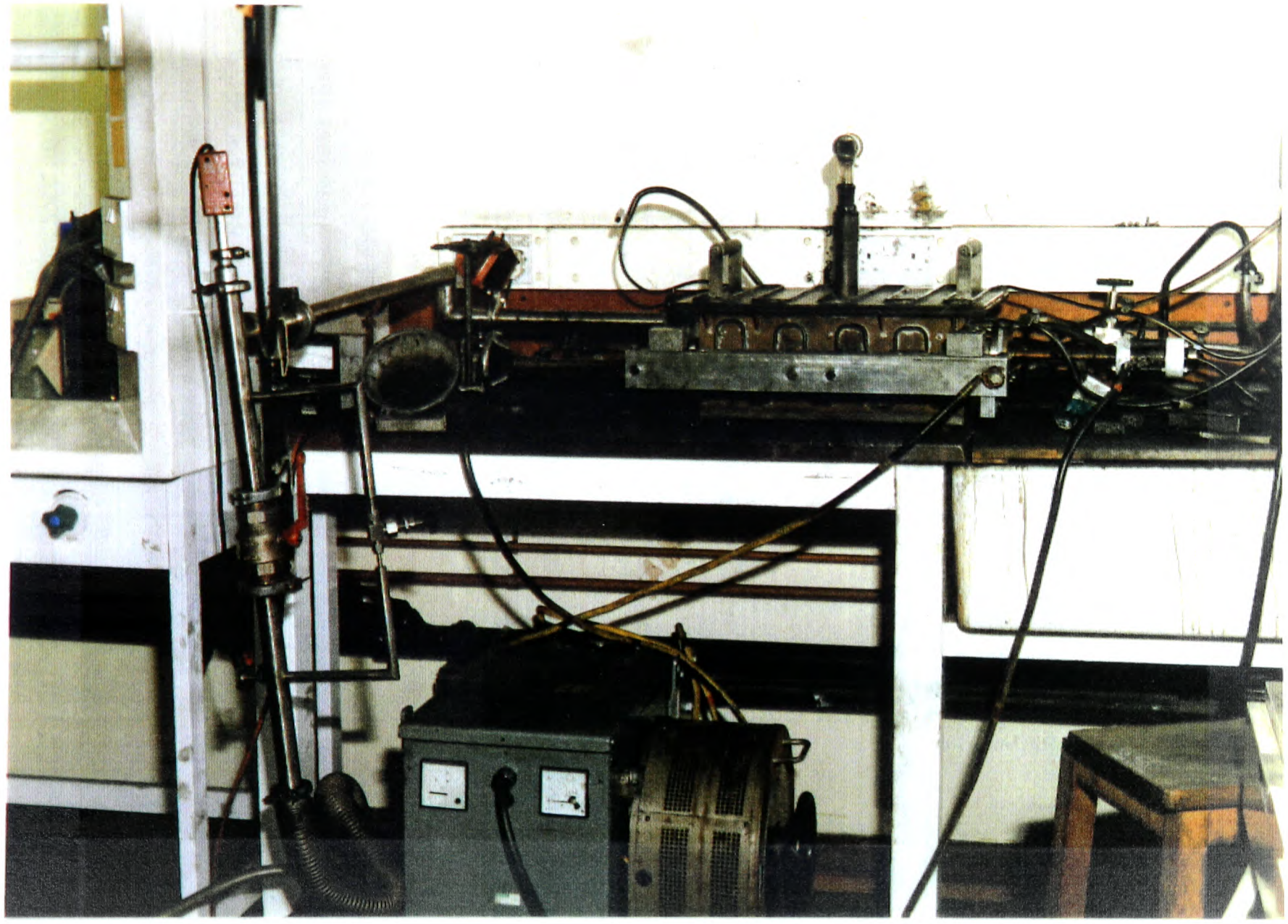


Figure 1.13.1.1a. Photograph of the soot generator and power supply.

On completion of the preparation the chamber was isolated from the pump by closing the needle valve and the electrodes were allowed to cool over a period of 10 minutes. Helium was then allowed to enter the chamber to atmospheric pressure and the flow of cooling water could be ceased. Removal of the chamber lid revealed a very short (10mm) anode and an extended cathode (80mm) due to carbon deposit. On the walls and lid of the chamber the fullerene rich soot was deposited and was collected using a dust pan and brush. Collected soot was transferred to a jar and placed in a refrigerator at -25°C. Yield (from anode) = 10g (70%).

Troubleshooting.

Occasionally the two rods would fuse together causing the rods to heat significantly and the current to increase off-scale. This is rectified by quickly winding out the anode away from contact with the cathode or by switching off the power.

During the course of the preparation the rate at which the anode vaporised decreased due to a glassy carbon deposit that forms on the cathode. Increasing the voltage and hence the current allowed accelerated vaporisation of the anode.

On initiation of the plasma the pressure in the chamber decreased due to formation of soot. This was not a problem as long as the total pressure did not exceed 300 Torr.

The effectiveness of the pump diminishes over time because the very fine soot enters the pump oil, even with a pre-trap. The pump oil must be regularly changed (typically every 100 rods) to maintain optimum pump efficiency.

1.13.2. Column Chromatography of Fullerene Containing Soot.

C_{60} was separated from the soot and higher fullerenes by eluting soot direct from the synthesis chamber with hot hexane on a neutral alumina column using the apparatus as shown in figure 1.13.2.1. and 1.13.2.1a.

Typically the column was constructed by pouring 1 litre of neutral alumina via a large funnel into the central region of the columning apparatus previously charged with 2.5 litres of hexane (technical grade). Some of the hexane was run into the round bottomed flask to settle the column packing, retaining 50mm of solvent above the alumina surface. 8 - 10g of soot was then carefully poured via a large funnel into the central region of the column to avoid dispersing the very fine sooty material. More hexane was run through the column to allow the soot to settle retaining 10mm of hexane above the soot surface. Hexane above the soot appeared red in colour.

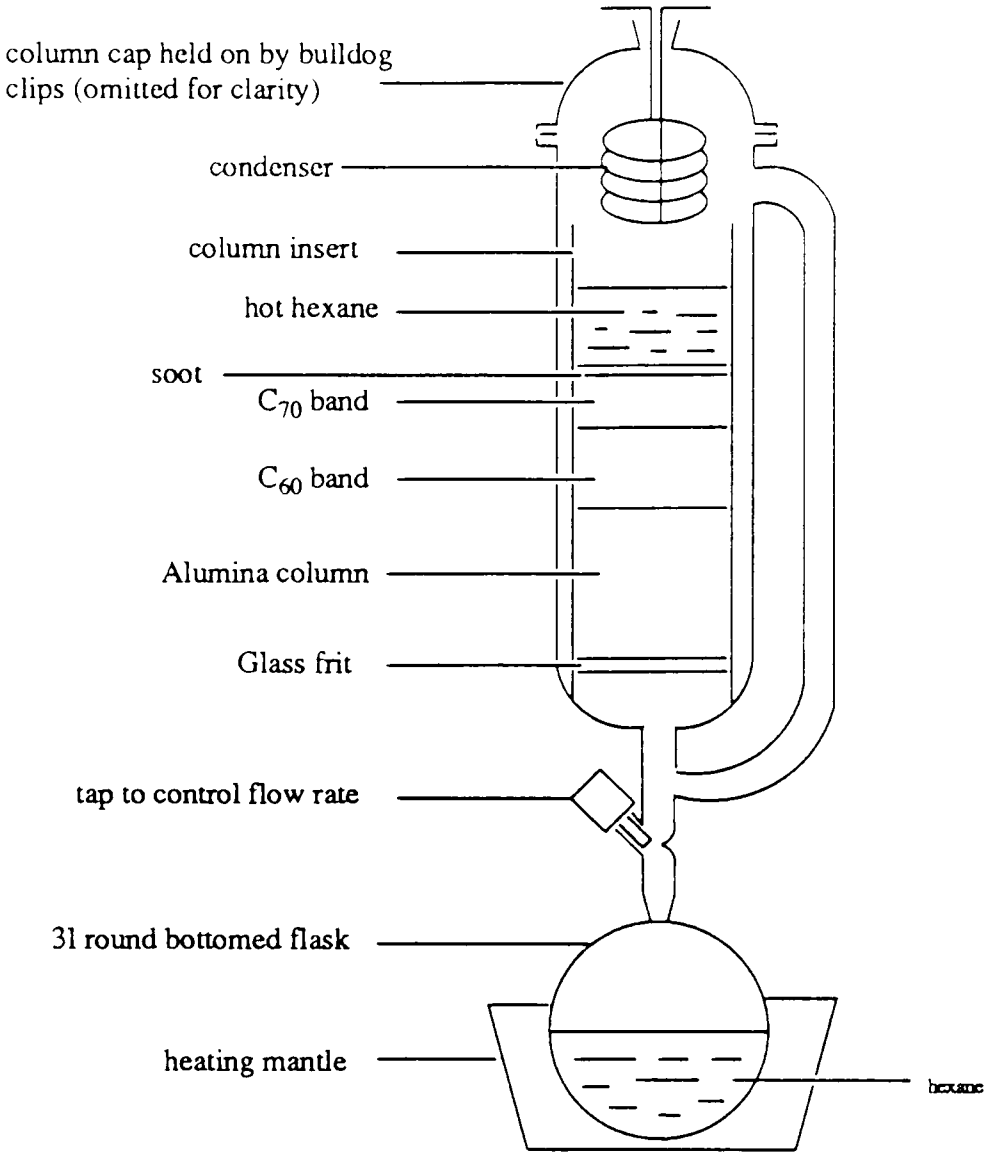


Figure 1.13.2.1. Column used for the extraction of C_{60} from raw soot.

The round bottomed flask was then heated via the mantle and a very slow (dropwise) flow of hexane was initiated. Once the hexane begins to condense on top of the column a larger flow rate was initiated while maintaining a constant head of solvent above the surface of the soot. At this stage a purple C_{60} band and above it a red C_{70} band was apparent. Depending on the flow rate; the exact length of the column and more importantly the condition of the alumina a purple C_{60} band will be eluted in 18 - 36 hours. If the alumina was fresh, and hence dry, elution was slow. If the alumina had been exposed to air for approximately two weeks (this depended on the humidity) elution was fast. Complete separation between C_{60} and C_{70} was not achieved on this length of column. Removal of the red C_{70} band and residual C_{60} was achieved by allowing all the hexane to run into the round bottomed flask and replacing it with a flask containing 2.5 litres of toluene. The column was then stripped of all toluene soluble material by eluting with hot toluene over a period of 24 hours.

1.13.3. Isolation of C_{60}.

The flask containing the mixture of a purple hexane C_{60} solution, solid C_{60} and a small amount of alumina was condensed to a dark solid under reduced pressure on a rotary evaporator. The residue was extracted with toluene, typically 500ml, filtered and

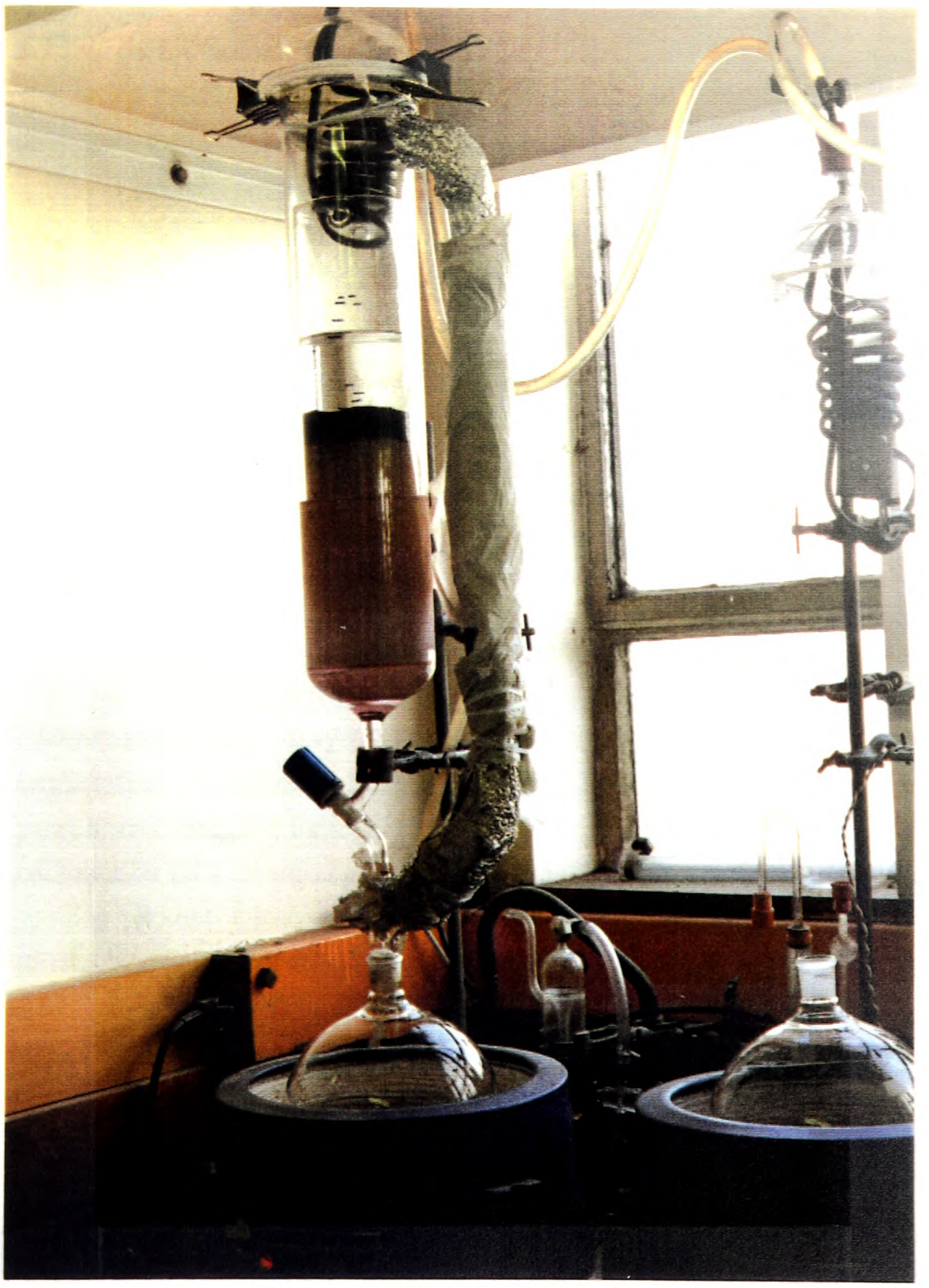


Figure 1.13.2.1a. Photograph of the column used for the extraction of C_{60}. The pink band in the bottom fifth of the column is C_{60} and the orange band above is C_{70}.

condensed under reduced pressure on a rotary evaporator yielding C_{60} as a dark solid. The solid was then washed with thf (2 x 30ml), pentane (2 x 30ml) and finally dried under reduced pressure for 2 hours.

1.13.4. Sublimation of C_{60}.

To produce ultrapure C_{60}, free from occluded solvents and gases, primarily dioxygen, sublimation is required.

Typically, a silica tube 12mm in diameter was charged with 200 - 300mg of C_{60} and connected directly to a vacuum pump via a Swage lock and glass tubing. Heating then took place in a tube furnace for the following times and temperatures.

Temperature/°C	Time/ Hours
150	2
300	2
450	2
550	overnight

Ramping the temperature in such a manner allowed occluded gases and solvents to be removed effectively and avoided bumping. The yield was typically 80-90%. Some decomposition to a sooty black deposit was always observed. The most plausable explanation is that of radical initiated decomposition. ESR measurements[230] of presublimed material indicate paramagnetic species present to a small degree. Upon sublimation ESR measurements indicate a vast reduction in the amount of paramagnetic species present. Ultrapure C_{60} should be stored under Ar or He. A powder X-ray difffraction pattern of asample of sublimed C_{60} is shown in figure 1.13.4.1.

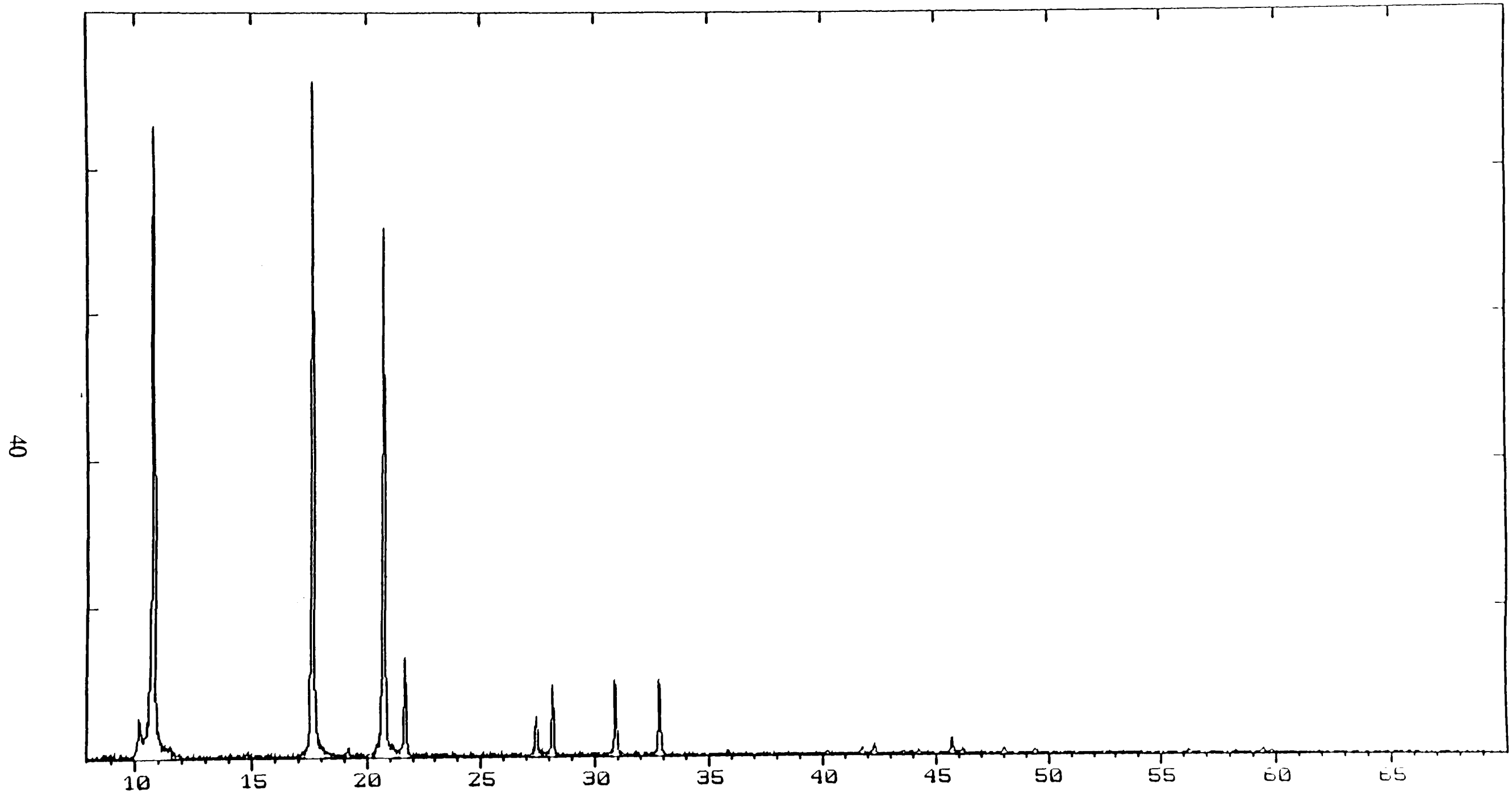


Figure 1.13.4.1. Powder X-ray diffraction pattern of a sample of sublimed C_{60}. λ = 1.5406Å.

References

1. *The Fullerenes. New Horizons for the Chemistry, Physics and Astrophysics of Carbon.*; Kroto, H. W.; Walton, D. R. M., Ed.; Cambridge University Press: Cambridge, 1993, pp 154.
2. *The Fullerenes*; Kroto, H. W.; Fischer, J. E.; Cox, D. E., Ed.; Pergamon: Oxford, 1993, pp 314.
3. Kroto, H. W. *Angew. Chem. Int. Ed. Engl.* 1992, ***31***, 111.
4. Kroto, H. W.; Allaf, A. W.; balm, S. P. *Chem. Rev.* 1991, ***91***, 1213.
5. Kroto, H. *Science* 1988, ***242***, 1139.
6. Kroto, H. W.; Heath, J. R.; O'Brien, S. C.; Curl, R. F.; Smalley, R. E. *Nature* 1985, ***318***, 162.
7. Kratschmer, W.; Lamb, L. D.; Fostiropolous, K.; Huffman, D. R. *Nature* 1990, ***347***, 354.
8. Koruga, D.; Hamerloff, S.; Withers, J.; Loutfy, R.; Sundaresham, M. *Fullerene C60. History, Physics, Nanobiology, Nanotechnology.* ; Elsevier: Amsterdam, 1993.
9. *Buckminsterfullerenes*; Billups, W. E.; Ciufolini, M. A., Ed.; VCH Publishers: New York, 1993, pp 339.
10. Ohsawa, Y.; Saji, T. *J. Chem. Soc., Chem. Comm.* 1992, 781.
11. Weeks, D. E.; Harter, W. G. *J. Chem. Phys.* 1989, ***90***, 4744.
12. Taylor, R.; Hare, J. P.; Abdul-Sada, A. K.; Kroto, H. W. *J. Chem. Soc., Chem. Comm.* 1990, 1423.
13. Hawkins, J. M.; Meyer, A.; Lewis, T. A.; Loren, S.; Hollander, F. J. *Science* 1991, ***252***, 312.
14. Balch, A. L.; Lee, J. W.; Olmstead, M. M. *Angew. Chem. Int. Ed. Engl.* 1992, ***31***, 1356.
15. Kikuchi, K.; Nakahara, N.; Wakabayashi, T.; Honda, M.; Matsumiya, H.; Moriwaki, T.; Suzuki, S.; Shiromaru, H.; Saito, K.; Yamauchi, K.; Ikemoto, I.; Achiba, Y. *Chem. Phys. Lett.* 1992, ***188***, 177.
16. Kikuchi, K.; Nakahara, N.; Wakabayashi, T.; Suzuki, S.; Shiromaru, H.; Miyake, Y.; Saito, K.; Ikemoto, I.; Kainosho, M.; Achiba, Y. *Nature* 1992, ***357***, 142.
17. Ettl, R.; Chao, I.; Diederich, F.; Whetten, R. L. *Nature* 1991, ***353***, 149.
18. Diederich, F.; Ettl, R.; Rubin, Y.; Whetten, R. L.; Beck, R.; Alvarez, M.; Anz, S.; Sensharma, D.; Wudl, F.; Khemani, K. C.; Koch, A. *Science* 1991, ***252***, 548.
19. Diederich, F.; Whetten, R. L.; Thilgen, C.; Ettl, R.; Chao, I.; Alvarez, M. *Science* 1991, ***254***, 1768.

20. Diederich, F.; Whetten, R. L.; Thilgen, C.; Ettl, R.; Chao, I.; Alvarez, M. M. *Science* 1991, ***254***, 1768.
21. Fowler, P. W.; Manolopoulos, D. E.; Ryan, R. P. *Carbon* 1992, ***30***, 1235.
22. Bochvar, D. A.; Gal'pern, E. G. *Dokl. Akad. Nauk. SSSR* 1973, ***209***, 610.
23. Davidson, R. A. *Theor. Chem. Acta.* 1981, ***58***, 193.
24. Haymet, A. D. *J. Chem. Phys. Lett.* 1985, ***122***, 421.
25. Stankevich, I. V.; Nikerov, M. V.; Bochvar, D. A. *Russ. Chem. Rev.* 1984, ***53(7)***, 640.
26. Echegoyen, L.; Xie, Q.; Perez-Cordero, E. *J. Am. Chem. Soc.* 1992, ***114***, 3978.
27. McEwen, C. N.; McKay, R. G.; Larsen, B. S. *J. Am. Chem. Soc.* 1992, ***114***, 4412.
28. Bundy, F. P. *Physica A* 1989, ***156***, 169.
29. Beckhaus, H.-D.; Verevkin, S.; Ruchardt, C.; Diederich, F.; Thilgen, C.; Meer, H.-U. t.; Mohn, H.; Müller, W. *Angew. Chem. Int. Ed. Engl.* 1994, ***33***, 996.
30. Ruchardt, C.; Beckhaus, H.-D.; Kao, M.; Diederich, F.; Foote, C. S. *Angew. Chem. Int. Ed. Engl.* 1992, ***31***, 63.
31. Bakowies, D.; Thiel, W. *J. Am. Chem. Soc.* 1991, ***113***, 3704.
32. Armitage, D. A.; Bird, C. W. *Tetrahedron Lett.* 1993, ***34***, 5811.
33. Allinger, N. L.; Yuh, Y. H.; Lii, J.-H. *J. Am. Chem. Soc.* 1989, ***111***, 8551.
34. Pan, C.; Sampson, M. P.; Chal, Y.; Hauge, R. H.; Margrave, J. L. *J. Phys. Chem.* 1991, ***95***, 2944.
35. Heiney, P. A. *J. Phys. Chem. Solids* 1992, ***53***, 1333.
36. Chase, B.; Herron, N.; Holler, E. *J. Phys. Chem.* 1992, ***96***, 4262.
37. Narasimhan, L. R.; Stoneback, D. N.; Hebard, A. F.; Haddon, R. C.; Patel, C. K. N. *Phys. Rev.* 1992, ***B46***, 2591.
38. Neumann, D. A.; Copley, J. R. D.; Cappelletti, R. L.; Kamitakahara, W. A.; Lindstrom, R. M.; Creegan, K. M.; Cox, D. M.; Romanow, W. J.; Coustel, N.; McCauley, J. P.; Maliszewskyj, N. C.; Fischer, J. E.; III, A. B. S. *Phys. Rev. Letts.* 1992, ***64***, 3808.
39. Yannoni, C. S.; Johnson, R. D.; Meijer, G.; Bethune, D. S.; Salem, J. R. *J. Phys. Chem.* 1991, ***95***, 9.
40. Johnson, R. D.; Yannoni, C. S.; Dorn, H. C.; Salem, J. R.; Bethune, D. S. *Science* 1992, ***255***, 1235.
41. Heiney, P. A.; Fischer, J. E.; McGhie, A. R.; Romanow, W. J.; Denenstein, A. M.; Jr, J. P. M.; III, A. B. S.; Cox, D. E. *Phys. Rev. Letts.* 1991, ***66***, 2911.

42. Tycko, R.; Dabbagh, G.; Fleming, R. M.; Haddon, R. C.; Makhija, A. V.; Zahurak, S. M. *Phys. Rev. Lett.* 1991, ***67***, 1886.
43. Dworkin, A.; Fabre, C.; Schuta, D.; Kriza, G.; Ceolin, R.; Szwarc, H.; Bernier, P.; Jerome, D.; Leach, S.; Rassat, A.; Hare, J. P.; Dennis, T. J.; Kroto, H. W.; Taylor, R.; Walton, D. R. M. *C. R. Acad. Sci. Paris* 1991, *313 II*, 1017.
44. Sachidanandam, R.; Harris, A. B. *Chem. Phys. Lett.* 1991, ***183***, 1467.
45. Milliken, J.; Keller, T. M.; Baronavski, A. P.; McElvany, S. W.; Callahan, J. H.; Nelson, H. H. *Chem. Mater.* 1991, *3*, 386.
46. Assink, R. A.; Schirber, J. E.; Loy, D. A.; Morosin, B.; Carlson, G. A. *J. Mat. Res.* 1992, *7*, 2136.
47. Vijayakrishnan, V.; Santra, A. K.; Pradeep, T.; Seshadri, R.; Nagarajan, R.; Rao, C. N. R. *J. Chem. Soc., Chem. Comm.* 1992, 198.
48. Haufler, R. E.; Conceicao, J.; Chibante, L. P. F.; Chai, Y.; Byrne, N. E.; Flanagan, S.; Haley, M. M.; O'Brien, S. C.; Pan, C.; Xiao, Z.; Billups, W. E.; Ciufolini, M. A.; Hauge, R. H.; Margrave, J. L.; Wilson, L. J.; Curl, R. F.; Smalley, R. E. *J. Phys. Chem.* 1990, ***94***, 8634.
49. Olah, G.; Bucsi, I.; Lambert, C.; Aniszfeld, R.; Trivedi, N. J.; Sensharma, D. K.; Prakash, G. K. S. *J. Am. Chem. Soc.* 1991, ***113***, 9385.
50. Olah, G.; Bucsi, I.; Lambert, C.; Aniszfeld, R.; Trivedi, N. J.; Sensharma, D. K.; Prakash, G. K. S. *J. Am. Chem. Soc.* 1991, ***113***, 9387.
51. Banks, M. R.; Dale, M. J.; Gosney, I.; Hodgson, P. K. G.; Jennings, R. C. K.; Jones, A. C.; Lecoultre, J.; Langridge-Smith, P. R. R.; Maier, J. P.; Scrivens, J. H.; Smith, M. J. C.; Smyth, C. J.; Taylor, A. T.; Thorburn, P.; Webster, A. S. *J. Chem. Soc., Chem. Comm.* 1993, 1149.
52. An, Y.-Z.; Rubin, Y.; Schaller, C.; McElvany, S. W. *J. Org. Chem.* 1994, ***59***, 2927.
53. Wudl, F.; Suzuki, T.; Li, Q.; Khemani, K. C.; Almarsson, O. *J. Am. Chem. Soc.* 1992, ***114***, 7300.
54. Hirsch, A.; Skiebe, A. *J. Chem. Soc., Chem. Comm.* 1994, 335.
55. Vasella, A.; Uhlmann, P.; Waldraff, C. A. A.; Diederich, F.; Thilgen, C. *Angew. Chem. Int. Ed. Engl.* 1992, ***31***, 1388.
56. Tsuda, M.; Ishida, T.; Nogami, T.; Kurono, S.; Ohashi, M. *Tetrahedron Lett.* 1993, ***34***, 6911.
57. Isaacs, L.; Diederich, F. *Helv. Chim. Acta.* 1993, ***76***, 2454.
58. Tokuyama, H.; Nakamura, M.; nakamura, E. *Tetrahedron Lett.* 1993, ***34***, 7429.
59. Beer, E.; Feuerer, M.; Knorr, A.; Mirlach, A.; Daub, J. *Angew. Chem., Int. Ed. Engl.* 1994, ***33***, 1087.

60. Maggini, M.; Scorrano, G.; Prato, M. *J. Am. Chem. Soc.* 1993, ***115***, 9798.
61. Prato, M.; Suzuki, T.; Foroudian, H.; Li, Q.; Khemani, K.; Wudl, F. *J. Am. Chem. Soc.* 1993, ***115***, 1594.
62. Belik, P.; Gugel, A.; Spikermann, J.; Müllen, J. *Angew. Chem., Int. Ed. Engl.* 1993, ***32***, 78.
63. Rubin, Y.; Khan, S. I.; Freedberg, D. I.; Yeretzian, C. J. *J. Am. Chem. Soc.* 1993, ***115***, 344.
64. Zhang, X.; Romero, A.; Foote, C. S. *J. Am. Chem. Soc.* 1993, ***115***, 11024.
65. Wudl, F.; Prato, M.; Suzuki, T.; Foroudian, H.; Li, Q.; Khemani, K.; Leonetti, J.; Little, R. D.; White, T.; Rickborn, B.; Yamago, S.; Nakamura, E. *J. Am. Chem. Soc.* 1993, ***115***, 1594.
66. Mullen, K.; Belik, P.; Gugel, A.; Spickermann, J. *Angew. Chem. Int. Ed. Engl.* 1993, ***32***, 78.
67. Rubin, Y.; An, Y.-Z.; Anderson, J. L. *J. Org. Chem.* 1993, ***58***, 4799.
68. Rubin, Y.; Kahn, S.; Freedberg, D. I.; Yeretzian, C. *J. Am. Chem. Soc.* 1993, ***115***, 344.
69. Rubin, Y.; Kahn, S. I.; Oliver, A. M.; Paddon-Row, M. N. *J. Am. Chem. Soc.* 1993, ***115***, 4919.
70. Schlueter, J. A.; Seaman, J. M.; Taha, S.; Cohen, H.; Lykke, K. R.; Wang, H. H.; Williams, J. M. *J. Chem. Soc., Chem. Comm.* 1993, 972.
71. Tsuda, M.; Ishida, T.; Nogami, T.; Kurono, S.; Ohashi, M. *J. Chem. Soc., Chem. Comm.* 1993, 1296.
72. Bingel, C. *Chem. Ber.* 1993, ***126***, 1957.
73. Fagan, P. J.; Krusic, P. J.; Evans, D. H.; Lerke, S. A.; Johnston, E. *J. Am. Chem. Soc.* 1992, ***114***, 9697.
74. Yamago, S.; Yanagawa, M.; Nakamura, E. *J. Chem. Soc., Chem. Comm.* 1994, 2093.
75. Kenyon, G. L.; Friedman, S. H.; DeCamp, D. L.; Sijbesma, R. P.; Srdanov, G.; Wudl, F. *J. Am. Chem. Soc.* 1993, ***115***, 6506.
76. Frechet, J. M. J.; Wooley, K. L.; Hawker, C. J.; Wudl, F.; Srdanov, G.; Shi, S.; Li, C.; Kao, M. *J. Am. Chem. Soc.* 1993, ***115***, 9836.
77. Cooks, R. G.; II, S. H. H.; Molstad, J.; Dilettato, D.; Jay, M. J.; Carlson, D.; Kahr, B. *J. Org. Chem.* 1992, ***57***, 5069.
78. Rao, A. M.; Zhou, P.; Wang, K.-A.; Hager, G. T.; Holden, J. M.; Wang, Y.; Lee, W.-T.; Bi, X.-X.; Eklund, P. C.; Cornett, D. S.; Duncan, M. A.; Amster, I. J. *Science* 1993, ***259***, 955.
79. Luh, T.-Y.; Shui, L.-L.; Lin, T.-I.; Peng, S.-M.; Her, G.-R.; Ju, D. D.; Lin, S.-K.; Hwang, J.-H.; Mou, C. Y. *J. Chem. Soc., Chem. Comm.* 1994, 647.

80. Suzuki, T.; Li, Q.; Khemani, K. C.; Wudl, F.; Almarsson, Ö. *Science* 1991, ***254***, 1186.
81. Meier, M. S.; Poplawska, M. *J. Org. Chem.* 1993, ***58***, 4524.
82. Wudl, F.; Prato, M.; Li, Q. C.; Lucchini, V. *J. Am. Chem. Soc.* 1993, ***115***, 1148.
83. Deiderich, F.; Ettl, R.; Rubin, Y.; Whetten, R. L.; Beck, R.; Alvarez, M.; Anz, S.; Sehsharma, D.; Wudl, F.; Khemani, K. C.; Koch, A. *Science* 1991, ***252***, 548.
84. Henderson, C. C.; Cahill, P. A. *Science* 1993, ***259***, 1885.
85. Ballenweg, S.; Gleiter, R.; Krätschmer, W. *Tetrahedron Lett.* 1993, ***34***, 3737.
86. Henderson, C. C.; Cahill, P. A. *Chem. Phys. Lett.* 1992, ***198***, 570.
87. Matsuzawa, N.; Dixon, D. A.; Fukunaga, T. *J. Phys. Chem.* 1992, ***96***, 7594.
88. Foote, C. S.; Elemes, Y.; Silverman, S. K.; Sheu, C.; Kao, M.; Alvarez, M. M.; Whetten, R. L. *Angew. Chem. Int. Ed. Engl.* 1992, ***31***, 351.
89. Cox, D. M.; Creegan, K. M.; Robbins, J. L.; Robbins, W. K.; Millar, J. M.; Sherwood, R. D.; Tindall, P. J.; III, A. B. S.; McCauley, J. P.; Jones, D. R.; Gallagher, R. T. *J. Am. Chem. Soc.* 1992, ***114***, 1103.
90. Balch, A. L.; Costa, D. A.; Lee, J. W.; Noll, B. C.; Olmstead, M. M. *Inorg. Chem.* 1994, ***33***, 2071.
91. Fagan, P. J.; Calabrese, J. C.; Malone, B. *Science* 1991, ***252***, 1160.
92. Fagan, P. J.; Calabrese, J. C.; Malone, B. *J. Am. Chem. Soc.* 1991, ***113***, 9408.
93. Fagan, P. J.; Lerke, S. A.; Parkinson, B. A.; Evans, D. H. *J. Am. Chem. Soc.* 1992, ***114***, 7807.
94. Balch, A. L.; Catalano, J. C.; Lee, J. *J. Inorg. Chem.* 1991, ***21***, 3980.
95. Shapley, J. R.; Koefod, R. S.; Hudgens, M. F. *J. Am. Chem. Soc.* 1991, ***113***, 8957.
96. Balch, A. L.; Catalano, V. J.; Lee, J. W.; Olmstead, M. M. *J. Am. Chem. Soc.* 1992, ***114***, 5455.
97. Balch, A. L.; Lee, J. W.; Noll, B. C.; Olmstead, M. M. *J. Am. Chem. Soc.* 1992, ***114***, 10984.
98. Stephens, A. H. H. *Personal Comunication.*
99. Balch, A. L.; Lee, J. W.; Noll, B. C.; Olmstead, M. M. *Inorg. Chem.* 1993, ***32***, 3577.
100. Douthwaite, R. E.; Green, M. L. H.; Stephens, A. H. H.; Turner, J. F. C. *J. Chem. Soc., Chem. Comm.* 1993, 1522.
101. Claridge, J. B.; Douthwaite, R. E.; Green, M. L. H.; Lago, R. M.; Tsang, S. C.; York, A. P. E. *J. Mol. Cat.* 1993, ***89***, 113.

102. Rasinkangas, M.; Pakkanen, T. T.; Pakkanen, T. A. *J. Organomet. Chem.* 1994, ***476***, C6.

103. Pakkanen, T. A.; Rasinkangas, M.; Pakkanen, T. T.; Ahlgren, M.; Rouvinen, J. *J. Am. Chem. Soc.* 1993, ***115***, 4901.

104. Compton, R. N.; Tuinman, A. A.; Gakh, A. A.; Adcock, J. L. *J. Am. Chem. Soc.* 1993, ***115***, 5885.

105. Cox, D. M.; Kniaz, K.; Fischer, J. E.; Selig, H.; Vaughan, G. B. M.; Romanow, W. J.; Chowdhury, S. K.; McCauley, J. P.; Strongin, R. M.; III, A. B. S. *J. Am. Chem. Soc.* 1993, ***115***, 6060.

106. Cox, D. M.; Cameron, S. D.; Tuinman, A.; Gakh, A.; Adcock, J. L.; Compton, R. N.; Hagaman, E. W.; Kniaz, K.; Fischer, J. E.; Stronglin, R. M.; Cichy, M. A.; SmithIII, A. B. *J. Am. Chem. Soc.* 1994, ***116***, 1115.

107. Fagan, P. J.; Krusic, P. J.; McEwen, C. N.; Lazar, J.; Parker, D. H.; Herron, N.; Wasserman, E. *Science* 1993, ***262***, 404.

108. Gakh, A. A.; Tuinman, A. A.; Adcock, J. L.; Sachleben, R. A.; Compton, R. N. *J. Am. Chem. Soc.* 1993, ***116***, 819.

109. Holloway, J. H.; Hope, E. G.; Taylor, R.; Langley, G. J.; Avent, A. G.; Dennis, T. J.; Hare, J. P.; Kroto, H. W.; Walton, D. R. M. *J. Chem. Soc., Chem. Comm.* 1991, 966.

110. Selig, H.; Lifshitz, C.; Peres, T.; Fischer, J. E.; McGhie, A. R.; Romanow, W. J.; Jr, J. P. M.; III, A. B. S. *J. Am. Chem. Soc.* 1991, ***113***, 5475.

111. Taylor, R.; Holloway, J. H.; Hope, E. G.; Avent, A. G.; Langley, G. J.; Dennis, T. J.; Hare, J. P.; Kroto, H. W.; Walton, D. R. M. *J. Chem. Soc., Chem. Comm.* 1992, 665.

112. Taylor, R.; Langley, G. J.; Brisdon, A. K.; Holloway, J. H.; Hope, E. G.; Kroto, H. W.; Walton, D. R. M. *J. Chem. Soc., Chem. Comm.* 1993, 875.

113. Tebbe, F. N.; Becker, J. Y.; Chase, D. B.; Firment, L. E.; Holler, E. R.; Malone, B. S.; Krusic, P. J.; Wasserman., E. *J. Am. Chem. Soc.* 1991, ***113***, 9900.

114. Birkett, P. R.; Avent, A. G.; Darwish, A. D.; Kroto, H. W.; Taylor, R.; Walton, D. R. M. *J. Chem. Soc., Chem. Comm.* 1993, 1230.

115. Tebbe, F. N.; Harlow, R. L.; Chase, D. B.; Thorn, D. L.; Campbell, G. C.; Calabrese, J. C.; Herron, N.; Young, R. J.; Wasserman, E. *Science* 1992, ***256***, 822.

116. Kroto, H. W.; Birkett, P. R.; Hitchcock, P. B.; Taylor, R.; Walton, D. R. M. *Nature* 1992, ***357***, 479.

117. Zhu, Q.; Cox, D. E.; Fischer, J. E.; Kniaz, K.; McGhie, A. R.; Zhou, O. *Nature* 1992, ***355***, 712.

118. Miller, J. S.; Epstein, A. J. *Angew. Chem., Int. Ed. Engl.* 1994, ***33***, 385.

119. Miller, J. S. *Adv. Mat.* 1991, *3*, 262.
120. Wudl, F.; Allemand, P.-M.; Srdanov, G.; Koch, A.; Khemani, K. *J. Am. Chem. Soc.* 1991, ***1991***, 2780.
121. Penicaud, A.; Perez-Benitez, A.; V., R. G.; P., E. M.; Escudero, R. *J. Am. Chem. Soc.* 1993, ***115***, 10392.
122. Bilow, U.; Jansen, M. *J. Chem. Soc., Chem. Comm.* 1994, 403.
123. Foss, C. A.; Feldheim, D. A.; Lawson, D. R.; Dorhout, P. K.; Elliot, C. M.; Martin, C. R.; Parkinson, B. A. *J. Electrochem. Soc.* 1993, ***140***, L84.
124. Kobayashi, H.; Moriyama, H.; Kobayashi, A.; Watanabe, T. *J. Am. Chem. Soc.* 1993, ***115***, 1185.
125. Reed, C. A.; Penicaud, A.; Hsu, J.; Koch, A.; Khemani, K. C.; Alemand, P.-M.; Wudl, F. *J. Am. Chem. Soc.* 1991, ***113***, 6698.
126. Bossard, C.; Rigaut, S.; Astruc, D.; Deville, M.-H.; Felix, G.; Fevrier-Bouvier, A.; Amiell, J.; Flandrois, S.; Delhaes, P. *J. Chem. Soc., Chem. Comm.* 1993, 333.
127. Reed, C. A.; Stinchcombe, J.; Penicaud, A.; Bhyrappa, P.; Boyd, P. D. W. *J. Am. Chem. Soc.* 1993, ***115***, 5212.
128. Parimal, P.; Xie, Z.; Bau, R.; Boyd, P. D. W.; Reed, C. A. *J. Am. Chem. Soc.* 1994, ***116***, 4145.
129. Izuoka, A.; Tachikawa, T.; Sugawara, T.; Suzuki, Y.; Konno, M.; Saito, Y.; Shinohara, H. *J. Chem. Soc., Chem. Comm.* 1992, 1472.
130. Pradeep, T.; Singh, K. K.; Sinha, A. P. B.; Morris, D. E. *J. Chem. Soc., Chem. Comm.* 1992, 1747.
131. Allemand, P.-M.; Khemani, K. C.; Koch, A.; Wudl, F.; Holczer, K.; Donovan, S.; Grüner, G.; Thompson, J. D. *Science* 1991, ***253***, 301.
132. Wudl, F.; Thompson, J. D. *J. Phys. Chem. Solids* 1992, ***53***, 1449.
133. Douthwaite, R. E.; Green, M. L. H.; Heyes, S. J.; Rosseinsky, M. J.; Turner, J. F. C. *J. Chem. Soc., Chem. Comm.* 1994, 1367.
134. Locke, I. W.; Darwish, A. D.; Kroto, H. W.; Prassides, K.; Taylor, R.; Walton, D. R. M. *Chem. Phys. Lett.* 1994, ***225***, 186.
135. Balch, A. L.; Lee, J. W.; Noll, B. C.; Olmstead, M. M. *J. Chem. Soc., Chem. Comm.* 1993, 56.
136. Meidine, M. F.; Hitchcock, P. B.; Kroto, H. W.; Taylor, R.; Walton, D. R. M. *J. Chem. Soc., Chem. Comm.* 1992, 1534.
137. Oszlanyi, G.; Bortel, G.; Faigel, G.; Pekker, S.; Tegze, M. *Solid State Comm.* 1994, ***89***, 417.
138. Crane, J. D.; Hitchcock, P. B.; Kroto, H. W.; Taylor, R.; Walton, D. R. M. *J. Chem. Soc., Chem. Comm.* 1992, 1764.

139. Xiang, X.-D.; Hou, J. G.; Briceno, G.; Vareka, W. A.; Mostovoy, R.; Zettl, A.; Crespi, V. H.; Cohen, M. L. *Nature* 1992, ***256***, 1190.

140. Serizawa, S.; Gabrielova, I.; Fujimoto, T.; Shido, T.; Ichikawa, M. *J. Chem. Soc., Chem. Comm.* 1994, 799.

141. McCauley, J. P.; Zhu, Q.; Coustel, N.; Zhou, O.; Vaughan, G.; Idziak, S. H. J.; Fischer, J. E.; Tozer, S. W.; Groski, D. M.; Bykovetz, N.; Lin, C. L.; McGhie, A. R.; Allen, B. H.; Romanow, W. J.; Denenstein, A. M.; III, A. B. S. *J. Am. Chem. Soc.* 1991, ***113***, 8537.

142. Murphy, D. W.; Rosseinsky, M. J.; Fleming, R. M.; Tycko, R.; Ramirez, A. P.; Haddon, R. C.; Seigrist, T.; Dabbagh, G.; Tully, J. C.; Walstedt, R. E. *J. Phys. Chem. Solids* 1992, ***53***, 1321.

143. Tanigaki, K.; Ebbesen, T. W.; Saito, S.; Mizuki, J.; Tsai, J. S.; Kubo, Y.; Kuroshima, S. *Nature* 1991, ***352***, 222.

144. Tycko, R.; Dabbagh, G.; Rosseinsky, M. J.; Murphy, D. W.; Ramirez, A. P.; Fleming, R. M. *Phys. Rev. Letts.* 1992, ***68***, 1912.

145. Tycko, R.; Dabbagh, G.; Rosseinsky, M. J.; Murphy, D. W.; Fleming, R.; Ramirez, A. P.; Tully, J. C. *Science* 1991, ***253***, 884.

146. Tycko, R.; Dabbagh, G.; murphy, D. W.; Zhu, Q.; Fischer, J. E. *Phys. Rev. B* 1993, ***48***, 9097.

147. Tycko, R. *J. Phys. Chem. Solids* 1994, ***54***, 1713.

148. Fleming, R. M.; Ramirez, A. P.; Rosseinsky, M. J.; Murphy, D. W.; Haddon, R. C.; Zahurak, S. M.; Makhija, A. V. *Nature* 1991, ***352***, 787.

149. Rosseinsky, M. J.; Murphy, D. W.; Fleming, R. M.; Tycko, R.; Ramirez, A. P.; Siegrist, T.; Dabbagh, G.; Barrett, S. E. *Nature* 1992, ***356***, 416.

150. Zhou, O.; Fleming, R. M.; Murphy, D. W.; Rosseinsky, M. J.; Ramirez, A. P.; Dover, R. B. v.; Haddon, R. C. *Nature* 1993, ***362***, 433.

151. Kortan, A. R.; Kopylov, N.; Glarum, S.; Gyorgy, E. M.; Ramirez, A. P.; Thiel, F. A.; Haddon, R. C. *Nature* 1992, ***355***, 529.

152. Kortan, A. R.; Kopylov, N.; Glarum, S.; Gyorgy, E. M.; Ramirez, A. P.; Fleming, R. M.; Zhou, O.; Thiel, F. A.; Trevor, P. L.; Haddon, R. C. *Nature* 1992, ***360***, 566.

153. Tanigaki, K.; Hirosawa, I.; Ebbesen, T. W.; Mizuki, J.; Shimakawa, Y.; Kubo, Y.; Tsai, J. S.; Kuroshima, S. *Nature* 1992, ***356***, 419.

154. Yildirim, T.; Zhou, O.; Fischer, J. E.; Bykovetz, N.; Strongin, R. A.; Cichy, M. A.; III, A. B. S.; Lin, C. L.; Jelinek, R. *Nature* 1992, ***360***, 569.

155. Chauvet, O.; Oszlanyi, G.; Forro, L.; Stephens, P. W.; Tegze, M.; Faigol, G.; Janossy, A. *Phys. Rev. Lett.* 1994, ***72***, 2721.

156. Pekker, S.; Janossy, A.; Mihaly, L.; Chauvet, O.; Carrard, M.; Forro, L. *Science* 1994, ***265***, 1077.

157. Yildirim, T.; Fischer, J. E.; Harris, A. B.; Stephens, P. W.; Liu, D.; Brard, L.; Strongin, R. M.; III, A. B. S. *Phys. Rev. Lett.* 1993, ***71***, 1383.
158. Regueiro, M. N.; Monceau, P.; Hodeau, J.-L. *Nature* 1992, ***355***, 237.
159. Tutt, L. W.; Kost, A. *Nature* 1992, ***356***, 225.
160. Iwasa, Y.; Arima, T.; Fleming, R. M.; Siegrist, T.; Zhou, O.; Haddon, R. C.; Rothberg, L. J.; Lyons, K. B.; Carter, H. L.; Hedard, A. F.; Tycko, R.; Dabbagh, G.; Krajewski, J. J.; Thomas, G. A.; Yagi, T. *Science* 1994, ***264***, 1570.
161. Loy, D. A.; Assink, R. A. *J. Am. Chem. Soc.* 1992, ***114***, 3977.
162. Wudl, F.; Shi, S.; Khemani, K. C.; Li, Q. *J. Am. Chem. Soc.* 1992, ***114***, 10656.
163. Wang, Y. *Nature* 1992, ***356***, 585.
164. Wei, Y.; Tian, J.; MacDiarmid, A. G.; Masters, J. G.; Smith, A. L.; Li, D. *J. Chem. Soc., Chem. Comm.* 1993, 603.
165. Bergbreiter, D. E.; Grey, H. N. *J. Chem. Soc., Chem. Comm.* 1993, 645.
166. Chen, K.; Caldwell, W. B.; Mirkin, C. A. *J. Am. Chem. Soc.* 1993, ***115***, 1193.
167. Curl, R. F.; Smalley, R. E. *Science* 1988, ***242***, 1017.
168. Garvey, J. F.; Stry, J. J.; Coolbaugh, M. T.; Turos, E. *J. Am. Chem. Soc.* 1992, ***114***, 7914.
169. Gross, M. L.; Caldwell, K. A.; Giblin, D. E. *J. Am. Chem. Soc.* 1992, ***1992***, 3743.
170. Freiser, B. S.; Jiao, Q.; Huang, Y.; Lee, S. A.; Gord, J. R. *J. Am. Chem. Soc.* 1992, ***114***, 2726.
171. Bohme, D. K.; Petrie, S.; Javahery, G. *J. Am. Chem. Soc.* 1993, ***115***, 1445.
172. Bohme, D. K.; Petrie, S.; Javahery, G.; Wang, J. *J. Am. Chem. Soc.* 1992, ***114***, 6268.
173. Bohme, D. K.; Becker, H.; Javahery, G.; Petrie, S.; Cheng, P.-C.; Schwartz, H.; Scott, L. T. *J. Am. Chem. Soc.* 1993, ***115***, 11636.
174. Freiser, B. S.; Roth, L. M.; Huang, Y.; Schwedler, J. T.; Cassidy, C. J.; Ben-Amotz, D.; Kahr, B. *J. Am. Chem. Soc.* 1991, ***113***, 6298.
175. Bohme, D. K.; Wang, J.; Javahery, G.; Petrie, S.; Hopkinson, A. C. *Angew. Chem. Int. Ed. Engl.* 1994, ***33***, 206.
176. Zybill, C. *Angew. Chem. Int. Ed. Engl.* 1992, ***31***, 173.
177. Schwarz, H.; Weiske, T.; Bohme, D. K.; Hrusak, J.; Kratschmer, W. *Angew. Chem. Int. Ed. Engl.* 1991, ***30***, 884.
178. Leigh, D. A.; Davey, S. N.; Moody, A. E.; Tetler, L. W. *J. Chem. Soc., Chem. Comm.* 1994, 7.

179. Chiang, L. Y.; Swirczewski, J. W.; Hsu, C. S.; Chowdhury, S. K.; Cameron, S.; Creegan, K. *J. Chem. Soc., Chem. Comm.* 1992, 1791.
180. Bethune, D. S.; Johnson, R. D.; Salem, J. R.; Vries, M. S. d.; Yannoni, C. S. *Nature* 1993, ***366***, 123.
181. Shinoahara, H.; Yamaguchi, H.; Hayashi, N.; Sato, H.; Ohkohchi, M.; Ando, Y.; Saito, T. *J. Phys. Chem.* 1993, ***97***, 4259.
182. Beyers, R.; Kiang, C.-H.; Johnson, R. D.; Salem, J. R.; Vries, M. S. d.; Yannoni, C. S.; Bethune, D. S.; Dorn, H. C.; Burbank, P.; Harich, K.; Stevenson, S. *Nature* 1994, ***370***, 196.
183. Kikuchi, K.; Nakao, Y.; Suzuki, S.; Achiba, Y.; Suzuki, T.; Maruyama, Y. *J. Am. Chem. Soc.* 1994, ***116***, 9367.
184. Nagase, S.; Kobayashi, K. *J. Chem. Soc., Chem. Comm.* 1994, 1837.
185. Sanders, M.; Jimenez-Vazquez, H. A.; Cross, R. J.; Mroczkowski, S.; Freedberg, D. I.; Anet, F. A. L. *Nature* 1994, ***367***, 256.
186. Sanders, M.; Jimenez-Vazquez, H. A.; Bangerter, B. W.; Cross, R. J.; Mroczkowski, S.; Freedberg, D. I.; Anet, F. A. L. *J. Am. Chem. Soc.* 1994, ***116***, 3621.
187. Sanders, M.; Jimenez-Vazquez, H. A.; Cross, R. J.; Mroczkowski, S.; Gross, M. L.; Giblin, D. E.; Poreda, R. J. *J. Am. Chem. Soc.* 1994, ***116***, 2193.
188. Braun, T. *Angew. Chem. Int. Ed. Engl.* 1992, ***31***, 588.
189. Meier, M. S.; Selegue, J. P. *J. Org. Chem.* 1992, ***57***, 1924.
190. Chatterjee, K.; Parker, D. H.; Wurz, P.; Lykke, K. R.; Gruen, D. M.; Stock., L. M. *J. Org. Chem.* 1992, ***57***, 3253.
191. Darwish, A. D.; Kroto, H. W.; Taylor, R.; Walton, D. R. M. *J. Chem. Soc., Chem. Comm.* 1994, 15.
192. Mullen, K.; Gugel, A.; Becker, M.; Hammel, D.; Mindach, L.; Rader, J.; Simon, T.; Wagner, M. *Angew. Chem. Int. Ed. Engl.* 1992, ***31***, 644.
193. Parker, D. H.; Wurz, P.; Lykke, K. R.; Hunt, J. E.; Pellin, M. J.; Heminger, J. C.; Gruen, D. M.; Stock, L. M. *J. Am. Chem. Soc.* 1991, ***113***, 7499.
194. Reed, C. A.; Bhyrappa, P.; Penicaud, A.; Kawamoto, M. *J. Chem. Soc., Chem. Comm.* 1992, 936.
195. Schnering, H. G. v.; Mittelbach, A.; Honle, W.; Carlsen, J.; Janiak, R.; Quast, H. *Angew. Chem. Int. Ed. Engl.* 1992, ***31***, 1640.
196. Taylor, R.; Hare, J. P.; Abdul-Sada, A. K.; Kroto, H. W. *J. Chem. Soc., Chem. Comm.* 1990, 1423.
197. Vassallo, A. M.; Palmisano, A. J.; Pang, L. S. K.; Wilson, M. A. *J. Chem. Soc., Chem. Comm.* 1992, 60.
198. Suzuki, T.; Nakashima, K.; Shinkai, S. *Chem. Lett.* 1994, 699.
199. Atwood, J. L.; Koutsantonis, G. A.; Raston, C. L. *Nature* 1994, ***368***, 229.

200. Wudl, F.; Khemani, K. C.; Prato, M. *J. Org. Chem.* 1992, *57*, 3254.
201. Andersson, T.; Nilsson, K.; Sundahl, M.; Westman, G.; Wennerstrom, O. *J. Chem. Soc., Chem. Comm.* 1992, 604.
202. Ermer, O.; Robke, C. *J. Am. Chem. Soc.* 1993, ***115***, 10077.
203. Asmus, K.-D.; Hungerbuhler, H.; Guldi, D. M. *J. Am. Chem. Soc.* 1993, ***115***, 3386.
204. Schuth, F.; Gugel, A.; Mullen, K.; Reichert, H.; Schmidt, W.; Schon, G.; Spickermann, J.; Titman, J.; Unger, K. *Angew. Chem. Int. Ed. Engl.* 1993, ***32***, 556.
205. Morton, J. R.; Preston, K. F.; Krusic, P. J.; Hill, S. A.; Wasserman, E. *J. Phys. Chem.* 1992, ***96***, 3576.
206. Morton, J. R.; Preston, K. F.; Krusic, P. J.; Wasserman, E. *J. Chem. Soc., Perkin Trans.* 1992, 1425.
207. Krusic, P. J.; Hill, S. A.; Wasserman, E.; Morton, J. R.; Preston, K. F. *J. Am. Chem. Soc.* 1992, ***114***, 5454.
208. Krusic, P. J.; Wasserman, E.; Parkinson, B. A.; Malone, B.; Jr, E. R. H.; Keizer, P. N.; Morton, J. R.; Preston, K. F. *J. Am. Chem. Soc.* 1991, ***113***, 6274.
209. Krusic, P. J.; Wasserman, E.; Keizer, P. N.; Morton, J. R.; Preston, K. F. *Science* 1991, ***254***, 1183.
210. Iijima, S. *Nature* 1991, ***354***, 56.
211. Ajayan, P. M.; Iijima, S. *Nature* 1993, ***361***, 333.
212. Tsang, S. C.; Chen, Y. K.; Harris, P. J. F.; Green, M. L. H. *Nature* 1994, ***372***, 159.
213. Tsang, S. C.; Harris, P. J. F.; Green, M. L. H. *Nature* 1993, ***362***, 520.
214. Saito, T.; Yoshikawa, T.; Okuda, M.; Fujimoto, N.; Sumiyama, K.; Suzuki, K.; Kasuya, A.; Nishina, Y. *J. Phys. Chem. Solids* 1993, ***54***, 1849.
215. Murakami, Y.; Shibata, T.; Okuyama, K.; Arai, J.; Suematsu, H.; Yoshida, Y. *J. Phys. Chem. Solids* 1993, ***54***, 1861.
216. Griffin, J.1994, *PartII Thesis*, University of Oxford
217. Zhou, O.; Fleming, R. M.; Murphy, D. W.; Chen, C. H.; Haddon, R. C.; Ramirez, A. P.; Glarum, S. H. *Science* 1994, ***263***, 1744.
218. Iijima, S.; Ichihashi, T. *Nature* 1993, ***363***, 603.
219. Bethune, D. S.; Kiang, C. H.; Vries, M. S. d.; Gorman, G.; Savoy, R.; Vazquez, J.; Beyers, R. *Nature* 1993, ***363***, 605.
220. Subramoney, S.; Ruoff, R. S.; Lorents, D. C.; Malhotra, R. *Nature* 1993, ***364***, 637.
221. Dresselhaus, M. S.; Dresselhaus, G.; Eklund, P. C. *J. Mater. Res.* 1993, *8*, 2054.

222. Dresselhaus, M. S.; Dresselhaus, G.; Saito, R. *Phys. Rev. B* 1992, ***45***, 6234.
223. Saito, R.; Dresselhaus, G.; Dresselhaus, M. S. *Chem. Phys. Lett.* 1992, ***195***, 537.
224. Smalley, R. *Mater. Sci. Eng. B* 1993, ***B19***, 1.
225. Iijima, S.; Ichihashi, T.; Ando, Y. *Nature* 1992, ***356***, 776.
226. Tsang, S. C.; Harris, P. J. F.; Claridge, J. B.; Green, M. L. H. *J. Chem. Soc., Chem. Comm.* 1993, 1519.
227. Iijima, S.; Ichihashi, T.; Ando, Y. *Nature* 1992, ***356***, 776.
228. Harris, P. J. F.; Green, M. L. H.; Tsang, S. C. *J. Chem. Soc., Faraday Trans.* 1993, ***89***, 1189.
229. Ugarte, D. *Nature* 1992, ***359***, 707.
230. Werner, H.; Bublak, D.; Gobel, U.; Henschke, B.; Bensch, W.; Schlogl, R. *Angew. Chem., Int. Ed. Eng.* 1992, ***31***, 868.

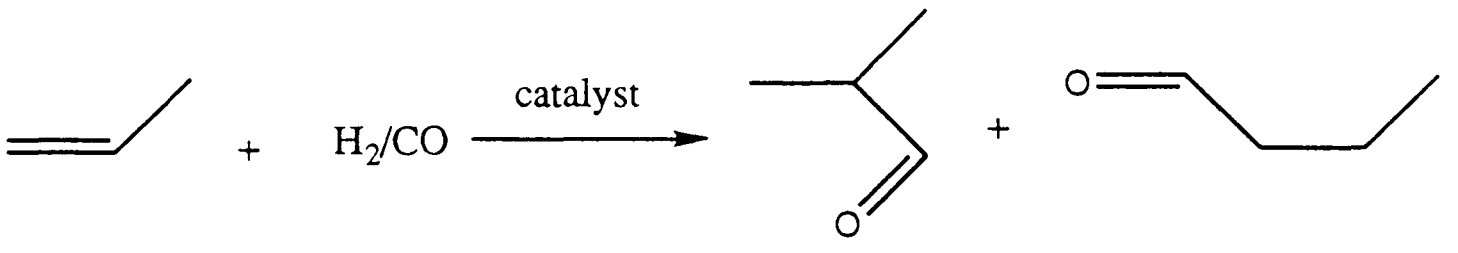
Chapter 2

C_{60} and the Hydroformylation Process

2.1. Introduction.

Hydroformylation is an important industrial process providing oxo-aldehydes and alcohols on the billion kilogram scale every year.[1-3] A great deal of work has been undertaken in the area of hydroformylation and numerous excellent reviews on the subject have been published and developments patented.[4-9] This section will concentrate on the role of relevant rhodium catalyst precursors, particularly $Rh(CO)(H)(PPh_3)_3$, and will attempt to place them into context of the hydroformylation process as a whole.

Hydroformylation is the conversion of alkenes and syn gas (H_2/CO) to aldehydes. This reaction will not take place in the absence of a suitable catalyst.



equation 2.1.1.

Many metal complexes are active hydroformylation catalysts with varying degrees of activity and selectivity.[5, 10] Two positional isomers are possible for the reaction with an unsymmetrical alkene as shown in equation 2.1.1. For industrially important terminal alkenes the useful product is the n-(normal) straight chain isomer with the iso-branched isomer of little or no use. Currently there is great interest in asymmetric hydroformylation for the synthesis of chiral isomers which are precursors for natural product synthesis.

The majority of catalysts are based on electron rich platinum group metals in low formal oxidation states,[4, 5] but only two metal systems are used industrially to date, those of cobalt and rhodium. By far the most important industrial hydroformylation process is the conversion of propene to *n*-butanal accounting for over 60% of aldehyde production.[9]

2.2. The Industrial Hydroformylation Process.

In 1938 Otto Roelen,[7] during his investigation of the effect of alkenes on Fischer-Tropsch catalysis, discovered a cobalt system capable of the catalytic hydroformylation of alkenes. A specific surface was thought to be required for the reaction; however, it was later discovered that the actual catalytic species was a homogeneous cobalt carbonyl complex.[11] Industrially the catalytic process is operated at temperatures of 150-180^{o}C and at pressures of 200-400 atm resulting in a mixture of normal and branched chain isomers in an approximate ratio of 3:1.[12] Byproducts, including alcohols and hydrogenated alkenes, are also produced resulting in approximately 15% loss of the alkene. Separation of the catalyst from the required

products is problematic since a volatile intermediate, believed to be a catalytically active species, $HCo(CO)_4$, is present. The catalyst is recovered usually as a cobalt salt and subsequently recycled.

A development of the cobalt carbonyl system has been the introduction of tertiary alkyl phosphine ligands which results in a number of advantages over the non-phosphine system. An 8:1 increase in the selectivity to linear over branched aldehydes is observed and the catalyst has increased thermal stability and lower volatility compared to the carbonyl system, reducing the need for extraction and regeneration.[12] The process is also performed at much lower pressures, typically 100 atm. Disadvantages are the greater production of hydrogenated byproducts and a reduction in reaction rates.

In 1965 Wilkinson and co-workers discovered a much more effective catalytic system based on rhodium tertiary phosphine complexes.[6] With the catalytic precursor $Rh(CO)(H)(PPh_3)_3$, shown in figure 2.2.1, hydroformylation can occur at room temperature and atmospheric pressure with a greater selectivity towards the normal isomer.

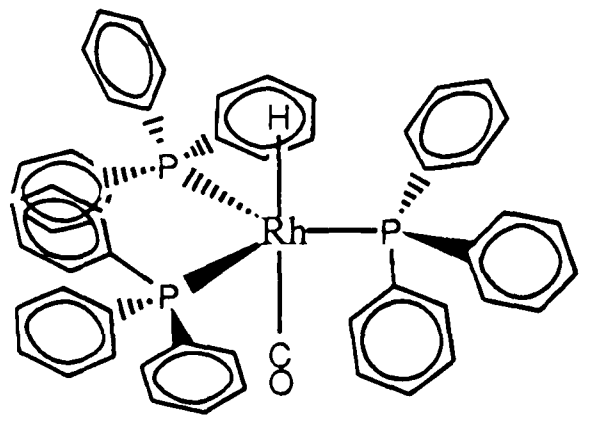


figure 2.2.1. Industrial catalytic precursor for the hydroformylation process.

The rhodium based catalytic hydroformylation system has several other advantages over its cobalt counterpart. Industrially the temperatures and pressures required are much lower in the case of rhodium and no volatile intermediate is present. Major advantages are the high selectivity of linear over branched aldehyde typically of the order of 15:1 for rhodium, in comparison to 4:1 for cobalt, and the lack of hydrogenation products and alcohols.[9, 13] The industrial process (Union Carbide) operates at approximately 90°C and 2-5 atms producing insignificant amounts of hydrogenation byproducts and in the case of propylene the major product is the useful normal isomer, *n*-butanal.[13]

However rhodium is a very expensive metal requiring a very efficient system for the process to be profitable. Great care must be taken to recover all the spent rhodium catalyst, and the retardation of catalyst poisoning and intrinsic deactivation, caused by cluster formation, is required as discussed in section 2.4 Rhodium catalysed hydroformylation has become profitable because of technology developed by Johnson-

Matthey which is capable of recovering spent rhodium from the catalytic system.[14] With recovery of spent rhodium, the catalyst must be capable of producing 10^6 - 10^7kg of aldehyde per kg of rhodium for economic viability.[9]

The best catalyst precursor with respect to activity and selectivity is the complex $Rh(CO)(H)(PPh_3)_3$.[10, 13] In conjunction with an excess of triphenylphoshine, which promotes the associative mechanism[10] discussed in section 2.2., excellent selectivity for the n-isomer is achieved. The process can be performed in molten triphenylphosphine[15] as the solvent to further improve the n/iso isomer ratio. Other rhodium catalytic precursors have been studied by variation of the oxidation state of the metal, the ligating atoms, the bulk of the ligands and the charge on the rhodium complex. However, none of these catalyst precursors have yet matched the performance of $Rh(CO)(H)(PPh_3)_3$.

Water soluble derivatives of $Rh(CO)(H)(PPh_3)_3$, in the form of a trimetasulfonatotriphenylphosphine sodium salt, as shown in figure 2.2.2, have allowed hydroformylation to be observed in the aqueous phase with the reactant, propylene, and product, n-butanal, in the organic phase.[16] Separation is straightforward and selectivity is on the order of 19:1 in favour of the straight chain aldehyde.

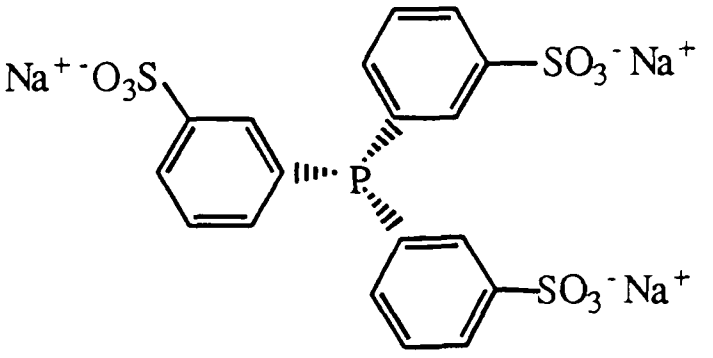
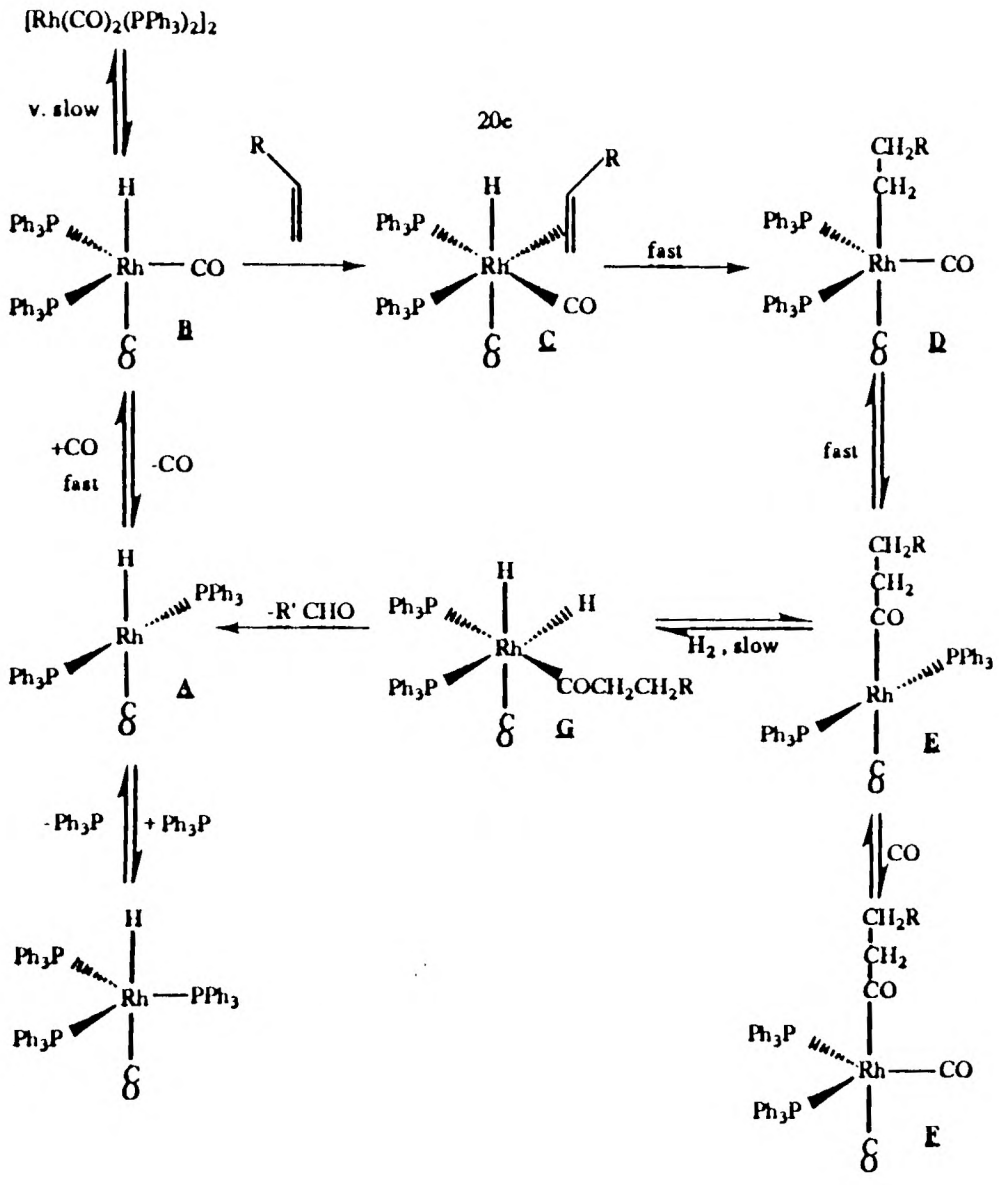


Figure 2.2.2.

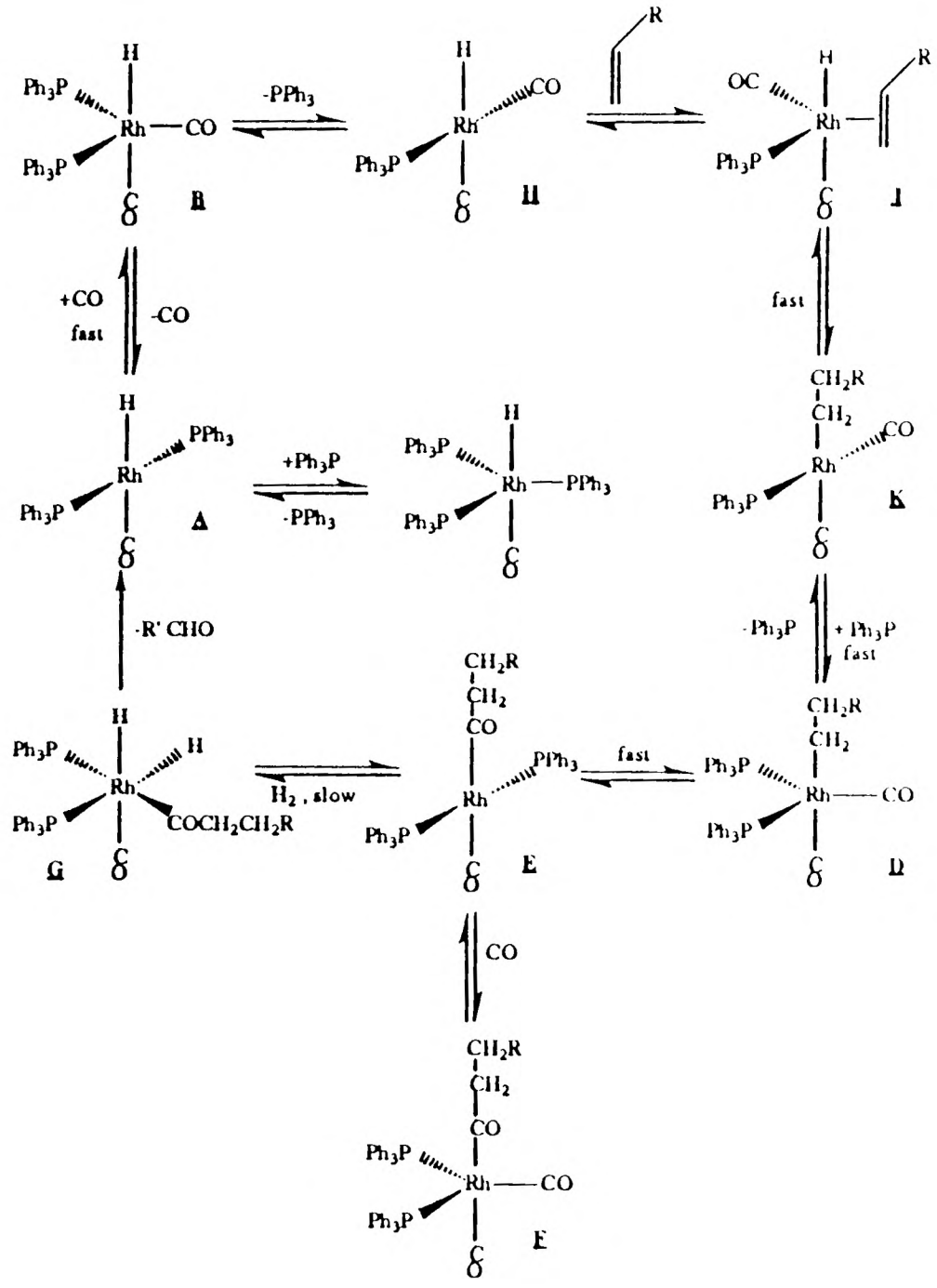
Finally, much effort has been extended to heterogenise the hydroformylation process based on homogeneous catalysts.[17] This should allow more efficient industrial scale production but so far this has been met with limited success.

2.3. The Mechanisms of Hydroformylation Catalysis Using Rhodium Tertiary Phosphine Complexes.

The mechanism of the catalytic hydroformylation process is by no means completely certain. A number of reports advocating various critical intermediates and rate determining steps have been published utilising techniques such as high pressure infra-red spectroscopy, ^{13}C and ^{31}P variable temperature NMR and the synthesis of stable analogues of postulated short lived intermediates. Some of the mechanistic



Associative mechanism



Dissociative mechanism

Scheme 2.3.1. Postulated mechanistic pathways for catalytic hydroformylation.

studies have been performed under stoichiometric rather than catalytic conditions which has resulted in product distributions that are invariably different from the catalytic distributions.

The easiest framework in which to discuss the mechanism is that proposed by Evans, Osborn and Wilkinson.[10] Mechanistically the hydroformylation process can be described by two routes, the associative and dissociative pathways as shown in scheme 2.3.1.

The two pathways were postulated on the basis of factors effecting the rate and selectivity on a number of alkene substrates. It is the associative pathway that provides the selectivity towards linear over branched aldehydes discussed further section 2.3.2.

Both pathways require dissociation of triphenylphosphine from $Rh(CO)(H)(PPh_3)_3$ to produce the square planar $16e^-$ intermediate (**A**). This accounts for the observation that excess triphenylphosphine, or very high catalyst concentrations result in lower activity than pure catalyst precursor at nominal concentrations (mmol). Subsequent addition of CO provides the catalytically active species (**B**) in both the associative and dissociative pathways.

Wilkinson and coworkers postulated $Rh(CO)_2(H)(PPh_3)_2$ (**B**), to be the catalytically active species in the hydroformylation process based on data from hydrogenation and hydroformylation experiments.[10, 18, 19] The concentration of this intermediate is effected by the partial pressures of H_2 and particularly CO, the total pressure, the concentration of free triphenylphosphine and the concentration of catalyst precursor. The nature of the alkene substrate, with respect to steric and electronic factors, also plays a prominent role with regard to activity and selectivity.

From **B** the mechanistic pathways diverge. In the associative case addition of alkene substrate is postulated, resulting in a short lived $20e^-$ intermediate (**C**) which immediately undergoes insertion to the five coordinate alkyl (**D**). In the dissociative route, (**B**) dissociates a triphenylphosphine ligand resulting in the coordinatively unsaturated $16e^-$ intermediate (**H**) which subsequently adds alkene substrate to form (**J**). Rapid insertion into the rhodium hydride bond yields (**K**) and addition of triphenylphosphine the five coordinate alkyl (**D**). Both associative and dissociative mechanisms progress via carbonyl insertion to form the acyl (**E**) followed by oxidative addition of H_2 (**G**) and subsequent aldehyde elimination completing the catalytic cycle.

The concentration of free triphenylphosphine is the major factor determining whether the mechanism is associative or dissociative. The associative pathway is favoured in conditions of high free triphenylphosphine concentration, which can occur on addition of excess phosphine to the catalytic system or high precursor catalyst concentration which effectively increases the amount of free phosphine present.

Mechanisms resulting in hydrogenation and isomerisation products can compete with hydroformylation if the concentration of the square planar complex **A** is significant. **A** is an efficient catalyst for hydrogenation and isomerisation of a wide variety of alkenes; since there is little significant hydrogenation and isomerisation

products (1-4%) from catalytic hydroformylation it was concluded that **B**, and not **A**, was the significant intermediate. Factors affecting the concentration of **A** and the relative rates of hydrogenation/isomerisation and hydroformylation will be discussed in sections 2.3.1. and 2.3.2.

2.3.1. Factors Affecting the Rate of Hydroformylation.

All experimental observations concerning the rate of the hydroformylation are consistent with the mechanism(s) proposed by Brown and Wilkinson. The parameters which affect the rate are the free triphenylphosphine concentration, catalyst concentration, temperature, partial pressures of CO and H_2, the total applied pressure and the concentration/partial pressure of the alkene substrate. Brown and Wilkinson postulated their mechanism(s) mainly from the study of the hydroformylation of hex-1-ene and to a lesser extent that of styrene. The nature of the alkene substrate, with regard to functionalities and stereoelectronic requirements, also plays a prominent role.

Excess triphenylphosphine reduces the rate by retarding the initial dissociation of a phosphine ligand from $Rh(CO)(H)(PPh_3)_3$, preventing the rhodium complex entering the catalytic cycle. The effect is not prohibitive and the reaction can be performed in molten triphenylphosphine if the temperature and pressure are increased.

Increasing the catalyst concentration increases the rate linearly above *ca.* 6mM suggesting pseudo-first order behaviour, below this value a more complex rate law operates. This has been interpreted as a change in mechanism from the associative to the dissociative pathway.

The rate increases with temperature but derivation of a rate law is not possible due to complex equilibria simultaneously occurring. Increasing the temperature above *ca.* 110°C results in a reduction of the rate due to catalyst decomposition via several routes as discussed in section 2.4.

Dependence on the total pressure and partial pressures of CO and H_2 is complex due to dimer formation and the formation of unreactive acyl intermediates such as **F**.

The effect of total pressure upon the rate can be separated into high and low pressure regimes. On increasing the total pressure, by addition of N_2 to a 1:1 ratio of CO and H_2, a reduction in rate is observed. This also occurs when increasing the total pressure, by increasing the partial pressures of CO and H_2.

The most prominent adverse effect on the rate of hydroformylation is an increase in the partial pressure of CO. At high partial pressures of CO the oxidative addition of H_2 is hindered due to formation of the acyl **F**. It could be argued that other products, particularly those from hydrogenation, are being formed at the expense of those from hydroformylation, but no increase in byproducts is observed. If high concentrations of catalyst are used in conjunction with high partial pressures of CO relative to H_2 precipitation of the dimer $[Rh(CO)_2(PPh_3)_2]_2$ occurs, accompanied by a

reduction in the rate. Increasing the concentration of triphenylphosphine and the partial pressure of hydrogen allow catalytic hydroformylation to be operated at higher temperatures by retarding dimer formation, shown in equation 2.3.1.1.

$$2RhH(CO)_2(PPh_3)_2 \underset{+H_2}{\overset{-H_2}{\rightleftharpoons}} [Rh(CO)_2(PPh_3)_2]_2$$

Equation 2.3.1.1. Dimer formation occurs on a drop in the partial pressure of H_2.

A small dependence of the rate of hydroformylation with the partial pressure of hydrogen is observed. On increasing the partial pressure of H_2, the rate of hydrogenation and isomerisation increase and compete seriously with hydroformylation.

The oxidative addition of H_2 is considered as the most probable rate determining step because it requires a change in the formal oxidation state of the metal in addition to a change in coordination number.

A wide variety of alkenes with a range of functionalities are amenable to hydroformylation, as shown in table 2.3.1.1. Sterically unhindered alk-1-enes e.g. allyl alcohol and styrene have a high rate of hydroformylation relative to alk-2-enes and cyclic olefins. Conjugated substrates such as penta-1,3-diene, butadiene and allylamine react with the catalyst precursors forming stable compounds. Cyclohexene and methyl acrylate yield no detectable hydroformylation products.

A further consideration is the solubility of the catalyst as the concentration of aldehyde increases within the reaction medium. Generally, solubility of the catalyst drops as the concentration of aldehyde increases, decreasing the rate of hydroformylation.

Table 2.3.1.1.

Substrate	Rate (ml/min)
Allyl alcohol	7.05
Styrene	4.32
Allyl cyanide	3.72
Hex-1-ene	3.52
Dodec-1-ene	3.18
Ethyl vinyl ether	0.20
2-Methylpent-1-ene	0.06

Conditions: Rate as uptake of H_2 + CO (1:1) in ml min^{-1} at 10psi gas pressure, 25°C; catalyst concentration 2.5mM, substrate concentration 1.0M in benzene.

A range of catalyst precursors, based on rhodium and triphenylphosphine, can be used in the hydroformylation process, but all are converted under reaction conditions

to $Rh(CO)(H)(PPh_3)_3$ or to the intermediate, $Rh(CO)_2(H)(PPh_3)_2$, **B**.[10] There is thus an induction period and consequently a decrease in the measured rate as determined by gas uptake or product formation.

Other phosphines and arsines have been investigated but none have had the selectivity or activity of $Rh(CO)(H)(PPh_3)_3$.[4, 5, 10]

2.3.2. Factors Affecting the Selectivity of Hydroformylation.

The selectivity of the hydroformylation process is of prime concern since the industrially useful products are the anti-Markownikoff straight chain isomers. Aldehydes generally have no direct practical application, but are efficient precursors to detergents and plasticisers.[9, 13] Byproducts resulting from hydrogenation and isomerisation must be kept to a minimum if the process is to be economically viable unless they can be recycled as in the case of iso-butanal.[20]

The catalytic species postulated as being responsible for the selectivity is $Rh(CO)_2(H)(PPh_3)_2$ (**B**). Straight chain isomers predominate for the associative pathway whereas a mixture of branched and straight chain isomers, depending on the alkene substrate, are produced by the dissociative pathway.

A range of selectivities is observed for differing alkene substrates depending upon electronic factors and non-bonding interactions of the incoming olefin with the rhodium complex It is agreed that non-bonding interactions are generally dominant, but electronic and non-bonding effects for a particular alkene are difficult to quantify, resulting in the selectivity being a qualitative observation.

Excess triphenylphosphine undoubtedly has a beneficial effect on selectivity.[15] On increasing the concentration, the extent of dissociation of triphenylphosphine from **B** is reduced resulting in the dominant catalytic pathway being associative. Although this is at the expense of the rate, as mentioned in section 2.3.1, the effect is not significant in comparison to the reduction in rate observed for hydrogenation and isomerisation. Triphenylphosphine is a bulky ligand having a cone angle typically on the order of 145° subtended at the metal depending upon the metal, the formal oxidation state of the metal and other ligands that are present in the primary coordination sphere.[21] Complex **B** has two triphenylphosphine ligands in a mutually *cis* orientation which results in unfavourable non-bonding interactions with an olefin approaching the rhodium centre. This 'directing effect' causes the olefin to orient in the least sterically hindered position leading to selective insertion into the rhodium hydrogen bond.

An increase in the catalyst concentration effectively increases the concentration of free triphenylphosphine, and hence an increase in the selectivity.

The temperature dependence of the selectivity is not well understood but it is generally agreed that the selectivity increases at higher temperatures until the onset of catalyst decomposition.

Increasing the partial pressure of CO results in a reduction in selectivity whereas the reverse is true for an increase in the partial pressure of H_2, however, hydrogenation and isomerisation begin to dominate. On increasing the total pressure, greater selectivity for the straight chain aldehyde results.

J. M. Brown and coworkers studied, by ^{1}H, ^{13}C and ^{31}P NMR spectroscopy, the hydroformylation of styrene and other bulky terminal alkenes.[22, 23] It was observed that the catalytic rate of the hydroformylation of 1,2-D_2 styrene at ambient temperature and pressure with 1:1 CO/H_2 was slower with respect to isomerisation. However, on addition of an atmosphere of CO or a 5 fold molar excess of triphenylphosphine relative to the catalyst, the reverse was true, the rate of isomerisation being surpressed 100 fold. They postulated that (**A**) could not mediate the hydroformylation pathway because it is trapped too efficiently by CO or PPh_3 and that (**H**) was more likely.

Consideration of variable temperature ^{13}C NMR using ^{13}CO and 1-^{13}C styrene led Brown and coworkers to further postulate that the isomerisation of unsaturated acyl species such as (**E**) could be responsible for the isomer selectivity in catalytic hydroformylation rather than the associative versus dissociative mechanisms. The acyl species in equilibrium for the hydroformylation of styrene are shown in figure 2.3.2.1.

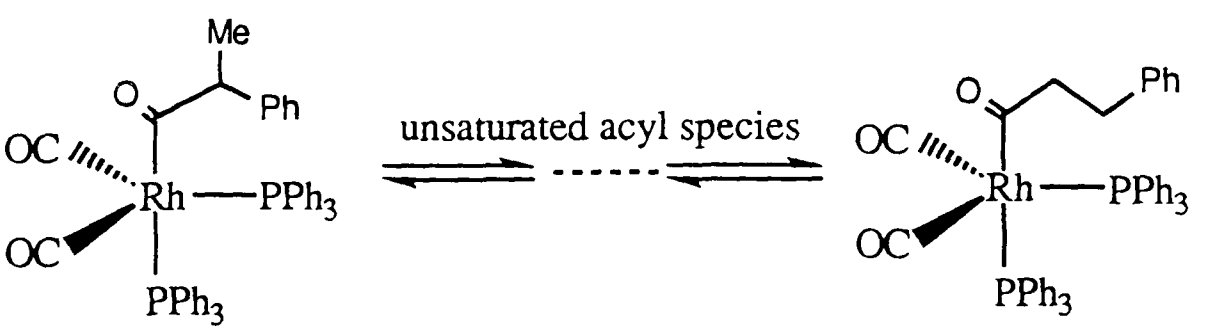


Figure 2.3.2.1. Acyl equilibrium that may be the cause of the selectivity in the hydroformylation of styrene.

Further contributions, in an attempt to understand the mechanism of hydroformylation, and other related mechanisms, have been reported by J. Halpern and coworkers.[24-28] Particular emphasis is made on the critical importance kinetic measurements have in the elucidation of a catalytic mechanism.[24, 26]

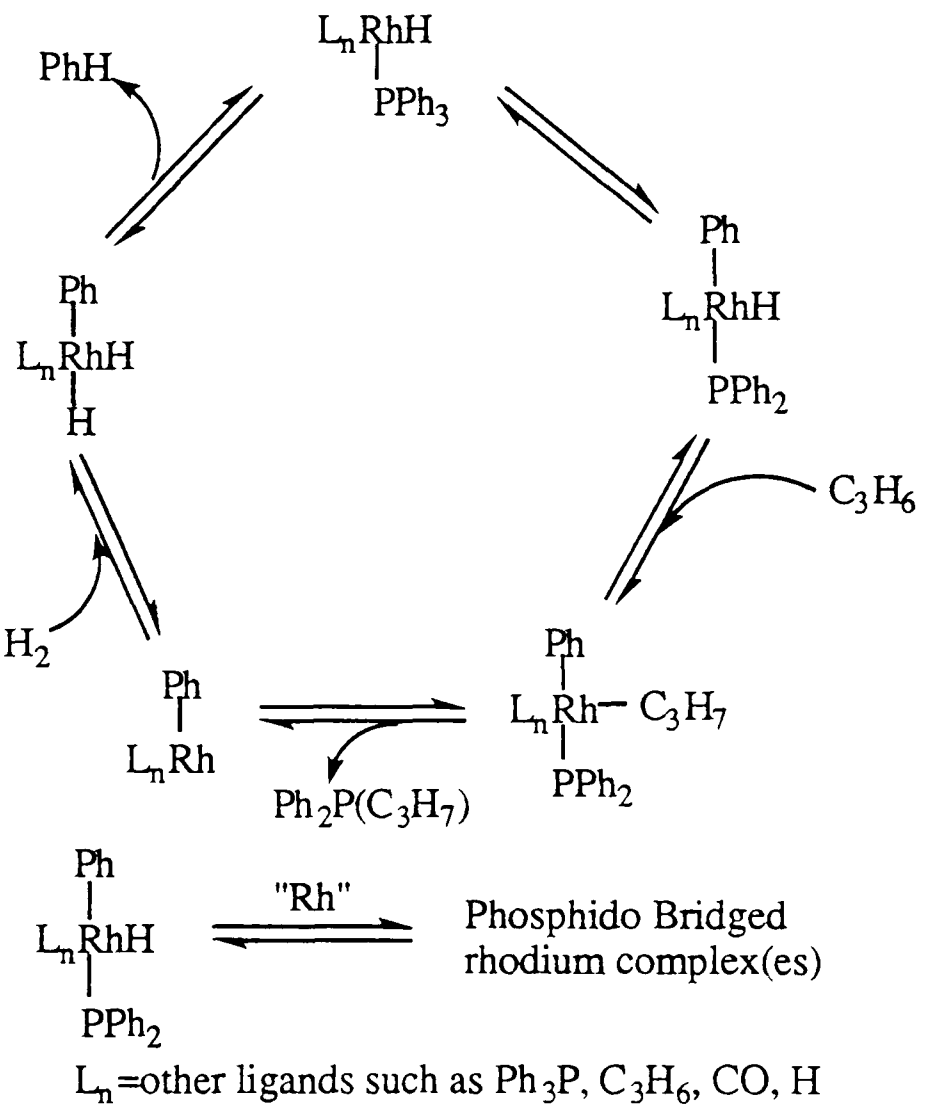
Detailed kinetic studies of a number of reactions, particularly asymmetric hydrogenation led to the conclusion that the species that accumulate to a sufficiently high concentration to be detected by techniques such as IR and NMR spectroscopies, are not generally responsible for major product formation, but instead are 'reservoirs' for the actual catalytic intermediates. For instance product ratios in asymmetric hydrogenation are often reported as a consequence of a good match between substrate and 'catalyst' which results in the matched pair product being the predominant isomer. Kinetic measurements by Halpern have shown that in fact the predominant isomer results from the unmatched pair, which has a rate greater than that of the matched pair,

and that the matched pair acts as a 'reservoir' effectively preventing catalyst decomposition.

2.4. Thermal Decomposition of $Rh(CO)(H)(PPh_3)_3$.

The rate of the hydroformylation process is limited thermally by the decomposition of the catalyst at elevated temperatures (>90°C). The mechanism(s) of deactivation and the relevant species and conditions involved have been the subject of considerable interest, due to the industrial economic implications.

Deactivation of the catalyst occurs during hydroformylation because at elevated temperatures monomeric electron rich rhodium complexes react with triphenylphosphine leading to clustered rhodium phosphido complexes,[29] alkylated phosphines[30] and benzene[31] as shown in scheme 2.4.1.



Scheme 2.4.1. Postulated thermal decomposition pathway occurring during hydroformylation.

The initial reaction between triphenylphosphine and the rhodium centre appears to be either orthometalation or oxidative addition of the phosphorus carbon bond. Experiments performed with *ortho*-deutero triphenylphosphine indicate the oxidative addition of a carbon phosphorus bond was favoured when CO is present but orthometallation when it is not.[31] Decomposition is not significant, at 105°C, without the presence of a small amount of H_2 and higher partial pressures do not significantly

effect the rate of decomposition. Increasing the concentration of alkene prevents the formation of rhodium clusters and the concomitant decrease in the rate of hydroformylation. Large excesses of triphenylphosphine cause a decrease in the rate of decomposition by reducing the concentration of active unsaturated rhodium complexes present.

Abatjoglou[31] and coworkers proposed the mechanism shown in scheme 2.4.1.

The reversibility in the proposed decomposition route shown in scheme 2.4.1. is accounted for by the observation that rhodium complexes have been shown to scramble the arene substituent in triphenylphosphine derivatives.

2.5. The Hydroformylation of C_{60}

To date the reactivity of C_{60} can largely be described as a multifunctional electron withdrawing olefin. This is especially true with respect to organometallic reactions of C_{60}. Comparisons have been drawn with the electron deficient olefin tetrafluoroethylene.[32] There are thirty carbon-carbon bonds on the surface of C_{60}, each of which can be described as electron deficient olefins. This has consequences for the number of possible products and isomers which could exist.

The reaction between tetrafluoroethylene and $Rh(CO)(H)(PPh_3)_3$ gives the square planar fluoroalkyl complex $Rh(C_2F_4H)(CO)(PPh_3)_2$,[33] and has been investigated by NMR and IR spectroscopy with a view to understanding the mechanism of hydroformylation. The square planar complex reacts with H_2 and HCl producing $C_2F_4H_2$ and reaction with CO gives di- and tricarbonyl rhodium complexes $Rh(C_2F_4H)(CO)_2(PPh_3)_2$ and $Rh(C_2F_4H)(CO)_3(PPh_3)$.[33]

Reaction of $Rh(C_2F_4H)(CO)(PPh_3)_2$ with H_2/CO 1:1 appeared to yield di- and tricarbonyl species in equilibrium. No mention was made of hydrogenation or hydroformylation products. Other fluorinated olefins such as vinylfluoride, 3, 3, 3 - trifluoropropene and pentafluorostyrene have however been successfully hydroformylated using $Rh(CO)(H)(PPh_3)_3$ as the catalytic precursor.[34]

Conceivably C_{60} could insert into a Rh-H bond producing a square planar alkyl, as in the analogous case of C_2F_4 facilitating the first step towards the hydroformylation of C_{60}. However, to date there is no precedent for the insertion of CO into a metal C_{60} bond. A likely intermediate in the hydroformylation of C_{60} would be an acyl complex such as **E** or **F** shown in scheme 2.3.1. The existence of this intermediate maybe doubtful since perfluoroacyl complexes are known to readily undergo decarbonylation to form perfluoroalkyl metal carbonyls.[35] The distinct possibility exists that hydrogenation and not hydroformylation would be the dominant mechanism.

Hydrogenation of C_{60} has been performed using BH_3.thf,[36] $(Cp)_2Zr(H)(Cl)$[37] and via Birch reduction.[38] The reaction with $(Cp)_2Zr(H)(Cl)$ is particularly relevant as

the species, $[(Cp)_2ZrCl]_2C_{60}H_n$ shown in equation 2.5.1 is the likely intermediate on route to hydrogenation products formed after quenching with dilute acid.

$$(\eta^5\text{-}C_5H_5)_2Zr(H)Cl + C_{60} \xrightarrow[24h]{C_6H_6} [(\eta^5\text{-}C_5H_5)_2ZrCl]_nC_{60}H_n \xrightarrow[\text{-n"Cp}_2\text{ZrCl(OH)"}]{HCl/H_2O} C_{60}H_{2r}$$

Equation 2.5.1. The hydrozirconation of C_{60}.

2.6. Summary.

The hydroformylation process is undoubtedly complicated when one considers the number of variables involved and the complex equilibria that govern them. Understanding the intricacies of the mechanism(s), and the synthesis and testing of new catalysts, should aid in the development of improved catalytic performance and hence economic viability of the hydroformylation process.

With this in mind it was decided to investigate the possibility of the hydroformylation of C_{60} and the effect C_{60} may have on the catalytic cycle in the hydroformylation of alkenes.

2.7. The Hydroformylation of C_{60}.

The conversion of C_{60} into an aldehyde derivative is a very attractive proposition because of the versatility and well established synthetic methodology of organic carbonyl chemistry. A vast new area of C_{60} chemistry would be available to the synthetic chemist.

Methods commonly used to convert alkenes to aldehydes, e.g. ozonolysis and hydroboration, have been used in an attempt to introduce a carbonyl functionality directly bound to the surface of C_{60}, so far without success.

Hydroformylation is a well established process and is compatible with a wide range of functionalities which may be present on an alkene substrate. However, if C_{60} is to be considered as analogous to an electron deficient olefin such as C_2F_4, hydroformylation is not expected to be achieved readily, because of the reluctance of electron deficient olefins to insert into the Rh-CO bond, as discussed in section 2.5.

2.8. Synthesis of $Rh(C_{60})(CO)(H)(PPh_3)_2$.

On addition of a purple toluene solution of C_{60} to a pale yellow toluene solution of $Rh(CO)(H)(PPh_3)_3$ an intense emerald green solution results. Removal of the solvent under reduced pressure gives an emerald green solid soluble in thf, CH_2Cl_2 and slightly soluble in diethylether. C_{60} is completely insoluble in thf and diethylether.

Solution $^{31}P\{^1H\}$ NMR spectroscopy shows a doublet at δ36ppm ($^1J(^{103}Rh$-$^{31}P)$ = 140Hz) and a resonance at δ - 8ppm corresponding to one equivalent of free triphenylphosphine as shown in figure 2.8.1. This strongly indicates that substitution of a triphenylphosphine by C_{60} has occurred.

Isolation of the green solid from free triphenylphosphine is most readily performed by precipitation from a thf solution by the addition of ethanol and subsequent filtration. Elemental analysis gave a composition corresponding to the complex with the formulation $Rh(C_{60})(CO)(H)(PPh_3)_2$. The solid is stable, but decomposes slowly in solution.

$^{31}P\{H\}$ NMR spectroscopy shows only a doublet at δ 36ppm ($^1J(^{103}Rh$-$^{31}P)$ = 140Hz) as shown in figure 2.8.1. ^1H NMR spectroscopy shows multiplets at δ 6.95 and 7.61ppm assignable to triphenylphosphine and a triplet at δ -9.09ppm ($^2J(^{31}P$-$^1H)$ = 9Hz) corresponding to a hydride. No coupling between the rhodium and hydride could be resolved. The hydride in the precursor $Rh(CO)(H)(PPh_3)_3$ has a multiplet resonance at δ -9.5ppm due to fluxional processes occurring at room temperature. ^{13}C NMR spectroscopy at room temperature reveals peaks assignable to triphenylphosphine and a broad resonance at δ 141-145ppm corresponding to C_{60}. This broad resonance could be ascribed to a degree of lability of the C_{60} or possibly the rhodium moiety 'tracking' over the surface of the C_{60} molecule.

Low temperature ^{13}C NMR spectroscopy, at 125MHz, was kindly performed by Adam Stephens of The Inorganic Chemistry Laboratory, Oxford. Spectra were recorded at temperatures of -40, -10 and 10°C respectively. At -40 and -10°C 29 peaks

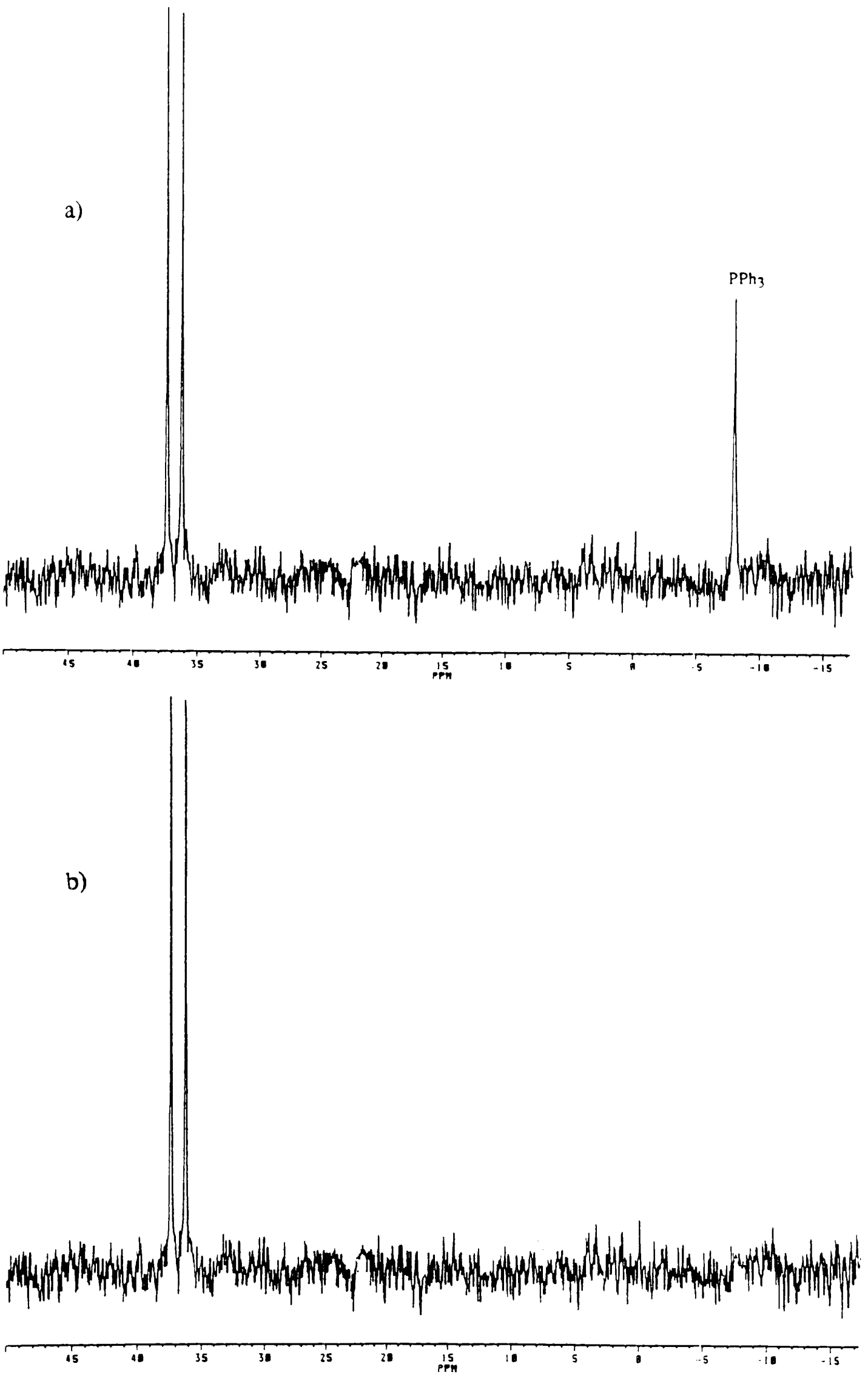


Figure 2.8.1. ^{31}P NMR (125MHz) of a) the reaction mixture of $Rh(CO)(H)(PPh_3)_3$ + C_{60} and b) of $Rh(\eta^2\text{-}C_{60})(CO)(H)(PPh_3)_2$.

are observed in the region between 128 and 165ppm that correspond ^{13}C resonances from C_{60}, as shown in figure 2.8.2. If the point symmetry of the complex is C_s, 32 peaks would be expected whereas a point symmetry of C_i would give 60 peaks in the ^{13}C NMR spectrum. Assuming some of the 32 peaks in the ^{13}C NMR spectrum overlap, or are concealed by triphenylphosphine resonances, the ^{13}C NMR spectra observed at -40 and -10°C are consistent with the point group C_s. If the plane describing the triphenylphosphines and the rhodium metal is designated P_2Rh, and the plane describing the rhodium and the two carbons on C_{60} closest in proximity to the metal is C_2Rh, then a dihedral angle, θ, can be defined between the planes. $\theta = 0$ would correspond to a point symmetry of C_s and $\theta \neq 0$ to a point group C_1.

The IR spectrum of the green solid shows a carbonyl stretch at 1986cm^{-1} and a rhodium-hydride stretch at 2056cm^{-1} which are shifted to longer wavelengths in comparison to $Rh(CO)(H)(PPh_3)_3$. Bands at 516 and 525cm^{-1} are also evident indicating the presence of C_{60}.

The green complex is formulated as $Rh(\eta^2\text{-}C_{60})(CO)(H)(PPh_3)_2$ having the structure as shown in figure 2.8.3.

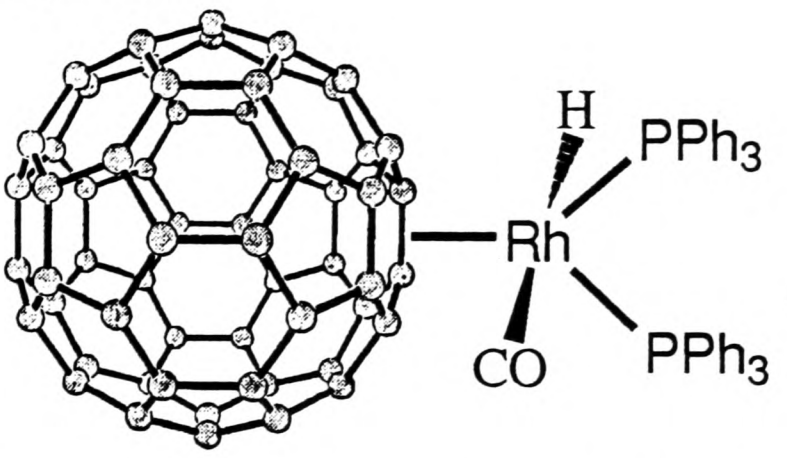


Figure 2.8.3. Postulated average solution structure of $Rh(\eta^2\text{-}C_{60})(CO)(H)(PPh_3)_2$ at room temperature.

The point group of the complex in figure 2.8.3. at room temperature is C_s which can account for the equivalence of the triphenylphosphines as indicated by ^{31}P NMR spectroscopy and the hydride resonance in the ^1H NMR spectrum at room temperature. At lower temperatures and probably in the solid state the point symmetry is E where the triphenylphosphines are not equivalent. A *cis* configuration of the tertiary phosphine and hydride ligands is indicated by the small value of the coupling constant ($^2J(^{31}P\text{-}^1H)$ = 9Hz) as compared to a typical value of 80- 160Hz[39, 40] in a *trans* arrangement of tertiary phosphine and hydride ligands at a rhodium centre. The nature of the C_{60}-rhodium bond is formulated as η^2 across a 6:6 ring fusion on the basis of bands at 516 and 525cm^{-1} and is consistent with all known C_{60} complexes of electron rich metals which bind in such a fashion. Considering C_{60} as a two electron donor satisfies the eighteen electron rule for the rhodium and comparison with electron deficient olefins is consistent with the shift to lower wavelengths of the carbonyl and rhodium-hydride stretches with respect to those in the complex $Rh(CO)(H)(PPh_3)_3$.

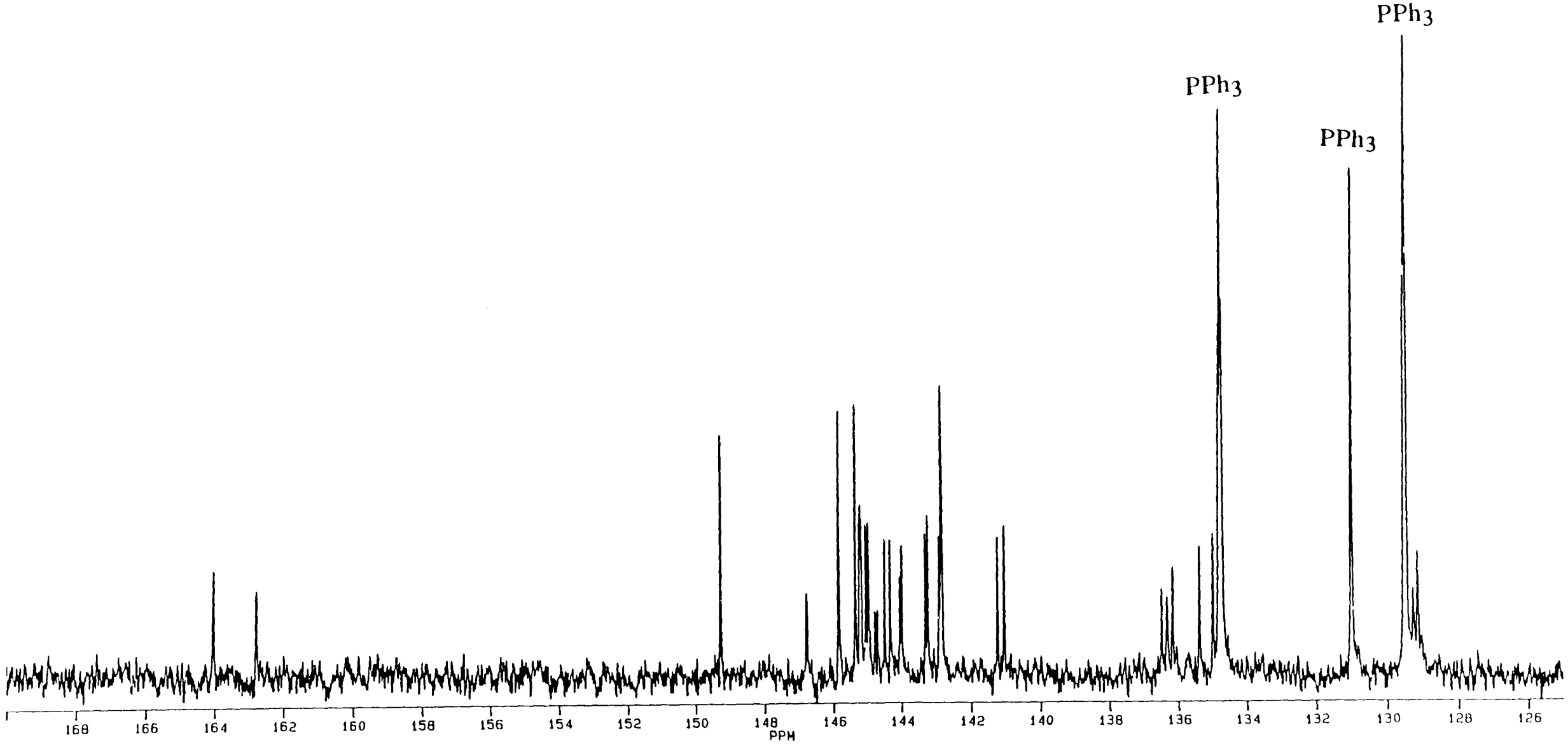


Figure 2.8.2. ^{13}C NMR (125MHz) of $Rh(\eta^2\text{-}C_{60})(CO)(H)(PPh_3)_2$ at -10°C.

2.8.1. The Single Crystal Structure of $Rh(\eta\text{-}C_{60})(CO)(H)(PPh_3)_2$.

The proposed low temperature solution structure determined by ^{13}C NMR spectroscopy was confirmed by Balch and coworkers[41] who independently reported the synthesis and single crystal structure determination of $Rh(\eta^2\text{-}C_{60})(CO)(H)(PPh_3)_2$. Single crystal structure determination at 100K showed that the dihedral angles between the P_2Rh and C_2Rh planes are 21.9 and 22.3° respectively for the two molecules in the unit cell giving molecular symmetry with point group C_1.

One month previously to this report, a single crystal of $Rh(\eta^2\text{-}C_{60})(CO)(H)(PPh_3)_2$ was obtained by slowly cooling a saturated dichloromethane solution to -80°C over a period of 3 months. A unit cell was determined prior to full data collection and was subsequently found to be identical to that obtained by Balch.

2.8.2. Some Reactivity of $Rh(\eta^2\text{-}C_{60})(CO)(H)(PPh_3)_2$.

The reaction of $Rh(\eta^2\text{-}C_{60})(CO)(H)(PPh_3)_2$ with $HBF_4.Et_2O$, anhydrous HCl in toluene, CS_2, or allene all resulted in the elimination of C_{60} as observed by ^{13}C NMR and IR spectroscopy.

2.9. The Study of $Rh(\eta^2\text{-}C_{60})(CO)(H)(PPh_3)_2$ as a Hydroformylation Catalyst.

All the catalytic experiments presented below were performed in collaboration with Rochel M. Lago and Dr. S. C. Tsang of The Inorganic Chemistry Laboratory, Oxford.

The catalytic activity of (**1**) towards the hydroformylation of ethene and propene was investigated to study the effect C_{60} has upon hydroformylation of these alkenes and also to gain insight into the possibility of the hydroformylation of C_{60}.

C_{60} has been compared to an electron deficient alkene and, to date, all transition metal C_{60} derivatives isolated are coordinated η^2 to the C_{60}. This is the case for the new rhodium complex $Rh(\eta^2\text{-}C_{60})(CO)(H)(PPh_3)_2$ (**1**). Alkenes are formally two electron donors and (**1**) can be modelled as an intermediate in the catalytic hydroformylation of alkenes. To date, no alkene analogues of (**1**) have been isolated due to the propensity of the olefin to insert into the rhodium-hydrogen bond. The reluctance of C_{60} to insert into the rhodium-hydrogen bond does not bode well for the hydroformylation of C_{60}, because it is one of the most facile steps towards the hydroformylation of an alkene.

A suitable solvent was required in which to test the catalytic activity and selectivity of (**1**) in comparison to that obtained with $Rh(CO)(H)(PPh_3)_3$ (**2**) and to allow the thermal degradation of the two catalysts to be studied under the reaction conditions or conditions as close as was possible. Characteristics required of the solvent are to impart, solubility of the catalysts, any free ligand(s) and the reactant

species concurrent with a high boiling point (low vapour pressure). A commonly available solvent which meets these requirements is di-n-butylphthalate.

This solvent is capable of dissolving both catalysts, triphenylphosphine, reactant gases and C_{60}, and has a boiling point of 340°C.

2.10. The Catalytic Hydroformylation of Ethene.

Ethene was the substrate chosen for the initial investigation into the hydroformylation activity by (**1**). It undergoes facile hydroformylation with respect to temperature and pressure with a wide variety of catalyst precursors. The reactant gases and the aldehyde product, propylaldehyde, are volatile and could be easily monitored quantitatively by an on-line GC.

Reactions were performed in a Pyrex column wrapped in heating tapes and fitted with a glass frit. A di-*n*-butylphthalate solution of the catalytic precursor was heated to 90°C and, once the solution had reached the reacting temperature, a 1:1:1 mixture of the reactant gases was bubbled through the frit and reaction solution.

2.10.1. Results of Ethene Hydroformylation

A typical GC trace is shown in figure 2.10.1.1. and the data is given in table 2.10.1.1.

Table 2.10.1.1. Hydroformylation of ethene at 90°C. Conditions: rhodium complex 0.07 mmol, solvent di-*n*-butylphthalate (20ml), ethene/CO/H_2 ratio 1:1:1, at flow rate of 30 ml/min and at 1 bar.

Catalyst Precursor	TN (h^{-1})[a]
$Rh(CO)(H)(PPh_3)_3$ (**2**)	172.1
$Rh(C_{60})(CO)(H)(PPh_3)_2$ (**1**)	169.8

[a]Turnover number to propylaldehyde.

Propanal is produced immediately on introduction of ethene and CO/H_2 to both catalytic solutions. A change in the colour of the reaction solution on addition of ethene is evident in both cases. The reaction solution containing (**2**) changes from pale yellow to a golden yellow upon introduction of ethene whereas the solution containing (**1**) is very dark green becoming very dark brown.

2.10.2. Discussion on the Hydroformylation of Ethene.

It is apparent that there is no difference, within experimental error, between the two catalysts at this temperature, concentration and flow rate of H_2/CO and ethene. The possibility exists that under the conditions of the catalytic hydroformylation of ethene the two processes contain the same catalytically active species which is probably

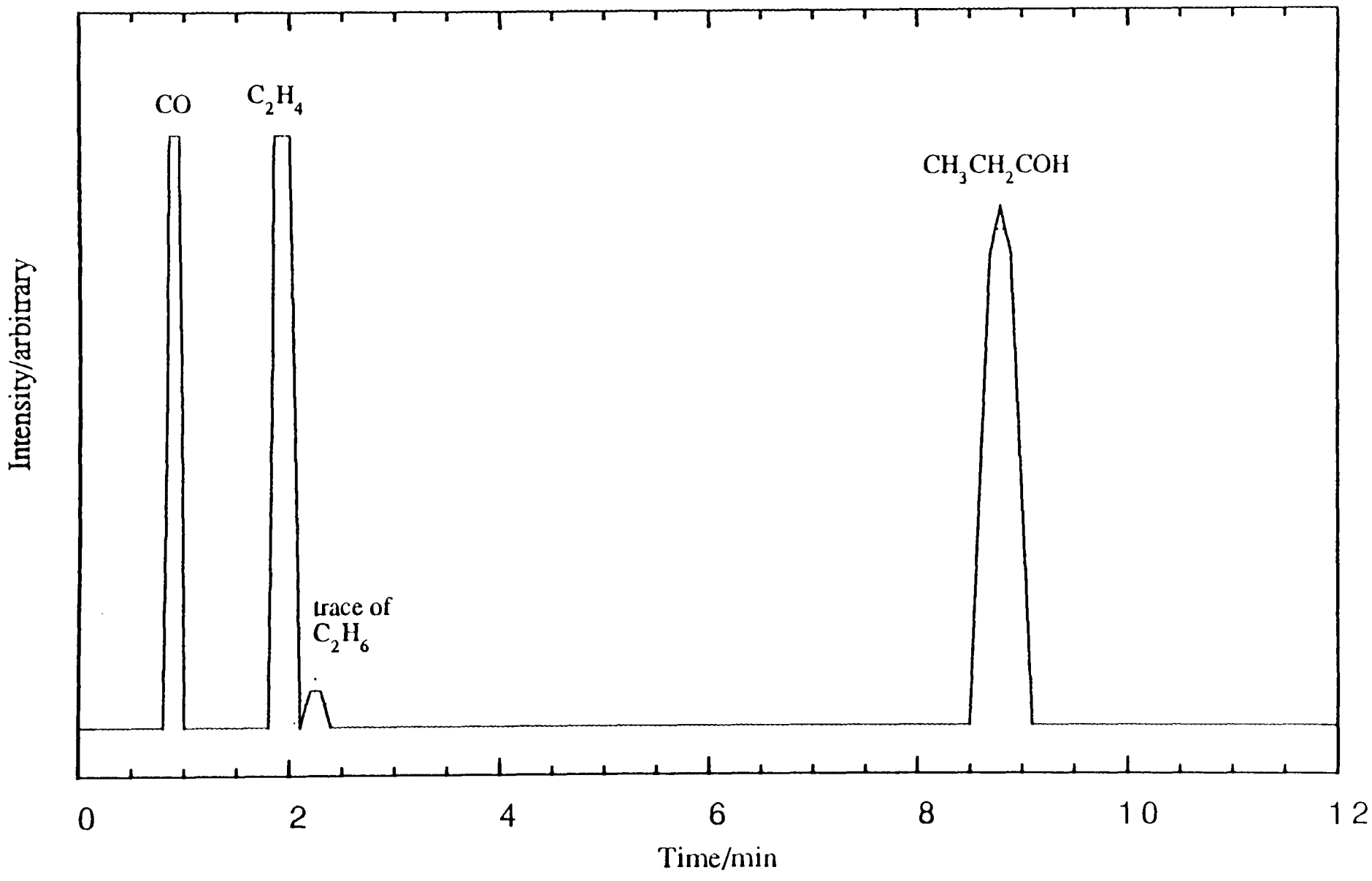


Figure 2.10.1.1. GC trace from the hydroformylation of ethene.

$Rh(CO)_2(H)(PPh_3)_2$ as discussed in section 2.2. This would indicate that C_{60} acts as a labile ligand in the same manner as the third triphenylphosphine ligand in the catalyst $Rh(CO)(H)(PPh_3)_3$ (**2**). There is no evidence to distinguish between a mechanistic pathway involving C_{60} and one that does not, or a combination of parallel mechanisms.

Ethene is not sterically demanding in the primary coordination sphere of the rhodium metal centre and would not be under the influence of non-bonding interactions from triphenylphosphine or C_{60} ligands (section 2.3.). Electronic factors are difficult to quantify and as there is no difference in the activity of the catalysts (**1**) and (**2**), no conclusions can be drawn.

In conclusion ethene undergoes hydroformylation at a rate, using (**1**) and (**2**) as catalyst precursors, that differences could not be detected within experimental error. As the only aldehyde product from the hydroformylation of ethene is propanal, no information with regards to selectivity is possible. However in the case of an unsymmetrical alkene, where the selectivity of straight over branched isomers can be investigated in addition to any difference in activity, the two catalysts (**1**) and (**2**) could exhibit different behaviour .

Therefore an unsymmetrical alkene, propene, was chosen for investigation.

2.11. The Catalytic Hydroformylation of Propene.

The compound $Rh(\eta\text{-}C_{60})(CO)(H)(PPh_3)_2$ (**1**) was also investigated as a catalytic precursor for the hydroformylation of propene. To allow comparison between (**1**) and the industrial catalyst precursor, $Rh(CO)(H)(PPh_3)_3$ (**2**), both compounds were tested under congruent conditions.

Propene is an unsymmetrical alkene, giving two possible product aldehyde positional isomers, and can therefore be used to probe the selectivity of a catalyst, as shown in figure 2.11.1.

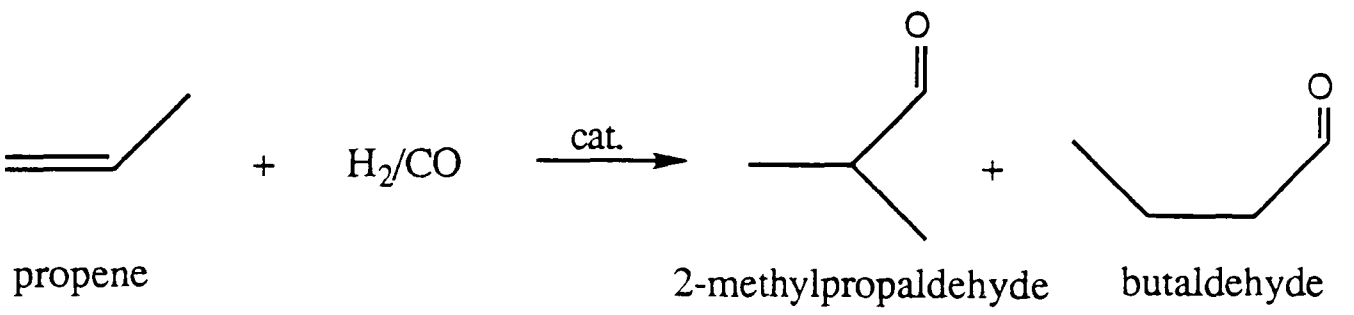


Figure 2.11.1. Possible positional isomers from the hydroformylation of propene

Typically, the catalytic precursor was dissolved in di-*n*-butylphthalate under dinitrogen and pressurised with propene/CO/H_2 in a high pressure autoclave at room temperature and heated to the reaction temperature. On termination of the experiment the solution was allowed to cool to room temperature, the excess pressure released and the contents quickly transferred to a Schlenk tube under an atmosphere of dinitrogen. Gas chromatography was performed with an internal standard of 2-pentanol to ascertain the

turnover number. Differences in solubility of the two product aldehydes in di-*n*-butylphthalate were assumed to be negligible.

2.11.1. Results of the Hydroformylation of Propene.

A typical GC trace is shown in figure 2.11.1.1. and the data in table 2.11.1.1.

Table 2.11.1.1 shows that (**1**) is also an effective catalyst for the hydroformylation of propene. At 90°C, the turnover number was found to be 57.3 h^{-1} and *n*-to-iso-aldehyde ratio was 1.38. However, this is significantly lower than that found for (**2**) which has a turnover number of 68.8h^{-1} with a *n*-to-iso-ratio of 1.63.

Table 2.11.1.1. Hydroformylation of propene. Conditions: rhodium complex 0.07 mmol, solvent di-*n*-butylphthalate (20ml), propene/CO/H_2 ratio 1:1:1 at initial pressure 11.0 bar at room temperature, reaction mixture is heated at 90°C for 5h.

Excess ligand/catalyst precursor	[L]/[Rh][a]	TN (h^{-1})[b]	n/iso Ratio[c]
-/$Rh(CO)(H)(PPh_3)_3$	0	68.8	1.63
-/$Rh(C_{60})(CO)(H)(PPh_3)_2$	0	57.3	1.38
PPh_3/$Rh(CO)(H)(PPh_3)_3$	13	64.6	2.91
C_{60}/$Rh(C_{60})(CO)(H)(PPh_3)_2$	13	44.8	1.19
PPh_3/$Rh(C_{60})(CO)(H)(PPh_3)_2$	13	55.3	3.00
PPh_3/$Rh(CO)(H)(PPh_3)_3$	40	64.8	4.23
PPh_3/$Rh(C_{60})(CO)(H)(PPh_3)_2$	40	49.5	4.25
-/$Rh(CO)(H)(PPh_3)_3$[d]	0	35.3	1.75
-/$Rh(C_{60})(CO)(H)(PPh_3)_2$[d]	0	23.0	1.53

[a] Molar ratio of excess ligand L to Rh catalyst.

[b] Turnover number to butanal.

[c] normal/isomer ratio.

[d] Rhodium complex 0.07 mmol, solvent di-*n*-butylphthalate (50ml).

Figure 2.11.1.2. clearly shows that addition of an excess of triphenylphosphine to the reaction mixture in propene hydroformylation caused a decrease in the turnover number as expected and discussed in section 2.2. Likewise, addition of an excess of C_{60} to the solution containing (**1**) decreased the propene hydroformylation activity from 57.3 to 44.8 h^{-1}.

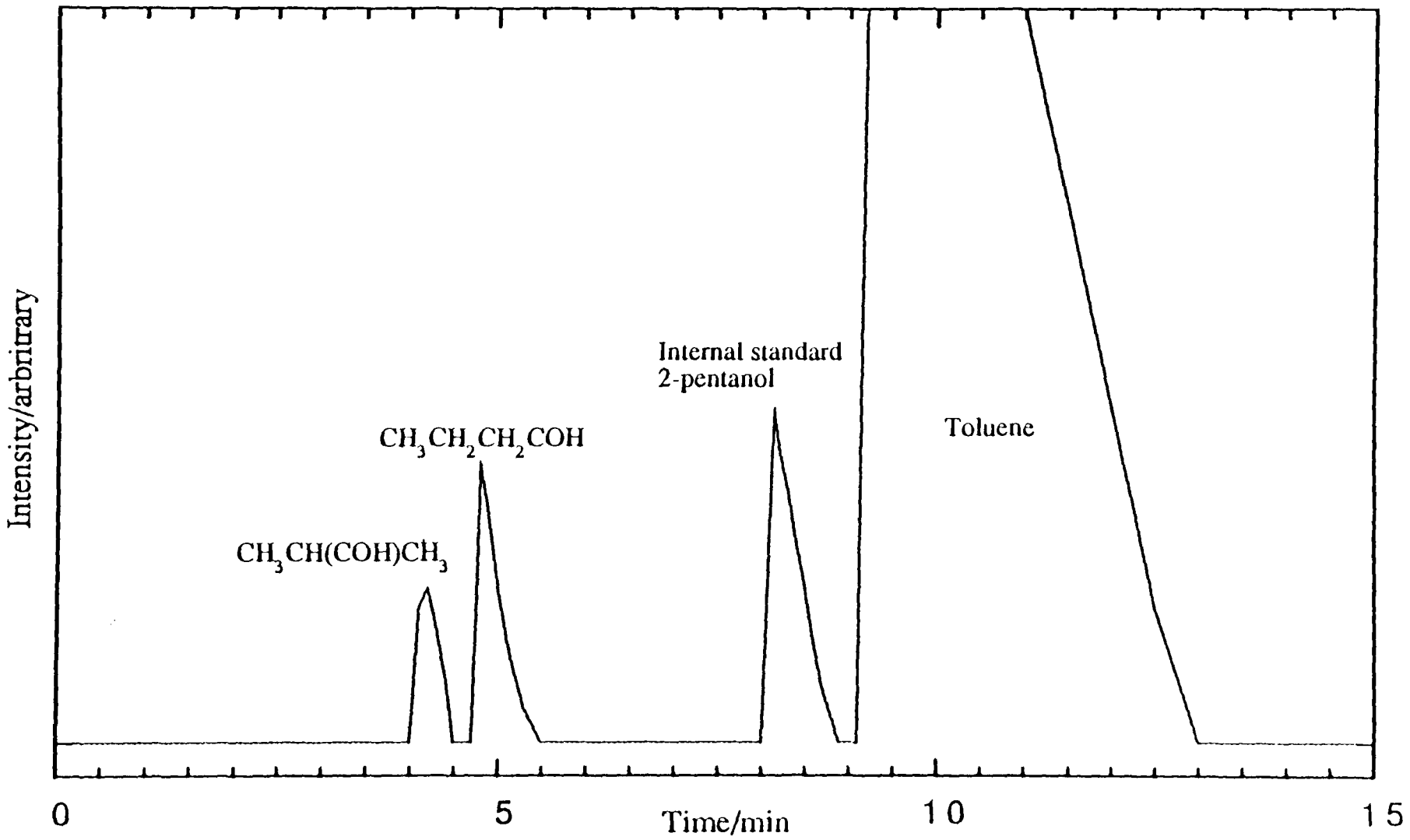


Figure 2.11.1.1. Typical GC trace from the hydroformylation of propene.

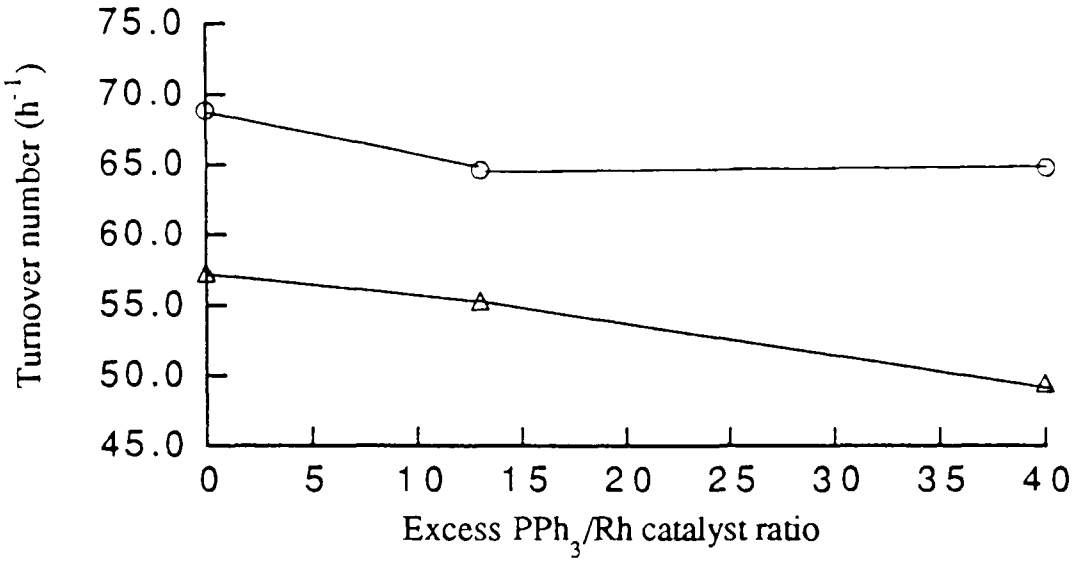


Figure 2.11.1.2. The effect of excess triphenylphosphine on the activity of $Rh(C_{60})(CO)(H)(PPh_3)_2$ (Δ) and $Rh(CO)(H)(PPh_3)_3$ (O) for the hydroformylation of propene at 90°C.

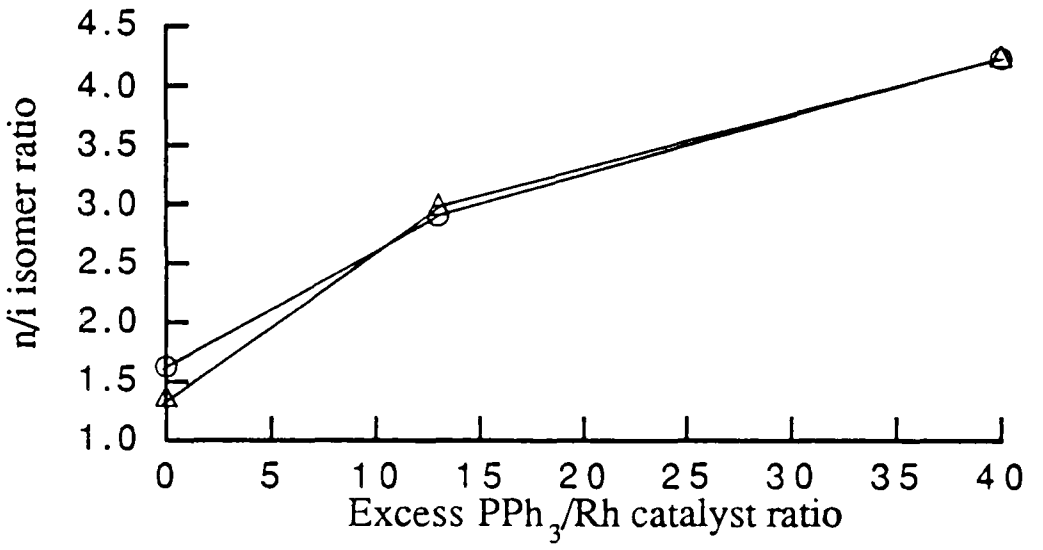


Figure 2.11.1.3. The effect of excess triphenylphosphine on the aldehyde n/i isomer ratio obtained in the hydroformylation of propene in the presence of $Rh(C_{60})(CO)(H)(PPh_3)_2$ (Δ) and $Rh(CO)(H)(PPh_3)_3$ (O) at 90°C.

Figure 2.11.1.3. shows that the addition of an excess of triphenylphosphine increased the propene hydroformylation selectivity to butaldehyde for both catalysts. Thus, the *n*-to-iso-ratio for the reaction catalysed by (**2**) increased from 1.63 to 4.23 when the free triphenylphosphine to rhodium ratio was increased from 0 to 40:1. Addition of an equivalent excess of free triphenylphosphine to (**1**) caused the *n*-to-iso-ratio to increase from 1.38 to 4.25 but addition of excess C_{60} (the ratio of free C_{60} to (**1**) was 1:13) caused a decrease from 1.38 to 1.19.

The colour of the reaction mixtures prior and after the experiments was as that in the case of ethene hydroformylation from an initial dark green to a dark orange/brown.

2.11.2. Discussion on the Hydroformylation of Propene.

The results in table 2.11.1.1 show a clear difference between the two catalysts in terms of selectivity and activity. The catalyst precursor $Rh(C_{60})(CO)(H)(PPh_3)_2$ (**1**) is less active and selective, towards butaldehyde, than $Rh(CO)(H)(PPh_3)_3$ (**2**) under the experimental conditions used.

A lower activity of (**1**) could be explained by an induction period that is required for the catalyst precursor to form the active catalytic species. This proposal would be consistent with the results of ethene hydroformylation as discussed in section 2.9.1, if C_{60} dissociated from (**1**) to yield the same intermediate as the dissociation of triphenylphosphine from (**2**) as shown in figure 2.11.2.1.

However if this was the case, though a difference in activity would be expected, a difference in the selectivity would not.

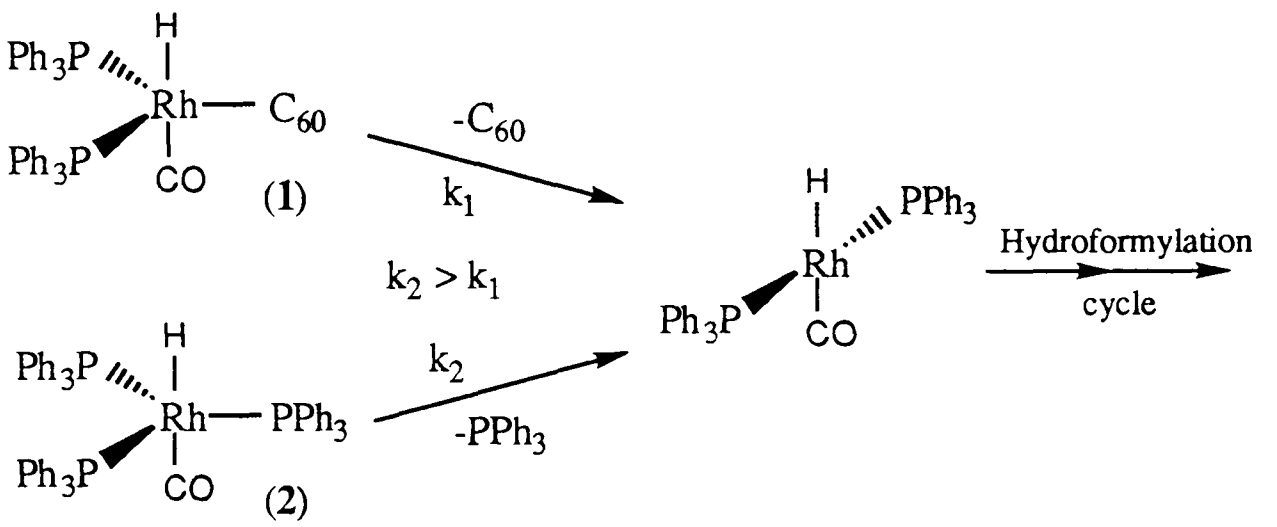


Figure 2.11.2.1. Possible reaction of catalytic precursors before the rhodium complex enters the catalytic cycle.

Previous studies on the effect of changing the Lewis acidity of the phosphine ligands on the rate of hydroformylation showed that the more acidic the ligand the lower the rate of hydroformylation. This is in accord with the IR and NMR spectroscopic data (section 2.6.1) for $Rh(C_{60})(CO)(H)(PPh_3)_2$, which indicate that C_{60} is a more electron withdrawing ligand than triphenylphosphine.

The lower selectivity using the catalytic precursor (**1**) as opposed to (**2**) can be explained if the catalytic intermediate or equilibrium responsible for selectivity is different.

It has been reported that the *n*-to- iso-aldehyde ratio of the product depends mainly on steric effects with a minor contribution from electronic effects. Thus, bulky donor ligands such as triphenylphosphine favour anti-Markovnikoff addition making the catalyst more selective towards the formation of the linear aldehyde. If it were the case that C_{60} were retained in the catalytic cycle and that C_{60} were less sterically demanding than triphenylphosphine then a lower activity and a lower selectivity would result. Comparison of the single crystal data of (**1**) and (**2**) show that a triphenylphoshine is more sterically demanding than a C_{60} moiety in the equivalent

rhodium complex. This is shown in the value of the cone angle, having a value of 75° for C_{60} in (**1**) and 140° for triphenylphosphine in (**2**).

The implication of the data in table 2.11.2.1. and previous work is that C_{60} is retained, at least to a degree, in the catalytic reactions of $Rh(C_{60})(CO)(H)(PPh_3)_2$ during propene hydroformylation at 90°C and that an equilibrium concentration of several catalytic species may be present. The possible mechanistic pathways involving C_{60} are probably very similar to those discussed and shown in section 2.2.

2.12. Thermal Decomposition Studies.

The catalyst $Rh(CO)(H)(PPh_3)_3$ is known to deactivate at elevated temperatures during the hydroformylation process. Side reactions of the triphenylphosphine ligands give products such as alkyldiphenylphosphines and benzene which mildly perturb the catalytic activity, and further decomposition gives rhodium clusters which severely reduces the catalytic performance, as discussed in section 2.5. These reactions have been postulated to occur via orthometallation or by the direct oxidative addition of a P-C bond to a rhodium metal centre. Statistically $Rh(C_{60})(CO)(H)(PPh_3)_2$ should have less propensity towards P-C bond activation because it has intrinsically less P-C bonds to activate than $Rh(CO)(H)(PPh_3)_3$. Due to the electron withdrawing effect of C_{60}, relative to triphenylphosphine, the electronic density at the rhodium centre is lower in the compound $Rh(C_{60})(CO)(H)(PPh_3)_2$ than $Rh(CO)(H)(PPh_3)_3$, which could also have a beneficial effect with regards to catalyst deactivation.

The thermal stability of the compounds $Rh(C_{60})(CO)(H)(PPh_3)_2$ (**1**) and $Rh(CO)(H)(PPh_3)_3$ (**2**), were studied by temperature-programmed decomposition. Experiments were performed using solutions of (**1**) and (**2**), in di-*n*-butylphthalate at the same concentration as was used in the catalytic experiments (sections 2.10.1. and 2.11.1.). These were heated from 50 to 180°C at a rate of 10°C/min in a stream of H_2/CO (1:1) and $H_2/CO/C_2H_4$. In particular, the formation of benzene was continuously monitored by an on-line quadrupole mass spectrometer with a mass selective detector. Control experiments were also performed without any rhodium complex present and using only triphenylphosphine.

2.12.1. Results of Thermal Decomposition Studies.

The data in figure 2.12.1.1. show that $Rh(C_{60})(CO)(H)(PPh_3)_2$ (**1**) is thermally more stable than $Rh(CO)(H)(PPh_3)_3$ (**2**).

Decomposition of (**2**) giving benzene starts at *ca.* 90°C and shows two maxima at *ca.* 125 and 175°C. However, with (**1**) benzene evolution is not detected until 140°C and the maximum at *ca.* 175°C is much less intense. The data in figure 2.12.1.1 suggests that there are two different processes for the decomposition of triphenylphosphine giving benzene. Both processes require the presence of rhodium since control experiments using only triphenylphosphine gave no benzene.

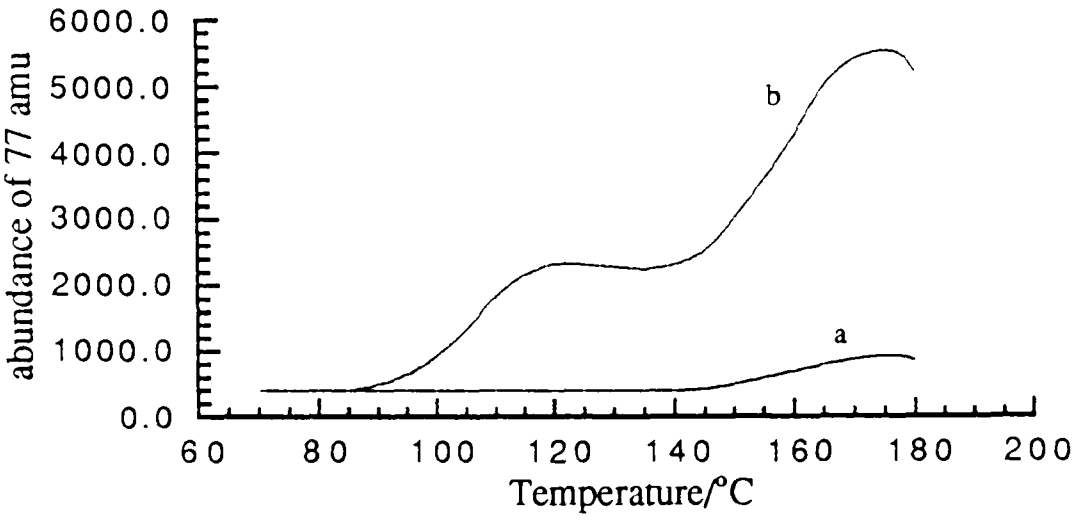


Figure 2.12.1.1. Benzene formation during the temperature-programmed decomposition of a) $Rh(C_{60})(CO)(H)(PPh_3)_2$ and (b) $Rh(CO)(H)(PPh_3)_3$ in the presence of H_2 and CO.

The stability of $Rh(C_{60})(CO)(H)(PPh_3)_2$ towards benzene evolution was also studied in the presence of H_2/CO and C_2H_4. The data is shown in figure 2.12.1.2. It was found that the lower temperature peak giving benzene at *ca.* 95°C reappeared and substantial benzene evolution occurs above 140°C.

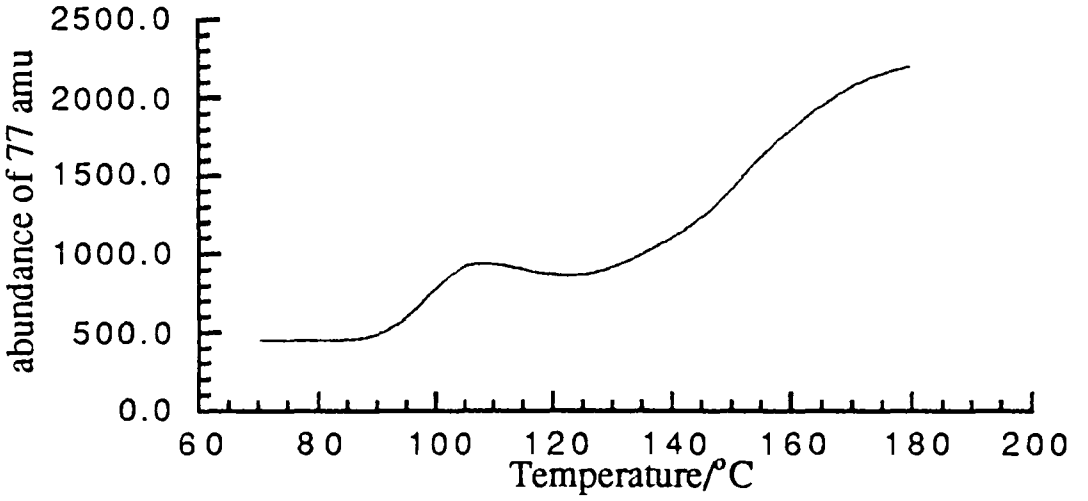


Figure 2.12.1.2. Benzene formation during the temperature-programmed decomposition of $Rh(C_{60})(CO)(H)(PPh_3)_2$ in the presence of H_2/CO and C_2H_4.

2.12.2. Disscusion on the Thermal Degradation Studies.

The results of the temperature-programmed decomposition show that replacement of a triphenylphosphine ligand, in $Rh(CO)(H)(PPh_3)_3$, by C_{60} can significantly reduce the rate of degradation of the catalyst at 90°C in the presence of a CO and H_2 gas mixture. However in the presence of a $CO/H_2/C_2H_4$ mixture the $Rh(C_{60})(CO)(H)(PPh_3)_2$ catalyst starts to evolve benzene at effectively the same temperature as for $Rh(CO)(H)(PPh_3)_3$. This suggests that C_{60} is displaced by ethene during the hydroformylation reaction.

The presence of a CO/H_2 gas mixture at 1 bar appears to have no effect on the two catalytic precursors and the decomposition is intrinsically due to the difference in

$Rh(C_{60})(CO)(H)(PPh_3)_2$ and $Rh(CO)(H)(PPh_3)_3$, i.e. the presence of a C_{60} ligand compared to a triphenylphosphine ligand. In this case increased stability is probably due in part to the decrease in electron density at the rhodium metal centre because of the electron withdrawing nature of the C_{60} ligand. This will tend to retard the oxidative addition of a P-C bond or orthometallation. As shown by the reaction used to synthesise $Rh(C_{60})(CO)(H)(PPh_3)_2$, the C_{60} complex is more stable than $Rh(CO)(H)(PPh_3)_3$, and hence decomposition would be expected to occur at a higher temperature.

In the presence of a $CO/H_2/C_2H_4$ gas mixture at 1 bar the two catalytic precursors have very similar decomposition profiles indicating that the decomposition route may be identical. Mechanisms postulated for the decomposition of $Rh(CO)(H)(PPh_3)_3$ involve unsaturated rhodium (I) complexes followed by intra- rather than intermolecular reaction of a P-C or C-H bond. The data in figures 2.12.1.1. and 2.12.1.2. seem to agree with this hypothesis if the unsaturated rhodium (I) complex is identical or very similar. In the presence of ethene dissociation of C_{60} from $Rh(C_{60})(CO)(H)(PPh_3)_2$ would lead directly to the same unsaturated rhodium (I) complex as the dissociation of triphenylphosphine from $Rh(CO)(H)(PPh_3)_3$ as shown in figure 2.10.2.1. Similar decomposition profiles would then be expected for the two complexes. It may be possible that the unsaturated rhodium (I) complex formed from $Rh(C_{60})(CO)(H)(PPh_3)_2$ by the dissociation of triphenylphosphine has similar energetics, with respect to intramolecular oxidative addition reactions, as the complex formed from dissociation of a triphenylphosphine ligand. However this seems unlikely given the significant effects a C_{60} ligand has upon the hydroformylation reaction, whose mechanism involves similar oxidative addition and alkyl migration/insertion steps as those postulated for the decomposition of $Rh(CO)(H)(PPh_3)_3$.

2.12.3. Reaction of $Rh(C_{60})(CO)(H)(PPh_3)_2$ with Excess C_{60}.

To remove the decomposition route via activation of a triphenylphosphine ligand an attempt was made to synthesise the compound $Rh(C_{60})_3(CO)(H)$ from $Rh(C_{60})(CO)(H)(PPh_3)_2$ and an excess of C_{60}. The reaction was unsuccessful based on evidence from ^{31}P and ^{13}C NMR spectroscopies, indicating no reaction had taken place.

2.13. The Hydroformylation of C_{60} from $Rh(C_{60})(CO)(H)(PPh_3)_2$.

On the addition of ethene or propene to a solution of $Rh(C_{60})(CO)(H)(PPh_3)_2$, C_{60} is dissociated, at least to a degree, and promotes catalyst decomposition above *ca.* 90°C (sections 2.10., 2.11. and 2.12.). However a CO/H_2 gas mixture at 1 bar does not appear to promote decomposition of $Rh(C_{60})(CO)(H)(PPh_3)_2$ to the same extent.

The stoichiometric hydroformylation of C_{60} using the complex $Rh(C_{60})(CO)(H)(PPh_3)_2$ was attempted by dissolving the complex in toluene and heating the solution at 75°C for 2 weeks under a gas mixture of H_2/CO at 30 bar.

Upon cooling and removal of the solution a change was observed from a dark green solution, prior to reaction, to a dark red solution with a pale brown precipitate. The pale brown precipitate (**3**) was insoluble in all common aqueous and organic solvents and the toluene solution, on removal of the volatiles, reduced to a very dark oily solid. Extraction with thf, of the oily solid, yielded an insoluble orange solid (**4**) and a dark red thf solution which, on removal of the volatiles, was reduced to a black oil (**5**).

IR of (**3**) showed the presence of C_{60} but no CO stretch was observed.

For the toluene soluble orange solid (**4**), ^1H NMR and IR spectroscopies were uninformative, other than CO stretches were not observed. FAB mass spectroscopy of (**4**) gave peaks to a maximum value of 731 but nothing could be assigned.

The highly soluble black oil (**5**) contains several CO stretching frequencies and characteristic C_{60} peaks. ^1H NMR showed several peaks between δ 7 and 8.5ppm. FAB mass spectroscopy showed the presence of triphenylphosphine but no peaks corresponding to C_{60} could be assigned. IBEI Mass spectroscopy did show C_{60} was present in the sample but nothing was observed that could be assigned to a hydroformylated product of C_{60}.

2.14. Summary.

The new complex $Rh(C_{60})(CO)(H)(PPh_3)_2$ (**1**) has been shown to be an effective catalytic precursor for the hydroformylation of ethene and propene at 90°C. In comparison to the industrial catalytic precursor, $Rh(CO)(H)(PPh_3)_3$ (**2**), (**1**) has a lower activity and a lower selectivity.

Thermal degradation studies of both (**1**) and (**2**) in the presence of a H_2/CO (1:1) gas mixture showed that the C_{60} containing complex (**1**) was more thermally robust than the industrial catalytic precursor. However, on introduction of ethylene to the gas mixture ($H_2/CO/C_2H_4$, 1:1:1) (**1**) decomposed at the same temperature as (**2**).

The hydroformylation of C_{60} using $Rh(C_{60})(CO)(H)(PPh_3)_2$ and a 2:1 H_2/CO gas mixture at 30 bar and 75°C, for 2 weeks, was unsuccessful.

2.15. General Experimental Details

2.15.1. Manipulations and Solvents

Manipulations of air and moisture sensitive materials were performed using standard Schlenk techniques, using dual nitrogen and vacuum manifolds. In house nitrogen was purified by passage over 'MnO' and 4Å molecular sieves. Solvents and solutions were transferred using stainless steel cannulae with an overpressure of dinitrogen and filtrations performed with modified cannulae fitted with paper and glass filters.

All other manipulations were performed in a dinitrogen filled drybox, with the dinitrogen purified over BASF catalyst and 4Å molecular sieves.

Solvents were predried by standing over 4Å molecular sieves followed by refluxing and distillation from a suitable drying agent under an atmosphere of dinitrogen. Solvents were degassed by the freeze/pump/thaw technique or by bubbling dinitrogen through the solvent for a few minutes.

The drying agents used were potassium (toluene and 100/120 petroleum ether), calcium hydride (dichloromethane, ethanol) and sodium/potassium alloy 1:3 w/w % (tetrahydrofuran, 40/60 petroleum ether, 30/40 petroleum ether, benzene and diethylether). Di-*n*-butylphthalate was dried over magnesium sulfate.

D_6-benzene for NMR was dried over potassium and transferred by vacuum distillation into an ampoule sealed with a Teflon stopcock.

2.15.2. Instrumental Methods.

Elemental analysis was performed by the microanalytical department of The Inorganic Chemistry Laboratory, Oxford.

Infra-red spectra were recorded on a Perkin-Elmer 1710 spectrophotometer (4000-400 cm^{-1}). Samples were prepared as a KBr disc.

Solution NMR were recorded on a Bruker AM-300 spectrometer fitted with an ASPECT 3000 computer at 300 MHz (^1H), 75.47 MHz (^{13}C) and 121.43 MHz (^{31}P). Spectra were referenced internally to residual protio-solvent resonances relative to tetramethylsilane for ^1H and ^{13}C, and externally relative to $PO(OMe)_3$ in D_2O for ^{31}P. Samples were contained in 10mm diameter NMR tubes.

A Bruker AMX500 spectrometer was used to record low temperature (-40, -10 and 10°C) ^{13}C spectra at 125 MHz. The samples were contained in 5mm diameter NMR tubes.

2.16. Synthesis and Reactions.

2.16.1. Synthesis of $Rh(CO)(H)(PPh_3)_3$. (1)

To a refluxing ethanol solution (100ml) of triphenylphosphine (2.7g, 10.3mmol) is added an ethanol solution (20ml) of $RhCl_3.xH_2O$ ($x \approx 3$, 0.28g, 1mmol). To this red solution, after a delay of 15s, was rapidly added successively 40% aqueous formaldehyde (10ml) and a hot ethanol solution (20ml) of KOH (0.8g). On addition of the basic ethanol solution the red solution formed a yellow precipitate with a yellow supernatant. The suspension was refluxed for 15 minutes, allowed to cool to room temperature, and filtered. The yellow residue was washed with ethanol (2 x 30ml), water (2 x 30ml) and hexane (30ml) and dried in vacuo to yield a pale yellow powder of analytical purity. Yield 90%.

^1H NMR spectroscopy (C_6D_6) δ 7.6, 6.9 (br, 45 H, PPh_3), -9.7 (br, 1 H, RhH)

IR spectroscopy (KBr disc) ν/cm^{-1} 1918 (CO), 2041 (RhH).

2.16.2. Synthesis of $Rh(C_{60})(CO)(H)(PPh_3)_2$. (2)

On addition of a pale yellow toluene solution (30ml) of $Rh(CO)(H)(PPh_3)_3$ (190mg, 0.21mmol) to a deep purple toluene solution (100 ml) of C_{60} (150mg, 0.21mmol), via cannula, an intense emerald colouration developed instantaneously. Removal of the solvent under reduced pressure revealed a dark green solid which was subsequently extracted with thf (3 x 40ml) and reduced in volume to *ca.*20ml. Precipitation, on addition of diethylether or ethanol (30ml), yielded a pale green microcrystalline powder of analytical purity. Yield > 95%.

^1H NMR spectroscopy (C_6D_6) δ 7.6, 6.9 (br, 30 H, PPh_3), -9.1 (t, 1 H, $^2J(^{31}P\text{-}^1H)$ = 9 Hz RhH); ^{13}C NMR spectroscopy (C_6D_6) at 293K δ 128.0, 129.5, 130.0, 133.5, (s, PPh_3) 141-145 (br, C_{60}), at 253K (d_8-thf) δ 129.5, 131.0, 134.7, 134.8, (s, PPh_3), 129.2, 129.3, 134.8, 135.0, 135.4, 136.2, 136.3, 136.5, 141.0, 141.2, 142.8, 142.9, 143.2, 143.3, 144.0, 144.3, 144.5, 144.7, 144.8, 144.9, 145.0, 145.1, 145.2, 145.3, 145.8, 146.5, 146.8, 149.3, 162.8, 164.1, (s, C_{60}); ^{31}P NMR spectroscopy (C_6D_6) δ 36.0 (d, $^1J(^{103}Rh\text{-}^{31}P)$ = 140 Hz, PPh_3).

IR spectroscopy (KBr disc) ν/cm^{-1} 1986 (CO), 2056 (RhH).

Analysis calculated for $C_{97}H_{31}O_1P_2Rh_1$, C 87.6, H 2.3; found C 87.4, H 2.5.

Properties

The green complex, $Rh(C_{60})(CO)(H)(PPh_3)_2$, is stable in air and over a period of several minutes the emerald green solution deposits a dark solid (C_{60}) with a pale orange supernatant.

The compound $Rh(C_{60})(CO)(H)(PPh_3)_2$ is soluble in benzene, toluene, dichloromethane, chloroform and slightly soluble in diethylether and 40/60 petroleum ether. The complex is insoluble in ethanol.

2.16.3. Reaction of $Rh(C_{60})(CO)(H)(PPh_3)_2$ with HCl.

To a toluene solution (20ml) of $Rh(C_{60})(CO)(H)(PPh_3)_2$ (10mg, 72μmol) was added 10 equivalents of HCl in toluene (1μl, 0.305M). Immediately the emerald green solution developed a pink colouration indicating the presence of free C_{60}. Extraction with thf (2 x 15ml) yielded a pale yellow solution and a thf insoluble tan solid (**3**). After filtration and removal of the volatiles under reduced pressure, the yellow solution yielded a brown solid (**4**). IR spectroscopy of (**4**) showed peaks cited in the literature as corresponding to $Rh(Cl)(CO)(PPh_3)_2$. ^{13}C NMR spectroscopy (C_6D_6) of (**3**) showed a peak at δ 143 corresponding to C_{60}.

2.16.4. Reaction of $Rh(C_{60})(CO)(H)(PPh_3)_2$ with $HBF_4.Et_2O$.

To a toluene solution (20ml) of $Rh(C_{60})(CO)(H)(PPh_3)_2$ (10mg, 72μmol) was added excess of 85% $HBF_4.Et_2O$ (30μl). After 30 seconds a pink colouration developed giving a very fine pale precipitate (**5**). Filtration and removal of the volatiles from the pink filtrate under reduced pressure gave a tan solid (**6**). IR spectroscopy of (**5**) showed no peaks corresponding to a CO stretch but did show peaks indicative of the BF_4 anion. ^{13}C NMR spectroscopy (C_6D_6) of (**6**) showed a peak at δ 143 corresponding to C_{60}.

2.16.5. Reaction of $Rh(C_{60})(CO)(H)(PPh_3)_2$ with CS_2.

$Rh(C_{60})(CO)(H)(PPh_3)_2$ (20mg, 144μmol) was dissolved in CS_2 to yield an intense emerald green solution which on standing for 30s developed into an intense brown/orange solution. ^{31}P NMR (C_6D_6) showed only free triphenylphosphine and triphenylphosphinesulfide. ^{13}C NMR spectroscopy (C_6D_6) showed a peak at δ 143ppm corresponding to free C_{60} and several peaks in a region associated with triphenylphosphine and its complexes/derivatives. ^{1}H NMR (C_6D_6) and IR spectroscopies did not reveal any conclusive information.

2.16.6. Reaction of $Rh(C_{60})(CO)(H)(PPh_3)_2$ with C_{60}.

To an intense emerald green toluene solution 30ml) of $Rh(C_{60})(CO)(H)(PPh_3)_2$ (25mg, 180μmol) was added a purple toluene solution (20ml) of C_{60} (26mg, 360μmol). The dichroic red/green solution was heated to 80°C for two days with no discernible change in the reaction solution. ^{31}P NMR spectroscopy (C_6D_6) showed only peaks assignable to $Rh(C_{60})(CO)(H)(PPh_3)_2$.

2.17. Hydroformylation Catalysis.

2.17.1. Procedure for Catalytic Reactions.

The ethene hydroformylation experiments were carried out by passing a 1:1:1 mixture of $CO/H_2/C_2H_4$, at a flow rate of 30 ml/min, continuously through the catalyst solution which was held in a 50cm high, 8mm internal diameter glass column. The

gases were passed through a sintered glass frit at the bottom of the column to disperse the bubbles, and the whole column was kept at 90°C using heating tapes. The reaction was carried out at ambient pressure.

Propene hydroformylation experiments were performed in a 100ml Parr high pressure autoclave, as shown in figure 2.17.1.1, using a batch mixture of $CO/H_2/C_3H_6$ (in the ratio 1:1:1) as the reactants, at a total pressure of 11 bar. The temperature was monitored and controlled (±2°C) by an internal thermocouple, and a Druck pressure transducer which allowed the pressure of the reactor to be measured continuously.

The products were analysed using a Pye-Unicam Gas Chromatograph, with 2-pentanol as an internal standard, and separation was achieved using a 3m Chromosorb P packed column. Detection of eluted gases was performed with a flame ionisation detector.

All the reactions were performed using di-*n*-butylphthalate (Aldrich) as a solvent, and the reactant gases (BOC) were all greater than 99% purity.

2.17.2. Hydroformylation Catalysis of Ethene Using $Rh(CO)(H)(PPh_3)_3$ and $Rh(C_{60})(CO)(H)(PPh_3)_2$.

67mg (0.07mmol) of $Rh(CO)(H)(PPh_3)_3$ was dissolved in 20ml of dry degassed di-*n*- butylphthalate and placed in a 50cm high, 8mm internal diameter Pyrex tube fitted with a sintered glass frit. The pale yellow solution was heated to 90°C (±2°C) using heating tapes wrapped around the column. A 1:1:1 mixture of $CO/H_2/C_2H_4$ was bubbled up through the tube at a rate of 30ml/min determined by a mass flow controller, the bubbles being dispersed by the sintered glass frit. On introduction of the reactant gases, the reaction solution changed from pale yellow to golden yellow.

The reaction was monitored via an on line Pye-Unicam Gas Chromatograph. Portions of gas from the reaction were sampled every 15min and separated on a 3m Chromosorb P column until a constant value of relative peak areas was obtained. This was to account for differing solubilities of the reactant gases and product.

100mg (0.07mmol) of $Rh(C_{60})(CO)(H)(PPh_3)_3$ was dissolved in 20 ml of dry degassed di-*n*- butylphthalate and placed in a 50cm high, 8mm internal diameter Pyrex tube fitted with a sintered glass frit. The resulting green solution was treated and analysed analogously as for $Rh(CO)(H)(PPh_3)_3$. On introduction of the reactant gases the dark green solution became an intense orange/brown.

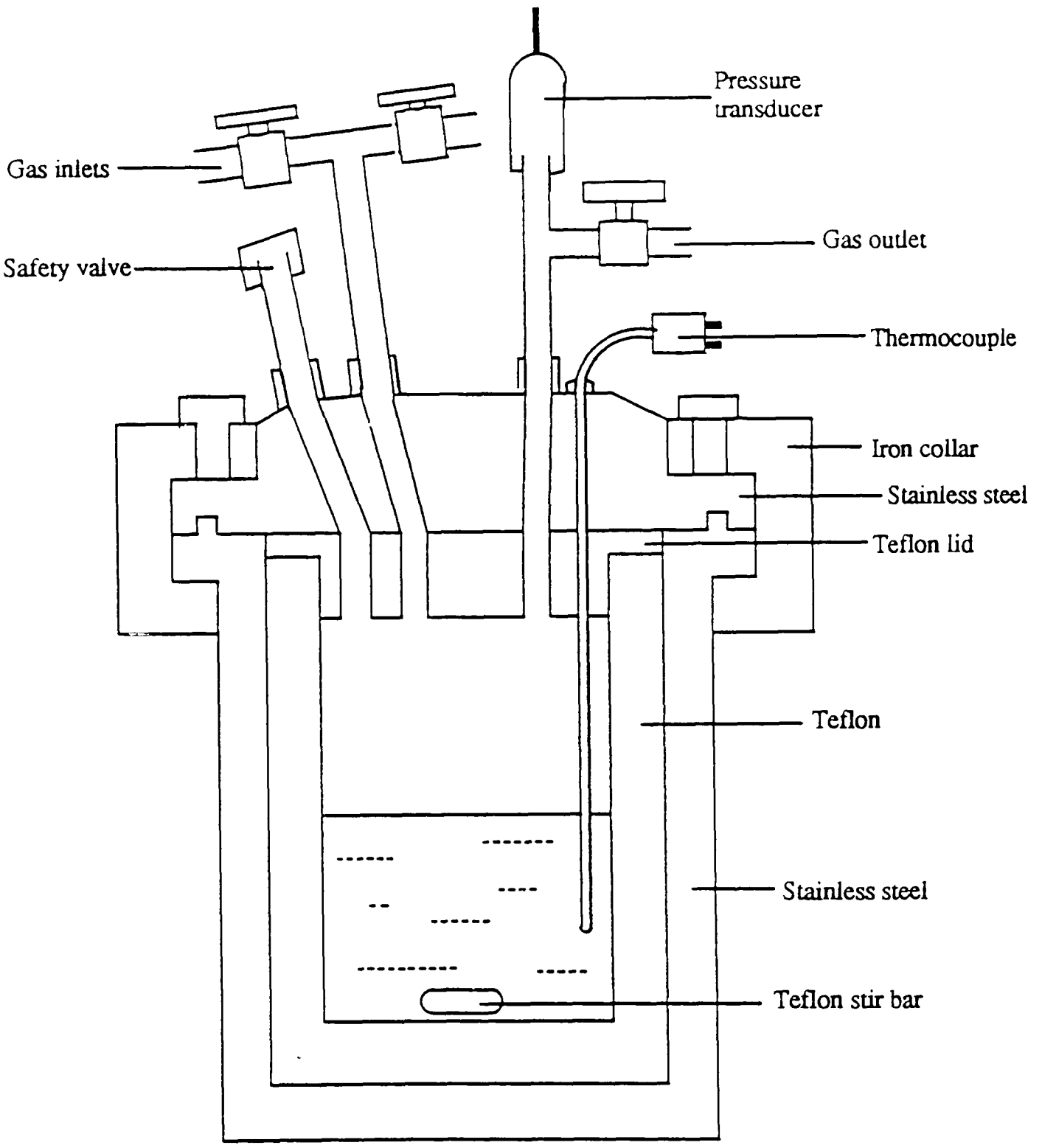


Figure 2.16.1.1. Autoclave used for the hydroformylation of propene.

2.17.3. Hydroformylation Catalysis of Propene Using $Rh(CO)(H)(PPh_3)_3$ and $Rh(C_{60})(CO)(H)(PPh_3)_2$.

In a Parr high pressure autoclave 67mg (0.07mmol) of $Rh(CO)(H)(PPh_3)_3$ was dissolved in 20ml of di-*n*-butylphthalate and placed under reduced pressure for 1 hour at room temperature. The autoclave was charged with 99% propene and stirred for 1 hour to saturate the solution. A static pressure of 3.67 bar was applied. A final static pressure of 11 bar at room temperature was achieved by the addition of 1:1 CO/H_2. The autoclave was heated to 90°C (± 2°C) using a preheated oil bath for 5 hours with stirring. The pressure of the system was monitored continually with a Druck pressure transducer.

In a Parr high pressure autoclave 100mg (0.07mmol) of $Rh(C_{60})(CO)(H)(PPh_3)_2$ was dissolved in 20ml of di-*n*-butylphthalate and placed under reduced pressure for 1 hour at room temperature. The sample was treated and analysed analogously as for $Rh(CO)(H)(PPh_3)_3$.

2.17.4. Analysis of the Products from Propene Hydroformylation.

To 20ml of the solution from the catalytic reaction was added an internal calibrant of 2-pentanol (1ml). Aliquots of this solution (0.5µl) were analysed using a Pye-Unicam Gas Chromatograph. A guard column of alumina was used to remove any of the catalyst, catalyst decomposition products and di-*n*-butylphthalate. Separation of hydroformylation products was achieved using a 3m Chromosorb P packed column and detection using a flame ionisation detector.

2.18. Temperature-Programmed Decomposition Studies of the Catalysts.

The effect of temperature on the lifetime of the two catalytic systems was determined Experiments were performed in the presence and absence of ethene.

Experiments without ethene were performed by passing CO/H_2, in the ratio of 1:1, through a di-*n*-butylphthalate solution of the catalyst precursor while ramping the temperature from 50°C to 180°C at a rate of 10°C/min. The exit gases were monitored continuously for benzene using an on-line quadrupole mass selective detector. The experiment with ethene was performed by bubbling a 1:1:1 mixture of $CO/H_2/C_2H_4$ through the catalytic solution at a heating rate of 1°C/min over the same temperature range. The apparatus is shown in figure 2.18.1.

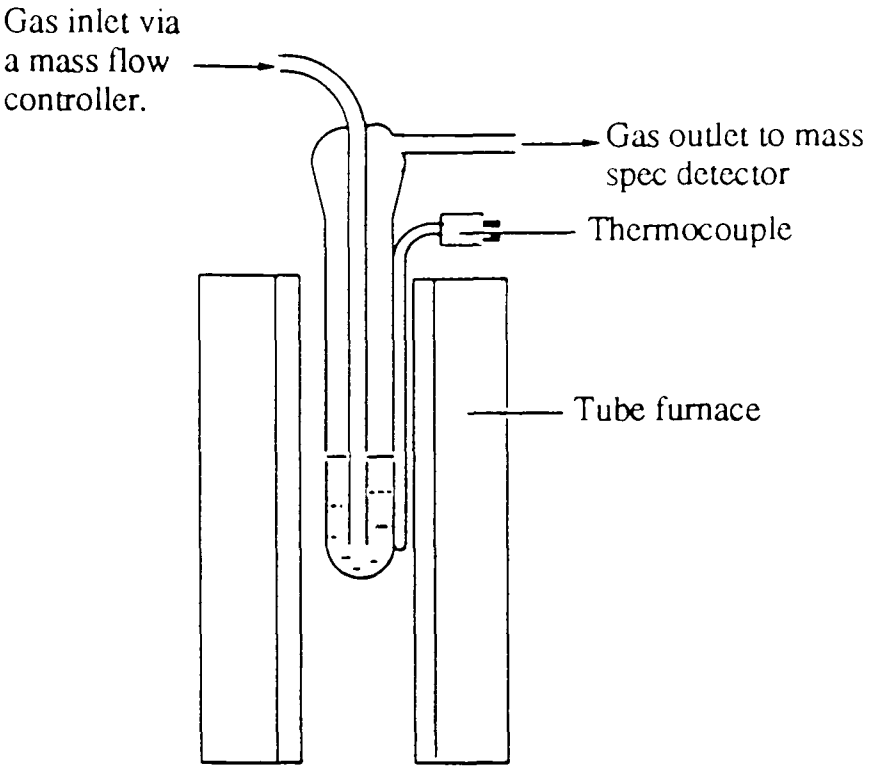


Figure 2.18.1.

2.18.1. Temperature-Programmed Decomposition of $Rh(C_{60})(CO)(H)(PPh_3)_2$ and $Rh(CO)(H)(PPh_3)_3$ in the Presence of CO and H_2.

10mg (0.007mmol) of $Rh(C_{60})(CO)(H)(PPh_3)_2$ was dissolved in 2ml of dry degassed di-*n*-butylphthalate. The green solution was purged for 30 minutes at room temperature with CO and H_2. A flow rate of 15ml/min was determined by a mass flow controller. The temperature was controlled by a Eurotherm Temperature Controller and monitored by a thermocouple at a rate of 10°C/min over the temperature range 50 to 180°C. Heating was achieved via a tube furnace. The reaction was monitored for benzene using an on-line quadrupole mass selective detector. On decomposition the green solution became a suspension of a dark solid in a red supernatant.

7mg (0.007mmol) of $Rh(CO)(H)(PPh_3)_3$ was dissolved in 2ml of dry degassed di-*n*-butylphthalate. The pale yellow solution was treated in the same manner as in for $Rh(C_{60})(CO)(H)(PPh_3)_2$. On decomposition the pale yellow solution became a dark brown solution with a little dark precipitate.

2.18.2. Temperature-programmed decomposition of $Rh(C_{60})(CO)(H)(PPh_3)_2$ and $Rh(CO)(H)(PPh_3)_3$ in the presence of CO, H_2 and C_2H_4.

10mg (0.007mmol) of $Rh(C_{60})(CO)(H)(PPh_3)_2$ was dissolved in 2ml of dry degassed di-*n*-butylphthalate. The green solution was purged for 30 minutes at room temperature with CO, H_2 and C_2H_4. On introduction of the reactant gases the green solution became orange/brown. The same conditions were used as in section 2.18.1. except that a heating rate of 1°C/min was used. On decomposition the green solution became a suspension of a dark solid in a red supernatant.

7mg (0.007mmol) of $Rh(CO)(H)(PPh_3)_3$ was dissolved in 2ml of dry degassed di-*n*-butylphthalate. The pale yellow solution was treated in exactly the same manner as for $Rh(C_{60})(CO)(H)(PPh_3)_2$. On decomposition the pale yellow solution became a dark brown solution with a little dark precipitate.

2.19. Attempted Hydroformylation of C_{60}.

100mg (0.07mmol) of $Rh(C_{60})(CO)(H)(PPh_3)_2$ was dissolved in 25ml of dry degassed toluene and placed in a Parr high pressure autoclave. The autoclave was charged with H_2/CO 2:1 at 30 bar at room temperature and then warmed to 70°C using a preheated oil bath. Over a 2 week period the pressure was observed to decrease at a constant rate to a final pressure of 20 bar indicating a small leak was present.

After cooling and release of the excess pressure the contents of the autoclave were transferred to a Schlenk tube, the sample consisted of a deep red supernatant and pale brown precipitate. The pale brown precipitate (**7**) was found to be insoluble in common organic and aqueous solvents such as toluene, thf, dichloromethane, acetonitrile, dimethylsulfoxide, water and dilute hydrochloric acid. Removal of the volatiles under reduced pressure from the toluene supernatant gave a dark oily solid which was subsequently extracted with thf. The thf insoluble material (**8**) was a pale orange solid and the thf solution deep red, which on removal of the volatiles under reduced pressure revealed a black oil (**9**).

All three products were analysed by FAB mass spectrometry revealing no useful information. ^1H NMR spectroscopy of (**8**) showed peaks which could be assigned to residual solvents, whereas (**9**) gave peaks between δ 7 and 8.5ppm which could be assigned to triphenylphosphine and toluene. IR spectroscopy showed that all three fractions could possibly contain C_{60} material but only (**9**) showed peaks consistent with CO stretching frequencies.

References

1. Falbe, J. *Carbon Monoxide in Organic Synthesis* ; Springer-Verlag: Berlin and New York, 1970.
2. *Chem. Market. Rep.* 1984, ***14***, 54.
3. *Chem. Market. Rep.* 1984, ***17***, 74.
4. Wilkinson, G.; Stone, F. G. A. Abel, E. W., Ed.; Pergamon Press: 1982; Vol. 8; p 115.
5. Wilkinson, G.; Gillard, R. G. McCleverty, J. A., Ed.; Pergamon Press: 1982; Vol. 6; p 258.
6. Osborn, J. A.; Wilkinson, G.; Young, J. F. *J. Chem. Soc., Chem. Comm.* 1965, 17.
7. Roelen, O. German Patent 1938, 849.
8. Roelen, O. U. S. Patent 1943, 2.
9. *Hydroformylation*; Pruett, R. L., Ed.; 1979; Vol. 17, pp 1.
10. Evans, D.; Osborn, J. A.; Wilkinson, G. *J. Chem. Soc. (A)* 1968, 3133.
11. Adkins, H.; Krsek, G. *J. Am. Chem. Soc.* 1948, ***71***, 3051.
12. Cotton, F. A. *Advanced Inorganic Chemistry* 5th ed.; John Wiley & Sons: 1988.
13. Pruett, R. L. *J. Chem. Ed.* 1986, ***63***, 196.
14. Brewster, E. A. V. *Chem. Eng.* 1976, ***83***, 90.
15. Brown, C. K.; Wilkinson, G. *J. Chem. Soc. (A)* 1970, 2753.
16. Jenck, J. F.; Kuntz, E. *Abstracts of the 187th ACS National Meeting,* Apr. 1984,
17. Wilkinson, G.; Stone, F. G. A. Abel, E. W., Ed.; Pergamon: 1982; Vol. 8; p 597.
18. Jardine, F. H.; Osborn, J. A.; Wilkinson, G. *J. Chem. Soc. (A)* 1967, 1574.
19. Osborn, J. A.; Jardine, F. H.; Young, J. F.; Wilkinson, G. *J. Chem. Soc. (A)* 1966, 1711.
20. Falbe, J.; Tummes, H.; Hahn, H. *U. S. Patent 4,039,584* 1977,
21. Tolman, C. A. *J. Am. Chem. Soc.* 1970, ***92***, 2956.
22. Brown, J. M.; Canning, L. R.; Kent, A. G.; Sidebottom, P. J. *J. Chem. Soc., Chem. Comm.* 1982, 721.
23. Brown, J. M.; Kent, A. G. *J. Ckem. Soc., Chem. Comm.* 1982, 723.
24. Halpern, J. *Inorg. Chim. Acta* 1981, ***50***, 11.
25. Halpern, J. *Acc. Chem. Res.* 1982, ***15***, 332.
26. Halpern, J. *Science* 1982, ***217***, 401.
27. Halpern, J.; Okamoto, T. *Inorg. Chim. Acta* 1984, ***89***, L53.
28. Webb, S. L.; Giandomenico, C. M.; Halpern, J. *J. Am. Chem. Soc.* 1985, ***108***, 345.
29. Bryant, D. R.; Billing, E. *U. S. Patent 4,283,304* 1981.

30. Bryant, D. R.; Galley, R. A. *U. S. Patent 4,283,304* 1981.
31. Abatjoglou, A. G.; Billig, E.; Bryant, D. R. *Organometallics* 1984, ***3***, 923.
32. Fagan, P. J.; Calabrese, J. C.; Malone, B. *Acc. Chem. Res.* 1992, ***25***, 134.
33. Yagupsky, G.; Brown, C. K.; Wilkinson, G. *J. Chem. Soc. (A)* 1970, 1392.
34. Botteghi, C.; Ponte, G. D.; Marchetti, M.; Paganelli, S. *J. Mol. Cat.* 1994, ***93***, 1.
35. Elschenbroich, C.; Salzer, A. *Organometallics: A Concise Introduction* 2nd ed.; VCH: 1992.
36. Henderson, C. C.; Cahill, P. A. *Science* 1993, ***259***, 1885.
37. Ballenweg, S.; Gleiter, R.; Krätschmer, W. *Tetrahedron Lett.* 1993, ***34***, 3737.
38. Haufler, R. E.; Conceicao, J.; Chibante, L. P. F.; Chai, Y.; Byrne, N. E.; Flanagan, S.; Haley, M. M.; O'Brien, S. C.; Pan, C.; Xiao, Z.; Billups, W. E.; Ciufolini, M. A.; Hauge, R. H.; Margrave, J. L.; Wilson, L. J.; Curl, R. F.; Smalley, R. E. *J. Phys. Chem.* 1990, ***94***, 8634.
39. Geoffroy, G. L.; Lehman, J. R. *Adv. Inorg. Chem. Radiochem.* 1978, ***20***, 190.
40. Green, M. L. H.; Jones, D. J. *Adv. Inorg. Chem. Radiochem.* 1965, ***7***, 115.
41. Balch, A. L.; Lee, J. W.; Noll, B. C.; Olmstead, M. M. *Inorg. Chem.* 1993, ***32***, 3577.

Chapter 3

Studies into Sodium Compounds of the Anions of C_{60} and Related Areas

3.1. Introduction to C_{60} Anions.

The observation of metallic behaviour, and superconductivity, in the simple molecular salt K_3C_{60}[1, 2] has generated a great deal of interest in the chemistry and physics of materials containing the anions of C_{60}.

It has been demonstrated, using electrochemical techniques, that up to six electrons per C_{60} molecule can be reversibly[3, 4] added into the LUMO filling the t_{1u} level, as shown in figure 3.1.1. and described in section 1.2.2.

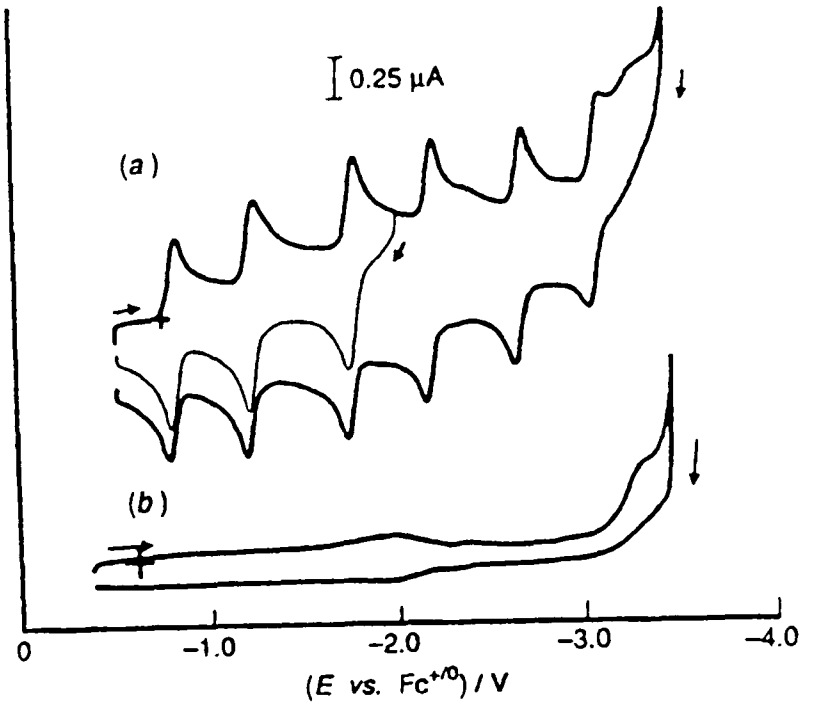


Figure 3.1.1. (a) Cyclic voltammogram of 0.3 mM C_{60} in DMF-toluene (2:3) containing 0.1 M Et_4NPF_6 at -88°C. (b) The corresponding background current in the absence of C_{60}. A platinum working electrode of *ca.* 0.08 cm^2 area was used.

A range of formal oxidation states are available allowing the possibility of tuning the properties of a particular material containing C_{60}. For instance binary rubidium C_{60} compounds show a range of electronic properties depending on the concentration of rubidium intercalated into the C_{60} lattice.

Intercalation of one equivalent of rubidium gives the compound Rb_1C_{60}, that is unusual in that it appears that neighbouring C_{60} molecules undergo polymerisation along one axis resulting in chains of C_{60}'s bonded through [2+2] psuedocyclobutane linkages.[5] 1-dimensional metallic behaviour has been postulated for this material which undergoes a phase transition above *ca.*100°C resulting in break up of the polymer and localised paramagnetic behaviour.[5-8] Addition of three equivalents of rubidium populates each of the orbitals in the triply degenerate t_{1u} level, assuming the anion is high spin, and overlap of these molecular orbitals throughout the C_{60} based fcc lattice results in a band structure in Rb_3C_{60} and metallic behaviour. On cooling below 29K Rb_3C_{60} becomes superconducting.[2, 9] On addition of a further equivalent of rubidium the semiconducting compound Rb_4C_{60} is formed[10] with a bct structure and two further equivalents give the insulator Rb_6C_{60}, which has a bcc structure.[2, 9] Materials

corresponding to the composition Rb_2C_{60}, Rb_5C_{60}, or intermediate solid solution phases have not been synthesised, to date.

A question arises as to whether the electronic wave function describing the electrons in the t_{1u} derived orbitals has significant density at the site of the alkali metal cation. Various experiments have been performed that indicate that these electrons are confined almost solely to the C_{60} lattice.[6, 11-13]

Alkali metal C_{60} intercalation compounds have been synthesised using a number of routes both in solution[14-17] and in the solid state.[2, 9, 10, 18-25] They are very sensitive to oxygen and moisture requiring rigorous handling in an inert atmosphere. Figure 3.1.2. illustrates the binary alkali metal C_{60} phases known to date at room temperature and pressure.

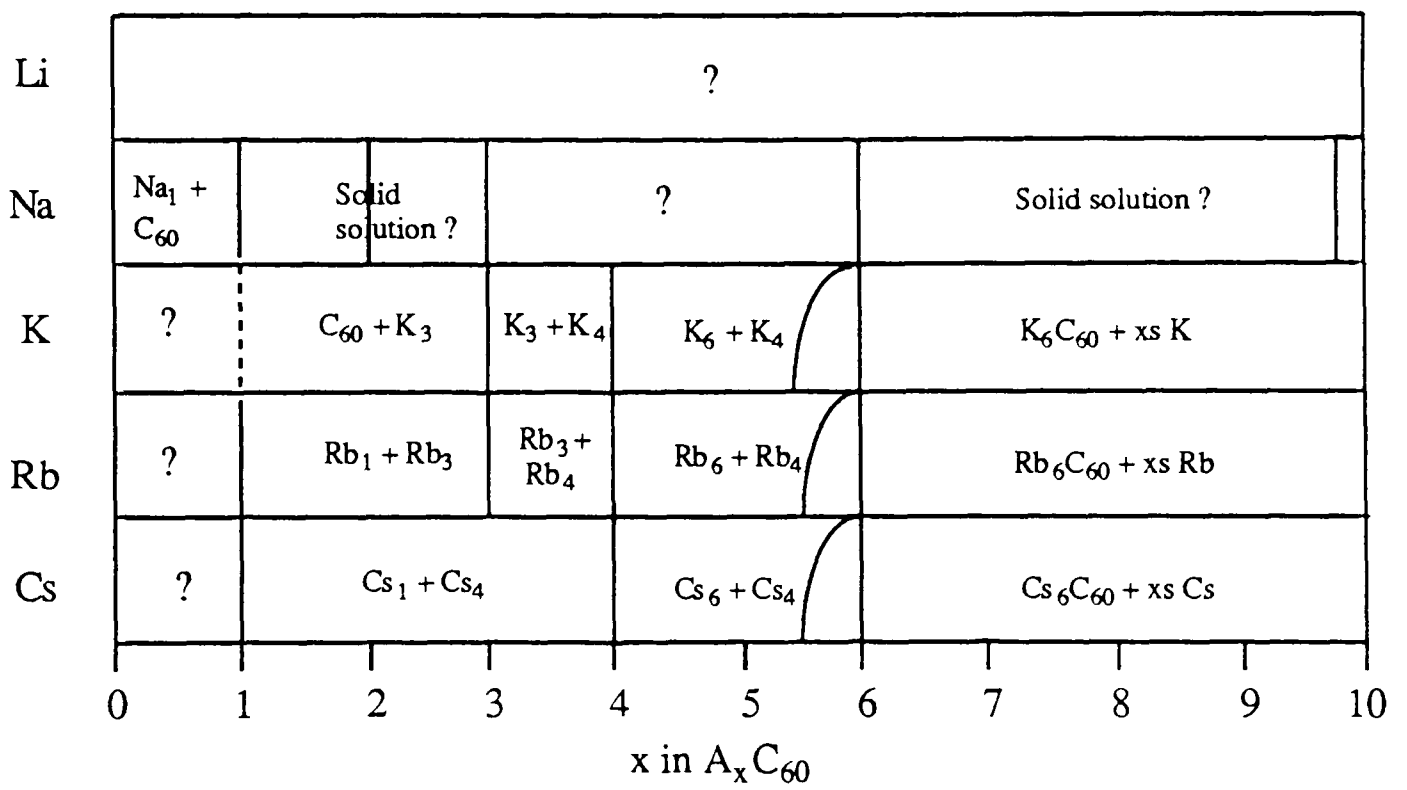


Figure 3.1.2. Proposed phase diagram based on the literature to date. Below the compositions KC_{60}, RbC_{60} and CsC_{60} two phases probably coexist, AC_{60} and C_{60}. KC_{60} is not an equilibrium phase but can be synthesised by quenching at high temperatures, but is contaminated with K_3C_{60} and C_{60}. No binary lithium C_{60} phases have been structurally characterised but Chabre[23] *et al* have synthesised and studied the binary lithium C_{60} system using a solid state electrochemical technique. The curved regions are meant to represent uncertainty in the phase boundary.

3.1.1. Solid State Synthetic Routes to Alkali Metal C_{60} Compounds.

Initially, synthesis was by direct combination of C_{60} and a stoichiometric amount of the relevant alkali metal. In the early days of macroscopic C_{60} chemistry only small amounts were available (~20 mg) for bulk chemical synthesis. This required very small quantities of alkali metal to be accurately measured, which was achieved by drawing molten metal into a capillary of small diameter (0.2mm), and from the known

density of the alkali metal, a length of the glass capillary could be cut containing the desired mass. Flame sealing the capillary length and C_{60} powder within a Pyrex tube under 10^{-5}mbar of helium, followed by several days heating, allowed synthesis of small quantities of these sensitive materials. This method only works for the lower melting alkali metals, potassium, rubidium and caesium which can be drawn into a capillary and not react with glass surfaces at the temperatures synthesis is performed.

In the case of sodium, copper or stainless steel containers are required which do not react with the alkali metal at the temperatures required for synthesis. Stoichiometric amounts of sodium and C_{60} are usually placed in a tube and then flame sealed within a silica or Pyrex tube at a helium pressure of 10^{-5}mbar. Some reactions have been performed in copper tubes sealed under an atmosphere of helium. To weigh accurately within a drybox a stoichiometric quantity of sodium metal requires at least a mass of 10mg, consequently large amounts of C_{60} (100-200mg) are required.

Another method which can be used in the cases of potassium, rubidium and caesium takes advantage of the fact that saturated phases of composition A_6C_{60} are formed. These phases can be easily synthesised by exposing C_{60} powder to alkali metal vapour. Sealing excess metal and C_{60} powder in a Pyrex tube and applying a small thermal gradient, at a mean temperature of 350°C, so that the C_{60} powder is at the hot end leads directly to the saturated phases. It is a simple matter to then dilute these compounds with pure C_{60} to the composition of choice. The major advantage in this method is that small quantities of metal need not be weighed out and the problem of reduction of glass surfaces does not occur at the temperatures required for efficient synthesis. However, experimentally the saturated phases appear to have the stoichiometry $A_{6+x}C_{60}$ where $x \sim 0.7$ which can cause problems in obtaining a phase pure material on initial dilution.

Sodium intercalates of C_{60} can be synthesised in a similar fashion but the composition A_6C_{60} is not the saturated phase. A phase corresponding to the composition $Na_{9.8}C_{60}$ has been structurally characterised[19] but it is not certain whether this is the saturated phase. The phase diagram of the binary sodium C_{60} system is by no means complete and uncertainty as to the existence of some of the postulated phases is present, as will be discussed in part of this chapter. The electronic structure of these materials is also unclear. Stoichiometric combination of sodium metal and C_{60} is probably still the most reliable route to the bulk synthesis of these compounds. The difficulty in the synthesis of sodium C_{60} compounds is probably reflected in the delay of the first report of the binary phases Na_2C_{60}, Na_3C_{60} and Na_6C_{60} compared to those of potassium, rubidium and caesium.

A more convenient synthesis of some of the alkali metal phases (Na_2C_{60}, Na_3C_{60} and K_3C_{60}) are from the respective hydrides and borohydrides,[9] as shown in equations 3.1.1.1. and 3.1.1.2.

$$xAH + C_{60} \longrightarrow A_xC_{60} + \frac{x}{2} H_2 \qquad \text{Eq. 3.1.1.1.}$$

$$xABH_4 + C_{60} \longrightarrow A_xC_{60} + \frac{x}{2} H_2 + \frac{x}{2} B_2H_6 \qquad \text{Eq. 3.1.1.2.}$$

This method is successful on account of the mechanism and temperature of decomposition of the hydride or borohydride, to dihydrogen and diborane. The temperatures of decomposition are similar to those required for efficient diffusion of the relevant alkali metal cation throughout the C_{60} lattice. In contrast to the intercalation of graphite with these precursors no ternary phases are observed. The disadvantage of this method is that large samples cannot be synthesised due to the volume of gas that would be liberated within the sealed reaction vessel.

Mercury amalgams have also been successfully used in the synthesis of sodium, potassium, rubidium and caesium binary phases of C_{60}.[9] Again no ternary phases were found in this study as is the case for similar intercalation reactions of graphite. However, at temperatures below *ca.* 400°C in the synthesis of Na_2C_{60}, it appears that some mercury is retained within the vacant octahedral site. However, if a thermal gradient is applied across the reaction vessel the mercury can be removed above *ca.* 200°C.[26]

$$Na_5Hg_2 + C_{60} \longrightarrow Na_2Hg_{0.2}C_{60} \longrightarrow Na_2C_{60}$$

In common with most solid state synthesis reaction times can be long, and in the case of alkali metal C_{60} compounds, especially sodium, reactions times of several weeks are typical. Synthesis of these materials can be divided into two time consuming steps, introduction of the metal to the C_{60} powder, and diffusion of the alkali metal cation throughout the C_{60} lattice. The time required for electron transfer is assumed to be negligible. Long times for the introduction of the metal to the C_{60} powder, due to low vapour pressures at the reaction temperature, can be circumvented by one of the routes described above. However, diffusion of alkali metal cations throughout the C_{60} lattice and subsequent annealing of the sample is not aided by the methods described above. Excessive heating of alkali metal C_{60} compounds to increase the rate of diffusion can result in deintercalation of a proportion of the metal, and decomposition of C_{60} occurs above *ca.* 600°C. However, a microwave induced argon plasma can increase the rate of diffusion dramatically, as described in chapter 4.

3.1.2. Solution Routes to Alkali Metal C_{60} Compounds.

Diffusion of alkali metal cations is not required, if the components of the C_{60} material can be mixed effectively on the molecular level, i.e. in solution, and subsequently deposited as a crystalline solid. Several routes have been reported that

describe the synthesis of solids from solution that contain alkali metal cations and C_{60} anions.[14, 15, 17, 27-29] Most work has centred on the superconducting phases of potassium and rubidium,[14-17] generally because very small amounts of superconducting material can easily be detected.

A major problem with all of these routes are that solvent molecules used in the synthesis tend to become occluded or are molecules of crystallisation. In favourable cases, long periods of heating under vacuum are required to remove the solvent. Generally solvent molecules remain up to the decomposition temperature of these materials or reaction with the solvent occurs. In effect the heating periods do not significantly increase the rate of synthesis of a phase pure material by comparison with all solid state routes, if a phase pure material is obtained at all.

The superconducting phases of potassium and rubidium have been detected, with varying success, from a number of solution phase preparations.

Addition of toluene to solid C_{60} and a large excess of potassium or rubidium metal, followed by refluxing for several hours, precipitated a solid that contained small amounts of the relevant superconducting phase.[15, 16] No other measurements were reported that could quantify the amount of A_3C_{60} phase present.

A more successful route, is the addition of a stoichiometric quantity of potassium or rubidium to a C_{60} suspension in liquid ammonia.[17] High values of the superconducting fractions have been reported and it is stated that the powder X-ray diffraction pattern shows only A_3C_{60} phases. Solid state ^{13}C and ^{87}Rb powder NMR show spectra very similar to those obtained from a conventional solid state techniques.

A third route utilises the method described later in this chapter. Alkali metal salts of the highly reducing 18-electron decamethylmanganocene anion can be used to selectively synthesise thf solvated alkali metal C_{60} materials.[14, 28] The thf molecules occluded in the isolated solid may be removed, depending on the alkali metal cation and/or the formal oxidation state of the C_{60} anion.

Reduction of C_{60} to the monoanion producing KC_{60}.thf has been achieved using 1-methylnaphthalene as the electron transfer catalyst.[27] Solid state ^{13}C powder NMR and ESR measurements indicate a monoanion is present although the elemental analysis found was vastly different from the calculated value for a stoichiometry of KC_{60}.thf.

Solution routes to materials containing C_{60} anions are very attractive because of the large variety of possible reagents and general ease of synthesis. Superconducting phases have been limited to alkali and alkaline earth metals because of the relatively high vapour pressures obtainable at temperatures amenable to C_{60} chemistry. Low temperature routes, which allow mixing of species with C_{60} on a molecular level, have the potential for the synthesis of a vast array of materials which would not be amenable

by traditional solid state techniques. However, to date the C_{60} anion containing materials, except those of alkali metals, which have been synthesised from solution, have not shown particularly interesting properties.

3.2. Electrochemical Routes to C_{60} Anions.

It was discovered early in C_{60} chemistry, that with a judicious choice of solvent(s), capable of solublising C_{60} anions and stable down to low reduction potentials, C_{60} can undergo six reversible one electron reductions.[3, 4] There has also recently been a report of a reversible one electron oxidation of C_{60}.[30]

Various techniques have been used to study solutions, containing C_{60} anions, either at an electrode surface or from bulk controlled potential electrolysis.[31-41] ESR spectroscopy is the most widely applied technique and has generated a debate in the literature on how to best interpret the experimental data. Charge transfer salts of C_{60} monoanions, as described in section 1.5, and electrochemically generated bulk solutions of the monoanions, have shown varying responses. As shown in figure 3.2.1. ESR spectroscopy on solids and frozen glasses of C_{60} monoanions have been reported showing features which have been ascribed to the effect of the cation in the ion pair, and an interplay of distortions about particular symmetry elements of C_{60}.[42] ESR spectroscopy of the monoanions of C_{60} show a temperature dependent linewidth, where narrowing of the linewidth occurs on cooling and sometimes a sharp 'spike' superimposed, at temperatures generally greater than 100K. At very low temperatures, on the order of 4K, anisotropy and a small increase in linewidth are observed depending on the associated cation and probably the nature of the solvent. A theory accounting for all the observed data has not been reported and it is not clear as to the origin of some features. This will be discussed in more detail in section 3.4.5.

Spectroelectrochemistry[35] and near i-r spectroscopy[42] have also been used extensively to probe bulk solutions of the anions. In the u-v spectra, red shifts are observed for the two bands associated with neutral C_{60} at 257 and 330nm upon population of the LUMO. Anions of C_{60} apparently also have distinctive absorption peaks in the near i-r spectrum depending on the degree of reduction.

As a method of preparation of materials containing C_{60} anions, electrocrystallisation has been investigated, as discussed in section 1.5. Various charge transfer salts have been prepared and structurally characterised and an interesting sodium salt which has been postulated as undergoing a metal-metal transition at low temperature.[29] This material will be discussed in more detail in section 3.5.

3.3. The Sodium C_{60} Phase Diagram.

The areas of the sodium C_{60} phase diagram investigated to date are by no means certain. Several problems become apparent on attempts to investigate this field, not least

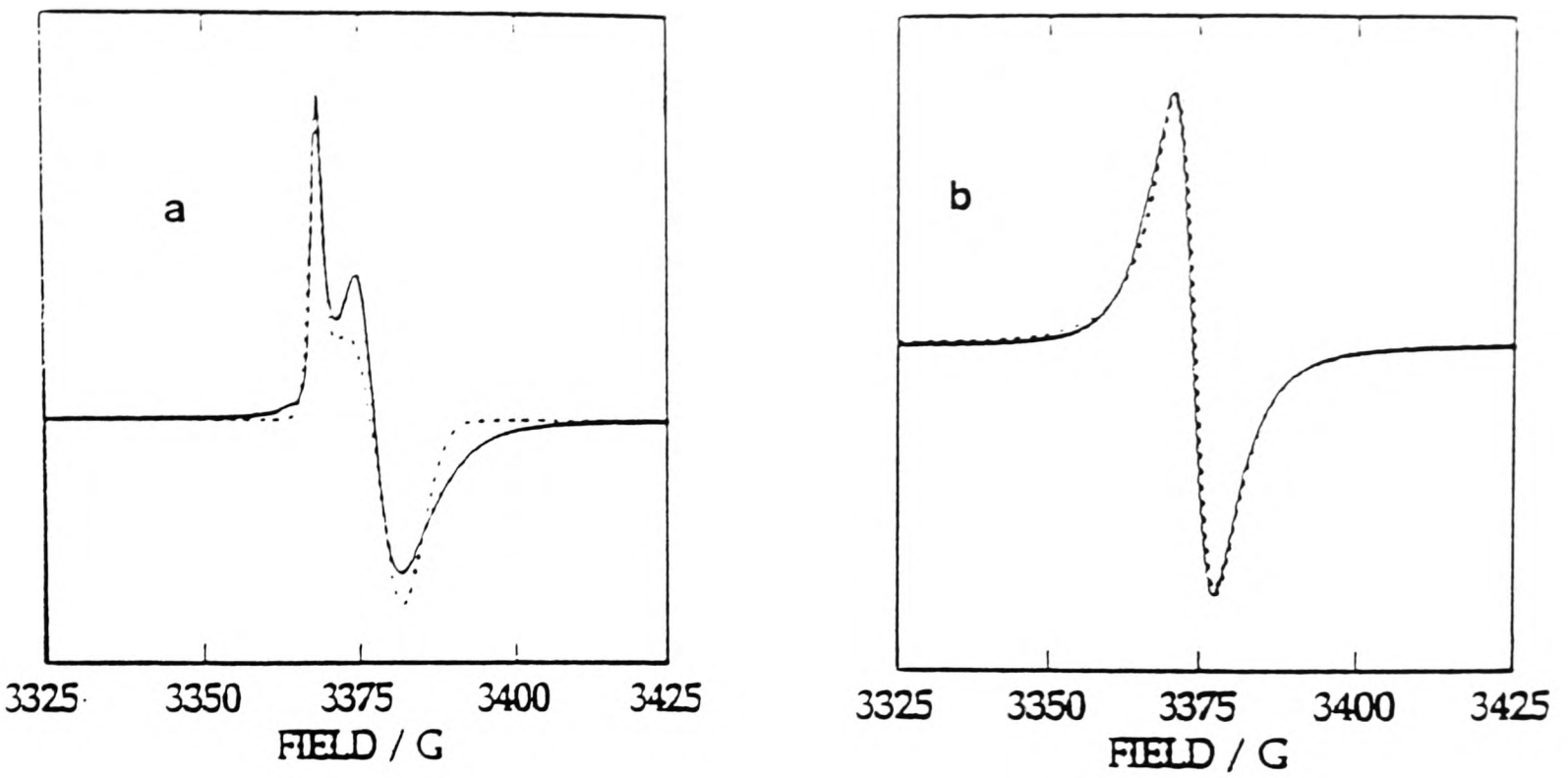


Figure 3.2.1. ESR spectroscopy studies at 4.5K of a) $Na(18\text{-}c\text{-}6)C_{60}.3thf$[57] in 2-Methf and b) $CoCp_2^+C_{60}^-$ [57] in thf. c) Variable temperature ESR spectra of $CoCp_2^+C_{60}^-$ exhibiting a 'spike' at temperatures above 70K. d) Variable temperature ESR spectra,[34] in pyridine, of C_{60}^- generated by bulk controlled electrolysis, exhibiting the spike at temperatures above 130K.

of which are the difficulty of reliable preparations and the array of characterisation techniques required to obtain sufficient evidence for proof of a successful synthesis.

Powder X-ray diffraction has a central role in the characterisation of sodium containing C_{60} phases, obviously as a structural probe, but it is has limitations in determining phase purity. Solid state ^{13}C powder NMR spectroscopy is useful in determining the dynamics of C_{60} molecules within the lattice, but large linewidths prevent determination of the number and quantity of phases present. This is also the case for ^{23}Na NMR spectroscopy. However, solid state ^{13}C MASNMR provides invaluable data with regards to the number of phases and the amount of each present, due to small linewidths, a relatively large chemical shift range, and generally excellent signal to noise. A combination of the techniques above must be utilised for confidence in a particular structural model.

Powder X-ray crystallography cannot be used solely for a number of reasons. The lattice is usually of cubic symmetry, consequently relatively few peaks are observed as reflections of the same d_{hkl} occur at the same 2θ value. Peaks are generally broad, as is the case for all alkali metal C_{60} structures, because of the relatively small domains of diffracting material and most importantly the lattice parameter changes very little on intercalation of successive amounts of sodium. This is because of the good size match between the sodium cation and the tetrahedral site in the fcc C_{60} lattice e.g. a = 14.17Å for C_{60} and a = 14.189Å for Na_2C_{60}. Due to the broadness and small lattice parameter differences, a two phase mixture may give a diffraction pattern which appears to be from a single phase.

A further consideration is that all phases do not have the same structure factors and so peak intensities from different phases are not a good indication of the amount of each phase present. This is most readily observed in comparing powder X-ray patterns and ^{13}C MASNMR spectroscopic data of K_4C_{60}, as shown in figure 4.15.4.4 and 4.15.1.5. ^{13}C MASNMR spectroscopy shows that the K_4C_{60} samples are at least 95% pure whereas from powder X-ray crystallography the level of impurities appears much greater estimated simply from visual comparison of the relative peak heights. The difference in structure factors could be due to a number of possible reasons such as static or dynamic disorder, due to a bad size match between the cation and the interstitial site. This would increase the thermal displacement factors and reduce structure factors, especially at higher angles. A probable explanation is that structure factors are accidentally smaller for the phase in question throughout the measured range. It should also be noted that for the heavier alkali metals (K, Rb and Cs) a reduction in symmetry is observed from fcc for A_3C_{60} to bct for A_4C_{60}. This would reduce the number of equivalent reflections at a given d-spacing. In contrast, Na_2C_{60} is fcc and has strong peaks because of the good size match between sodium cations and the tetrahedral interstitial site in the fcc C_{60} lattice, resulting in a well ordered structure.

Scattering from sodium C_{60} intercalates is dominated by the C_{60} lattice because of the large molecular weight of C_{60} compared to sodium, and its rigid constitution. The rigid carbon cage allows a simplification to be made in determining some structures, by considering C_{60} molecules as spherical shells of electron density.

Peculiar to sodium intercalates of C_{60} is that the fcc structure is maintained on doping above the composition A_3C_{60}.[19, 20] This is a consequence of the smaller size of the sodium atom, and its cation, relative to the heavier alkali metals, allowing clusters of sodium atoms to exist at the octahedral site, as will be discussed in the next section. Several X-ray peaks are sensitive to the concentration of sodium doping within the C_{60} lattice. Compositions have been postulated as ranging from NaC_{60} to $Na_{11}C_{60}$ with solution phases between particular dopant levels. On increasing the doping levels, low intensity peaks become apparent due to reflections from planes of intercalated sodium atoms, but the differences are small for significant (± 10%) variations in the dopant concentration, which can be explained on the basis of the low atomic number of sodium, and disorder present within the octahedral site.

On intercalation of low concentrations of sodium (<3 per C_{60}) into the C_{60} lattice, the lattice parameter, *a*, does not significantly alter. For example C_{60} has a lattice parameter of 14.17Å compared to a value of 14.189Å for the well characterised Na_2C_{60} phase and 14.183Å for Na_3C_{60}.[9] As discussed in section 3.8.5. this has consequences for the proposed solution phases in the range NaC_{60} to Na_3C_{60}.

As a consequence of the above considerations, refinement by the Rietveld method has lower confidence limits than for standard inorganic lattices, especially with regard to the concentration of sodium present within the C_{60} lattice.

Finally, due to inherent weak diffraction from sodium C_{60} intercalates, synchrotron powder X-ray crystallography has been extensively used, which gives data with enhanced signal to noise and hence greater confidence can be placed in a proposed structural model.

3.3.1. Postulated Binary Sodium C_{60} Phases at Room Temperature.

A number of studies[19, 20, 25, 43] on the phase diagram of sodium C_{60} intercalates have been reported postulating phases including, and intermediate, of the compositions NaC_{60} and $Na_{11}C_{60}$, as shown in figure 3.1.2. The methods used to determine the structures and properties of these phases have not included ^{13}C MASNMR but have been reliant primarily upon powder X-ray crystallography. For the reasons outlined in section 3.3. and work presented in this chapter, doubts as to the accuracy of parts of the postulated phase diagram are present.

In line with the other heavier alkali metals phases, the saturated phase Na_6C_{60} and the compositions Na_3C_{60} and Na_2C_{60} were reported early in the field. All sodium intercalates retained the fcc structure of the parent C_{60} lattice in contrast to the bct

structures of A_4C_{60} and bcc structures of A_6C_{60}, (where A = K, Rb, and Cs). Synthesis of the Na_6C_{60} phase was by exposure of C_{60} powder to excess sodium, in a stainless steel tube, followed by distillation of unreacted sodium from the product. Magnetisation measurements showed that the Na_3C_{60} phase did not superconduct above 2K, although a superconducting transition temperature, T_c, of 16K had been proposed based on interpolation from other superconducting fcc alkali metal phases, as described in section 1.6.2. This has been ascribed to a phase transition on lowering the temperature, probably resulting in disproportionation to Na_2C_{60} and Na_6C_{60}. The reason given for this disproportionation is thought to be a consequence of the particularly bad size match between a sodium cation and the octahedral interstitial site. At higher temperatures the thermal motion of the sodium cation in the octahedral site is great enough to maintain a stable structure by what has been termed 'chemical pressure'.[20] On lowering the temperature, the thermal amplitude of motion decreases, and the chemical pressure drops to a degree where the structure cannot be maintained and disproportionation occurs. In the heavier alkali metal analogues the cation in the octahedral site does not require such large thermal amplitudes of motion because of its inherently larger size and so the fcc structure is maintained at lower temperatures and superconductivity is observed. It has been shown that by effectively increasing the size of the sodium cation in the octahedral site, for example by the coordination of ammonia ligands to form the cation $Na(NH_3)_4^+$, as in the compound $Na(NH_3)_4NaCsC_{60}$,[44] superconductivity is observed. By replacement of Na in the octahedral site of Na_3C_{60}, by Cs, the Na_2CsC_{60} fcc structure is stabilised at lower temperatures and superconductivity is observed with a T_c in accordance with figure 1.6.2.1. The K analogue undergoes disproportionation but the Rb compound retains its fcc structure down to 10K having an anomalous low T_c of 3K. For compounds with the composition $Na_2Rb_xCs_{(1-x)}$ it has been shown that the linear relationship described in section 1.6.2. is not strictly applicable.[45] These phases have the space group Pa3 and do display a linear relationship between T_c and *a* but with a larger gradient than the other alkali metal superconducting phases which have a Fm3m space group. It has been extrapolated that an increase in lattice parameter of 0.1Å above the maximum known so far will result in a T_c at approximately 300K.

It was demonstrated in a later report that the saturated phase of the sodium C_{60} phase diagram at room temperature does not correspond to Na_6C_{60} but that greater concentrations of sodium can be accommodated within the fcc C_{60} lattice.[19] The small size of atomic sodium and its cation allows sodium clusters to exist at the octahedral site. A maximum of nine sodium atoms in a body centred cube arrangement at the octahedral site, in addition to a sodium atom at each of the tetrahedral sites, gives what appears to be the limiting composition of $Na_{11}C_{60}$, as shown in figure 3.3.1.2. Structural characterisation of this compound has not been achieved. However, a

composition corresponding to $Na_{9.8}C_{60}$, has been refined, using the $Na_{11}C_{60}$ structural model with partial occupancies of the octahedral cube. The X-ray powder diffraction patterns of reactions with the compositions $Na_{11}C_{60}$ and $Na_{12}C_{60}$ show peaks corresponding to metallic sodium indicating the saturated phase of sodium C_{60} intercalates is approximately $Na_{9.8}C_{60}$.

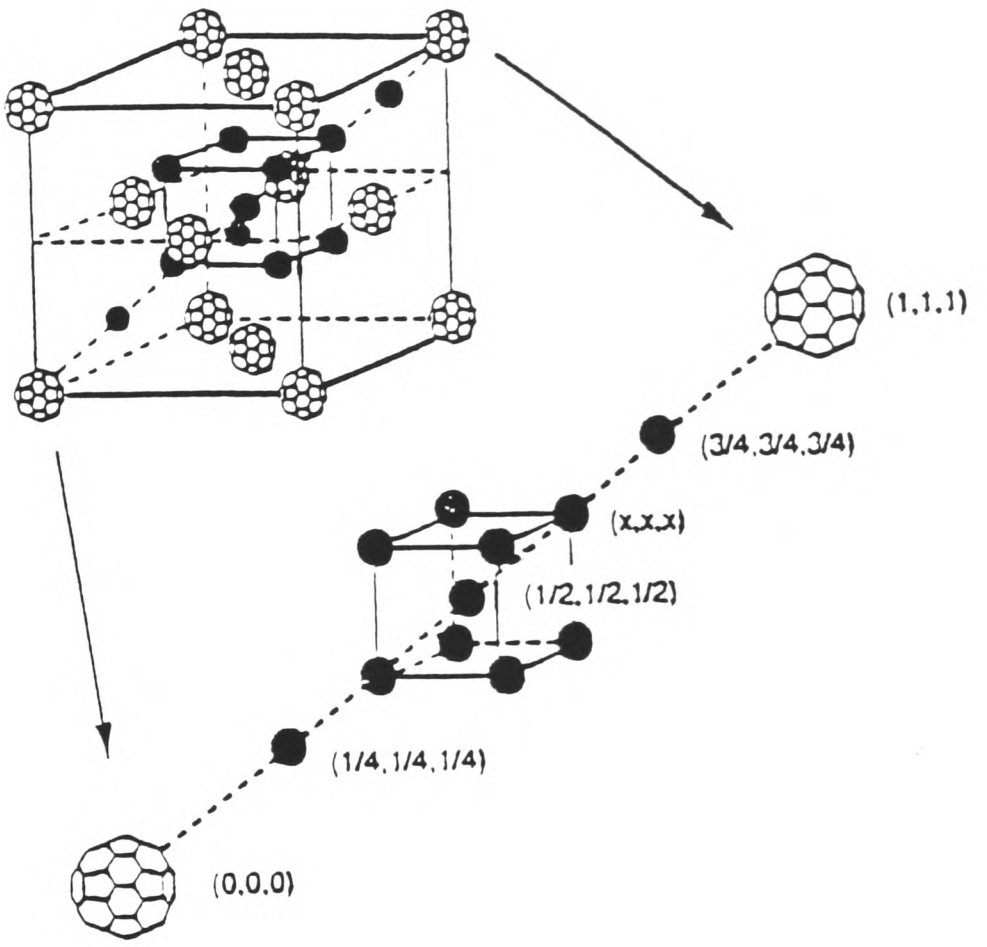


Figure 3.3.1.2. The powder X-ray crystal structure of $Na_{9.8}C_{60}$ is best refined by incorporating sodium clusters at the octahedral site.

It should also be noted that at sodium concentrations above Na_6C_{60} minority hexagonal phases can be observed in the powder X-ray diffraction patterns.

Throughout the whole range of sodium C_{60} intercalates the fcc structure is retained. This allows the possibility that solid solution phases may be possible and indeed this has been postulated as occurring between NaC_{60} and Na_3C_{60}, and possibly throughout the whole compositional range. One particular study[25] where phases with the gross composition between NaC_{60} and Na_3C_{60} has been reported, utilising variable temperature synchrotron X-ray crystallography and differential scanning calorimetry. Depending on the concentration of sodium the first order structural phase transition observed for pure C_{60}, from fcc to simple cubic, increased in temperature with

associated lower enthalpy changes. At the composition $Na_{2.8}C_{60}$ no transition was observed at all. Below the stoichiometry Na_1C_{60} disproportionation was observed to C_{60} and Na_1C_{60} but no data of this reaction was given.

3.4. Synthesis of Na_1C_{60}.5thf from Solution.

The solution chemistry of C_{60} has developed rapidly since the isolation of macroscopic quantities. However, solution chemistry of the anions is relatively unknown. Apart from charge transfer salts which are essentially reactions of C_{60} no chemistry has been reported of C_{60} anions in solution.

For instance, in the addition chemistry of inorganic substrates to C_{60} the only bonding mode observed to date is that of η^2 across a 6:6 ring fusion, as discussed in section 1.4. If a reagent such as NaC_{60} was used different bonding modes may result. The ionic nature of the anions would also allow homogeneous reactions in polar solvents such as thf, MeCN, DMSO and EtOH, in which C_{60} is completely insoluble.

There are several possible synthetic routes to Na_1C_{60} which would be rapid and efficient. Obvious candidates for the reduction of C_{60} are sodium mercury amalgam, sodium in liquid ammonia, sodium metal, and sodium naphthalide. However all of these reactions are essentially heterogeneous in as much as either the reducing species or C_{60} is insoluble in the reaction medium. This incompatibility leads to the unselective production of polyanions which can be insoluble or possibly react with the solvent medium, as shown schematically in figure 3.4.1.

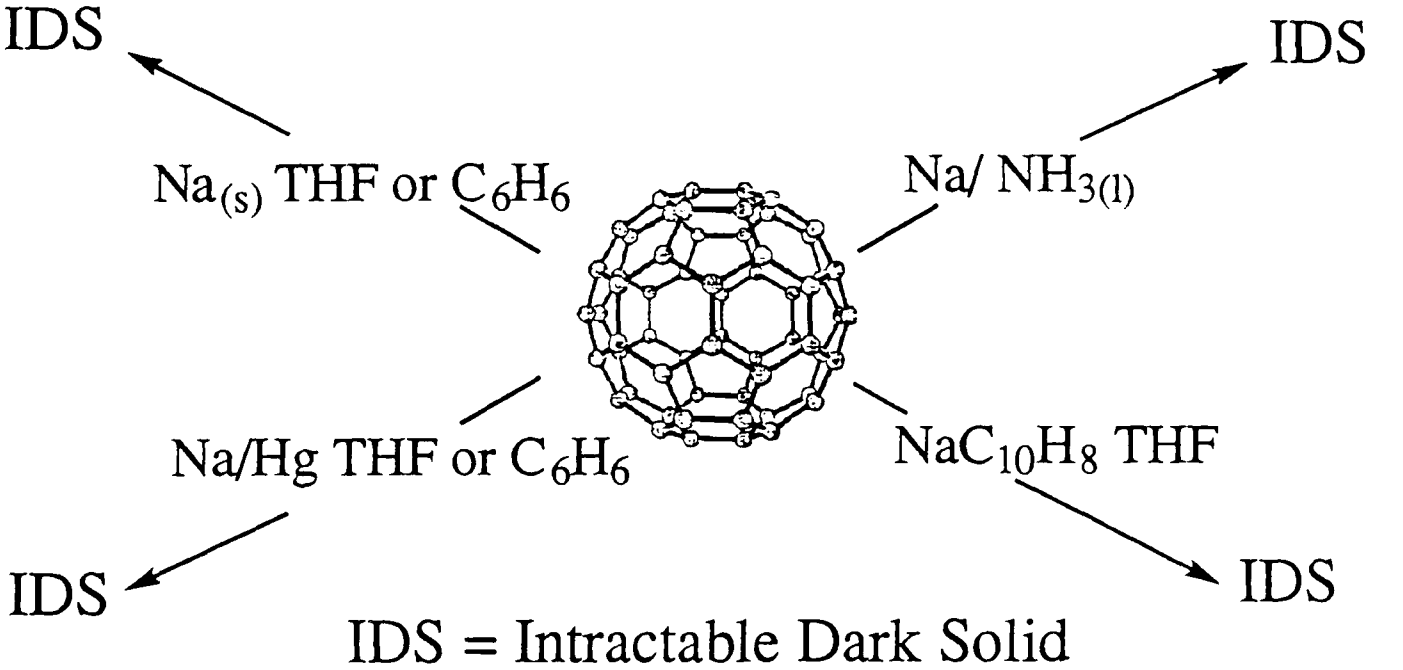


Figure 3.4.1. Routes attempted for the synthesis of NaC_{60} which gave inconclusive results.

To control the degree of reduction and hence the stoichiometry of the reaction a number of methodologies could be employed. The most obvious is to use a reagent which is only capable of reducing C_{60} to the oxidation state of choice, however, no such sodium reagent exists. A second method is to control the degree of reduction by kinetically trapping the desired product. This could be achieved by utilising the solubility characteristics of reagents and products in the reaction medium.

Solvents such as toluene, benzene and carbon disulfide are capable of

solublising C_{60} but more polar solvents such as thf, acetonitrile, diethyether, dimethysulfoxide and dimethylformamide are not. In contrast, salts containing C_{60} monoanions tend to have the opposite solubility characteristics. They dissolve in thf, acetonitrile, etc but are insoluble in aromatic solvents.

If a reagent capable of reducing C_{60} is soluble in, for instance toluene, then reaction in this medium would result in precipitation of a salt containing C_{60} anions. This is the general strategy used in the synthesis of charge transfer salts described in section 1.5. Electron transfer can be from an electron rich species in solution or from the surface of an electrode, and can be very solvent dependent. The product formed can depend on the reaction medium, with respect to the number of electrons transferred and solvent molecules possibly occluded in the solid, and on the rate of reaction, with respect to the dimensions and structure of a crystalline material.

A suitable reagent which is capable of reducing C_{60}, based on the electrochemical data available is the metallocene anion $Mn(Cp^*)_2^-$ which can be synthesised as the sodium salt.[46] Cyclic voltammetry of manganocene in solution shows it has two one electron reversible couples at -0.56V (+1/0) and -2.17V (0/-1) vs. SCE in MeCN, compared to C_{60} which has the first two reduction potentials at -0.4V (0/-1) and -0.8V (-1/-2) vs SCE in 1:1 CH_2Cl_2/toluene respectively. Assuming there are no drastic solvent effects, potentials indicate that a 1:1 mixture of C_{60} and $Mn(Cp^*)_2^-$ would result in a one electron reduction, as shown in equation 3.4.2.

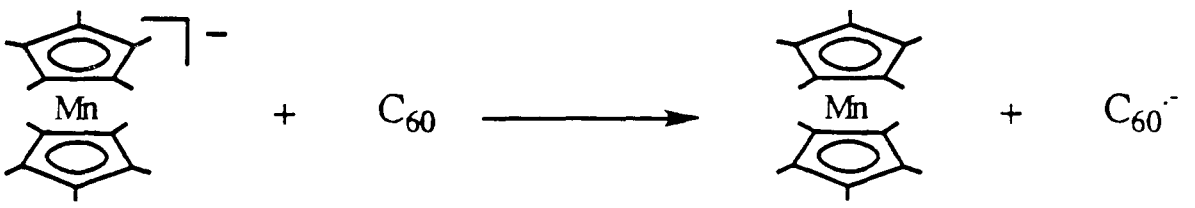


Figure 3.4.2. Electrochemical data suggests the above reaction should occur and that further reduction of a C_{60} monoanion by neutral manganocene should not occur.

The compound $Na\{Mn(Cp^*)_2\}$ is soluble in thf, reacts with MeCN, and is insoluble in aromatic and hydrocarbon solvents. However on addition of toluene to a concentrated thf solution, precipitation of $Na\{Mn(Cp^*)_2\}$ does not occur, presumably due to co-ordination of thf molecules to sodium cations. In the same ratio of thf:toluene, C_{60} can be solublised, permitting a homogeneous reaction.

On addition of a thf solution of one equivalent of $Na\{Mn(Cp^*)_2\}$ to a toluene solution of C_{60} a dark red solid immediately precipitates with a yellow supernatant. Subsequent characterisation of the supernatant by ^1H NMR spectroscopy and elemental analysis showed it contained all of the manganese in the form of $Mn(Cp^*)_2$.

The solid was extracted with thf giving a deep cherry red solution, and the remaining residue was a dark grey material that will be described in more detail in

section 3.5. On removal of the volatiles from the cherry red thf solution, a very dark purple microcrystalline solid precipitated. Subsequent analysis and characterisation showed this material to be NaC_{60}.5thf. It is very sensitive to dioxygen and moisture in solution and the solid state, and is soluble in thf, MeCN, DMSO, PhCN, EtOH and is slightly soluble in CH_2Cl_2.

3.4.1. Determination of the Quantity of thf Occluded in NaC_{60}.

Elemental analysis gave the stoichiometry as NaC_{60}.5thf. An independent method involved dissolving a known amount of NaC_{60}.*x*thf and ferrocene, in d_3-MeCN and integrating the subsequent ^1H NMR signals. Allowing a suitable relaxation delay of 20s integration of the signals, from two separately prepared samples, gave a stoichiometry of 4.9 and 5 thf molecules per formula unit assuming the other constituent species were sodium and C_{60}.

3.4.2. Structural Studies on NaC_{60}.5thf.

Analysis of the powder X-ray diffraction pattern of NaC_{60}.5thf was performed by Dr. M. J. Rosseinsky of the Inorganic Chemistry Laboratory, Oxford and molecular modelling using the BIOSYM software by Mark Green of the Inorganic Chemistry Laboratory, Oxford.

The capillary powder X-ray diffraction pattern of NaC_{60}.5thf, at 1.5406Å, shows a large number of closely spaced peaks that do not extend above 35° in 2θ, and signal to noise and resolution are poor. Using this data set indexing of the pattern was not successful.

Synchrotron radiation provides a method for improving signal to noise and resolution in powder X-ray diffraction studies. Data sets were collected at 0.8719Å over the range 2-30° in 2θ at Station 9.4 of the Daresbury Laboratory Synchrotron Radiation Source, Cheshire and the diffraction pattern is shown in figure 3.4.2.1. Indexing of the pattern gave a triclinic cell with the cell constants a = 12.68Å, b = 15.99Å, c = 10.09Å, α = 92.52°, β = 95.93Å and γ = 74.52Å, and V = 1962Å^3, which was the only good candidate found by the indexing program TREOR. The value of c, of 10.09Å, indicates that in this direction there could be a C_{60} - C_{60} contact. Comparison of this cell with a monoclinic cell proposed in the structure of tetrakis(dimethylamino)ethylene (TDAE) C_{60}[47] is shown in table 3.4.2.1. Cell constants reported[48] for (TDAE)C_{60} have been relabelled to allow comparison with the proposed cell for NaC_{60}.5thf.

The volume calculated from the unit cell dimensions of NaC_{60}.5thf indicates that two formula units comprise the unit cell. A C_{60} volume of 525Å^3 is calculated from a ball radius of 10Å, and assuming all non hydrogen atoms contribute 18Å^3 to the cell volume, a total estimated volume of 1986Å^3 is calculated for $(NaC_{60}.5thf)_2$. This is in good agreement with the value of 1962Å^3 obtained from the proposed unit cell.

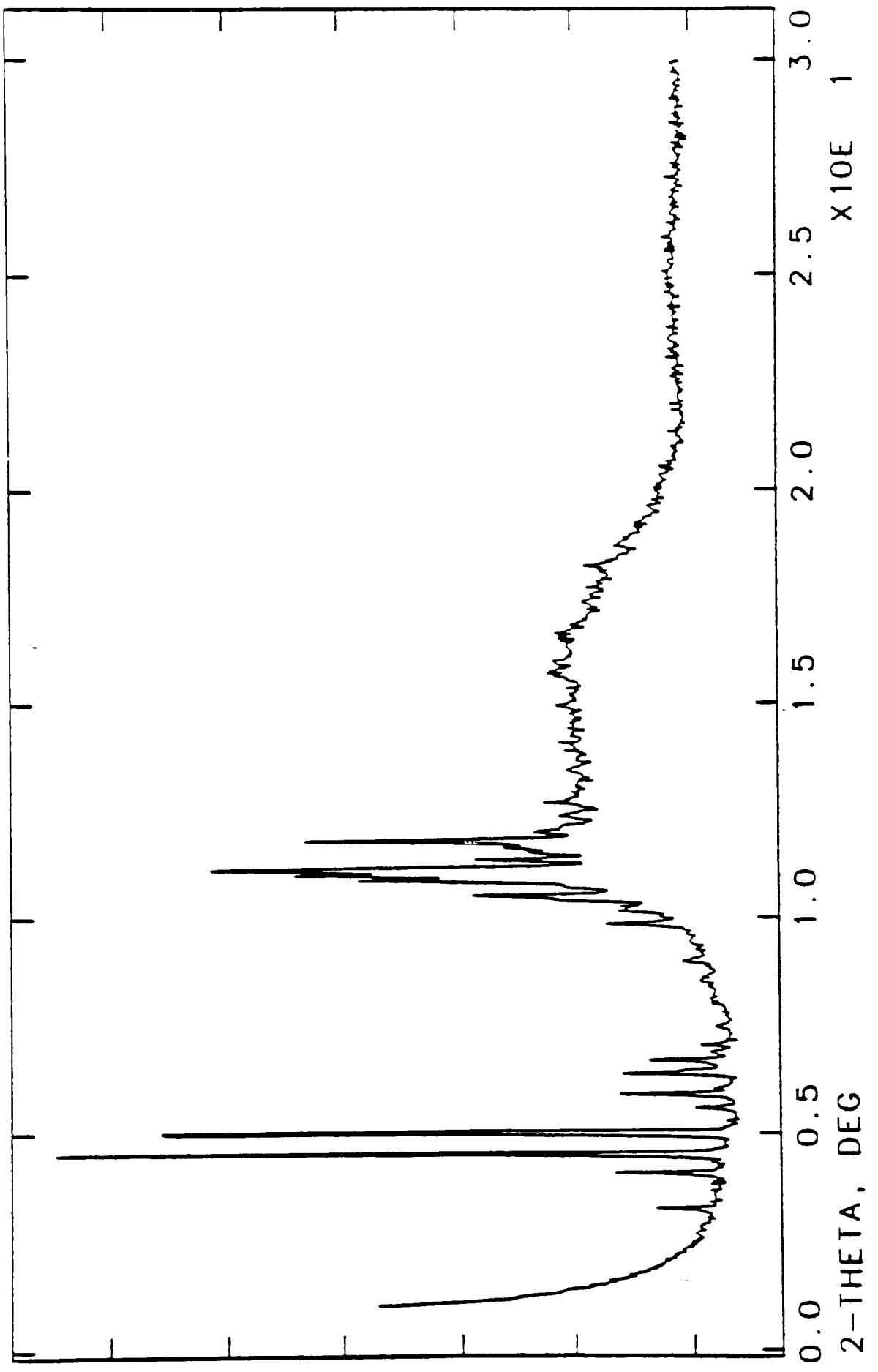


Figure 3.4.2.1. Synchrotron powder X-ray diffraction pattern of NaC_{60}.5thf collected with an incident wavelength of 0.8719Å.

BIOSYM software was used to construct various structural models and comparisons were made between calculated diffraction patterns and that obtained experimentally using synchrotron radiation. All analysis was done in the space group P1. Initial efforts were directed towards the positions of the C_{60} molecules as they tend to dominate the diffraction patterns of alkali metal compounds. A body centred arrangement of the C_{60} molecules within the unit cell did not give a satisfactory match between the calculated and experimental diffraction patterns. This was also the case for face centred models were C_{60} molecules were placed in the ac or bc faces of the cell or as close as possible to avoid the implication of bonding. However, on placing C_{60} molecules in the ab face calculation of the diffraction pattern showed marked similarities to the experimental powder diffraction pattern.

Table 3.4.2.1.

Cell constants	NaC_{60}.5thf	(TDAE)C_{60}
a	12.68	12.785
b	15.99	15.807
c	10.09	9.859
α	92.52	94.02
β	95.93	90
γ	74.52	90
V	1962	2052

Figure 3.4.2.2. shows (TDAE)C_{60} along two of the monoclinic axis and compares this with a possible C_{60} based lattice from the proposed cell dimensions of NaC_{60}.5thf.

Molecular modelling using BIOSYM to reproduce the synchrotron powder X-ray diffraction pattern of NaC_{60}.5thf show that the proposed unit cell is a good candidate as all of the major features are reproduced as shown in figure 3.4.2.3. The C_{60} molecules in the ab face of the unit cell are displaced along the c-axis due to steric constraints between C_{60} molecules, resulting in zig-zag chains along the ab face diagonal. Adjacent chains could be in contact because of the 10.09Å distance along the c-axis creating planes of C_{60} molecules in contact with each other. In contrast the cell of (TDEA)C_{60} allows a C_{60} molecule to fit in the ab face of the monoclinic cell and the only C_{60}-C_{60} contacts, at least at room temperature, are along the c-axis creating chains of C_{60} molecules throughout the structure. A recently reported structure describes a $Na(thf)_6^+$ cation with psuedooctahedral geometry at the sodium centre.[49] By analogy a $Na(thf)^+$ cation with psuedotrigonalbipyramidal geometry was constructed using BIOSYM software. Attempts to position two of these fragments within the unit cell proved impossible due to steric constraints. However two equivalents of Na^+ and ten equivalents of thf can fit into the vacant cell volume if it is assumed that some of the thf

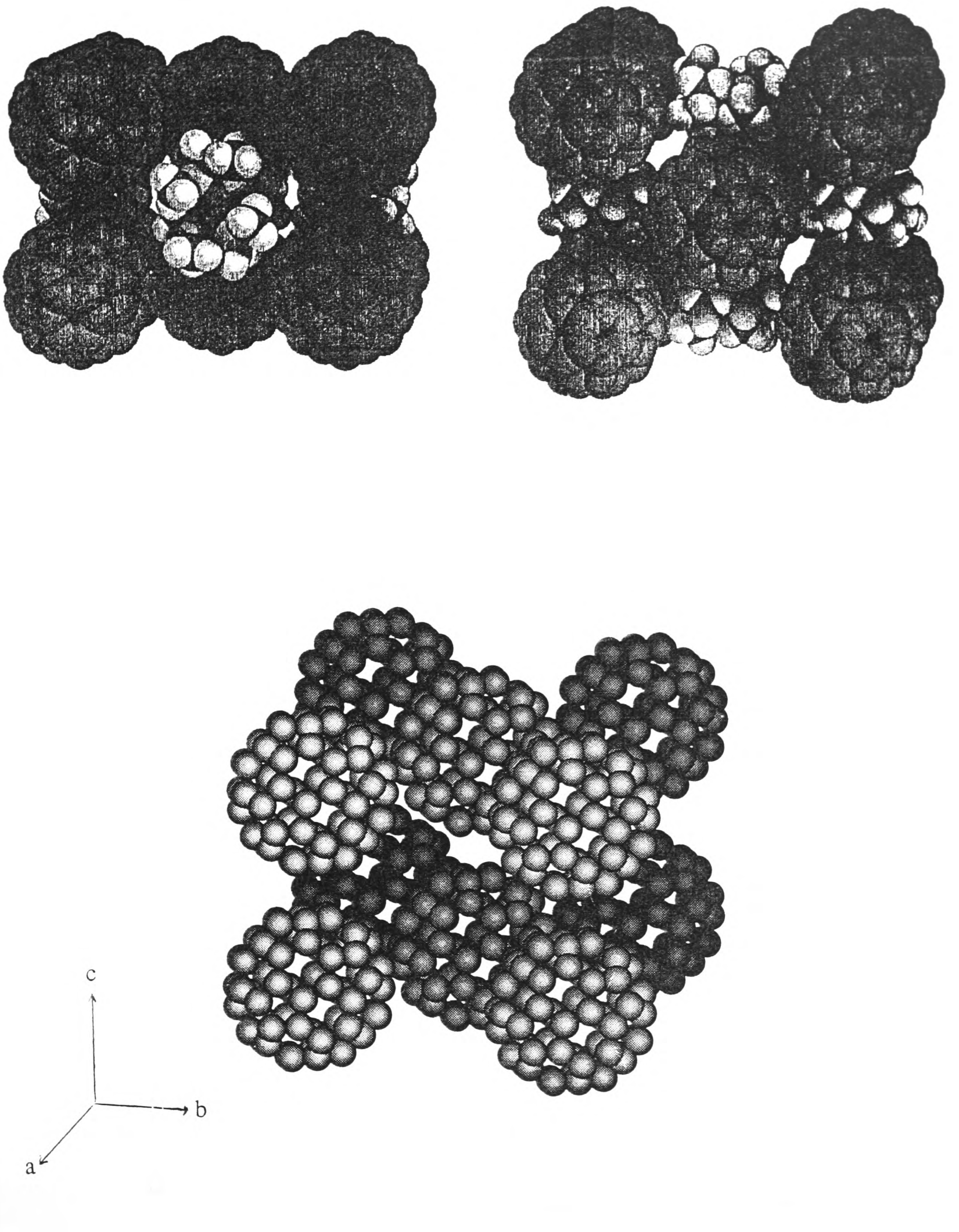


Figure 3.4.2.2. Comparison of the structure of TDAE-C_{60} and that proposed for NaC_{60}.5thf showing only the C_{60} lattice.

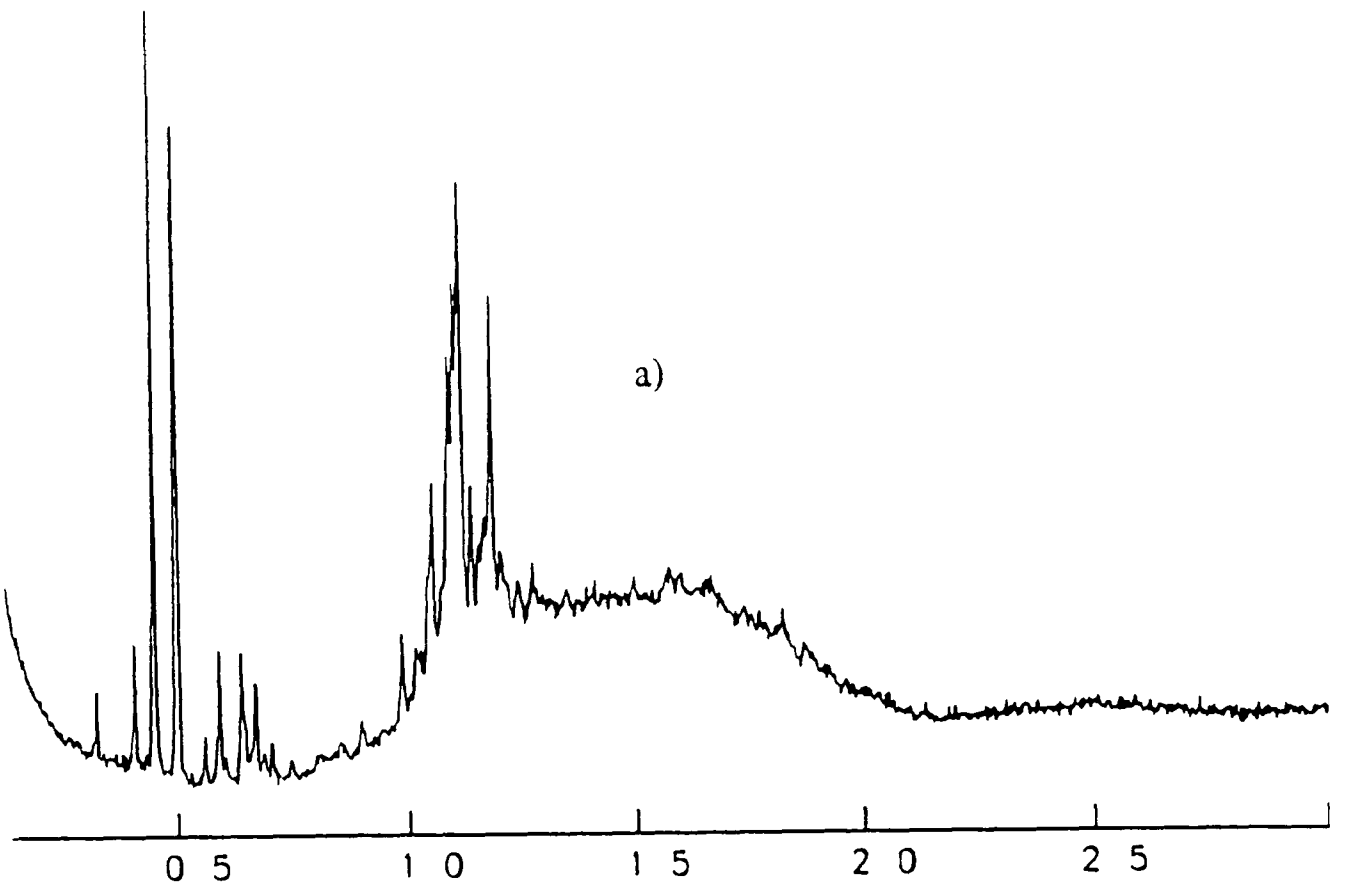


Figure 3.4.2.3. a) Experimental diffraction pattern and b) diffraction pattern from the proposed model generated using BIOSYM software.

molecules are not bound to a sodium cation. Location of the sodium cations is difficult due to the relatively low electron density of Na^+ and the presence of the solvent which appears to be somewhat disordered.

Further work to locate the thf molecules and sodium cations is in progress: the restricted diffraction range makes full structural characterisation difficult.

3.4.3. ^{13}C and ^{23}Na MAS and Powder NMR Spectroscopic Studies of NaC_{60}.5thf.

The NMR characteristics of C_{60} and its alkali metal intercalation compounds have been thoroughly investigated by ^{13}C, ^{23}Na, ^{87}Rb, and ^{133}Cs powder NMR spectroscopy and some work has also been reported on MASNMR spectroscopy. Powder NMR predominates for several reasons. Firstly, powder NMR, being a static technique, allows dynamic processes occurring within the solid sample to be investigated, and secondly sample containment is relatively straight forward being generally a sealed glass tube. This last point has two major advantages over MAS which requires, for sensitive materials, an air tight KEL-F container within the ceramic rotor, reducing the active volume and introducing background peaks from the carbon containing insert. Secondly, much lower temperatures can also be achieved with a static sample because differences in thermal expansion coefficients between rotor and rotor cap, and rotor and insert, are not a consideration. However, MASNMR provides far greater resolution than powder NMR, which is of primary consideration when relationships between chemical shift and structure, and sample purity, are the object of the investigation.

Variable temperature ^{13}C powder NMR spectra of NaC_{60}.5thf are shown in figure 3.4.3.1. At room temperature a single peak at δ 188ppm with a linewidth, υ, of 2kHz observed, corresponding to the ^{13}C's from C_{60} molecules. There is no apparent anisotropy to the lineshape and such a narrow line leads to the conclusion that the C_{60} molecules are spinning isotropically within the solid at ambient temperature. On cooling, anisotropy of the lineshape becomes evident indicating slower dynamics and a broad resonance centred at approximately δ 50ppm is apparent and tentatively assigned to the thf molecules. A large shift to lower field in the C_{60} resonance occurs on cooling due to a large change in the magnetic susceptibility consistent with a paramagnet.

If the change in chemical shift relative to C_{60} is plotted as a function of temperature a transition is evident at 170K, as shown in figure 3.4.3.2.

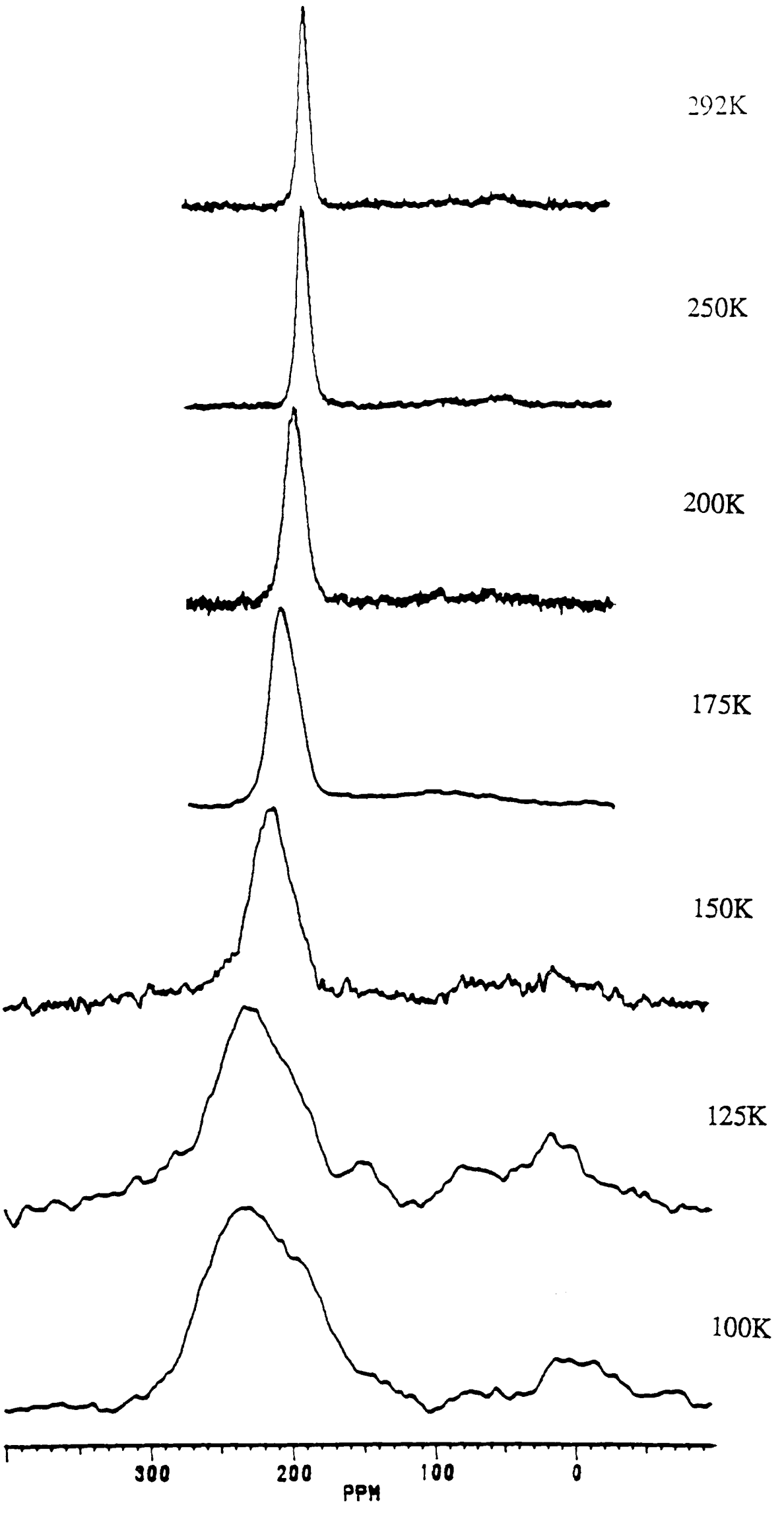
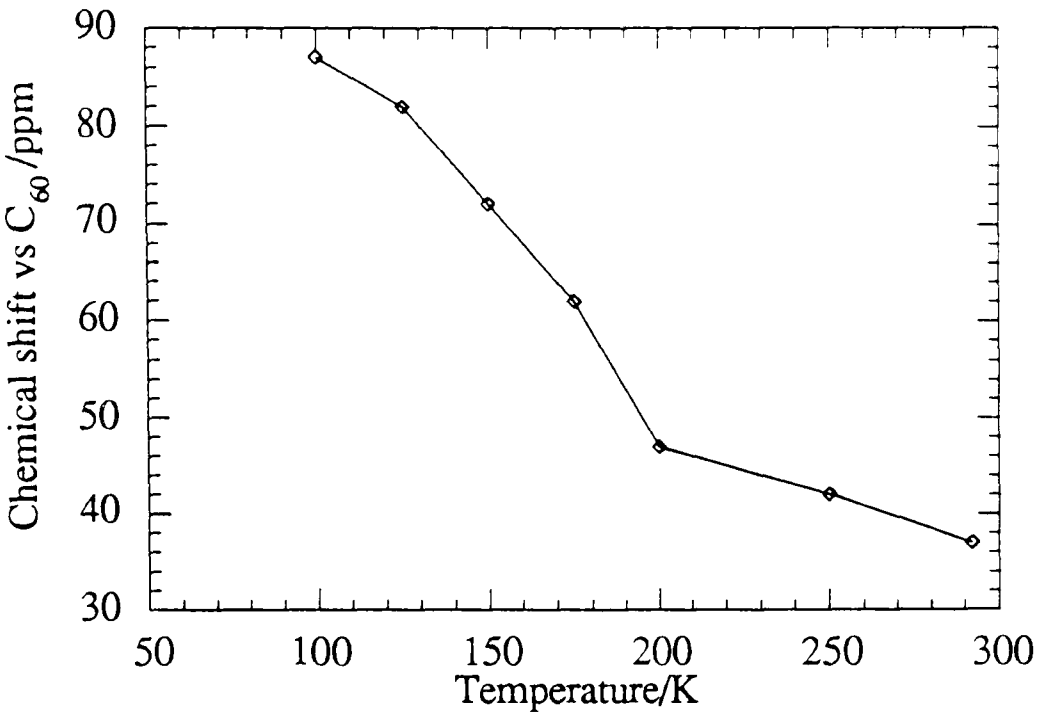


Figure 3.4.3.1. Variable temperature ^{13}C powder NMR spectra of $NaC_{60}.5thf$.



3.4.3.2. Chemical shift (relative to pure C_{60}) as a function of temperature for ^{13}C powder NMR spectra of NaC_{60}.5thf.

This transition will be discussed in more detail in the following sections.

^{13}C MASNMR spectroscopy at room temperature showed a single peak at δ 188ppm (υ < 100Hz), with no peaks apparent for the thf molecules present, as shown in figure 3.4.3.3. However, cross polarisation showed four peaks at δ 53ppm, δ 62ppm, δ 95ppm and δ 109ppm which may be assigned to the thf molecules, as shown in figure 3.4.3.3.

^{23}Na powder NMR spectroscopy yielded very little information apart from the observation that the sample contained sodium. A broad singlet is observed at δ 0ppm (υ = 12kHz) which remains unchanged on cooling to 100K, as shown in figure 3.4.3.4.

Figure 3.4.3.4. contains the ^{23}Na MASNMR spectrum of NaC_{60}.5thf which shows two major peaks, a sharp singlet at δ 9ppm and a broader resonance at δ -23ppm. At least two sodium sites are implied and a peak at δ -23ppm is consistent with Na^+ coordinated by oxygen ligands which have previously been reported to resonante in the range δ -3ppm to δ -32ppm. This resonance(s) could be attributed to $Na^+(thf)_x$ species. The peak at δ 9ppm cannot easily be assigned without knowledge of the crystal structure of this material but the small linewidth implies a symmetric site.

3.4.4. Magnetic Measurements of NaC_{60}.5thf.

A SQUID magnetometer was used to investigate the magnetic properties of NaC_{60}.5thf under an applied magnetic field as a function of the field strength and temperature.

Measurements of the bulk static magnetic susceptibility as a function of field

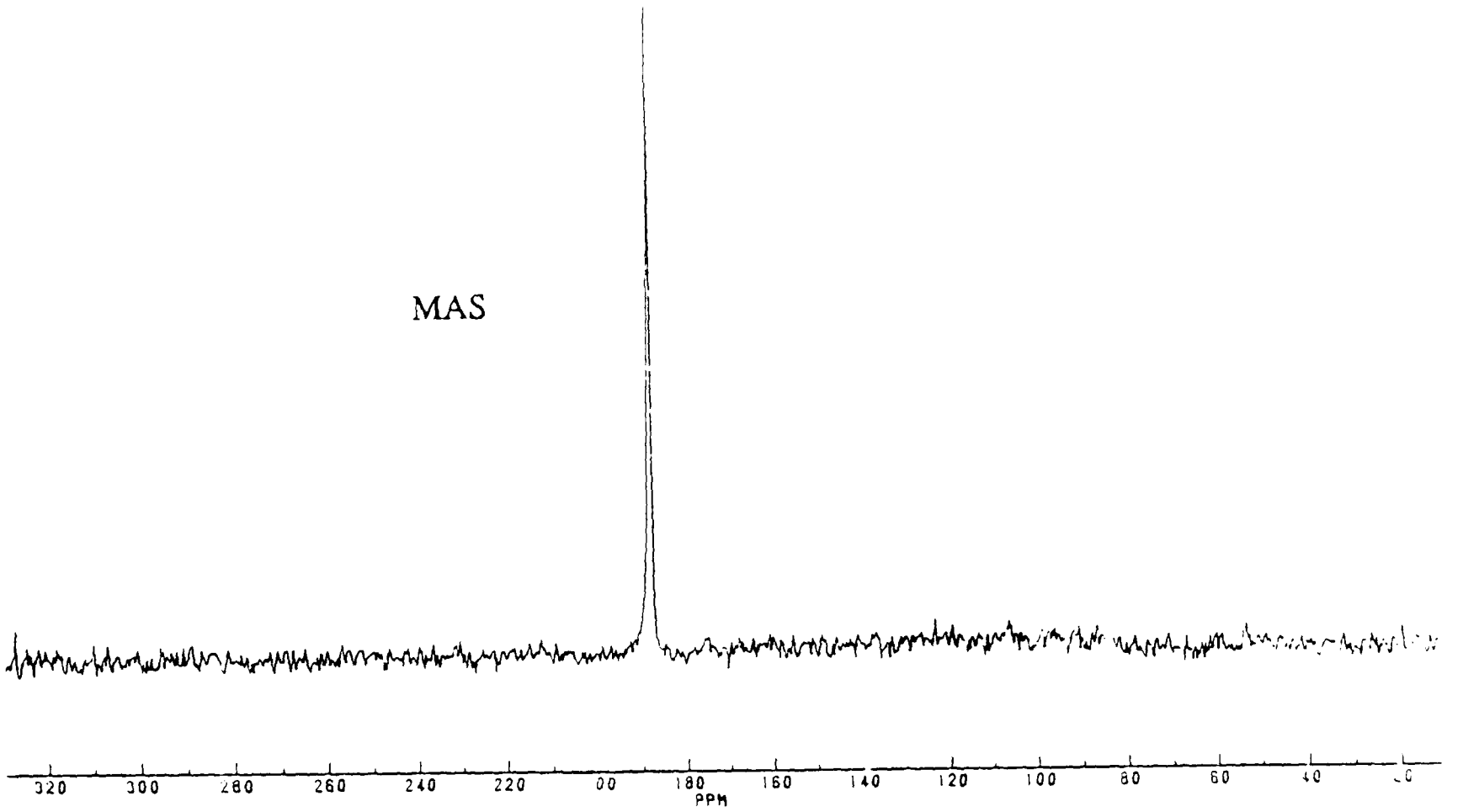


Figure 3.4.3.3. ^{13}C MASNMR and CPMASNMR of NaC_{60}.5thf.

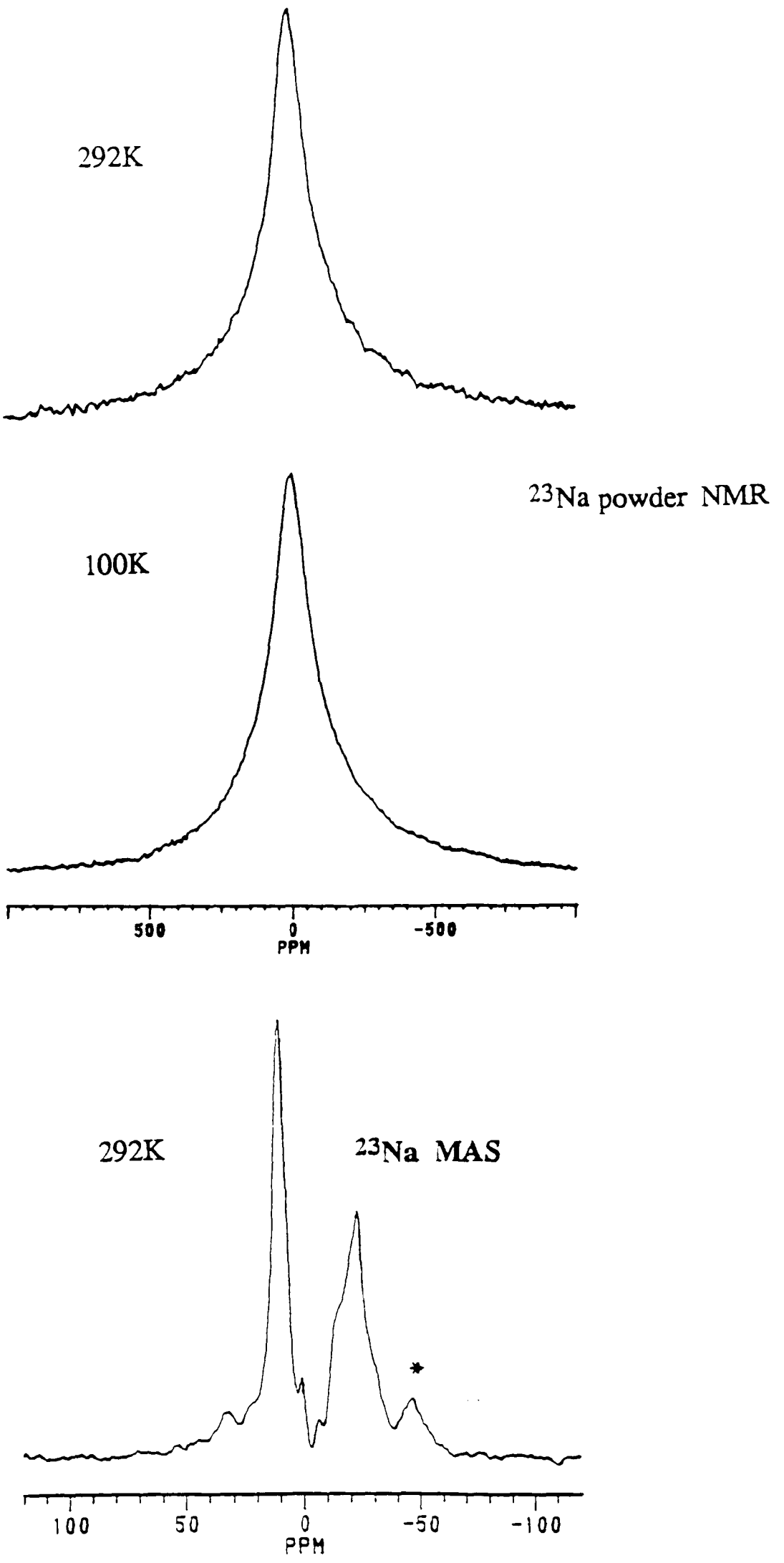


Figure 3.4.3.4. ^{23}Na powder and MASNMR of NaC_{60}.5thf at the temperatures indicated.

strength were also performed at 6 and 250K and showed a linear relationship with no hysterisis or saturation at high fields. Figure 3.4.4.1. shows the molar susceptibility as a function of temperature in a field of 0.5T.

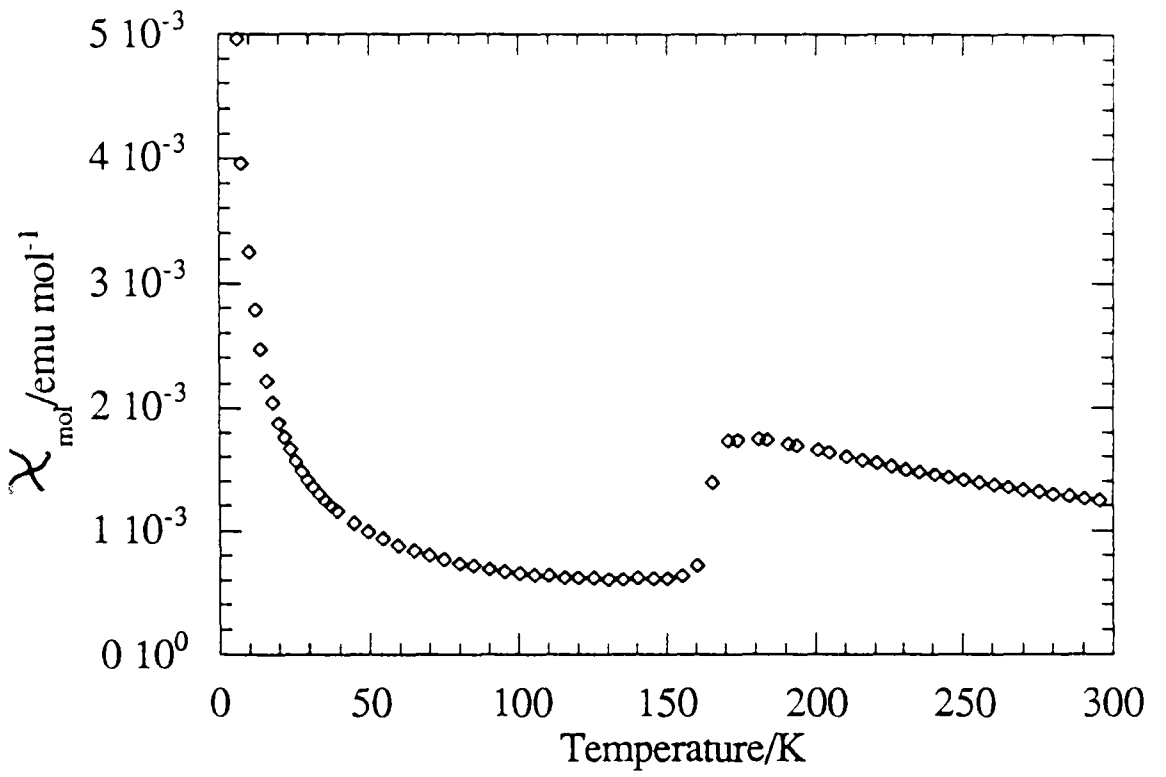


Figure 3.4.4.1 Molar susceptibility as a function of temperature for $NaC_{60}.5thf$, at an applied field of 0.5T.

On warming the sample from 6 - 300K a transition is evident at approximately 180K where the susceptibility suddenly increases. After correction for the diamagnetism of the sample and sample container, a plot of the inverse bulk static magnetic susceptibility versus temperature, above 200K, obeys the Curie-Weiss law,[50] shown in equation 3.4.4.1.

$$\chi = \frac{Ng^2\mu_B^2 S(S+1)}{3kT} \qquad \text{Equation 3.4.4.1.}$$

Where χ is the molar susceptibility, C is the Curie constant, θ is the Weiss constant , a measure of the short range interaction between paramagnetic ions, N is Avogadro's constant, g is the Lande factor, μ_B is the Bohr magneton, S is the total spin, and k is Boltzmann's constant.

The 'effective magnetic moment' can be calculated using equation 3.4.4.2.

$$\mu_{eff}^2 = \frac{3kT\chi}{N\mu_B^2} \qquad \sim 8C \qquad \text{Equation 3.4.4.2.}$$

Where μ_{eff} is the effective magnetic moment.

Above 200K the data fits for a S = 1/2 system with a Weiss temperature, θ, of -78K, as shown in figure 3.4.4.2.

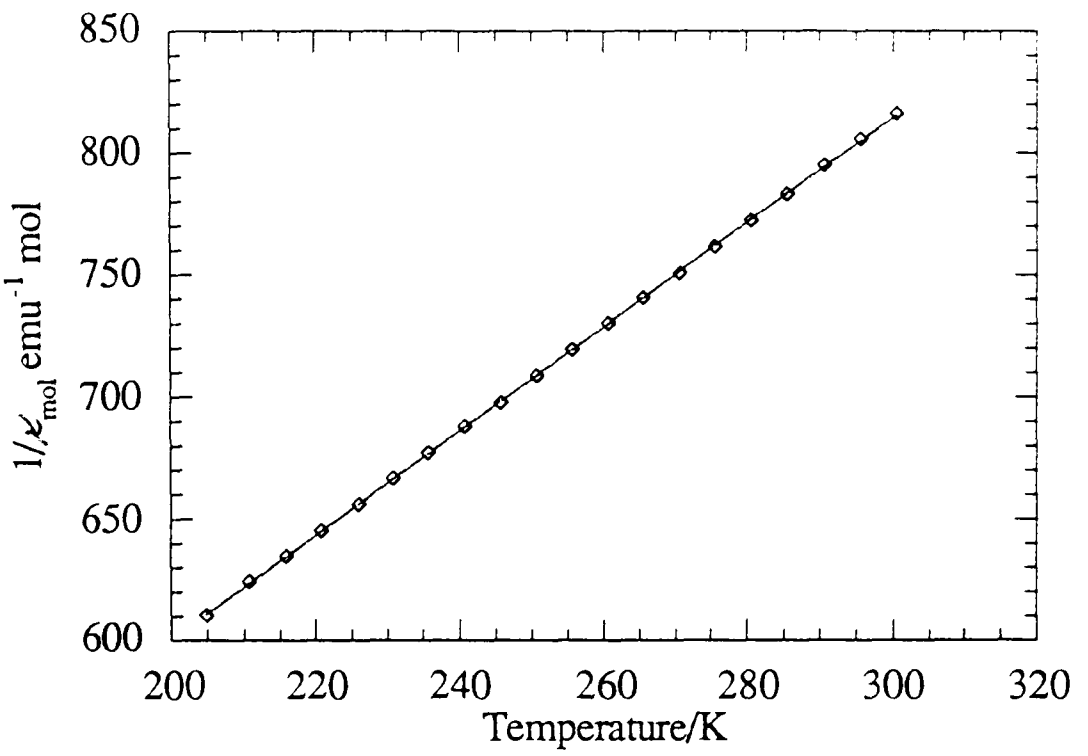


Figure 3.4.2.2. Plot of the inverse bulk static susceptibility as a function of temperature above 200K for NaC_{60}.5thf. The susceptibility has been corrected for the container, by a pre scan, and core electron diamagnetism, using a diamagnetic constant of -400 x 10^{-6} emu mol^{-1}.

A plot of the effective magnetic moment versus temperature is shown in figure 3.4.4.3. showing the marked transition at 180K, where the low temperature value is approximately half of that found at room temperature.

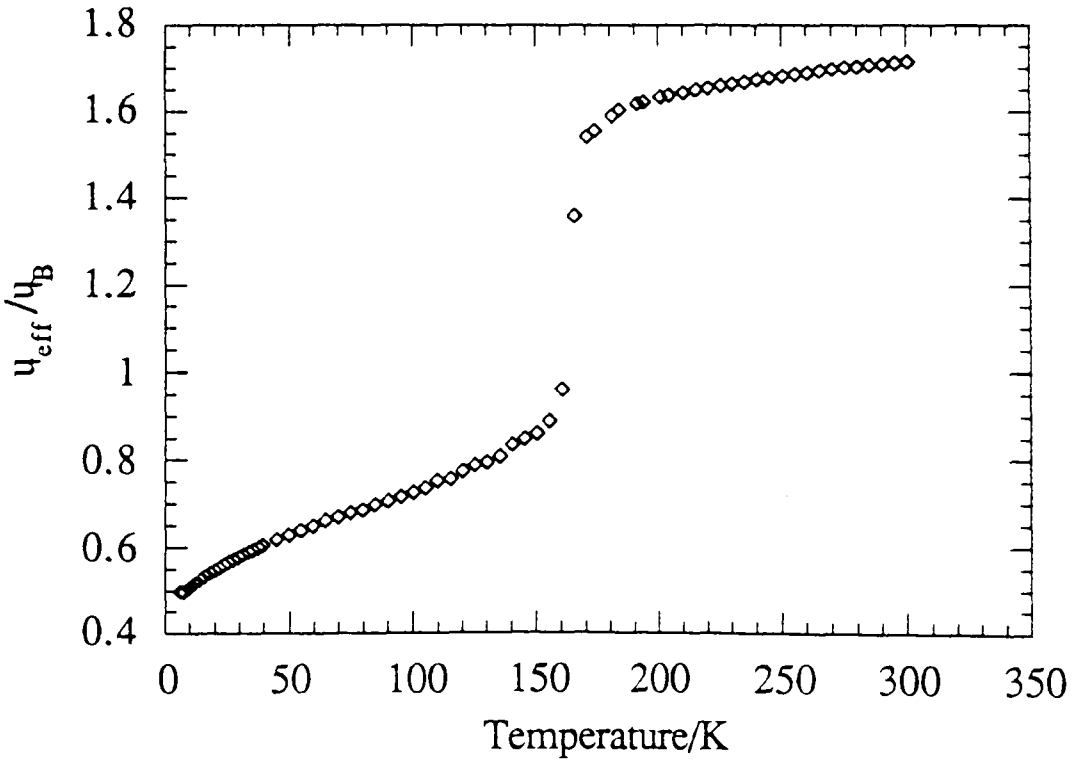


Figure 3.4.4.3. Effective moment as a function of temperature for NaC_{60}.5thf in an applied field of 0.5T.

It should be noted that even though the data above 200K seems to exhibit good Curie-Weiss behaviour, as shown in figure 3.4.4.2., the effective moment is not constant, reaching μ_{eff} =1.72 only at the highest temperature measured.

Below the transition the susceptibility as a function of temperature does not display Curie-Weiss behaviour, as shown in figure 3.4.4.4.

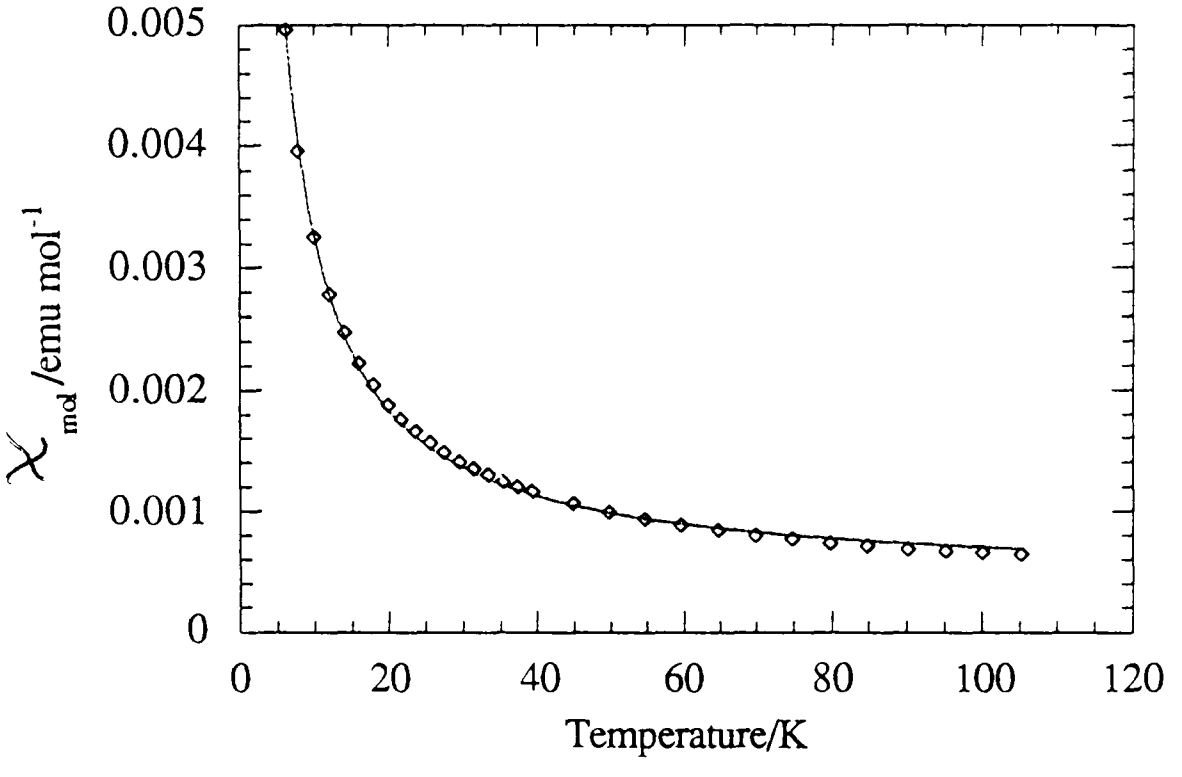


Figure 3.4.4.4. Susceptibility as a function of temperature below 110K for NaC_{60}.5thf and the fit (solid line) using equation 3.4.4.1., where A and C are the fitted parameters.

However, it is possible to fit the susceptibility (χ) data to equation 3.4.4.1.

$$\chi = A + \frac{C}{T} \qquad \text{Equation 3.4.4.1.}$$

Where A is a temperature independent susceptibility which may be due to a second order Zeeman effect which is the mixing of wavefunctions from excited states, that are not thermally populated, into the ground state wavefunction, or paramagnetism derived from a band structure. C is the Curie constant for a temperature dependent paramagnetism. Fitting these two parameters gave A = 3.20 x 10^{-4} emu mol^{-1} and C = 0.028 emu mol^{-1} K. Using equation 3.4.4.1, a value of C = 0.028 emu mol^{-1} K is equivalent to 7.8% of the sample being a paramagnetic species with S = 1/2 and g = 2.

It is very difficult to assign the temperature independent susceptibility to either a second order Zeeman interaction or paramagnetism due to band electrons without knowledge of the conductivity of the material. For comparison K_3C_{60} has a temperature independent paramagnetism of approximately 10 x 10^{-4} emu mol^{-1} in the normal

state.[51]

The high temperature data was also fitted to equation 3.4.4.1. and is shown in figure 3.4.4.5.

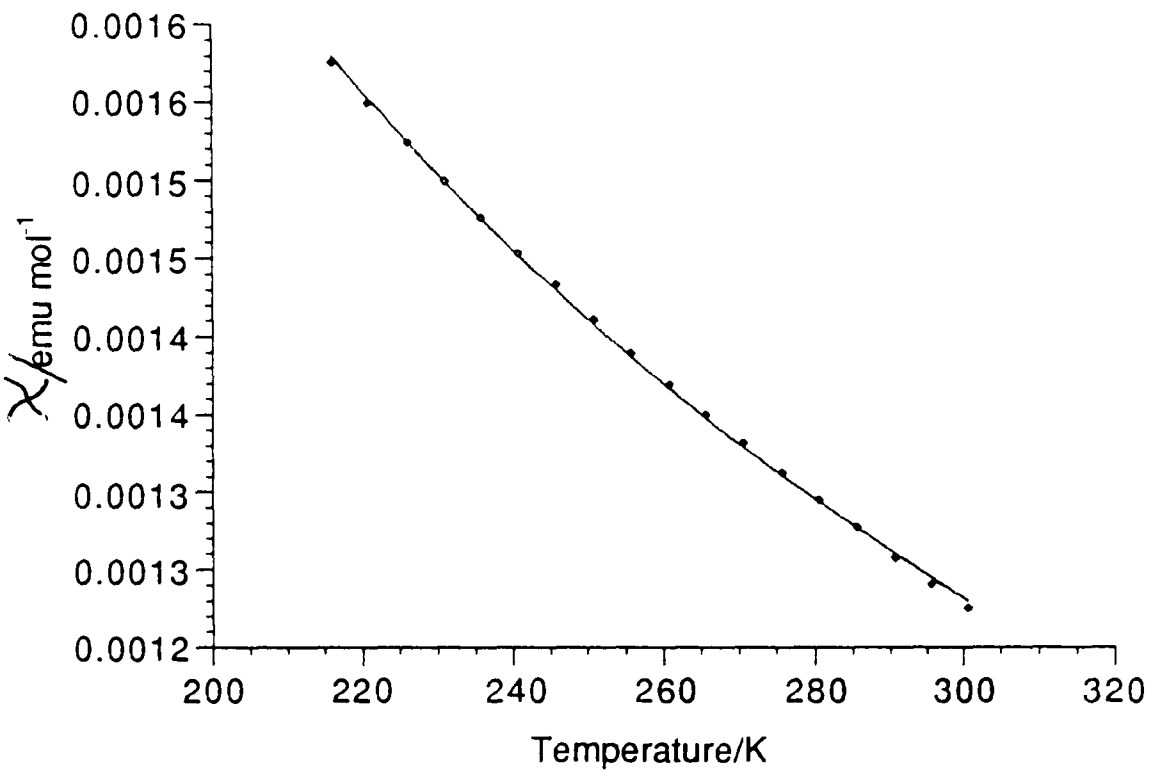


Figure 3.4.4.5. Fit of the susceptibility as a function of temperature using equation 3.4.4.1.

Values for the fitted constants are A = 3.4 x 10^{-4} emu mol^{-1} and C = 0.265 emu mol^{-1} K. A is in agreement with the low temperature data but C is only 70% of the value obtained when the high temperature data was fitted using the Curie-Weiss law.

If it is assumed the temperature independent paramagnetism is due to paramagnetism derived from a band structure then the observed molar susceptibility is a measure of the density of states at the Fermi level[52] and is described by equation 3.4.4.3.

$$n(E_f) = \frac{10e\chi_{mol}}{2\mu_B{}^2N_A} \qquad \text{Equation 3.4.4.3.}$$

Where $n(E_f)$ is the density of states at the Fermi level measured in orbital states per electron volt, e is the electron volt, μ_B is the Bohr magneton, and N_A is Avogadro's constant . The factor of 2 accounts for the fact we are dealing with orbital states not the total number of states and the factor 10 is a consequence of using χ_{mol} in cgs units.

The density of states calculation gives a value of 4.9 eV^{-1} using the value of A directly. Correction for the Landau diamagnetism associated with the band electrons assuming an effective electron mass equal to the free electron can easily be achieved using equation 3.4.4.3.

$$\chi_{Land} = -\frac{1}{3}\chi_{tip}$$

Equation 3.4.4.4.

A value of 6.6 eV^{-1} is now obtained. These are physically reasonable numbers. As a comparison, the density of states at the Fermi energy for the one dimensional metallic orthorhombic phases of Rb_1C_{60} and Cs_1C_{60}, estimated from NMR experiments, is $7eV^{-1}$,[6] whereas values of 17 and $21eV^{-1}$ are obtained for K_3C_{60} and Rb_3C_{60} respectively.[9]

Using the value for the density of states obtained from magnetisation measurements it is possible to calculate the magnitude of a possible Knight shift[53, 54] observed in the ^{13}C powder NMR spectra shown in figure 3.4.3.1. if an estimation of the hyperfine interaction can be calculated. The isotropic Knight shift is described by equation 3.4.4.5.

$$K_z = ha_{zz}\left(\frac{\gamma_e}{\gamma_n}\right)\chi^{(0)}$$

Equation 3.4.4.5.

$$\chi^{(0)} = \frac{1}{2}n(E_f)$$

Equation 3.4.4.6.

where K is the isotropic Knight shift, γ_e is the electron gyromagnetic ratio (1.768×10^7 rad $(sG)^{-1}$), γ_n is the nuclear gyromagnetic ratio ($^{13}C = 6.7263 \times 10^3$ rad$(sG)^{-1}$, and $\chi(0)$ is the normalised susceptibility calculated from the density of states as shown in equation 3.4.4.6. a_{zz} is the component of the hyperfine tensor parallel to the external field. In a powder the average isotropic hyperfine interaction, a, can be used but its value for NaC_{60}.5thf is not available. However it has been determined for Rb_3C_{60} and K_3C_{60} in their normal states and has a value of $2\pi \times 2.0 \times 10^6$ s^{-1}.[55] If this value is used in the calculation for the Knight shift for NaC_{60}.5thf then K = 72ppm. This is relative to the true chemical shift of NaC_{60}.5thf which is 180ppm at room temperature. At 100K the observed chemical shift is ~ 230ppm, 50ppm down field from the value at room temperature. In alkali metal fullerides the hyperfine interaction varies with crystal structure and on the degree of reduction of C_{60} molecules[13] which could account for the discrepancy between the calculated and experimental values.

3.4.5. ESR Measurements of NaC_{60}.5thf.

ESR measurements (X-band 9.5GHz) were performed on a solid sample of NaC_{60}.5thf and in a frozen thf matrix.

A few reports exist where the ESR spectrum of C_{60} monoanions have been recorded in the solid phase or in a glass solvent matrix.[34, 42, 56-63] Data for NaC_{60}.5thf is in qualitative agreement with observations reported to date. ESR spectra of NaC_{60}.5thf in a thf glass and the solid state at low and high temperature are shown in figure 3.4.5.1. In the frozen thf glass matrix two features are apparent, a broad signal with a temperature dependent linewidth and a narrow 'spike' , whereas the solid state ESR spectra does not show any evidence of the narrow resonance within the

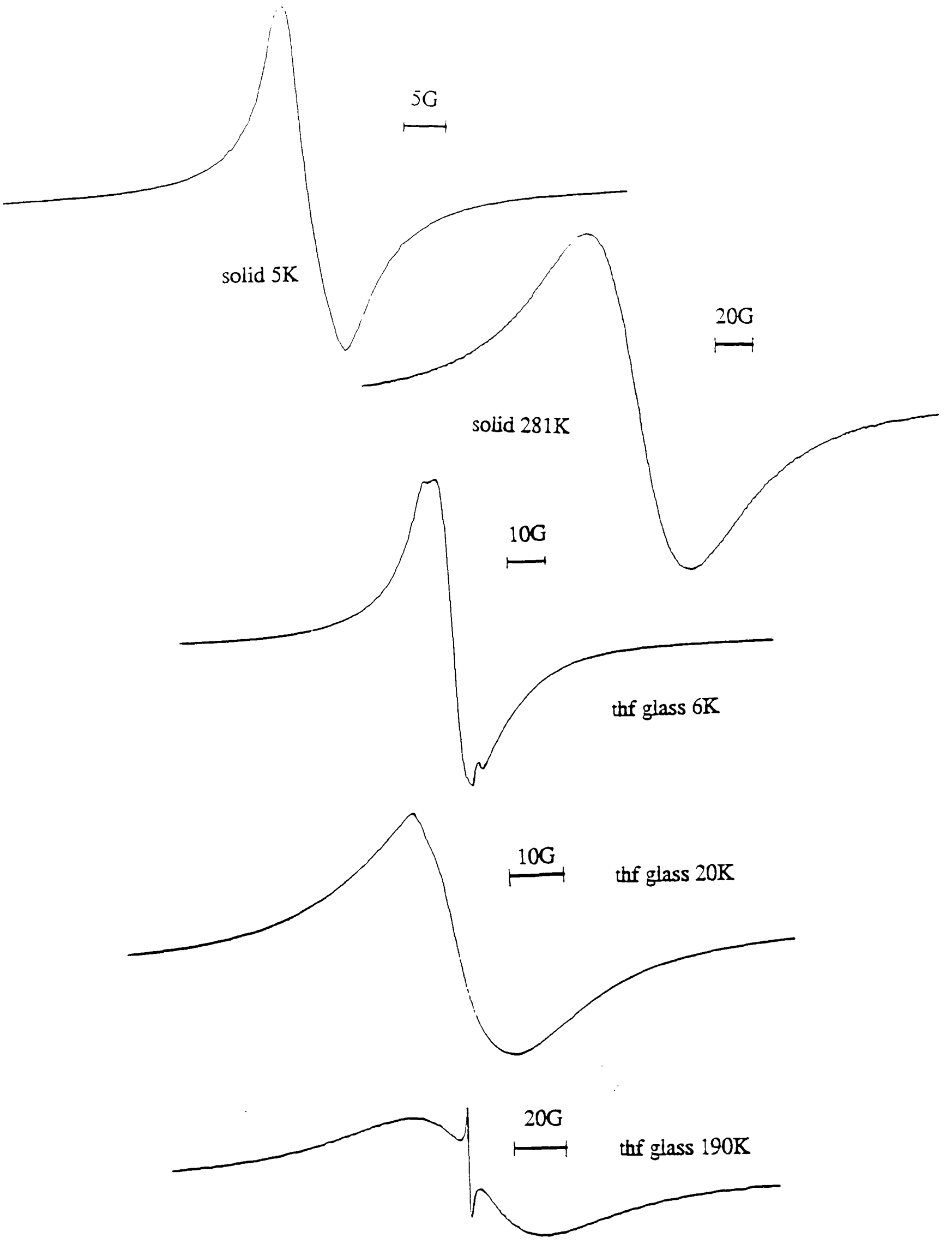
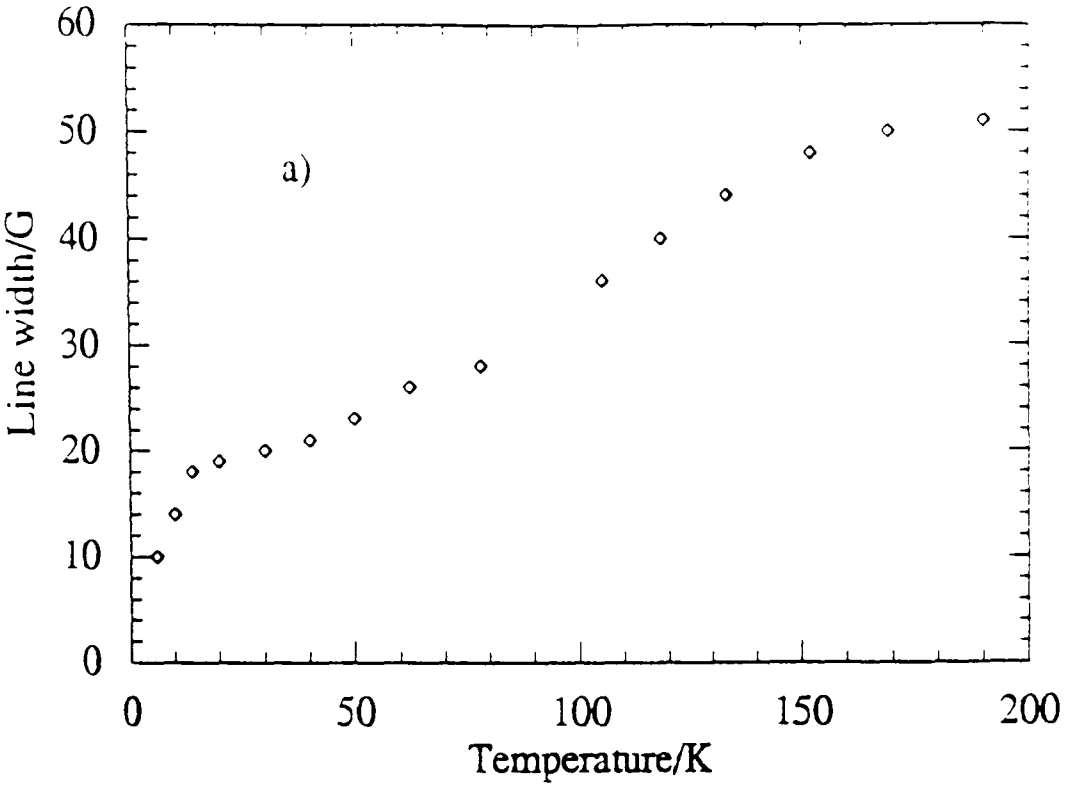


Figure 3.4.5.1. X-band ESR spectra of NaC_{60}.5thf in the solid state and as a thf glass at the temperatures indicated.



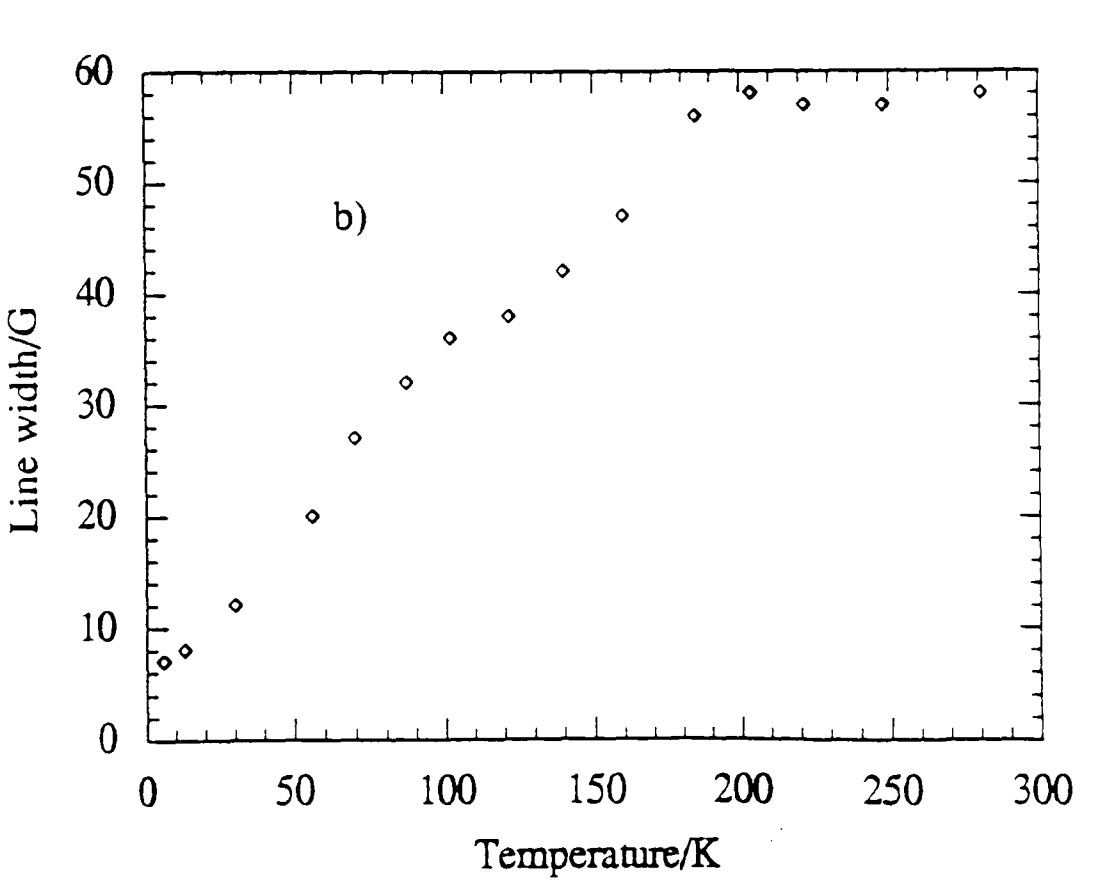


Figure 3.4.5.2.Linewidth as a function of temperature for $NaC_{60}.5thf$ in a) a thf glass matrix and in b) the solid state.

temperature range studied.

The most notable aspect of ESR spectra of C_{60} monoanions is the increase in the linewidth with increasing temperature, as shown in figure 3.4.5.2. for $NaC_{60}.5thf$ in the solid state and in a frozen thf glass respectively. It can be seen, in the thf glass the linewidth increases approximately linearly as a function of temperature whereas in the solid state the linewidth increases approximately linearly but is virtually constant above the transition. ESR spectral features, of C_{60} monoanions in a frozen solvent glass matrix, have been interpreted in terms of a distortion of the triply degenerate t_{1u} LUMO. Two possible situations could arise due to splitting of this level, as shown in figure 3.4.5.3.

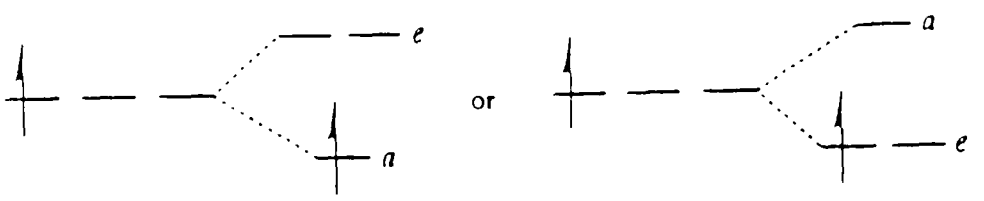


Figure 3.4.5.3. Possible frontier molecular orbital make-up of a C_{60} monoanion resulting from distortion of the C_{60} cage.

Intuitively the situation where the electron resides in a *a* state would be expected to occur because the alternative would be subject to a Jahn-Teller splitting. However, distortions due to compression or elongation of C_{60} along particular symmetry elements[57] can lead to the situation shown in figure 3.4.5.4.

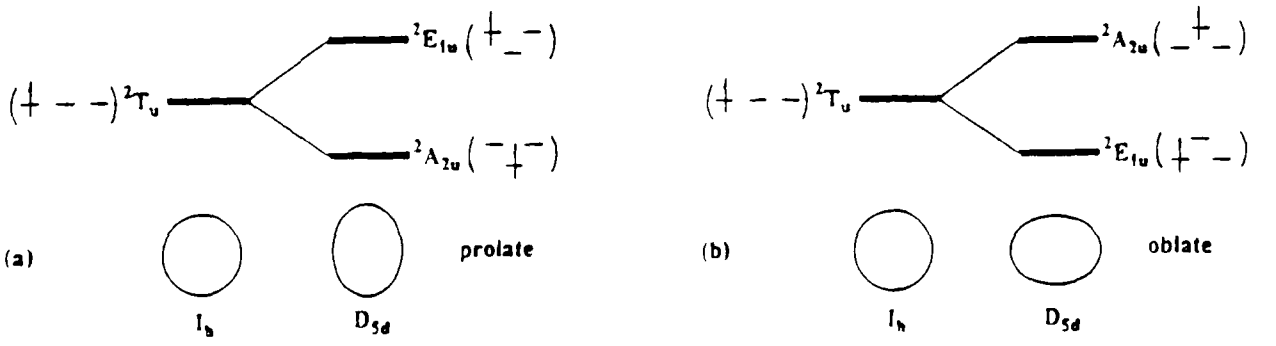


Figure 3.4.5.4. Possible splitting of the t_{1u} level from a Jahn-Teller distortion.

Kadish[34] and coworkers and Reed[57] and coworkers suggest distortion cannot explicitly be assigned to a Jahn-Teller effect because the C_{60} molecules are not in a totally symmetric environment. Environmental effects from the solvent and counterions were postulated as the probable cause of the distortion, probably in addition to an intrinsic Jahn-Teller distortion, and could account for discrepancies between various ESR spectra of the C_{60} monoanion derived from different sources, as shown in figure 3.2.1. It has also been noted that the broader feature does not saturate on increasing the power up to the maximum achievable with their instruments (200mW) whereas the sharp resonance does saturate.

Kadish[34] and coworkers reported that the narrow spike was due to an

equilibrium quantity of the C_{60} dianion, and that the temperature dependence of the linewidth of the broader feature is derived from lifetime broadening due to thermal averaging between the ground state and a low lying thermally accessible excited state .

However in a separate report Reed[57] and coworkers proposed that, in frozen glass matrices of C_{60} monoanions, the broad feature in the ESR spectrum is a consequence of a $^2E_{1u}$ ground state and the narrow 'spike' from a thermally populated $^2A_{2u}$ state, and that the calculations used to account for the spike by Kadish *et al*, on the basis of disproportionation, were incorrect by an order of magnitude. However the origin of the temperature dependence of the linewidth was not discussed.

With regard to the origin of the 'spike', in frozen glass matrices of the C_{60} monoanion, it is probably due to the thermal population of a $^2A_{2u}$ state rather than equilibrium disproportionation to C_{60} and C_{60} dianion because the equilibrium concentration of C_{60}^{2-} in a C_{60}^{-} solution derived from the Nernst equation is to small (<0.01%) to account for the concentration present (~1%).

The linewidth dependence of the broad feature, of frozen glass solvent and solid ESR spectra of the C_{60} monoanion is still unclear. Other possible causes for the broadening at high temperatures were explored by Kadish such as spin-spin exchange and electron transfer mechanisms but these were discounted on the basis of the low concentration of C_{60} monoanion present and the fact that the solution is frozen. The rotational correlation time for the ESR signal at 233K was calculated as approximately 10^{-9} s in agreement with the value obtained from ^{13}C powder NMR of solid C_{60} powder. Molecular rotation was discarded because 'there are no magnetic hyperfine interactions to be averaged or otherwise modulated by the rotation'. Solid state ^{13}C powder NMR of NaC_{60}.5thf does not show any evidence for the presence of thf unless cross polarisation techniques are used and even then the signal is very weak. Interaction between the paramagnetic C_{60} monoanion and ^{13}C's of the five equivalents of the thf present, via some mechanism or other, is the most probable reason for this observation. It should also be noted that in the ^{13}C powder NMR spectrum, as the temperature is lowered, rotation of the C_{60} monoanion molecules is reduced and a broad feature assigned to thf molecules becomes more evident, as shown in figure 3.4.3.1. It is probably conceivable that a spin-lattice relaxation mechanism mediated by molecular rotation of C_{60} molecules is responsible for line broadening observed in the solid state ESR spectrum of NaC_{60}.5thf and that by analogy the same is also the case for frozen solutions of C_{60} monoanions. A further point to note is that Kadish prepared solutions of C_{60} monoanions by bulk controlled potential electrolysis in various solvents and observed a solvent dependence in the linewidth

To date no detailed extensive studies on the ESR spectra of solids containing C_{60} monoanions has been performed. Variable temperature solid state ESR of the salt $PPh_4^+C_{60}^{\cdot-}.(PPh_4Cl)_2$, showed a linear variation in the linewidth of the ESR spectrum from 77 to 300K though saturation may becoming evident at higher temperatures. A

possible reason for saturation of the ESR linewidth in NaC_{60}.5thf at approximately 200K, is that the rapid rotation of the C_{60} molecules is reaching a limiting value. It has been noted that the correlation time of pure C_{60} powder obtained from ^{13}C powder NMR spectroscopy is only a third of the calculated gas phase value, as was discussed in section 1.2.2. Although coulombic interactions would be expected to slow the rotation of C_{60} monoanions in the solid state as observed by the ^{13}C powder NMR spectrum of NaC_{60}.5thf rotation is still remarkably rapid.

The intensity of the ESR signal is in qualitative agreement with SQUID measurements with a transition centred at 180K evident. At 6K, the solid state ESR spectrum has a slight asymmetry possibly resulting from metallic character of the sample and observation of a Dysonian signal.[64, 65]

The *g* value does not appreciably change with temperature being virtually constant at 1.996 for both the solid and solution state, slightly lower than the free electron value of 2.0023 and consistent with other reports.

3.4.6. Electrochemistry of NaC_{60}.5thf.

Investigation of NaC_{60}.5thf by electrochemical techniques was performed to confirm that the C_{60} cage was intact and that the C_{60} species present in solution was the monoanion.

The cyclic voltammogram of C_{60} has been recorded many times in the literature in a variety of solvents and supporting electrolytes. A CV of NaC_{60}.5thf recorded in thf with 0.1M tetra ^{n}butylammonium hexafluorophosphate showed that the only redox active species, within the voltage range of the experiment, had a trace consistent with that of C_{60}.

In a system such as C_{60}, where a number of reversible couples are present over a narrow voltage range, cyclic voltammetry is not very useful in determining the oxidation state of the species in solution. This is because where ever one begins the scan the applied potential will convert all the active species at the surface of the electrode to the oxidation state which is thermodynamically most stable. Assuming mass transport to the electrode surface is slow compared to the duration of the potential sweep, scanning over a particular voltage range, will produce very similar voltammograms no matter where the scan is initiated. This was found to be the case even at the highest scan rate used ($200mVs^{-1}$) with our equipment.

Linear sweep voltammetry would show that the C_{60} species was in a reduced form but identification of the oxidation state of the bulk solution species would not be readily possible.

A rotating disc electrode (RDE) works on the principle that by rotating an electrode rapidly, the rate of mass transport to the electrode surface can be varied in a controlled manner. Its application in the determination of the oxidation state of the

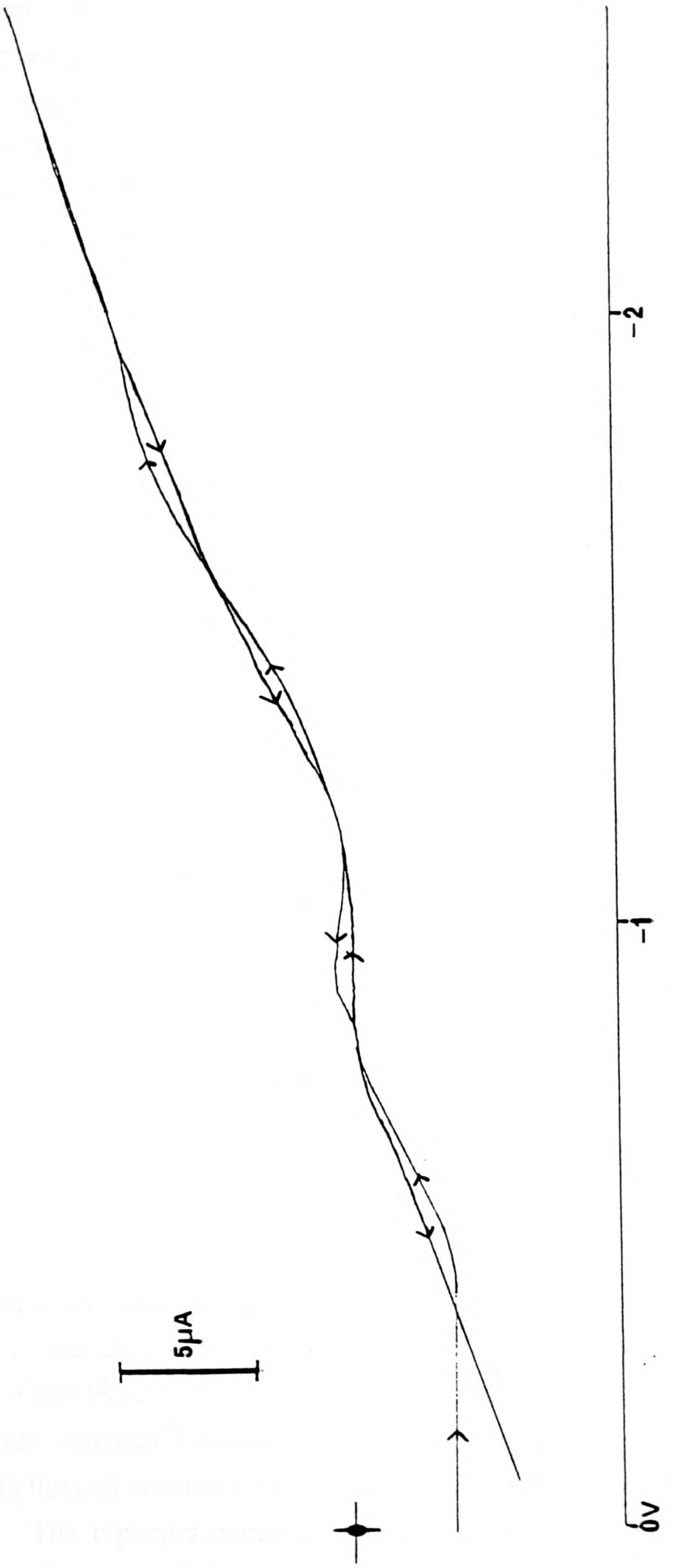


Figure 3.4.6.1. Rotating disc electrochemistry of $NaC_{60}.5thf$ in thf vs Ag/Ag^+, 900rpm.

electroactive C_{60} species in solution, derives from rapid mass transport of the bulk solution species to the electrode surface, compared to the duration of the potential sweep. At potentials where a C_{60} monoanion can be oxidised to neutral C_{60}, an anodic current will be recorded. As the potential approaches the 0/-1 couple the current decreases and remains zero over a certain potential range until the potential reaches the -1/-2 couple and a cathodic current is recorded. A current versus potential scan, of a thf solution of NaC_{60}.5thf, using a rotating disc electrode is shown in figure 3.4.6.1. This experiment was performed in collaboration with Zheng Chen of the Inorganic Chemistry Laboratory, Oxford. It can be seen that at the potential that corresponds to the 0/-1 couple of C_{60}, no current is observed, confirming that the bulk solution species is the monoanion of C_{60}. Irreversibility of the scan is attributed to adsorbed species at the electrode surface which has been observed previously.[31, 32]

3.4.7. UV-Vis Spectroscopy of NaC_{60}.5thf.

Spectroelectrochemical measurements of C_{60} in the mono-, di-, and trianion form have been recorded. Spectra of the monoanion of C_{60} do not significantly differ from that of neutral C_{60}, with a small red shift observed for the bands at 257 and 330nm respectively. UV-Vis spectroscopy of NaC_{60}.5thf was consistent with the reported data.[35]

3.5. Studies of the thf Insoluble Residue from the Synthesis of NaC_{60}.5thf.

After extraction of NaC_{60}.5thf from the reaction between C_{60} and $Na\{Mn(Cp^*)_2\}$ a dark grey residue remains that is insoluble in thf. This material was of interest because it caused losses in the yield of NaC_{60}.5thf. It is an air sensitive material decomposing essentially quantitatively to C_{60} as observed by ^{13}C MASNMR spectroscopy, as shown in figure 3.5.1.

3.5.1. Powder X-ray Crystallography and Formulation of 'The Residuals'.

Powder X-ray crystallography showed this material was highly crystalline having sharp peaks and a relatively excellent signal to noise ratio, as shown in figure 3.5.1.1 Indexing of the pattern was successful on a hexagonal unit cell of dimensions a = 15.338(2)Å, c = 9.933(3)Å and V = 2024Å^3. This is very similar to a recently reported material[29] formulated as $Na_xC_{60}thf_y$ where x = 0.39±0.03 and y = 2.2±0.7 having the cell constants a = 15.331(4)Å, c = 9.965(4)Å and V = 2049Å^3.

The reported material was synthesised by electrocrystallisation of C_{60} and $NaB(C_6H_5)_4$ in a chlorobenzene solution. Rod shaped 'single crystals' were harvested after 7 days but a single crystal structure determination has not as yet been reported.

Elemental analysis of these crystals proved to be variable with respect to the

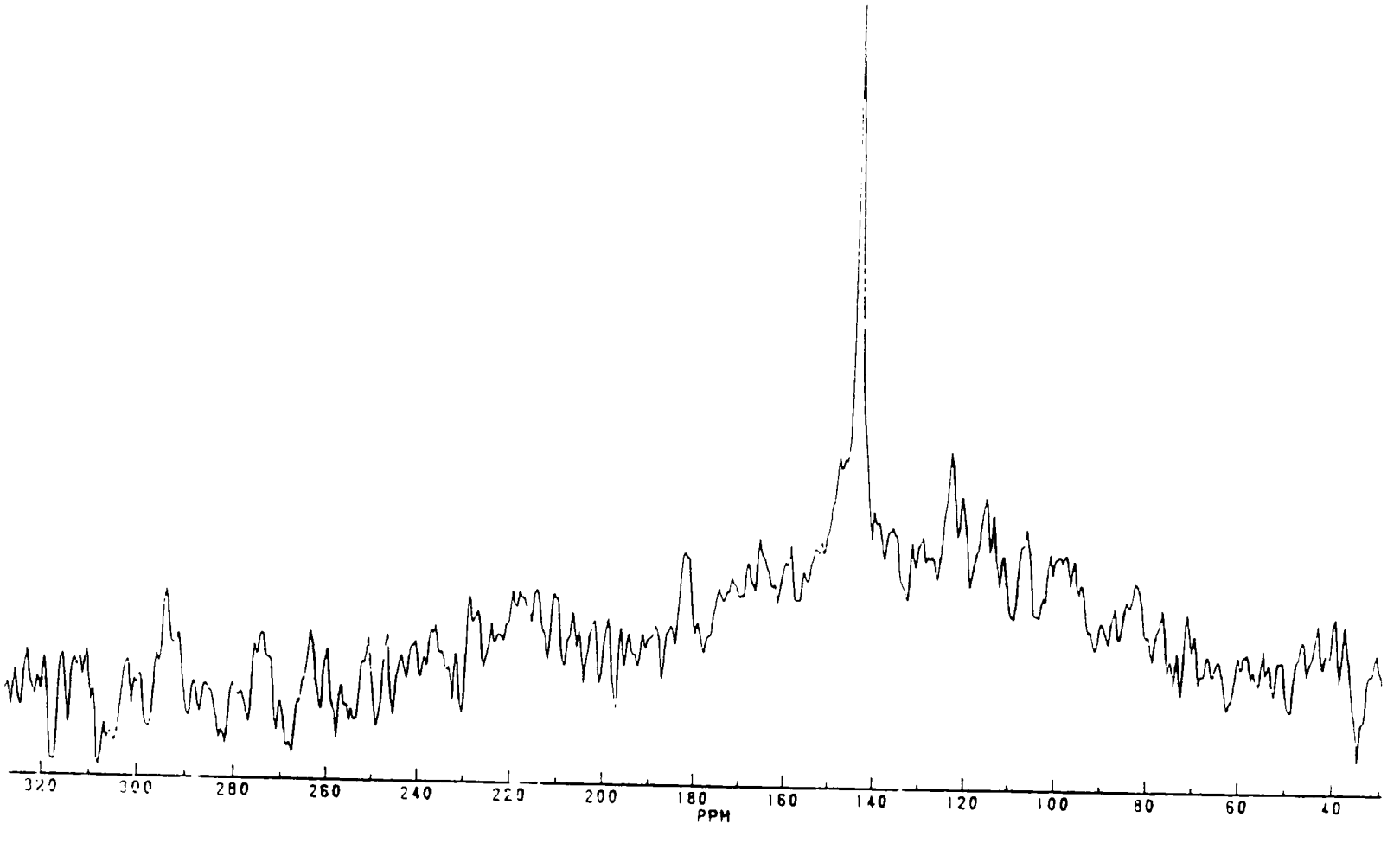


Figure 3.5.1. ^{13}C MASNMR of a sample of 'the residuals' exposed to air for several minutes.

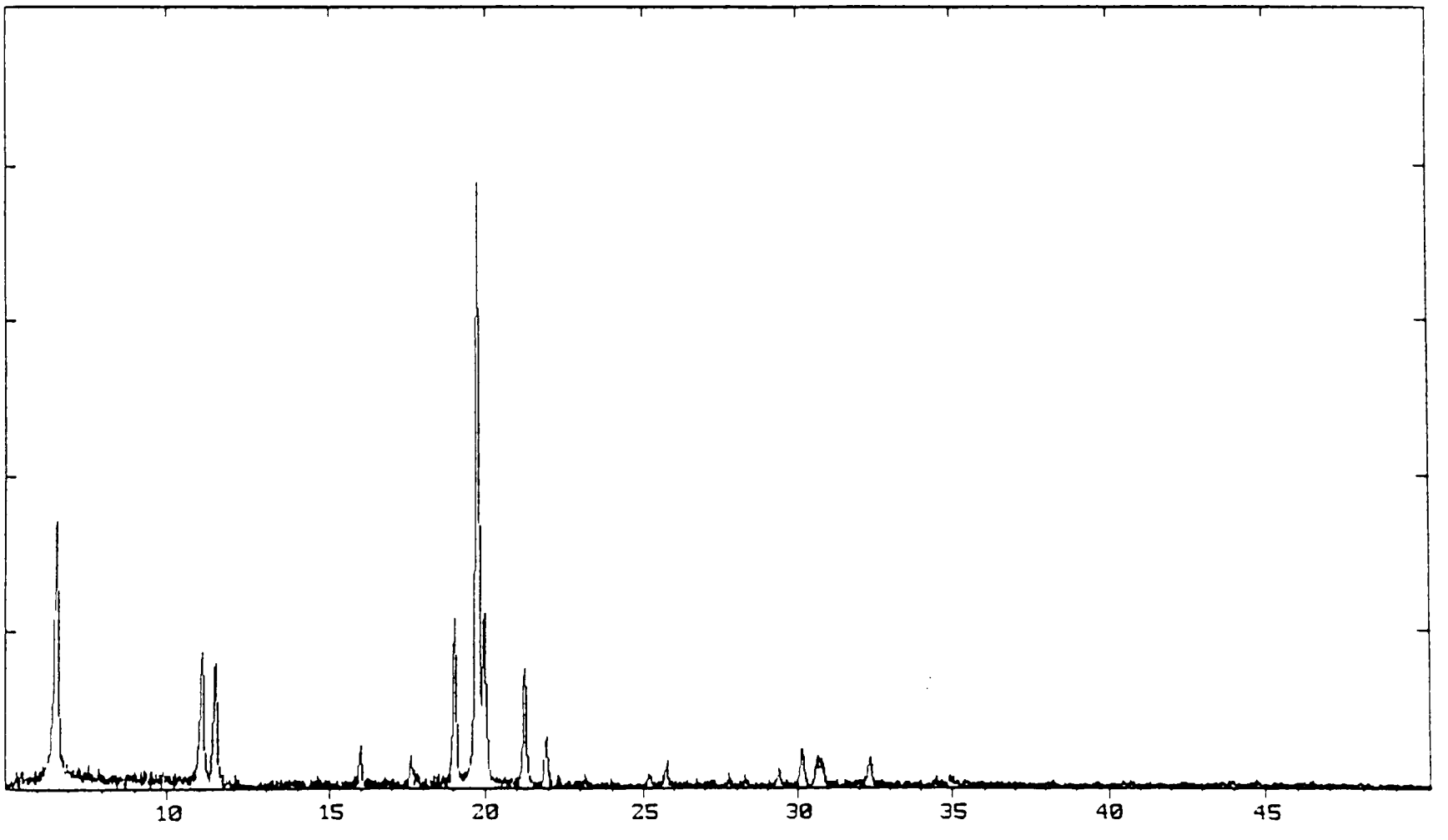


Figure 3.5.1.1. Powder X-ray diffraction pattern of 'the residuals'.

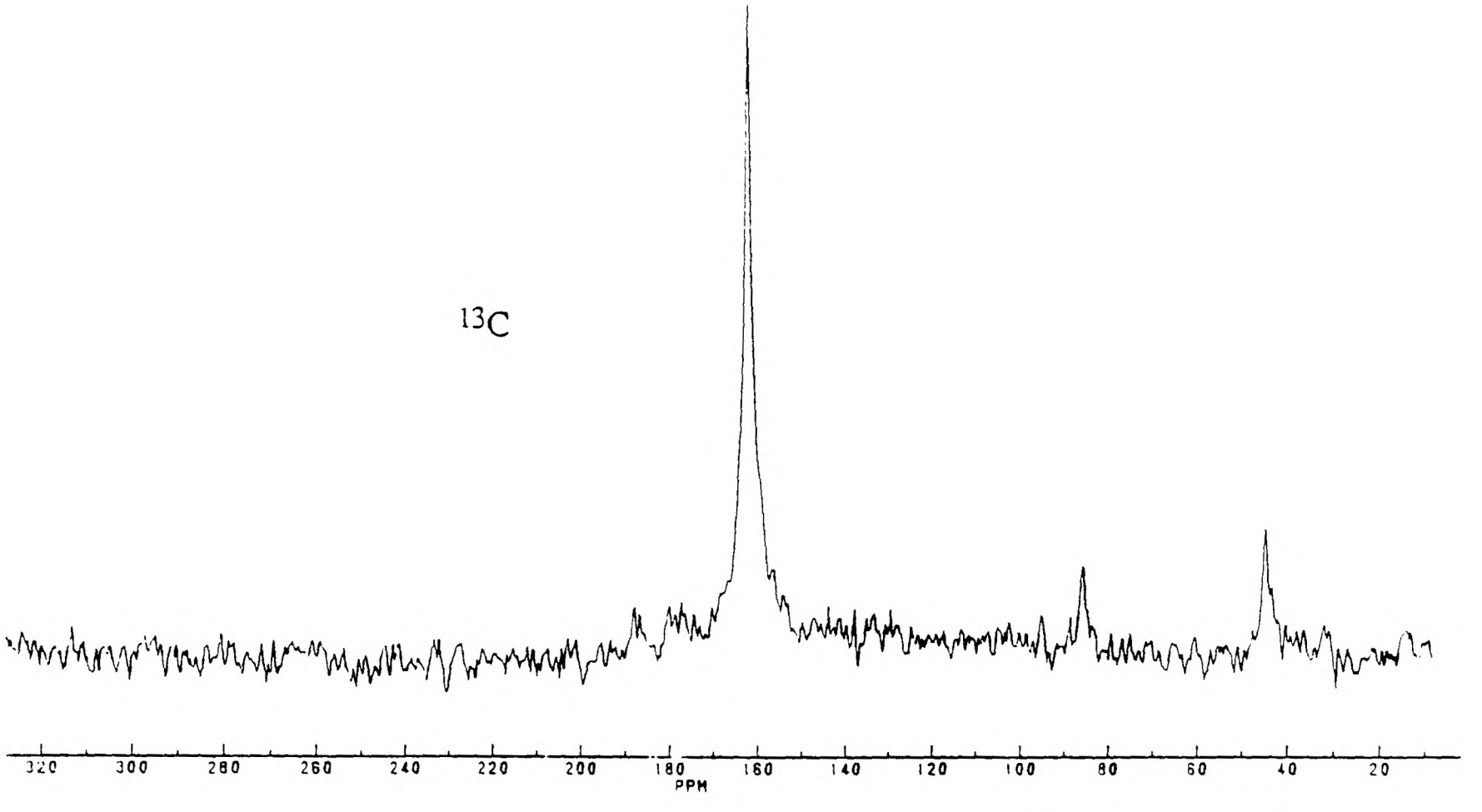
carbon and hydrogen content and the composition formulated does not correspond to any of the values reported, C (87.58, 92.45, 91.60) and H (2.58, 2.77, 1.53) respectively. Sodium analysis using an ICP method gave the sodium content as 1.01%. The residual material, referred to from now on as 'the residuals', from the synthesis of NaC_{60}.5thf had the following elemental analysis C (87.48, 87.37), H (2.36, 2.45) and from the ICP method Na(1.89, 2.10). Whilst carbon and hydrogen contents are comparable between the two materials the sodium content is vastly different. Elemental analysis of the residuals gives a composition $Na_{0.9}C_{60}$.3thf, giving the calculated element compositions as C = 90.3%, H = 2.5%, Na = 2.1%, on assuming the H and Na contents have a higher probability of being more accurate than the C content. This is because it is well known that C_{60} containing compounds consistently give low percentage C results due to incomplete combustion. The possibility of decomposition of the sample during the weighing procedure should also not be discounted.

Analysis of the solid obtained from removal of the volatiles from the yellow supernatant produced during the reaction of C_{60} and $Na\{Mn(Cp^*)_2\}$, showed that it contained a very small quantity of sodium (<0.1%) and probably thf but that the majority was $Mn(Cp^*)_2$.

3.5.2. ^{13}C and ^{23}Na MASNMR Spectroscopy of 'The Residuals'.

^{13}C MASNMR spectra of the residuals showed three peaks at δ 162, 85 and 44ppm respectively, as shown in figure 3.5.2.1. The peaks at higher field are due to the thf molecules present, and the low field resonance to C_{60} carbons. This is in comparison to the ^{13}C powder NMR spectrum of the electrocrystallisation product which has resonances at δ 158, 81 and 41ppm respectively. The small discrepancies observed in the chemical shift values could be due to reference differences or, more probably, on changing from powder to MAS spectroscopy, the centre of gravity of the peak, measured from the MAS spectrum, is different from the major feature chosen from the powder spectrum.

^{23}Na MASNMR of the residuals showed a single peak at δ -8ppm and a small peak at δ 9ppm, as shown in figure 3.5.2.1, in comparison to the powder NMR of the electrocrystallisation product which shows a peak at δ -6ppm. The ^{23}Na powder NMR spectrum of the electrocrystallisation product was not illustrated in the report but it is likely that the broadening observed in the comparison of MAS to static NMR spectroscopy could be responsible for the discrepancy. As mentioned in section 3.4.3, the chemical shift observed at δ -8ppm is consistent with sodium cations bound by oxygen containing ligands.



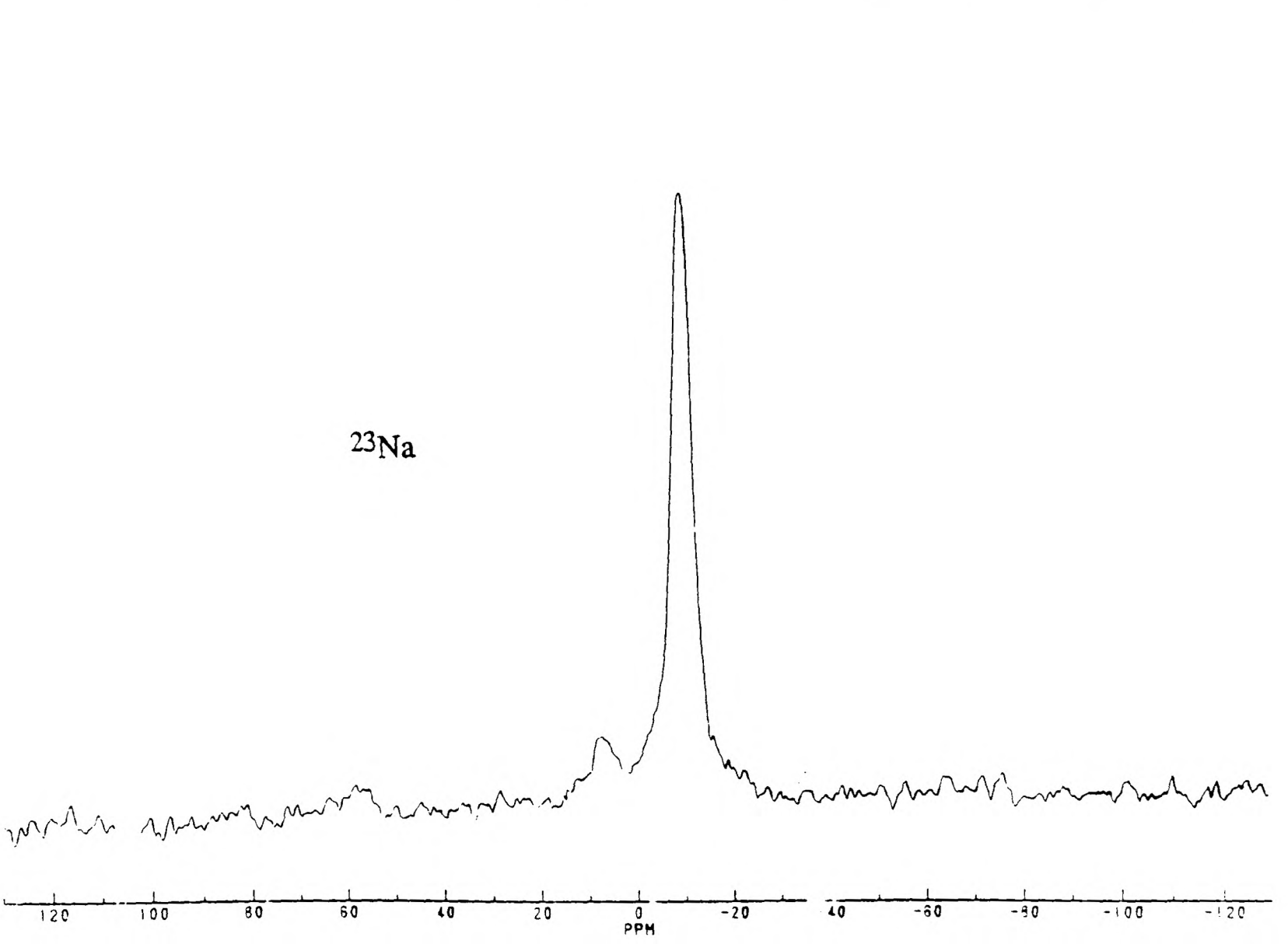
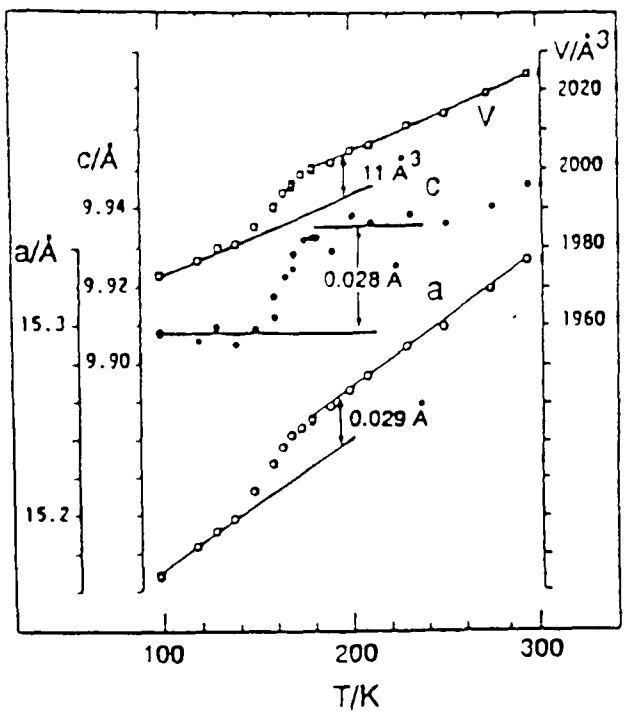


Figure 3.5.2.1. ^{13}C MASNMR and ^{23}Na MASNMR of 'the residuals'.

3.5.3. SQUID and ESR Measurements of 'The Residuals'.

Conductivity measurements along the c-axis of the crystals from the electrocrystallisation route showed that the material undergoes a transition at approximately 180K which was interpreted as a metal-metal transition, as shown in figure 3.5.3.1.



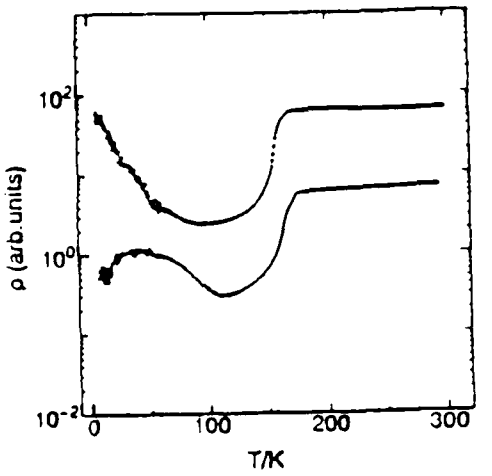


Figure 3.5.3.1. Dependence of the lattice constants, and resistivity measured along the c-axis for two different 'crystals', as a function of temperature for $Na_xC_{60}.thf_y$.

The conductivity between 300 and 180K is virtually constant at approximately 50 S cm^{-1} where below the transition conductivities of greater than 1000 S cm^{-1} were observed. Details of the transition and conductivity values were sample dependent and from the report it appears rigorous exclusion of oxygen and moisture was not employed. Associated with the conductivity transition is a decrease in the unit cell volume and the values of the a and c axis, as shown in figure 3.5.3.1.

ESR and SQUID measurements were eluded to, both showing transitions at the same temperature observed in the variable temperature X-ray crystallography, and conductivity measurements.

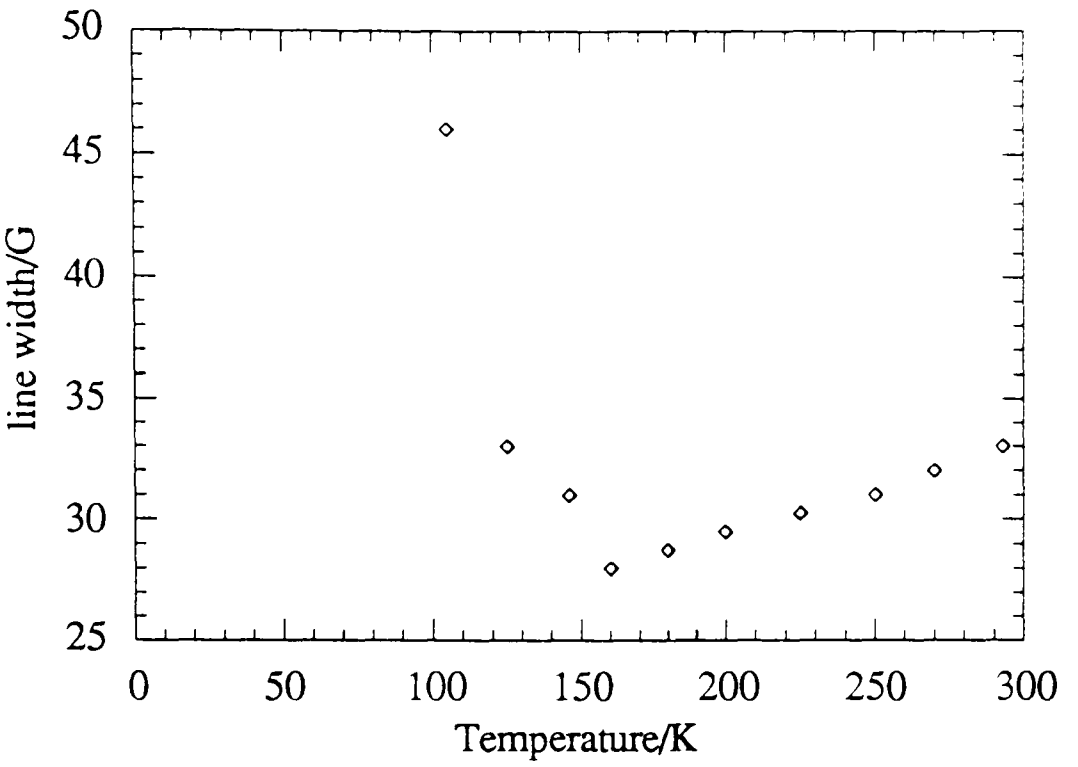


Figure 3.5.3.4. Temperature dependence of the line width of the broad feature in the ESR spectrum of 'the residuals'.

The variable temperature ESR spectra of 'the residuals' are shown in figure 3.5.3.2. and the power dependence of the ESR signal at 19K is shown in figure 3.5.3.3. At low temperatures a relatively sharp feature is observed which is asymmetric and has an approximately temperature independent linewidth of 6G. At temperatures above 19K a broad feature with a temperature dependent linewidth is observed. The spectrum at 44K appears anomalous, appearing to have a large broad component in contrast to the spectra recorded at 19 and 60K. A satisfactory reason for this is as yet unknown but the temperature at which this occurs appears to be the onset of the noisy conductivity data shown in figure 3.5.3.1. The line width of the broad feature as a function of temperature is shown in figure 3.5.3.4. The power dependence of the spectra at 19K show that the sharp low temperature feature saturates much more readily than the broad feature. Non saturation of C_{60} monoanion ESR spectra has been accounted for on the basis of rapid electron spin relaxation due to the thermally accessible excited state which may also be responsible for the temperature dependence of the linewidth as discussed in section 3.4.5.

The g-value was approximately constant at 1.997 over the temperature range studied.

A metal should have a reasonably constant, small, susceptibility with respect to a localised electron model, as a function of temperature. A plot of the arbitrary spin susceptibility from the unitless intensity of the ESR spectra at variable temperature is shown in figure 3.5.3.5.

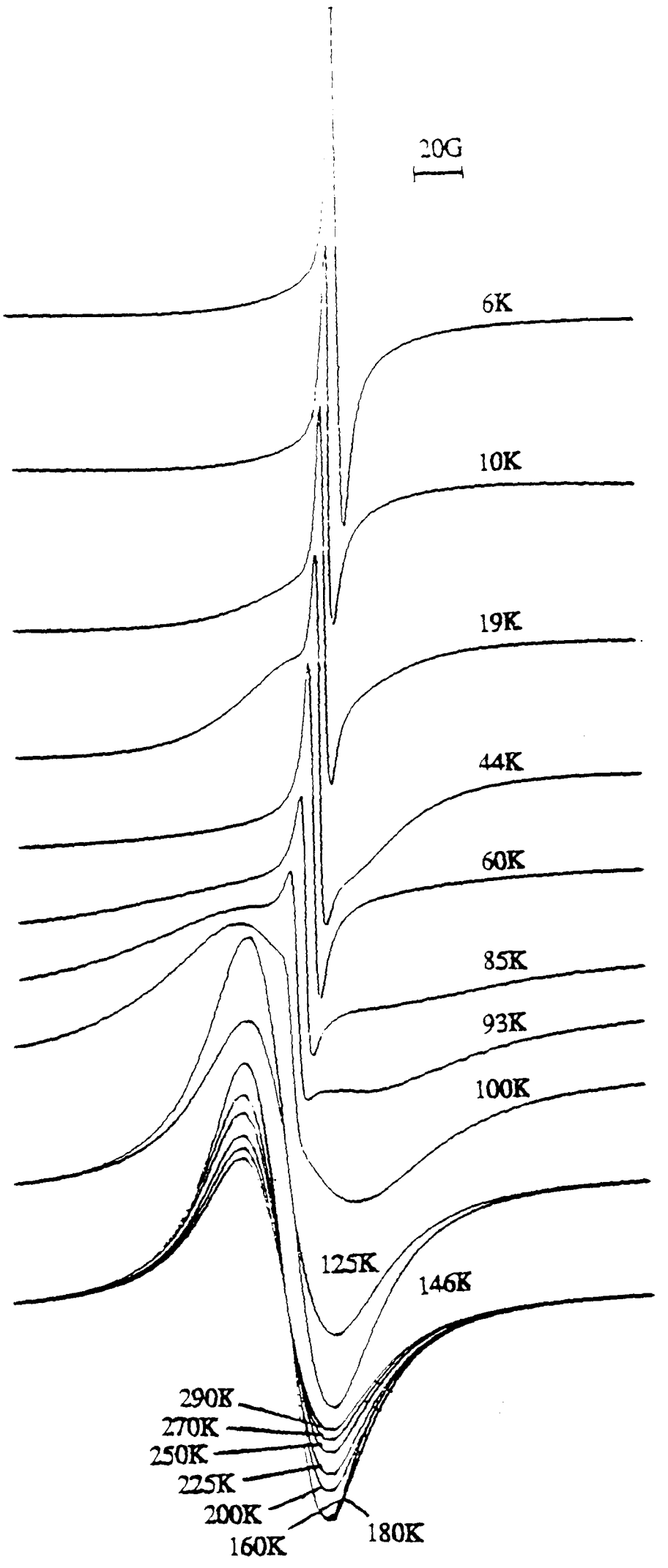
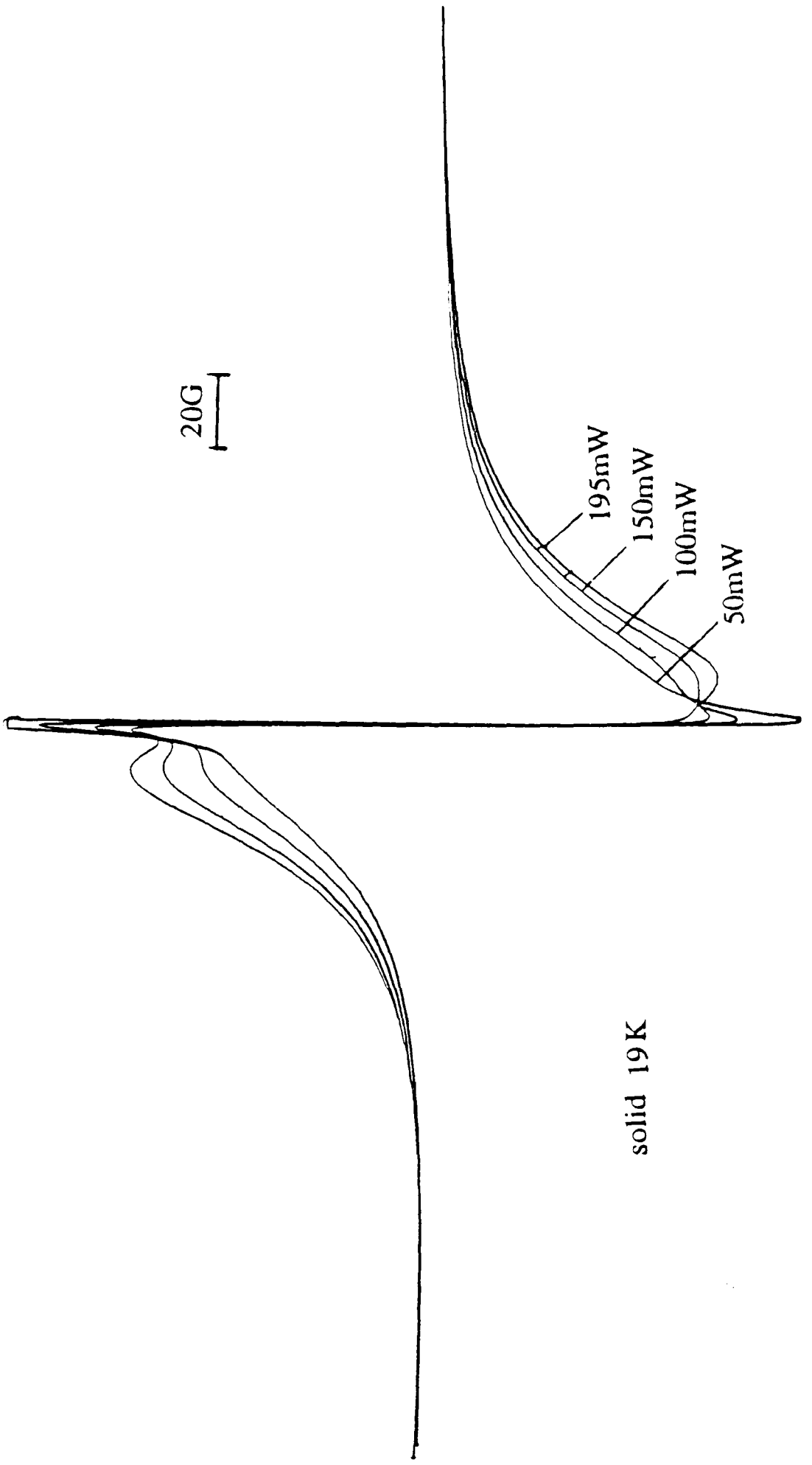


Figure 3.5.3.2. Temperature dependence of the ESR spectrum of 'the residuals'. Spectra are not normalised with respect to intensity. Spectra at 125 and 146K were recorded at the same sensitivity, as were spectra from 160 to 290K



solid 19K

Figure 3.5.3.3. Power dependence of the ESR spectrum of 'the residuals'.

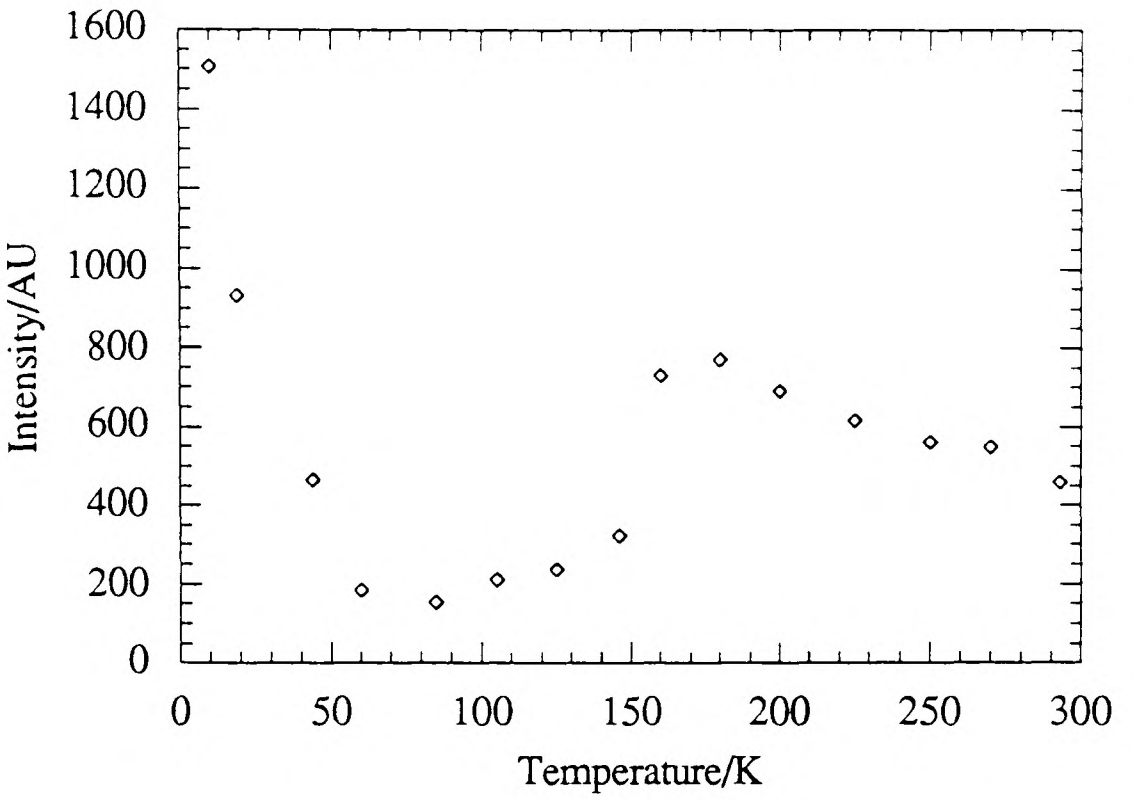


Figure 3.5.3.5. Temperature dependence of the ESR intensity of 'the residuals'.

SQUID magnetometry, kindly performed at the University of Edinburgh by Dr. Gavin Whittaker and Dr. Andrew Harrison, showed a transition at approximately 170K consistent with the ESR data, as shown in figure 3.5.3.6.

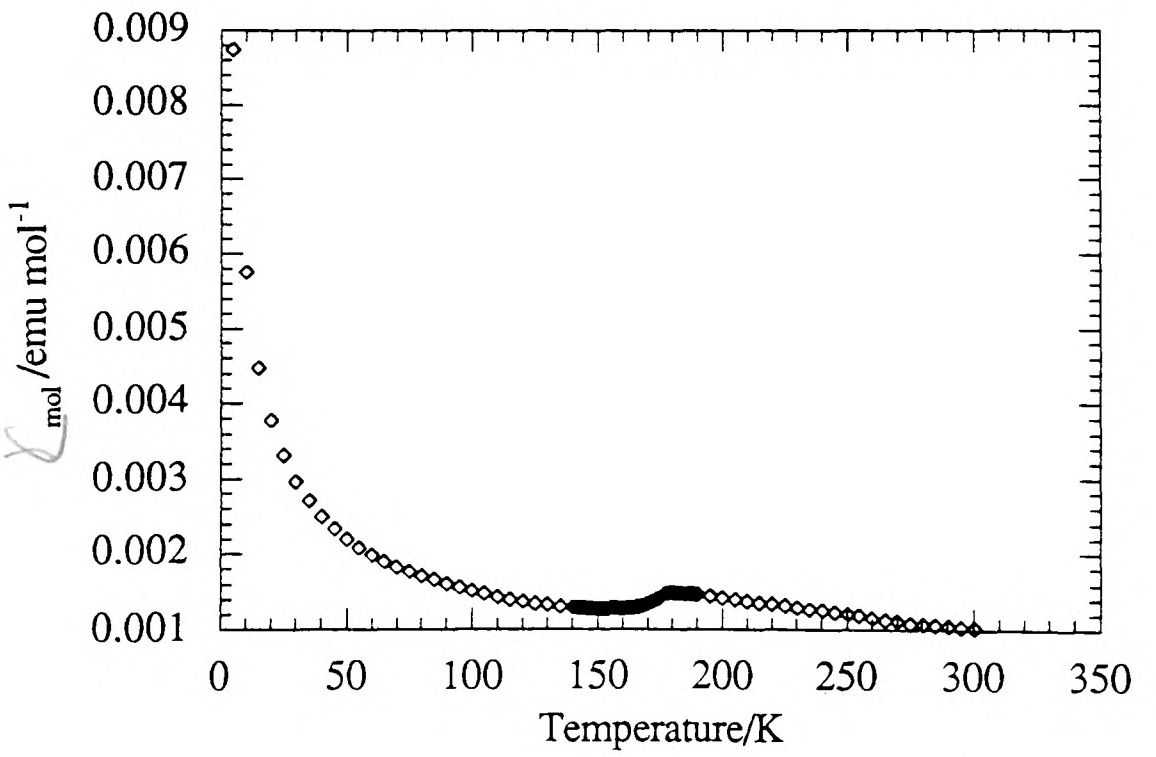


Figure 3.5.3.7. Molar susceptibility as a function of temperature for 'the residuals' in an applied field of 1T. Data was corrected for a ferromagnetic impurity, container diamagnetism and core electron diamagnetism (χ_d = -400 x 10^{-6} emu mol^{-1}).

Measurements of the magnetisation as a function of field, above and below the

transition showed saturation above 0.5T consistent with impurity from a nickel alloy spatula. Data was corrected by subtracting the saturation magnetisation, obtained by extrapolating to 0T using magnetisation data linear above saturation with respect to the applied field. Examination of the effective magnetic moment as a function of temperature shows that the high temperature moment is approaching the value expected for a localised S=1/2 spin system, as shown in figure 3.5.3.8.

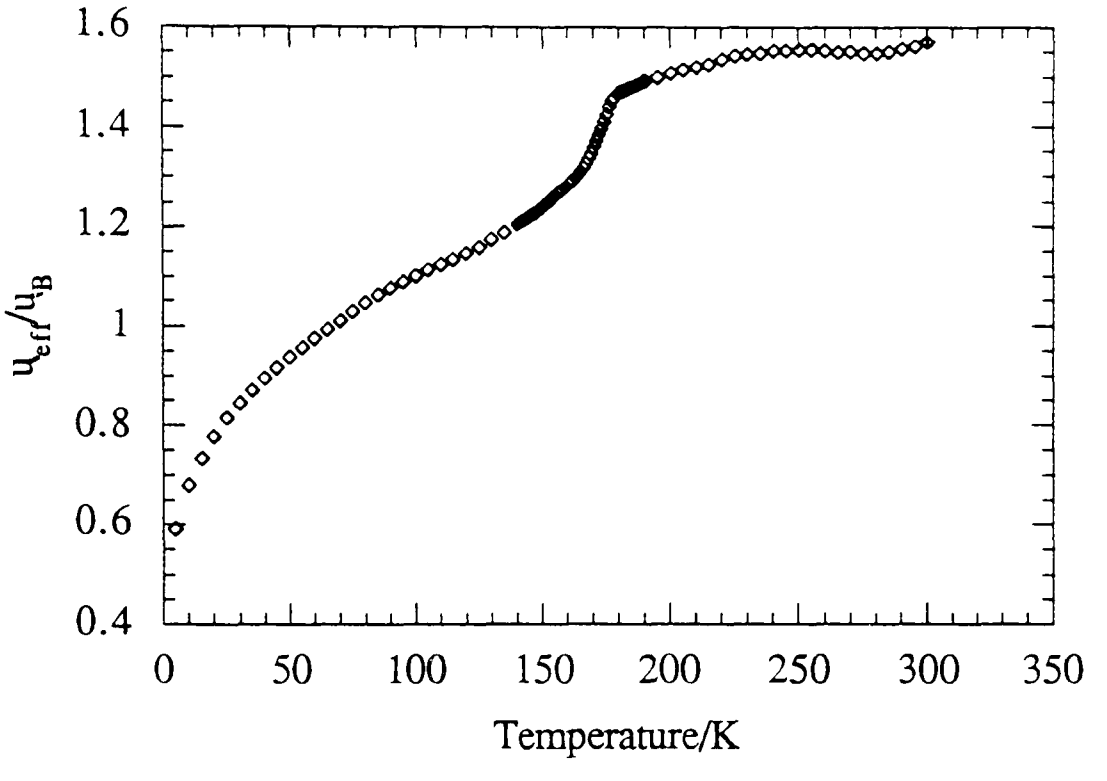


Figure 3.5.3.8. Effective magnetic moment as a function of temperature for 'the residuals'.

Neither above, or below, the transition at 170K does the bulk static susceptibility exhibit Curie-Weiss behaviour. A fit using equation 3.4.4.1. was not successful when applied to the susceptibility below 120K.

3.6. Discussion on the Na C_{60} thf System.

The synthesis of NaC_{60}.5thf has been demonstrated and some of its properties investigated. Without full structure determination, preferably at variable temperature, relationships between the magnetic data, specifically the transition at 180K, and the structure cannot be confidently made.

In solution, the characterising data is consistent with previously reported solutions containing C_{60} monoanions (ESR, UV-Vis) and the electrochemical data (RDE) is further confirmation.

Magnetic measurements in the solid state (SQUID, ESR), above 200K, indicate the presence of a paramagnetic material composed of single unpaired electrons localised on C_{60} molecules. In discussion of the origin of the transition centred at 180K, a variety of possibilities could be speculated upon including antiferromagnetic coupling of unpaired electrons, an insulator-metal transition, or 1-dimensional polymerisation as

observed at lower temperatures in Rb_1C_{60} and Cs_1C_{60}. Structural knowledge at a range of temperatures either side of the transition is required to distinguishing between the possibilities and single crystals to allow conductivity measurements would greatly aid interpretation of the magnetic data.

To date, as discussed in section 1.5, all non alkali metal C_{60} monoanion compounds exhibit Curie-Weiss behaviour. Of the alkali metal C_{60} monoanions known all seem to exhibit metallic behaviour in at least one of their structural phases.

^{13}C solid state NMR spectroscopy of NaC_{60}.5thf shows that at ambient temperatures C_{60} molecules are rotating isotropically within the solid and at lower temperature the dynamics become slower. No obvious transition in the dynamics is evident at 180K, as observed in the magnetic measurements, which probably rules out the possibility of 1-dimensional polymerisation, as a sudden decrease in the C_{60} dynamics would be expected. However a transition is observed in the chemical shift not inconsistent with a Knight shift observed for a metallic state.

^{23}Na MASNMR shows two major resonances which are due to two inequivalent sites in the unit cell of NaC_{60}.5thf. If the unit cell proposed in section 3.4.2. is basically correct it is tempting to assign the sharp resonance at δ 9ppm to a symmetric site at the body centre, and the broader resonance to sodium species centred in a pair of faces, most likely the bc face, of the unit cell or vice versa.

It is not particularly remarkable that two apparently very similar materials compositionally have different structures and probably as a result completely different solubilities. An attempt to dissolve 'the residuals' by refluxing in thf for several weeks was unsuccessful, as was an attempt to dissolve the parent dark red solid precipitated from the reaction solution.

However, magnetically the two solids behave in a very similar fashion showing a transition from a high effective moment state at high temperature to a low effective moment state at low temperature. Short range antiferromagnetic coupling could possibly account for the transition but the very sharp nature of the transition indicates this is not the case.

Characterisation of 'the residuals' indicates that this material is probably that reported by Kobayashi and coworkers prepared as 'single crystals' by electrocrystallisation.

Comparison of the SQUID and ESR measurements of 'the residuals' and NaC_{60}.5thf appear to show that the transition observed at approximately 170K in both materials could be very similar in nature. This would imply that NaC_{60}.5thf possibly undergoes an unprecedented metal-insulator transition at approximately 180K, but only conductivity measurements on single crystals would be definitive proof. Attempts to grow single crystal of NaC_{60}.5thf have to date been unsuccessful.

3.7. Some Reaction Chemistry of NaC_{60}.5thf.

The compound NaC_{60}.5thf has large potential as a possible synthon for a variety of reactions. Two of particular interest are cation metathesis for the synthesis of novel soluble materials with interesting magnetic, optical and electronic properties, and organometallic chemistry to ascertain whether the C_{60} monoanion can co-ordinate to a metal centre in anything but an η^2 fashion across a 6:6 ring fusion.

Exposure of NaC_{60}.5thf in the solid state or in solution, to air, results in decomposition in under 30 seconds. Some of the decomposition product is soluble in toluene producing a purple colouration and ^{13}C MASNMR spectroscopy shows a peak at δ 143ppm which corresponds to C_{60}, as shown in figure 3.7.1. Similar results occur on exposure of solid NaC_{60}.5thf to degassed deionised water.

Attempts were made to remove the five equivalents of thf molecules from the compound NaC_{60}.5thf. Heating for a variety of times, at a variety of temperatures and vacuums, both dynamic and static, did not yield a material free of hydrogen as determined by elemental analysis. ^{13}C MASNMR shows that phase separation or possibly decomposition is occurring at 200°C, as shown in figure 3.7.2.

Further reduction of NaC_{60}.5thf by two equivalents of a reducing agent would give a solid containing C_{60} trianions, which in some materials have resulted in superconductivity at low temperatures. Addition of a thf solution of two equivalents of sodium naphthalide to a thf solution of NaC_{60}.5thf resulted in immediate precipitation of a dark solid. The solid is soluble in MeCN but only partially soluble in thf. ^{13}C MASNMR spectroscopy shown in figure 3.7.2. showed two broad peaks indicating slow dynamics of C_{60} molecules within the solid. SQUID magnetometry showed no detectable superconducting material was present above 6K.

Reaction of one equivalent of NaC_{60}.5thf with one equivalent of $CpFe(CO)_2Cl$ in thf solution immediately resulted in precipitation of a brown solid with a very pale yellow supernatant. The brown solid was soluble in toluene giving a purple solution. Removal of the volatiles from the pale yellow solution, gave a pale orange solid, which ^1H NMR spectroscopy showed a peak at δ 4.2ppm corresponding to that of the dimer $Cp_2Fe_2(CO)_4$. It appears NaC_{60}.5thf acts as a reducing agent as shown in equation 3.7.1.

$$Na^+C_{60}^{\cdot -} + CpFe(CO)_2Cl \longrightarrow C_{60} + NaCl + \{CpFe(CO)_2\}_2 \qquad \text{Equation 3.7.1.}$$

Therefore reaction with substrates incapable of reduction by the C_{60} monoanion ($E_{1/2}$ 0/-1 = -0.4V vs SCE) should be used.

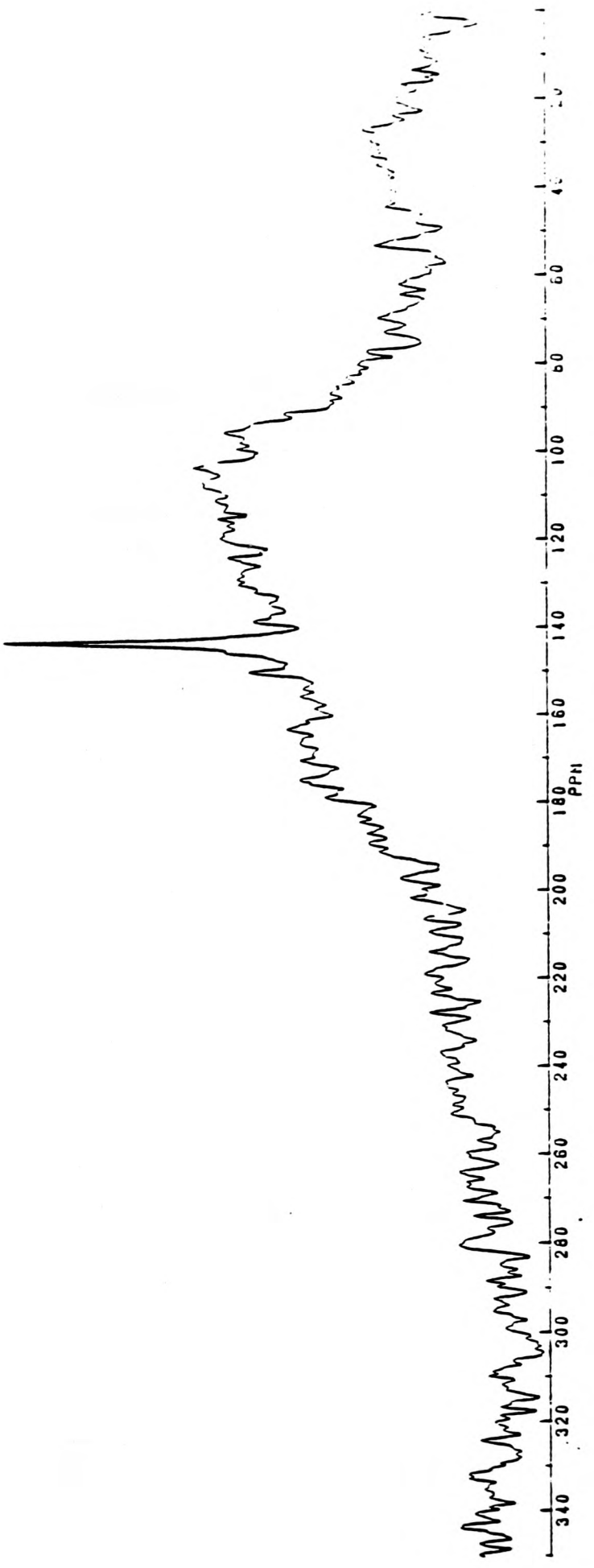


Figure 3.7.1. ^{13}C MASNMR spectrum of $NaC_{60}.5thf$ after exposure to air for a few seconds.

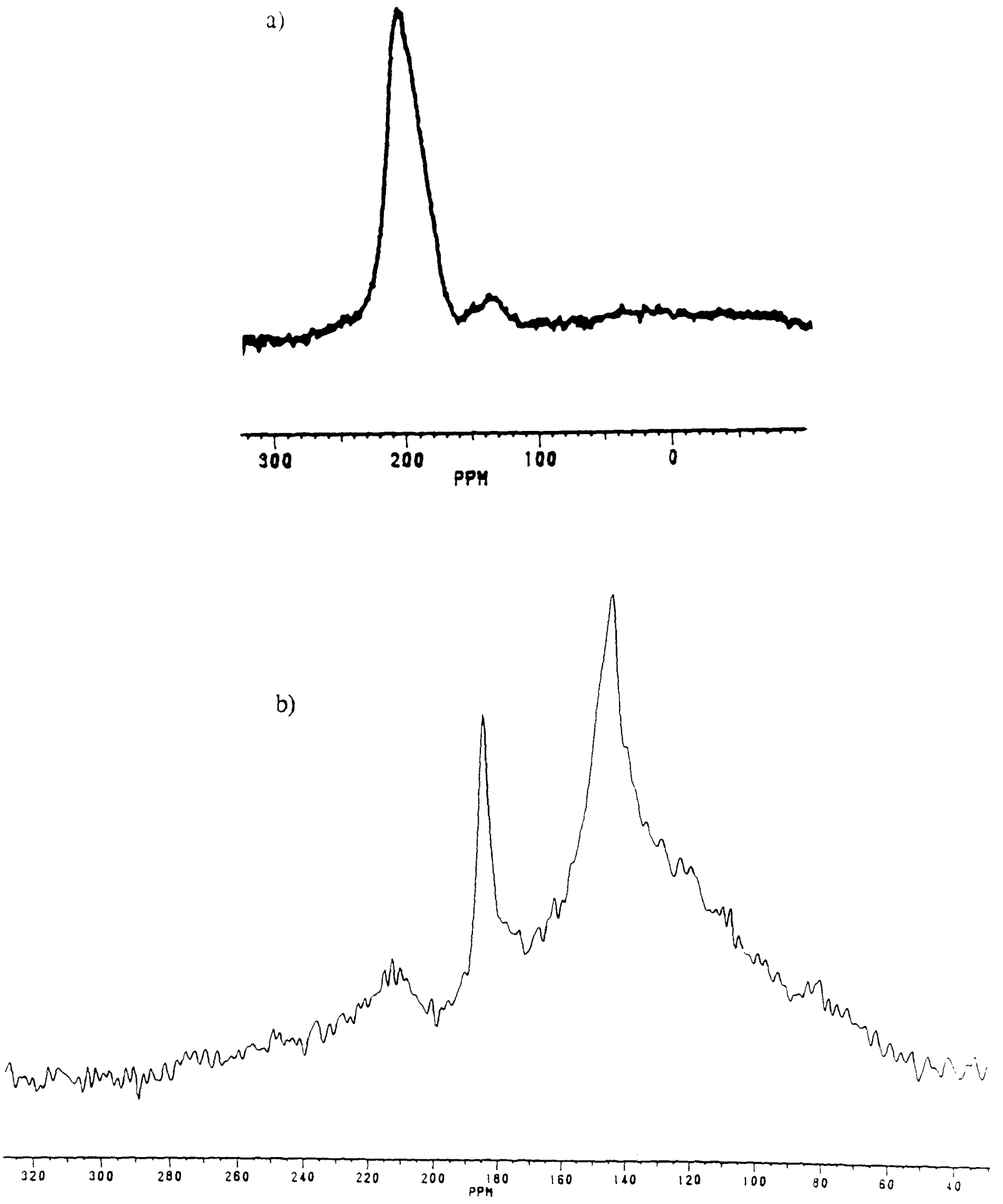


Figure 3.7.2. a) ^{13}C powder spectra of $NaC_{60}.5thf$ heated at 100°C for 24 hours under a dynamic vacuum of 10^{-5} mbar and b) ^{13}C MASNMR of reaction of two equivalents of sodium naphthalide with one equivalent of $NaC_{60}.5thf$.

A suitable substrate could be the dimer $Cp^*_2Co_2Cl_2$ where the electron rich fragment Cp^*Co^+ is very unlikely to undergo reduction by the C_{60} monoanion and subsequent dimerisation. On addition of one equivalent of a thf solution of $Cp^*_2Co_2Cl_2$ to two equivalents of NaC_{60}.5thf a dark precipitate formed almost immediately with a virtually colourless supernatant. The dark solid was found to be insoluble in all common organic solvents.

This reaction highlights a typical problem of C_{60} chemistry, insolubility of reaction products. Efforts should be made to use precursors that are likely to impeach solubility on C_{60} containing materials.

Several reactions were attempted with first row transition metal dichlorides and an appropriate quantity of NaC_{60}.5thf. Unfortunately reactions were generally inconclusive or deposited C_{60} and bulk metal.

Further work in the general area of organometallic of C_{60} anions is worth pursuing and a recent address[66] by Fagan where η^4-coordination of C_{60} to a Cp^*Ru^+ was implied seems to indicate this area of chemistry is beginning to show signs of success.

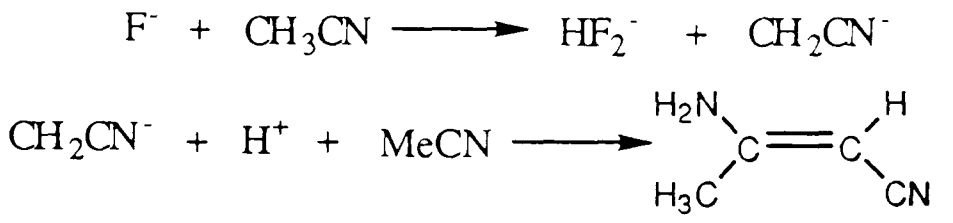
3.7.1. Synthesis of NMe_4C_{60}.1.5thf.

The extent of the relationship between the lattice parameter and T_c described in section 1.6.2, in fcc alkali metal C_{60} superconductors, is limited by the size of the alkali metal cations. Organic cations obviously have a wide variety of shapes and sizes, which when accommodated into the C_{60} lattice could allow higher T_c's to be obtained. As a preliminary step towards this goal cation metathesis of NaC_{60}.5thf with a suitable salt was attempted.

The cation of choice was NMe_4^+ because of its size and reasonable thermal robustness. Having a very similar size to $Na(NH_3)_4^+$, NMe_4^+ could be accommodated in the octahedral interstitial site of the fcc C_{60} lattice. If NMe_4C_{60} can be synthesised, and providing the organic cation can survive the high temperatures required, then traditional solid state techniques, to synthesise ternary salts containing the C_{60} trianion, could be employed.

For efficient cation metathesis it is desirable that both salt precursors be soluble and that either the desired product or side product be insoluble in the reaction medium. Due to the moisture sensitivity of NaC_{60}.5thf, ion-exchange columns are not practical. A good candidate for solution metathesis is NMe_4Cl, because the expected side product, NaCl, has a high lattice energy and the desired product, NMe_4C_{60}, is expected to be soluble in thf or MeCN, two suitable solvents for NaC_{60}.5thf. Unfortunately NMe_4Cl, NMe_4Br and NMe_4I, are all insoluble in thf or MeCN only displaying reasonable solubility in alcohols and aqueous solvent media. However, NMe_4F, though being insoluble in thf, is soluble in MeCN.[67] At room temperature NMe_4F reacts with MeCN, abstracting a proton to produce trans-3-amino-2-butenenitrile, as shown in

equation 3.7.1.1.



Equation 3.7.1.1.

At lower temperatures, 0 to -40°C, decomposition is very slow and can be disregarded at the lowest temperatures, allowing other kinetically faster reaction chemistry to occur.

Addition, at -5°C, of one equivalent of a MeCN solution of NMe_4F to a MeCN solution of NaC_{60}.5thf gave, after removal of the volatiles at -5°C, a dark purple solid indistinguishable from NaC_{60}.5thf in appearance. Extraction showed that the material was very soluble in thf (~50 $mgml^{-1}$) compared to NaC_{60}.5thf (5 $mgml^{-1}$) indicating a reaction had taken place. The residue, after extraction, appeared grey in colour and contained significant amounts of sodium as indicated by elemental analysis.

Concentration of the thf solution of NMe_4C_{60} and cooling at -80°C gave very dark needles that decomposed to a blue/black microcrystalline powder on removal of the mother liquor.

Elemental analysis gave a composition which could be formulated as NMe_4C_{60}.1.5thf. This was confirmed by integration of the relevant peaks in the ^1H NMR spectrum, as shown in figure 3.7.1.1. Elemental analysis showed that the sodium content was less than 0.1%.

The compound is very soluble in thf and also soluble in MeCN, PhCN and slightly in CH_2Cl_2.

3.7.2. Powder X-ray Crystallography of NMe_4C_{60}.1.5thf.

Powder X-ray diffraction at 1.54051Å showed only nine peaks between 8 and 55°, in 2θ, preventing structural characterisation, as shown in figure 3.7.2.1.

3.7.3. ^1H Solution and ^{13}C Powder and MASNMR Spectroscopy of NMe_4C_{60}.1.5thf.

At ambient temperature ^{13}C powder NMR spectroscopy shows that C_{60} molecules are spinning isotropically within the solid as was the case for NaC_{60}.5thf. A single peak at δ 185ppm ($\upsilon_{1/2}$ = 500Hz) is observed, and on cooling the dynamics of C_{60} molecules becomes progressively slower and a large temperature dependent chemical shift is observed to lower field, as shown in figure 3.7.3.1.

^{13}C MASNMR spectroscopy shows a sharp single resonance at δ 185ppm ($\upsilon_{1/2}$ < 100Hz) and no peaks corresponding to the thf molecules as was the case for NaC_{60}.5thf, as shown in figure 3.7.3.2. No peak(s) due to the NMe_4^+ cation or thf could be observed in any of the solid state spectra even using cross polarisation techniques.

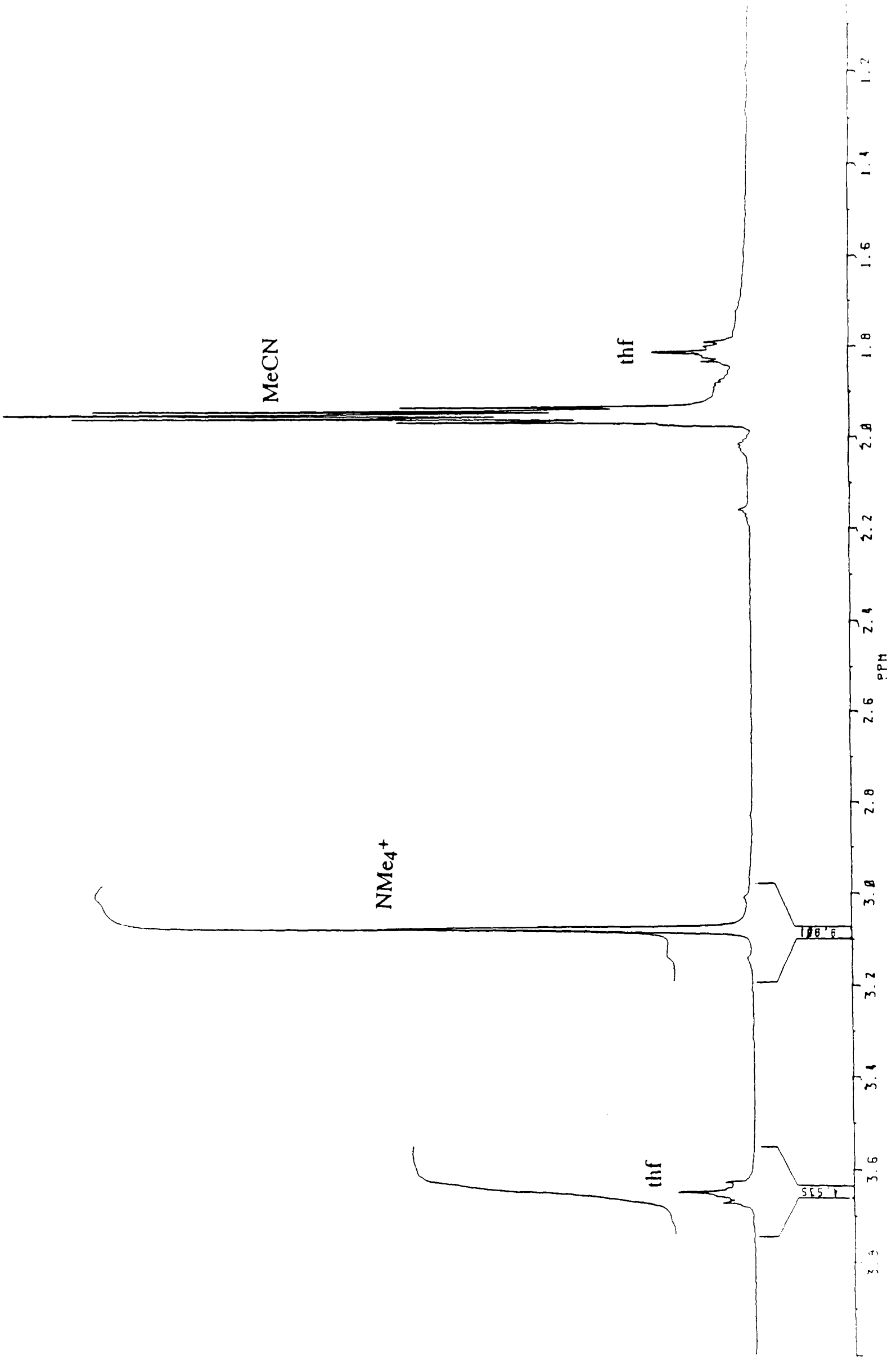


Figure 3.7.1.1. ^1H NMR (d_3-MeCN) of $NMe_4C_{60}.1.5thf$.

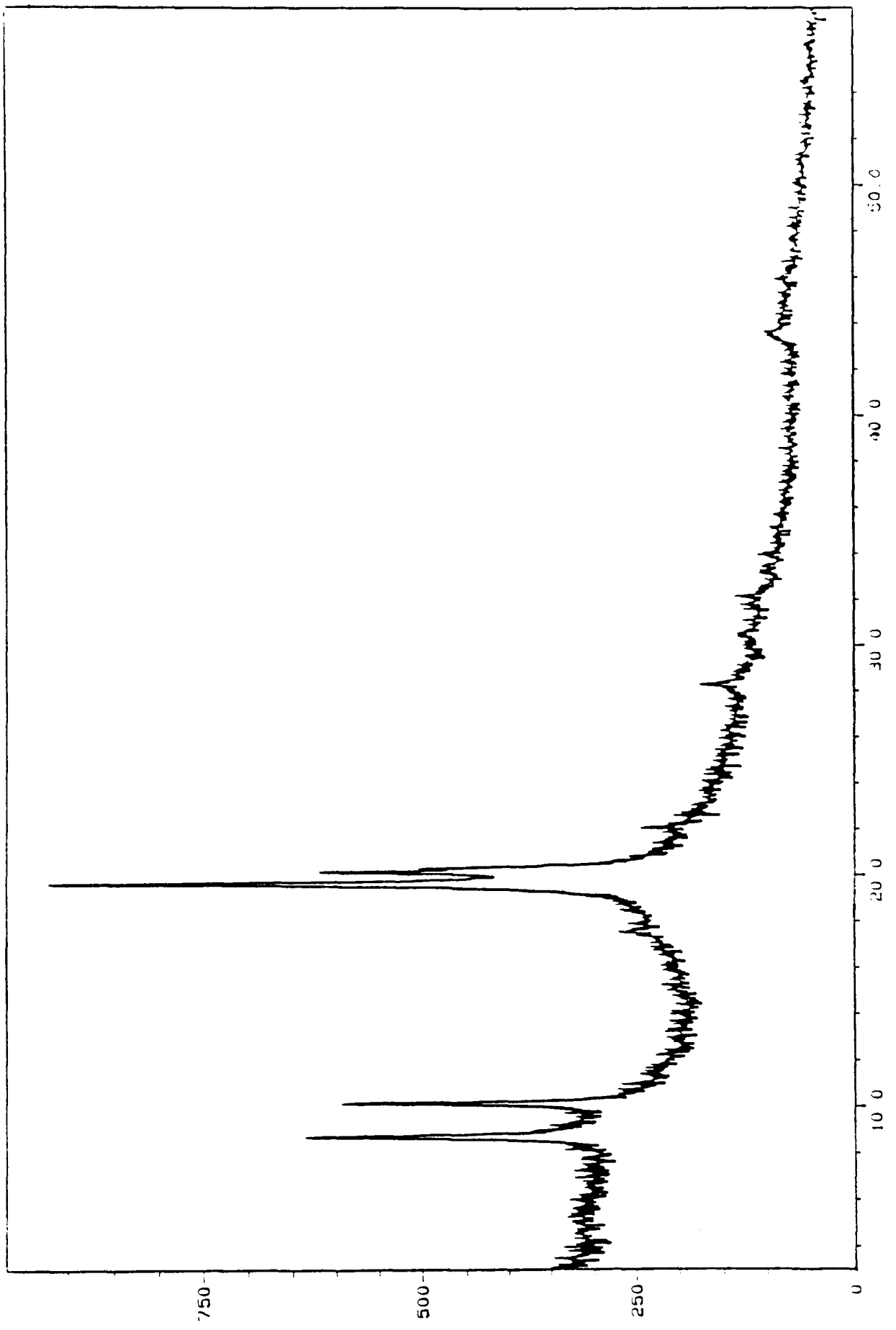


Figure 3.7.2.1. Powder X-ray diffraction pattern of $NMe_4C_{60}.1.5thf$.

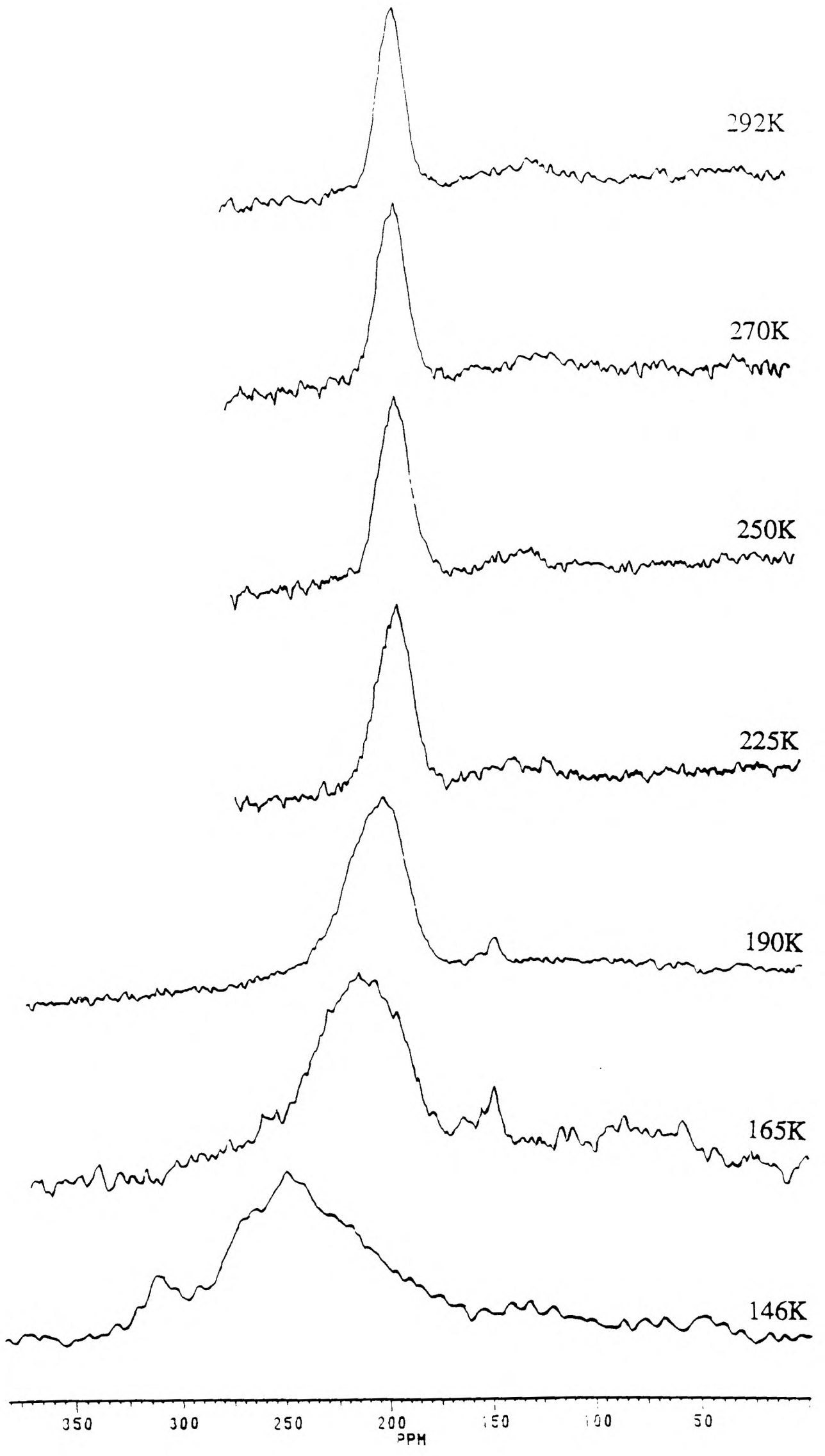


Figure 3.7.3.1. Variable temperature ^{13}C powder NMR spectra of $NMe_4C_{60}.1.5thf$ at the indicated temperatures.

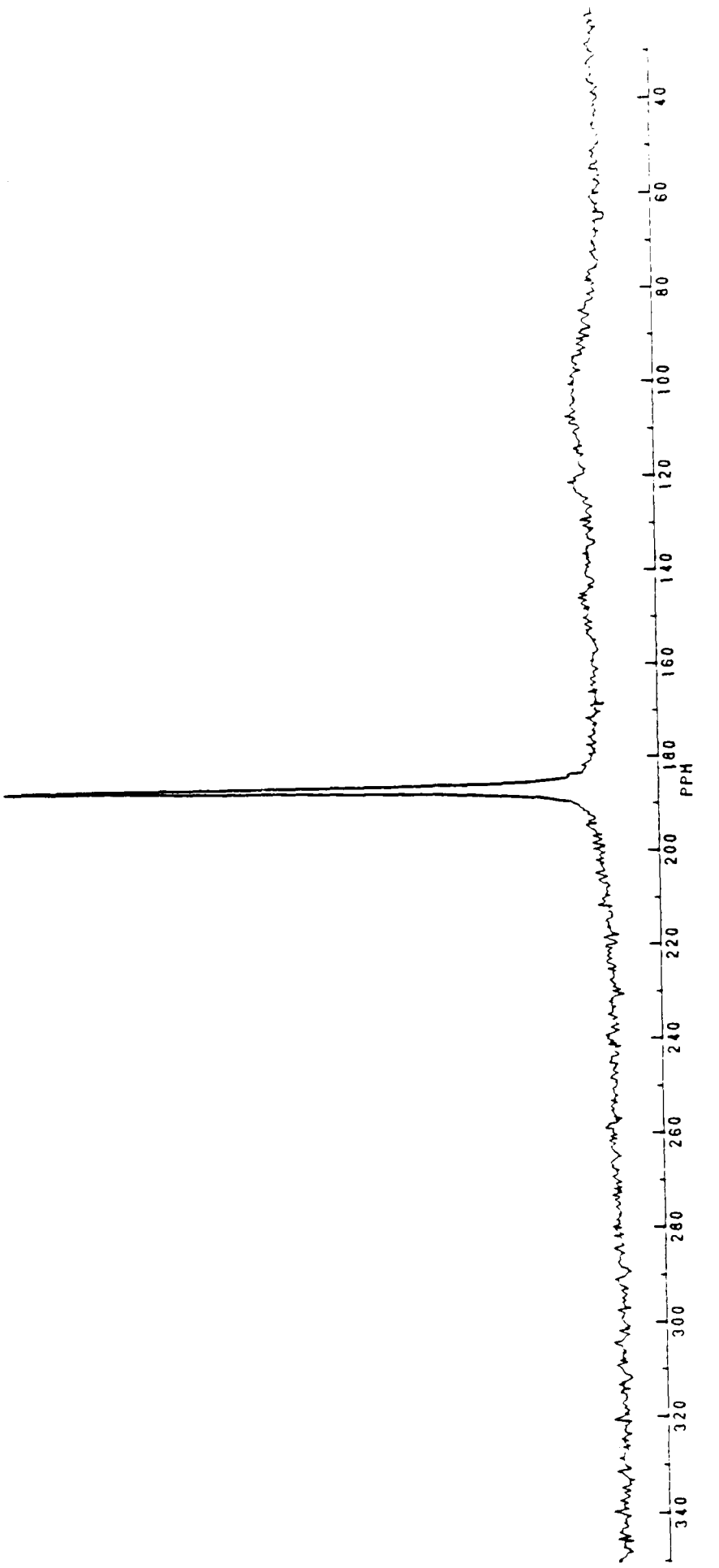


Figure 3.7.3.2. ^{13}C MASNMR spectrum of $NMe_4C_{60}.1.5thf$.

^{1}H solution NMR spectroscopy in d_3-MeCN showed the presence of NMe_4^+ cations and thf molecules in the sample, as shown in figure 3.7.1.1.

3.7.4. SQUID and ESR Measurements of NMe_4C_{60}.1.5thf.

Magnetic measurements, using a SQUID magnetometer, revealed basically the same results as for NaC_{60}.5thf, except that the transition was observed over a larger temperature range, as shown in figures 3.7.4.1 and 3.4.4.2.

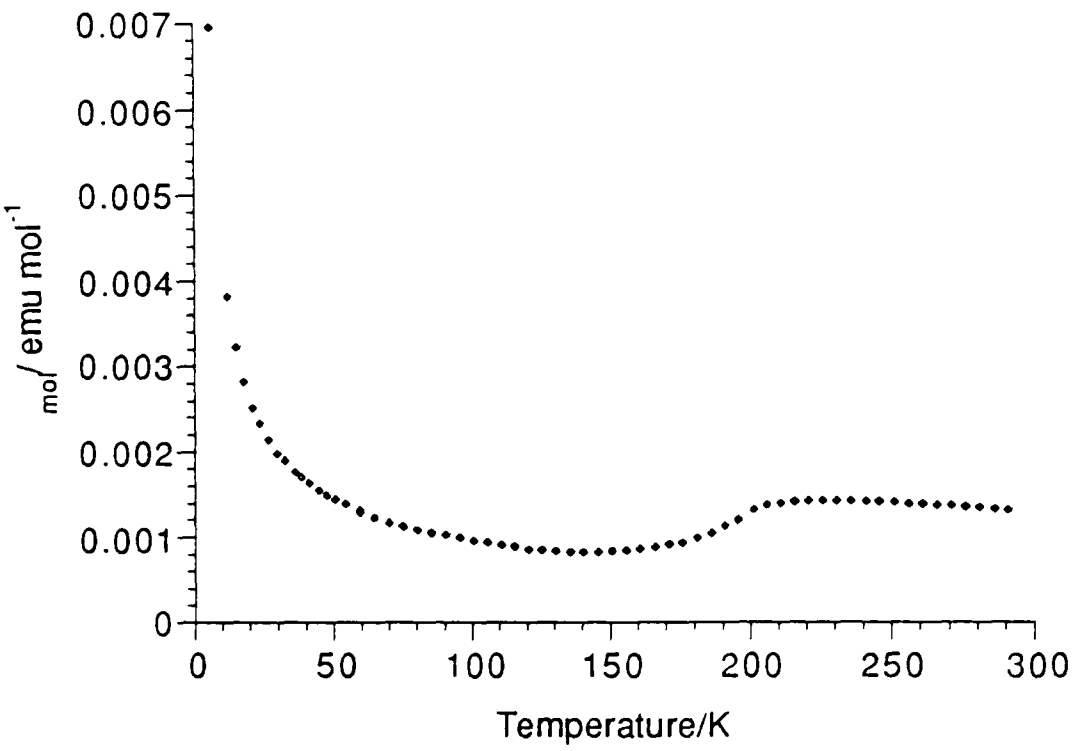


Figure 3.7.4.1. Bulk static susceptibility as a function of temperature for NMe_4C_{60}.1.5thf. data has been corrected for the container and the core electron diamagnetism (χ_d = -350 emu mol^{-1}).

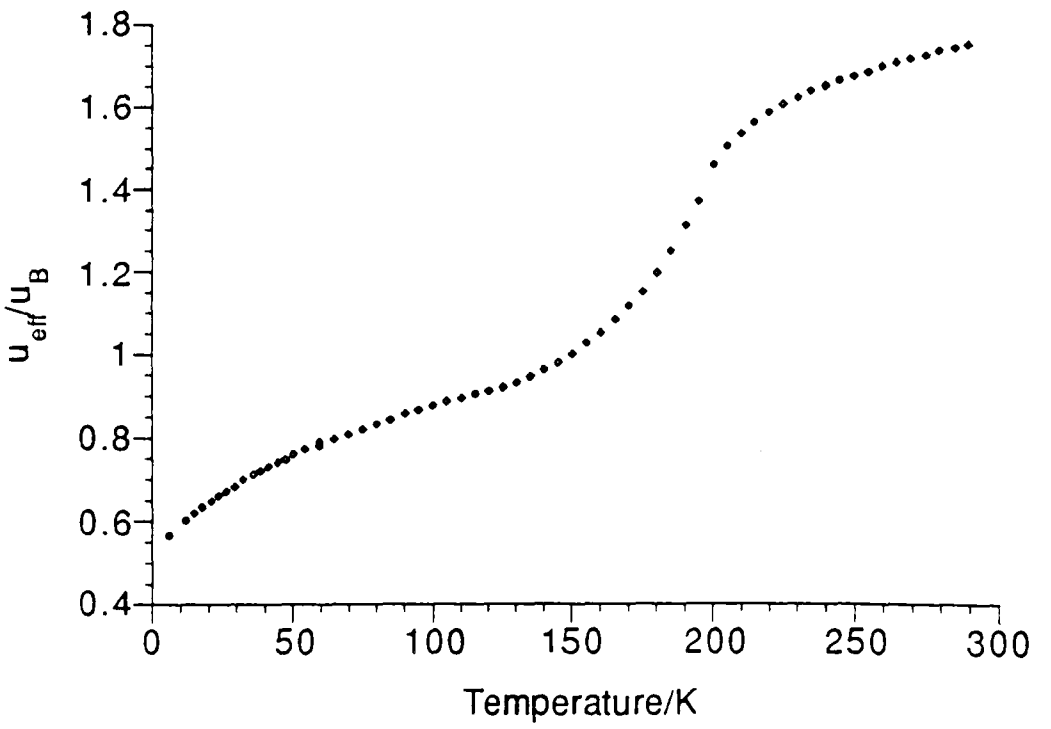


Figure 3.7.4.2. Effective magnetic moment as a function of temperature at 0.5T for NMe_4C_{60}.1.5thf.

Measurements of the magnetisation as a function of field strength at 6K and 250K showed that the material exhibited no hysterisis or saturation up to 2.4T. behaving as a good paramagnet. At temperatures above 230K data could be fitted to the Curie-Weiss law,with a Weiss constant θ = -300K, but the Curie constant is only 40% that expected for a localised spin system where S = 1/2 and the inverse susceptibility did display a slight curvature dropping below that predicted by the fitted line at the highest temperatures. The high temperature data could also be fitted with equation 3.4.4.1. with A = 8.0 x 10^{-4} emu mol^{-1} and C = 0.15 emu mol^{-1} K which is 40% of the S = 1/2 value and agrees with the value obtained when the data was fitted to the Curie-Weiss law. Below the transition the data can be fitted to equation 3.4.4.1. as for NaC_{60}.5thf, where A = 6.5 x 10^{-4} emu mol^{-1} and C = 0.037 emu mol^{-1} K. Following the same procedure as for NaC_{60}.5thf the value of C corresponds to 10% of the material being paramagnetic below 120K and a density of states of 10 states eV^{-1} from the measured static susceptibility and a value of 13 states eV^{-1} when a correction is made for the Landau diamagnetism.

Calculation of the isotropic Knight shift using 13 states eV^{-1} for the density of states gives a Knight shift of 140ppm. The observed chemical shift at 150K is 250ppm, 70ppm from the observed shift at room temperature.

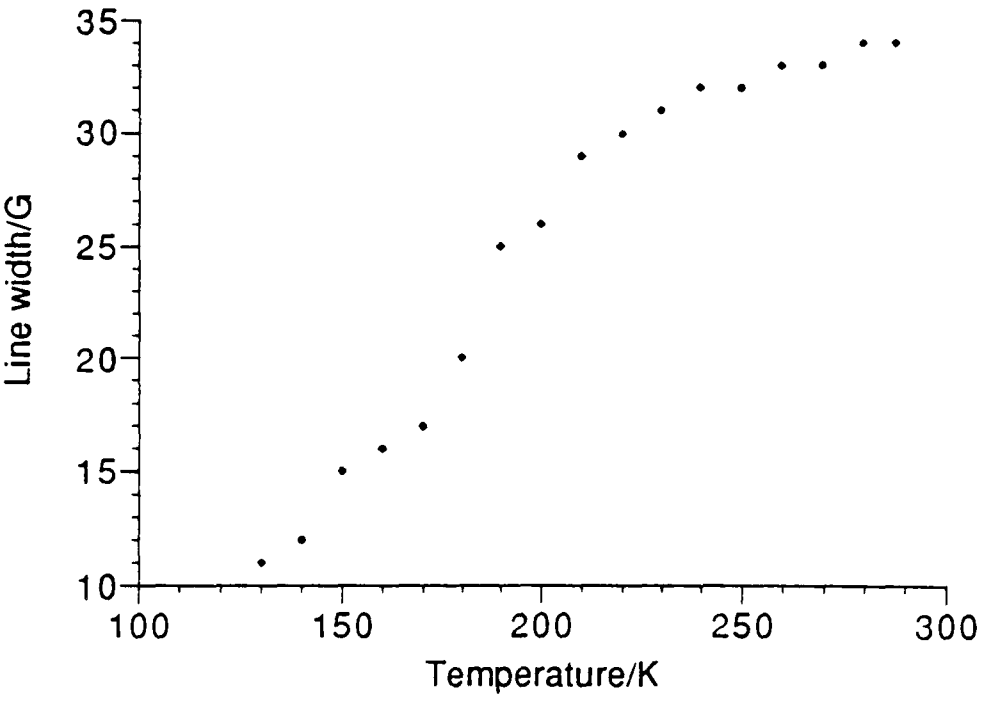


Figure 3.7.4.3. ESR linewidth as a function of temperature for solid NMe_4C_{60}.1.5thf.

ESR spectroscopy in the solid and solution state showed very similar behaviour to NaC_{60}.5thf with respect to linewidths, intensities and g-value. In a frozen thf glass a temperature dependent linewidth is observed from 21G at 135K, up to 40G at 190K. This is compared to 44G and 50G respectively at the same temperatures observed for NaC_{60}.5thf. In the solid state the temperature dependence of the linewidth is shown in

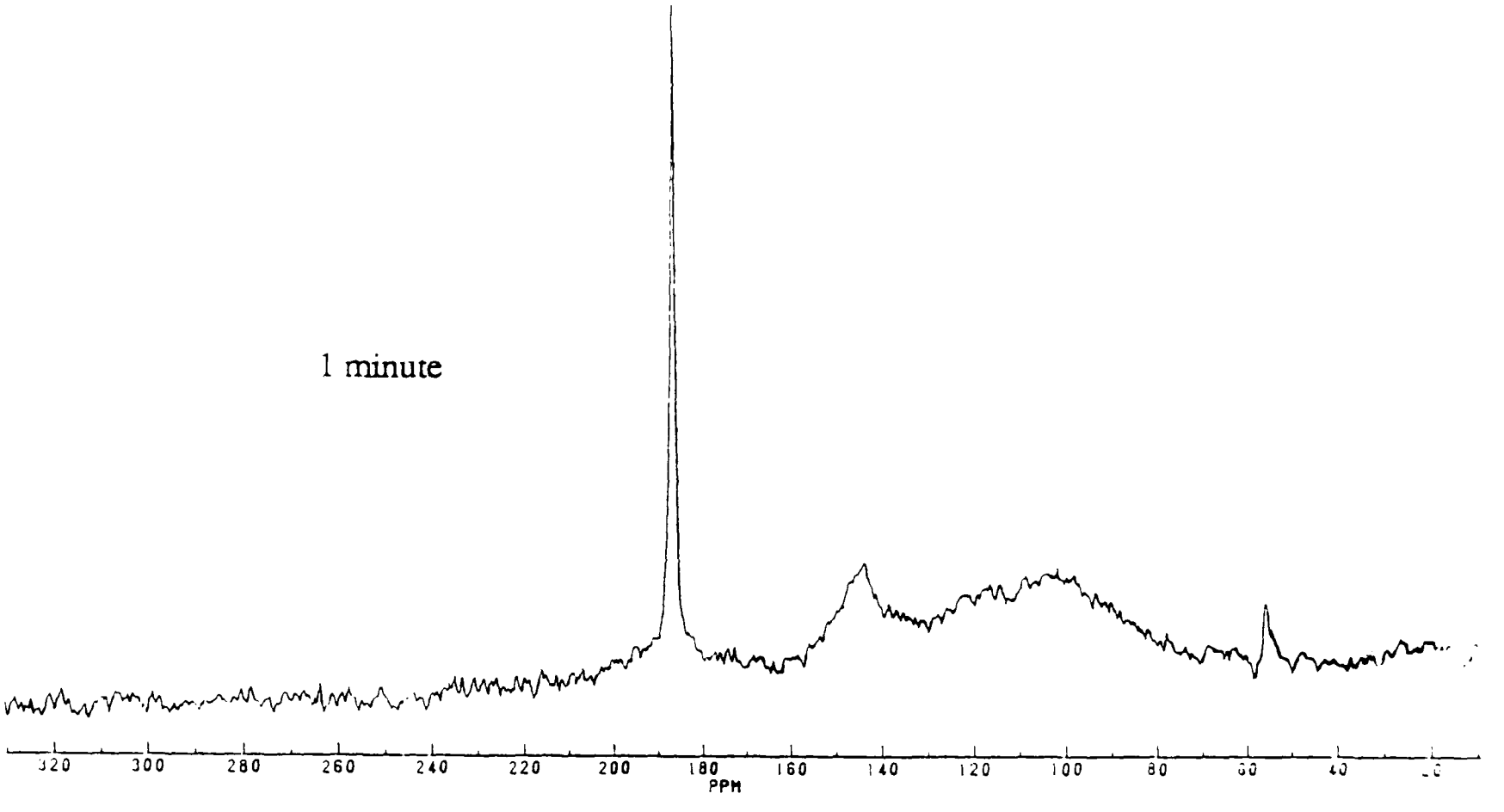
figure 3.7.4.2, again a plateau region being observed above approximately 200K, and the intensity data qualitatively corroborates the results obtained from SQUID magnetometry. A constant g-value of approximately 1.997 was observed at all temperatures.

3.7.5. Some Chemistry of NMe_4C_{60}.1.5thf.

On exposure of solid NMe_4C_{60}.1.5thf to oxygen and moisture, decomposition is very slow, in stark contrast to NaC_{60}.5thf. Decomposition can be followed by ^{13}C MASNMR spectroscopy as shown in figure 3.7.5.1. The compound NMe_4C_{60}.1.5thf is blue/black in colour but only after several months does the colour significantly change to brown, noting that in the ^{13}C MASNMR spectrum NMe_4^+ cations are clearly evident with a peak at δ 55ppm. Interestingly, the decomposition product is not C_{60}, as shown in figure 3.7.5.1, and this is also shown by the fact that the decomposition material is insoluble in all common solvents including toluene. If a thf solution is exposed to air a brown solid is precipitated in a matter of seconds, but a MeCN solution, exposed in an identical manner, decomposes from a deep cherry red to a deep orange solution (MeCN solutions of NaC_{60}.5thf decompose to a brown precipitate and colourless supernatant, analogous to thf solutions). On removal of the volatiles the material does not redissolve in any common organic solvent. ^{13}C NMR spectroscopy of a decomposed d_3-MeCN solution did not show any peaks other than those from the solvent. However ^{1}H NMR spectroscopy showed a broad peak centred at δ 2.3ppm, with no evidence of the NMe_4^+ cation resonance usually observed at δ 3.1ppm, as shown in figure 3.7.5.2. The origin of this peak is unclear. ^{13}C MASNMR of a decomposed MeCN solution after removal of the volatiles showed a spectrum very similar to the aerial decomposition product of NMe_4C_{60}, as shown in figure 3.7.5.3. Polymerisation of organic derivatives of C_{60} is known as discussed in section 1.7 and this could be a possible explanation but as the material is insoluble and ^{13}C MASNMR was not particularly informative characterisation of this material is a difficult task.

Attempts were made to remove the occluded thf molecules at a variety of temperatures and time durations, under dynamic and static vacuums. All of the thf molecules could be removed, as determined by ^{1}H NMR spectroscopy in d_3-MeCN and shown in figure 3.7.5.4. ^{13}C MASNMR spectroscopy of the solvent free material showed a small change in the chemical shift of the C_{60} resonance from δ 186 to 183 ppm, and the presence of an extra broad peak centred at δ 144ppm, as shown in figure 3.7.5.5. The process is irreversible as recrystallisation of the desolvated material from thf, showed that the broad peak at δ 144ppm remained, as shown in figure 3.7.5.5.

The compound NMe_4C_{60}.1.5thf was reacted with two equivalents of rubidium in an attempt to synthesise the salt $(NMe_4)Rb_2C_{60}$. Three samples of NMe_4C_{60}.1.5thf were flame sealed in Pyrex tubes with two equivalents of rubidium metal, measured by



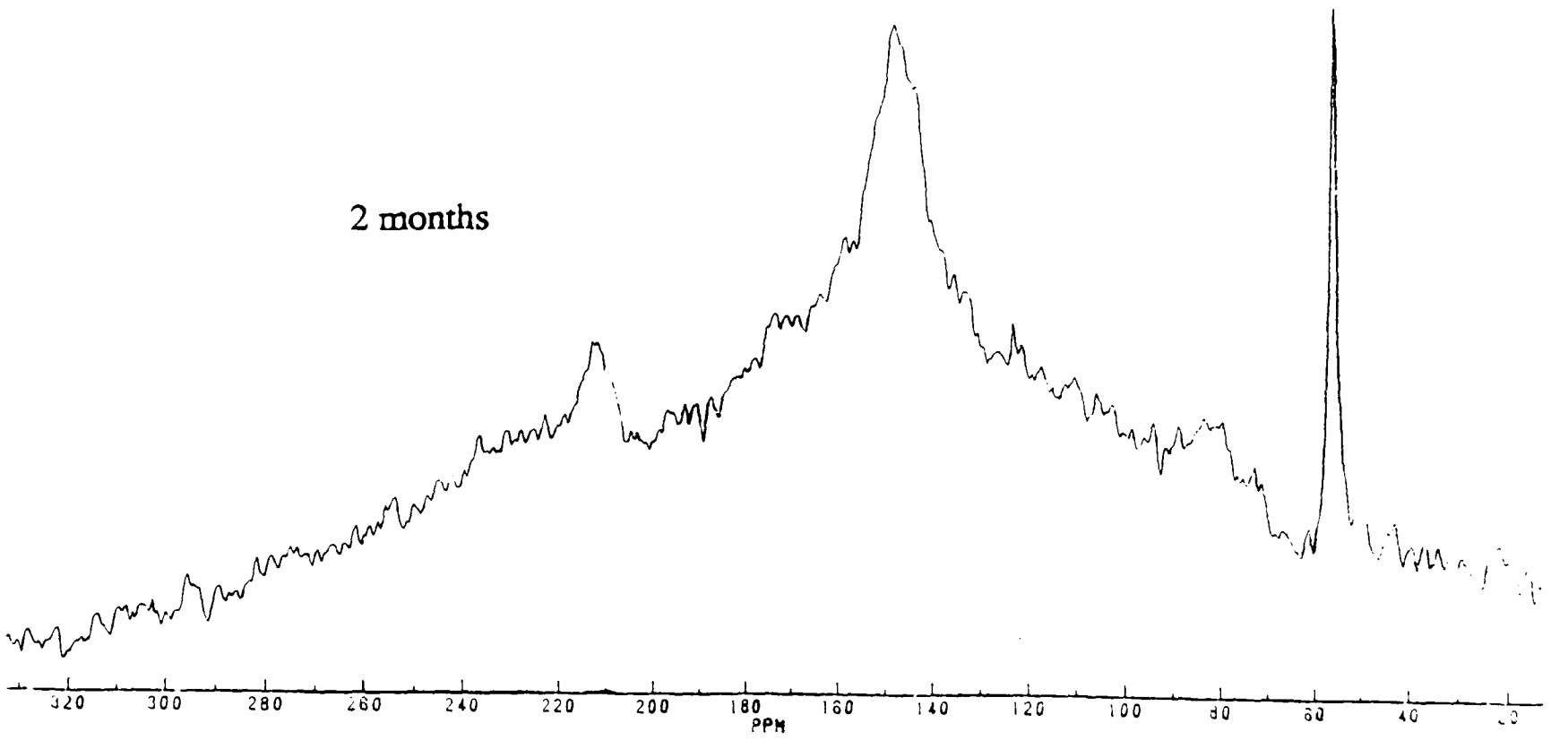


Figure 3.7.5.1. ^{13}C MASNMR spectra of $NMe_4C_{60}.1.5thf$ after exposure to air for the times indicated.

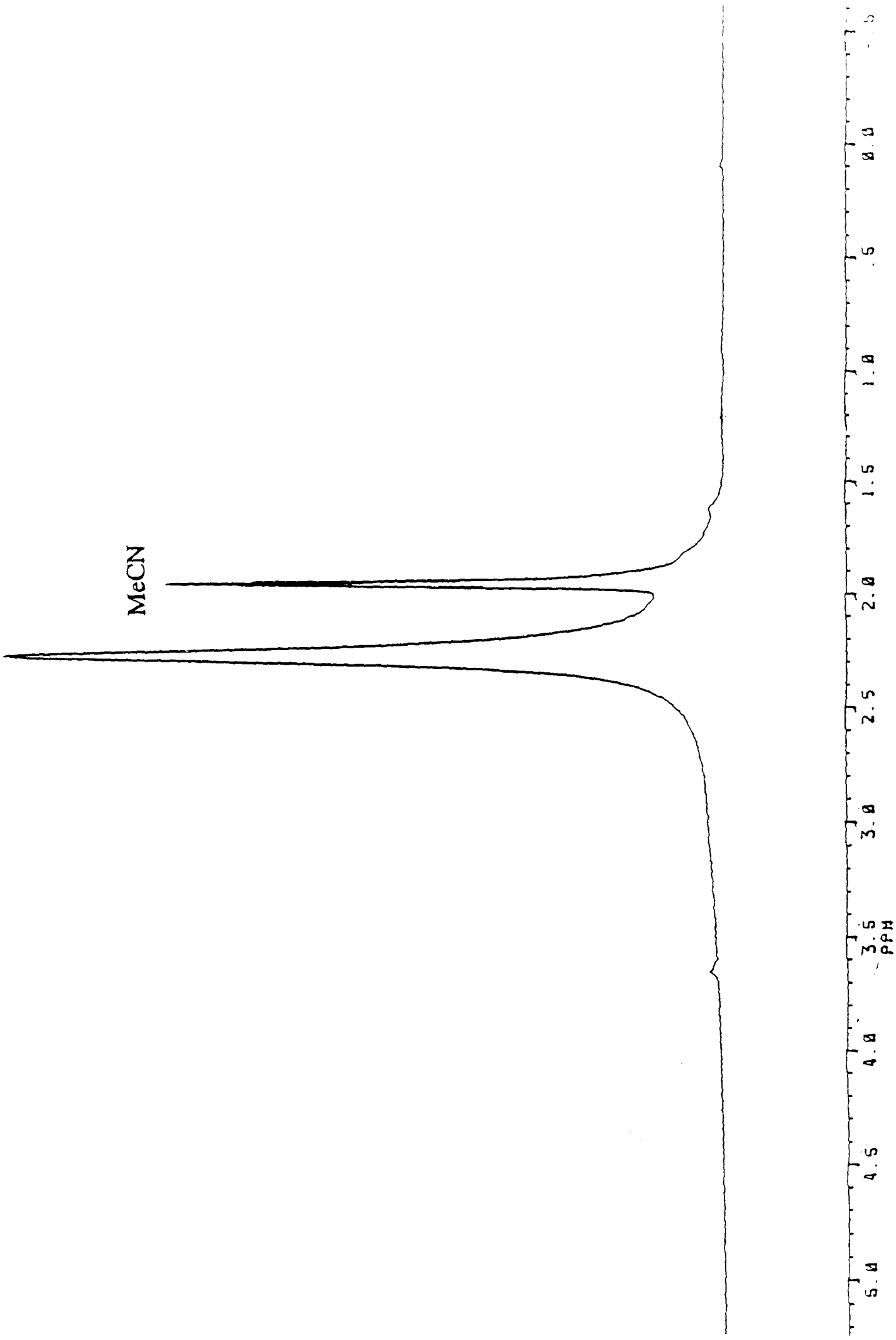


Figure 3.7.5.2. ^{1}H NMR spectrum of a d$_3$-MeCN solution of NMe_4C_{60}.1.5thf after exposure to air for 1 minute.

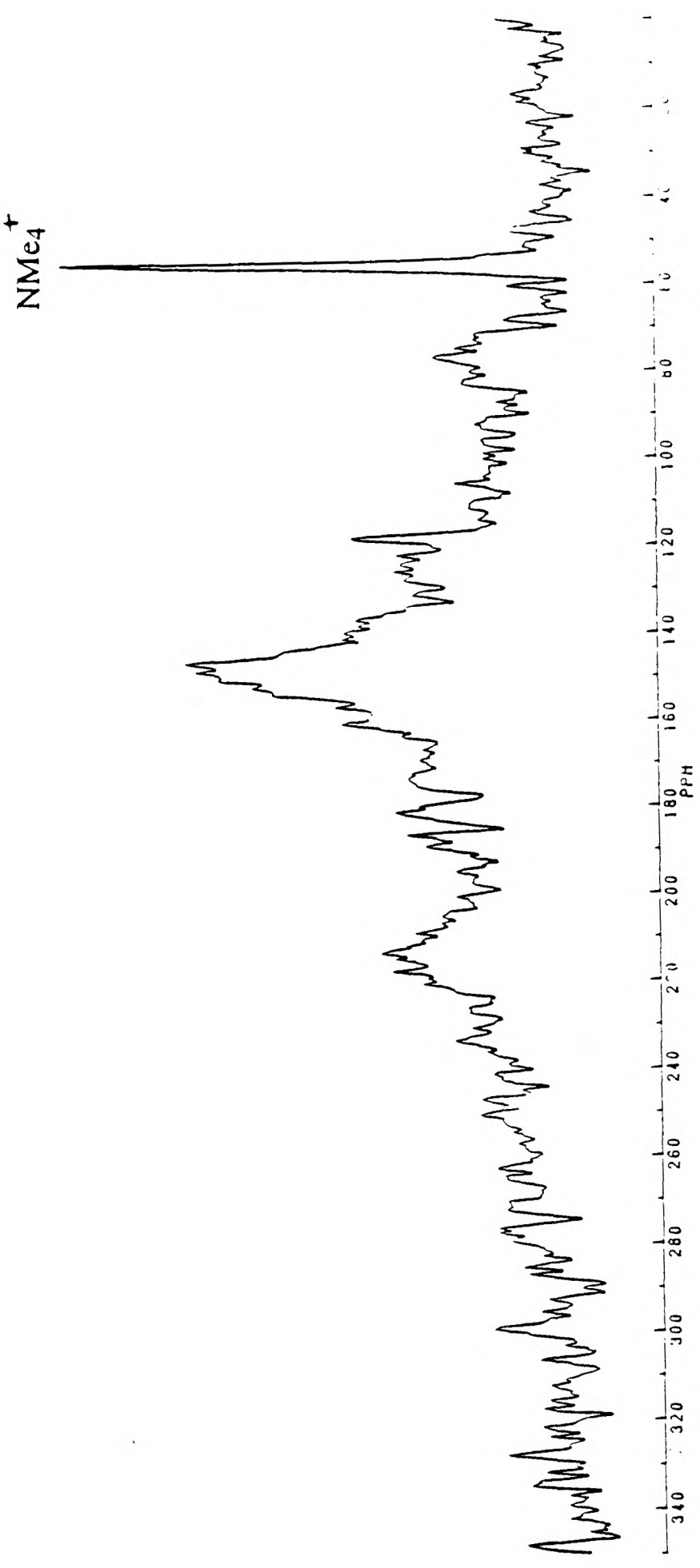


Figure 3.7.5.3. ^{13}C MASNMR spectrum of a sample prepared by allowing an intense cherry red MeCN solution of $NMe_4C_{60}.1.5thf$ to decompose to an intense orange solution and the volatiles subsequently removed under reduced pressure.

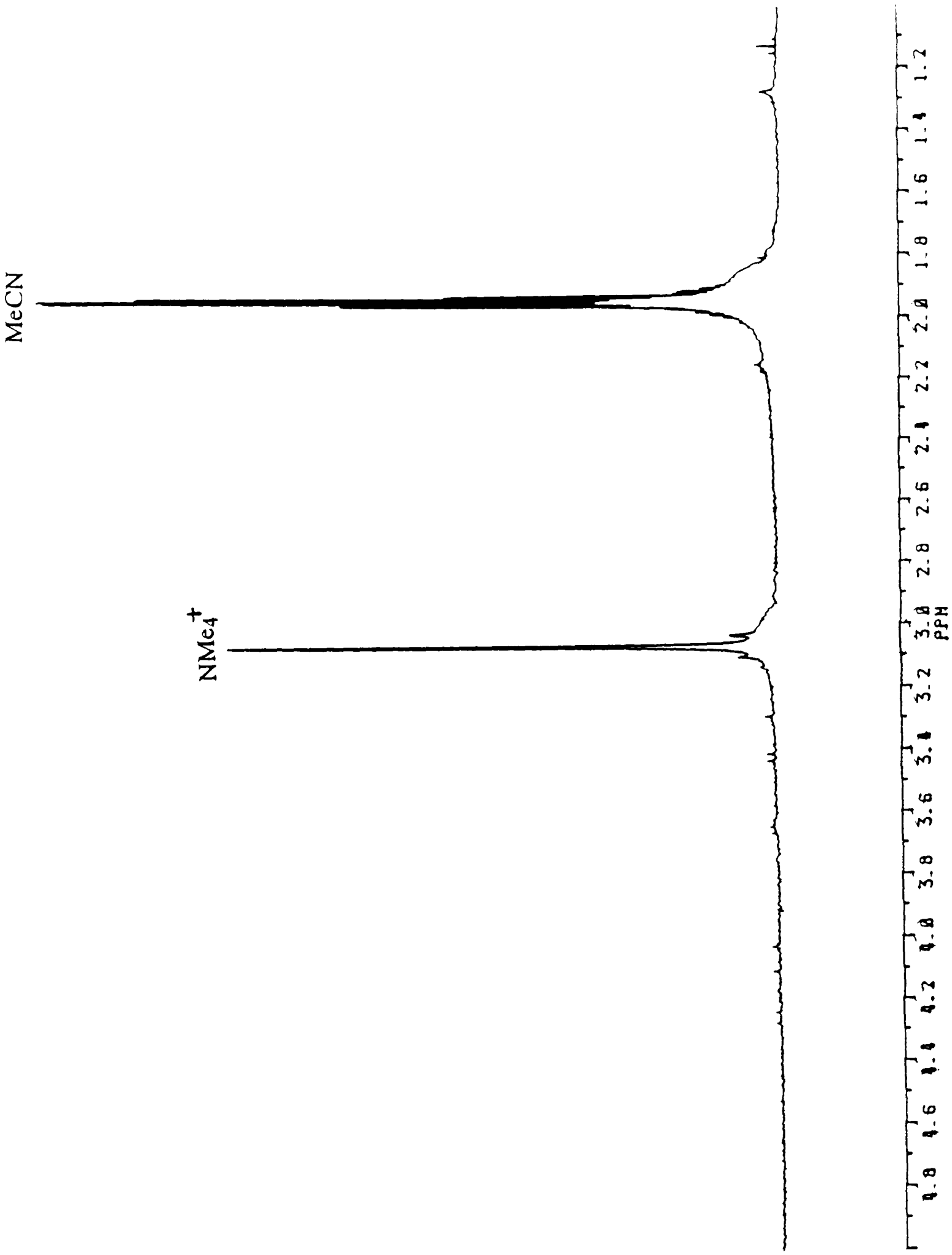


Figure 3.7.5.4. ^{1}H NMR (d_3-MeCN) of $NMe_4C_{60}.1.5thf$ after heating at 50°C for 12 hours under a dynamic vacuum of 10^{-5} mbar.

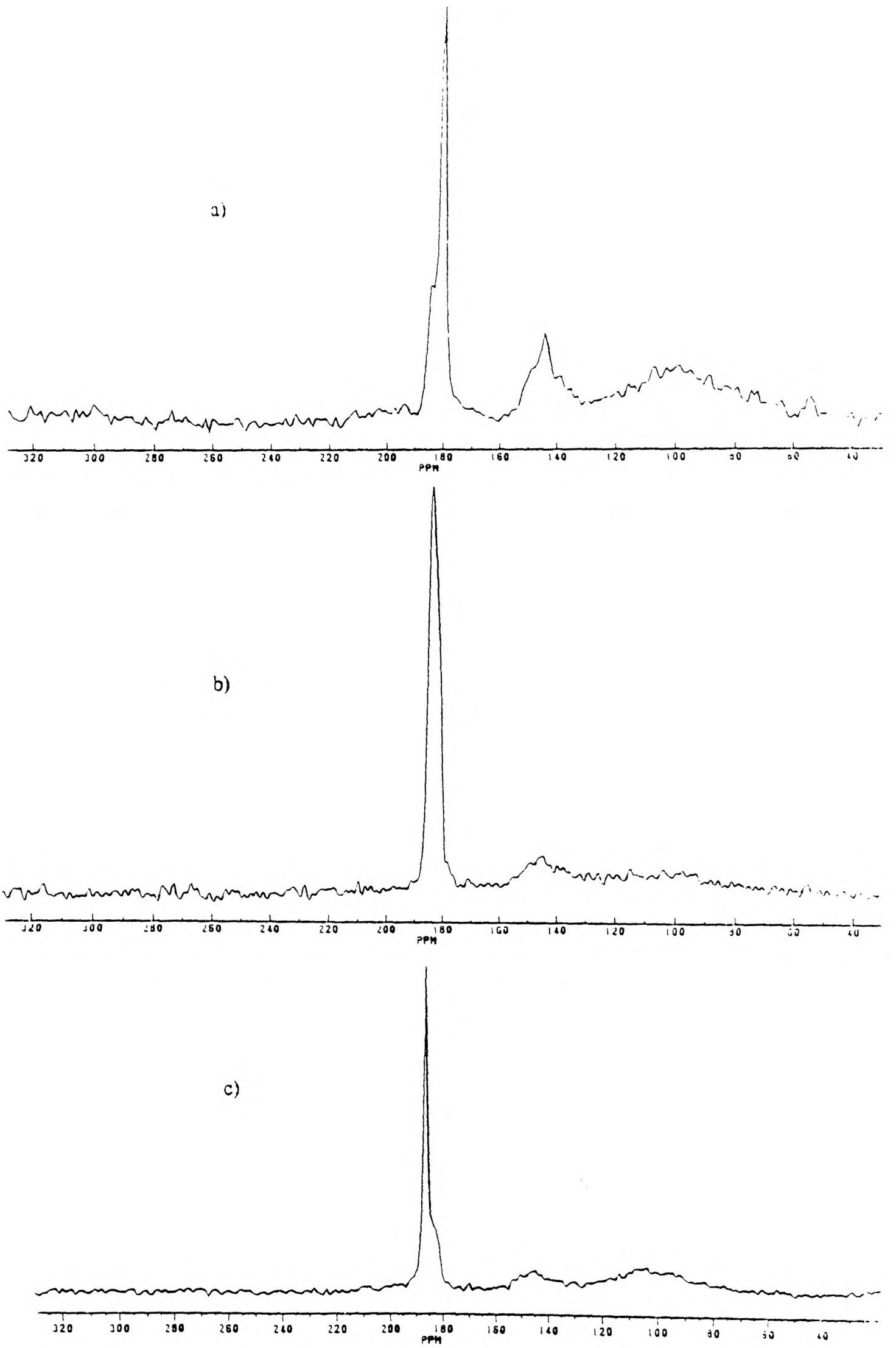


Figure 3.7.5.5. ^{13}C MASNMR spectra of a) desolvated NMe_4C_{60} b) intermediate solvation and c) the desolvated sample recrystallised from thf.

the capillary technique, under a pressure of 10^{-5}mbar of helium. These samples were heated at 150, 200 and 350°C respectively for 5 days. Analysis by ^{13}C MASNMR spectroscopy showed essentially the same result for each sample, two broad peaks at δ 186ppm and δ 145ppm, as shown in figure 3.6.5.6. The chemical shift of the peak at δ 186ppm could correspond to that of NMe_4C_{60}.1.5thf but the linewidth is approximately 10 times greater. SQUID magnetometry showed that no superconducting phase was present above the lowest attainable temperature of 6K. This observation is somewhat surprising as some fraction of the sample was expected to be impurity Rb_3C_{60}. Failure of the reaction could be due to the thermal instability of NMe_4^+ cations in the presence of rubidium atoms and/or C_{60} anions so low temperature intercalation was attempted.

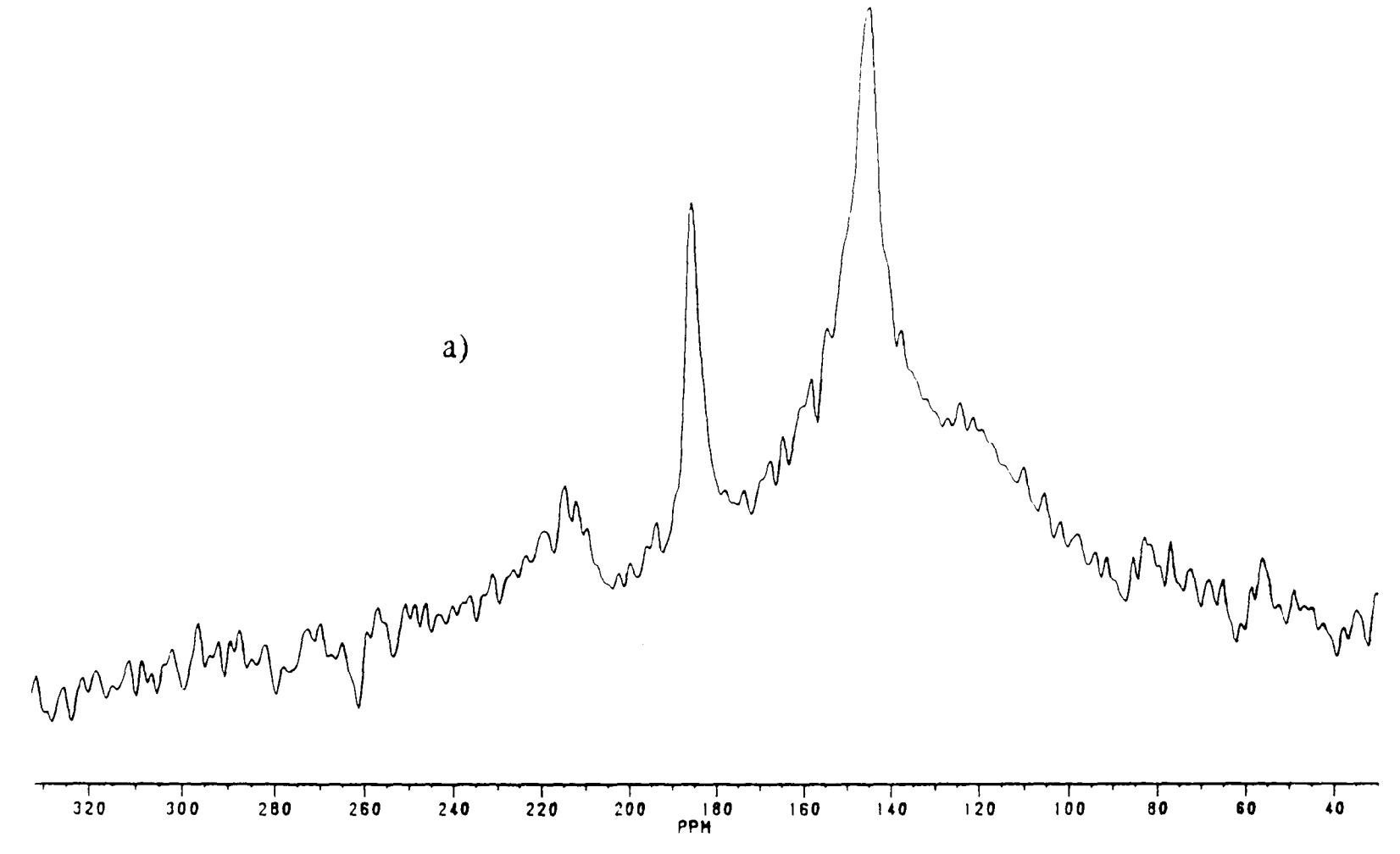
Low temperature intercalation of alkali metals can be achieved by the use of alkali metal alkyls such as ^{n}butyl lithium. The reaction is heterogeneous, and in the case of C_{60} materials this is especially necessary, as ^{n}butyl lithium acts as a nucleophile eventually producing alkyl-C_{60} isomers. A sample of NMe_4C_{60}1.5thf was suspended in hexane and an excess of 2.5M ^{n}butyl lithium in hexane was added to the stirring suspension. After stirring overnight the vast majority of the solid was still apparent, though an orange colouration had been imparted in the hexane supernatant. Isolation of the black solid and subsequent analysis by ^{13}C MASNMR showed that no NMe_4C_{60}.1.5thf remained and that two new peaks at δ 183 and δ 181 ppm were evident as shown in figure 3.7.5.6. ^7Li powder NMR spectroscopy at 77.77MHz showed an extremely broad resonance at δ 6ppm, $\upsilon_{1/2}$ = 7kHz, as shown in figure 3.6.5.7. ^7Li MASNMR spectroscopy at 77.77MHz showed a narrower peak at δ 3ppm, $\upsilon_{1/2}$ = 3kHz, with a shoulder at δ 15ppm, as shown in figure 3.7.5.7. ^7Li MASNMR spectroscopy performed at 155.54MHz showed essentially the same spectrum indicating that the ^7Li present in the sample is probably disordered and that the peak shape is not due to the possibly remaining second order quadrupolar interaction between ^7Li nuclei and the external magnetic field, that was not eliminated by MAS.

3.7.6. Discussion on NMe_4C_{60}.1.5thf.

Metathesis of NaC_{60}.5thf with NMe_4F in MeCN at -5°C gives the compound formulated as NMe_4C_{60}.1.5thf. This material is very soluble in thf, an advantage over all other C_{60} synthons and measurements indicate that it has very similar properties with respect to dynamics and magnetism as the parent compound NaC_{60}.5thf.

The similar magnetic properties indicate that the completely organic material NMe_4C_{60}.1.5thf could possess metallic character at low temperature. This is not completely surprising as it is expected that the electronic wave function is dominated by the C_{60} molecules and that the cations are essentially present only to preserve electroneutrality.

It has also been demonstrated that ^{n}BuLi dissolved in hexanes can be used to successfully intercalate lithium into alkali metal C_{60} compounds.



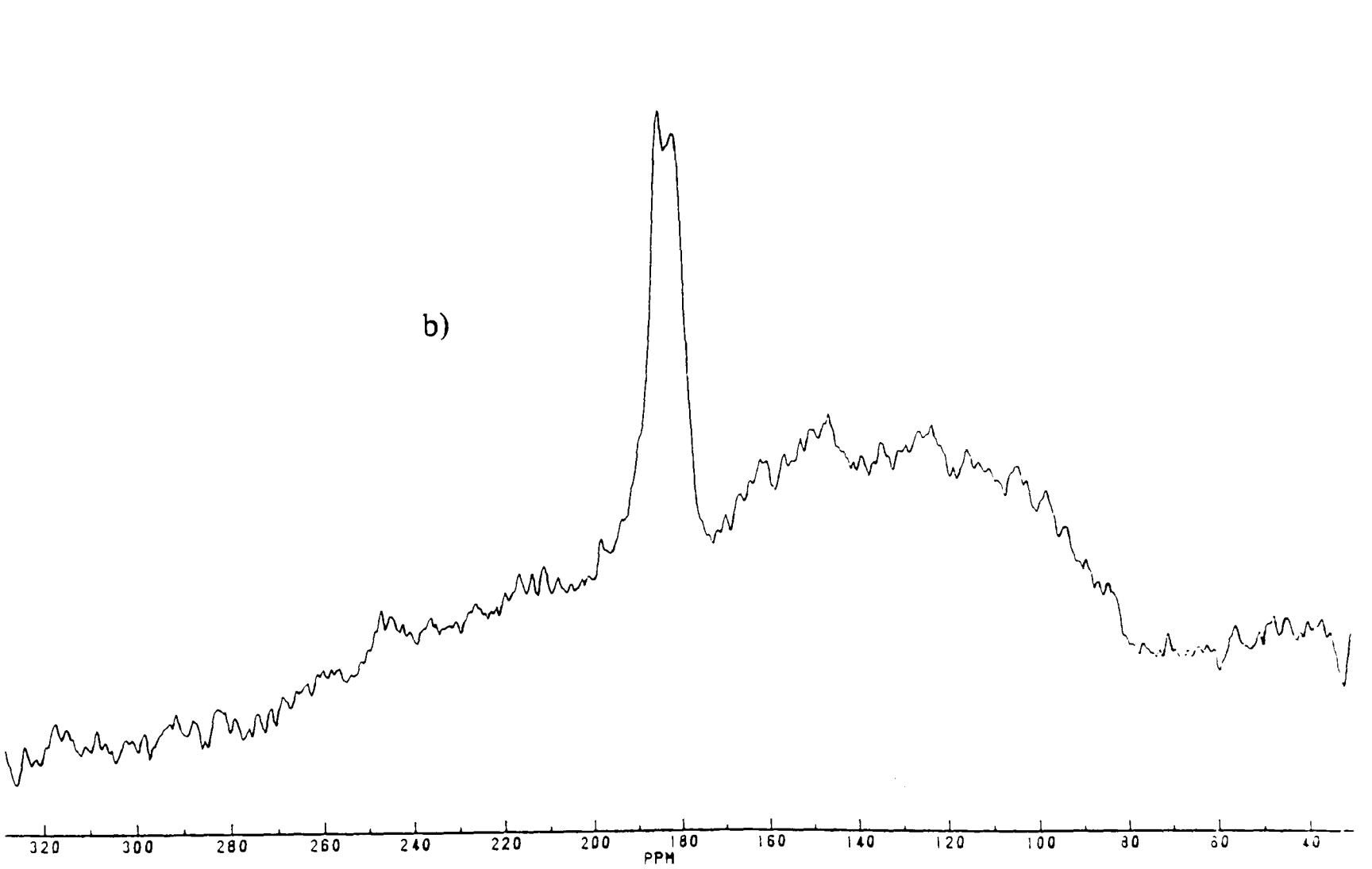
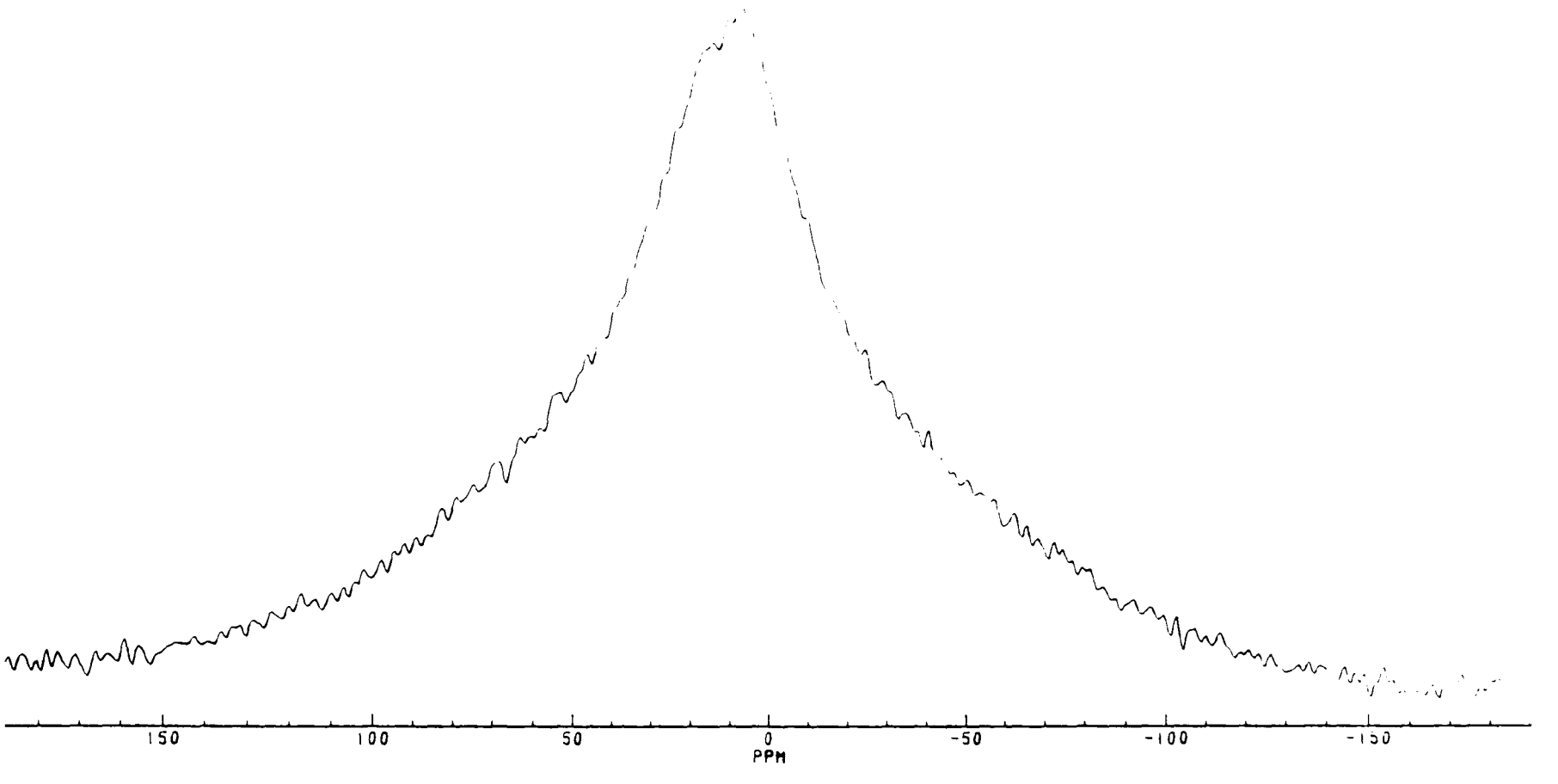


Figure 3.7.5.6. ^{13}C MASNMR spectra of a) reaction of $NMe_4C_{60}.1.5thf$ with two equivalents of rubidium metal at 150°C for 5 days and b) reaction of $NMe_4C_{60}.1.5thf$ with excess 2.5 M ^{n}butyl lithium in hexane at room temperature for 24 hours.



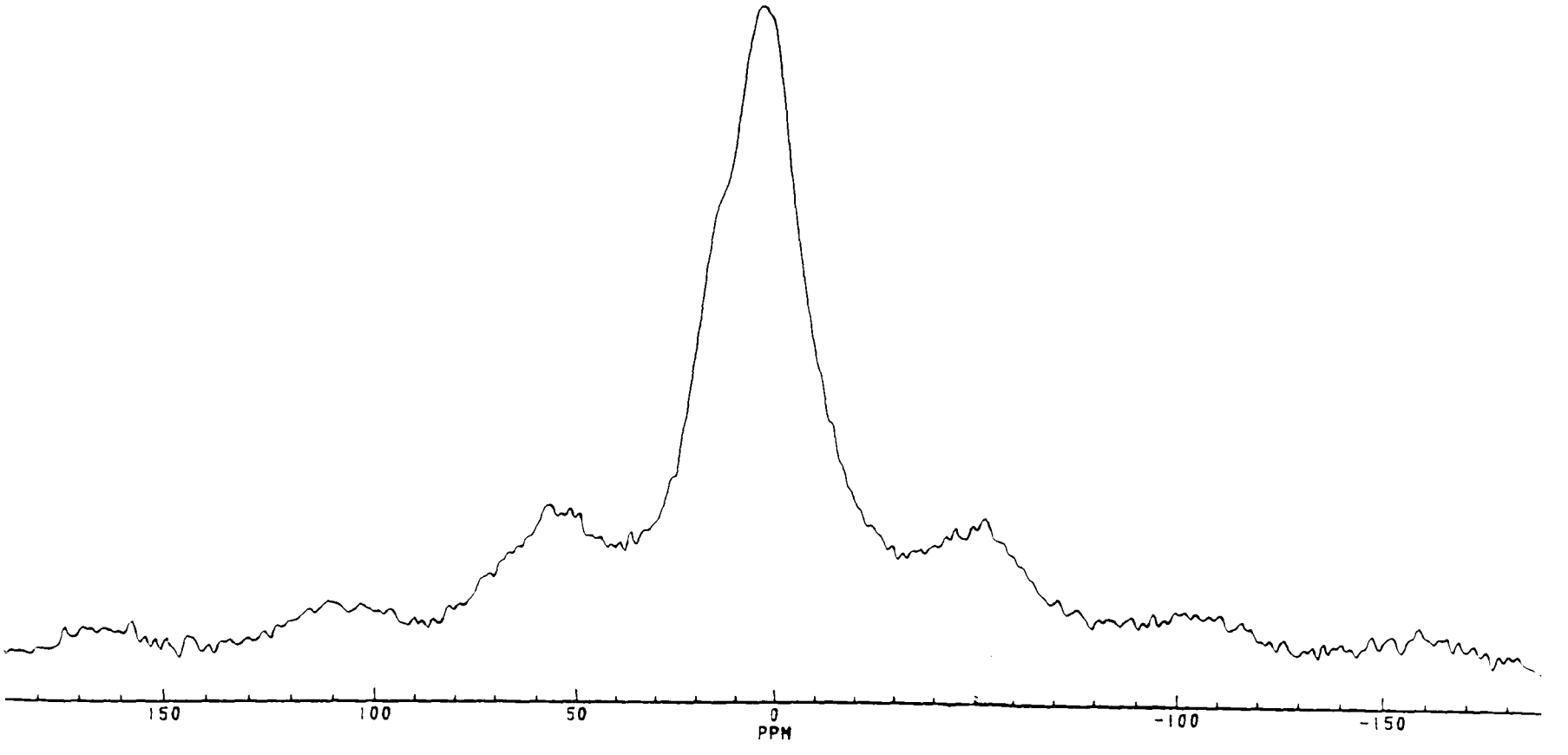


Figure 3.7.5.7. ^{7}Li powder and MASNMR spectra from reaction of $NMe_4C_{60}.1.5thf$ with excess 2.5 M ^{n}butyl lithium in hexane at room temperature for 24 hours.

3.8. Investigations into the Sodium C_{60} Phase Diagram.

The synthesis of Na_1C_{60} and solid solutions up to the composition Na_3C_{60} using a solid state technique has been reported.[25] Synthesis was accomplished by simply diluting Na_9C_{60} with the appropriate amount of C_{60} in an evacuated copper tube, and heating for several hours at temperatures up to 600°C.[19] Experimental evidence consisted of variable temperature synchrotron powder X-ray diffraction of a composition $Na_{1.3}C_{60}$ and DSC measurements plotting temperature and enthalpy change of the structural phase transition from fcc to simple cubic as a function of sodium concentration.

Synthesis of Na_1C_{60}, by solid state techniques, would provide a clean reaction route as no solvent is present. The proposed structure at room temperature is fcc, in contrast to the insoluble, 1-dimensional polymers Rb_1C_{60} and Cs_1C_{60}, which have orthorhombic phases. As a consequence, Na_1C_{60} may be rendered soluble in polar organic solvents such as thf.

3.8.1. Attempted Synthesis of Na_1C_{60}.

To avoid weighing out very small quantities of sodium metal (~1-2mg), or the use of large amounts of C_{60} (~300-500 mg), the strategy of synthesis of Na_2C_{60} followed by dilution to Na_1C_{60} was attempted. Very high confidence is placed in the existence of Na_2C_{60}; it has a documented and refined powder X-ray pattern,[20] a well defined ^{13}C MASNMR spectrum and has been successfully synthesised repeatedly in other laboratories including the Inorganic Chemistry Laboratory, Oxford.

After successful synthesis of Na_2C_{60}, a 50 mg sample was diluted with one equivalent of C_{60}, ground in an agate mortar and pestle, placed in a stainless steel tube, and flame sealed in a silica tube under 10^{-5} mbar of He, as shown in figure 3.8.1.1.

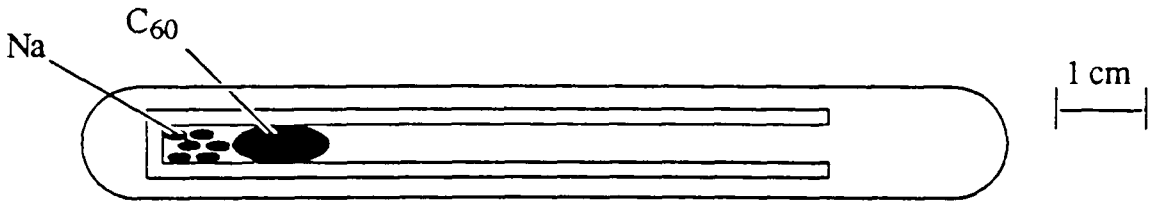
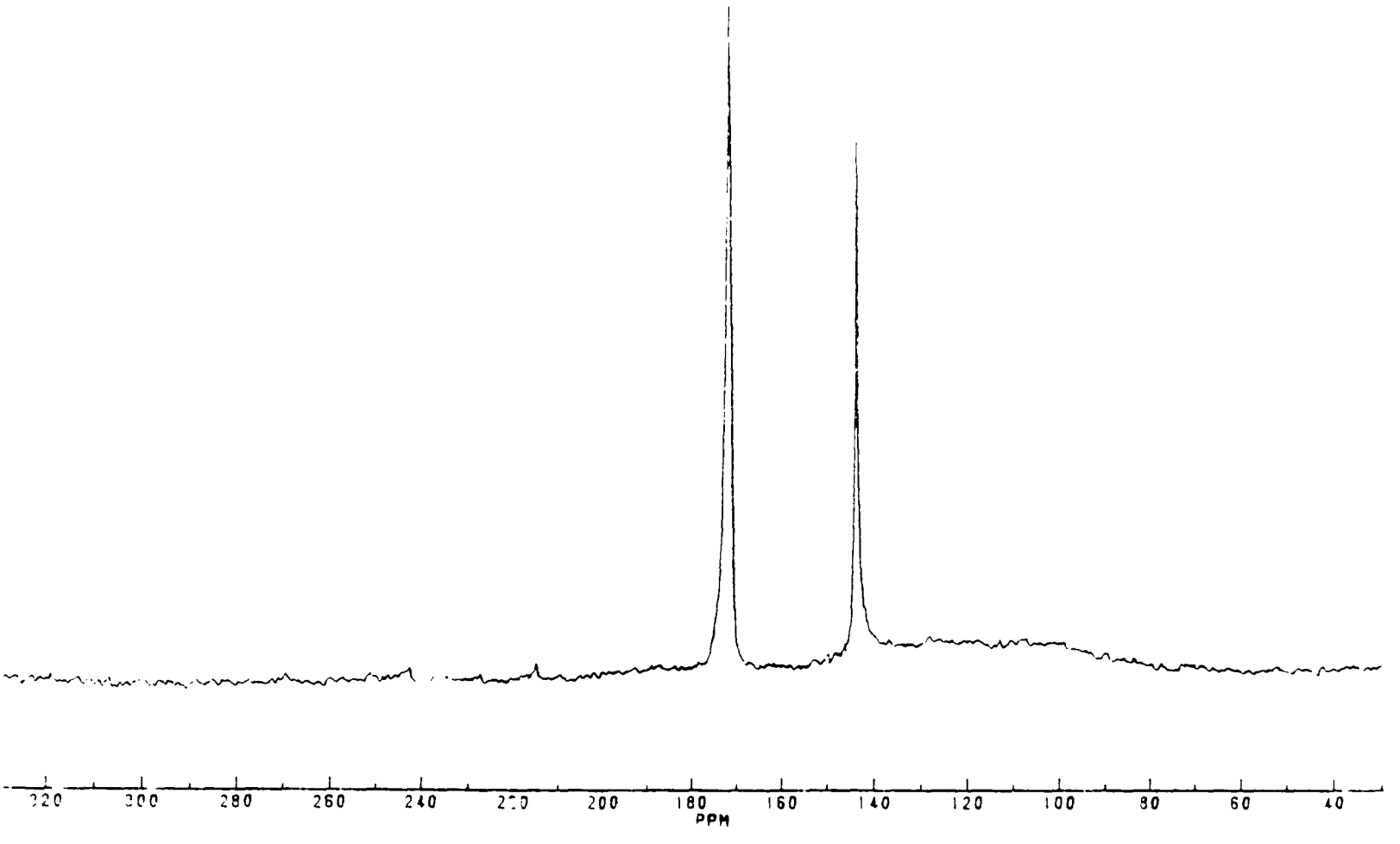


Figure 3.8.1.1. Apparatus used for the synthesis of Na_xC_{60} phases.

This was then heated in stages from 100 to 500°C and annealed at 500°C for 5 days. As shown in figure 3.8.1.2. ^{13}C MASNMR spectroscopy shows peaks at δ 143ppm and δ 172ppm which correspond to pure C_{60} and Na_2C_{60} respectively. On heating for a further 7 days at 600°C no difference was observed in the ^{13}C MASNMR spectrum. The ^{13}C MASNMR data implies no further reaction has taken place.

Synchrotron powder X-ray diffraction was the main evidence for the phase $Na_{1.3}C_{60}$ and did not show obvious evidence at 300K that the peaks could be indexed using a multiphase model. A lattice parameter of 14.184Å was calculated from indexing the pattern on a fcc lattice in contrast to 14.17Å for pure C_{60}. One can easily calculate



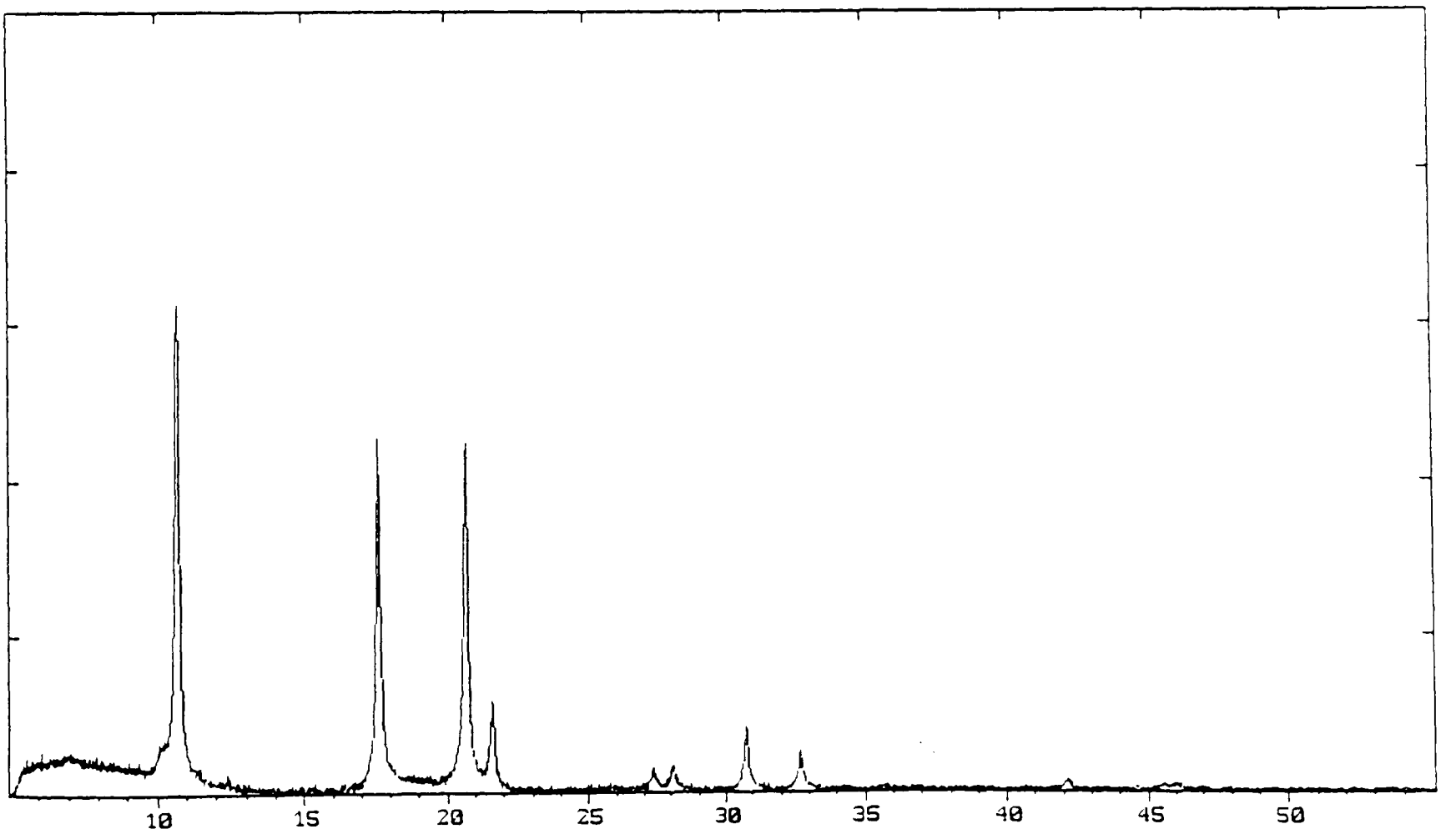


Figure 3.8.1.2. ^{13}C MASNMR and powder X-ray diffraction pattern from reaction of Na_2C_{60} and one equivalent of C_{60} at 550°C for 5 days.

the position of a particular reflection from the lattice parameter and wavelength of the incident radiation within a cubic lattice using equation 3.8.1.1.

$$\sin^2\theta = \frac{\lambda}{2a}(h^2 + k^2 + l^2)$$

Equation 3.8.1.1.

Where θ is the position of the reflection, λ is the wavelength of the incident radiation, *a* is the lattice parameter and (hkl) are the Miller indices of the reflection at position θ.

It can be seen that taking the literature values[9] of 14.184Å for the lattice parameter of $Na_{1.3}C_{60}$ and 1.15Å for the wavelength of the incident synchrotron X-ray radiation, and comparing the (220) reflection with that of pure C_{60}, a difference of only one hundredth of a degree is calculated. No explicit mention is made of the step size used during data collection, but close examination of illustrations of the data, and a sensible step size to maximise resolution and the signal to noise ratio, favour a step size of at least 0.01° to be expected.

The compound Na_2C_{60} has a lattice parameter of 14.189Å which gives a discrepancy of 16 thousandths of a degree for the (220) reflection. Taking into account other line broadening effects such as the domain sizes of the microcrystalline sample, and errors in measurement of the lattice parameter, the discernment of peaks from a multiphase sample containing Na_2C_{60} and C_{60} would not be possible at the resolution implied in the report of the structure of $Na_{1.3}C_{60}$. It is also worth noting that the compound Na_3C_{60} has a value for the lattice parameter of 14.183Å.

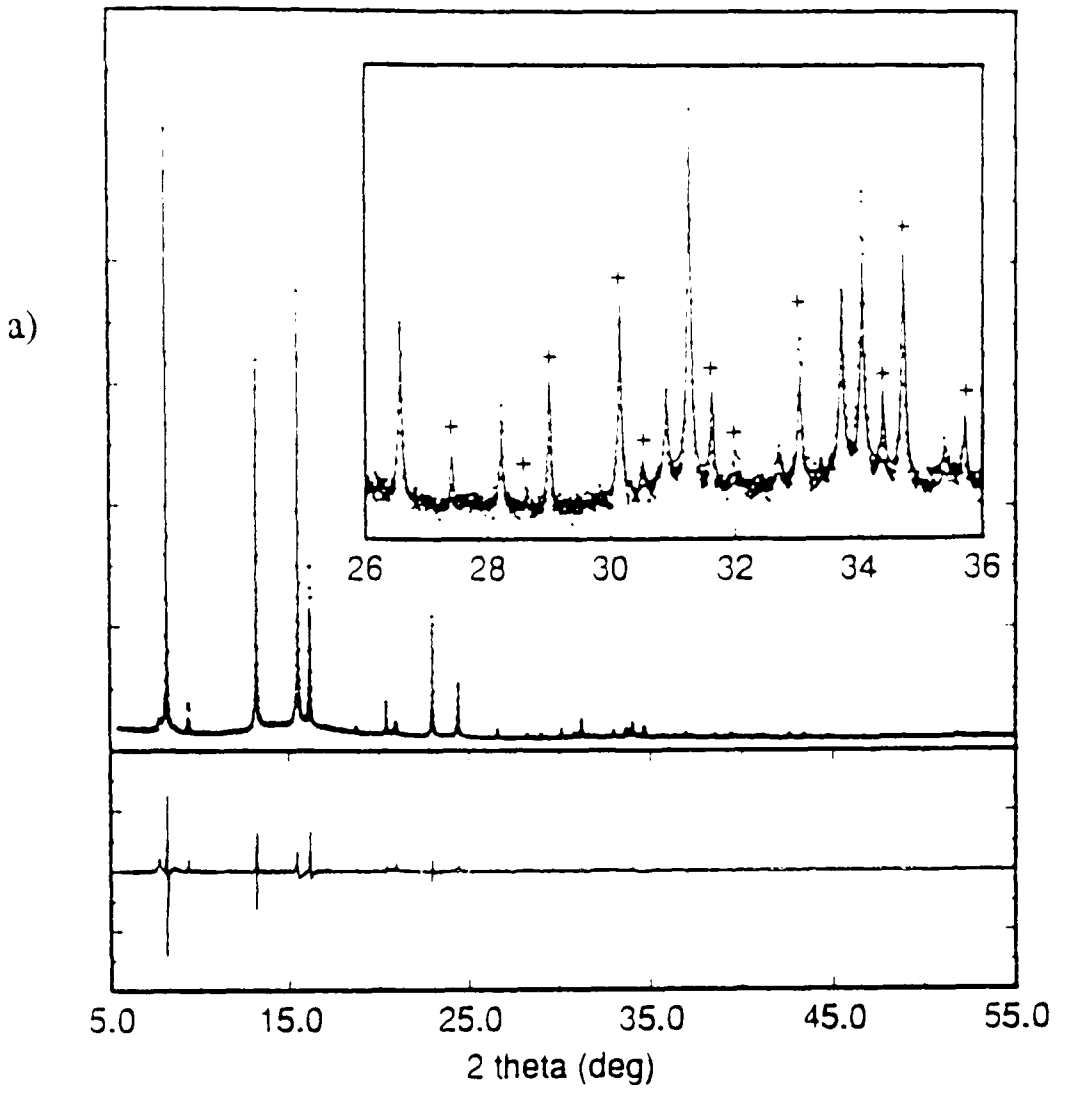
At lower temperatures it can be noted that a large asymmetry is evident in some of the peaks of the synchrotron powder X-ray pattern of $Na_{1.3}C_{60}$, possible indication of a multiphase sample where the phases have differing thermal coefficients of expansion.

Unfortunately the differential scanning calorimetry data eluded to in the report is not presented in detail and no comment can be made with respect to the broadness of the transition or exactly how measurements were performed.

3.8.2. Attempted Synthesis of $Na_{1.3}C_{60}$.

An attempt to synthesise $Na_{1.3}C_{60}$ from C_{60} and sodium metal gave similar results. The only peaks visible in the ^{13}C MASNMR spectrum were at δ 143ppm and δ 172ppm which correspond to C_{60} and Na_2C_{60}. Powder X-ray diffraction showed a pattern very similar to that reported for $Na_{1.3}C_{60}$ within the resolution and signal to noise of our instrument, as shown in figure 3.8.2.1. The small intensity differences seen in some of the peaks reflect the uncertainty in the exact sodium concentration.

Figure 3.8.2.2. shows a powder X-ray diffraction pattern of Na_2C_{60} and C_{60} with the composition $Na_{1.3}C_{60}$ which have been ground together in an agate mortar and pestle at room temperature and placed directly into a capillary for X-ray diffraction obtained at 1.54051Å in a 0.5mm capillary with a step size of 0.02°. No discernible



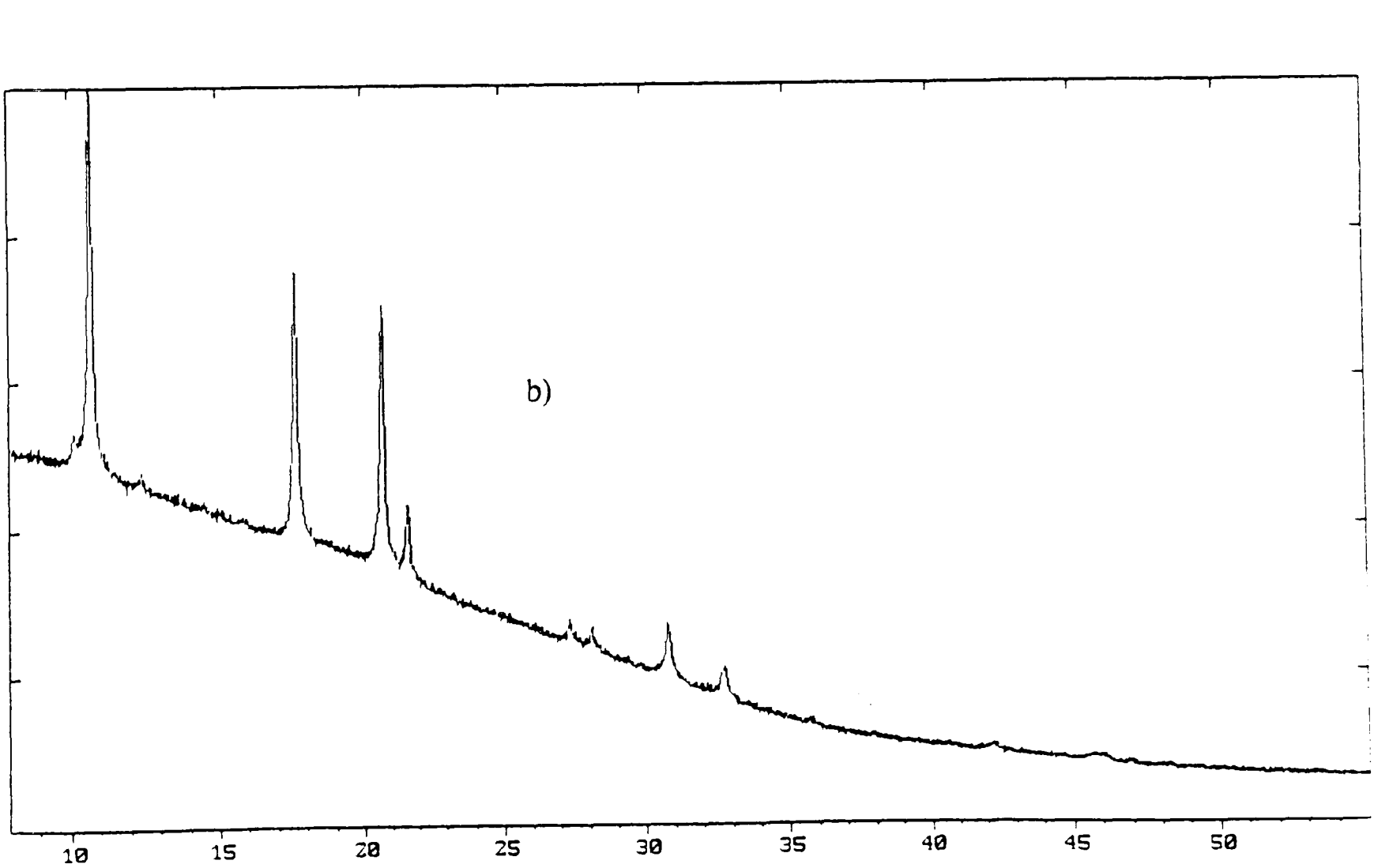


Figure 3.8.2.1. Powder X-ray diffraction pattern of '$Na_{1.3}C_{60}$' a) literature sample using synchrotron radiation at 1.15Å and b) sample prepared in the Inorganic Chemistry Laboratory , Oxford using Cu $K\alpha_1$ radiation at 1.54051Å.

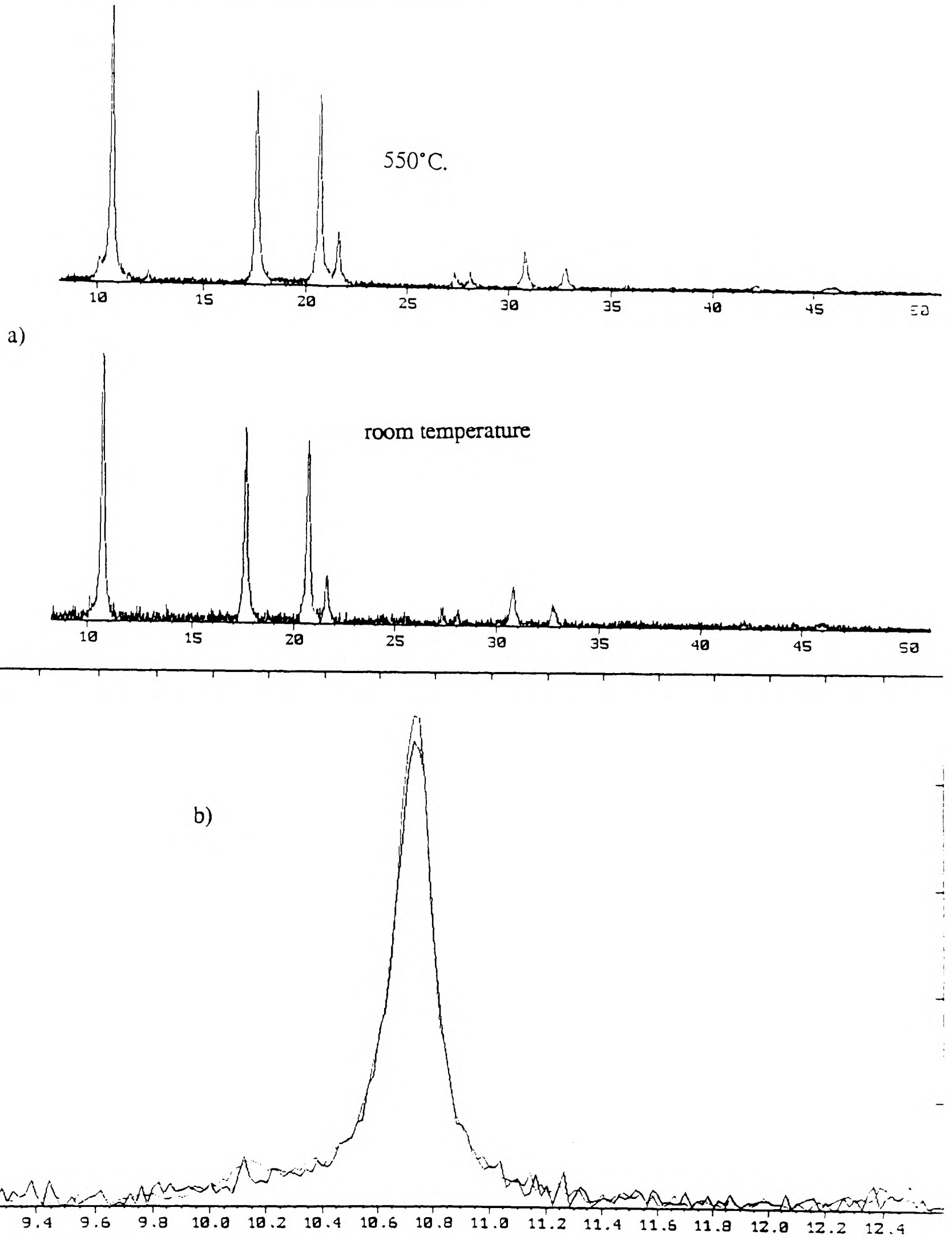


Figure 3.8.2.2. a) Comparison of powder X-ray diffraction of samples of '$Na_{1.3}C_{60}$' prepared at 550°C and at room temperature and b) expanded view of the (111) reflection of the two samples.

difference between the two samples is evident and superposition of the (111) reflection from both samples shows the linewidths at half the intensity are identical.

3.8.3. Attempted Synthesis of Na_1C_{60} and $Na_{1.3}C_{60}$ via Quenching.

It is possible that solid solution phases of sodium intercalates of C_{60} could be stabilised at high temperatures and that by rapid quenching the structure could be effectively 'frozen in' to form a metastable phase. This has been demonstrated to a certain extent for K_1C_{60}, but the sample is only approximately 60% pure due to impurity equilibrium phases of C_{60} and K_3C_{60}. Quenching was achieved by heating the sample in a tube furnace positioned vertically above the bench to allow a bath of quenching oil to be positioned underneath, as shown in figure 3.8.3.1.

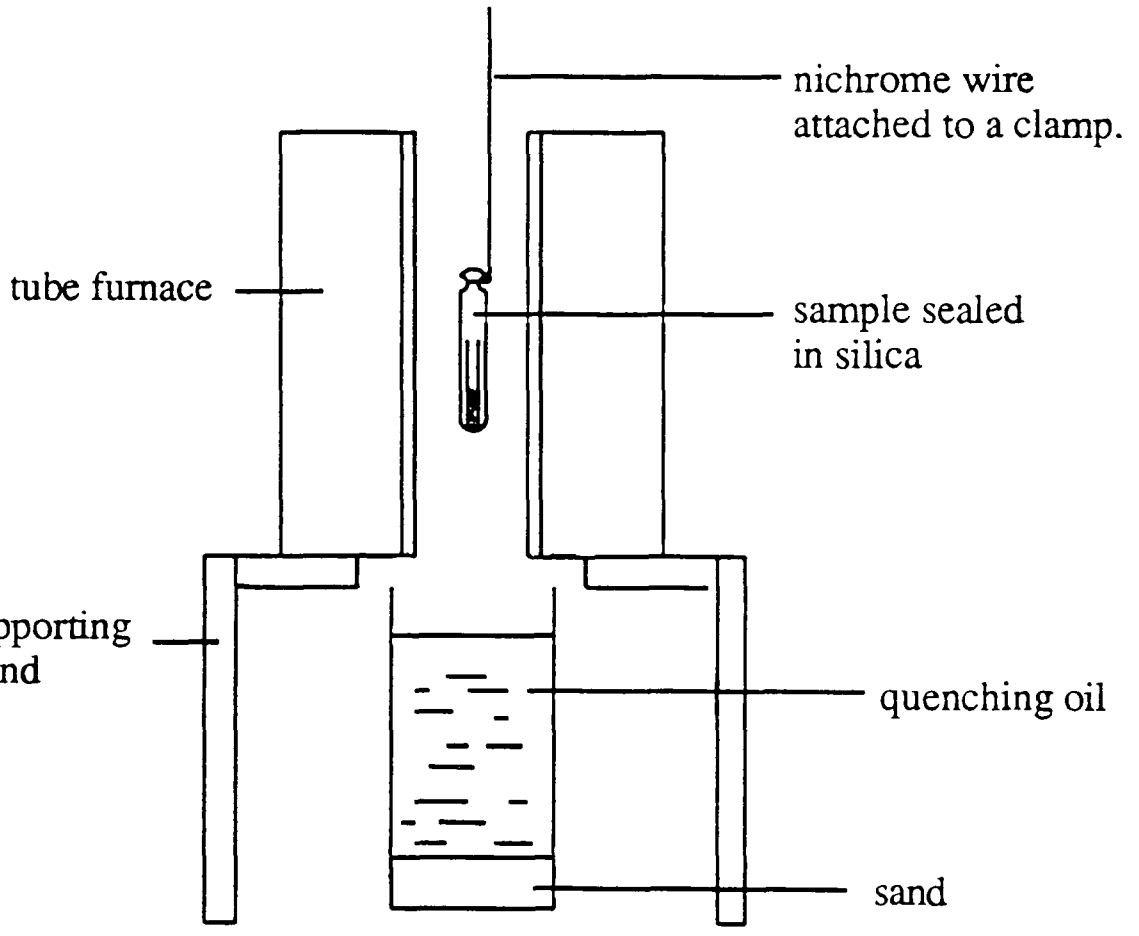


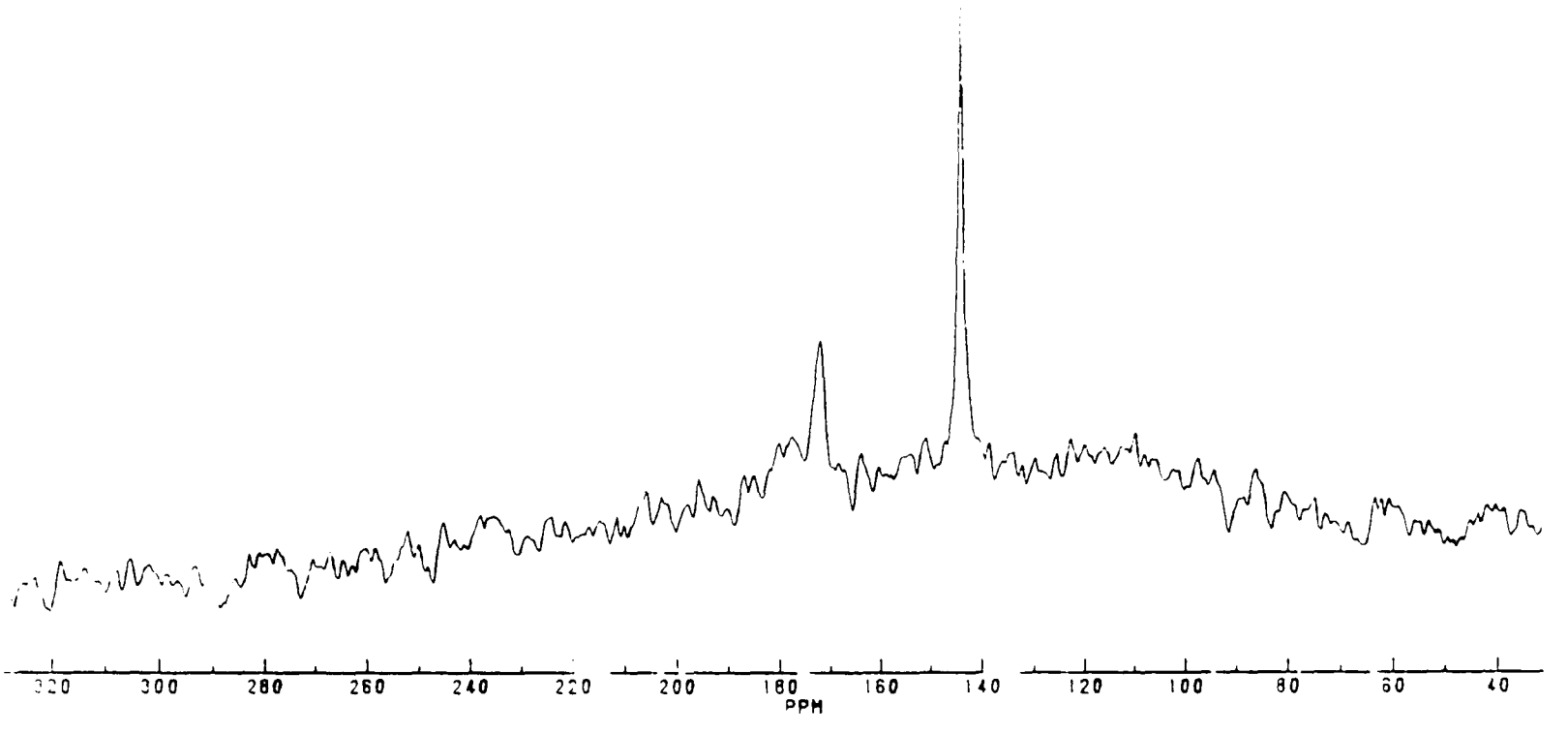
Figure 3.8.3.1. Apparatus used for quenching $Na_{1.3}C_{60}$ and Na_1C_{60}.

On cutting the suspension wire, the sample drops into the oil cooling at a rate which can kinetically stabilise thermodynamic metastable states.

From ^{13}C MASNMR data no reaction appears to have taken place in either case, as shown in figure 3.8.3.2.

3.8.4. Synthesis of $Na_{2.5}C_{60}$.

In an attempt to understand the possibility of solid solution phases between the compositions Na_1C_{60} and Na_3C_{60}, synthesis of a phase between Na_2C_{60} and Na_3C_{60} was attempted. To 2.5 equivalents of freshly cut sodium metal was added a 55mg sample of powdered C_{60} which was then placed in a stainless steel tube and flame sealed in a tube of silica under a pressure of 10^{-5} mbar of He. The sample was heated up to 500°C for 5 days but the reaction had not reached equilibrium as observed by ^{13}C



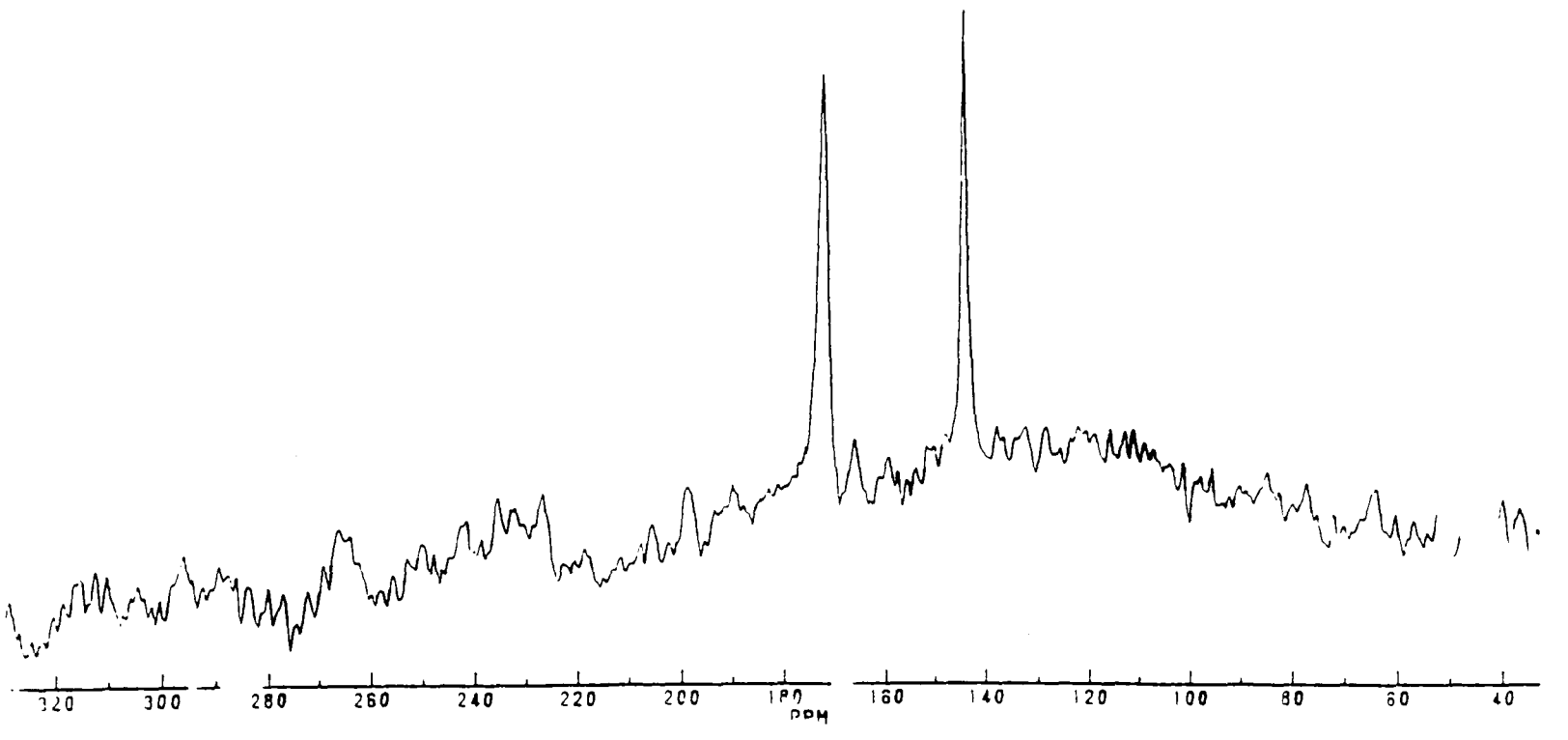


Figure 3.8.3.2. ^{13}C MASNMR of samples of composition Na_1C_{60} and $Na_{1.3}C_{60}$ quenched from 550°C.

MASNMR spectroscopy. After regrinding and further heating at 550°C for 7 days ^{13}C MASNMR spectroscopy showed only one peak at δ 179ppm, as shown in figure 3.8.4.1. A peak at this position has been observed previously but not solely. In the preparation of Na_2C_{60} and other unsuccessful synthesis of sodium C_{60} intercalates this peak can be observed with varying intensities.

Powder X-ray diffraction, shown in figure 3.8.4.1, shows peaks that cannot be indexed on a fcc structure. Attempts at indexing all the peaks within one space group have so far been unsuccessful.

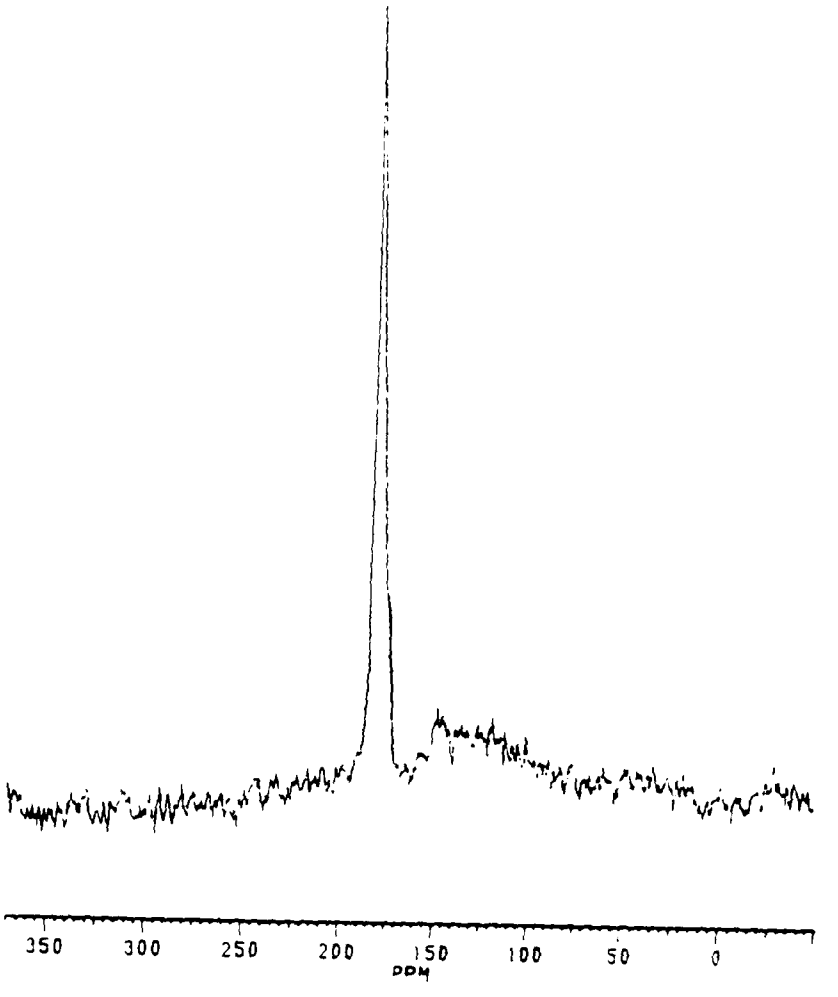
3.8.5. Discussion on Solid Solution Phases Between the Compositions Na_1C_{60} and Na_3C_{60}.

The data described in sections 3.8.1. to 3.8.4. indicate that Na_1C_{60} and the postulated solid solution phases up to the composition Na_2C_{60} do not exist. For a solid solution to be the thermodynamically equilibrium state at a particular temperature and pressure it must have a lower free energy than any other phase or assemblage of phases with the same composition. This would imply that $Na_{1.3}C_{60}$ would have to be the thermodynamic equilibrium state with respect to Na_2C_{60} and C_{60}.

Structurally Na_2C_{60} can be described as the intercalation of sodium atoms into both tetrahedral sites of the fcc C_{60} lattice with the octahedral site vacant. $Na_{1.3}C_{60}$ was refined with essentially partial occupation of the tetrahedral sites.

In solid solutions, if a change in structure, or other property, with temperature can be measured then the temperature of this change usually varies with composition of the solid solution. In the case of C_{60} a structural transition from fcc to simple cubic occurs at 260K. On intercalation of sodium this phase change is proposed to have a maximum temperature and enthalpy change at Na_1C_{60}. As the composition is increased a decrease in the transition temperature and enthalpy change occurs until at the composition $Na_{2.8}C_{60}$ no phase change is observed at all. Without the data available it is not possible to comment on the data from DSC measurements used to probe the enthalpy change in the observed phase transition between the compositions Na_1C_{60} and Na_3C_{60}. However other thermodynamic data is available at higher temperatures (> 433K) in the form of EMF measurements[43] of Na_xC_{60} compositions in a Na β-alumina solid electrolyte between the compositional range 0-6. The authors conclude that solid solution behaviour exists between the compositions $2 < x < 3$ and $x > 3.7$ and not between $1 < x < 2$. If both reports are correct this implies that phase separation occurs at high temperatures for compositions below Na_2C_{60}. However, synthesis of $Na_{1.3}C_{60}$ was performed at temperatures far in excess of 433K.

Reaction of 2.5 equivalents of sodium metal and C_{60} appears to yield a single phase product as observed by a single peak at a previously unobserved frequency in the ^{13}C MASNMR spectrum At δ 179ppm. Solid solution behaviour between the compositions Na_2C_{60} and Na_3C_{60} is not contradicted by ^{13}C MASNMR spectroscopy



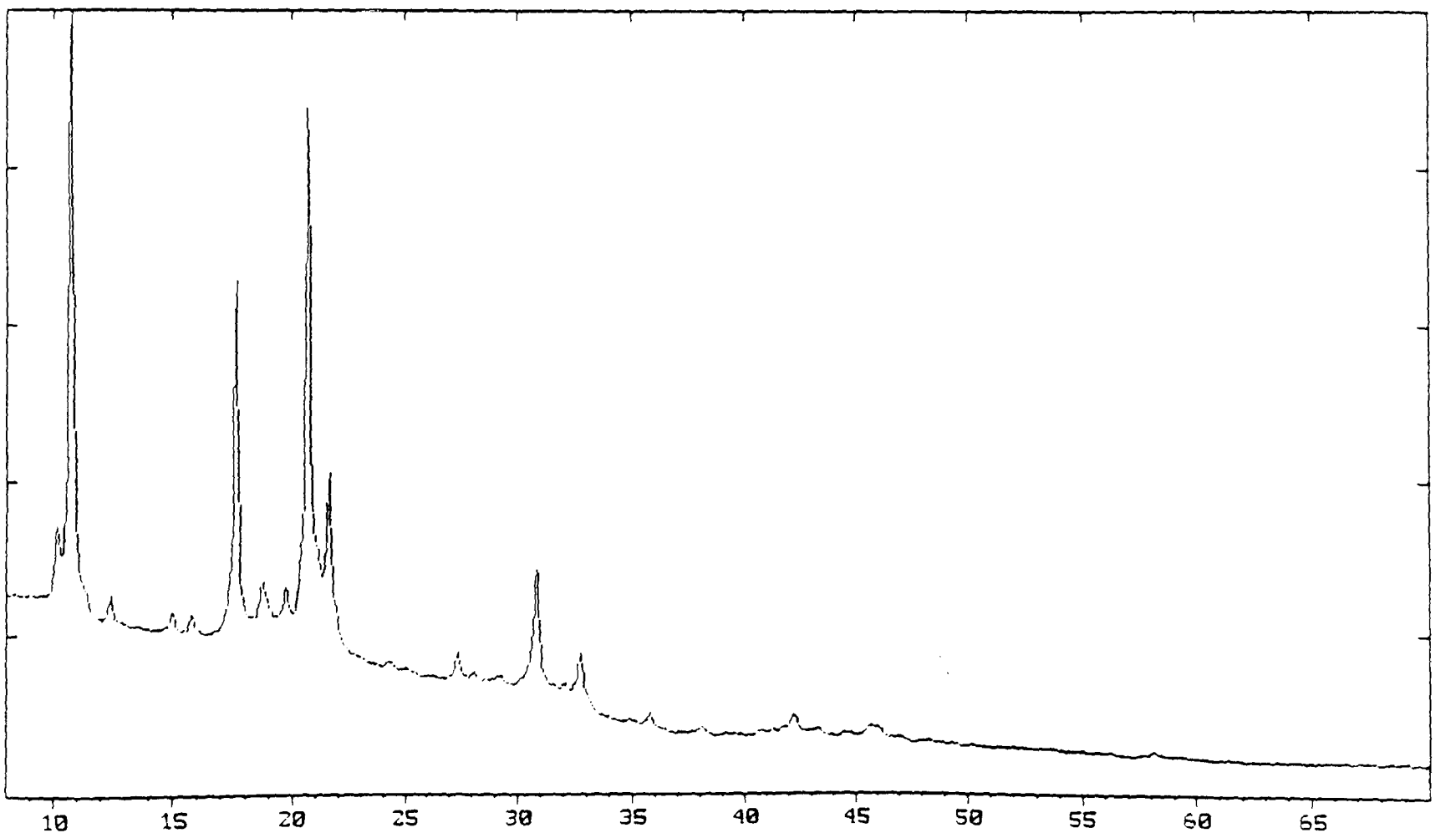


Figure 3.8.4.1. ^{13}C MASNMR and powder X-ray diffraction pattern of a sample with the composition $Na_{2.5}C_{60}$ prepared from sodium metal and C_{60} powder at 550°C.

and can be rationalised as partial population of the octahedral site. Na_3C_{60} is known to undergo phase separation[19] at approximately 250K which is thought to prevent superconductivity at lower temperatures and is thought to be a consequence of a lower 'chemical pressure' from the reduced thermal vibrations of the octahedral sodium. The same authors in a subsequent paper[25] proposing solid solution behaviour between Na_1C_{60} and Na_3C_{60}, do not indicate whether phase separation occurs between the compositions Na_2C_{60} and Na_3C_{60}.

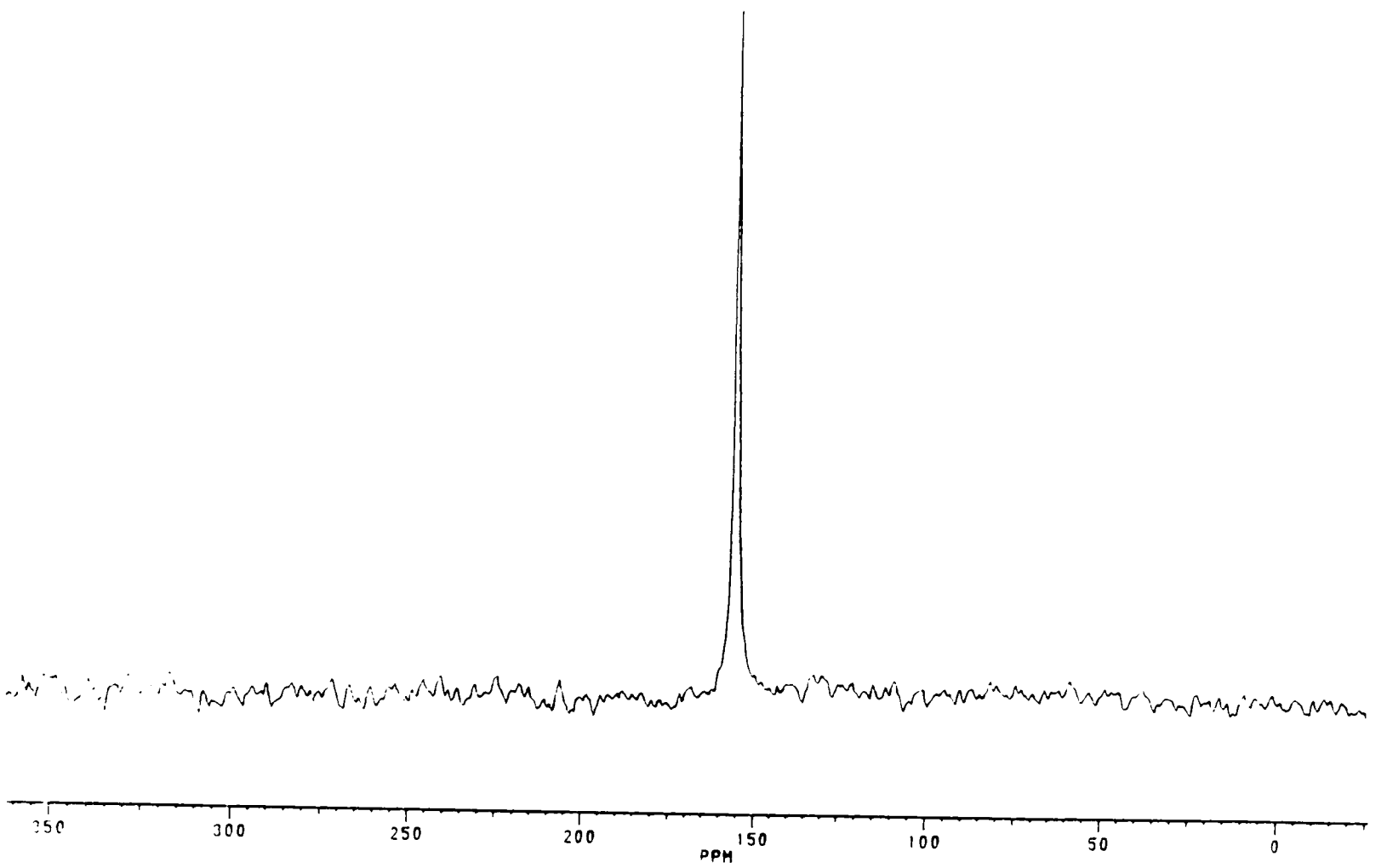
During the synthesis of various sodium C_{60} intercalates, several peaks in the ^{13}C MASNMR spectra have been observed that cannot be assigned to any of the known phases Na_2C_{60}, Na_3C_{60} or Na_6C_{60}. As indicated by the relative intensities these peaks appear to lie between the gross compositions Na_1C_{60} and Na_4C_{60}. One of these peaks at δ179 ppm may belong to the composition $Na_{2.5}C_{60}$ as discussed in section 3.8.5, but other peaks at δ 180ppm, δ176ppm and δ192ppm cannot yet be accounted for.

3.8.6. Synthesis of Hexagonal Close Packed Na_6C_{60} and Na_9C_{60}.

The synthesis of fcc Na_6C_{60} is described in the literature by exposing powdered C_{60} to sodium vapour under 1 atm of He in a sealed stainless steel tube and subsequent distillation of excess sodium away from the reaction products.[20] Powder X-ray diffraction showed a pure fcc phase and refinement of the structure gave the composition Na_6C_{60} where the tetrahedral sites were filled and the octahedral site consisted of Na_4 tetrahedra in two disordered orientations.

In an attempt to synthesise Na_6C_{60}, six equivalents of freshly cut sodium metal were placed in a stainless steel tube with a sample of powdered C_{60}, and flamed sealed in a silica tube under a pressure of 10^{-5}mbar of He. The vessel was heated in stages to a maximum temperature of 450°C and held at this temperature for 5 days. The appropriate weight gain was observed. Powder X-ray diffraction showed peaks which could not be indexed on a fcc lattice but could successfully on a hcp lattice, with a=10.281Å and c=16.666Å, V = 1525Å^3, as shown in figure 3.8.6.1. Refinement of the structure is in progress. ^{13}C MASNMR spectroscopy showed a single peak at δ 156ppm in contrast to that of δ 165ppm for fcc Na_6C_{60}, as shown in figure 3.8.6.1. SQUID magnetometry showed no superconducting material was present above 6K.

Further reaction of a sample of hcp Na_6C_{60} with three equivalents of freshly cut sodium metal at 450°C gave the appropriate weight gain and showed by powder X-ray crystallography that the hcp structure was retained with a=10.168Å and c=16.651Å, V =1491Å^3, as shown in figure 3.8.6.2. Refinement of the structure is in progress. ^{13}C MASNMR spectroscopy showed a peak at δ 156ppm, no perceptible difference in shift or linewidth from hcp Na_6C_{60}, as shown in figure 3.8.6.2. Figure 3.8.6.3. shows the powder X-ray diffraction patterns of Na_6C_{60} and Na_9C_{60} for comparison. SQUID magnetometry showed no superconducting material was present above 6K.



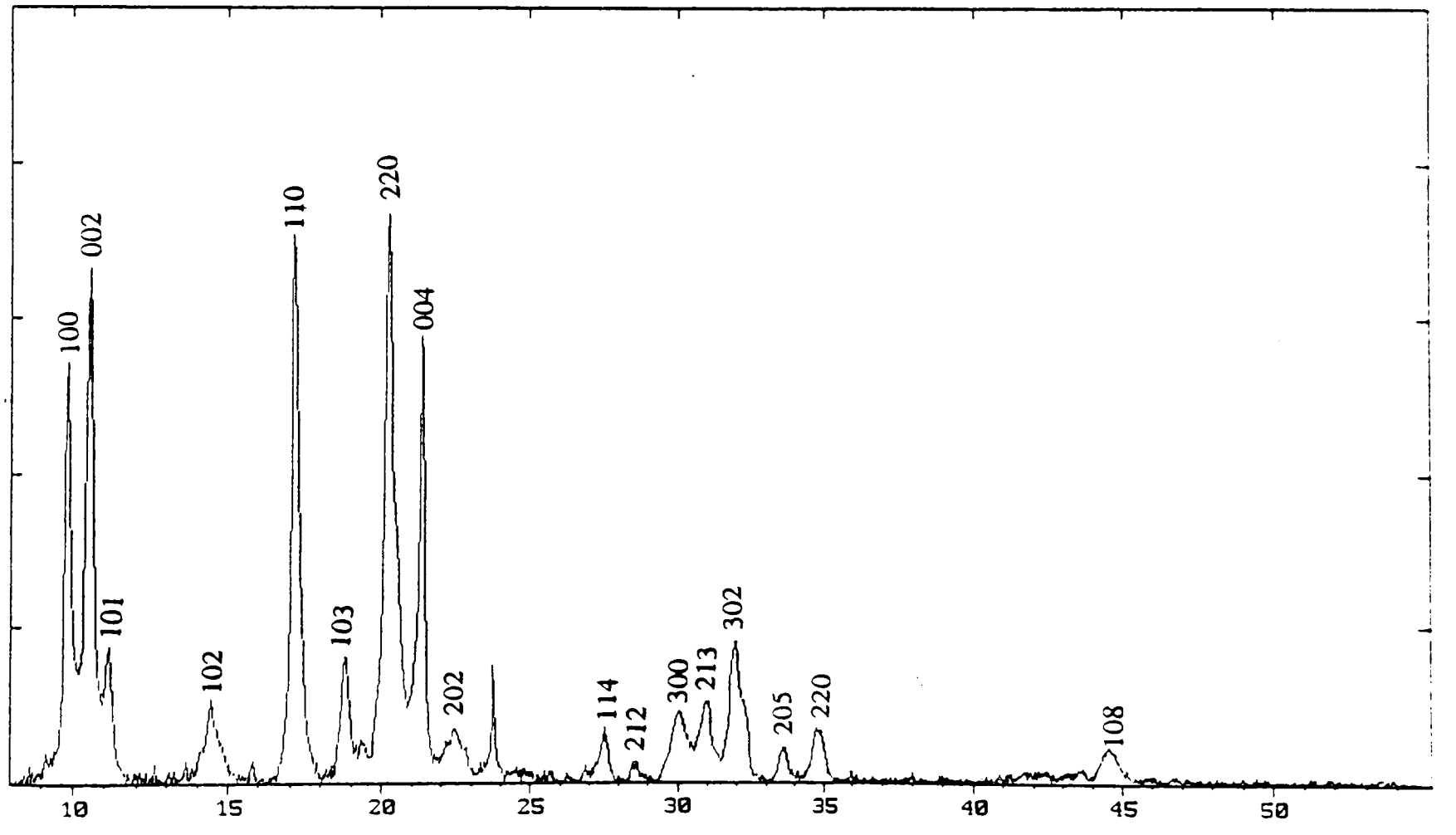
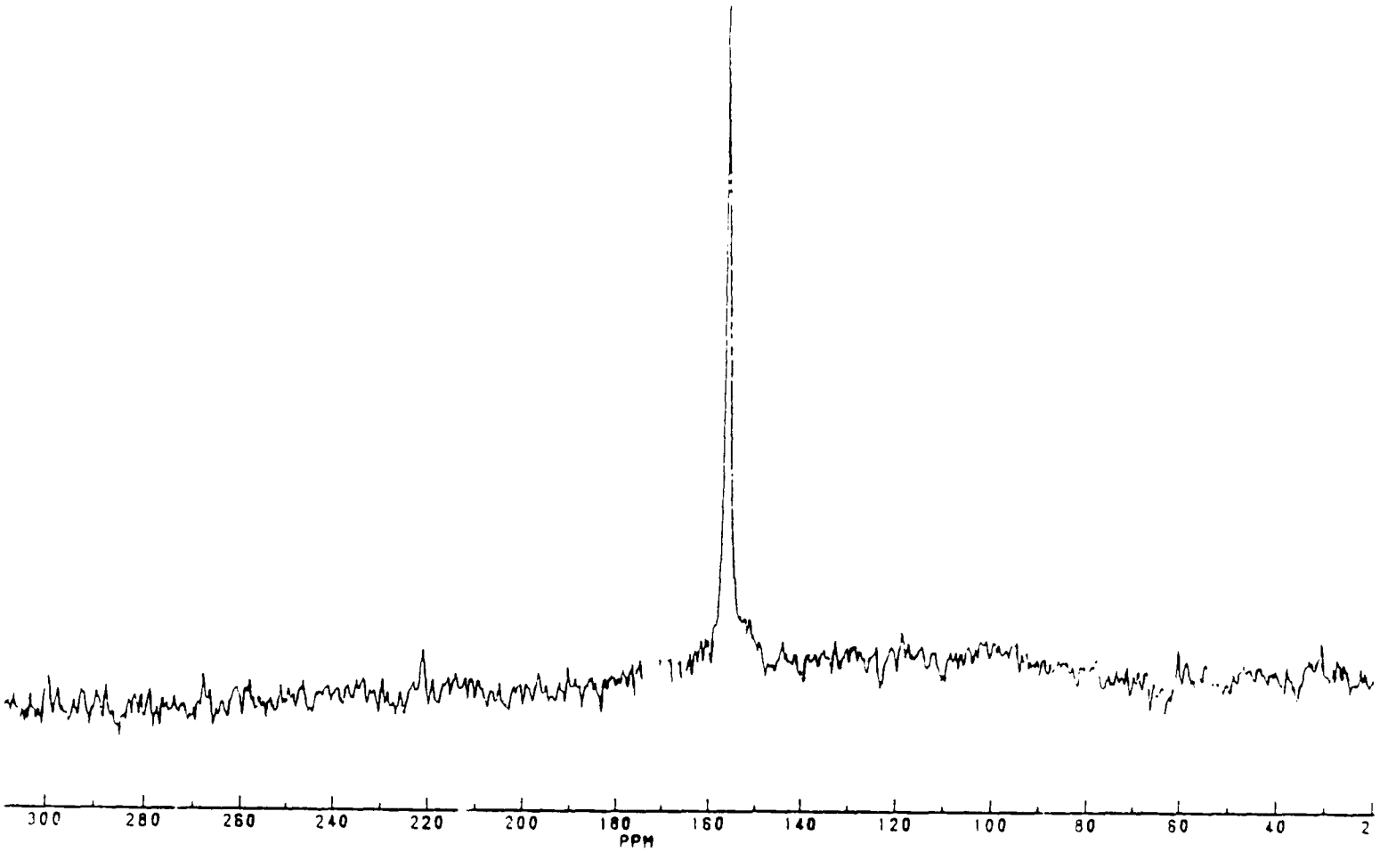


Figure 3.8.6.1. ^{13}C MASNMR and powder X-ray diffraction pattern of a sample with composition Na_6C_{60} prepared from sodium metal and C_{60} powder at 450°C.



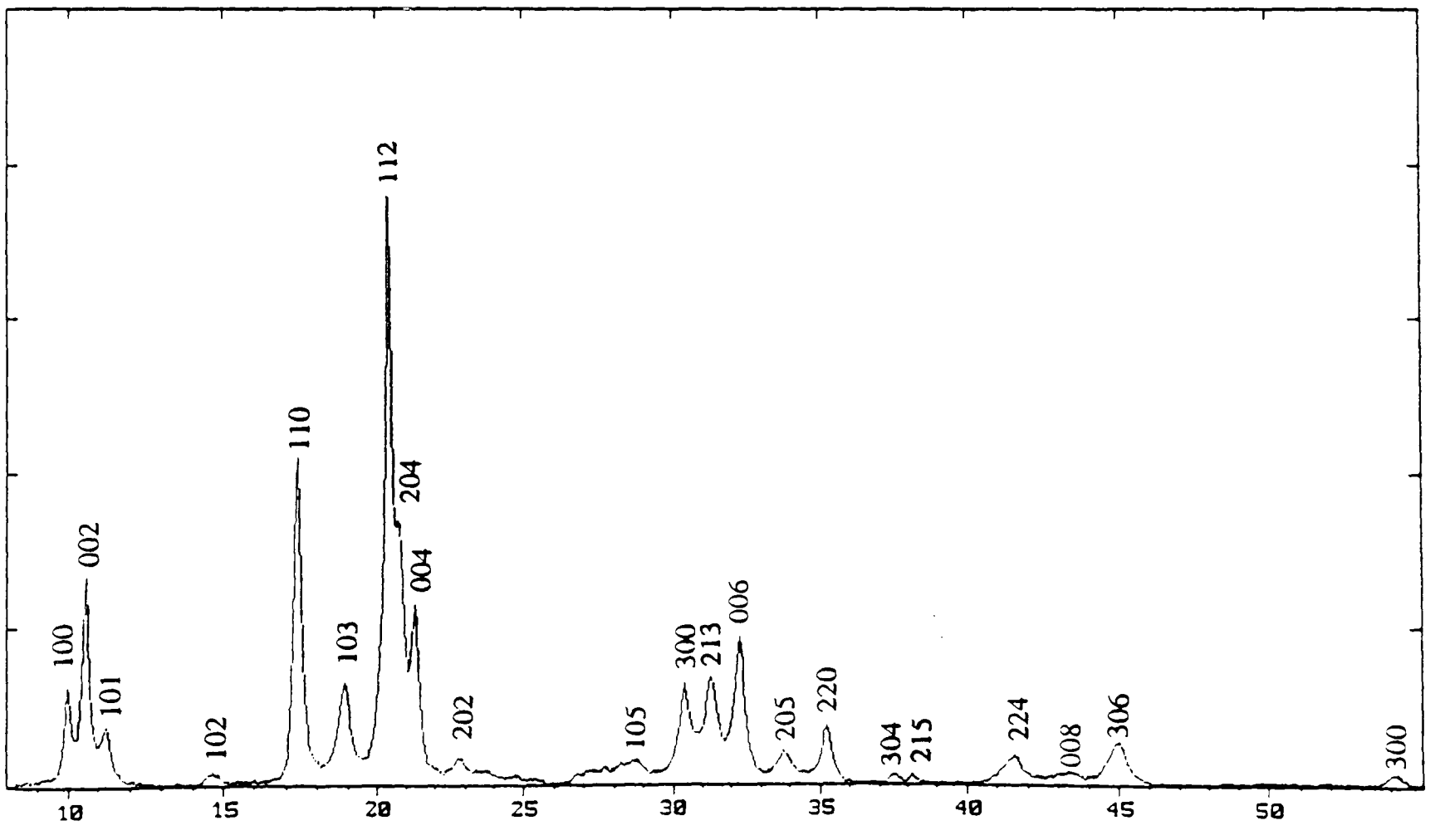


Figure 3.8.6.2. ^{13}C MASNMR and powder X-ray diffraction pattern of a sample with composition Na_9C_{60} prepared from sodium metal and Na_6C_{60} powder at 350°C.

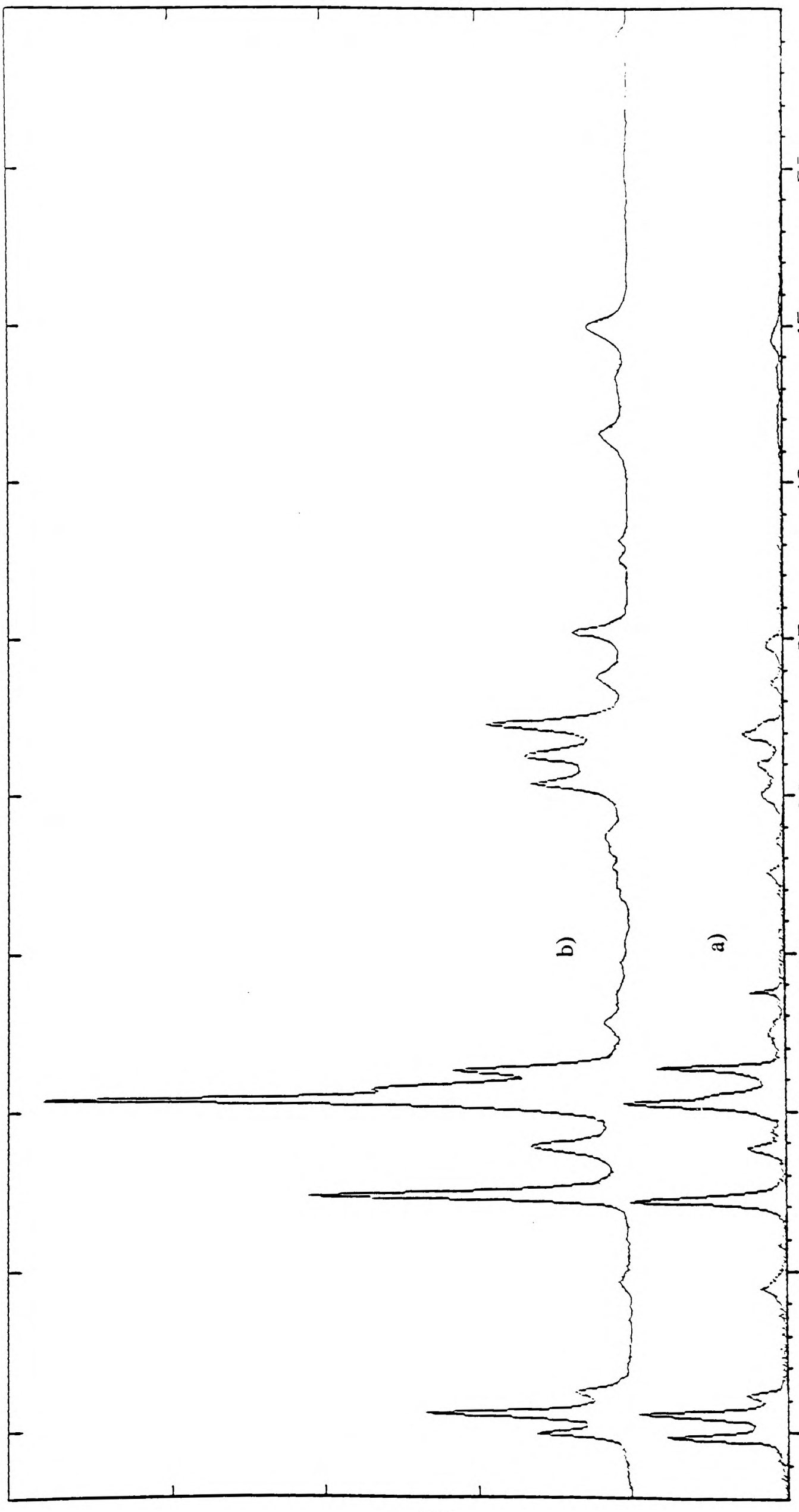


Figure 3.8.6.3. Comparison of powder X-ray diffraction patterns of a) hcp Na_6C_{60} and b) hcp Na_9C_{60}.

Reaction of hcp Na_6C_{60} with one equivalent of C_{60} powder at 350°C showed by powder X-ray diffraction peaks that could be indexed on a fcc lattice and not hcp with a lattice parameter of 14.190(2)Å, *c.f.* Na_3C_{60} a = 14.183(3)Å.

3.8.7. Discussion of the Sodium C_{60} Phase Diagram.

From published work and evidence produced in this chapter, the phase diagram of sodium C_{60} intercalates is far from complete and more data is required from independent sources to verify those materials already postulated.

With respect to solid solution behaviour between Na_1C_{60} and Na_2C_{60} serious consideration should be given to the proposal that disproportionation occurs to Na_2C_{60} and C_{60}. ^{13}C MASNMR spectroscopy clearly shows that attempts to synthesis Na_1C_{60} gave only Na_2C_{60} and C_{60}. The very similar lattice parameters observed in the sodium C_{60} intercalate phases mean that ^{13}C MASNMR spectroscopy is superior to powder X-ray diffraction in ascertaining phase purity.

Reports of structures of sodium C_{60} intercalation phases at, and above, the composition Na_6C_{60} have always shown minority hcp impurities. However, the hcp phases of Na_6C_{60} and Na_9C_{60} described in this chapter do not show fcc impurities. It should also be noted that synthesis of the hcp phases involved longer reaction times at temperatures comparable to the synthesis of the fcc analogues. This tends to indicate that the hcp phases are probably the thermodynamic equilibrium phases for these compositions at room temperature and pressure and the fcc phases are the kinetic products. At the composition Na_3C_{60}, and below, the fcc structure is probably the equilibrium phase as shown by reaction of hcp Na_6C_{60} with C_{60} to form an fcc material.

Based on the observations described in this chapter an alternative sodium C_{60} phase diagram at room temperature and pressure is shown in figure 3.8.7.1. and compared to that based on the literature reports to date.

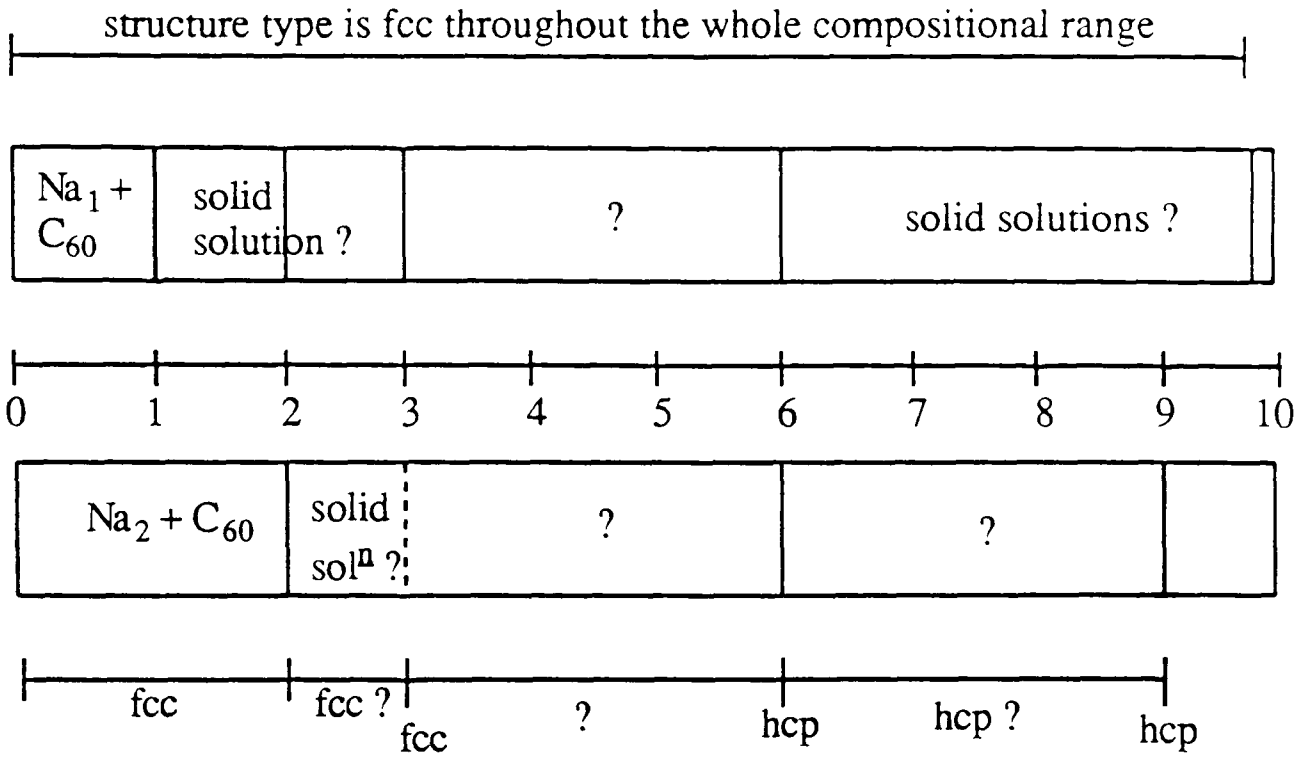


Figure 3.8.7.1. Comparison of the equilibrium compositional phase diagram of Na_xC_{60} intercalates at room temperature and pressure top) literature data reported to date and bottom) possible alternative from work in this thesis. The numbered bar in the centre of the diagram represents the composition x in Na_xC_{60} and the dashed line represents uncertainty in the phase boundary.

Experimental Details for Chapter 3

3.9. Manipulations and Solvents

Manipulations of air and moisture sensitive materials were performed using standard Schlenk techniques, using dual nitrogen and vacuum manifolds. In house nitrogen was purified by passage over 'MnO' and 4Å molecular sieves. Solvents and solutions were transferred using stainless steel cannulae with an over pressure of dinitrogen and filtrations performed with modified cannulae fitted with paper and glass filters.

All other manipulations requiring solvents were performed in a dinitrogen filled drybox, with the dinitrogen purified over BASF catalyst and 4Å molecular sieves.

Solid manipulations were performed in a He filled drybox with the He purified over a hot copper catalyst and 4Å molecular sieves.

Solid state reactions were performed in a home built tube furnace controlled by a Eurotherm temperature controller. Stainless steel tubes used to contain the reactants were cleaned by refluxing in 100/120 petrol for several hours followed by washing with dilute acid and water and then finally conditioned by heating in a flame sealed Pyrex tube under a pressure of 10^{-5} mbar of He at 500°C for several days.

Solvents were predried by standing over 4Å molecular sieves followed by refluxing and distillation from a suitable drying agent under an atmosphere of dinitrogen. The drying agents used were potassium (toluene and 100/120 petroleum ether), calcium hydride (acetonitrile, dichloromethane, ethanol, nitrobenzene and benzonitrile), sodium/potassium alloy 1:3 w/w % (tetrahydrofuran, 40/60 petroleum ether, 30/40 petroleum ether, benzene and diethylether).

Deuterated solvents for NMR were dried over a suitable drying agent and transferred by vacuum distillation into ampoules sealed with a Teflon stopcock. Drying agents used were potassium (d_6-benzene and d_8-thf) and calcium hydride (d_3-acetonitrile).

All reactions were performed either using sublimed C_{60} prepared as described in section 1.13 and stored in a He drybox, or C_{60} dried at 200°C for 48 hrs under a dynamic vacuum and stored under dinitrogen.

3.10. Instrumental Methods.

Elemental analysis was performed by the microanalytical department of The Inorganic Chemistry Laboratory, Oxford and Analytische Laboratorien, Gummersbach, Germany.

Infra-red spectra were recorded on a Perkin-Elmer 1710 spectrophotometer (4000-400 cm^{-1}). Samples were prepared as a KBr disc.

Ultra-Violet/Visible spectra were recorded on a Perkin Elmer lambda 3 UV-Vis spectrometer (190-900nm). Samples were contained in quartz cuvettes of 1mm path

length sealed with a Teflon stopper to prevent exposure to moisture and oxygen.

Electrochemical Measurements were performed using a rotating disc electrode in thf, 0.1M tetrabutylammonium hexafluorophosphate, 900ppm, 20mVs^{-1} *vs* Ag/Ag^{+}.

Magnetic Measurements were recorded using a Cryogenic Consultants S600C SQUID magnetometer fitted with a Lakeshore temperature controller. Samples were sealed in gelatine capsules or 2mm quartz capillaries under an atmosphere of He.

Electron Spin Resonance spectra were recorded on a Varian E-line century series X-band electron spin resonance spectrometer. Samples were contained in quartz tubes, supplied by Spectrasil, sealed with a Teflon stopper and spectra were referenced externally to α, α' diphenyl-β-picrylhydrazyl radicals (DPPH). Measurement of the linewidth was performed using a ruler and pencil and taken as the peak to peak width in the first derivative of the spectrum. Integration was by the cut and weigh method.

Solid State NMR spectra were recorded on a Brucker MSL200 at 50 MHz (^{13}C), 53 MHz (^{23}Na), 77 MHz (^{7}Li) and on a Brucker MSL400 at 100 MHz (^{13}C), 105 MHz (^{23}Na) and 155 MHz (^{7}Li). For MASNMR spectroscopy, samples were contained in a KEL-F insert within a 7mm zirconia rotor. For powder NMR spectroscopy, samples were flame sealed in 5mm diameter NMR tubes 30mm in length with 10mm of the length filled with glass wool at both ends. Spectra were referenced to adamantane (^{13}C), 1M aqueous NaCl (^{23}Na) and 1M aqueous LiCl (^{7}Li). Linewidths were measured as the full width at half the peak intensity.

Solution NMR were recorded on a Brucker AM-300 fitted with an ASPECT 3000 computer at 300MHz (^{1}H) and 75MHz (^{13}C). Spectra were referenced internally to residual protio-solvent resonances (^{1}H) and ^{13}C resonances (^{13}C) relative to tetramethylsilane. Samples were contained in 5mm screw-top NMR tubes.

Powder X-ray Diffraction data was collected in transmission geometry on samples sealed in quartz capillaries, using a Siemens D5000 instrument with a position sensitive detector and Cu Kα_1 radiation.

Synchrotron X-ray powder crystallography was performed at the Synchrotron Radiation Source, Daresbury Laboratories, station 9.4, at an incident wavelength of 0.8179Å in capillaries sealed under He.

3.11. Preparation of $Mn(Cp^*)_2$

The method used was that of Robbins[46] and coworkers. In a typical preparation Cp^*H (2g, 14.7 mmol) was dissolved in thf (150ml) and cooled to -78°C in an acetone/CO_2 bath. To this n-butyl lithium in hexanes (2.5M, 6ml) was added via a syringe and the reaction vessel allowed to warm to room temperature. A white precipitate of $LiCp^*$ resulted. The suspension was cooled to -78°C and anhydrous $MnCl_2$ (1.34g, 10.6mmol) was added against a counter flow of dinitrogen. The stirring suspension was allowed to warm to room temperature over approximately 1 hour and

then further heated at 40°C for 1 hour yielding an orange solution. Removal of the solvent under reduced pressure gave an orange solid which was subsequently sublimed (100°C, 10^{-5} Torr) yielding a very air sensitive bright orange solid. Yield 1.50g, 61%. ^{1}H NMR (C_6D_6) -4.7ppm (bs)

3.12.Synthesis of Na[Mn(Cp*)$_2$]

The method used was that of Robbins[46] and co-workers. Naphthalene (0.53g, 4.12mmol) was dissolved in thf (30ml) and stirred over sodium (230mg, 10mmol) for 1hr giving a deep green solution of sodium naphthalide. The dissolution of sodium could be accelerated with the aid of an ultrasound bath. The sodium naphthalide solution was transferred quickly via cannula onto Mn(Cp*)$_2$ (1.34g, 4.12mmol) and stirred for 15mins. Removal of the solvent under reduced pressure and washing with hexane (3 x 30ml) and toluene (2 x 30ml) yielded a pale orange pyrophoric solid of Na[Mn(Cp*)$_2$]. Yield 1.34g, 94%. ^{1}H NMR (d_8-thf) 1.80ppm (s).

3.13. Synthesis of Solvated Sodium Salts of C_{60}.

All the solvated sodium salts described were prepared from the same route by addition of a thf solution of Na[Mn(Cp*)$_2$] to a toluene solution of C_{60}.

In a typical preparation, C_{60} (150mg, 0.21mmol) in toluene (125ml) was treated with Na[Mn(Cp*)$_2$] (72mg, 0.21mmol) in thf (10ml). Addition was performed quickly via a stainless steel cannula. Immediately a dark precipitate separated leaving a yellow supernatant of Mn(Cp*)$_2$. After filtration the dark red precipitate was washed with hexane (3x20ml). The washings were colourless.

Removal of the volatiles under reduced pressure from the yellow supernatant, gave the orange solid Mn(Cp*)$_2$ which was sublimed and recycled.

3.13.1. Extraction of NaC_{60}.5thf.

The dark red solid produced in section 3.13. was extracted with thf (1 x 50ml, 2 x 25ml) to give an intense cherry red solution. Removal of the volatiles gave a very dark red microcrystalline solid, which on subsequent characterisation, was formulated as NaC_{60}.5thf in *ca.* 75% Yield.

^{13}C powder NMR δ 188ppm, $\upsilon_{1/2}$ = 2kHz.

^{23}Na powder NMR δ 0ppm, $\upsilon_{1/2}$ = 12kHz.

^{13}C MASNMR δ 188ppm, $\upsilon_{1/2}$ = <100Hz.

^{23}Na MASNMR δ -23ppm and δ 9ppm.

ESR (thf glass and solid) were performed on freshly prepared solutions or solid, by first cooling in zero field to 4K and then warming to a particular temperature, allowing the sample to equilibrate for 5 minutes, and a spectrum recorded. Spectra at 6 and 290K were also recorded for DPPH. A modulation frequency of 100 kHz and a microwave power of 2mW were used. Measurements showed a temperature dependent

line width for both solid and solvent glass samples, with saturation of the line width observed above approximately 200K in the solid state. A broad resonance at all temperatures, and a sharp 'spike' at higher temperatures was observed in the frozen glass spectra. In the solid state ESR spectra consisted of a broad peak at all temperatures. The solid state ESR spectrum recorded at 6K was very asymmetric reminiscent of a Dysonian[64, 65] indicative of metallic character.

SQUID (gelatine capsule) 80mg sample mass, diamagnetic constant determined using Pascal's constants, χ_d = -400 x 10^{-6} emu cgs g^{-1}. At 0.5T Curie-Weiss behaviour above 200K, for S = 1/2, μ = 1.70, θ = -58K. Abrupt drop in susceptibility at 170K to μ = 0.8, non Curie-Weiss behaviour below this temperature. Behaviour is field independent. Low temperature data can be fitted for a temperature independent paramagnetism plus 7.8% of a paramagnetic species with S = 1/2. At 6 and 250K the magnetisation vs field strength is linear between 0 and 3T, with no hysteresis or saturation observed, consistent with a good paramagnet.

Synchrotron X-ray powder crystallography was tentatively indexed on a triclinic lattice with the unit cell dimensions of a = 12.684Å, b = 15.992Å, c = 10.092Å, α = 92.524°, β = 95.932°, γ = 74.516°, and V = 1960Å^3.

UV-Vis shows two major features at 262 and 340 nm

Rotating disc electrochemistry was performed in thf with ^{n}Bu$_4$NPF$_6$ 0.1 mol dm^{-3} as supporting electrolyte vs Ag/Ag^+ at a scan rate of 20 mV s^{-1} and a disc speed of 900rpm. Decomposition of the sample was avoided by immersing the cell in an atmosphere of argon. Sweeping from a positive potential relative to the 0/-1 couple of C_{60} gave an anodic current and above the -1/-2 couple, a cathodic current. Between the 0/-1 and -1/-2 couples of C_{60} no current flowed. The scan was not reversible due to adsorbed species on the working electrode surface.

^{1}H NMR (d_3-MeCN) was performed on a sample made up from 2.7mg of NaC_{60}.5thf and 1.3mg of ferrocene. A relaxation delay of 30s was used and integration was performed by the computer using software as supplied by Brucker. Two independently prepared samples gave a stoichiometry of NaC_{60}.4.9thf and NaC_{60}.5thf.

Analysis calculated for $C_{80}H_{40}O_5Na_1$, C 87.0, H 3.0, Na 2.0; found C 86.3, H 3.6, Na 2.0. No manganese was detected in the sample.

Properties

Soluble, giving a cherry red solution in thf, MeCN, PhCN, DMSO, EtOH, and is slightly soluble in CH_2Cl_2. The compound NaC_{60}.5thf is very moisture and oxygen sensitive as a solid and in solution. Solutions precipitate a brown solid.

3.13.2. Studies of the thf Insolubles: 'The Residuals'.

After extraction of NaC_{60}.5thf from the precipitate a dark grey solid remains., which was dried under reduced pressure at 10^{-1}mbar. On the basis of elemental analysis

the composition is formulated as $Na_{0.9}C_{60}.3thf$.

^{13}C MASNMR δ 162ppm (C_{60}), δ 85 and 44ppm (thf).

^{23}Na MASNMR δ -8ppm.

ESR (solid) were performed by first cooling in zero field to 4K and then warming to a particular temperature, allowing the sample to equilibrate for 5 minutes, and a spectrum recorded. Spectra at 6 and 290K were also recorded for DPPH. A modulation frequency of 100 kHz and a microwave power of 2mW were used. At 19K spectra were recorded as a function of power from 2 to 200mW.Measurements showed a temperature dependent line width, with saturation of the line width observed above approximately 200K in the solid state. The solid state ESR spectra consisted of a sharp slightly asymmetric peak at low temperature and a broader peak at higher temperatures. At 19K the sharp peak showed saturation at high power levels whereas the broad resonance did not.

SQUID (gelatine capsule) 17mg sample mass, diamagnetic constant χ_d = -400 x 10^{-6} emu cgs g^{-1}. Abrupt drop in susceptibility at 170K to $\mu = 0.8\mu_B$, non Curie-Weiss behaviour below this temperature. Behaviour is field independent. At 6 and 250K the magnetisation vs field is linear between 0 and 3T, with no hysteresis or saturation observed consistent with a good paramagnet.

Powder X-ray crystallography was indexed on a hexagonal lattice with the unit cell dimensions of a = 15.338Å, c = 9.933Å, and V = 2024$Å^3$.

Analysis calculated for $C_{72}H_{24}O_3Na_{0.9}$, C 90.3, H 2.5, Na 2.1; found C 87.4, H 2.4, Na 2.0. No manganese was detected in the samples.

3.14. Synthesis of $NMe_4C_{60}.1.5thf$.

At -5°C (ice/ammonium chloride slush), one equivalent of a MeCN solution (20ml) of NMe_4F (4.2mg, 0.045mol) was added to a MeCN solution (30ml) of $NaC_{60}.5thf$ (50mg, 0.045mmol) quickly via a cannula. The volatiles were removed at -5°C under reduced pressure giving a dark purple solid. Extraction with thf (1 x 20, 2 x 10ml) at room temperature gave an intense cherry red solution with a pale grey residue. After filtration the thf solution was reduced in volume to *ca.* 1-2ml and cooled to -80°C overnight. Very dark needles precipitated which on removal of the red supernatant decomposed to a dark microcrystalline powder subsequently formulated as $NMe_4C_{60}.1.5thf$. Yield > 90%.

^{13}C MASNMR δ 186ppm (C_{60}), δ 85 and 44ppm (thf).

ESR (solid) were performed by first cooling in zero field to 100K and then warming to a particular temperature, allowing the sample to equilibrate for 5 minutes, and a spectrum recorded. A spectrum at 290K was also recorded for DPPH. A modulation frequency of 100 kHz and a microwave power of 2mW were used. Measurements showed a temperature dependent line width for both solid and solvent glass samples, with saturation of the line width observed above approximately 200K in

the solid state. A broad resonance at all temperatures, and a sharp 'spike' at higher temperatures was observed in the frozen glass spectra. In the solid state ESR spectra consisted of a broad peak at all temperatures.

SQUID (gelatine capsule) 50mg sample mass, diamagnetic constant χ_d = -350 x 10^{-6} emu cgs g^{-1}. Abrupt drop in susceptibility at 170K to μ = 0.8, non Curie-Weiss behaviour below this temperature. Behaviour is field independent. At 6 and 250K the magnetisation vs field is linear between 0 and 3T, with no hysteresis or saturation observed consistent with a good paramagnet.

^{1}H NMR (d_3-MeCN) was performed on a sample with a relaxation delay of 2s and integration was performed by the computer using software as supplied by Brucker. Various samples showed that the ration of NMe_4^+ to thf was approximately 1:1.5.

Analysis calculated for $C_{70}H_{24}N_1O_{1.5}$, C 93.1, H 2.7, N 1.6; found C 90.4, H 2.6, N 1.5.

Properties

Very soluble in thf and soluble in MeCN, PhCN and slightly in CH_2Cl_2. It is slightly moisture and oxygen sensitive as a solid. In solution decomposition occurs in less than one minute giving an intense orange solution in MeCN and precipitating a brown solid from thf.

3.15. Synthesis of Some Na Phases of C_{60} Using a Furnace.

Reactions were performed in stainless steel or iron tubes (70 x 7 o.d. (5 i.d.)) flame sealed in silica tubes under 10^{-5} mbar of He, as shown in figure 3.15.1. Silica tubes allowed temperatures over 500°C to be used, which is approximately the glass transition temperature of Pyrex, and the steel container prevented reaction of the glass walls by sodium liquid.

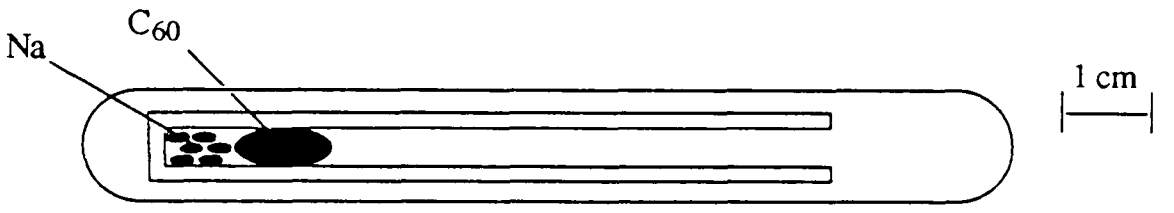


Figure 3.15.1. Apparatus used for the synthesis of sodium C_{60} intercalates.

Na_2C_{60} was synthesised by the combination of C_{60} (200mg, 0.278mmol) and two equivalents of freshly cut sodium (12.8mg). The C_{60} was placed on top of the sodium metal to eliminate loss of sodium vapour before it could react with the C_{60} powder. Heating temperatures and times are shown in table 3.15.1.

Table 3.15.1.1.

Temperature/°C	Time/hrs
200	12
350	24
500	48
^{13}C MASNMR and regrind	
300	24
550	72

^{13}C MASNMR showed a single peak at δ 172ppm.

Powder X-ray crystallography was consistent with previously prepared samples.

3.15.1. Attempted Synthesis of NaC_{60}.

A sample of Na_2C_{60} (50mg, 0.065mmol) was diluted with one equivalent of C_{60} (47mg) to yield the gross composition NaC_{60}. The sample was ground in an agate mortar and pestle, placed in a stainless steel tube, and flame sealed in a silica tube under 10^{-5} mbar of He. Table 3.15.1.1. shows the temperatures and duration of heating of the sample.

Table 3.15.1.1.

Temperature/°C	Time/hrs
200	12
350	24
500	120 (5 days)
^{13}C MASNMR and regrind	
300	24
550	168 (7 days)

^{13}C MASNMR spectroscopy showed two peaks at δ 172 and 143ppm indicating that a reaction had not occurred.

Synthesis from stoichiometric quantities of C_{60} and sodium metal was also performed in an analogous procedure with the same result.

3.15.2. Attempted Synthesis of $Na_{1.3}C_{60}$.

Two samples of Na_2C_{60} (30mg, 0.039mmol) were diluted with the appropriate amounts of C_{60} to obtain the gross stoichiometry $Na_{1.3}C_{60}$. After grinding in an agate mortar and pestle one of the samples was flame sealed as described in section 3.15. and heated for the times and temperatures shown in table 3.15.1.1. The other was placed directly into an X-ray capillary and sealed under He.

Powder X-ray crystallography and ^{13}C MASNMR spectroscopy showed there was no difference between the two samples.

3.15.3. Attempted Synthesis of Na_1C_{60} and $Na_{1.3}C_{60}$ via Quenching.

Two samples of Na_2C_{60} (30mg, 0.039mmol) were diluted with the appropriate amounts of C_{60} to obtain the gross stoichiometries Na_1C_{60} and $Na_{1.3}C_{60}$. After grinding in an agate mortar and pestle the samples flame sealed as described in section 3.15. and heated in apparatus shown in figure 3.15.3.1. for the temperatures and times in table 3.15.3.1.

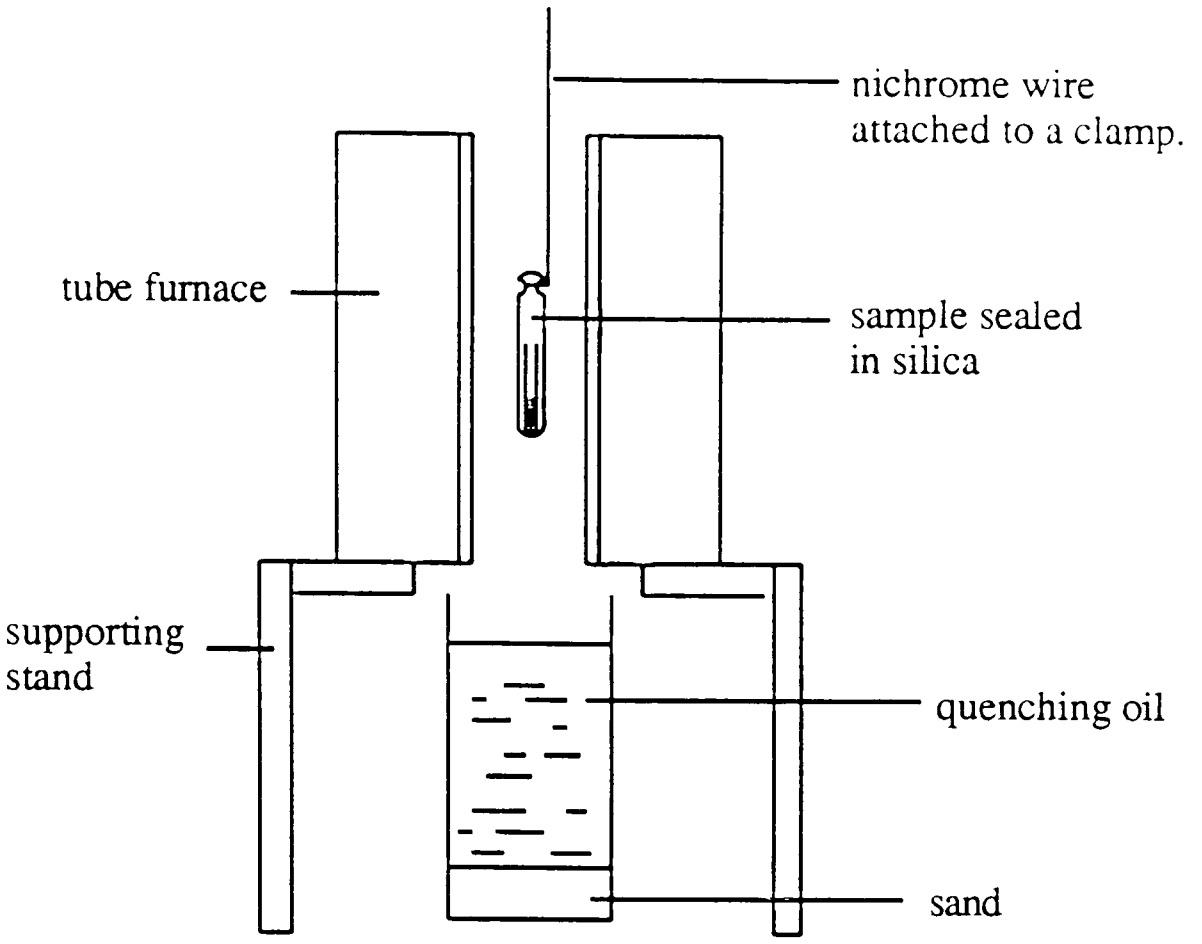


Figure 3.15.3.1. Apparatus used to quench reactions from high temperatures.

Table 3.15.3.1.

Temperature/°C	Time/hrs
200	12
350	24
500	48
550	168 (7 days)

The samples were then allowed to fall into quenching oil in an attempt to kinetically stabilise a metastable state. ^{13}C MASNMR spectroscopy showed that no new phases were apparent.

3.15.4 Synthesis of $Na_{2.5}C_{60}$.

As described in section 3.15. C_{60} (55.1mg, 0.077mmol) and 2.5 equivalents of freshly cut sodium metal (4.4.mg) were heated for the times and temperatures shown in table 3.15.4.1.

Table 3.15.4.1.

Temperature/°C	Time/hrs
200	12
350	24
500	120 (5 days)
^{13}C MASNMR and regrind	
300	24
550	168 (7 days)

^{13}C MASNMR spectroscopy showed a single peak at δ 179ppm, υ < 200Hz.

Powder X-ray crystallography gave data that could not be indexed on cubic or hexagonal lattices. Further work is in progress.

3.15.5. Synthesis of hcp Na_6C_{60} and Na_9C_{60}.

To a sample of powdered C_{60} (125mg,0.17mmol) was added six equivalents of sodium (24mg) as described in section 3.15. The sample was heated for the times and temperatures shown in table 3.15.5.1.

Table 3.15.5.1.

Temperature/°C	Time/hrs
100	24
150	24
250	24
350	24
450	72

^{13}C MASNMR δ 156ppm, $\upsilon_{1/2}$ = <200Hz.

^{23}Na MASNMR δ -13ppm $\upsilon_{1/2}$ ~ 1400Hz.

Powder X-ray diffraction showed peaks which could be indexed as hcp with a hexagonal unit cell of dimensions a = 10.280Å and c = 16.666Å, V = 1525Å^3.

The synthesis of hcp Na_9C_{60} was performed by the addition of three equivalents of sodium metal (4mg) to hcp Na_6C_{60} (50mg, 0.058mmol) as described in section 3.15.1. and the reaction vessel heated at the times and temperatures shown in table 3.15.5.1.

^{13}C MASNMR δ 156ppm, $\upsilon_{1/2}$ = <200Hz..

^{23}Na MASNMR δ -8ppm $\upsilon_{1/2}$ ~ 1000Hz.

Powder X-ray diffraction showed peaks which could be indexed as hcp with a hexagonal unit cell of dimensions a = 10.168Å and c = 16.651Å, V = 1496Å^3 .

3.15.6. Reaction of hcp Na_6C_{60} and C_{60}.

To hcp Na_6C_{60} (15mg,), one equivalent of powdered C_{60} was added and the sample ground and sealed as described in section 3.15. The reaction was heated for the times and temperatures shown in table 3.15.6.1.

Table 3.15.6.1.

Temperature/°C	Time/hrs
100	24
150	24
250	24
300	24
350	72

^{13}C MASNMR δ 177 and 180 ppm, $\upsilon_{1/2}$ < 500Hz in each case.

^{23}Na MASNMR δ 60ppm and δ -37ppm, $\upsilon_{1/2}$ ~ 3500 and 1000Hz respectively.

Powder X-ray diffraction showed peaks which could be indexed as fcc with a lattice parameter of 14.19Å.

References

1. Hebbard, A. F.; Rosseinsky, M. J.; Haddon, R. C.; Murphy, D. W.; Glarum, S. H.; Palstra, T. T. M.; Ramirez, A. P.; Kortan, A. R. *Nature* 1991, ***350***, 600.
2. McCauley, J. P.; Zhu, Q.; Coustel, N.; Zhou, O.; Vaughan, G.; Idziak, S. H. J.; Fischer, J. E.; Tozer, S. W.; Groski, D. M.; Bykovetz, N.; Lin, C. L.; McGhie, A. R.; Allen, B. H.; Romanow, W. J.; Denenstein, A. M.; III, A. B. S. *J. Am. Chem. Soc.* 1991, ***113***, 8537.
3. Echegoyen, L.; Xie, Q.; Perez-Cordero, E. *J. Am. Chem. Soc.* 1992, ***114***, 3978.
4. Ohsawa, Y.; Saji, T. *J. Chem. Soc., Chem. Comm.* 1992, 781.
5. Chauvet, O.; Oszlanyi, G.; Forro, L.; Stephens, P. W.; Tegze, M.; Faigol, G.; Janossy, A. *Phys. Rev. Lett.* 1994, ***72***, 2721.
6. Tycko, R.; Dabbagh, G.; murphy, D. W.; Zhu, Q.; Fischer, J. E. *Phys. Rev. B* 1993, ***48***, 9097.
7. Winter, J.; Kuzmany, H. *Solid State Commun.* 1993, ***84***, 935.
8. Janossy, A.; Chauvet, O.; Pekker, S.; Cooper, J. R.; Forro, L. *Phys. Rev. Lett.* 1993, ***71***, 1091.
9. Murphy, D. W.; Rosseinsky, M. J.; Fleming, R. M.; Tycko, R.; Ramirez, A. P.; Haddon, R. C.; Seigrist, T.; Dabbagh, G.; Tully, J. C.; Walstedt, R. E. *J. Phys. Chem. Solids* 1992, ***53***, 1321.
10. Fleming, R. M.; Rosseinsky, M. J.; Ramirez, A. P.; Murphy, D. W.; Tully, J. C.; Haddon, R. C.; Siegrist, T.; Tycko, R.; Glarum, S. H.; Marsh, P.; Dabbagh, G.; Zahurak, S. M.; Makhija, A. V.; Hampton, C. *Nature* 1991, ***352***, 701.
11. Tycko, R.; Dabbagh, G.; Rosseinsky, M. J.; Murphy, D. W.; Fleming, R.; Ramirez, A. P.; Tully, J. C. *Science* 1991, ***253***, 884.
12. Tycko, R.; Dabbagh, G.; Rosseinsky, M. J.; Murphy, D. W.; Ramirez, A. P.; Fleming, R. M. *Phys. Rev. Letts.* 1992, ***68***, 1912.
13. Tycko, R. *J. Phys. Chem. Solids* 1994, ***54***, 1713.
14. Liu, X.; Wan, W. C.; Owens, S. M.; Broderick, W. E. *J. Am. Chem. Soc.* 1994, ***116***, 5489.
15. Wang, H. H.; Kini, A. M.; Savall, B. M.; Carlson, K. D.; Williams, J. M.; Lykke, K. R.; Parker, D. H.; Wurz, P.; Pellin, M. J.; Gruen, D. M.; Welp, U.; Kwok, W.-K.; Fleshler, S.; Crabtree, G. W. *Inorg. Chem* 1991, ***30***, 2838.
16. Wang, H. H.; Kini, A. M.; Savall, B. M.; Carlson, K. D.; Williams, J. M.; Lathrop, M. W.; Lykke, K. R.; Parker, D. H.; Wurz, P.; Pellin, M. J.; Gruen, D. M.; Welp, U.; Kwok, W.-K.; Fleshler, S.; Crabtree, G. W.; Schirber, J. E.; Overmyer, D. L. *Inorg. Chem.* 1991, ***30***, 2962.

17. Ziebarth, R. P.; Buffinger, D. R.; Stenger, V. A.; Recchia, C.; Pennington, C. H. *J. Am. Chem. Soc.* 1993, ***115***, 9267.
18. Pekker, S.; Janossy, A.; Mihaly, L.; Chauvet, O.; Carrard, M.; Forro, L. *Science* 1994, ***265***, 1077.
19. Yildirim, T.; Zhou, O.; Fischer, J. E.; Bykovetz, N.; Strongin, R. A.; Cichy, M. A.; III, A. B. S.; Lin, C. L.; Jelinek, R. *Nature* 1992, ***360***, 569.
20. Rosseinsky, M. J.; Murphy, D. W.; Fleming, R. M.; Tycko, R.; Ramirez, A. P.; Siegrist, T.; Dabbagh, G.; Barrett, S. E. *Nature* 1992, ***356***, 416.
21. Tanigaki, K.; Ebbesen, T. W.; Saito, S.; Mizuki, J.; Tsai, J. S.; Kubo, Y.; Kuroshima, S. *Nature* 1991, ***352***, 222.
22. Weaver, J. H.; Poirier, D. M.; Ohno, T. R.; Kroll, G. H.; Chen, Y.; Benning, P. J.; Chibante, L. P. F.; Smalley, R. E. *Science* 1991, ***253***, 646.
23. Chabre, Y.; Djurado, D.; Armand, M.; Romanow, W. R.; Coustel, N.; McCauley, J. P.; Fischer, J. E.; III, A. B. S. *J. Am. Chem. Soc.* 1992, ***114***, 764.
24. Fischer, J. E.; McCauley, J. P.; Zhu, Q.; Coustel, N.; Zhou, O.; Vaughn, G.; Idziak, S. H. J.; Tozer, S. W.; Groski, D. M.; Bykovetz, N.; Lin, C. L.; McGhie, A. R.; Allen, B. H.; Romanow, W. J.; Denenstein, A. M.; III., A. B. S. *J. Am. Chem. Soc.* 1991, ***113***, 8537.
25. Yildirim, T.; Fischer, J. E.; Harris, A. B.; Stephens, P. W.; Liu, D.; Brard, L.; Strongin, R. M.; III, A. B. S. *Phys. Rev. Lett.* 1993, ***71***, 1383.
26. M. J. Rosseinsky, *unpublished results*
27. Chen, J.; Huang, Z.-E.; Cai, R.-F.; Shao, Q.-F.; Chen, S.-M.; Ye, H.-J. *J. Chem. Soc., Chem. Comm.* 1994, 2177.
28. Douthwaite, R. E.; Brough, A. R.; Green, M. L. H. *J. Chem. Soc., Chem. Comm.* 1994, 267.
29. Kobayashi, H.; Tomita, H.; Moriyama, H.; Kobayashi, A.; Wanatabe, T. *J. Am. Chem. Soc.* 1994, ***116***, 3153.
30. Echegoyen, L.; Xie, Q.; Arias, F. *J. Am. Chem. Soc.* 1993, ***115***, 9818.
31. Compton, R. G.; Spackman, R. A.; Wellington, R. G.; green, M. L. H.; Turner, J. *J. Electroanal. Chem.* 1992, ***327***, 337.
32. Compton, R. G.; Spackman, R. A.; Riley, D. J.; Wellington, R. G.; Eklund, J. C.; Fischer, A. C.; Green, M. L. H.; Douthwaite, R. E.; Stephens, A. H. H.; Turner, J. F. C. *J. Electroanal. Chem.* 1993, ***344***, 235.
33. Wudl, F.; Li, Q.; Thilgen, C.; Whetten, R. L.; Diederich, F. *J. Am. Chem. Soc.* 1992, ***114***, 3994.
34. Kadish, K. M.; Dubois, D.; Jones, M. T. *J. Am. Chem. Soc.* 1992, ***114***, 6446.
35. Kadish, K. M.; Dubois, D.; Flanagan, S.; Haufler, R. E.; Chibante, L. P. F.; Wilson, L. J. *J. Am. Chem. Soc.* 1991, ***113***, 4364.

36. Kadish, K. M.; Dubois, D.; Flanagan, S.; Wilson., L. J. *J. Am. Chem. Soc.* 1991, ***113***, 7773.
37. Goldenberg, L. M.; Williams, G.; Bryce, M. R.; Monkman, A. P.; Petty, M. C.; Hirsch, A.; Soi, A. *J. Chem. Soc., Chem. Comm.* 1993, 1310.
38. Bard, A. J.; Mirkin, M. V.; Bulhoes, L. O. S. *J. Am. Chem. Soc.* 1993, ***115***, 201.
39. Bard, A. J.; Jehoulet, C.; Obeng, Y. S.; Kim, Y.-T.; Zhou, F. *J. Am. Chem. Soc.* 1992, ***114***, 4237.
40. Bard, A. J.; Zhou, F.; Jehoulet, C. *J. Am. Chem. Soc.* 1992, ***114***, 11004.
41. Bard, A. J.; Jehoulet, C.; Wudl, F. *J. Am. Chem. Soc.* 1991, ***113***, 5456.
42. Reed, C. A.; Bhyrappa, P.; Paul, P.; Stinchcombe, J.; Boyd, P. D. W. *J. Am. Chem. Soc.* 1993, ***113***, 11004.
43. Kim, J. H.; Petric, A.; Ummat, P. K.; Datars, W. R. *J. Phys., Cond. Mat.* 1994, ***6***, 5387.
44. Zhou, O.; Fleming, R. M.; Murphy, D. W.; Rosseinsky, M. J.; Ramirez, A. P.; Dover, R. B. V.; Haddon, R. C. *Nature* 1993, ***362***, 433.
45. Yildirim, T.; Fischer, J. E.; Dinnebier, R.; Stephens, P. W.; Lin, C. L. *Solid State Commun.* 1995, in press.
46. Robbins, J. L.; Edelstein, N. M.; Cooper, S. R.; Smart, J. C. *J. Am. Chem. Soc.* 1979, ***101***, 3853.
47. Allemand, P.-M.; Khemani, K. C.; Koch, A.; Wudl, F.; Holkzer, K.; Donovan, S.; Gruner, G.; Thompson, J. D. *Science* 1991, ***253***, 301.
48. Stephens, P. W.; Cox, D.; Lauher, J. W.; Mihaly, L.; Wiley, J. B.; Allemand, P.-M.; Hirsch, A.; Holczer, K.; Li, Q.; Thompson, J. D.; Wudl, F. *Nature* 1992, ***355***, 331.
49. Gornitzka, H.; Stalke, D. *Angew. Chem. Int. Ed. Eng.* 1994, ***33***, 693.
50. Carlin, R. L. *Magnetochemistry* ; Springer-Verlag: 1986.
51. Ramirez, A. P.; Rosseinsky, M. J.; Murphy, D. W.; Haddon, R. C. *Phys. Rev. Lett.* 1992, ***69***, 1687.
52. Ashcroft, N. W.; Mermin, N. D. *Solid State Physics* ; Holt-Saunders: 1976.
53. Slichter, C. P. *Principles of Magnetic Resonance* 3rd ed.; Springer: Berlin, 1989.
54. Abragam, A. *The Principles of Nuclear Magnetism* ; Clarendon Press: Oxford, 1961.
55. Kuzmany, H.; Fink, J.; Mehring, M.; Roth, S. *Electronic Properties of Fullerenes* ; Springer-Verlag: Berlin, 1993, p 321.
56. Howard, J. A.; Tomietto, M.; Wilkinson, D. A. *J. Am. Chem. Soc.* 1991, ***113***, 7870.
57. Reed, C. A.; Stinchcombe, J.; Penicaud, A.; Bhyrappa, P.; Boyd, P. D. W. *J. Am. Chem. Soc.* 1993, ***115***, 5212.

58. Wudl, F.; Allemand, P.-M.; Srdanov, G.; Koch, A.; Khemani, K. *J. Am. Chem. Soc.* 1991, ***1991***, 2780.

59. Krusic, P. J.; Wasserman, E.; Parkinson, B. A.; Malone, B.; Jr, E. R. H.; Keizer, P. N.; Morton, J. R.; Preston, K. F. *J. Am. Chem. Soc.* 1991, ***113***, 6274.

60. Reed, C. A.; Penicaud, A.; Hsu, J.; Koch, A.; Khemani, K. C.; Alemand, P.-M.; Wudl, F. *J. Am. Chem. Soc.* 1991, ***113***, 6698.

61. Penicaud, A.; Perez-Benitez, A.; V., R. G.; P., E. M.; Escudero, R. *J. Am. Chem. Soc.* 1993, ***115***, 10392.

62. Bossard, C.; Rigaut, S.; Astruc, D.; Deville, M.-H.; Felix, G.; Fevrier-Bouvier, A.; Amiell, J.; Flandrois, S.; Delhaes, P. *J. Chem. Soc., Chem. Comm.* 1993, 333.

63. Dinse, K.-P.; Ruebsam, M.; Plueschau, M.; Fink, J.; Kraetschmer, W.; Fostiropoulos, K.; Taliani, C. *J. Am. Chem. Soc.* 1992, ***114***, 10059.

64. Dyson, F. J. *Phys. Rev.* 1955, ***98***, 349.

65. Feher, G.; Kip, A. F. *Phys. Rev.* 1955, ***98***, 337.

66. Fagan, P. J. *XVIth International Conference of Organometallic Chemistry* 1994,

67. Christie, K. O.; Wilson, W. W.; Wilson, R. D.; Bau, R.; Feng, J.-A. *J. Am. Chem. Soc.* 1990, ***112***, 7619.

Chapter 4

Application of Microwave Techniques to the Synthesis of Metal Fullerides

4.1. General Introduction to Microwave Techniques

The use of microwave techniques in chemical synthesis has become increasingly popular over the last decade.[1-5] Microwave techniques are applicable in all reaction media ranging from the gas phase to homogeneous solutions, the solid state, and thin film technology.[1-7]

The primary condition, for heating, is that at least one of the reaction components, or the medium of the reaction, absorb microwave radiation at the wavelength(s) applied. By this means energy transfer to the system is achieved.

The region of the electromagnetic spectrum that is deemed microwave radiation lies in the wavelength region 1cm to 1m which is between the near infra-red and radio frequencies. Commercially available domestic microwave ovens operate at 12.2cm (2.45GHz) or 33.3cm (900MHz). These wavelengths are chosen to avoid interference with telecommunications and RADAR instrumentation which also use microwave frequencies. The oven used in this thesis operated at 2.45GHz. Modifications to domestic microwave ovens and the construction and optimisation of microwave generators and cavities, to provide a range of wavelengths and powers available for chemical synthesis, have been reported.[8-13] Operation at frequencies other than 2.45GHz and 900MHz requires shielding to prevent interference with telecommunications and RADAR.

Microwave techniques, as far as the chemist is concerned, have generally been used to accelerate the rate of a reaction by effectively superheating the system. The mechanisms by which energy can be transferred from the microwave radiation to the system are discussed in the following sections. Dielectric loss is the most common method of heating, but this mechanism does not play a dominant role in this thesis and so only a very brief account will be given. However conduction losses and heat generated by a microwave induced plasma play a significant role and therefore will be dealt with in more detail.

The absorption of microwave, or other high frequency radiation, by a system arises from the coupling of the motion of charged species with the oscillating electric field. These charged species can take the form of dipoles in a liquid or ions and electrons in a solid or gas. For absorbtion to take place it is necessary that the frequency of the field is of the same order of magnitude as the response of the absorbing material, whether it be the alignment of dipoles in a liquid, the polarization of charged particles in a solid or the build up of charge between surfaces.

4.2. The Heating Effect Caused by Dielectric Losses

Bulk heating of liquid and solid phases, via dielectric loss, has been investigated by many workers especially in the area of food technology and has been placed on a more theoretical basis by workers such as Debye,[14] Frolich,[15] Daniel,[16] Cole and Cole,[17] Hill[18] and Hasted.[19]

Heating of a system, caused by dielectric loss, is most readily explained by

considering the effect of the applied oscillating electric field on the polarisation of the absorbing dielectric medium. The total polarisation of a dielectric can be described by the sum of the individual polarisations caused by the field.[20] Each component to the total polarisation has an associated time constant and it is only those components which are on the same timescale as the frequency of the applied microwave radiation that will cause significant amounts of energy to be absorbed. This is shown in figure 4.2.1.

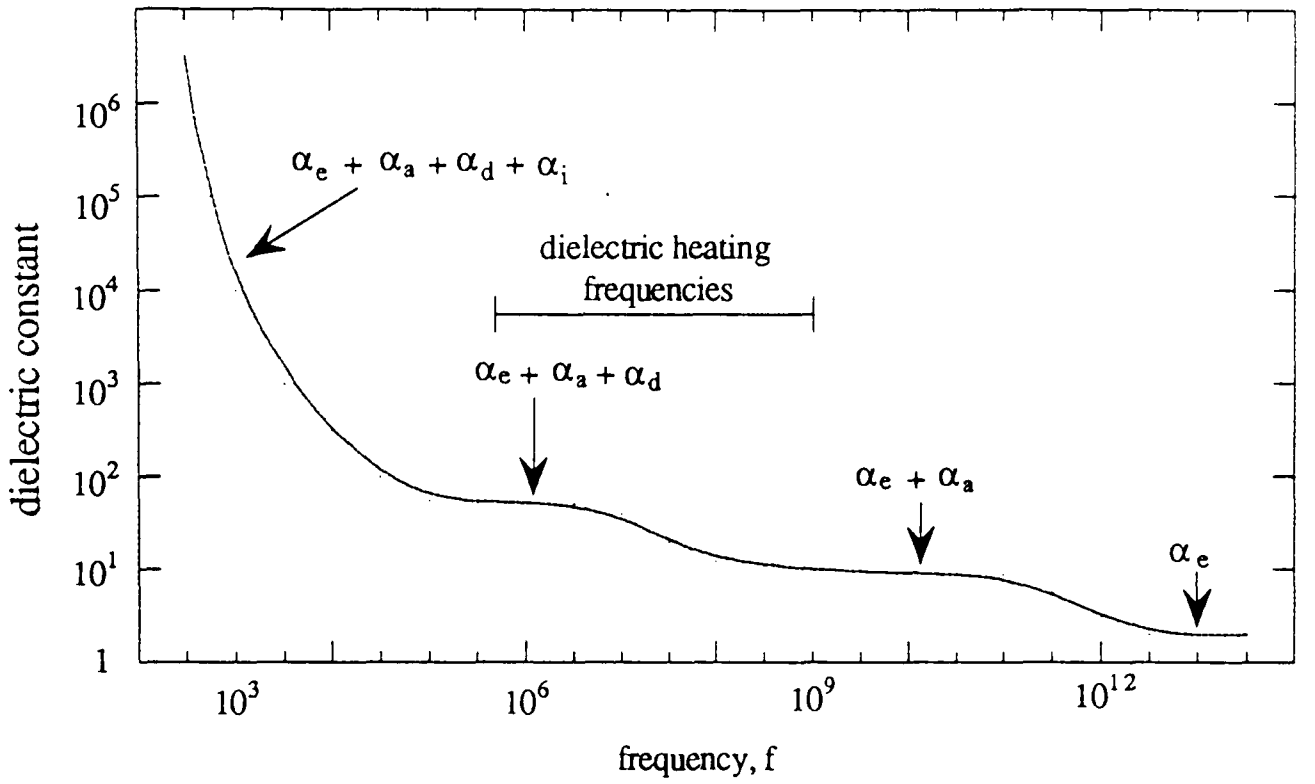


Figure 4.2.1. Polarisation effects in a dielectric. The α terms are defined in the main text.

The total polarisation, α_T, can be described by the simple equation:

$$\alpha_T = \alpha_e + \alpha_a + \alpha_d + \alpha_i$$

α_e is the electronic polarisation which occurs due to the polarisation of electrons with respect to the nuclei, α_a is the atomic polarisation which arises from the relative displacement of nuclei with respect to the unequal distribution of charge within the dielectric. Neither of these effects contribute to the heating of a system in a microwave cavity because they respond faster than the frequency of radiation.

α_i is the interfacial polarisation which is also known as the Maxwell-Wagner effect. This polarisation occurs when there is a build up of charge at the interfaces of particles and is important for conducting particles in a non-conducting medium. Wire wool will spark and melt when irradiated in a conventional household microwave oven as a consequence of interfacial polarisations.

α_d is the dipolar polarisation and is responsible for the heating effect utilised in accelerating the majority of chemical reactions studied to date. It results from the time dependent reorientation of permanent dipoles with respect to an applied oscillating electric field.

If the electric field oscillates at a very high frequency the charged particles cannot respond at a rate fast enough for significant quantities of energy to be absorbed. At low frequencies, because the charged particles can adequately reorientate themselves with the field, again no significant net absorption of energy occurs, as is the case for the electronic and atomic polarisations. At intermediate frequencies, which correspond to the microwave region, the response of the charged particles is such that as the field changes direction the particles are still experiencing the forces from the previous direction of the field. The delay indicates that energy is being absorbed by the system and heating is occurring via dielectric loss . An analogy is that of a child on a swing. As the child moves his or hers centre of gravity the swing takes a finite time to respond to the torque applied. As with an oscillating field, energy is transferred from the childs body causing the swing to gain in kinetic energy.

The heating caused by dipolar polarisation can be placed on a more quantitative basis by defining the dielectric loss tangent.[20] This is the ratio of the dielectric loss, determined by measuring the efficiency of heating by the microwave radiation, to the dielectric constant which describes the ability of the molecule to be polarised by the electric field.[3] The dielectric loss tangent is frequency dependent as shown in figure 4.2.2. for water.[21]

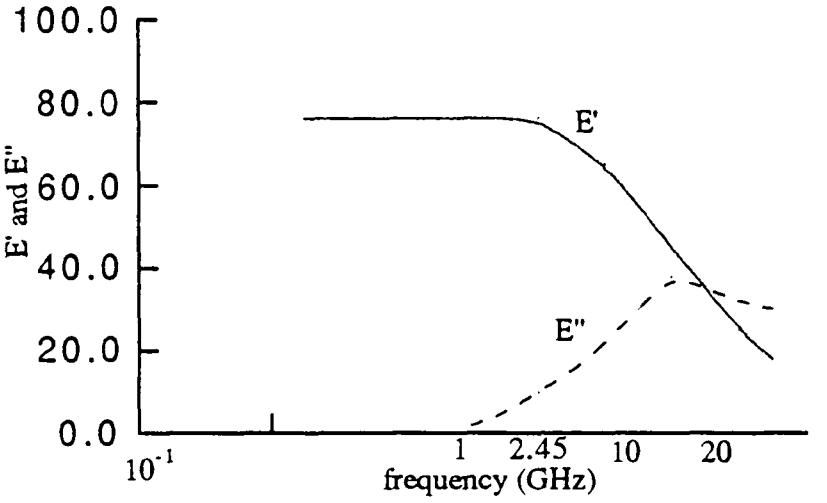


Figure 4.2.2. Dielectric properties of water as a function of frequency. E' is the measured dielectric constant and E" the dielectric loss.

The quantitative treatment for the rise and decay of polarisation in liquids and solids is essentially the same. In describing the reorientation of the dipole there are severe restrictions in the solid state and the dipole is simply treated as assuming one of two possible orientations parallel with the field direction.[15]

The dipolar polarisation is dependent on such factors as the temperature, viscosity (in liquids), the shape and size of the system, and intrinsic factors such as static and high frequency dielectric constants and relaxation time constants. It is therefore very difficult to treat dipolar polarisation mathematically, though empirical equations have been constructed.[22] The dielectric loss tangents at various frequencies for some common solvents[21] are given in table 4.2.1.

Table 4.2.1. Dielectric constant and dielectric loss of some common solvents with varying frequency.

	Frequency					
	3×10^8 Hz		3×10^9 Hz		1×10^{10} Hz	
Solvent	ε'	ε''	ε'	ε''	ε'	ε''
Water	77.5	1.2	76.7	12.0	55.0	29.7
0.1M NaCl	76	59	75.5	18.1	54	30
Heptane	1.97		1.97	$2x10^{-4}$	1.97	$3x10^{-3}$
Ethanol	22.3	6.0	6.5	1.6	1.7	0.11
Ethylene glycol	39	6.2	12	12	7	5.5
Carbon tetrachloride	2.2		2.2	$9x10^{-4}$	2.2	$3x10^{-3}$

4.3. The Heating Effect Caused by Conduction Losses

Heating caused by conduction losses can be described within the framework of general dielectric heating effects and Maxwell-Wagner theory.[3, 16, 23-25] Maxwell[26] considered layers of material with differing dielectric constants and conductivities as part of a parallel plate capacitor and calculated the field generated between the plates as a function of current. Maxwell showed that this model could be used to describe the dielectric relaxation in a heterogeneous dielectric material. Wagner[27] later extended this theory describing the effect microwave radiation exerts on a heterogeneous mixture of particles suspended within a medium of differing dielectric constant and conductivity. The model consisted of small spheres (relative to the wavelength of the radiation) dispersed so that electrostatic interactions were negligible. Its role in explaining conduction losses is when one considers the interactions when the conducting particles are in close proximity to each other.

The mathematical approach is too complex to consider here but the total Maxwell-Wagner theory realises the equation.

$$\varepsilon_i^* = \varepsilon'_\infty + \frac{(\varepsilon'_0 - \varepsilon'_\infty)}{(1 + i\omega t)} - \frac{i\sigma}{\omega\varepsilon_0}$$

Where ε_i^* is the complex permitivity, ε'_∞ is the high frequency dielectric constant, ε'_0 is the static dielectric constant, ω is the angular frequency (the build up and decay of polarisation), t is time, ε_0 is the permitivity of free space, and σ is the conductivity.

The complex dielectric constant is a composite of a real part corresponding to that of simple Debye theory which describes, and is equivalent to, the measured dielectric constant. The imaginary part which describes the 'lossiness' of the dielectric, contains the third term of the equation, and describes a D.C. conductivity contribution to the dielectric loss. The more conducting the dielectric the larger the conductive loss

effects will become.

Dielectric materials are electrical insulators. It is therefore sometimes necessary to pretreat the dielectric, for example by heating the material, to promote conduction and hence conduction losses. This could be achieved by immersing the dielectric in a microwave induced plasma as discussed in sections 4.5. and 4.6.

4.4. Thermal Runaway in Ceramics.

The sintering of ceramic materials, using microwave radiation has been studied extensively by a number of workers.[1, 5, 28-37] This work was used as a basis to determine new approaches to the rapid synthesis of known alkali metal fullerides and investigations into novel lanthanide metal fullerides. In this thesis a piece of sintered alumina was used as a furnace to sublime metals, because of its mechanical and thermal robustness and its propensity to undergo thermal runaway.

The interaction of microwave radiation with ceramic materials can result in a heating phenomenon known as thermal runaway.[32, 33, 38] Thermal runaway is a sudden rapid increase in the temperature of a material due to a non-linear absorption of microwave energy with respect to time. The effect can be very dramatic, resulting in heating rates greater than 100°C/s in some materials.[32]

The origin of thermal runaway in ceramics has been considered on the microscopic level to be caused by absorbers of microwave radiation that will only absorb when released from a potential well by thermal fluctuations. As the number of absorbers increases, the total amount of energy absorbed by the material will also increase, and further absorbers will be liberated from their potential wells. This 'cascade' of events results in a rapid rise in temperature as the sample absorbs increasing amounts of microwave radiation.[5]

If the ceramic is perfectly transparent to microwave radiation, absorption will not occur and the material remains at room temperature. However, as is usually the case, there are defects in the lattice of the ceramic, or small amounts of impurity, then these may act as absorbers of microwave radiation and initiate thermal runaway. A perfectly transparent material can undergo thermal runaway by pretreatment before being exposed to microwave radiation. By simply heating the sample, sufficient absorbers can be liberated from potential wells, initiating thermal runaway. Another method, is to impregnate the microwave transparent material with a strongly absorbing material. This will enhance the coupling of the microwaves to the transparent matrix via the local heating of the occluded absorbers.

Initially there maybe an induction period where the ceramic does not heat at a large rate, as shown for chroma[39] in figure 4.4.1.

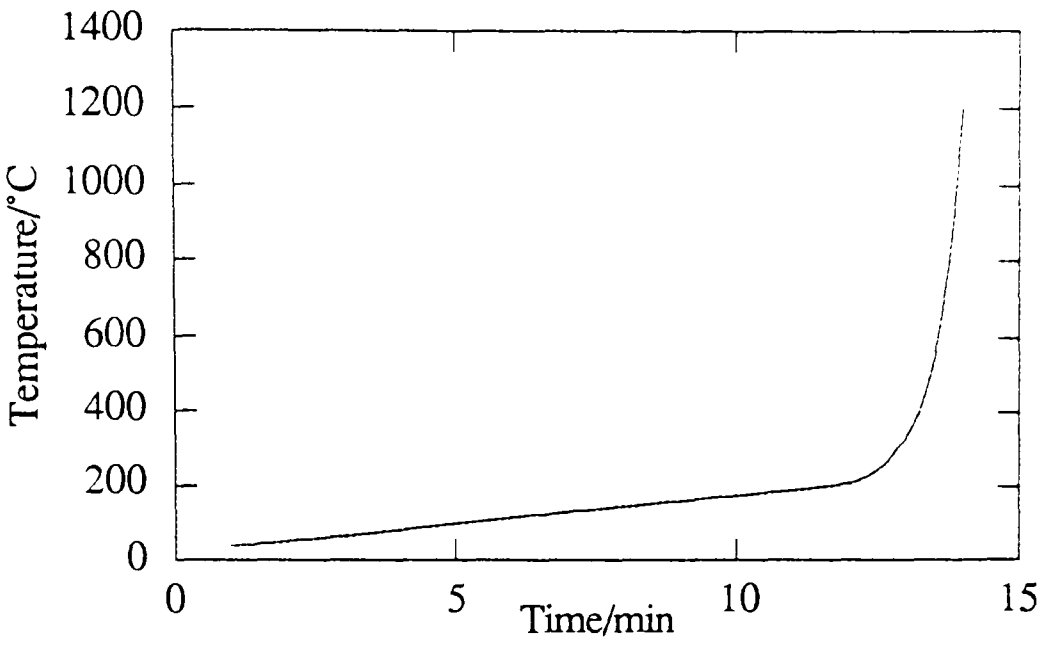


Figure 4.4.1. The heating of chroma when exposed to 500W of microwave radiation.

The profile of temperature versus time for a ceramic is dependent on the constituent elements, the previous history of the sample, how efficient heat can be transferred from the sample to its environment, and the frequency of the applied radiation. An efficient heat transfer mechanism from the sample to the environment results in saturation of the temperature versus time curve, as shown in figure 4.4.2. The dominant mechanism for the saturation of thermal runaway appears to be from radiative heat losses.

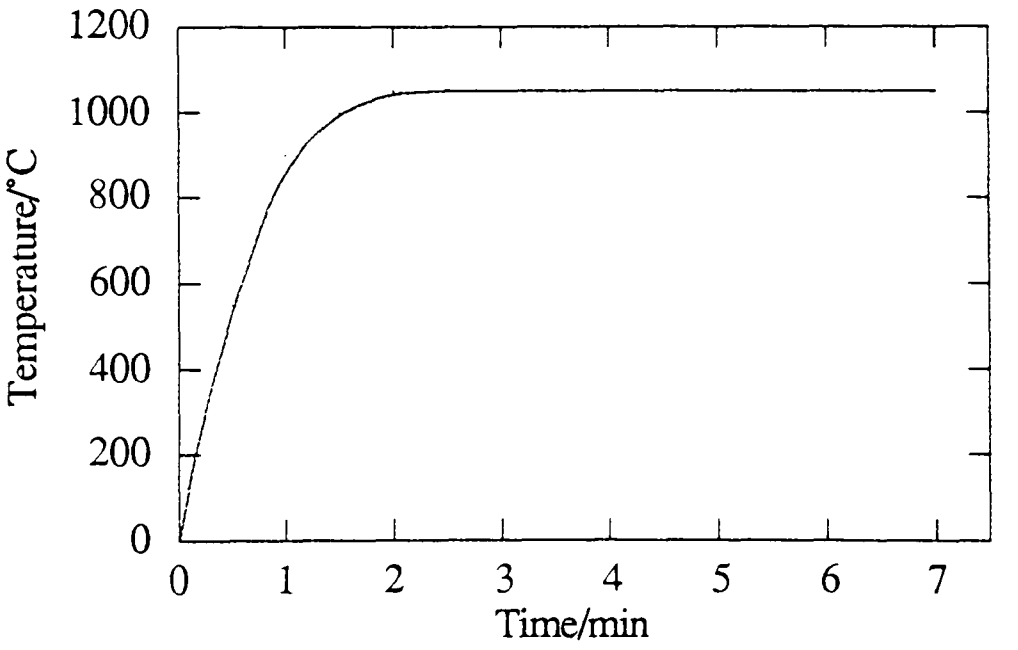


Figure 4.4.2. Microwave heating of iron oxide.[39]

It can be seen from a comparison of figures 4.4.1. and 4.4.2. that for iron oxide the initial period of slow temperature rise is absent, or very short, and that saturation is not observed in chroma, for the duration of the experiment. Alumina has a temperature versus time profile intermediate between chroma and iron oxide as shown in figure 4.4.3.

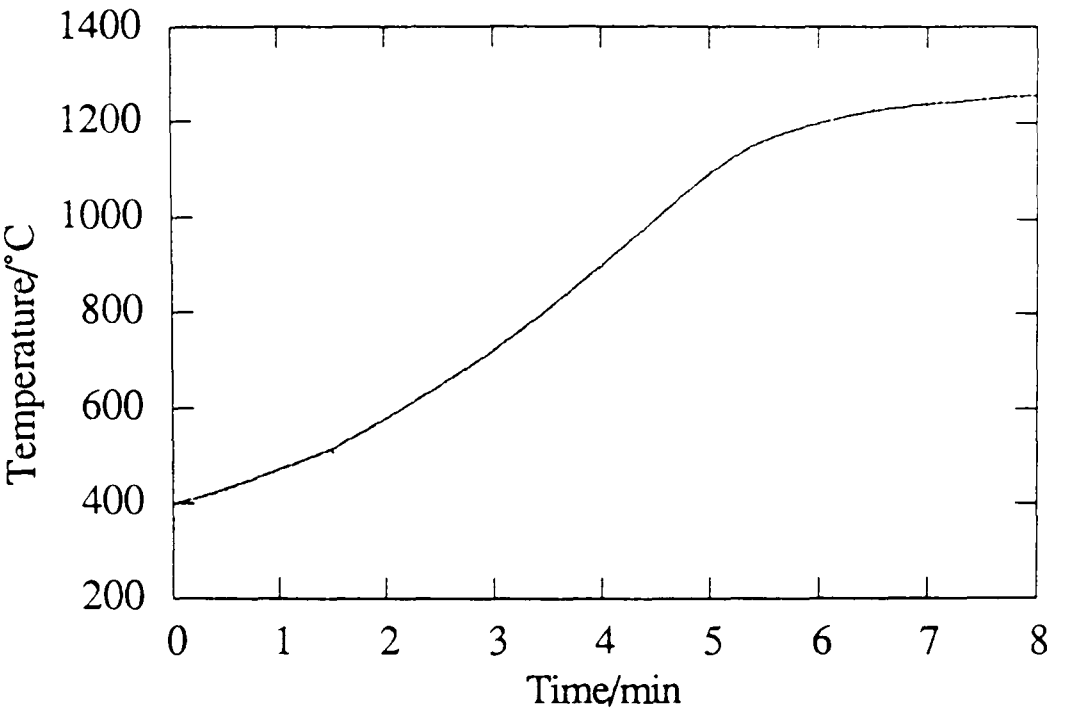


Figure 4.4.3. Microwave heating profile of alumina.[40] Note that preheating of the sample was required for absorption of microwave radiation to occur.

Thermal runaway in alumina is based on the promotion of electrons from the 2p based oxygen orbital to a 3s3p conduction band. The resulting conduction losses, as discussed in section 4.2., become larger with increasing temperature because the number of conduction electrons increases. Saturation occurs at *ca.* 1200°C due to radiative losses.

4.5. Microwave Induced Plasmas.

Microwave induced plasmas, or discharges, have been investigated for over 45 years.[41] They have been applied to thin film technology in the form of microwave plasma chemical vapour deposition (MPCVD)[6, 7, 42, 43] and in the generation of species *in situ* for deposition, e.g. arsine from arsenic and dihydrogen.[6] Microwave plasma induced sintering (MPIS) has been demonstrated for alumina and other ceramics where temperatures in excess of 1600°C have been readily achieved[1, 5, 28, 29] and microwave plasma etching has shown considerable promise.[44] An example of the decomposition of cobalt carbonyl in a series of zeolites has also been reported.[45] Other applications have been suggested in the areas of laser discharges and RF heating in thermonuclear fusion research.[46] It has even been proposed that ball lightning is a consequence of microwave interference generated from instabilities in atmospheric electricity.[47]

A plasma is a gas consisting of ions, electrons and neutral particles at essentially electrical neutrality. Above absolute zero any gas has a certain percentage of ionised atoms, though the percentage may be extremely small. As the concentration of ionised particles increases the interactions between them causes their motion to be restricted. If the partial volume of ionised gas approaches the total volume of the gas, the restrictions become such that any disturbances of macroscopic neutrality induce strong magnetic fields which rapidly restore neutrality. An ionised gas at such concentration was termed

a plasma by Langmuir in 1923.[46]

A plasma may be generated in various ways including electrical discharges between electrodes, and laser plasmas, but this thesis was concerned with a plasma generated by a high frequency electric field in a microwave oven. An argon plasma such as was used in this thesis is shown in figure 4.5.1.

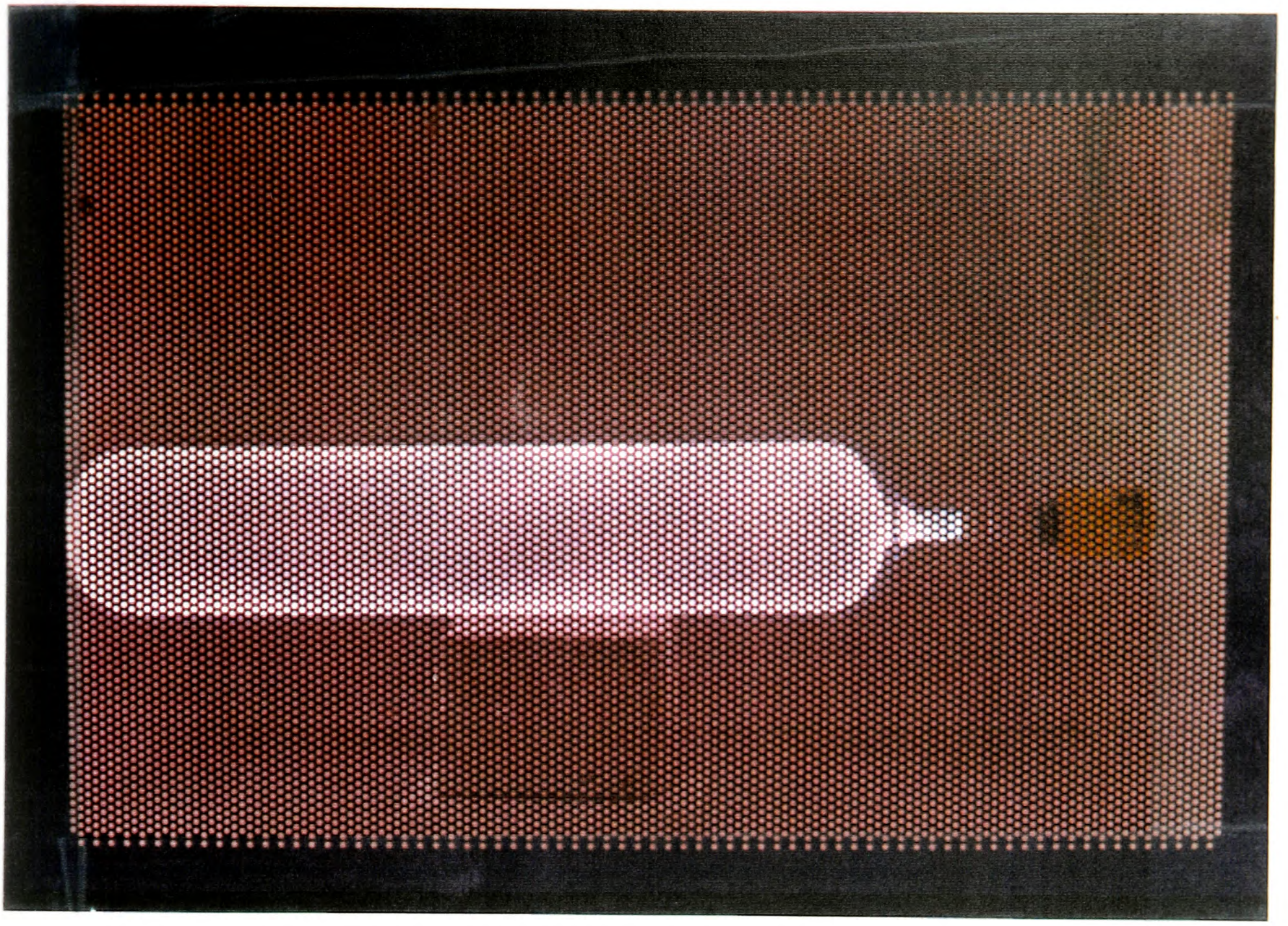


Figure 4.5.1. Microwave induced argon plasma generated in a conventional household microwave oven. The plasma is confined by the walls of an ampoule.

A microwave plasma is generated by the absorption of microwave energy in an ionised gas. There is therefore the prerequisite that a portion of the gas must be ionised prior to absorption of microwave energy and generation of a plasma.[4] A plasma may be induced from an outside source such as a Tesla coil or the incident microwave power may suffice.

4.6. The Heating Effect Caused by a Microwave Induced Plasma.

There are two basic characteristics of a plasma that can make it useful for chemical processes. High energy electrons that can break chemical bonds by collision with a gas molecule, and secondly, plasma ions bombarding a surface can effect the composition and microstructure, for instance significantly altering film growth and the sintering process.[4]

Microwave induced plasmas have been known for sometime to cause rapid increases in temperature of reaction vessel walls and solid samples contained within them.[29, 48] The heating effect is due to ion bombardment of the surfaces bounding the plasma.

The maximum temperature that can be achieved depends on several factors not least of which are the pressure of the gas, the nature of the gas, the power of the applied radiation and the frequency of the radiation. Factors intrinsic to the sample are also critical such as the morphology and composition. All studies concerning the heating effect of a microwave induced plasma have concentrated on the sintering process, invariably that of ceramic materials. Various gases have been investigated including dinitrogen, dihydrogen, dioxygen and argon.[8, 10, 28, 49] The best characteristics, with respect to sintering temperature and stability, was exhibited by dinitrogen followed by dihydrogen and dioxygen. Argon showed the lowest sintering temperature and instabilities at low pressures (1 kPa).[28] Higher temperatures for the diatomic gases has been attributed to the heat of association of dissociated atoms which occurs at the surface of the plasma immersed sample. It should be noted that these experiments were performed under a dynamic pressure of the plasma gas. A static pressure was used for the experiments performed in this thesis.

4.7. Conventional Solid State and Other Synthetic Routes to Alkali Metal Fullerides.

The observation of superconductivity in A_3C_{60} (A = K, Rb) alkali metal fullerides, has generated considerable interest in this class of materials.[50, 51] Initially, the methods of preparation were based on solid state synthetic techniques using stoichiometric quantities of alkali metals and C_{60} (Na, K, Rb, Cs) or dilution of saturated alkali metal C_{60} phases with an appropriate amount of C_{60} (K, Rb, Cs).[51, 52] In common with most synthesis performed in the solid state reaction times are long, typically on the order of 10 - 14 days, because of slow diffusion rates and the procedure is only applicable to metals with reasonable vapour pressures ($\sim 10^{-2}$ mbar) below the decomposition temperature of C_{60} (~ 600°C).

Other synthetic routes, in the solid state and solution, have been sought to circumvent the problems of diffusion and vapour pressure.

Solid state routes have used mercury amalgams (Na), hydrides and borohydrides (Na, K)[52] and, with limited success, an advanced electrochemical intercalation technique to study lithium C_{60} intercalates.[53]

Solution synthesis of alkali metal fullerides has been applied to the superconducting phases of potassium and rubidium. Both K_3C_{60} and Rb_3C_{60} can be detected from reaction of excess K or Rb with a toluene solution of C_{60},[54, 55] or from reaction with a stoichiometric ammonia solution of the alkali metal with C_{60}.[56] The reaction with excess metal does not result in phase purity and only small amounts of superconducting material are present. Phase purity of K_3C_{60} and Rb_3C_{60} synthesised

via liquid ammonia is not certain as crystallographic details are absent and the ^{13}C NMR data reported is a static rather than a MAS spectrum and hence of lower resolution. However, large quantities of superconducting material were present. Based on the synthesis of $NaC_{60}.5thf$,[57] K_3C_{60} has also been prepared from C_{60} and $K\{Mn(\eta\text{-}C_5Me_5)_2\}$.[58] The phase purity of this material is also uncertain as no X-ray diffraction or NMR spectroscopic data was reported.

All the synthetic methods reported to date require a period of heating for at least a day, and typically several days, to anneal the sample and/or remove occluded solvent.

4.8. Possible New Fullerides and Their Potential Properties.

There are no structurally characterised binary fullerides containing Li and no C_{60} fullerides containing a lanthanide or transition metal. The major reason is the low vapour pressures available within the working range of C_{60}. Temperatures above *ca.* 600°C cause C_{60} to decompose.

Electropositive elements have shown to readily intercalate into the C_{60} lattice with reduction of C_{60} molecules and population of the t_{1u} LUMO. In the case of alkali metals, the composition A_3C_{60} (where A = K, Rb), or alkali metal ternaries $A_2B_1C_{60}$ (where A = Na, K, Rb and B = K, Rb, Cs in various combinations), are superconducting, at various temperatures depending on the lattice parameter of the fcc structure,[59] as discussed in section 1.6.2. The alkaline earth compositions Ca_5C_{60}[60] and Ba_6C_{60}[61] are also superconducting.

Lanthanide and transition metal fullerides are an attractive proposition because of their potential electronic, magnetic and optical properties. Intrinsically, the possible C_{60} intercalate structures should be simple, and would be an opportunity to gain insight into structure-property relationships. Alkali and alkaline earth cations have a closed shell electronic configuration, but this is not necessarily the case for lanthanide and transition metal cations. Interactions between magnetic cations and C_{60} anions might be particularly interesting.

4.9. Application of Microwave Techniques to the Synthesis of Alkali Metal Fullerides.

Alkali metal fullerides are air and moisture sensitive and so all reactions were performed in flame sealed Pyrex or silica vessels.

Synthesis were conducted in a Hinari 'Lifestyle' 1000W microwave oven operating at a frequency of 2.45 GHz, modified to incorporate a variable power unit as shown in figure 4.24.2. Reaction vessels were supported on fire bricks to prevent thermal contact with the oven walls.

4.10. Preliminary Investigations.

4.10.1. The Effect of Microwave Radiation on C_{60} and Potassium.

A few milligrams of C_{60} were flame sealed in a Pyrex tube under dinitrogen and exposed to microwave radiation for 10 minutes, at the maximum power obtainable. Intermittently the magnetron would cease to operate due to reflected power entering the waveguide. Too much reflected power engages a safety cutout mechanism, indicating that the microwaves were not being absorbed in the cavity to a significant degree. The temperature of the reaction vessel did not appreciably increase during exposure, and the C_{60} sample appeared unchanged. Decomposition did not occur as demonstrated by complete dissolution of the sample in toluene to produce a purple solution.

Heating of the C_{60} sample did not take place because there is no mechanism by which energy can be transferred from the impinging microwave radiation to a solid sample of C_{60}. C_{60} is apparently transparent to microwave radiation at 2.45 GHz.

In an analogous manner 10 mg of freshly cut potassium was exposed to maximum power for 10 minutes. No heating occurred presumably because, potassium being a metal, the microwave radiation was reflected and not enough metal was present to cause heating by conduction losses.

4.10.2. Attempted Volumetric Heating of Potassium Metal in the Presence of C_{60}.

Metal powders are known to have high dielectric loss tangents at 2.45 GHz and have successfully been used in solid state synthesis. Coupling with the microwave radiation results in volumetric heating of the sample, and occurs via conduction mechanisms and possibly additional local plasma effects. However, sufficient sample must be present (>1g)[62, 63] and the size of the metal particles above a minimum size (>100 mesh).

If volumetric heating of potassium metal powder is to be achieved, then gram quantities of potassium would be required. Consequently, for a stoichiometric reaction between potassium and C_{60}, prohibitive amounts of C_{60} would also be needed. The use of large excesses of potassium is not desirable since separation of unreacted metal from a K_xC_{60} phase will be required. Metal particles are known to arc between each other, if excessive power is applied, due to the build up of large electric field gradients.[64] This

could possibly act as a source of heat causing potassium to vaporise and diffuse into the C_{60} sample. If a phase assemblage of K_xC_{60} also effectively couples with the microwave radiation the resulting heating effect would cause diffusion of potassium atoms throughout the C_{60} particle.

25mg of C_{60} and 50mg of potassium metal, in the form of 10 freshly cut chips, were flame sealed in a Pyrex tube under 10^{-1} mbar of dinitrogen as shown in figure 4.10.2.1.

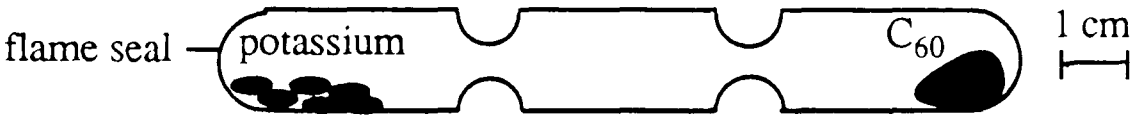


Figure 4.10.2.1. Pyrex vessel used in the initial investigation into the synthesis of K_3C_{60}. The kinks in the tube are to prevent molten potassium from reaching the C_{60} powder.

On exposure to maximum microwave power an orange dinitrogen discharge was produced almost immediately. After approximately 5 seconds the potassium metal began to melt, immediately followed by a purple potassium discharge and rapid vaporisation of the metal. Exposure to microwaves was ceased immediately. The tube was hot to the touch (~ 150°C) with a thin film of potassium metal covering some of the surface of the inner wall and some of the C_{60} powder. Further exposure, for 10 seconds, at maximum power immediately resulted in a purple potassium discharge associated with a green discharge over the C_{60} region. Recovery of the C_{60} sample was problematic due to portions of the powder being embedded in potassium metal and the presence of small potassium fragments. An accurate mass balance was impractical. However, 20mg of a dark powder was recovered which did not significantly differ in appearance from C_{60}. Solubility tests indicated that C_{60} anions may be present as some of the material was partially soluble in acetonitrile imparting a red colouration. C_{60} also appeared evident as addition of toluene partially solublised the solid to give a purple solution.

^{13}C MASNMR spectroscopy revealed a peak at δ 143 ppm assignable to C_{60} but no other clearly discernible peaks were apparent. D. C. bulk susceptibility measurements using a SQUID magnetometer showed that a small amount (<1%) of some superconducting phase was present. The superconducting transition temperature (T_c) of 19K observed, corresponds to that of K_3C_{60}.[50]

4.10.3. Exposure of C_{60} to a Dinitrogen/Potassium Discharge.

The small amount of superconducting K_3C_{60} found in the experiment in section 4.10.2. could possibly be due to the reaction of C_{60} and the potassium plasma. The amount of potassium in the vapour phase, which is responsible for the discharge, is small and could account for the small percentage of superconducting material found.

The modified apparatus used to expose C_{60} powder to a potassium discharge is

shown in figure 4.10.3.1.

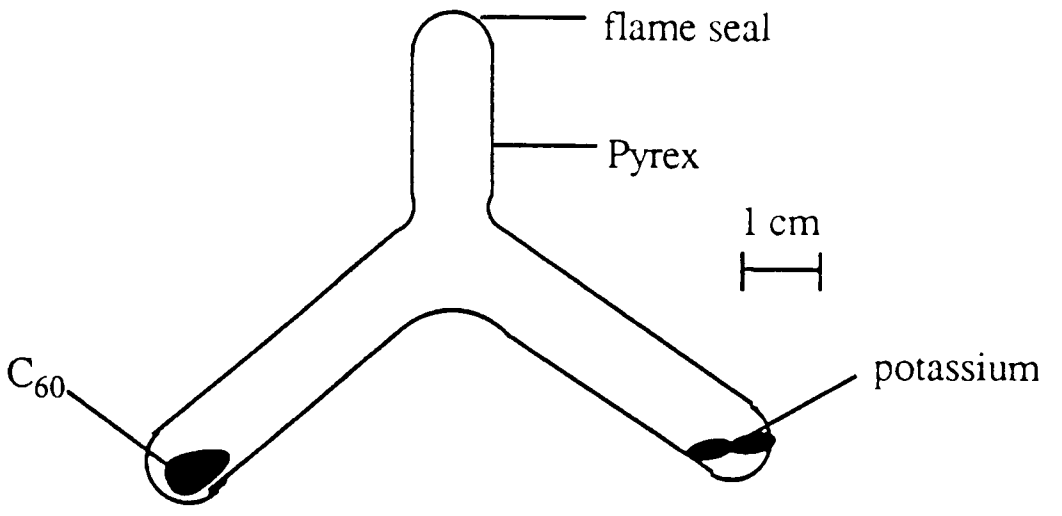


Figure 4.10.3.1. 'Y' shaped tube used to expose the C_{60} powder to a potassium discharge.

On exposure to the microwave radiation an orange dinitrogen discharge formed immediately which resulted almost instantaneously in the formation of a purple potassium discharge. However after approximately 2 seconds the plasma extinguished. Heating the tube with a heat gun outside of the cavity, and quickly transferring it back into the oven, had the desired effect resulting in a purple plasma that appeared stable on exposure to the microwaves. The C_{60} powder was exposed to the potassium plasma for 10 seconds. A green discharge was present over the C_{60} region during the experiment and no potassium was apparent on the walls of the reaction vessel in the proximity of the C_{60} powder.

The C_{60} containing dark powder did not appreciably gain in weight and was analysed using ^{13}C MASNMR spectroscopy revealing only a peak at δ 143 ppm assignable to C_{60} and SQUID magnetometry showing no detectable superconducting material. On addition of a sample of the solid to acetonitrile no colouration was observed.

The C_{60} sample was flame sealed with a fresh quantity of potassium and exposed to the purple potassium discharge for 1 minute. This resulted in vaporisation of a portion of the potassium metal and softening of the reaction vessel wall due to the heat generated by the plasma. A green discharge again was apparent over the C_{60} region and no potassium metal was in close proximity to the C_{60}.

Analysis via ^{13}C MASNMR spectroscopy and SQUID magnetometry showed no discernible change in the sample.

4.10.4. Choice of Initiating Plasma Gas.

The experiments described in 4.10.1. to 4.10.3. which utilised 10^{-1} mbar of dinitrogen as the atmosphere suffered from problems concerning the initiation of the plasma. A dinitrogen plasma is required to generate enough heat to vaporise a quantity of potassium sufficient to sustain a potassium plasma discharge. Preheating the

potassium with a heat gun outside of the microwave cavity aids in forming a plasma, but it is not reliable or satisfactory. Another gas was sought which could easily form a discharge over a range of pressures to obviate problems of stringent pressure control. Argon proved to be suitable forming a pale green plasma very easily over a wide range of pressures from 10^{-1} - 10^{-5} mbar. Above 10^{-1} mbar a lightning effect is observed as shown in figure 4.10.4.1.

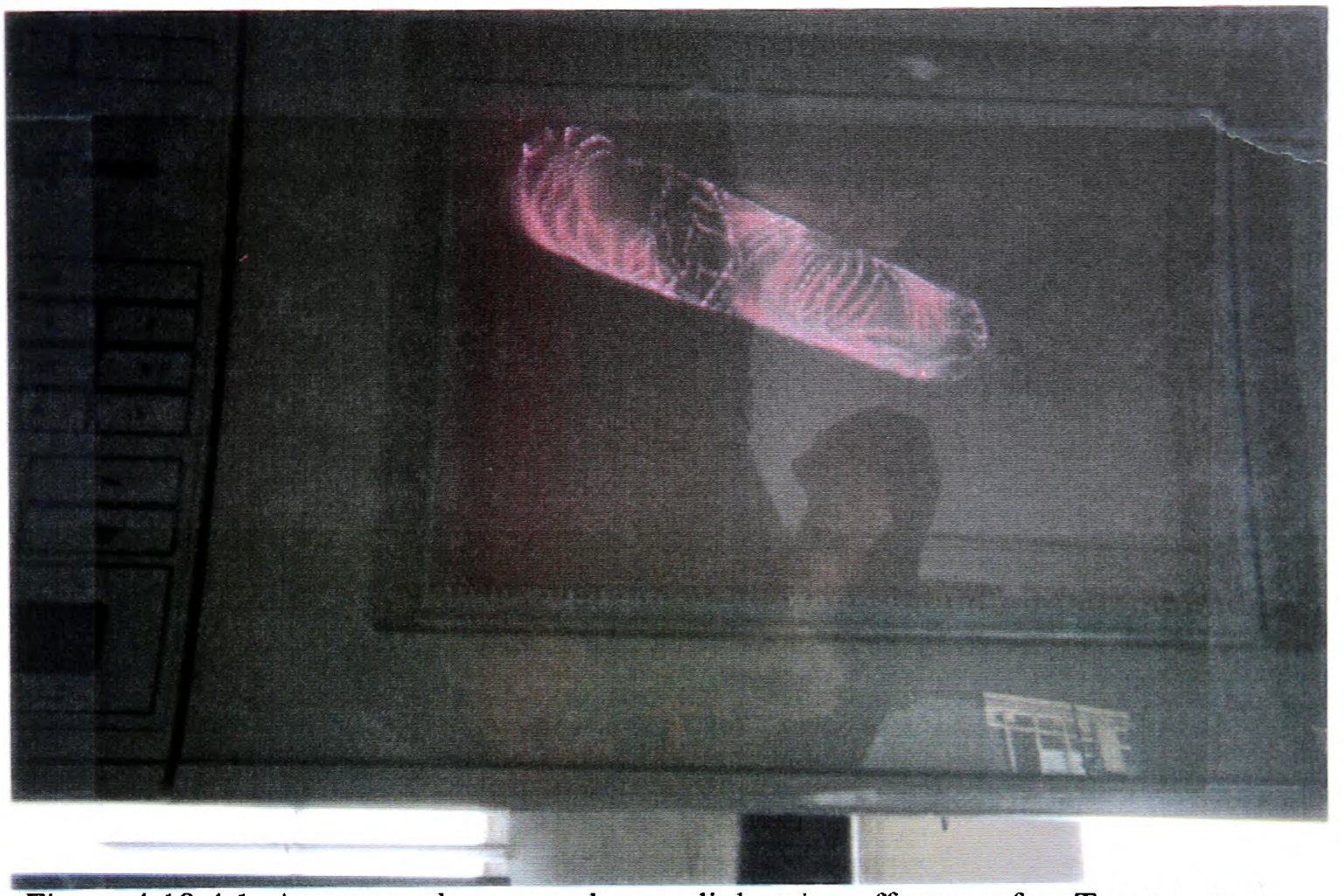


Figure 4.10.4.1. An argon plasma produces a lightening effect at a few Torr pressure.

4.10.5. Reaction of C_{60} and Excess Potassium in an Argon/Potassium Discharge.

A 50mg sample of C_{60} was placed in a Pyrex tube and was intimately mixed with potassium metal (50mg) in the form of 5 freshly cut chips and the tube was flame sealed under 10^{-1} mbar of argon. On exposure to microwave radiation, for 20 seconds, a green argon discharge immediately resulted followed by a purple potassium discharge. The heat generated by the plasma caused the potassium to melt and vaporise violently and project C_{60} throughout the reaction vessel. Further exposure for 2 x 20 seconds, to avoid melting the Pyrex reaction vessel, gave similar results. Removal of the sample was problematic due to the liberal spread of potassium metal throughout the vessel. However, 38mg of a black material was recovered.

^{13}C MASNMR spectroscopy revealed a phase assemblage of C_{60}, K_4C_{60} and K_6C_{60}. Integration by the cut and weigh method revealed the relative percentages as 25, 20 and 55% respectively as shown in figure 4.10.5.2.

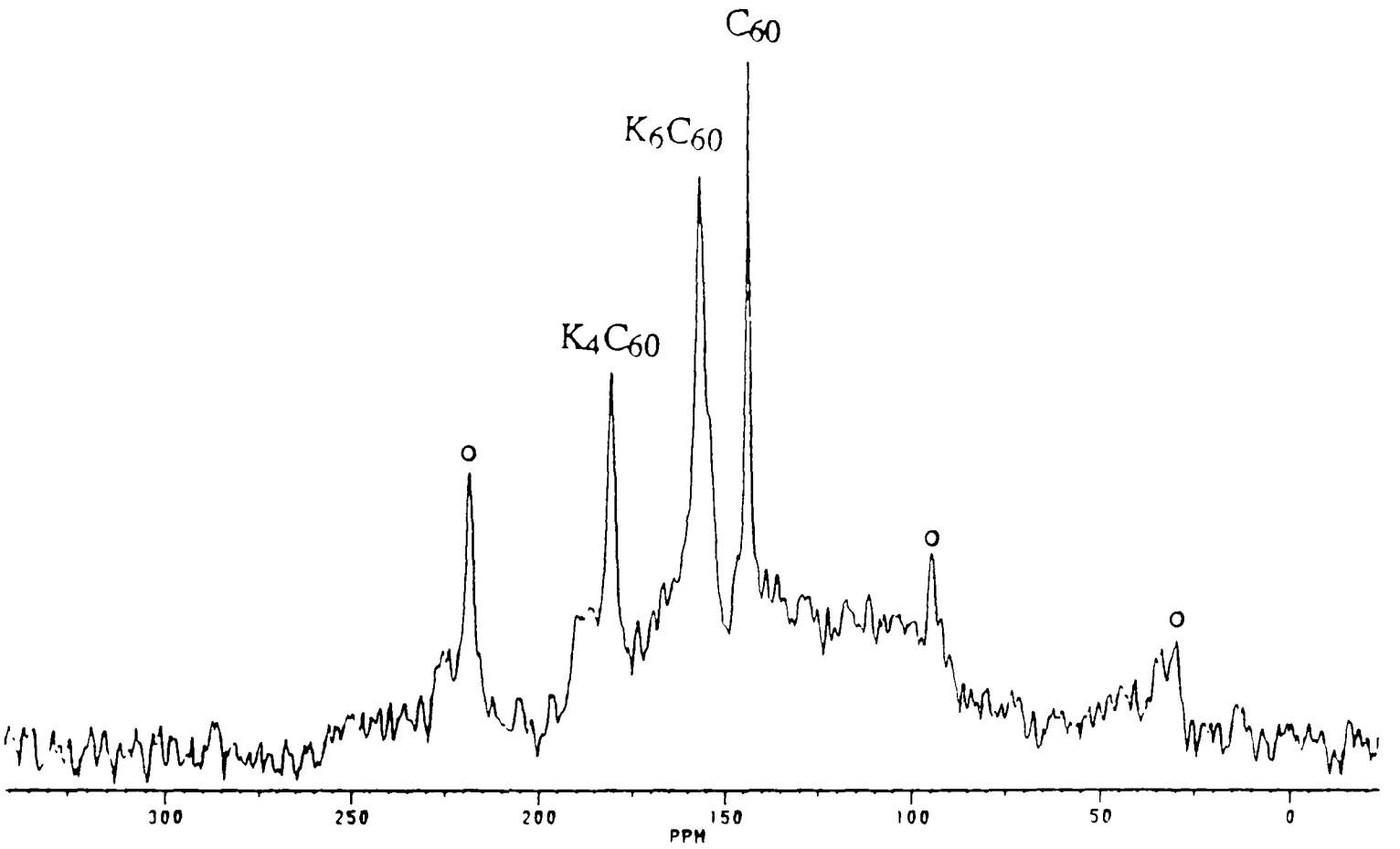


Figure 4.10.5.2. ^{13}C MASNMR spectrum of a K_xC_{60} phase assemblage synthesised in a microwave oven. Spinning side bands of K_6C_{60} are denoted by an 'o'.

K_3C_{60}

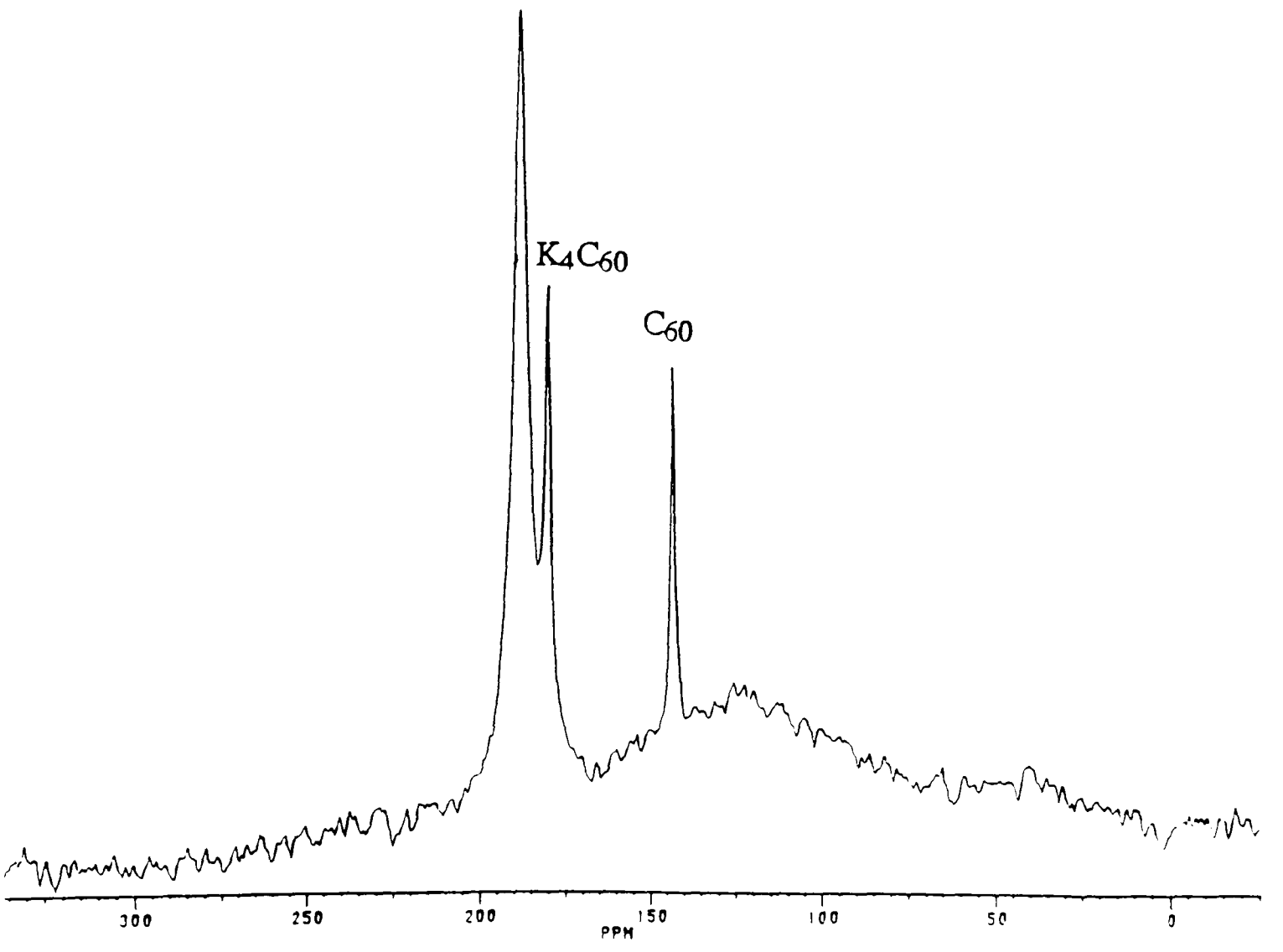


Figure 4.10.6.1. ^{13}C MASNMR spectrum of a K_xC_{60} phase assemblage and C_{60} sample exposed to a microwave induced argon plasma.

4.10.6. Reaction of a K_xC_{60} Phase Assemblage and C_{60} to form K_3C_{60}.

If the K_xC_{60} phase assemblage effectively coupled with microwave radiation enough energy may be absorbed to cause diffusion of potassium atoms throughout the C_{60} lattice and effectively anneal the sample to a phase pure material.

A K_xC_{60} phase assemblage as produced in section 4.8.5. was ground with an appropriate quantity of C_{60} to obtain the gross stoichiometry K_3C_{60}. The sample was flame sealed in a Pyrex tube under 10^{-1} mbar of argon. On exposure to microwave radiation a green argon plasma immediately formed and became extinguished after 5 seconds. The sample was exposed to 3 x 10 mins without a plasma being initiated.

^{13}C MASNMR spectroscopy revealed the sample contained C_{60} (10%), K_4C_{60} (15%) and K_3C_{60} (75%), as shown in figure 4.10.6.1.

The sample was reground and flame sealed under 10^{-1} mbar of argon and exposed to microwave radiation. The plasma did not initiate and the sample was exposed for 3 x 10 mins.

^{13}C MASNMR spectroscopy revealed the sample was unchanged.

4.10.7. Discussion of the Preliminary Reactions.

The synthesis of K_3C_{60} using microwave techniques is possible if the appropriate conditions are met. None of the reaction components, C_{60}, potassium metal (in the quantities used in these experiments) or a K_xC_{60} phase assemblage effectively couples with microwave radiation at 2.45 GHz at room temperature. Therefore dielectric heating is not useful in the synthesis of potassium fullerides. However, by use of a plasma discharge, sufficient heat is generated to melt and vaporise potassium and cause diffusion of potassium atoms throughout the C_{60} lattice.

Choice of plasma gas was determined by the stability of the plasma. An argon plasma has greater stability than dinitrogen at the pressures and volumes used in these experiments. Higher temperatures are thought to be achieved when diatomic gases are used in microwave plasma techniques as opposed to monatomics, but temperatures above *ca.* 600°C would destroy a C_{60} sample, and so the lower temperatures achieved with argon may in fact be advantageous.

To avoid excessive loss of C_{60} containing material, because it can be embedded in potassium metal, a method by which potassium can be introduced into the C_{60} lattice avoiding this problem, would be advantageous. This approach will be discussed in the next section.

4.11. The Use of Ceramics as Microwave Furnaces.

An attractive proposition would be to use a ceramic crucible, containing potassium metal, as a source of a potassium vapour that could react with C_{60} under the action of a microwave induced plasma. If the ceramic only couples with the microwave radiation at elevated temperatures, as in the case of sintered alumina, the plasma could

also act to mediate absorption of microwave energy by preheating the ceramic.

4.11.1. Sublimation of Potassium from an Alumina Crucible Aided by an Argon Plasma.

A crucible of sintered alumina was fashioned from a rod with the dimensions (10 x 50 x 100mm). Alumina is a very hard material but can be sawn and, with difficulty, drilled with a diamond bit. The crucible is shown in figure 4.11.1.1.

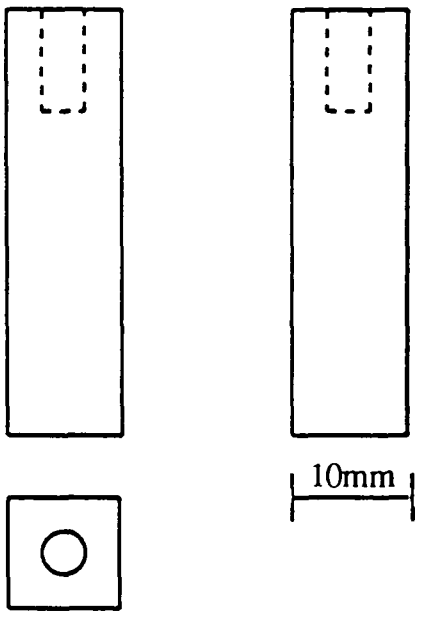


Figure 4.11.1.1. Projection of an alumina crucible used to vaporise potassium metal.

The crucible was filled with 50 mg of freshly cut potassium metal and flame sealed in a Pyrex tube under 10^{-5} mbar of argon as shown in figure 4.11.1.2. A firebrick was used as a support by drilling an appropriately sized hole capable of receiving the tube.

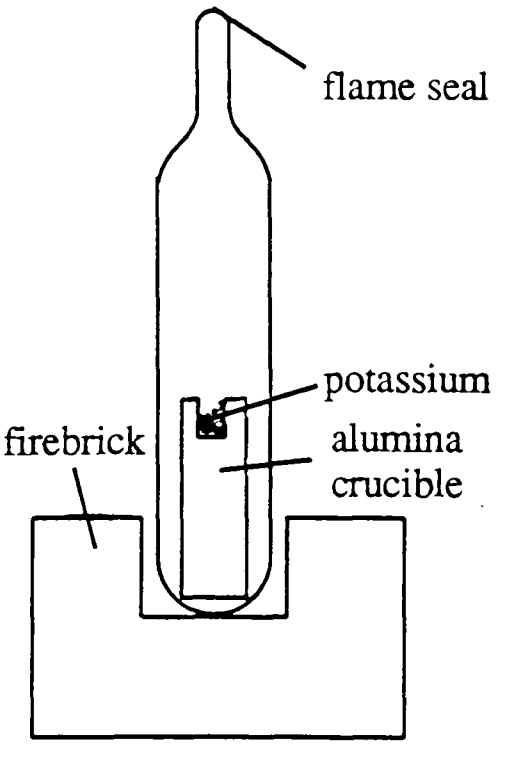


Figure 4.11.1.2. Apparatus to test the viability of potassium vaporisation using an alumina crucible and microwave induced argon plasma.

On exposure to microwave radiation a green argon plasma formed immediately,

enveloping the crucible but not the volume above. After 30 seconds the top of the alumina crucible began to get visibly hot. A purple glow became apparent followed by distillation of the potassium metal onto the walls of the reaction vessel. The heat generated by the plasma caused the potassium to sublime to the cooler top of the tube, and bronzing, due to reaction of potassium with Pyrex occurred in isolated patches on those areas of the walls, which were particularly hot. After 10 seconds the Pyrex failed due to the heat, producing a hole in the wall of the reaction vessel. The heat generated by a microwave induced plasma can easily reach the softening temperature of Pyrex causing the reaction vessel to fail. Silica was used in subsequent reactions because of its much higher temperature threshold (~ 1050 vs 550°C) and its transparency to microwave radiation

4.12. Design of a Suitable Microwave Reactor for the Synthesis of a K_xC_{60} Phase Assemblage.

Continually sealing and resealing tubes of silica capable of passing a crucible of 10 mm^2 in cross section is obviously arduous and time consuming. A reusable simple apparatus was designed for the synthesis of K_xC_{60} phases and is shown in figure 4.12.1.

Important aspects that needed to be taken into consideration were where to place the C_{60} powder relative to the potassium metal, the ease of recovery of the sample, and the geometry of the vessel with respect to the cavity and the microwave radiation.

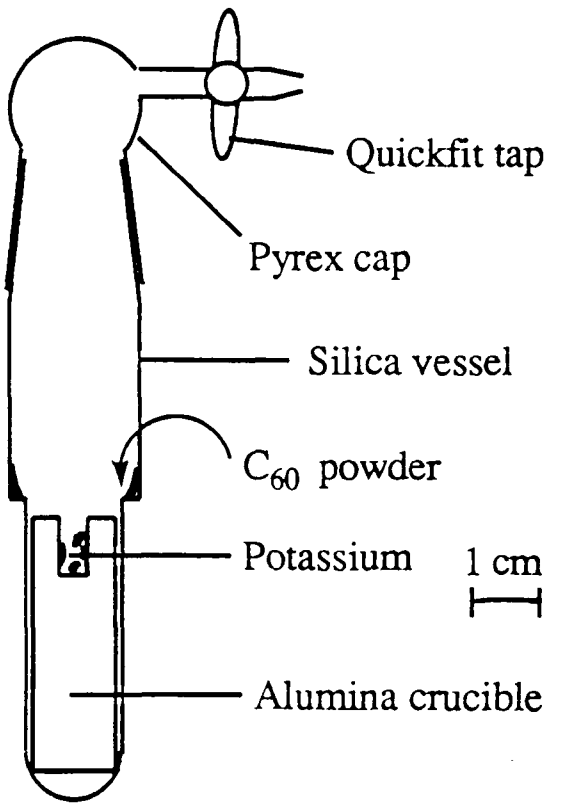


Figure 4.12.1. Reusable apparatus for the synthesis of a K_xC_{60} phase assemblage.

On vaporisation, the potassium vapour will attempt to fill the available volume until it condenses on a sufficiently cool surface i.e. the reaction vessel walls. The position of the bulk potassium metal relative to the C_{60} powder should be such that a large proportion of the metal vapour condenses on the C_{60} powder which may be achieved by trying to direct the vapour over a short path length. However, the path

length cannot be too short or significant decomposition of C_{60} would occur, due to the heat generated by the plasma.

Microwave ovens generate a standing wave within the cavity unless a paddle is used to 'disperse' the incoming microwave radiation. A turntable is commonly used in microwave ovens to account for the standing wave allowing even cooking throughout the food. The microwave oven used in this thesis had the turntable removed and was not fitted with a paddle, therefore a standing wave was present. The position of various nodes and antinodes that are present can be determined simply by exposing a small volume of water for a constant time throughout the volume of the cavity and measuring the increased temperature. Microwave power was at a maximum in the central region of the cavity used in this thesis. Reactions were performed in the centre of the microwave cavity and no account of the waveform was made in the design of the reusable apparatus shown in figure 4.12.1.

4.13. Synthesis of a K_xC_{60} Phase Assemblage Using a Reusable Microwave Reactor.

Typically, freshly cut potassium metal (75mg) was placed in the crucible and C_{60} powder was deposited in the trough via a funnel made from a Pasteur pipette. The atmosphere of the reactor was replaced with argon by a pump/fill procedure and reduced to a pressure of 10^{-5} mbar via a turbomolecular pump. The apparatus was then supported on the fire brick and placed in the microwave cavity, as shown in figure 4.13.1.

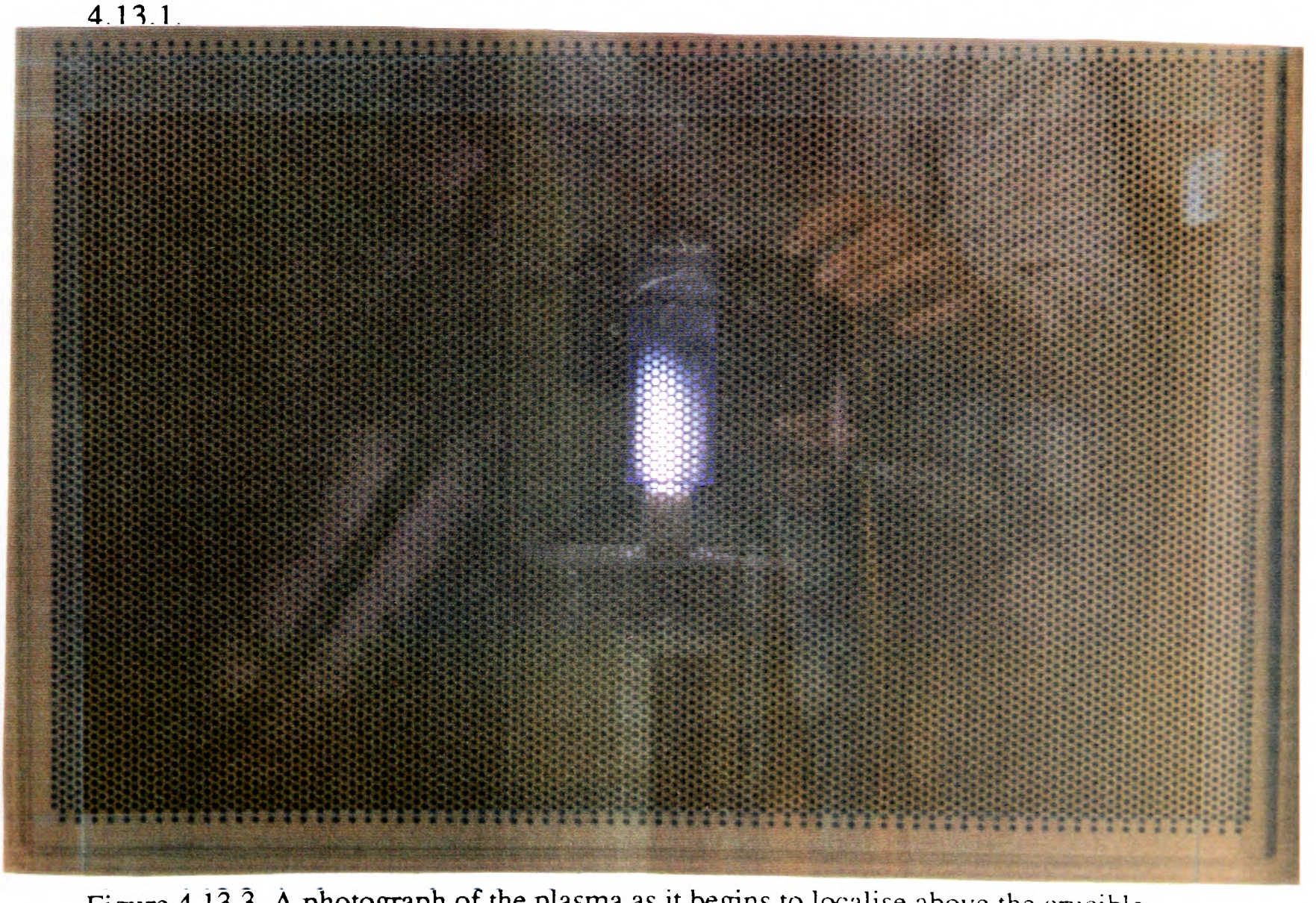


Figure 4.13.3. A photograph of the plasma as it begins to localise above the crucible.

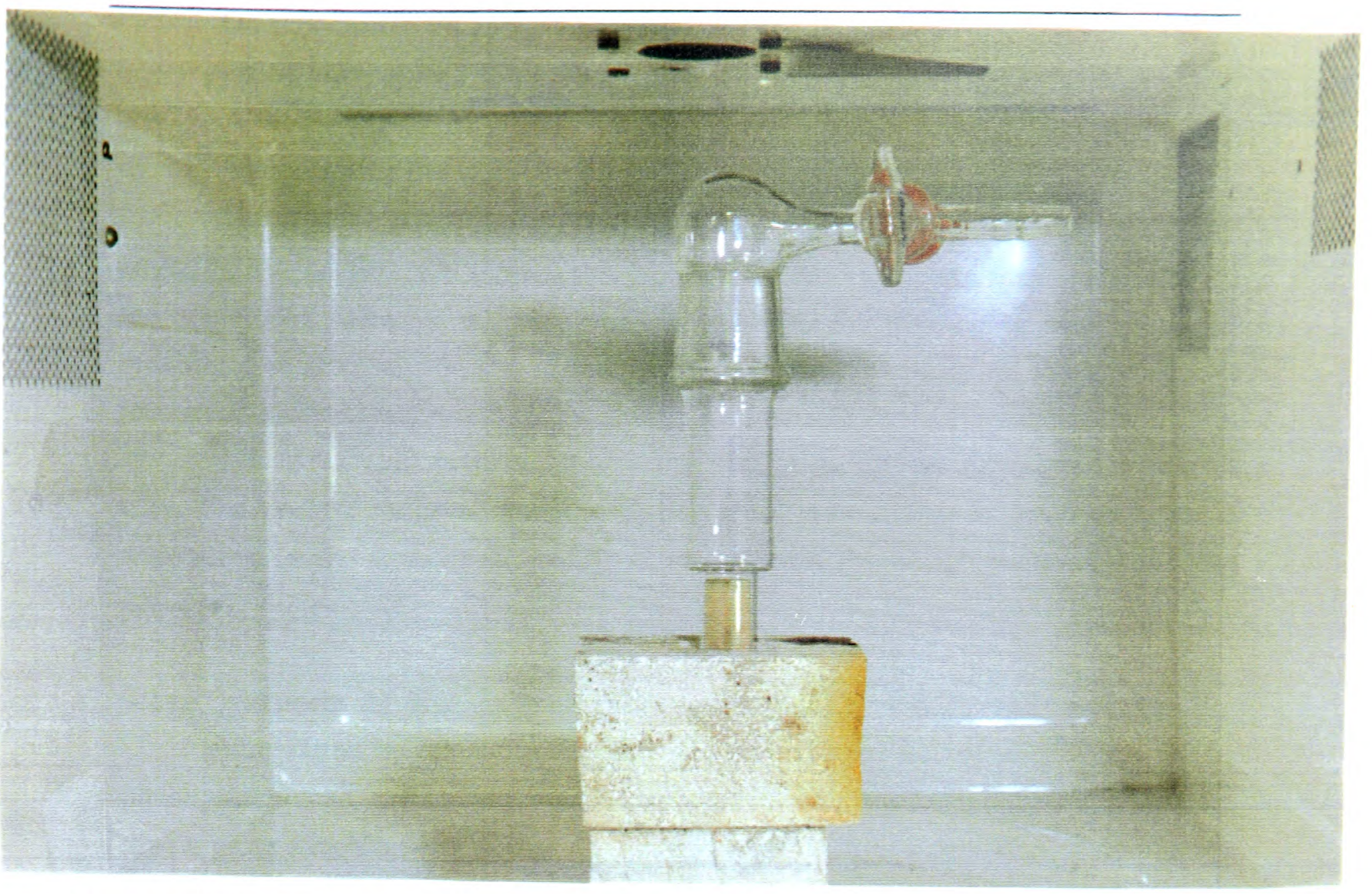


Figure 4.11.1. Apparatus and microwave cavity prior to application of microwave radiation.

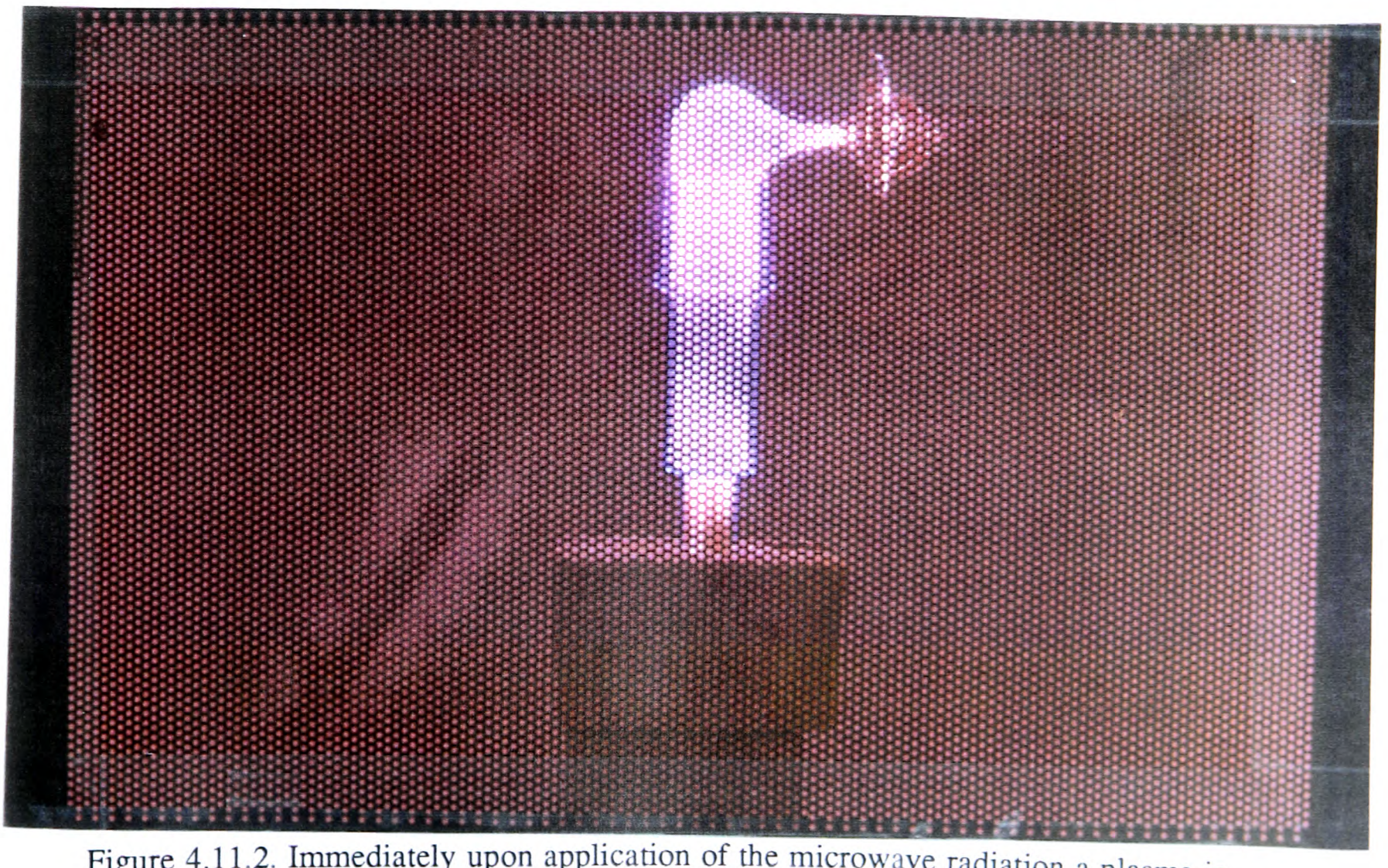


Figure 4.11.2. Immediately upon application of the microwave radiation a plasma is initiated thorughout the reaction vessel.

On exposure to microwave radiation, at the maximum power available, a green argon plasma immediately formed throughout the whole apparatus as shown in figure 4.13.2. After 5 seconds the plasma localised around the crucible, partially immersing the trough containing the C_{60} powder as shown in figure 4.13.3.

The crucible became visibly hot and the potassium vaporised within 30 seconds, covering the reaction vessel walls and in the vicinity of the C_{60} powder. Exposure to the microwave radiation was continued for a further 5 seconds after which time the reaction was stopped and the vessel allowed to cool. Virtually all the sample was recovered and the sample was black.

^{13}C MASNMR reveals the presence of K_3C_{60}, K_4C_{60}, K_6C_{60} and unreacted C_{60}. The average value of x in the K_xC_{60} phase assemblage is between 4 and 6 depending on the amount of potassium that reaches the trough containing the C_{60} powder.

4.14. Synthesis of K_3C_{60} from C_{60} and a K_xC_{60} Phase Assemblage.

Integration by the cut and weigh method provided the value of x in a K_xC_{60} phase assemblage, and so long as the value exceeds 3 a quantity of C_{60} can be added to give a gross stoichiometry of K_3C_{60}. The experiments in section 4.10.6. show that the presence of a plasma is required if the reaction is to proceed due to the lack of intrinsic coupling between C_{60} or K_xC_{60} and microwave radiation at a frequency of 2.45 GHz.

Typically, a material of bulk composition K_3C_{60} was formed from C_{60} and K_xC_{60}, and was ground using an agate mortar. The sample was flame sealed in a Pyrex tube under 10^{-1} mbar of argon and exposed to increasing microwave power for 10 seconds and held at maximum power for a further 3 seconds. A green plasma formed immediately throughout the tube and gave rise to a orange glow above the C_{60} region on application of maximum microwave power. If the radiation was prolonged much longer the sample became agitated and violently dispersed throughout the tube.

^{13}C MASNMR spectroscopy revealed the product was almost pure K_3C_{60} together with a little K_4C_{60} impurity, as shown in figure 4.14.1. On regrinding, resealing and exposure to a further 13 second period in the microwave cavity, pure K_3C_{60} was obtained.

A sample of K_3C_{60} synthesised by conventional furnace techniques over a two week period was compared to the sample produced via microwave radiation.

^{13}C MASNMR spectra are shown in figure 4.14.2. and capillary powder X-ray diffraction patterns are shown in figure 4.14.3. There does not appear to be any difference between the sample produced in the furnace or that in the microwave cavity with regards to NMR characteristics or crystallinity.

The superconducting properties of the sample produced in the microwave oven were investigated using SQUID magnetometry.

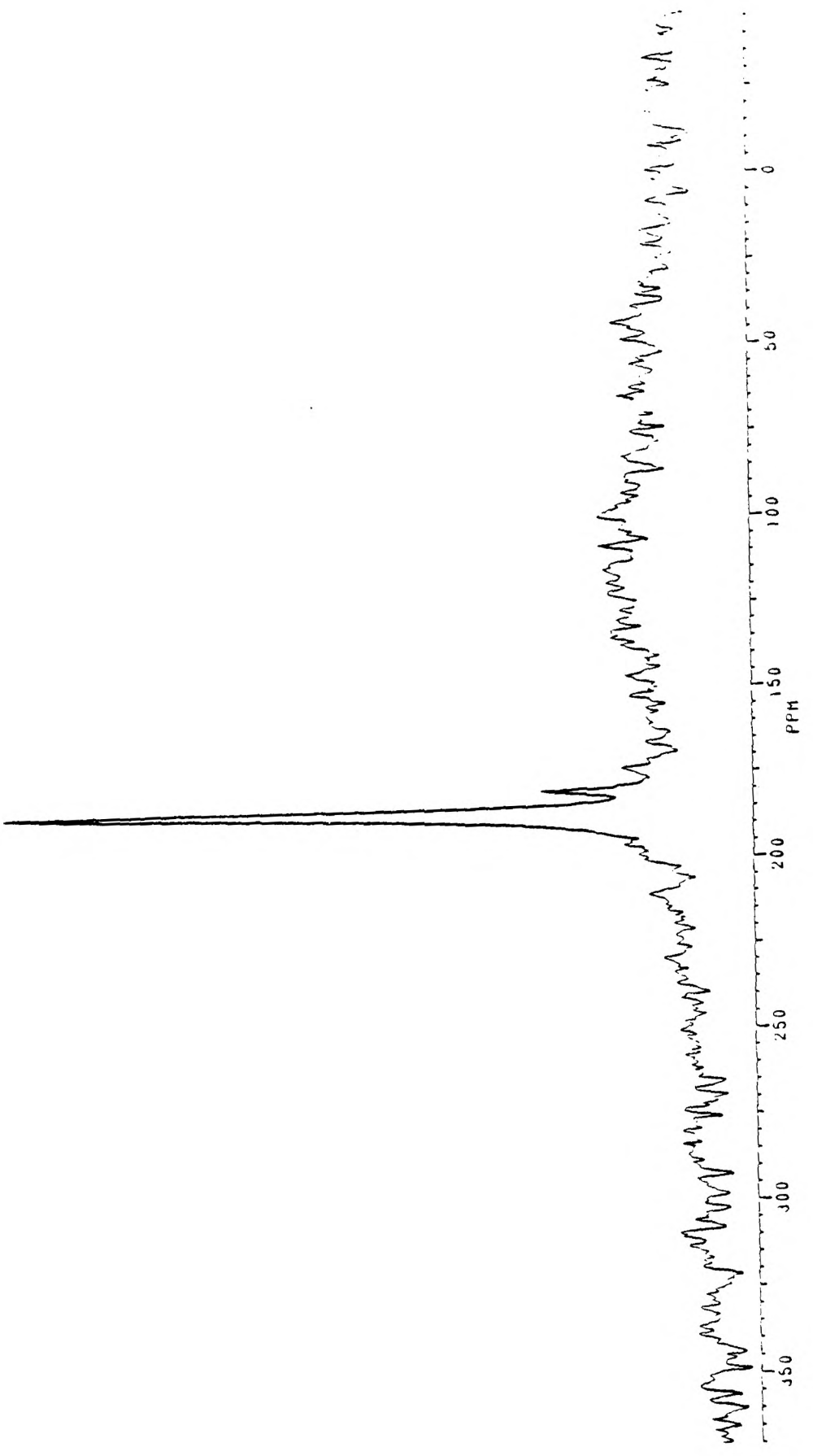
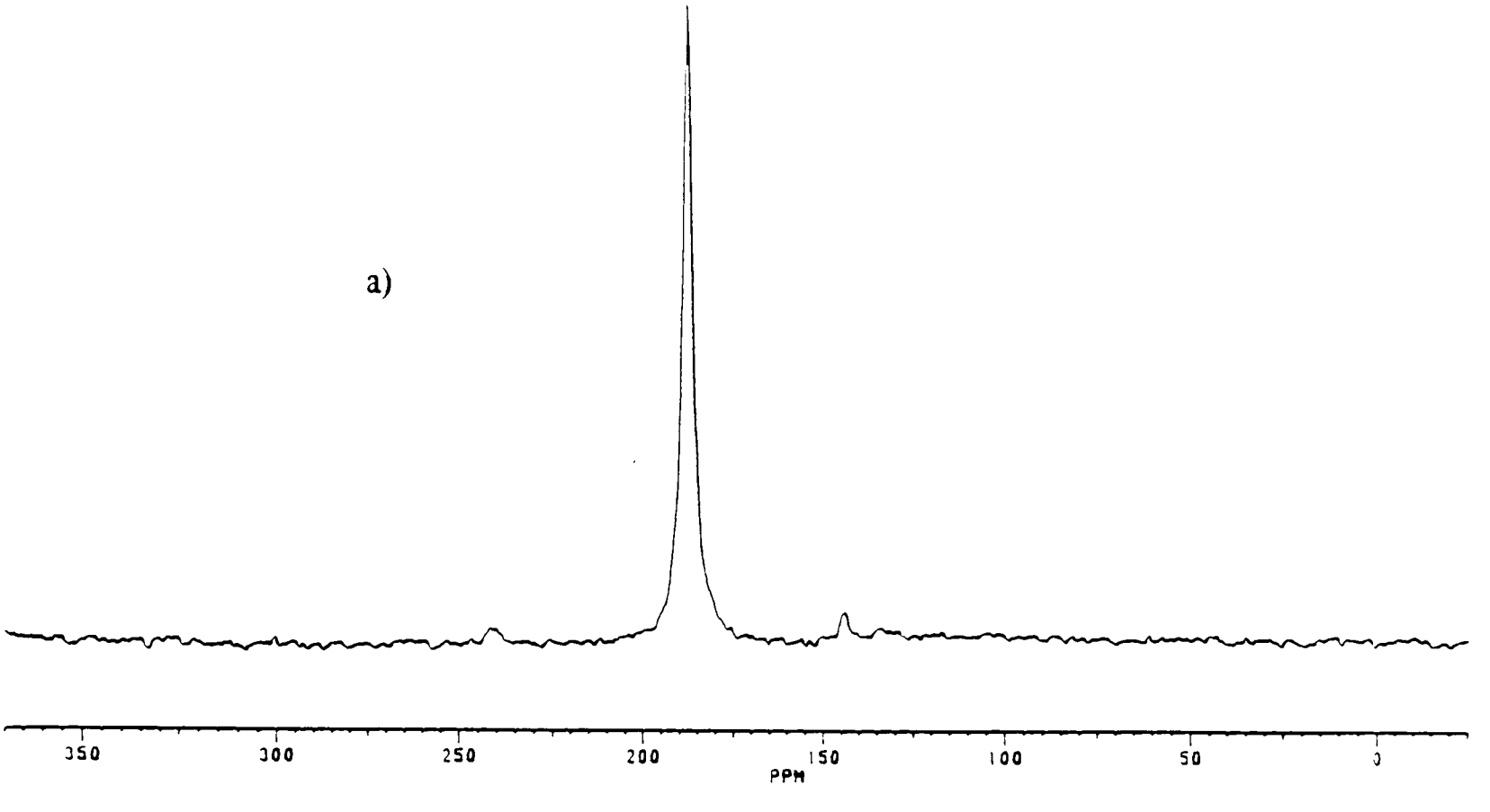


Figure 4.14.1. ^{13}C MASNMR spectrum of a sample of K_3C_{60} synthesised in a microwave oven from a K_xC_{60} sample and the appropriate quantity of C_{60}.



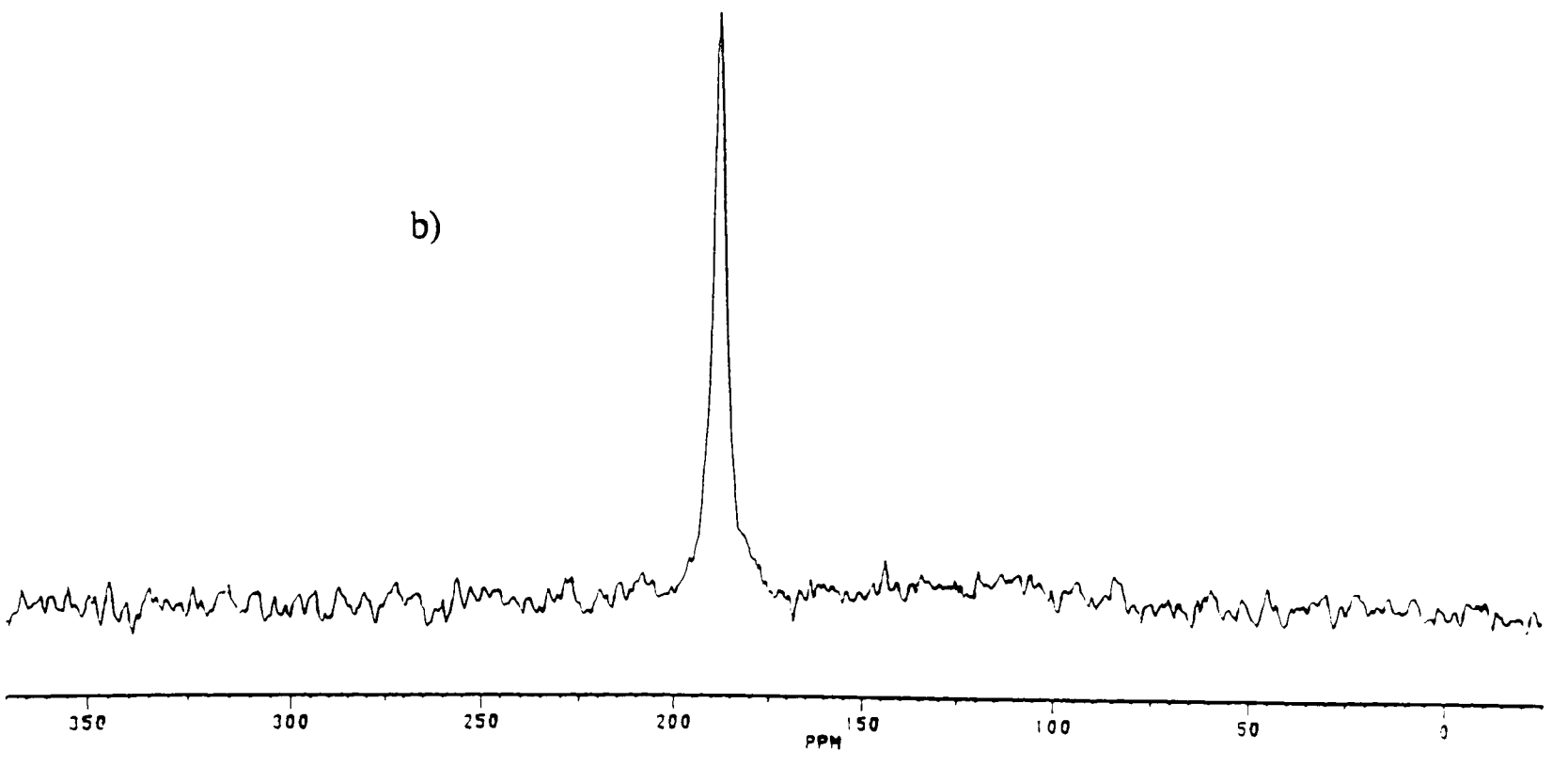


Figure 4.14.2. ^{13}C MASNMR spectrum of samples of K_3C_{60} prepared a) thermally in a furnace and, b) in the microwave oven.

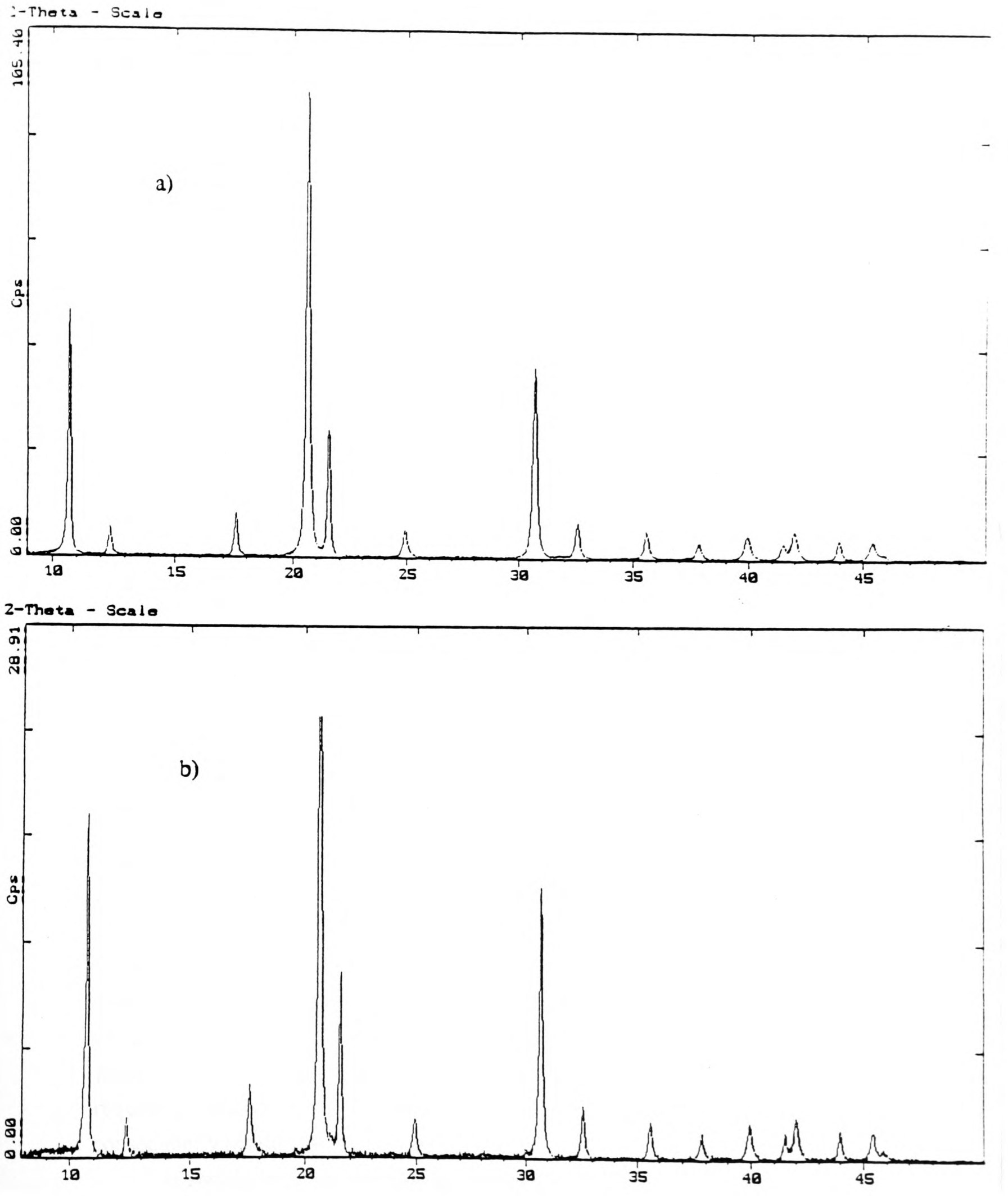


Figure 4.14.3. Capillary powder X-ray powder diffraction patterns of samples of K_3C_{60} prepared a) thermally in a furnace and, b) in the microwave oven.

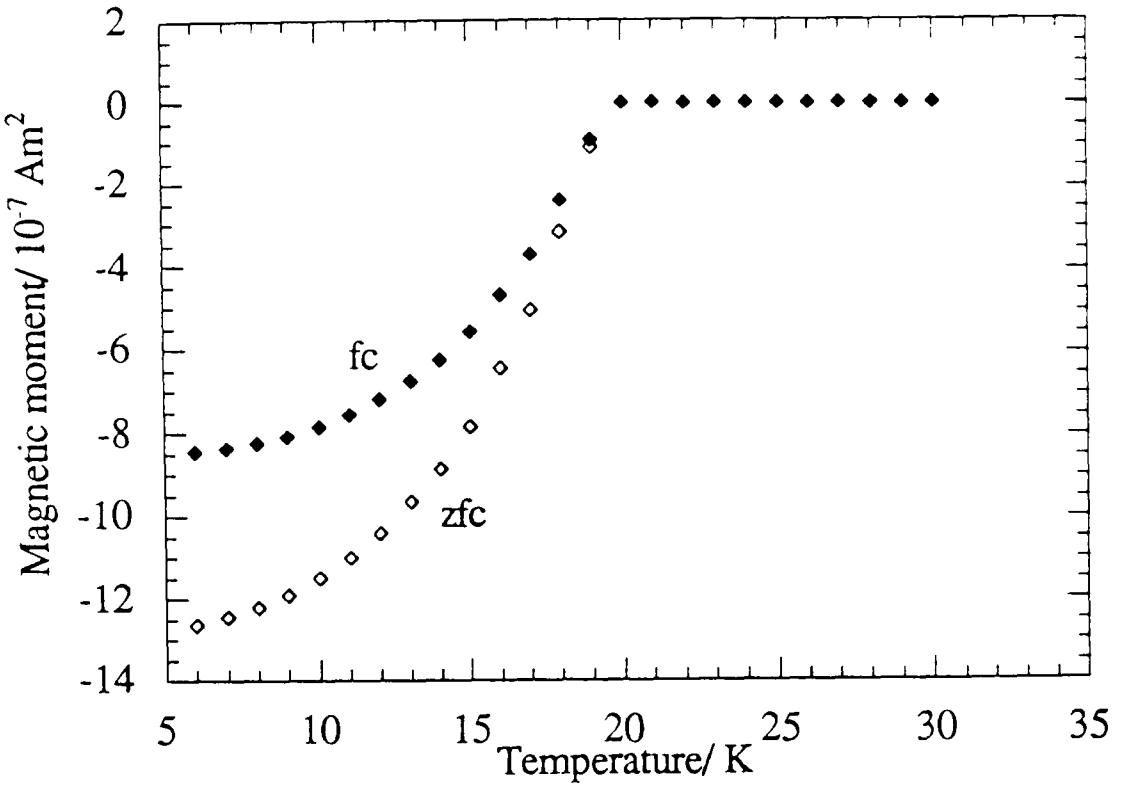


Figure 4.14.4. Zero field cooled (zfc) and field cooled (fc) (10G) magnetization as a function of temperature for K_3C_{60} synthesised in a microwave oven.

As can be seen from figure 4.14.4. superconductivity is observed below 19K which is consistent with that reported for K_3C_{60} and a superconducting shielding fraction of 18% can be calculated in comparison to a perfect diamagnet, as shown in appendix D.

Shielding fractions between 10 and 40% are typically achieved in a furnace reaction.

4.15. Synthesis of Other Alkali Metal Fullerides.

The synthesis and characterisation of alkali metal C_{60} phases of phase purity is very time consuming not least because of the techniques required (MASNMR and powder x-ray crystallography) for their characterisation. The saturated A_6C_{60} phases (where A = K, Rb and Cs) are readily synthesised from excess metal and C_{60} powder, but because of the small sample sizes used, synthesis of the nonsaturated phases from stoichiometric quantities of C_{60} and alkali metal are problematic. This is because a slight excess of metal or C_{60}, incurred during weighing, causes a deviation from the desired stoichiometry and hence a further reaction is required to rectify the error. Each reaction requires, on average, 3 - 7 days to ensure the components are at equilibrium, consequently resulting in large delays.

It should be noted that A_6C_{60} phases seem to be best formulated as $A_{6.7}C_{60}$ from the experience of various workers.

No binary lithium C_{60} compounds are known to date, the only C_{60} material containing lithium, which is structurally characterised, is Li_2CsC_{60}. In the case of

sodium the saturated phase is not well characterised and may not even have been synthesised. This is because the small size of sodium allows clusters of sodium atoms to exist at the octahedral interstitial site in the fcc C_{60} lattice. Refinement of a X-ray diffraction pattern corresponding to the composition $Na_{9.8}C_{60}$ has been reported.

It was decided to study the application of a microwave induced argon plasma to the synthesis of the known potassium, rubidium and caesium C_{60} phases from C_{60} powder and the saturated A_6C_{60} phases synthesised by conventional thermal methods. Using ^{13}C MASNMR spectroscopy and powder X-ray crystallography, comparisons between microwave preparations and conventional thermal preparations were made. In the case of sodium, a sample of hcp Na_6C_{60} described in section 3.9.5. was diluted with C_{60} and exposed to a microwave induced argon plasma and compared to the analogous conventional thermal reaction also described in section 3.9.5. The synthesis of new binary Li C_{60} compounds was also briefly investigated.

4.15.1. Synthesis of K_3C_{60} and K_4C_{60} from K_6C_{60} and C_{60}.

Typically, a sample of K_6C_{60} (25mg) was diluted with C_{60} to afford the required stoichiometry and ground using an agate mortar. The sample was transferred to a Pyrex tube sealed with a Pyrex stopcock with a Teflon seal under 10^{-1} mbar of argon, as shown in figure 4.15.1.1. Flame sealing of the sample is not required as the plasma does not degrade the Teflon seal during the period of the experiment.

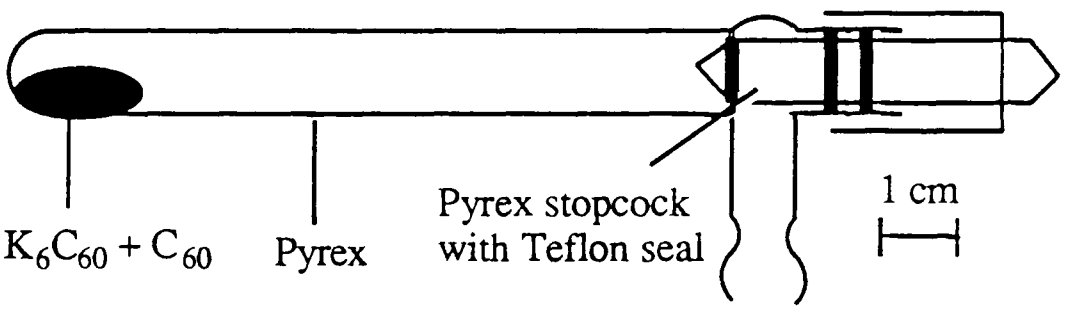


Figure 4.15.1.1. Apparatus used for the rapid synthesis of K_3C_{60} from K_6C_{60} and C_{60}.

A green argon plasma was initiated immediately on application of the microwaves. On ramping the power to the maximum available over 3 seconds and continuing for a further 10 seconds the sample was agitated and tended to cling to the walls of the reaction vessel. After the reaction the region containing the sample was hot to the touch, and hotter than the remainder of the tube. The appearance of the sample changed from a dark brown to a black solid.

^{13}C MASNMR spectroscopy and powder X-ray diffraction patterns of samples of K_3C_{60} and K_4C_{60} produced thermally and in the microwave cavity are shown in figures 4.15.1.2. to 4.15.1.5.

From figures 4.15.1.2. to 4.15.1.5. it can be seen that a microwave induced plasma is an effective and efficient route to K_3C_{60} and K_4C_{60}.

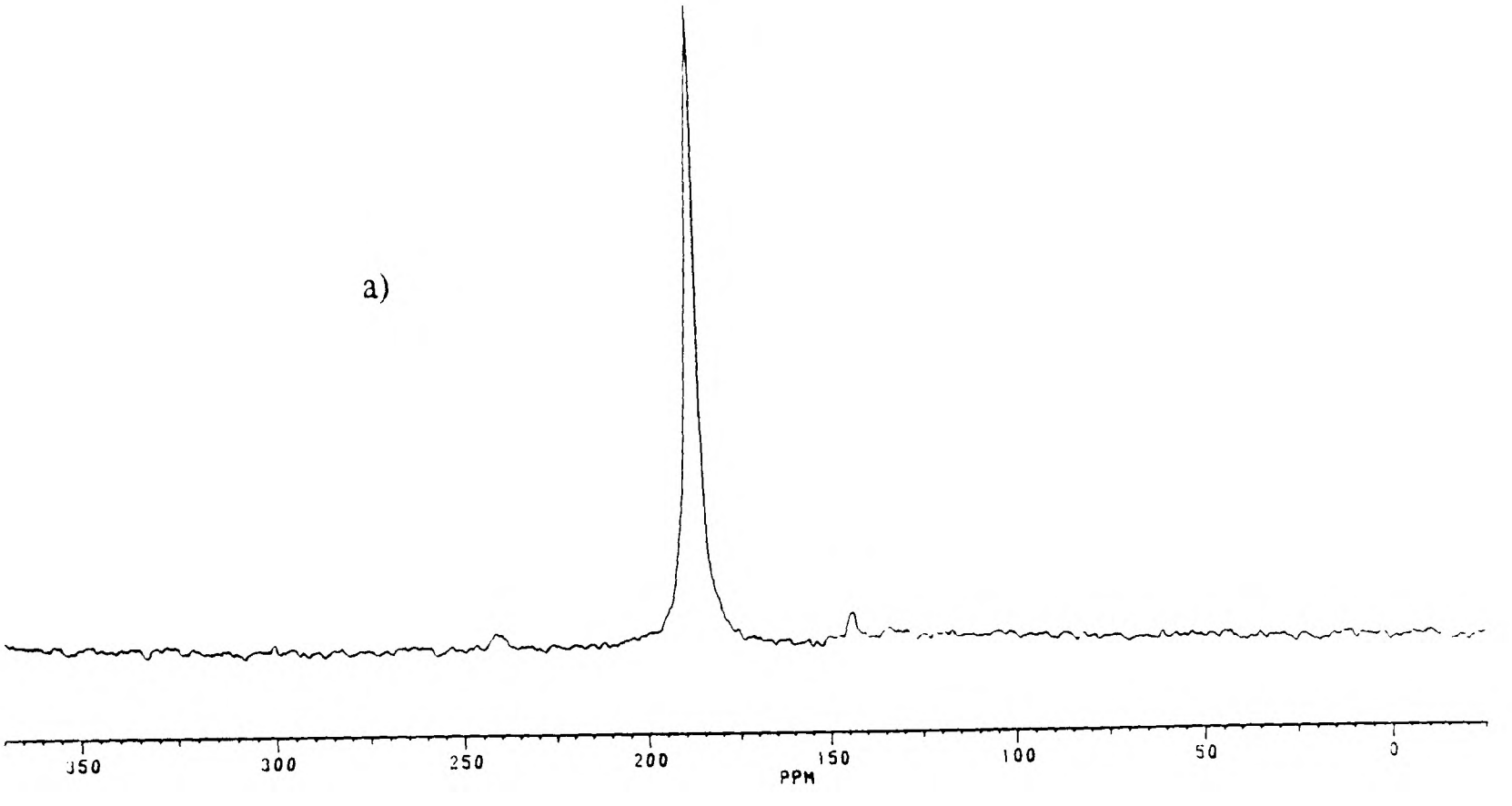


Figure 4.15.1.2. ^{13}C MASNMR spectrum of samples of K_3C_{60} prepared from K_6C_{60} and C_{60} a) thermally in a furnace and, b) in the microwave oven.

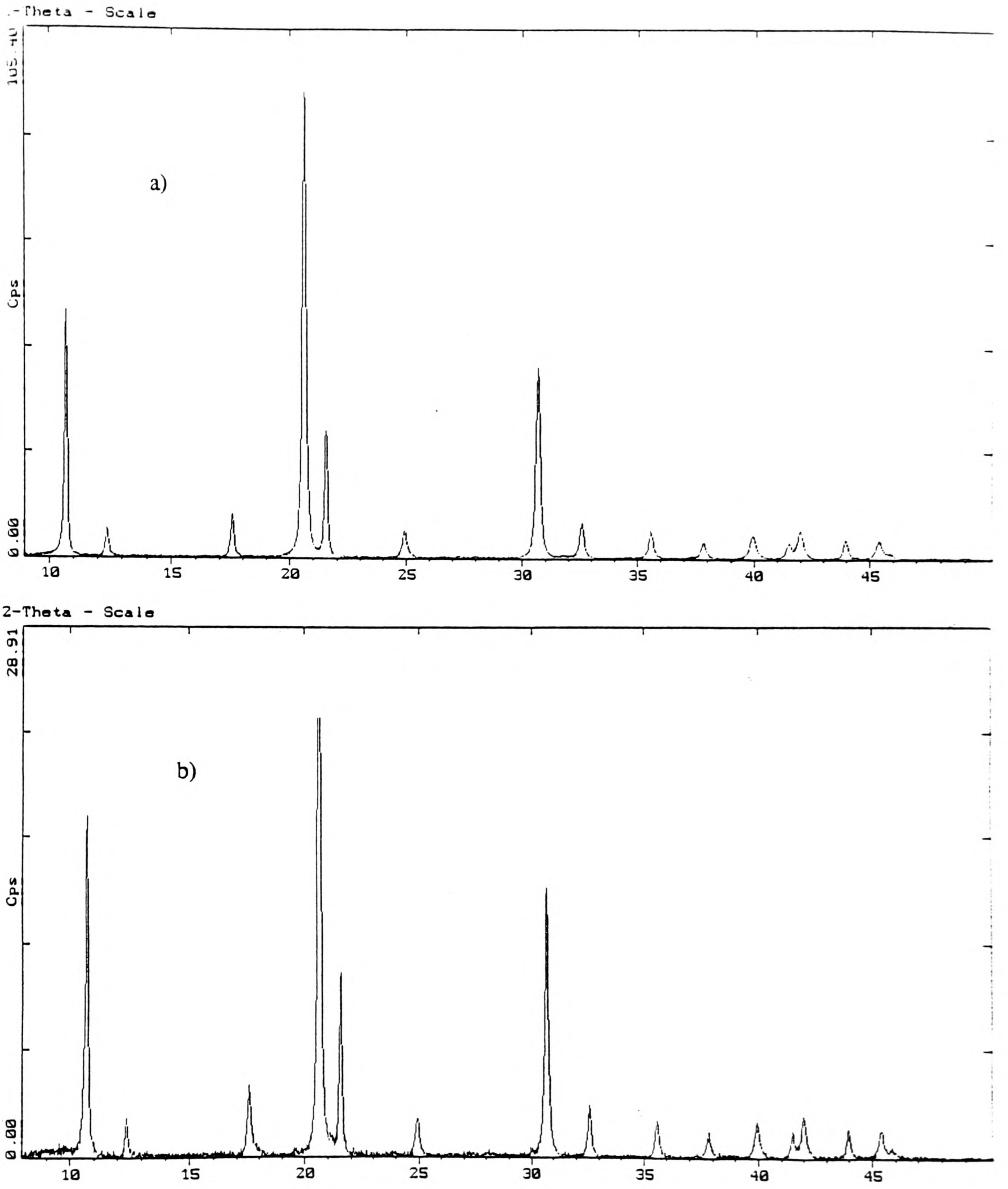


Figure 4.15.1.3. Capillary powder X-ray powder diffraction patterns of samples of K_3C_{60} prepared from K_6C_{60} and C_{60} a) thermally in a furnace and, b) in the microwave oven.

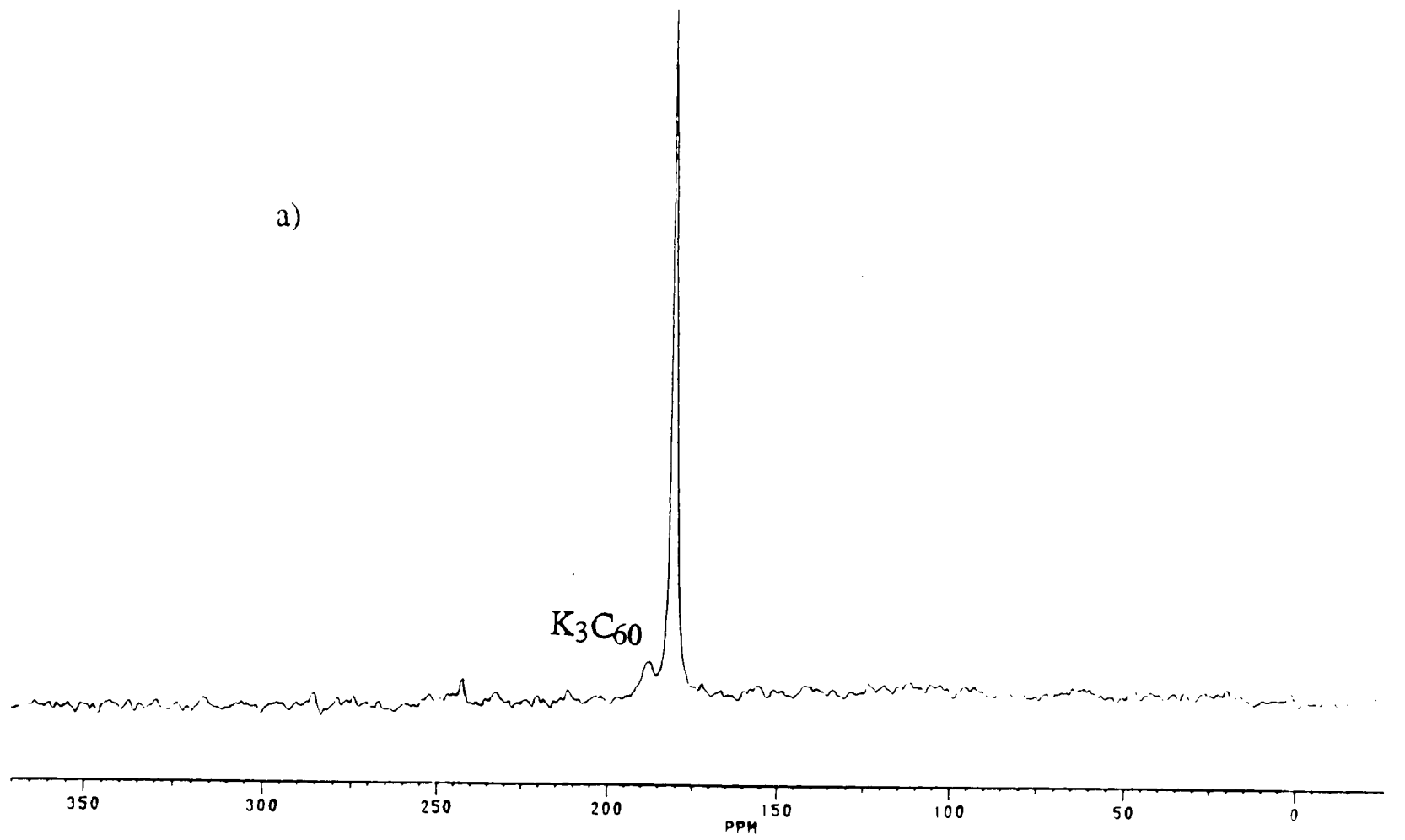


Figure 4.15.1.4. ^{13}C MASNMR spectrum of samples of K_4C_{60} prepared from K_6C_{60} and C_{60} a) thermally in a furnace and, b) in the microwave oven.

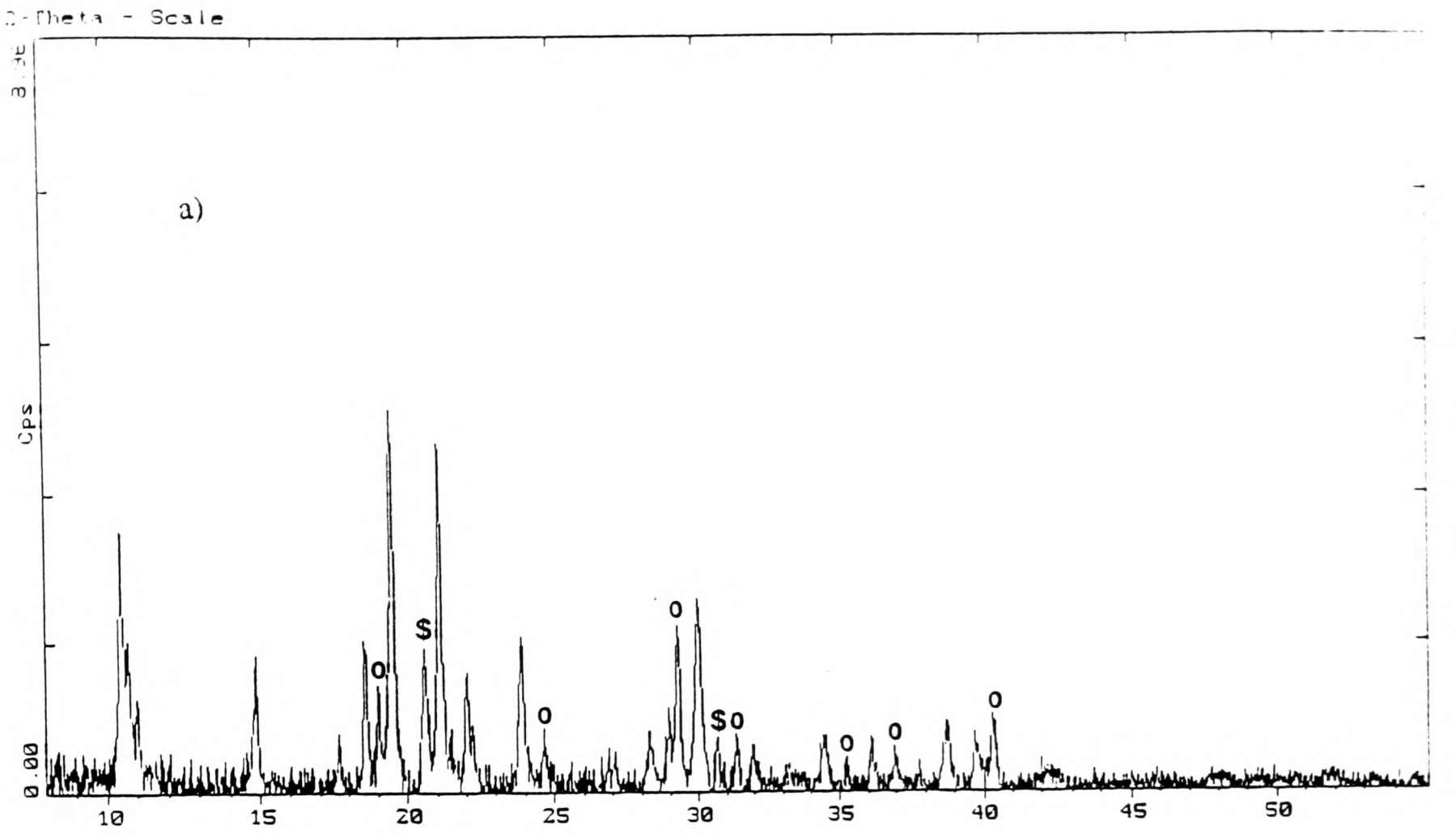


Figure 4.15.1.5. Capillary powder X-ray powder diffraction patterns of samples of K_4C_{60} prepared from K_6C_{60} and C_{60} a) thermally in a furnace and, b) in the microwave oven. 'o' denotes K_6C_{60} and '$' denotes K_3C_{60} impurity peaks.

4.15.2. Synthesis of Rb_1C_{60}, Rb_3C_{60} and Rb_4C_{60} from Rb_6C_{60} and C_{60}.

An analogous procedure as that outlined for the potassium phases was used but the Rb_1C_{60} sample required an intermediate regrinding and further exposure to 2 x 10 seconds at the maximum power available.

^{13}C MASNMR spectroscopy and powder X-ray diffraction patterns of Rb_3C_{60} and Rb_4C_{60} from a conventional furnace reaction and the microwave preparation are shown in figures 4.15.2.1. to 4.15.2.4.

Rb_1C_{60} is a particularly interesting fulleride because the synchrotron powder X-ray diffraction pattern can be best refined using a structural model consisting of 1-dimensional polymer chains of C_{60}. Within the chain each C_{60} is bonded through a [2+2] cyclobutane linkage to two other C_{60}'s. The polymer is postulated to break up into its monomer constituents above 150°C.[65, 66]

Static variable temperature solid state ^{13}C NMR spectroscopy of the product shows a sharp peak at δ 180ppm and a broad peak centred at δ 100ppm.[66] These are apparently due to two phases, a low temperature (δ 100ppm) and a high temperature (δ 180ppm) phase which have differing variable temperature NMR characteristics. The high temperature phase has a weakly temperature dependent shift similar to A_2C_{60}, A_3C_{60}, and A_4C_{60} compounds and a small linewidth consistent with isotropic rotational averaging of C_{60} molecules. In contrast, the low temperature phase has a temperature dependent shift much smaller than that observed in any alkali metal fullerides, or even C_{60} itself, and the linewidth indicates rotational averaging is not occurring at least on a timescale of 100μs. Measurements of T_1 at variable temperature indicate that the high temperature phase is a paramagnet. The low temperature phase has a much reduced spin susceptibility consistent with a metal. As shown in figure 4.15.2.5.

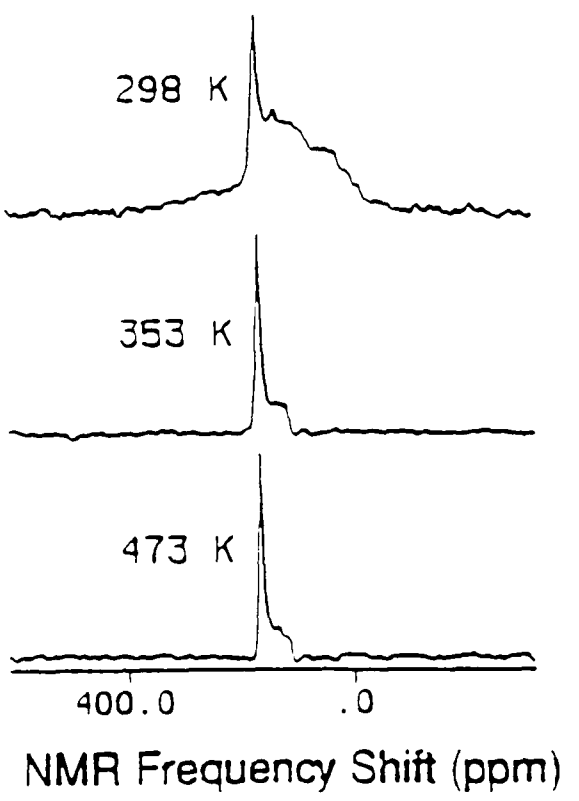


Figure 4.15.2.5. Variable temperature powder ^{13}C NMR spectroscopy of Rb_1C_{60}.

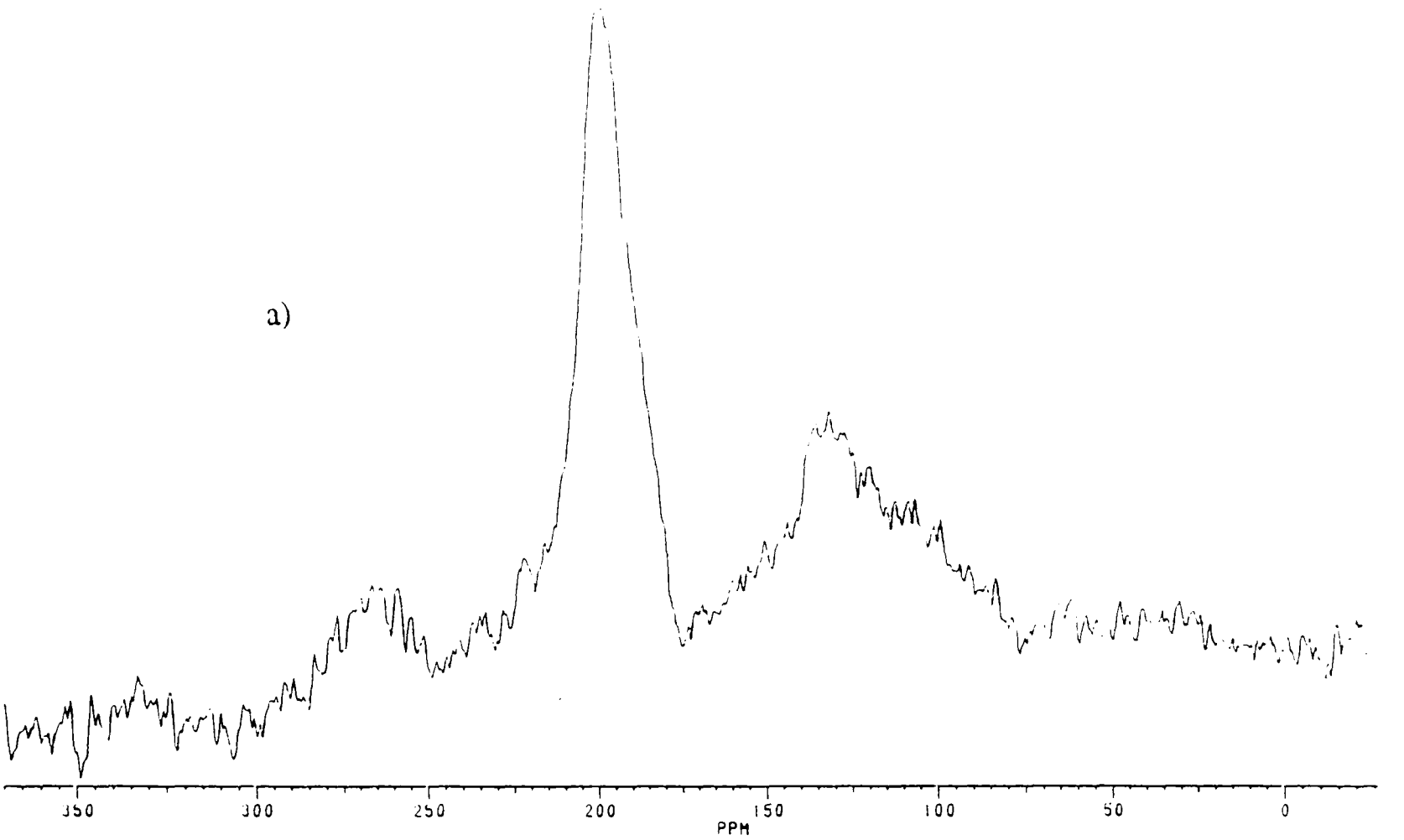


Figure 4.15.2.1. ^{13}C MASNMR spectrum of samples of Rb_3C_{60} prepared from Rb_6C_{60} and C_{60} a) thermally in a furnace and, b) in the microwave oven.

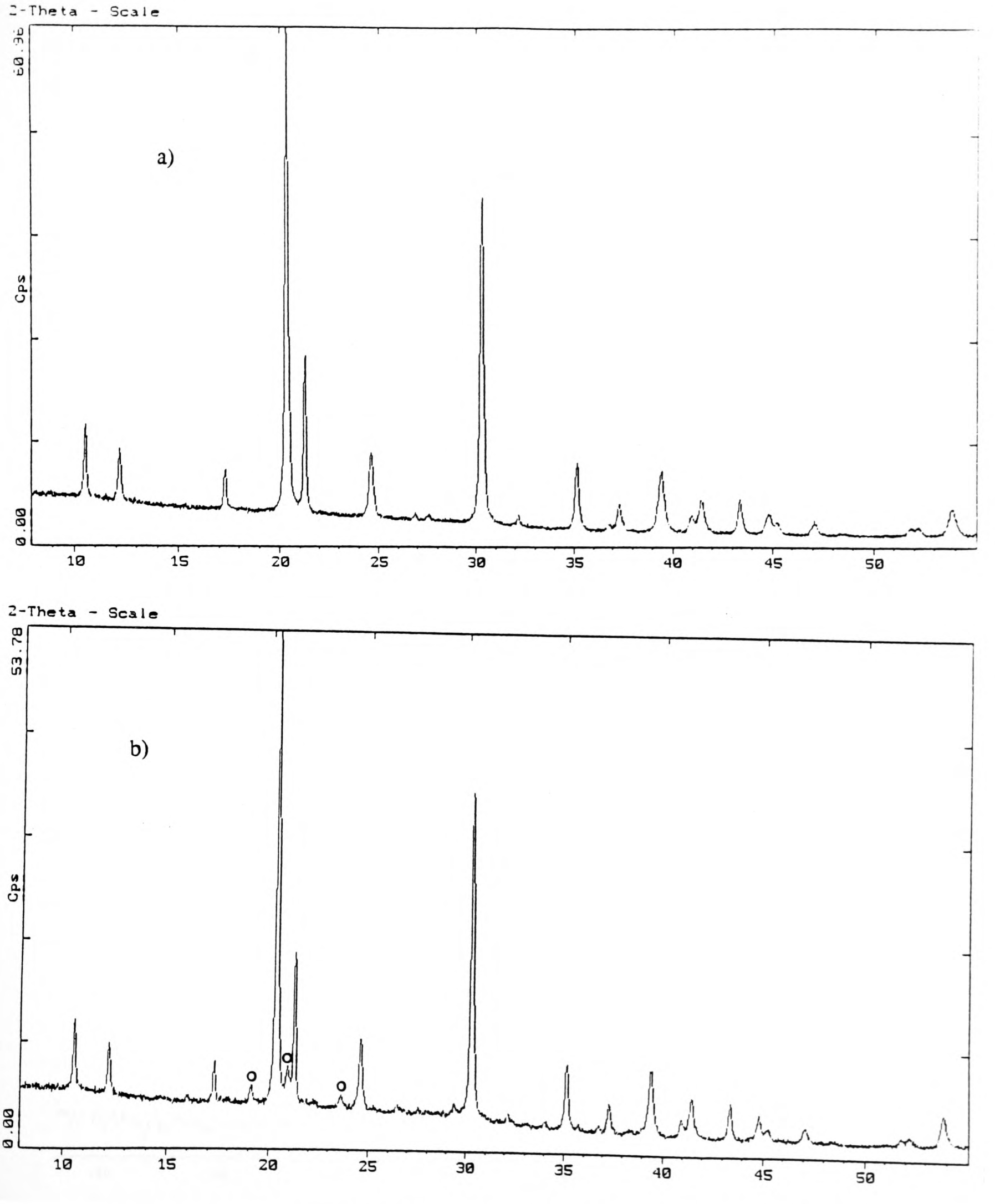


Figure 4.15.2.2. Capillary powder X-ray powder diffraction patterns of samples of Rb_3C_{60} prepared from Rb_6C_{60} and C_{60} a) thermally in a furnace and, b) in the microwave oven. 'o' denotes Rb_4C_{60} impurity peaks.

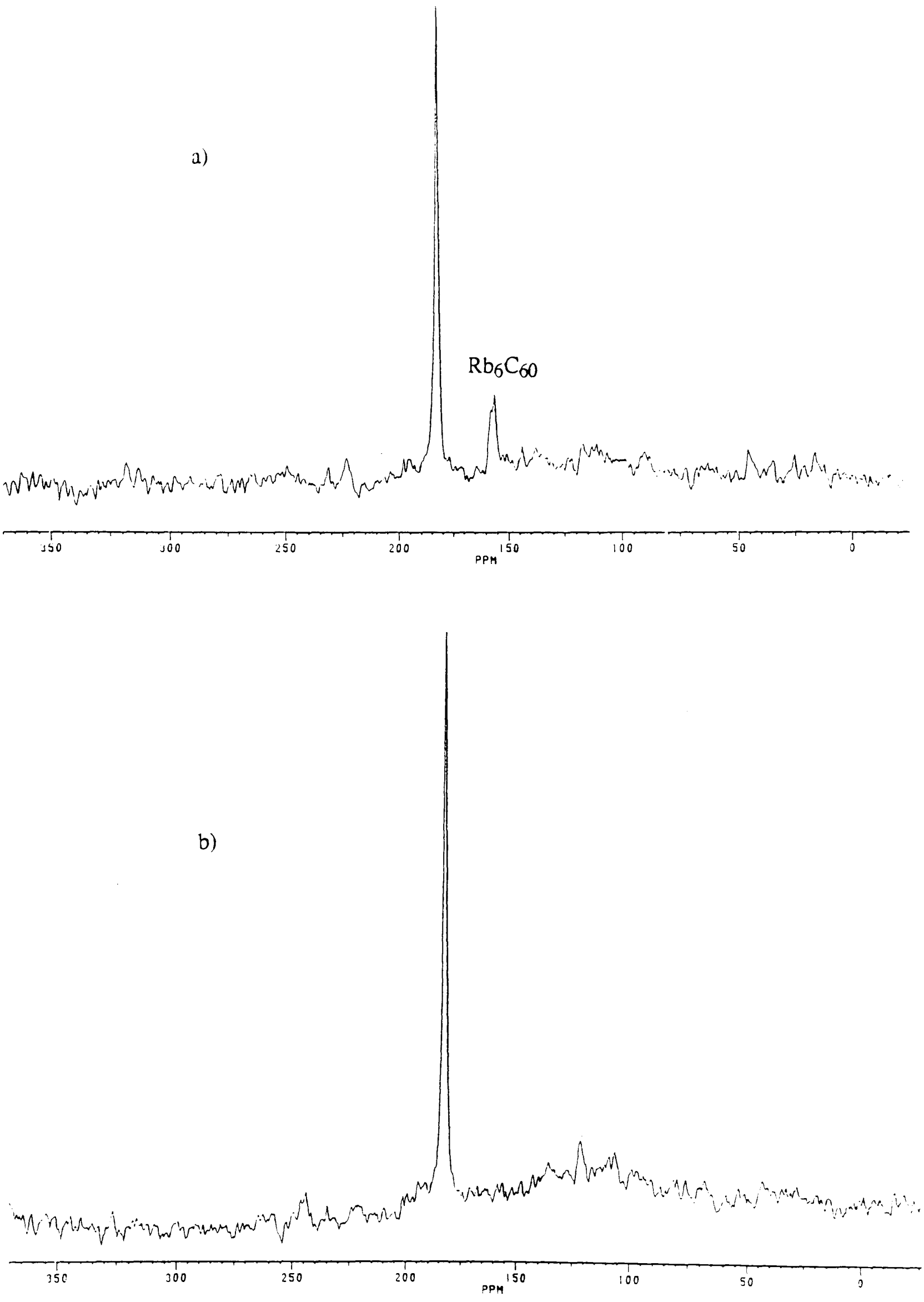


Figure 4.15.2.3. ^{13}C MASNMR spectrum of samples of Rb_4C_{60} prepared from Rb_6C_{60} and C_{60} a) thermally in a furnace and, b) in the microwave oven.

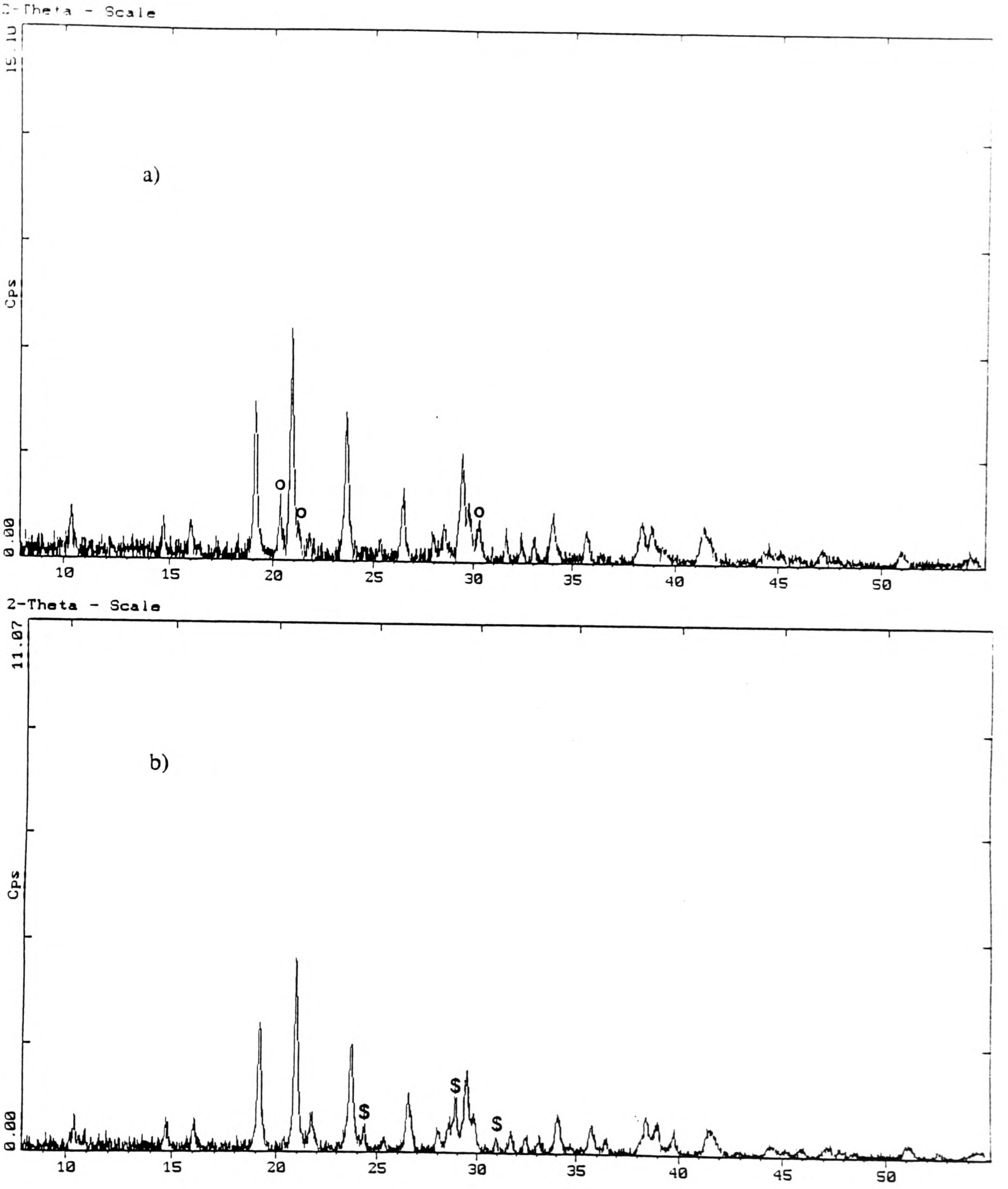


Figure 4.15.2.4. Capillary powder X-ray powder diffraction patterns of samples of Rb_4C_{60} prepared from Rb_6C_{60} and C_{60} a) thermally in a furnace and, b) in the microwave oven. 'o' denotes Rb_6C_{60} and '$' denotes Rb_3C_{60} impurity peaks.

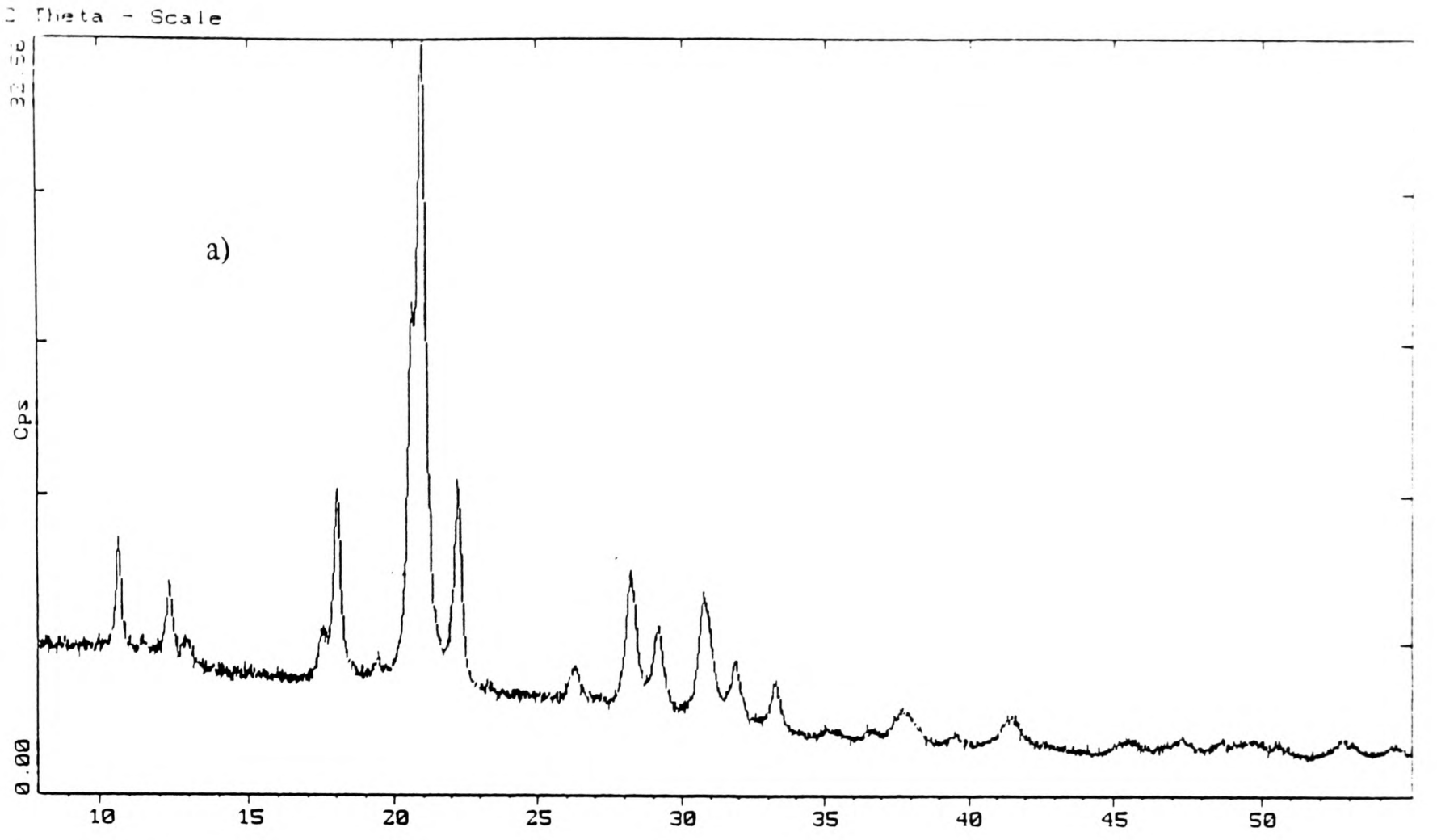


Figure 4.15.2.6. Capillary powder X-ray powder diffraction patterns of samples of Rb_1C_{60} prepared from Rb_6C_{60} and C_{60} a) thermally in a furnace and, b) in the microwave oven. 'o' denotes C_{60} impurity peaks.

^{13}C powder NMR spectroscopy shows that both phases are present at room temperature and at least that the high temperature phase is very evident.

Early, synchrotron X-ray diffraction studies at variable temperature and DSC measurements, again showed the presence of a low and high temperature phase. However the phase transition was broad with an onset temperature of approximately 350°C. Quenching of the high temperature phase, is implied in these studies which could account for the apparent discrepancy. Experimental details are absent in both reports, such as the rate of cooling and the time between synthesis and characterisation. It is also evident that the experiments were also performed once and on one sample only.

^{13}C MASNMR spectroscopy shows, for both microwave and thermally prepared samples, no peaks that can be assigned to anything but the Kel-F insert used to contain the air sensitive material within the ceramic rotor. Powder X-ray diffraction of the thermally prepared material shows a phase pure material corresponding to the low temperature rhombohedral phase and the microwave sample some C_{60} impurity, as shown in figure 4.15.2.6.

4.15.3. Synthesis of Cs_1C_{60} and Cs_4C_{60} from Cs_6C_{60} and C_{60}.

The synthetic procedures were analogous to those performed in section 4.15.2.

^{13}C MASNMR spectroscopy and powder X-ray diffraction data for both thermal and microwave prepared samples are shown in figures 4.15.3.1. to 4.15.3.3.

A number of peaks are observed in the ^{13}C MASNMR spectrum of Cs_4C_{60}, that correspond to crystallographically inequivalent carbon atoms of the C_{60} molecule within the bct unit cell. Nine carbon positions are present in the bct unit cell[67] of Cs_4C_{60} but only six peaks are observed in the ^{13}C MASNMR spectrum, though of varying intensity. The ^{13}C MASNMR spectrum of Cs_4C_{60} has not been reported previously, the small differences in intensity observed between the thermal and microwaved samples are of unknown origin, but are not consistent with the known caesium C_{60} intercalate phases. A sample of Cs_4C_{60} prepared thermally and subsequently quenched gave an identical spectrum to that for the conventional thermally prepared sample.

The structure of Cs_1C_{60} at room temperature has not been investigated to the same degree as Rb_1C_{60} but it appears to contain very similar characteristics. ^{13}C MASNMR spectroscopic studies[66] have the same high temperature fcc phase and low temperature rhombohedral phase. The T_1 behaviour is again indicative of a metal in the low temperature phase.

Comparing the ^{13}C MASNMR of the microwave and thermally prepared samples of Cs_1C_{60} was again not informative as no discernible peaks, other than the broad resonance from the KEL-F insert were present, as shown in figure 4.15.3.4. Powder X-ray diffraction showed the thermally prepared sample was virtually all rhombohedral with a little of the fcc phase present and the microwaved sample was identical except for a very small amount of C_{60}.

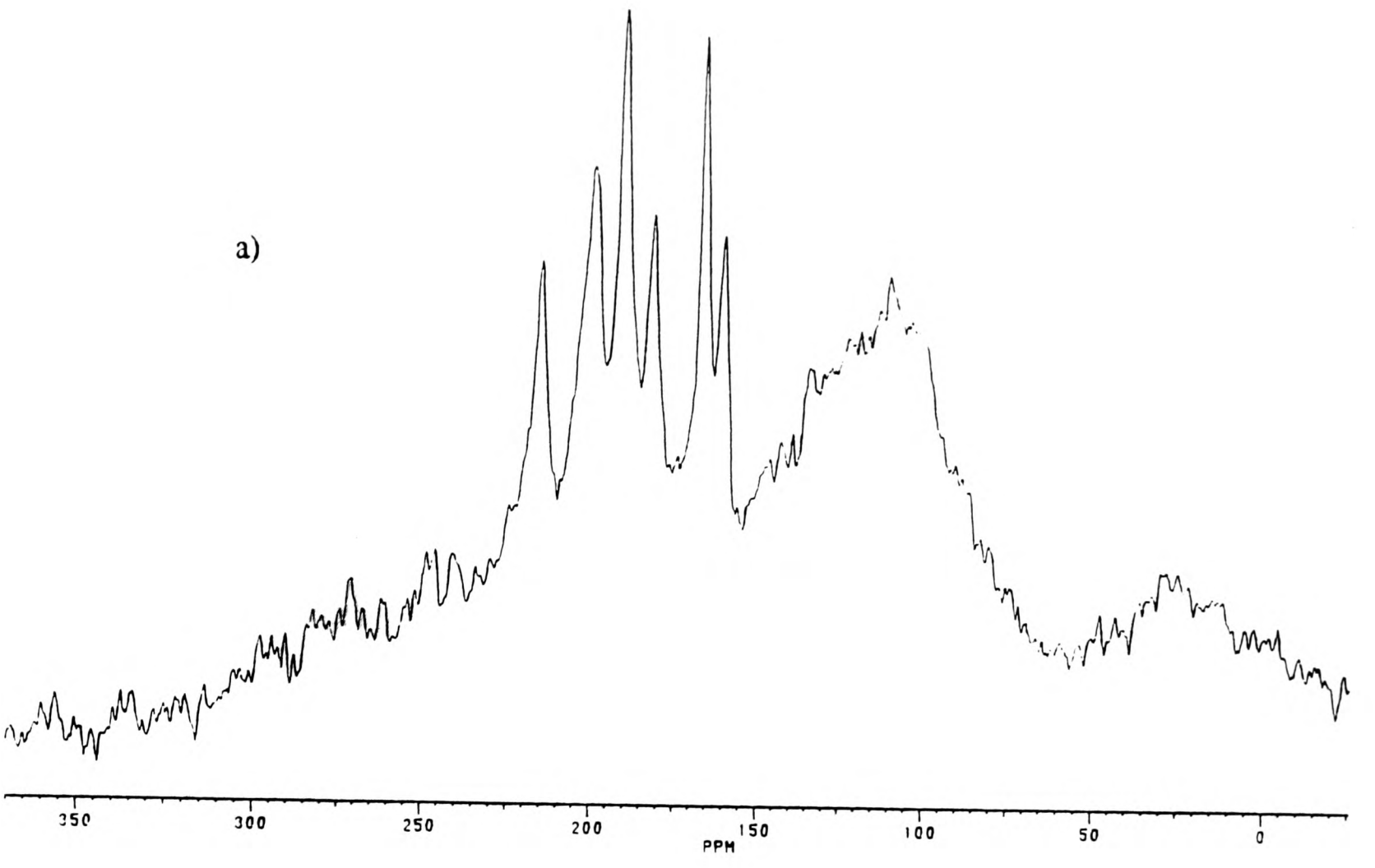


Figure 4.15.3.1. ^{13}C MASNMR spectrum of samples of Cs_4C_{60} prepared from Cs_6C_{60} and C_{60} a) thermally in a furnace and, b) in the microwave oven.

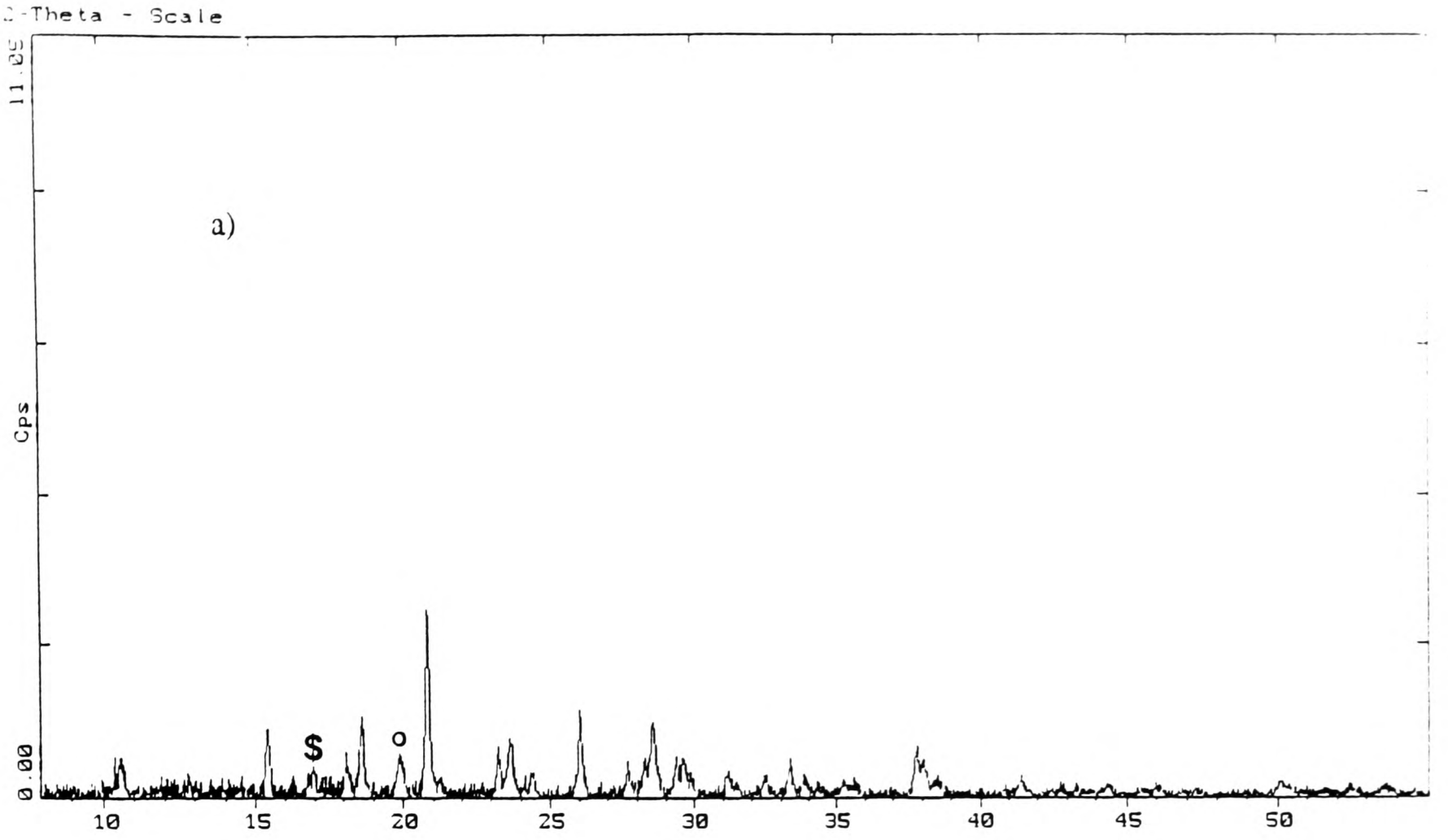


Figure 4.15.3.2. Capillary powder X-ray powder diffraction patterns of samples of Cs_4C_{60} prepared from Cs_6C_{60} and C_{60} a) thermally in a furnace and, b) in the microwave oven. 'o' denotes Cs_6C_{60} and '$' denotes C_{60} impurities.

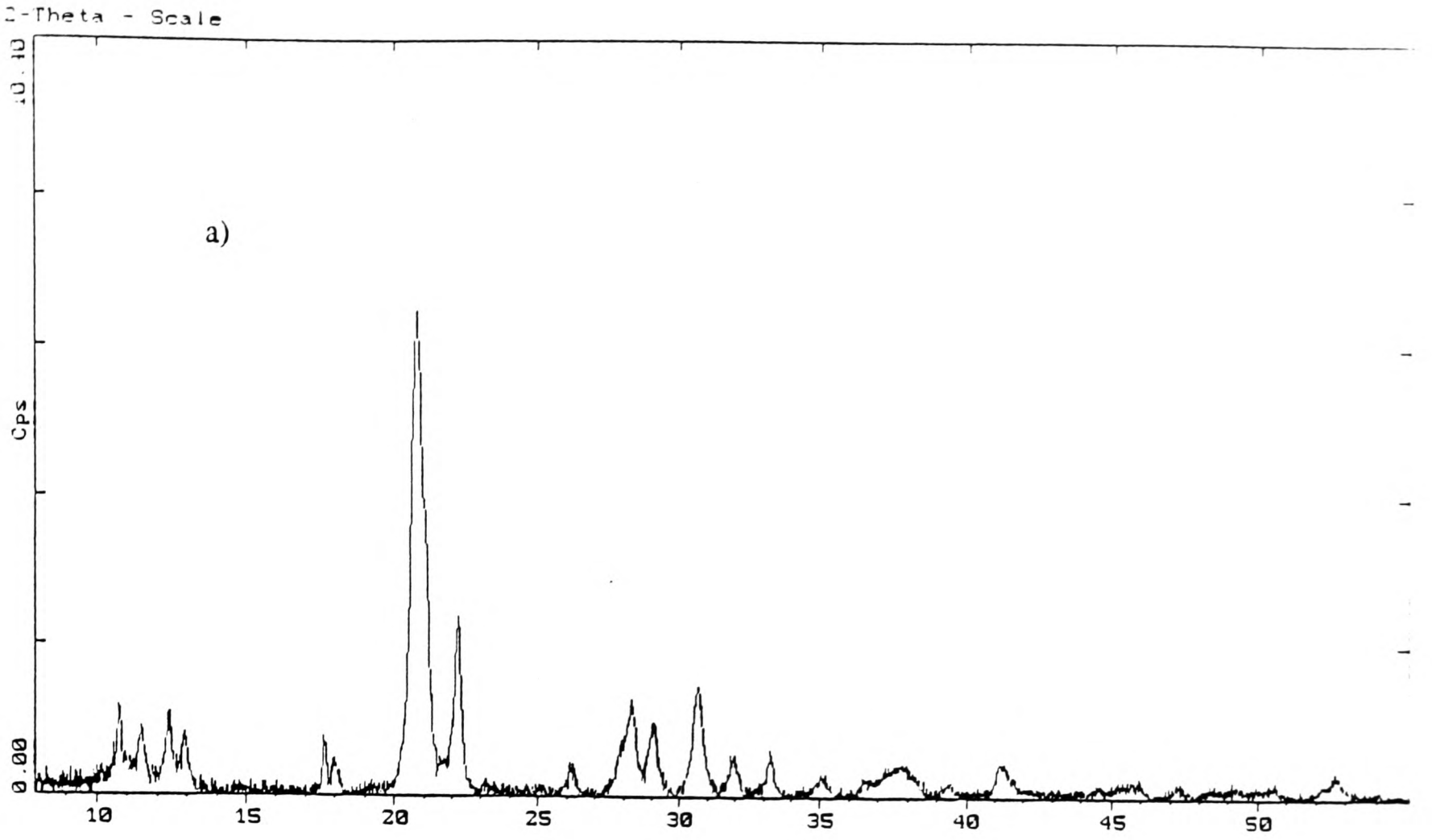


Figure 4.15.3.3. Capillary powder X-ray powder diffraction patterns of samples of Cs_1C_{60} prepared from Cs_6C_{60} and C_{60} a) thermally in a furnace and, b) in the microwave oven. 'o' denotes C_{60} impurity peaks.

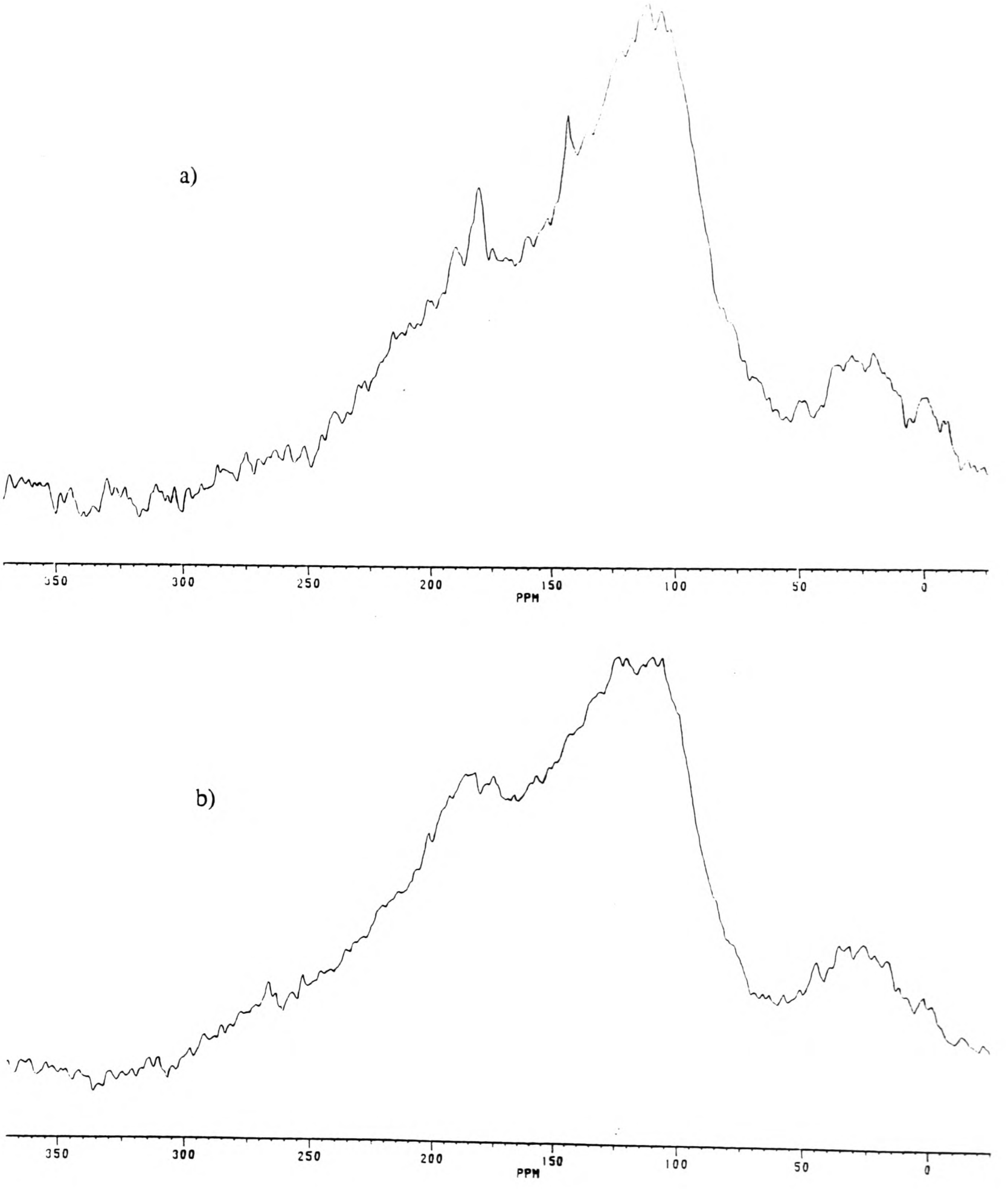


Figure 4.15.3.4. ^{13}C MASNMR spectrum of a sample of a) Cs_1C_{60} and b) an empty insert and rotor.

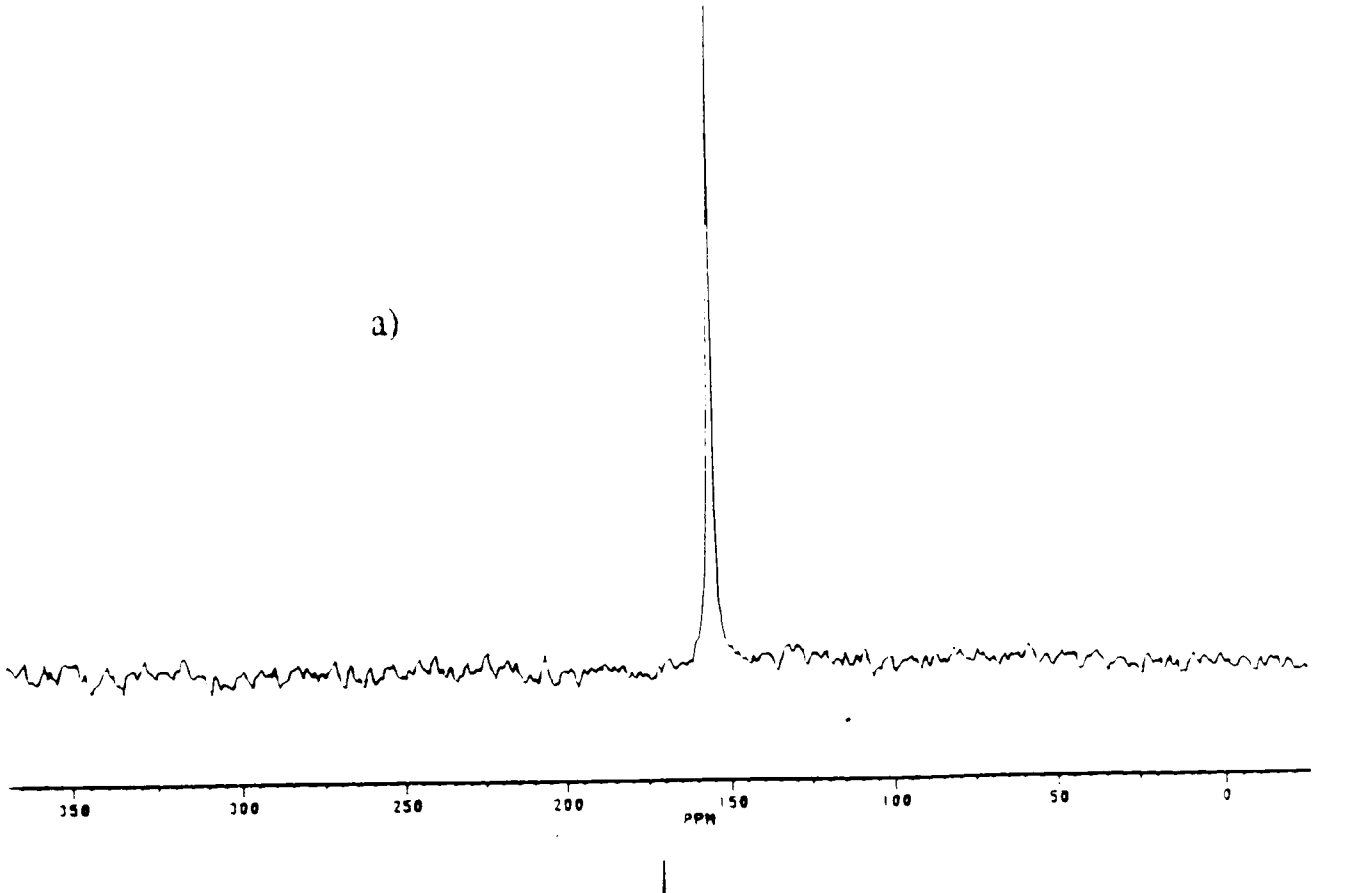


Figure 4.16.1. ^{13}C MASNMR spectrum of samples of a) 'Na_6C_{60}' and 'Na_3C_{60}' prepared from 'Na_6C_{60}' and C_{60} b) thermally in a furnace and, c) in the microwave oven.

4.16. Reaction of hcp Na_6C_{60} With One Equivalent of C_{60}.

The phase diagram of Na and C_{60} is incomplete and under considerable debate and investigation as discussed in section 3.9. A sample of nominal composition Na_6C_{60} was diluted with one equivalent of C_{60} to obtain Na_3C_{60}, or the same composition as was observed in the analogous furnace reaction.

After exposure to a microwave induced argon plasma for 3 x 5 seconds at maximum power the sample was removed to reveal a black powder visually indistinguishable from the sample prepared in a furnace.

^{13}C MASNMR spectroscopy showed that diffusion of sodium atoms throughout the C_{60} lattice had occurred, and powder X-ray diffraction showed the structure had changed from hexagonal to a cubic close packed structure as was also observed from a furnace preparation. Figure 4.16.1. compares the ^{13}C MASNMR spectroscopic data obtained for a microwave versus furnace preparation. It can be seen that using microwave radiation the reaction has not reached equilibrium, as three Na_xC_{60} phases are present in addition to C_{60}. In the case of the thermal reaction (550°C, 7 days) equilibrium has been reached as only two phases are present, Na_3C_{60}, and another phase as yet not completely characterised. It appears that an argon induced plasma cannot heat the system greater than 500°C due to heat losses, or that quenching may be occurring. Grinding and subsequent exposure of the multiphase sample did not result in any change, as observed by ^{13}C MASNMR spectroscopy.

4.17. Preliminary Investigations into the Synthesis of Binary Lithium C_{60} Compounds.

No binary lithium C_{60} compounds exist that have been structurally characterised. Lithium has a boiling point of 1326°C at 1 atmosphere,[68] considerably higher than the other alkali metals, and can easily reduce silica and Pyrex restricting the containers used in preparation. However, the rate at which a plasma can heat a system may be rapid enough to vaporise lithium metal and, if the lithium was submerged in the C_{60} powder, prevent excessive reduction of the walls. No account of the possibility of C_{60} decomposition was made.

Six equivalents of freshly cut lithium metal, in the form of four chips, were added to a powdered C_{60} sample (50mg) and flame sealed in a Pyrex tube under an argon atmosphere at a pressure of 10^{-1}mbar. On exposure to microwave radiation at maximum power, for various lengths of time, no plasma resulted. The sample was then exposed to maximum power for 99 mins and abandoned. On returning to the sample it was observed that vaporisation of the lithium had occurred and the previously brown C_{60} powder had become black. No reduction of the Pyrex tube was apparent on removal of the sample and no lithium metal chips remained.

^{13}C MASNMR spectroscopy showed only a peak at δ 143ppm corresponding to C_{60}. Powder X-ray diffraction showed that new C_{60} phases, presumably containing lithium could be present, in addition to pure C_{60}, due to the observation of at least two

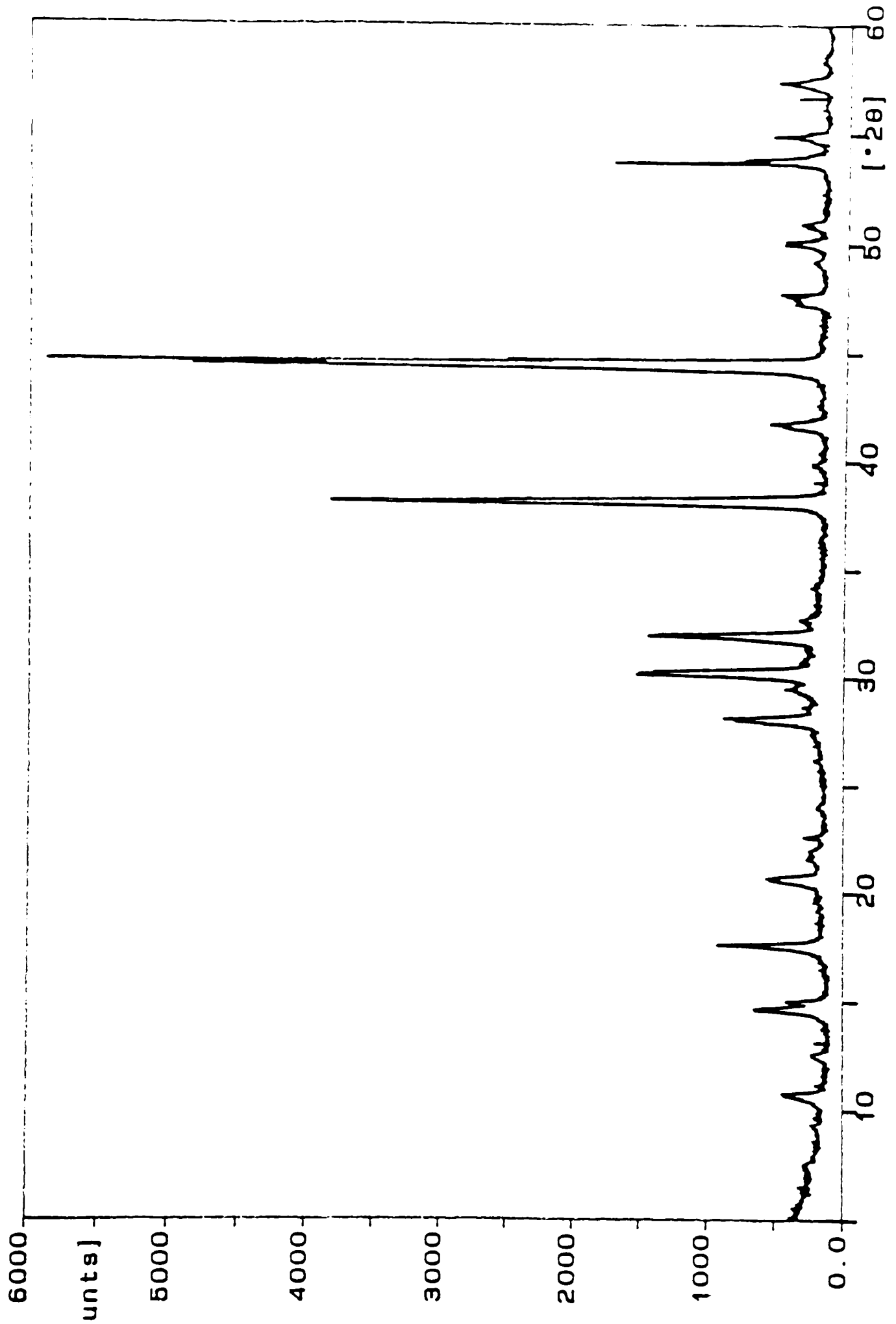


Figure 4.17.1. Capillary powder X-ray powder diffraction pattern from a reaction of six equivalents of lithium metal with C_{60} powder under the action of microwave radiation.

peaks at *ca.* 15° which can be tentatively indexed as (200) in a fcc lattice, as shown in figure 4.17.1.

4.18. Preliminary Investigations into the Synthesis of Lanthanide Fullerides Using Microwave Techniques.

Initially, it was necessary to determine if it was possible to vaporise a lanthanide using the techniques developed. Two lanthanides, europium and ytterbium, have the lowest boiling points (at 1 atmosphere) of 1439 and 1427°C respectively with thulium at 1727°C the next lowest.[68] Ytterbium also has the potential advantage that one of its most common oxidation states is +2, corresponding to the closed shell f^{14} electronic configuration. ^{13}C MASNMR spectroscopy could then be used in the characterisation of new phases.

Therefore, freshly cut ytterbium was placed into an alumina crucible and flame sealed in a silica tube under an argon pressure of 10^{-1} mbar, as shown in figure 4.18.1.

On exposure to an argon plasma at maximum power for 3 x 30 seconds, a brilliant green flash occurred, and ytterbium vapour condensed onto the walls of the reaction vessel. Unfortunately, the thermal shock, or the vigour of ytterbium vaporisation, caused the alumina crucible to fracture. The crucible appeared severely blackened in the location of the metal.

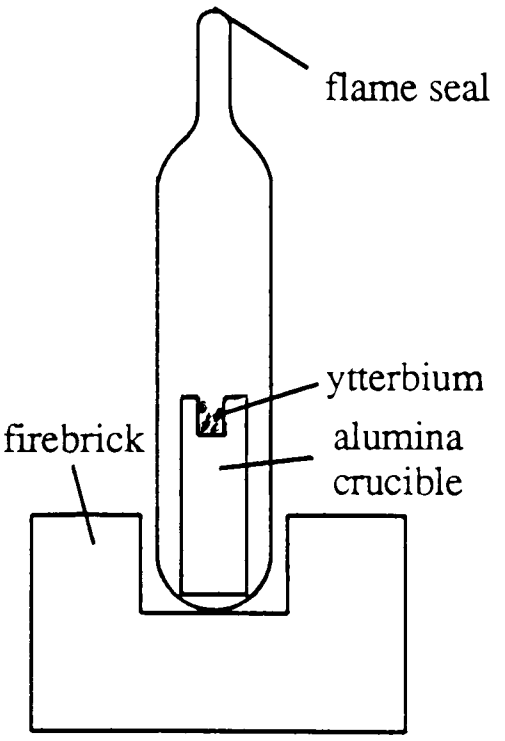


Figure 4.18.1. Apparatus used to test the viability of ytterbium vaporisation using a ceramic furnace and argon microwave induced plasma.

An argon plasma, sustained for approximately 90 seconds, at maximum power, decomposes a C_{60} sample, as shown by its insolubility in toluene and its amorphous nature as shown by electron microscopy. An alternative ceramic was sought which could increase the rate of vaporisation and survive the large, rapid, temperature variations involved in exposure to a plasma. Zirconia stabilised with magnesia, has a working upper continuous temperature of 2200°C,[69] undergoes thermal runaway, and is available in the form of a rod which can be made into a crucible. It also has good

resistance to concentrated acids and alkalis needed in cleaning processes.

An analogous experiment to that above, using a zirconia/magnesia, rather than an alumina crucible, was performed. Vaporisation of a ytterbium sample occurred after 15 seconds. The zirconia/magnesia crucible was severely blackened and fractured, at the position of the metal prior to vaporisation.

4.18.1. Reaction of Ytterbium Metal and C_{60}.

The apparatus was set up analogously to the synthesis of a K_xC_{60} phase assemblage. A zirconia/magnesia crucible was used to increase the rate of vaporisation and prevent decomposition of C_{60}. The sample was exposed to an argon plasma, at maximum power, for 20 seconds. After 15 seconds a green flash signified vaporisation of ytterbium metal and condensation of the metal vapour onto the walls of the reaction vessel occurred. The area where the ytterbium condensed was not the location of the C_{60} powder, as shown in figure 4.18.1.1.

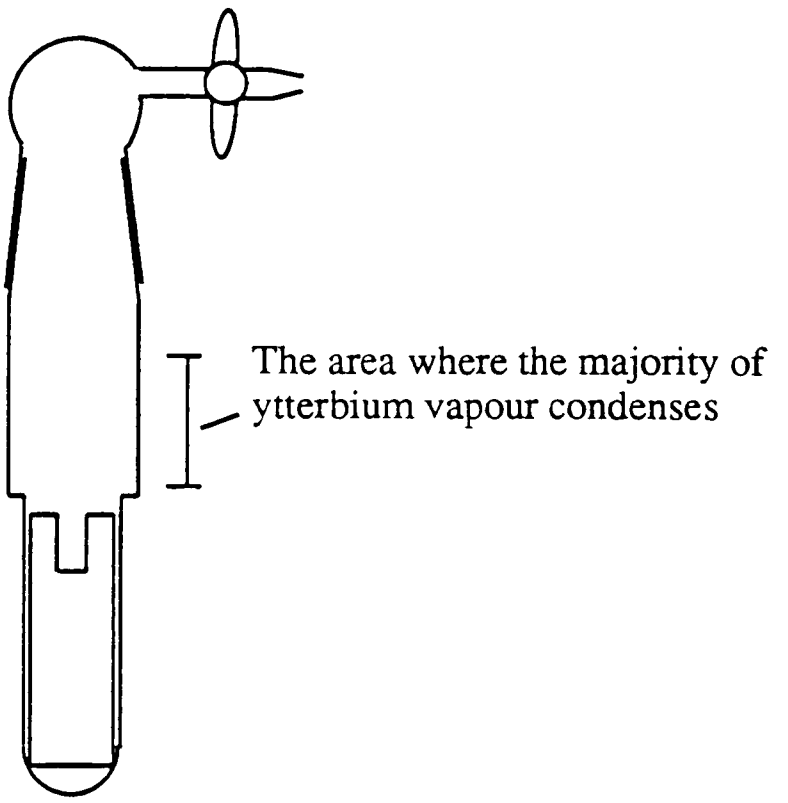


Figure 4.18.1.1. On vaporisation the ytterbium missed the C_{60} powder and condensed where indicated in the diagram.

To maximise the interaction between C_{60} and ytterbium vapour, the reaction was repeated, but a thin film of C_{60} was used. Where condensation of ytterbium vapour had occurred in the previous experiment, a sample of C_{60} was sublimed and condensed on the walls of the reaction vessel. After 15 seconds exposure to an argon plasma, the ytterbium vaporised onto the C_{60} film and was exposed to a further 5 seconds to anneal the sample. On removal, the sample appeared black, and the reaction vessel was bronzed in areas where ytterbium vapour had condensed and where there was no C_{60} present. The zirconia/magnesia crucible was fractured and blackened in the area where the metal was housed prior to vaporisation.

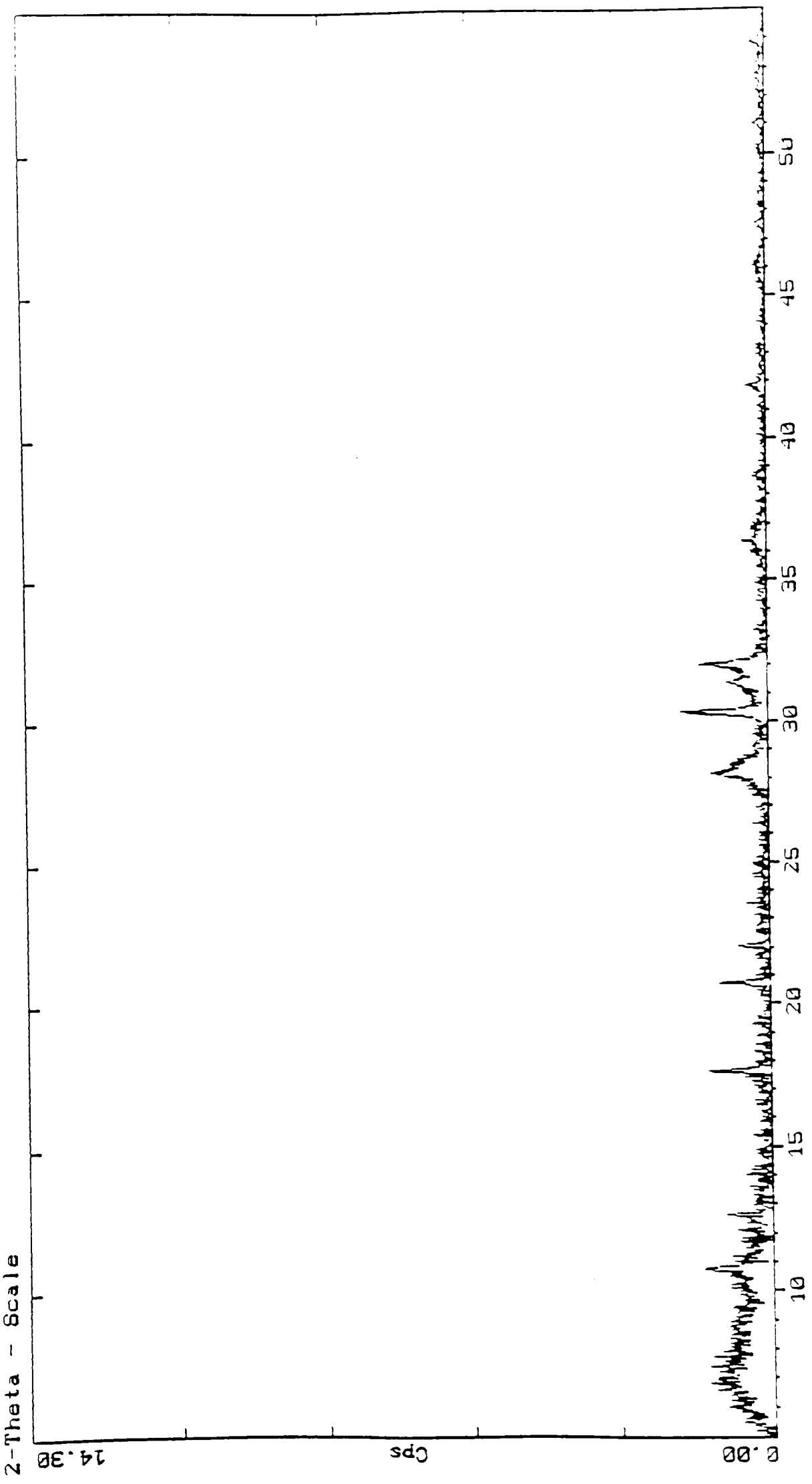


Figure 4.18.2. Capillary powder X-ray powder diffraction pattern from a reaction of ytterbium metal with C_{60} powder under the action of a microwave induced argon plasma.

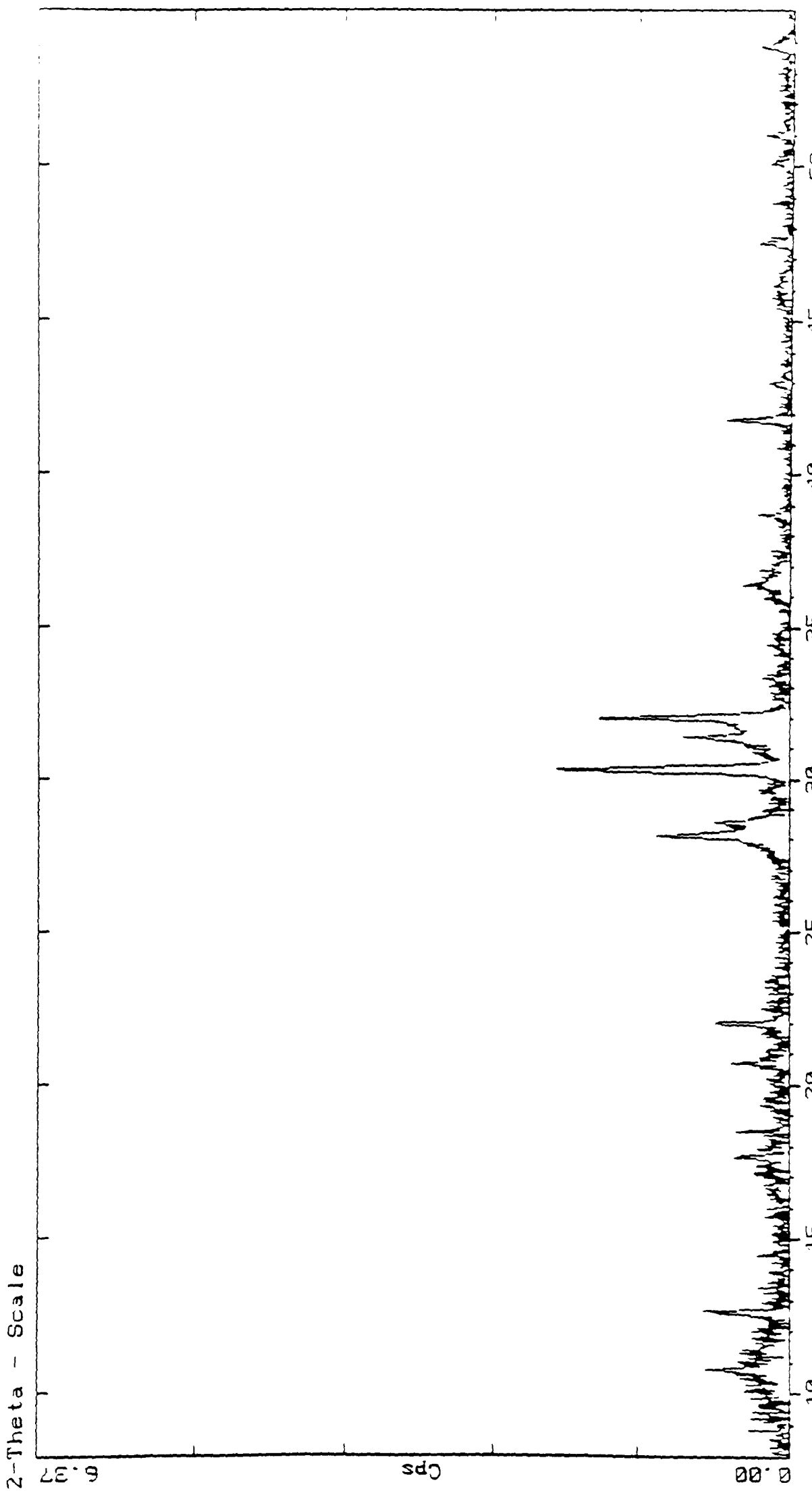


Figure 4.18.3. Capillary powder X-ray powder diffraction pattern from annealing of an ytterbium C_{60} sample under the action of a microwave induced argon plasma.

The black sample was flaky and on grinding using an agate mortar appeared as a fine black powder. Powder X-ray crystallography showed the presence of peaks other than C_{60} but they appeared broad and diffuse as shown in figure 4.18.1.2. SQUID magnetometry showed a paramagnetic response down to 6K and no significant difference between field cooled (50G) and zero field cooled data below 60K. This indicates the paramagnetic species is most likely to be due to an amount of a Yb(III) species being present.

Annealing of the Yb_xC_{60} phase assemblage was performed to improve the crystallinity of the sample. Exposure to 3 x 10 seconds and subsequent powder X-ray crystallography showed that the crystallinity had improved, as shown in figure 4.18.1.3., but attempts at indexing the pattern have so far been unsuccessful.

4.19. Discussion and Summary.

The synthesis of known sodium, potassium, rubidium and caesium binary phases of C_{60}, using a microwave induced argon plasma, has been demonstrated. Using an microwave induced argon plasma, reduces the time required for reaction, from several days to less than a minute as compared to conventional thermal techniques.

Reaction using a microwave induced argon plasma of lithium or ytterbium metal with C_{60} showed that a microwave induced argon plasma can be used in the synthesis of new C_{60} containing materials of lithium and ytterbium.

The heat generated by a microwave induced argon plasma derives from the interaction of ions, that constitute a plasma, and the substance bounding or immersed within it. Bombardment of a plasma immersed sample, by plasma ions, causes kinetic energy of the ions to be converted to heat energy of the immersed substance. This heat provides enough energy for excitation of an interstitial cation, to jump randomly into an adjacent vacant site. i.e. diffusion of cations throughout the C_{60} lattice occurs.

There is no reason why this technique cannot be used in the synthesis of other solid state materials that do not effectively couple with microwave radiation at 2.45GHz. It has been shown that temperatures in excess of those achieved in this thesis are possible by using different gases.[28]

Experimental Details for Chapter 4.

4.20. Manipulations and Solvents

Manipulations of air and moisture sensitive materials were performed using standard Schlenk techniques, and dual nitrogen (or argon) and vacuum manifolds. In house nitrogen was purified by passage over 'MnO' and 4Å molecular sieves and argon used as provided by BOC.

All manipulations requiring solvents were performed in a dinitrogen filled drybox, with the dinitrogen purified over BASF catalyst and 4Å molecular sieves.

Solid manipulations were performed in a He filled drybox with the He purified over a hot copper catalyst.

Solvents were predried by standing over 4Å molecular sieves followed by refluxing and distillation from a suitable drying agent under an atmosphere of dinitrogen. The drying agents used were potassium (toluene) and calcium hydride (acetonitrile).

All reactions were performed using sublimed C_{60} prepared as described in section 1.13. and stored in a He drybox.

4.21. Instrumental Methods

Magnetic Measurements were recorded using a Cryogenic Consultants S600C SQUID magnetometer fitted with a Lakeshore temperature controller. Samples were sealed in 2 mm quartz capillaries under an atmosphere of He.

Solid State NMR spectra were recorded on a Bruker MSL200 with a Bruker HP WB 73A MAS 7DB probe. Samples were contained in a KEL-F insert within a 7mm zirconia rotor and referenced externally to adamantane.

Powder X-ray Diffraction data was collected in transmission geometry on samples sealed in quartz capillaries, using a Siemens D5000 instrument with a position sensitive detector and Cu $K\alpha_1$ radiation.

4.22. Synthesis of the Saturated K, Rb and Cs Phases of C_{60}.

Synthesis of the saturated C_{60} phases of K, Rb, and Cs was performed in Pyrex tubes, flame sealed under a helium pressure of 10^{-5}mbar, as shown in figure 4.22.1, via a turbomolecular pump. A homemade tube furnace, controlled by a Eurotherm temperature controller and thermocouple, was used to heat the reactants. The furnace had previously been calibrated along its length at various set temperatures using an external thermocouple, allowing control of the temperature gradient over the reaction vessel.

Typically, 75mg of C_{60} was placed in a Pyrex tube with approximately a 10 fold molar excess of the alkali metal. A temperature gradient of approximately $1Kcm^{-1}$ was applied along the length of the reactant vessel with the alkali metal at the cooler end.

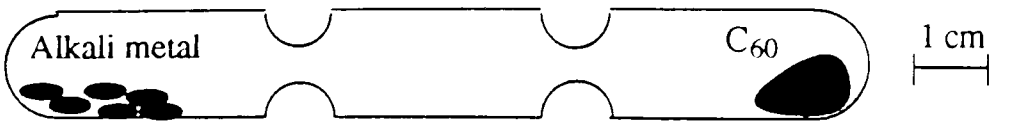


Figure 4.22.1.

Samples were heated at temperatures and times as shown in table 4.22.1. After a suitable length of time the intercalate of alkali metal and C_{60} was removed, ground in an agate mortar and pestle, resealed in a fresh Pyrex tube, and placed back in the furnace to anneal.

Table 4.22.1.

K		Rb		Cs	
Temp/°C	Time/days	Temp/°C	Time/days	Temp/°C	Time/days
100	1	75	1	75	1
175	1	150	1	150	1
275	2	200	2	200	2
350	3	250	3	250	3
Intermediately ground with an agate mortar and pestle and annealed.					
350	7	350	7	350	7

The samples was characterised by mass uptake of the relevant alkali metal and by ^{13}C MASNMR spectroscopy.

4.23. Conventional Thermal Synthesis of K, Rb and Cs Fullerides.

Reactions were performed in Pyrex tubes flame sealed under 10^{-5}mbar of He. All the known phases stable at room temperature and pressure were synthesised by heating the samples at 350°C for 7 days with an intermediate grinding and further heating for 5 days as required. The phases synthesised were K_3C_{60}, K_4C_{60}, Rb_1C_{60}, Rb_3C_{60}, Rb_4C_{60}, Cs_1C_{60} and Cs_4C_{60}. Typically, a sample of a saturated alkali metal C_{60} phase was diluted with the appropriate quantity of C_{60} to give the required composition, and then the mixture ground using an agate mortar . Total sample masses of 30 - 50mg were typically aimed for.

Characterisation was by powder X-ray crystallography and ^{13}C MASNMR spectroscopy.

4.24. Synthesis of Alkali Metal Fullerides using Microwave Techniques.

All reactions described were performed in a 1kW (2.45 GHz) Hinari 'Lifestyle' microwave oven fitted with a variable power unit to allow continuous microwave irradiation at variable power. Fire bricks were used to support reaction vessels to avoid heating the cavity floor and also to allow the vessels to be positioned in the required

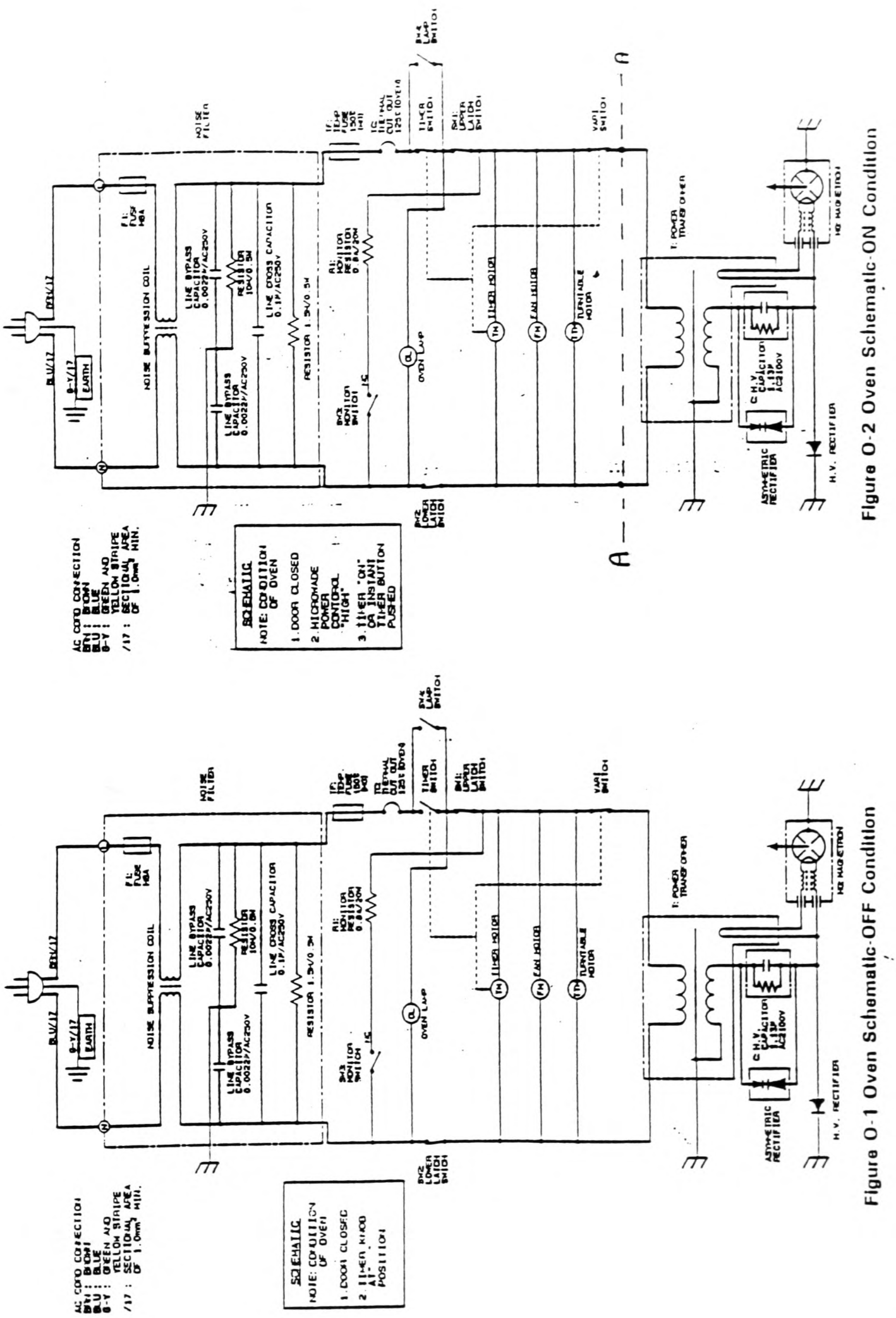


Figure 4.24.1. Microwave oven circuit diagram for the supply of microwave radiation at 2.45GHz.

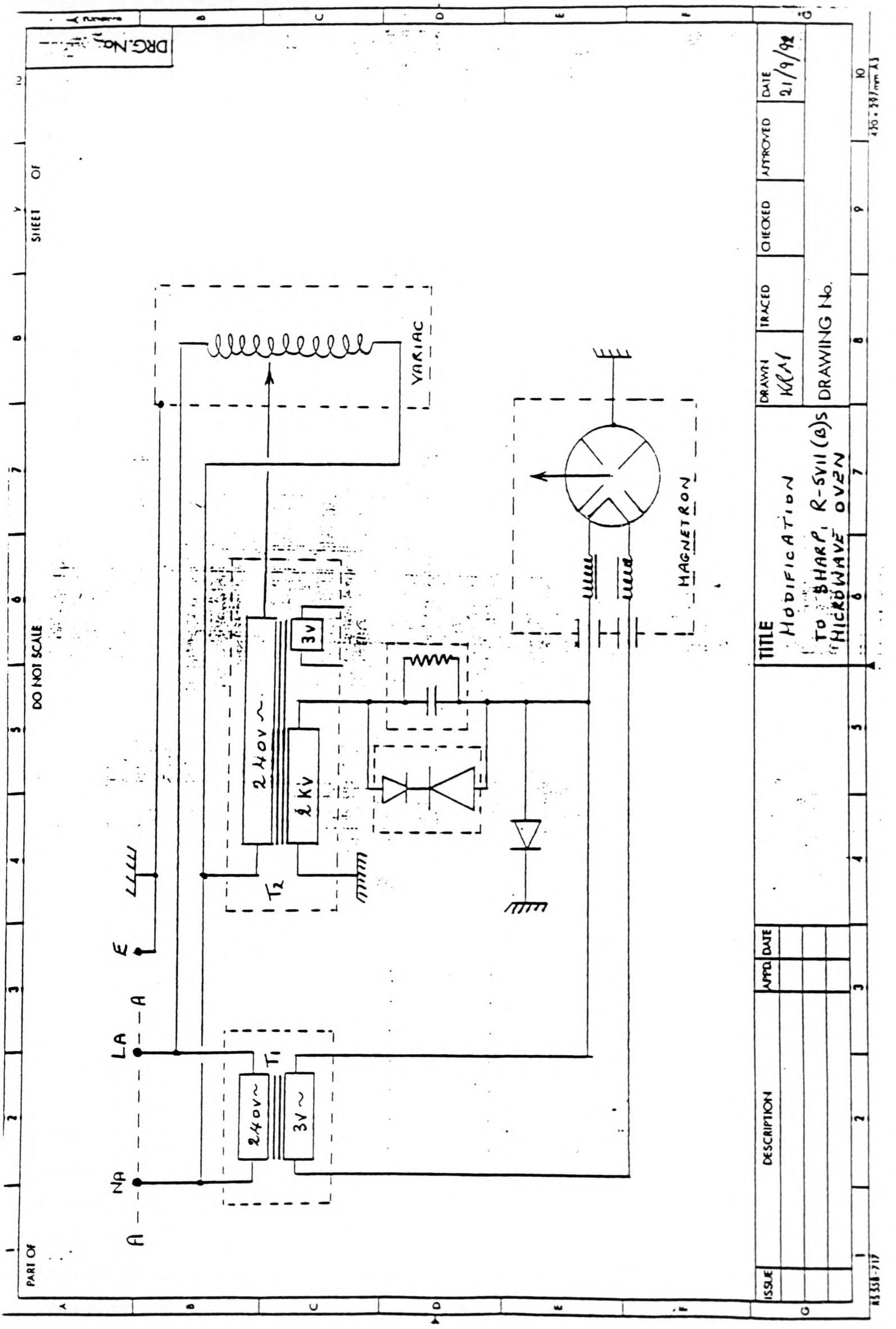


Figure 4.2.4.2. Modification to allow continuous microwave radiation at variable power controlled by an external Variac.

region of microwave radiation. Relevant circuit diagrams of the original and modified oven are given in figures 4.24.1. and 4.24.2.

4.25. Synthesis of a K_xC_{60} Phase Assemblage from K and C_{60} using an Argon Microwave Induced Plasma.

The apparatus used is shown in figure 4.25.1. Typically, freshly cut potassium (100mg) was placed in the alumina crucible and loaded into the reaction vessel. Ground C_{60} powder (40mg) was then carefully transferred into the trough of the reaction vessel using a funnel fashioned from a Pasteur pipette. The reaction vessel must be kept upright at all times which was most easily achieved using a suitable sized conical flask. To obtain a small pressure of argon, which is the source of the plasma, the vessel was pump/filled three times with argon to a final pressure of 10^{-1} mbar. The apparatus was then attached to a turbomolecular pump and the pressure reduced slowly to 10^{-5} mbar to avoid C_{60} powder being dispersed.

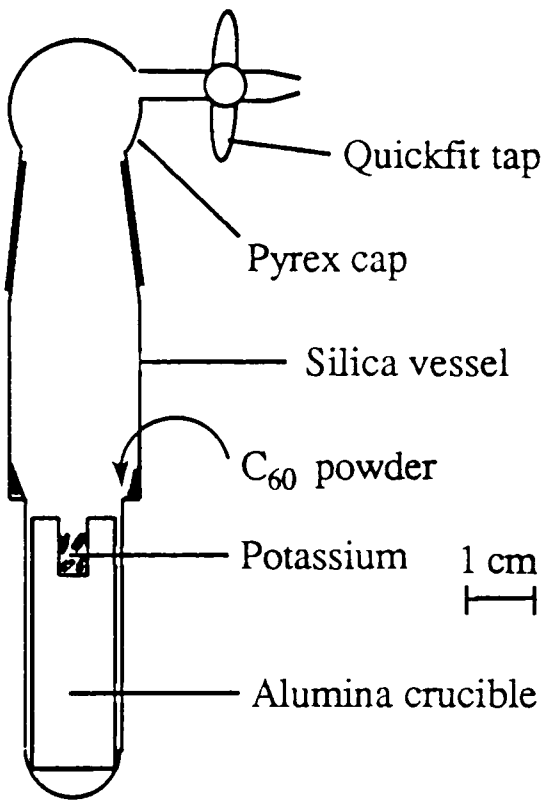


Figure 4.25.1. Reusable apparatus for the synthesis of a K_xC_{60} phase assemblage.

Firebricks, one drilled to accommodate the bottom inch of the reaction vessel, were used as a support and to position the apparatus in the microwave oven.

The microwave power was gradually increased, until a plasma was struck, and then quickly increased to maximum power. Initially the argon plasma was present in the whole of the reaction vessel volume but, after approximately 5 seconds, the plasma concentrated around the alumina crucible and partially covered the trough containing the C_{60} powder. Continual application of maximum power led to the alumina crucible becoming very hot as was indicated by the crucible glowing red. At this point the potassium vaporised from the crucible onto both the walls and the C_{60} powder. Further irradiation was continued for 5 seconds to partially anneal the product. After allowing the vessel to cool some bronzing can be observed on the vessel walls, and the crucible was partially black, particularly in the area where the potassium was initially located.

Taking care to keep the apparatus in an upright position the glass cap was twisted in order to determine whether it would be possible to remove the cap in the drybox. Occasionally the heat generated during the reaction can cause the cap to stick onto the main body of the reaction vessel. This can be rectified by connecting the vessel to an argon manifold with exit bubbler, introducing argon into the reaction vessel, and heating the affected area quickly with a blow torch. The different coefficients of expansion of Pyrex and silica, result in the dislocation of the joint. Quickly regreasing the joint and pump filling with argon several times allows recovery of the air sensitive product.

The product is black. Virtually all the C_{60} containing material can be recovered, with mass uptake indicating the K_xC_{60} sample has a value for x between 4 and 6.

The reaction vessel can be reused after cleaning with 20% aqueous hydrofluoric acid and the crucible by soaking in aqua regia overnight. However the crucible never returns to its original pale yellow colour and occasionally the alumina crucible can fracture during reaction or on cooling.

^{13}C MASNMR spectroscopy gives the composition of the phase assemblage and allows the determination of the percentage of potassium in the sample by integration of the peak areas, using the cut and weigh method.

4.26. Synthesis of K_3C_{60} from C_{60} and a K_xC_{60} Phase Assemblage.

A sample of a K_xC_{60} phase assemblage (30mg) of which x had been determined via ^{13}C MASNMR spectroscopy, was diluted with C_{60} to obtain the composition K_3C_{60}. The sample was ground using an agate mortar and placed in a Pyrex tube and sealed with a glass stopcock fitted with a Teflon seal under an argon atmosphere, at a pressure of 10^{-1} mbar, as shown in figure 4.26.1.

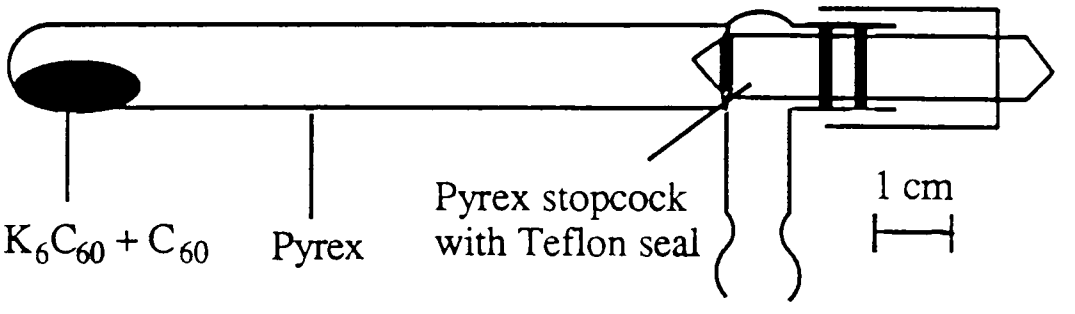


Figure 4.26.1. Simple apparatus for the synthesis of K_3C_{60}.

Exposure to a microwave induced argon plasma for 2 x 5 seconds at maximum power changed the sample from a brown to a black powder.

Characterisation was by ^{13}C MASNMR spectroscopy, powder X-ray crystallography and SQUID magnetometry.

4.27. Synthesis of K_3C_{60} and K_4C_{60} from $K_{6.7}C_{60}$ and C_{60}.

$K_{6.7}C_{60}$ (25mg, 0.039mmol) and the appropriate mass of C_{60} were ground together using an agate mortar and placed in a Pyrex tube under an argon atmosphere at

a pressure of 10^{-1} mbar The vessel was then sealed with a glass stopcock fitted with a Teflon seal. The dark brown mixture was exposed to a microwave induced argon plasma at maximum power for 5 seconds. On initiation of the plasma the sample tended to become fluidised which results in material being spread over the vessel walls. Occasionally orange sparks were observed on the surface of the powdered sample. On exposure to the plasma the vessel became hot (*ca.* 100-150°C) at the place where the sample was present. The product is a black microcrystalline solid consistent with all other alkali fullerides.

The vessel was positioned in the oven so that the plasma was localised around the sample region. This was necessary to avoid degradation of the Teflon seal, which occurs rapidly on exposure to a microwave induced argon plasma.

Characterisation was by ^{13}C MASNMR spectroscopy and powder X-ray crystallography.

4.28. Synthesis of Rb_1C_{60}, Rb_3C_{60} and Rb_4C_{60} from $Rb_{6.7}C_{60}$ and C_{60}.

$Rb_{6.7}C_{60}$ (20mg, 0.015mmol) and the required quantity of C_{60} were ground together using an agate mortar and placed in a Pyrex tube under an argon atmosphere at a pressure of 10^{-1}mbar sealed with a glass stopcock fitted with a Teflon seal. The dark brown solid was exposed to a microwave induced argon plasma at maximum power for 2 x 5 seconds. On initiation of the plasma the sample became fluidised which resulted in the sample being spread over the vessel walls and occasionally orange sparks could be observed on the surface of the powdered sample. After exposure the walls of the vessel were hot (*ca.* 100-150°C) where the sample was located and slightly above room temperature elsewhere. Rb_1C_{60} required an intermediate regrinding and further exposure to the plasma for 2 x 5 seconds. The products are black microcrystalline solids consistent with all other alkali fullerides.

Characterisation was by ^{13}C MASNMR spectroscopy and powder X-ray crystallography.

4.29. Synthesis of Cs_1C_{60} and Cs_4C_{60} from $Cs_{6.7}C_{60}$ and C_{60}.

$Cs_{6.7}C_{60}$ (20mg, 0.012mmol) and the required mass of C_{60} were ground together in an agate mortar and placed in a Pyrex tube under an argon atmosphere at a pressure of 10^{-1} mbar. The tube was sealed with a glass stopcock fitted with a Teflon seal. The dark brown solid was exposed to a microwave induced argon plasma at maximum power for 2 x 5 seconds. On initiation of the plasma the sample is prone to excitation which results in material being spread over the vessel walls and occasionally orange sparks could be observed on the surface of the powdered sample. After exposure the vessel was hot (*ca.* 100-150°C) where the sample was located. Cs_1C_{60} required an intermediate regrind and further exposure to the plasma for 2 x 5 seconds. The products are black microcrystalline solids consistent with all other alkali fullerides.

Characterisation was by ^{13}C MASNMR spectroscopy and powder X-ray crystallography.

4.30. Reaction of Na_6C_{60} and One Equivalent of C_{60}.

A sample of Na_6C_{60} (15mg) was diluted with one equivalent of C_{60} (12.6mg), ground using an agate mortar and sealed in a Pyrex tube with a glass stopcock fitted with a Teflon seal under argon at a pressure of 10^{-1} mbar. The sample was exposed at maximum power for 3 x 5 seconds to a microwave induced argon plasma. After 7 seconds the sample became agitated and spread onto the walls of the reaction vessel. On removal of the sample it had changed from brown to black and on grinding using an agate mortar the sample still appeared black.

^{13}C MASNMR spectroscopy showed diffusion of sodium within the C_{60} lattice had occurred, but the reaction was not at completion. The reactants were flame sealed, under 10^{-1}mbar of argon, in a silica tube to avoid tube failure, which had occurred on a previous occasion. Exposure of the sample to 3 x 10 seconds at maximum power followed by ^{13}C MASNMR spectroscopy revealed the sample had not changed.

4.31. Reaction of Li Metal and C_{60}.

Powdered C_{60} (50mg, 0.07mmol) was flame sealed in a Pyrex tube under an argon atmosphere at a pressure of 10^{-1} mbar with 6 equivalents of freshly cut Li metal (2.9mg). On exposure to microwave radiation at maximum power for 1 minute, a plasma discharge did not result and the sample and reaction vessel remained at room temperature. A plasma would not initiate even after preheating the sample with a heat gun or exposure to a Tesla coil. The sample was returned to the oven and exposed to full power for the maximum time available of 99 mins. During this period sufficient heat was generated, presumably from a plasma, to melt the lithium metal and to cause rapid vaporisation. The reaction vessel was expanded, at one end, to approximately twice its volume. Previous failures of reaction tubes, both Pyrex and silica, had resulted in collapse of the tube wall, until a hole was formed. The sample appeared black and was apparently sealed under an argon atmosphere. Removal of the sample showed no obvious signs that reaction of the Pyrex tube with lithium metal had occurred.

Characterisation of the sample was by ^{13}C MASNMR spectroscopy and powder X-ray crystallography. ^{13}C MASNMR showed only a broad resonance centred around δ 155ppm and a small peak at δ 143ppm attributable to C_{60}. Powder X-ray crystallography showed peaks attributable to C_{60} and peaks at *ca.* 15° which could be tentatively be indexed as (200) and belong to at least two new binary phases of lithium C_{60} intercalates. Indexing of the diffraction pattern has so far been unsuccessful.

4.32. Vaporisation of Ytterbium Metal in an Alumina Crucible using a Microwave Induced Argon Plasma.

Freshly cut ytterbium metal (50mg) was placed inside an alumina crucible and

flame sealed in a silica tube at an argon pressure of 10^{-5} mbar as shown in figure 4.32.1. A firebrick which had had a hole drilled into it to accommodate the tube was used as a support.

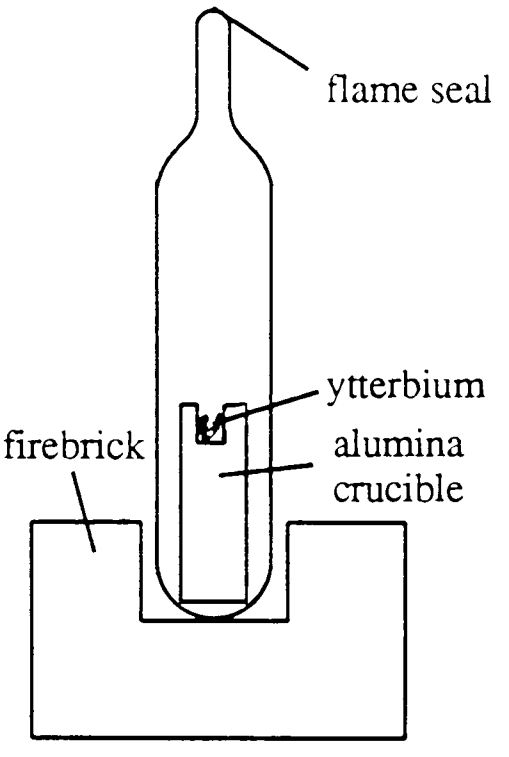


Figure 4.32.1. Apparatus used to test the viability of vaporising ytterbium metal.

Exposure to microwave radiation at maximum power for 2 x 30 seconds caused the alumina to glow red but the ytterbium did not sublime. On application of a further 30 seconds a brilliant green flash occurred and the walls of the reaction vessel became covered with ytterbium vapour. The reaction vessel was allowed to cool to room temperature, and on removal from the oven, bronzing of the vessel walls was evident and the alumina crucible appeared black at the top.

4.33. Vaporisation of Ytterbium Metal in a Zirconia/Magnesia Crucible using a Microwave Induced Argon Plasma.

A piece of zirconia rod stabilised with 8% magnesia (50mm x 10mm dia) as supplied by Goodfellow was fashioned into a crucible by drilling a hole (7mm x 5mm dia) with a diamond drill bit.

Freshly cut ytterbium metal (50mg) was placed inside a zirconia/magnesia crucible and contained in the same apparatus as used for the synthesis of a K_xC_{60} phase assemblage described in section 4.23. The apparatus was put under an argon pressure at 10^{-5} mbar and treated with microwave radiation at the maximum power available. After 15 seconds a brilliant green flash occurred and ytterbium vapour began to condense on the walls of the reaction vessel. After cooling the crucible had fractured where the metal had been located prior to vaporisation and severe blackening of the crucible had also occurred.

4.34. Reaction of Ytterbium Metal and Powdered C_{60}.

Freshly cut ytterbium (75mg) was contained in a zirconia/magnesia crucible and placed in the reaction vessel with powdered C_{60} (30mg), as described in section 4.21.

On application of the microwaves at full power for 15 seconds a brilliant green flash occurred and ytterbium vapour condensed on the walls of the reaction vessel. The large majority of vapour did not condense onto the C_{60} powder. On removal from the vessel the sample appeared unchanged and on grinding using an agate mortar revealed a solid which had the tan colouration of C_{60}.

Characterisation by X-ray crystallography showed the majority of the product was essentially C_{60}.

4.34.1 Reaction of Ytterbium Metal and a Film of C_{60} and Subsequent Annealing.

The reaction described in 4.34 was repeated, with the exception that prior to vaporisation of the metal the C_{60} sample was sublimed onto the walls of the reaction vessel, where most of the ytterbium had condensed in the previous reaction, as shown in figure 4.34.1.

After 15 seconds of exposure to a microwave induced argon plasma at maximum power, the ytterbium metal vaporised, and it condensed onto the C_{60} film and also onto the bare walls of the reaction vessel. Removal of the sample, by scrapping with a Pasteur pipette, gave a black solid that on grinding using an agate mortar remained black.

Powder X-ray crystallography of the product showed C_{60} was present together with other diffracting material that could not be indexed. SQUID magnetometry on a 5mg sample sealed in a quartz capillary under He did not show any superconducting phase to be present.

The sample was annealed by sealing the sample in a Pyrex tube under an argon atmosphere of 10^{-1} mbar with a glass stopcock fitted with a Teflon seal. On exposure to microwave radiation at maximum power for 3 x 10 seconds, the sample became agitated under the action of the microwave induced argon plasma. On removing the vessel from the oven the Pyrex tube was very hot (*ca.* 200°C) where the sample was residing

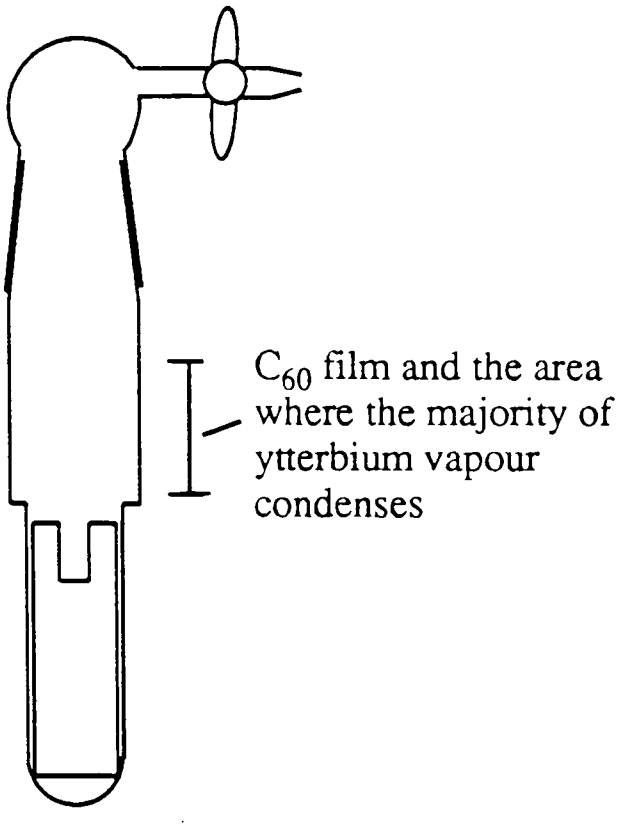


Figure 4.34.1.

Powder X-ray crystallography still showed peaks corresponding to C_{60}, but the other phase(s) had undergone annealing as could be seen from the increased crystallinity of the sample.

References

1. Das, S.; Curlee, T. R. *Ceram. Bull.* 1987, ***66***, 1093.
2. Hamblyn, S. M. L.; Rueben, B. G. *Adv. Inorg. Chem. Radiochem.* 1975, ***17***, 90.
3. Mingos, D. M. P.; Baghurst, D. R. *Chem. Soc. Rev.* 1991, ***20***, 1.
4. Musil, J. *Vacuum* 1986, ***36***, 161.
5. Sutton, W. H. *Ceram. Bull.* 1989, ***68***, 376.
6. Omstead, T. R.; Annapragada, A. V.; Jensen, K. F. *Appl. Phys. Lett.* 1990, ***57***, 2543.
7. Vinckier, C.; Dumoulin, A.; Cortouts, J.; Jaegere, S. D. *J. Chem. Soc., Faraday Trans.* 1988, ***84***, 1725.
8. Asmussen, J.; Mallavarpu, R.; Hamann, J. R.; Park, H. C. *Proceedings of the IEEE* 1974, ***62***, 109.
9. Meiners, L. G.; Alford, D. B. *Rev. Sci. Instrum.* 1986, ***57***, 164.
10. Goode, S. R.; Buddin, N. P.; Chambers, B.; Baughman, K. W.; Deavor, J. P. *Spectrochimica. Acta.* 1985, ***40B***, 317.
11. Moisan, M.; Barbeau, C.; Claude, R.; Ferreira, C. M.; Margot, J.; Paraszczak, J.; Sa, A. B.; Suave, G.; Wertheimer, M. R. *J. Vac. Sci. Technol. B* 1991, ***9***, 8.
12. Pagnotta, M.; Nolan, A.; Kim, L. *J. Chem. Ed.* 1992, ***69***, 599.
13. Rau, H.; Trafford, B. *J. Phys. D: Appl. Phys.* 1990, ***23***, 6137.
14. Debye, P. *Polar Molecules* ; New York, 1929.
15. Frolich, H. *Theory of Dielectrics* 2nd ed.; Oxford University Press: London, 1958.
16. Daniel, V. *Dielectric Relaxation* ; Academic Press: New York, 1967.
17. Cole, K. S.; Cole, R. H. *J. Chem. Phys.* 1941, ***9***, 341.
18. Hill, N.; Vaughan, W. E.; Price, A. H.; Davies, M. *Dielectric Properties and Molecular Behaviour* ; van Nonstrand: New York, 1969.
19. Hasted, J. B. *Aqueous Dielectrics* ; Chapman and Hall: London, 1973.
20. West, A. R. *Solid State Chemistry and its Applications* ; John Wiley & Sons: 1987.
21. Hippel, A. R. v. *Dielectric Materials and Applications* ; MIT Press: 1954.
22. Bottcher, C. J. F. *Theory of Electric Polarisation* ; Elsevier: Amstrerdam, 1952.
23. Coelho, R. *Physics of Dielectrics for the Engineer* ; Elsevier: Amsterdam, 1979.
24. Anderson, J. C. *Dielectrics* ; Chapamn and Hall: London, 1964.
25. Kharaldy, M. M. Z.; Jackson, W. *Proc. Institute of Electrical Engineers* 1953, ***100***, 199.
26. Maxwell, J. C. *A Treatise on Electricity and Magnetism* ; Dover Publications: Dover, 1954.
27. Wagner, K. W. *Arch. Elekrotech* 1914, ***2***, 371.

28. Kemer, E. L.; Johnson, D. L. *Am. Ceram. Soc. Bull.* 1985, ***64***, 1132.
29. Bennett, C. E. G.; McKinnon, N. A.; Williams, L. S. *Nature* 1968, ***217***, 1287.
30. Samuels, J.; Brandon, J. R. *J. Mat. Sci.* 1992, ***27***, 3259.
31. Holcombe, C. E.; Meek, T. T.; Dykes, N. L. *J. Mat. Sci. Lett.* 1988, *7*, 881.
32. Kenkre, V. M.; Skala, L.; Weiser, M. W.; Katz, J. D. *J. mat. Sci.* 1991, ***26***, 2481.
33. Kriegsmann, G. A. *J. Appl. Phys.* 1992, ***71***, 1960.
34. Meek, T. T. *J. Mat. Sci. Lett.* 1987, ***6***, 638.
35. Robertson, W. W.; Arjavalingham, G.; Shinde, S. L. *J. Appl. Phys.* 1991, ***70***, 7648.
36. Wright, R. A.; Cocks, F. H.; Vaniman, D. T.; Blake, R. D.; Meek, T. T. *J. Mat. Sci.* 1989, ***24***, 1337.
37. Holcombe, C. E.; Dykes, N. L. *J. Mat. Sci.* 1991, ***26***, 1730.
38. Kenkre, V. M.; Kus, M.; Katz, J. D. *Phys. Stat. Sol. (B)* 1992, ***172***, 337.
39. Sheppard, I. M. *Ceram. Bull.* 1988, ***67***, 1656.
40. Varadan, V. K.; Ma, Y.; Lakhtakia, A.; Varadan, V. V. *Materials Research Society,* 1988, 199.
41. Brown, S. C. *Basic Data in Plasma Physics* ; MIT Press: Cambridge Mass., 1959.
42. Kieser, J.; Neush, M. *Thin Solid Films* 1984, ***118***, 203.
43. Wertheimer, M. R.; Klemberg-Sapieha, J. E.; Schreiber, H. P. *Thin Solid Films* 1984, ***115***, 109.
44. Suzuki, K.; Okundaira, S.; Sakudo, N.; Kanomata, I. *Jap. J. Appl. Phys.* 1977, ***16***, 1979.
45. Zerger, R. P.; McMahon, K. C.; Seltzer, M. D.; Michel, R. G.; Suib, S. L. *J. Catal.* 1985, ***99***, 494.
46. Golant, V. E.; Zhilinsky, A. P.; Sakharov, I. E.; Brown, S. C. *Fundamentals in Plasma Physics* ; John Wiley & Sons: 1977.
47. Ohtsuki, Y. H.; Ofuruton, H. *Nature* 1991, ***350***, 139.
48. Allison, J.; Cullen, A. L.; Zavody, A. *Nature* 1962, ***193***, 156.
49. Knecht, J. P.; Micci, M. M. *AIAA Journal* 1988, ***26***, 188.
50. Hebbard, A. F.; Rosseinsky, M. J.; Haddon, R. C.; Murphy, D. W.; Glarum, S. H.; Palstra, T. T. M.; Ramirez, A. P.; Kortan, A. R. *Nature* 1991, ***350***, 600.
51. McCauley, J. P.; Zhu, Q.; Coustel, N.; Zhou, O.; Vaughan, G.; Idziak, S. H. J.; Fischer, J. E.; Tozer, S. W.; Groski, D. M.; Bykovetz, N.; Lin, C. L.; McGhie, A. R.; Allen, B. H.; Romanow, W. J.; Denenstein, A. M.; III, A. B. S. *J. Am. Chem. Soc.* 1991, ***113***, 8537.
52. Murphy, D. W.; Rosseinsky, M. J.; Fleming, R. M.; Tycko, R.; Ramirez, A. P.; Haddon, R. C.; Seigrist, T.; Dabbagh, G.; Tully, J. C.; Walstedt, R. E. *J.*

Phys. Chem. Solids 1992, ***53***, 1321.

53. Chabre, Y.; Djurado, D.; Armand, M.; Romanow, W. R.; Coustel, N.; McCauley, J. P.; Fischer, J. E.; III, A. B. S. *J. Am. Chem. Soc.* 1992, ***114***, 764.
54. Wang, H. H.; Kini, A. M.; Savall, B. M.; Carlson, K. D.; Williams, J. M.; Lathrop, M. W.; Lykke, K. R.; Parker, D. H.; Wurz, P.; Pellin, M. J.; Gruen, D. M.; Welp, U.; Kwok, W.-K.; Fleshler, S.; Crabtree, G. W.; Schirber, J. E.; Overmyer, D. L. *Inorg. Chem.* 1991, ***30***, 2962.
55. Wang, H. H.; Kini, A. M.; Savall, B. M.; Carlson, K. D.; Williams, J. M.; Lykke, K. R.; Parker, D. H.; Wurz, P.; Pellin, M. J.; Gruen, D. M.; Welp, U.; Kwok, W.-K.; Fleshler, S.; Crabtree, G. W. *Inorg. Chem* 1991, ***30***, 2838.
56. Ziebarth, R. P.; Buffinger, D. R.; Stenger, V. A.; Recchia, C.; Pennington, C. H. *J. Am. Chem. Soc.* 1993, ***115***, 9267.
57. Douthwaite, R. E.; Brough, A. R.; Green, M. L. H. *J. Chem. Soc., Chem. Comm.* 1994, 267.
58. Liu, X.; Wan, W. C.; Owens, S. M.; Broderick, W. E. *J. Am. Chem. Soc.* 1994, ***116***, 5489.
59. Fleming, R. M.; Ramirez, A. P.; Rosseinsky, M. J.; Murphy, D. W.; Haddon, R. C.; Zahurak, S. M.; Makhija, A. V. *Nature* 1991, ***352***, 787.
60. Kortan, A. R.; Kopylov, N.; Glarum, S.; Gyorgy, E. M.; Ramirez, A. P.; Thiel, F. A.; Haddon, R. C. *Nature* 1992, ***355***, 529.
61. Kortan, A. R.; Kopylov, N.; Glarum, S.; Gyorgy, E. M.; Ramirez, A. P.; Fleming, R. M.; Zhou, O.; Thiel, F. A.; Trevor, P. L.; Haddon, R. C. *Nature* 1992, ***360***, 566.
62. Whittaker, A. G.; Mingos, D. M. P. *J. Chem. Soc., Dalton Trans.* 1993, 2541.
63. Whittaker, A. G.; Mingos, D. M. P. *J. Chem. Soc., Dalton Trans.* 1992, 2751.
64. Baziard, Y.; Breton, S.; Toutain, S.; Gourdenne, A. *Eur. Polym. J.* 1988, ***24***, 521.
65. Chauvet, O.; Oszlanyi, G.; Forro, L.; Stephens, P. W.; Tegze, M.; Faigol, G.; Janossy, A. *Phys. Rev. Lett.* 1994, ***72***, 2721.
66. Tycko, R.; Dabbagh, G.; Murphy, D. W.; Zhu, Q.; Fischer, J. E. *Phys. Rev. B* 1993, ***48***, 9097.
67. Zhou, O.; Cox, D. E. *J. Phys. Chem. Solids* 1992, ***53***, 1373.
68. Gordon, A. J.; Ford, R. A. *The Chemist's Companion* ; John Wiley & Sons: 1972.
69. Goodfellow Catalogue ; 1994/5.

Appendices

Appendix A

Refinement of Cell Parameters for NaC_{60}.5thf

Unit Cell Parameters after 5 cycles of refinement

a(Å)	b(Å)	c(Å)	ALPHA	BETA	GAMMA
12.705(20)	15.981(8)	10.093(9)	92.52(9)	95.92(10)	74.50(13)

Incident wavelength = 0.87190Å Cell volume = 1962Å^3

TWO THETA(degrees)

OBS	CALC	H	K	L
3.2619	3.2447	0	1	0
4.0785	4.0993	1	0	0
4.5064	4.5061	1	1	0
4.9763	4.9787	0	0	1
6.3781	6.3780	-1	-1	1
6.6877	6.7003	1	2	0
7.0437	7.0396	1	1	1
7.4786	7.4756	-1	1	1
9.8543	9.8472	2	1	1
10.4124	10.4133	-1	0	2
10.4828	10.4871	-1	-3	1
10.5235	10.5278	-1	-1	2
10.7090	10.7304	2	2	1
10.8732	10.8714	0	-3	1
10.9938	11.0057	1	3	1
11.1196	11.1363	1	0	2
11.3569	11.3427	1	1	2

Appendix B

Refinement of Cell Parameters for Na_6C_{60}

Unit Cell Parameters after 5 cycles of refinement

a(Å)	b(Å)	c(Å)	ALPHA	BETA	GAMMA
10.280(12)	10.280(12)	16.666(16)	90	90	120

Incident wavelength = 1.54051Å Cell volume = 1525Å^3

TWO THETA(degrees)

OBS	CALC	H	K	L
9.8930	9.9262	1	0	0
10.5670	10.6071	0	0	2
14.5410	14.5467	1	0	2
17.2010	17.2361	1	1	0
18.8460	18.8116	1	0	3
20.3070	20.2809	1	1	2
21.2890	21.3064	0	0	4

Appendix C

Refinement of Cell Parameters for Na_9C_{60}

Unit Cell Parameters after 5 cycles of refinement

a(Å)	b(Å)	c(Å)	ALPHA	BETA	GAMMA
10.168(4)	10.168(4)	16.651(9)	90	90	120

Incident wavelength = 1.54051Å Cell volume = 1525Å^3

TWO THETA(degrees)

OBS	CALC	H	K	L
10.0130	10.0359	1	0	0
10.5930	10.6172	0	0	2
17.3960	17.4275	1	1	0
18.8960	18.8834	1	0	3
20.4470	20.4501	1	1	2
21.3130	21.3270	0	0	4
22.3970	22.3277	2	0	2
23.6530	23.6206	1	0	4
30.4370	30.4253	3	0	0
31.3250	31.3095	2	1	3
33.3200	33.3376	1	0	6
35.2480	35.2753	2	2	0

Appendix D
Calculation of the Superconducting Shielding Fraction of K_3C_{60} Prepared by Microwave Techniques.

For a perfect superconducting sphere, the flux exclusion (zfc) produces a magnetic moment m.

$$\frac{m}{V} = M = -\frac{3}{2}\frac{B}{\mu_0}$$

$$m = -1.194 \times 10^{-6} \times B \times V$$

Where V is the volume (m^3), M is magnetisation (Am^{-1}) (or magnetic moment per unit volume), B is the field (T), μ_0 is the permeability of free space ($4\pi \times 10^{-7}$ TmA^{-1}), and the factor of 3/2 is a consequence of treating the particles as spheres.

The superconducting volume fraction is derived by comparing the measured value of the magnetic moment with the 100% calculation.

For 2.6mg of K_3C_{60} the measured values of m(Am^2) at the fields indicated (zfc) were

$m(38G) = -1.97 \times 10^{-6}\ Am^2$ $\qquad$ $m(29G) = -1.699 \times 10^{-6}\ Am^2$

Subtracting the two values to allow for remnant field, trapped flux in solenoid etc.

$$m(9G) = -0.271 \times 10^{-6} Am^2$$

Calculation of the theoretical moment for 2.6mg of K_3C_{60} with 100% flux exclusion requires the volume of 2.6mg of K_3C_{60} which has cubic symmetry, a lattice parameter of 14.24Å, and 4 formula units per unit cell.

$$V(m^3) = \frac{m(g)}{\rho(gm^{-3})}$$

$$K_3C_{60}\ m(\text{unit cell}) = \frac{(39 \times 3 + 60 \times 12) \times 4}{6 \times 10^{23}}\ g = 5.58 \times 10^{-21}\ g$$

$$V(\text{unit cell}) = (14.24 \times 10^{-10})^3\ m^3 = 2.74 \times 10^{-27}\ m^3$$

$$\therefore \rho = \frac{5.58 \times 10^{-21}}{2.74 \times 10^{-27}} = 1.937 \times 10^6\ gm^3$$

$$V = \frac{0.0026}{1.937 \times 10^6} = 1.37 \times 10^{-9}\ m^3$$

$$m(Am^2) = -1.194 \times 10^{-6} \times 0.0009 \times 1.37 \times 10^{-9}$$

$$= -1.47 \times 10^{-6}\ Am^2$$

The volume fraction if therefore the ratio.

$$\therefore \text{Volume fraction} = \frac{0.27}{1.47} = 18.4\%$$